Techno-Economic and Environmental Assessment of Electricity-Based Renewable Hydrogen and its Derivatives

Zur Erlangung des akademischen Grades eines

Doktors der Ingenieurwissenschaften
(Dr.-Ing.)

von der KIT-Fakultät für Wirtschaftswissenschaften
des Karlsruher Instituts für Technologie (KIT)

genehmigte

Dissertation

von

Uwe Langenmayr, M.Sc.

Tag der mündlichen Prüfung:	17.03.2026
Referent:	Prof. Dr. Wolf Fichtner
Korreferent:	Prof. Dr. Dominik Möst

Acknowledgment

This dissertation bears my name, but it would not have been possible without the support of colleagues, co-authors, friends, and family, whom I would like to thank here.

First of all, I would like to express my sincere gratitude to Professor Fichtner for allowing me to conduct my research at his chair, for his supervision, and for his valuable feedback over the years. I especially appreciated his supervision style, which combined close engagement with the freedom to pursue my own ideas, as well as his reliability and the thoroughness of his feedback.

I want to thank my group leaders, Viktor, Manuel, Katrin, Patrick, and Armin, whom I frequently approached with questions and requests, and who never lost patience with me.

I particularly want to thank the four people who became good friends during my time at the institute, starting with those I shared an office with. First of all, Paul, with whom I worked on projects and publications, and who supported me with his infinite knowledge on chemical engineering. Jule, who spread her never-ending motivation and joy in our office, and contributed to my work with her research and writing skills. Alex, who kept spirits high with his snack supply, was always open to methodological discussions and didn't say no to a well-earned closing-time beer. Finally, my longtime office neighbor and friend Nina, for her sympathetic ear and reliability in staying true to her values and speaking up when it matters.

But the good relationships didn't just start at my office door. I want to thank all my institute colleagues for their support, for sharing struggles and achievements, and for always being up for a good laugh. Here, particularly Alexandra, Andreas, Anthony, Axel, Christian, David, Eric, Flo, Johannes, Leandra, Marina, Max, Nora, Sabrina, Simon G., Tim, Thomas, Thorben, and Thorsten. Thanks also go out to the colleagues who keep the institute running.

I also want to thank all my friends outside the institute, who helped me switch off stress and recharge my batteries. Finally, but most importantly, I want to thank my family for their constant support, not just during my PhD, but in the past and future. Thanks to my sisters Jenny and Lisa, my father Gust'l, my mother Brigitte, and Gertrud. I also want to thank my brother David. I hope you are doing well out there.

Abstract

Climate change mitigation requires transforming the energy system through the adoption of low-carbon technologies, such as renewable electricity generation and electrification. Yet, electrification has limits. Hard-to-abate sectors require high-temperature heat or specific energy carriers, and areas such as long-distance aviation remain infeasible to electrify. Low-carbon hydrogen and its derivatives, produced, among others, from low-carbon electricity via power-to-X applications, can replace fossil-based energy carriers in these sectors. Their development involves many stakeholders, ranging from end-users to policy-makers, who shape the future hydrogen economy while raising technical, economic, and environmental challenges.

This thesis advances research on the hydrogen economy through techno-economic and environmental assessments of electricity-based renewable hydrogen and its derivatives. The first part examines how regulated electricity supply conditions influence renewable kerosene production in a German power system model. Due to limited renewable potential in industrialized countries, large-scale imports of hydrogen and derivatives are expected. The second part develops a comprehensive, multi-method approach for modeling and evaluating stand-alone power-to-X facilities, optimizing technical setups in terms of both economic and environmental objectives. This enables multi-objective optimization across global sites, generating Pareto-optimal trade-offs for decision-making on costs, carbon intensity, and capacity needs. To address renewable variability, the optimization is developed using adaptive robust optimization, focusing on production costs to ensure reliable system operation under uncertain weather conditions. Computational expenses are addressed using representative data. The final contribution introduces a heuristic-inspired branch-and-bound algorithm that identifies the most cost-efficient transport and conversion routes among seven commodities and three transport modes, with high spatial resolution and global coverage of production sites and infrastructure.

The German power system analysis shows that electricity supply conditions closely link electrolysis demand to renewable generation. Reduced capacity factors necessitate additional electrolysis and storage capacities to maintain steady synthesis; however, this results in only slight increases in carbon abatement costs. The stand-alone facility assessment reveals that locations with windy conditions achieve lower costs and emissions, while those with sunny conditions have higher emissions due to carbon-intensive module production and lower capacity factors. The cost advantage of windy locations persists under robust optimization, though long-term uncertainties increase costs. Locations with mixed capacity factors benefit from combining low-cost wind electricity with stable solar generation. The infrastructure analysis highlights natural gas pipelines as key assets for supplying large volumes of low-cost, low-carbon hydrogen and derivatives. With Germany as a destination, imports from Northern Africa, the Middle East, Central Asia, and Northern Europe can be achieved at low costs, especially if pipelines are retrofitted for hydrogen. Ammonia and methanol emerge as preferred commodities for seaborne transport.

List of included articles

1. Paper A: Langenmayr, U. and Ruppert, M. Renewable origin, additionality, temporal and geographical correlation – eFuels production in Germany under the RED II regime. *Energy Policy*, 183:113830, Dec. 2023. ISSN 03014215. doi:10.1016/j.enpol.2023.113830. URL `https://linkinghub.elsevier.com/retrieve/pii/S0301421523004159`
2. Paper B: Langenmayr, U., Heinzmann, P., Schneider, A., Ruppert, M., Rudi, A., and Fichtner, W. Stand-alone power-to-X production dynamics: A multi-method approach to quantify the emission-cost reduction trade-off. *Journal of Industrial Ecology*, page jiec.70085, July 2025a. ISSN 1088-1980, 1530-9290. doi:10.1111/jiec.70085. URL `https://onlinelibrary.wiley.com/doi/10.1111/jiec.70085`
3. Paper C: Langenmayr, U., Slednev, V., Ruppert, M., and Fichtner, W. An adaptive robust optimization approach using scenario-based uncertainty sets for stand-alone power-to-X facilities. *Submitted to a scientific journal*, 2025c
4. Paper D: Langenmayr, U., Schuler, J., Slednev, V., and Fichtner, W. Mapping Tomorrow's Energy Journeys – A Global Perspective on the Transport of Synthetic Energy Carriers. *Submitted to a scientific journal*, 2025b

Contents

List of figures

List of tables

List of abbreviations

AEL	alkaline electrolysis
ARO	adaptive robust optimization
BEV	battery-electric vehicle
CCS	carbon capture and storage
CCU	carbon capture and utilization
DAC	direct air capture
eFuels	electricity-based hydrogen and its derivatives
EU	European Union
FT	Fischer-Tropsch
GHG	greenhouse gas
GIS	geographic information system
iRES	intermittent renewable energy sources
LCA	life cycle assessment
LC-H2D	low-carbon hydrogen and its derivatives
LH2	liquefied hydrogen
LNG	liquefied natural gas
LOHC	liquid organic hydrogen carrier
MOO	multi-objective optimization
PEM	proton exchange membrane electrolysis
PS	pointsource
PtX	power-to-X
PV	photovoltaic
REDII	renewable energy directive II
RES-E	renewable energy sources
RFNBO	renewable fuels of non-biological origin
SNG	synthetic natural gas
SOEL	solid oxide exchange electrolysis
Syngas	synthesis gas
TEA	techno-economic assessment
TRL	technology readiness level

Part I

Framework

1 Introduction

Mitigating climate change requires transforming our energy system by adopting low-carbon approaches and technologies. The replacement of fossil-based electricity generation by low-carbon technologies, such as renewable energy and nuclear power, and the electrification of applications, have been the primary approaches to reducing carbon emissions. However, electrification has its limitations, especially in the case of hard-to-abate sectors, where energy carriers are used to provide high-temperature heat or materials for industrial processes, or where electrification faces technical infeasibility, such as in parts of the aviation sector. In recent years, hydrogen and its derivatives have gained prominence as their advantages have become increasingly apparent. First, they can be applied in hard-to-abate sectors, allowing for the direct replacement of their conventional counterparts without fundamentally altering downstream value chains. Second, hydrogen can be produced in a low-carbon fashion via electrolysis using low-carbon electricity in the so-called power-to-X (PtX) process, from biomass, and using fossil energy carriers combined with carbon capture and storage (CCS). Subsequently, hydrogen can be used as a feedstock for various synthesis routes to convert it into hydrogen derivatives. These properties could make low-carbon hydrogen and its derivatives (LC-H2D) key components of the future energy system since they increase the share of low-carbon energy in hard-to-abate applications. LC-H2D could play such an important role that scenarios calculate a demand of up to 844 TWh in 2050 for Germany (Kopp et al., 2022).

While these characteristics highlight the technical potential of LC-H2D, their deployment extends far beyond technological considerations. A wide range of stakeholders, including technology developers, energy producers, investors, industrial consumers, policy makers, infrastructure operators, and end-users, are directly affected by and involved in shaping the emerging LC-H2D economy. This results in complex interactions among the technological, environmental, and socio-economic dimensions of this evolving system (Figure 1.1), raising numerous research questions.

The technological dimension encompasses the entire value chain, from production and conversion to storage, transport, and end-use applications. The technological complexity begins with the number of production paths for LC-H2D, including biogenic, electricity-based, and CCS methods. These production paths have different requirements, technological alternatives, and feedstock options. Significant infrastructure questions are raised, as different production paths require distinct infrastructure, such as terminals and pipelines for hydrogen, its derivatives, or feedstocks. Next to infrastructure, end-user applications might result in the transformation of entire sectors, such as the mobility, heating, and industrial sectors, which are further coupled to the electricity sector through the use of electrolysis. This complex interplay of production, infrastructure, and end-use requires assessments from a system planner's perspective, considering security of supply, resilience, resource adequacy, and decarbonization.

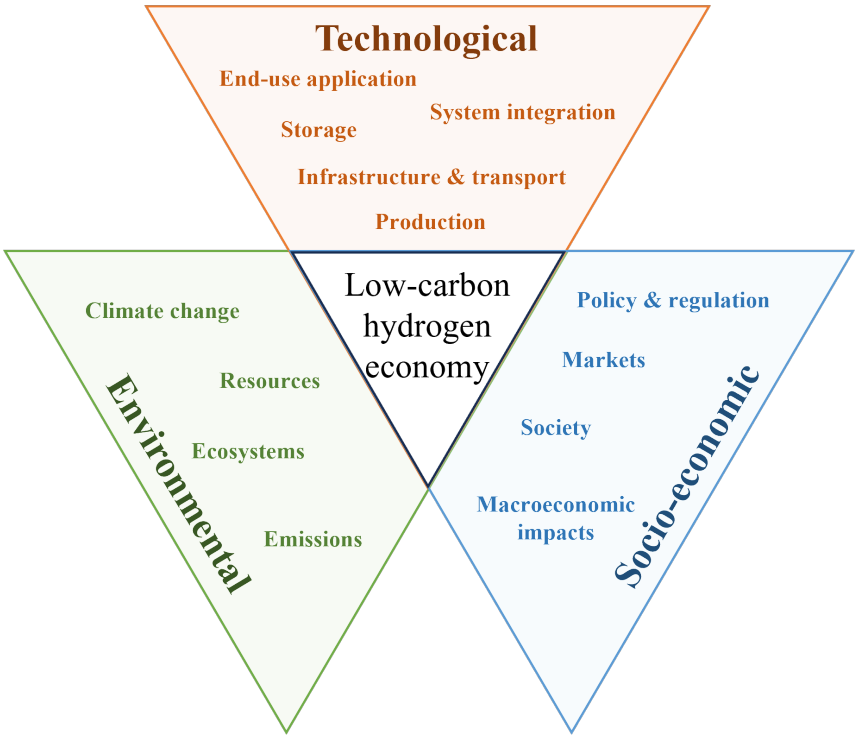

Figure 1.1: The technological, environmental, and socio-economic dimension of the low-carbon hydrogen economy.

The environmental dimension focuses on ensuring that the large-scale deployment of LC-H2D contributes to substantial reductions in greenhouse gas (GHG) emissions while avoiding unintended environmental burdens. Key aspects include the responsible use of scarce resources such as rare earth elements, precious metals, land, and water, which must be considered in holistic sustainability assessments. Environmental evaluations should therefore extend beyond carbon intensity to encompass broader impacts on resources and ecosystems.

The socio-economic dimension captures the institutional and societal context shaping the LC-H2D economy. It includes markets, policy, society, and macroeconomic impacts. Currently, no LC-H2D market exists, and open questions exist about how a future market might develop. Here, whole countries position themselves to play a role in the future LC-H2D economy, either to exploit the renewable potential within their countries for LC-H2D exports or to secure a low-cost, low-carbon supply for their future demand. The complexity is further exacerbated by regulation, which plays a crucial role in shaping the future hydrogen economy. Incentives and quotas could foster the application of LC-H2D, while bans pose barriers. Standards and certification implement a clear framework for production and markets. The stakeholders' perspectives play another vital role. Acceptance of regulations, technologies, and applications could support or slow down the implementation. These analyses are as important as the question of consumer willingness to pay. Finally, a broad range of macroeconomic analyses is required, including topics such as industrial competitiveness, employment, technology leadership, energy independence, or the overall economic benefits of the LC-H2D economy.

This thesis contributes to the existing research on the hydrogen economy by conducting techno-economic and environmental assessments of electricity-based renewable hydrogen and its derivatives. In general, it examines the PtX systems within integrated energy systems and as stand-alone facilities, as well as the global LC-H2D transport infrastructure. In the first study, the regulatory framework for renewable fuels of non-biological origin (RFNBO) is assessed within a German power system analysis to evaluate the mutual impact between the power system and electricity-based kerosene production, assuming compliance with the regulation (Paper A). The second study investigates stand-alone PtX facilities in terms of their technological, economic, and environmental performance using a multi-method approach, and quantifies the trade-off between production costs and GHG emissions by applying multi-objective optimization (MOO) (Paper B). With a sole focus on production costs, this model is developed into a robust optimization model to investigate the impact of location-specific renewable electricity generation uncertainties on different technologies, with the aim of achieving robust facility capacities (Paper C). Finally, the global transport of LC-H2D is modeled, considering highly resolved spatial hydrogen production costs and transport infrastructure. This model is solved using a heuristic-inspired branch-and-bound method that has been developed (Paper D).

This thesis comprehensively analyzes the production and transport of LC-H2D using the four above-mentioned contributions. Compared to other research, this thesis has an interdisciplinary approach, considering technological, economic, and environmental dimensions using methods from operations research, economics, and chemical engineering. In addition, the publications are closely related by exchanging methods, data, and results of the individual approaches, allowing for a comprehensive analysis of the LC-H2D supply chain, from production to supply to the consumer, with consistent data and methods. This research provides key insights and tools for stakeholders along the supply chain, as well as for policy makers to derive well-founded policy decisions. Developed models and applied data are publicly available. While detailed research questions are raised within the individual contributions, this thesis will answer the following research questions:

- What is the mutual impact of the RFNBO kerosene production on the energy system, and how does the impact change with the application of the electricity purchase conditions of the renewable energy directive II (REDII)? (Paper A)
- What are the trade-offs between production costs and greenhouse gas emissions for PtX production across different locations and energy carriers with varying flexibility and renewable generation capacity factors? (Paper B)
- How does the consideration of renewable generation uncertainties of wind and solar photovoltaic (PV) affect the optimal capacities and production costs? (Paper C)
- Which global export locations are favorable regarding total supply costs to Germany and the transported quantity of LC-H2D? (Paper D)

This thesis is organized into two parts. Part I contains the framework of the thesis. In this framework, Chapter 2 provides the necessary background on the energy transition with a special focus on the future demand and application of LC-H2D (Section 2.1), production (Section 2.2) and infrastructure (Section 2.3). Afterward, the current barriers to the hydrogen economy, including regulatory, technical, and economic barriers, are presented and discussed (Section 2.4). This chapter is followed by the methodology chapter (Chapter

3), which describes the applied and developed methods for energy system modeling (Section 3.1), modeling the stand-alone RFNBO production (Section 3.2), and the modeling of RFNBO transport (Section 3.4). In Chapter 4, Papers A to D are summarized, each including a motivation and objective, methodology, and key findings section. The critical reflection on applied methods, developments, and potential further research is presented in Chapter 5. Part I is completed with the summary of this thesis, derived conclusions, and an outlook (Chapter 6). Part II contains the manuscript versions of Papers A to D.

2 Background

Hydrogen is the lightest element, is a colorless and odorless gas when unbound, and is the most common element in the universe. It is bound chiefly on Earth, creating water (H_2O) and organic materials (C-H bonds). What makes hydrogen particularly interesting for the energy sector is the ability to use it as an energy carrier, either in its pure form or as parts of hydrocarbons, like alkanes (C_nH_{2n+2}) or alcohols ($C_nH_{2n+1}OH$), or other hydrogen compounds like ammonia (NH_3). Especially within the last years, hydrogen has risen in popularity, since many processes depend on conventional energy carriers, such as crude oil or natural gas. Replacing these with LC-H2D would allow us to reduce CO_2 emissions while retaining infrastructure and applications that currently use conventional energy carriers.

Even though the chemical element hydrogen remains the same, different hydrogen production routes exist, and a differentiation is necessary, since their properties, such as costs, GHG emissions, and production technologies, differ significantly. Political decision makers need this distinction to promote advantageous characteristics relating to the energy transition. Usually, a color scheme is used to allow visual distinction, shown in Figure 2.1. From these options, the LC-H2D are particularly interesting, since they can achieve a significant reduction of GHG emissions. In the following, the most promising LC-H2D options are explained, since other approaches are still at an early research stage (Arcos and Santos, 2023).

Providing low-carbon or GHG-neutral hydrogen can be achieved through three main approaches. The first approach is the use of biogenic energy carriers, such as biomethane or biofuels. Successful examples are the fuel type E10, which uses a biogenic ethanol share of up to 10% on the supply of gasoline, or the biogenic energy supply share of 31.3% on the total energy supply in Brazil (IEA Bioenergy, 2024). The usage of biomass, however, is not without critical discussions. The main disadvantages of biomass are the limited potential due to land use competition, monocultures, and the tank-or-table discussion[1], especially affecting the first generation[2] biofuels. These disadvantages caused the European Union (EU) to limit the use of first-generation biomass, especially critical ones like soy- or palm oil-based biofuels (Heimann et al., 2024). The main disadvantage of the second[3] and third[4] generation biofuels is the even more limited potential, and technical and economic hurdles exist (Sing et al., 2024).

The second approach is CCS. Here, separated CO_2 is captured and stored within underground storage like old gas and oil reservoirs, or saline aquifers. In the context of hydrogen, CCS is typically discussed using steam reforming to obtain hydrogen from natural gas. The

[1]The term tank-or-table describes the competition of using biomass as fuel (tank) or as food (table).
[2]Produced from food and forage crops
[3]Produced from byproducts, residual and waste material of biomass processing
[4]Produced from algae

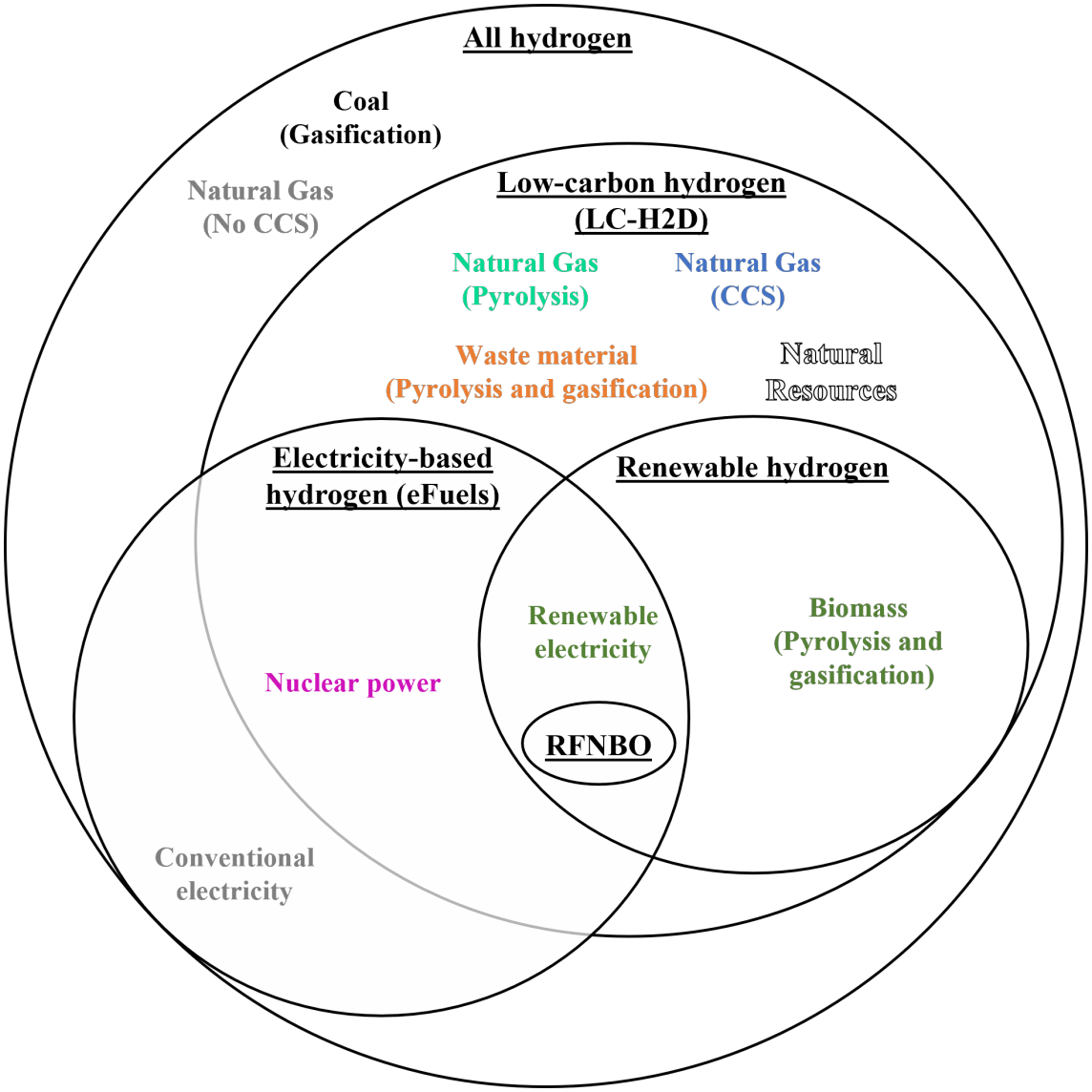

Figure 2.1: Hydrogen color scheme categorized by categories, processes, and feedstocks. Categories are shown in underlined. All types of hydrogen within the electricity-based hydrogen category are based on the electrolysis process. The scheme also applies to hydrogen derivatives.

main advantage of CCS is the continued use of conventional energy carriers, infrastructure, and the existing and mature steam reforming plants, since the post-combustion technology can be equipped to existing facilities without further modifications. However, only minor applications use CCS since the implementation faces several challenges. The main challenge is the necessary CO_2 infrastructure, including the capturing facilities, transport, and permanent storage. In addition, CCS contains uncertainties like the long-term reliability of CO_2 storage and potential CO_2 leakage.(Leung et al., 2014)

The production of electricity-based hydrogen and its derivatives (eFuels) is referred to as PtX and uses the electrolysis technology, which splits water into oxygen and hydrogen

using electricity. However, even if the production process is specified, major distinctions between eFuels can be made, which is particularly important when the regulatory framework is defined. To achieve low-carbon hydrogen, low-carbon electricity is required, usually stemming from renewable energies or nuclear power. The first option results in electricity-based, renewable hydrogen, while the second option only results in electricity-based, low-carbon hydrogen. Electricity-based, renewable hydrogen can further be defined as RFNBO when the REDII electricity supply conditions are considered. This thesis focuses on hydrogen using electrolysis and renewable electricity, as well as hydrogen derivatives produced from it. The distinction between different types of hydrogen is only applied if the specification is necessary, for example, in the case of production or policies. The transport or application is usually not affected by the type of hydrogen since the chemical properties are identical.

The following background chapter provides a comprehensive overview of key aspects of the hydrogen economy. In Section 2.1, the transformation of the German energy system is discussed, and how LC-H2D might contribute to this transformation. The potential demand could exert a pull effect on the LC-H2D supply chain, triggering production and transport. Therefore, electrolysis technologies, the conversion into hydrogen derivatives, and the required feedstock are presented in Section 2.2 to give an overview of the production of eFuels. The subsequent Section 2.3 provides details on the existing trade, infrastructure, and transport properties of energy carriers and chemical products, as well as potential developments such as retrofitting, expansion, and new implementations of infrastructure capacities. These sections demonstrate that a potential LC-H2D supply chain could emerge from a technical perspective. However, barriers exist that hinder scaling up the hydrogen economy, which are discussed in Section 2.4. This section also includes a detailed examination of the regulatory framework for RFNBO production (Section 2.4.1) and a critical discussion on the barriers (Section 2.4.4).

2.1 Hydrogen and its derivatives in the future energy system

The energy transition is in full swing. Especially the transition in the electricity sector changes the primary energy demand in Germany significantly since energy carriers like uranium, coal, and lignite are replaced by renewable generators like wind and solar PV, visible in Figure 2.2.

The increased renewable electricity generation supports not only the electricity sector transition. The term sector coupling defines the approach to use technologies like electric vehicles or heat pumps, which allow for the electrification of applications and increase renewable energy shares in the transport and heating sectors. Despite this opportunity, renewable electricity still plays a minor role in the heating and transport sector, while biomass supplies the majority of renewable energy with 81 % in the heating sector and 78 % in the transport sector (Umweltbundesamt, 2025). Two exemplary reasons for the slow electrification of these sectors are the high investment in the equipment and the necessary installation of infrastructure like battery-electric vehicle (BEV) charging stations (Agora Verkehrswende, 2024). Other challenges arise in the power system, where electrification increases the electricity demand while the capacity expansion of intermittent renewable energy sources (iRES) increases generation uncertainties like volatility and availability. This uncertainty increases demand for short- and long-term storage and electricity demand

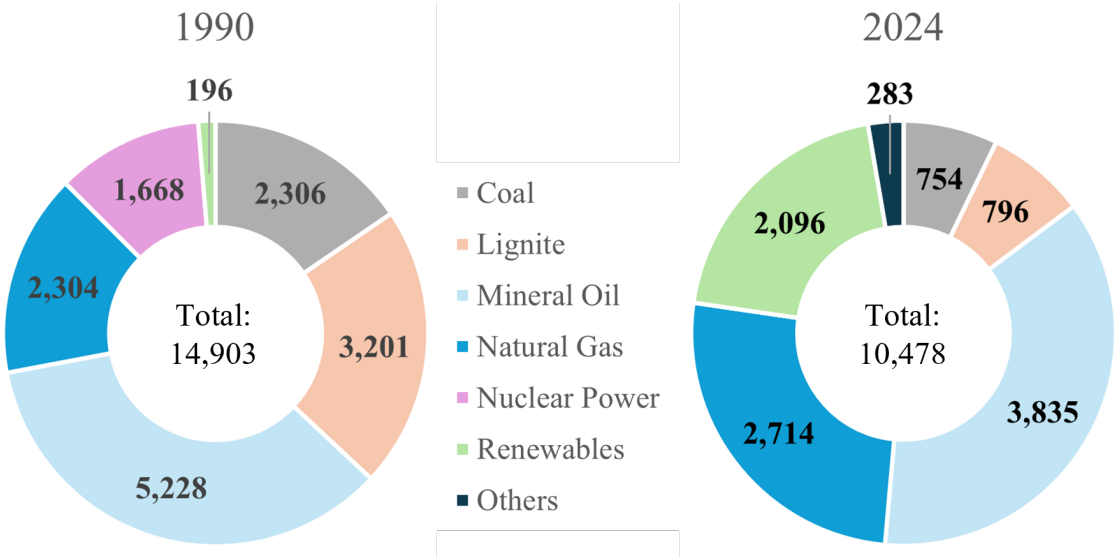

Figure 2.2: Primary energy demand (PJ) in Germany for the years 1990 and 2024 based on AG Energiebilanzen e.V. (2025a) and AG Energiebilanzen e.V. (2025b).

flexibility (Sterchele et al., 2020). The limits of electrification are shown by looking at hard-to-decarbonize applications, which define applications where electrification faces high financial expenditures or might still be technically impossible, so that alternatives to electrification are interesting or necessary. These include shipping, aviation, the supply of high-temperature heat, and the direct application of energy carriers as feedstock of industrial processes (Koller et al., 2021).

LC-H2D could complement the electrification of the energy system since their properties allow long-term storage, flexible production, and supplying hard-to-decarbonize applications while potentially being produced in a low-carbon fashion using biomass, CCS, and PtX. These properties fuel interest in hydrogen, which is why it is increasingly being considered in energy system studies. However, the extent of LC-H2D application is uncertain, shown by the range of potential LC-H2D applications and required quantities. To address this uncertainty, several studies included LC-H2D in their energy system studies (Koller et al., 2021; Prognos, Öko-Institut, Wuppertal-Institut, 2021; Sterchele et al., 2020; Fleiter et al., 2024; Energiewirtschaftliches Institut an der Universität zu Köln (EWI), 2021) to calculate requirements and optimal paths to achieve a low-carbon future energy systems.

These studies typically use scenarios and parameter assumptions to consider various applications, technologies, and behaviors. For example, electrification scenarios assume high penetration of electric vehicles and heat pumps. Parameters of such scenarios often limit capacity expansion of electrolysis units or the import of LC-H2D while electricity demand for electrified applications increases. Scenarios focusing on hydrogen replace current energy carriers with hydrogen and its derivatives in most applications, and scenarios based on persistence on specific technologies like internal combustion engine vehicles or oil and gas heating have an increased demand for LC-H2D. Technology scenarios are often combined with import limits of electricity and LC-H2D to model the availability of LC-H2D or the energy system's autarky levels. If such limits exist, increased domestic generation and production occur, which often result in higher domestic electricity demand in LC-H2D

scenarios compared to electrification scenarios since LC-H2D need to be produced domestically with a lower total efficiency of the LC-H2D supply chain compared to direct electrification. Finally, sufficiency scenarios assume decreasing demand, especially for energy and transportation, reducing the overall demand for electricity and LC-H2D, while nonacceptance scenarios, including slow thermal renovations of buildings, result in higher heating demands that could be covered by LC-H2D. However, the quantity is uncertain, visible at the extensive range of demand in the different studies and scenarios assessing the German energy system (Figure 2.3).

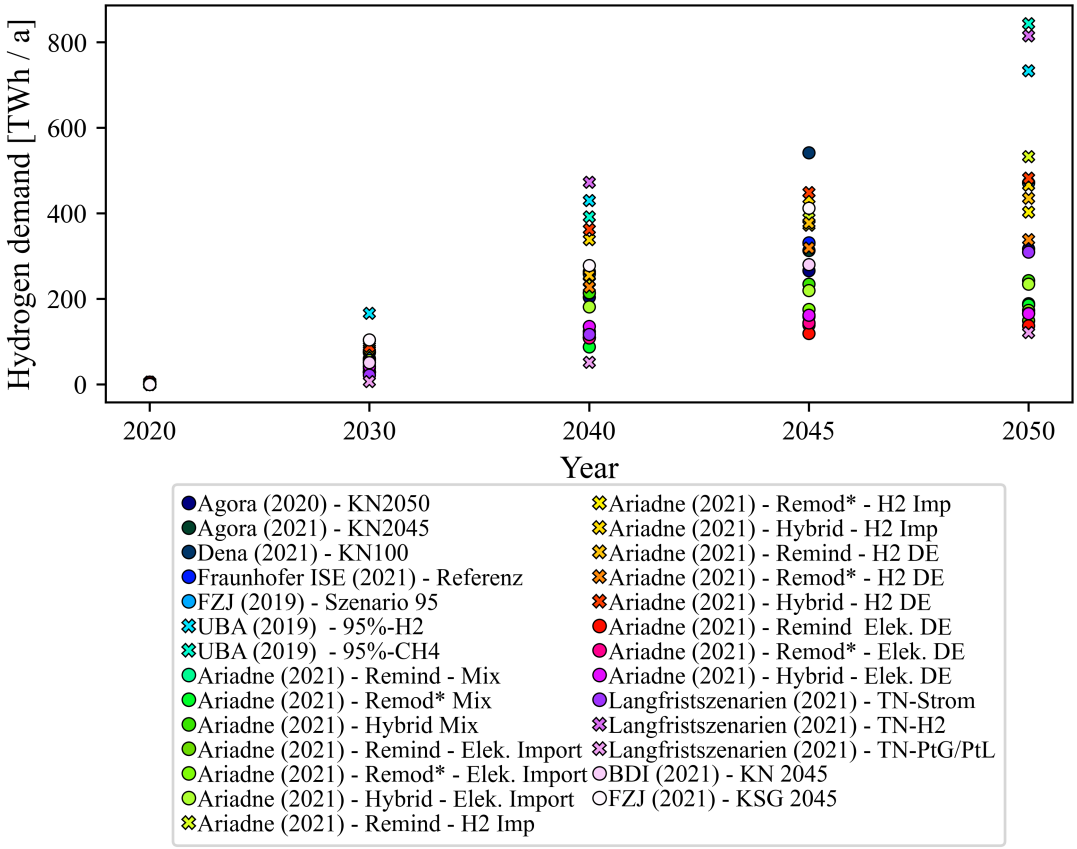

Figure 2.3: German hydrogen and hydrogen derivative demand of different studies and scenarios. Studies and scenarios marked with *X* assume increased hydrogen and hydrogen derivative demand (Kopp et al., 2022).

The use of LC-H2D in the electricity, building, industry, and mobility sectors differs significantly, and each of these sectors faces challenges that can be addressed with various technologies and approaches. A closer look at their potential transformation gives insights into the possible application of LC-H2D in the future.

2.1.1 The transformation of the electricity sector and the potential contribution of hydrogen and its derivatives

The GHG emissions of the electricity generation in Germany are steadily decreasing and contributed 163 Mio. t of the total 649 Mio. t CO_2 (25.12%) in 2024 (Icha and Lauf, 2025). The primary approach to reduce GHG emissions is the expansion of renewable electricity generation capacities to replace electricity generated from conventional energy carriers, such as lignite, coal, oil, and gas. Expanding renewable generation capacities will increase the uncertainty of electricity generation volatility and availability, while electrified applications increase demand. This challenge shows the need for flexibility on the supply and the demand side of the electricity sector, which might result in a complex interaction between components on both sides using the application of short-term electrical storage, controllable and uncontrollable electricity generation, load shifting, and demand response (Sterchele et al., 2020). The future application of LC-H2D in the electricity sector depends mainly on the power generation from gas turbines, the interaction of electrolysis systems with the electricity system, and the potential application of direct air capture (DAC) in CCS applications. Here, hydrogen could play a key role since long-term storage could be necessary to balance seasonal shifts in electricity generation or to cover long dark doldrums where battery storage capacities could be insufficient.

Concerning the eFuels production in Germany, Koller et al. (2021) have calculated the electrolysis capacities in Germany between 6 and 50 GW in 2050, depending on the underlying scenario. Since the investment in electrolysis units is still high, units maximize utilization to decrease the fixed costs of the products. With decreasing investment, electrolysis is operated more flexibly to utilize low electricity prices or participate in electricity network supporting mechanisms like the electricity balancing market to create additional revenues (Sterchele et al., 2020).

With the decommissioning of the last nuclear power plant in 2023 in Germany and the future phase-out of coal and lignite power, a significant amount of controllable power plant output will drop out. The German government planned to implement the *Kraftwerksicherheitsgesetz* (power plant safety act) to support the installation of controllable power generation from gas turbines, which, in the long term, use hydrogen to provide a backup electricity supply. The strategy aimed for 12.5 GW of generation capacities until 2028, consisting of 10 GW of generation units that would have been able to use both natural gas and hydrogen, 2 GW of modernization of existing gas turbines to allow the application of hydrogen, and 500 MW of gas turbines that already use hydrogen as fuel.(Deutscher Bundestag, 2024a) However, with the split of the *Ampel* coalition in 2024, the act was not adopted. System studies agree on the necessary expansion of gas turbines. Their numbers differ based on scenarios and approaches. For example, Prognos, Öko-Institut, Wuppertal-Institut (2021) calculate a gas turbine demand of 72 GW in 2050, while Energiewirtschaftliches Institut an der Universität zu Köln (EWI) (2021) state 50 GW. Some scenarios reach up to 150 GW to cover peak electricity demand when dark doldrums occur (Sterchele et al., 2020).

2.1.2 The potential role of hydrogen and its derivatives in the mobility sector

The German transport sector has not achieved significant GHG emission reduction since GHG emission savings from efficiency improvements in this sector are outweighed by the

increasing weight of passenger vehicles as well as the passenger and ton kilometers increase (Koller et al., 2021). This circumstance led to 143.1 Mio. t CO_2 emissions in 2024, which is only 20.3 Mio. t lower than in 1990 (12.42% reduction) (Umweltbundesamt, 2025). The long-term development of the transport sector depends particularly on the diffusion of BEV, with passenger vehicles currently being the primary focus of electric vehicle application. Other factors also play a role in transforming the transport sector: Both passenger and goods transport are subject to modal split. Foot, bicycle, and public transport might play an increasing role in passenger transport. The shift to rail transport of goods might also result in lower road transport. Other measurements like speed limits, emission limits, and carbon prices could further affect covered road distances and the diffusion of BEV.(Energiewirtschaftliches Institut an der Universität zu Köln (EWI), 2021) In contrast to passenger and light-duty vehicles, heavy-duty vehicles and aviation might rely on combustion processes in the short and medium term since batteries' low energy density results in high battery weight and space demand for such vehicles. Ships, on the other hand, could prefer liquid energy carriers to avoid the loss of space due to the large battery capacities required. LC-H2D have higher gravimetric and volumetric energy densities, allowing the propulsion of heavy vehicles over long distances. The application of hydrogen in fuel cells or combustion engines is discussed. However, this application requires the modification of the vehicles and the installation of infrastructure like hydrogen fuel stations. Applying renewable gasoline, diesel, and kerosene would avoid significant changes since they are identical to their conventional counterparts.(Koller et al., 2021)

2.1.3 The potential application of hydrogen and its derivatives in buildings

The German building sector emitted 101 Mio. t CO_2 in 2024 (15.56%) in 2024 (Umweltbundesamt, 2025), with the majority of energy demand stemming from the provision of space and water heating. Studies agree on two major approaches to reduce GHG emissions. First, the energy efficiency of the building stock has to improve to reduce the heating demand in general. Building insulation, in particular, allows a significant reduction in heating demand. Second, a switch of heating technologies and energy carriers is necessary. Technologies like heat pumps or electric boilers allow efficient heat supply, and several studies see them as key technologies to achieve carbon neutrality in the heating sector. In comparison, the application of LC-H2D is seen as more costly due to the increased operational costs from CO_2 pricing or hydrogen purchase.(Koller et al., 2021)

2.1.4 Hydrogen and its derivatives in selected industry sectors

With 153 Mio. t CO_2 eq. in 2024, the industry sector emits 24.35 % of the total German GHG emissions (Umweltbundesamt, 2025). The GHG emission reduction to 122 Mio. t CO_2 eq. until 2030 and climate neutrality in 2045 (Koller et al., 2021) is a special challenge in the case of the industry sector since conventional energy carriers are applied not only to supply energy, but are converted into downstream products like plastics, chemicals, and pharmaceuticals. Furthermore, new applications of LC-H2D might replace existing processes that rely on conventional energy carriers. Finally, high-temperature process heating might require LC-H2D since electrical alternatives have not yet matured or are not cost-competitive. Before going into the potential application of LC-H2D in the industry sector, it is necessary to mention that alternative routes, such as the application of DAC

using CCS to decarbonize the industry sector, exist, but are not within the scope of this thesis.

The steel production faces changes from different directions with partially contrary effects on the LC-H2D demand. First, by directly reducing iron ore instead of the current most widely applied processing in blast furnaces, steel production would move from using coal-based coke as a reducing agent to natural gas and, in the long term, hydrogen. Second, the circular economy could increase the share of recycled steel to up to 60% of the total steel production. Recycling steel is already an established process using electric arc furnaces, reducing the demand for primary produced steel. Third, some studies see a general decline in steel demand and the option to import low-carbon steel, reducing domestic production and potential LC-H2D demand further.(Prognos, Öko-Institut, Wuppertal-Institut, 2021)

Most emissions in the chemical industry emerge from the production of base chemicals like methanol, ammonia, and olefins, and can be divided into energy and process-related emissions. Process-related emissions stem from the material application of conventional energy carriers as feedstock within processes. Since direct electrification cannot replace this feedstock, continued supply is necessary if existing processes and infrastructure are to stay in place. Methanol and ammonia production rely on synthesis gas, which, in both cases, uses hydrogen that predominantly stems from the steam reforming of natural gas or gasification of coal, emitting considerable amounts of CO_2. Olefins rely on naphtha, a by-product of processing crude oil or other conventional energy carriers. Like steel production, the circular economy could affect the energy carrier demand since recycling could partially cover the feedstock demand. Energy-related emissions, on the other hand, stem mainly from the supply of process heat, which could be covered using electric heating technologies, biomass, or LC-H2D depending on the desired heat level.(Agora Industry, 2023)

Process and energy-related emissions exist in the production of mineral materials as well. For example, the processing of lime in the cement production emits process-related CO_2, which can only be reduced by lowering the clinker amount in the production process. However, since a particular share of clinker is necessary, some residual CO_2 emissions will occur. In such cases, studies suggest CCS to avoid emitting CO_2 into the atmosphere. High-temperature heat for drying and firing, which is based on the combustion of conventional energy carriers or waste materials, emits large quantities of emissions. In the future, particularly high-temperature heat might be supplied using LC-H2D if electric heating devices cannot provide the necessary temperatures or are not cost-competitive with LC-H2D.(Prognos, Öko-Institut, Wuppertal-Institut, 2021)

The industry and the other three sectors show the complex challenges of the system transformation to achieve carbon neutrality, and the LC-H2D application could contribute to this transformation. However, at the beginning of the supply chain stands the production, which is discussed in the following section.

2.2 The production of electricity-based hydrogen and its derivatives

Figure 2.1 describes the different production paths of hydrogen. Renewable hydrogen is only produced using biomass-based processes or electrolysis combined with renewable electricity. The following section defines and compares electrolysis technologies, and explains the proton exchange membrane electrolysis (PEM) in detail. Afterward, different hydrogen derivatives are described, followed by the feedstock materials necessary to produce eFuels.

2.2.1 Hydrogen

Hydrogen is the most prominent LC-H2D, which itself is a feedstock for all otherPtX processes. In 2023, global hydrogen demand reached 97 Mta, which was majorly produced using fossil energy carriers like natural gas or coal, or was a byproduct of refineries or petrochemical processes. Only 1 Mta of low-carbon hydrogen is produced, mostly stemming from CCS processes. However, the production could increase to up to 49 Mta per year in 2030 based on current project announcements. Around 100 kt of hydrogen is produced using electrolytic processes like electrolysis, splitting molecular water into hydrogen and oxygen by applying an electric voltage (Equation 2.1).(International Energy Agency (IEA), 2024)

$$2\ H_2O\ (l) \rightarrow 2\ H_2\ (g) + O_2\ (g) \tag{2.1}$$

The main difference between electrolysis technologies is the decision on the electrolyte material. The electrolytes differ regarding their charge carriers, pH value, and operation temperature, with some electrolytes demanding high-temperature heat to activate the ionic conductivity of the electrolyte. Both temperature and pH value affect the decision on cell structure, electrode, and membrane material, as all components in the electrolysis cell must withstand either acidic or alkaline electrolyte, and potentially high temperatures. This key component led to the development of the three main technologies alkaline electrolysis (AEL), PEM, and solid oxide exchange electrolysis (SOEL).(Lange et al., 2023)

Each of the different electrolysis technologies has individual properties, allowing for specific applications. For example, AEL is the most mature technology and has already been installed in industrial scales. The technology achieves the lowest investment and the highest lifetime of all technologies. However, the application in the context of iRES could be difficult since low partial loads and fast load changes are challenging. Therefore, applications with a steady electricity supply would be suitable for AEL.(Tüysüz, 2024)

The SOEL needs steam instead of water, which makes this technology especially suitable in integrated systems where waste heat can be supplied to evaporate the water. In such environments, SOEL would achieve the highest efficiency of the three electrolysis systems, especially if high temperatures are provided. Another major advantage of SOEL is the potential co-electrolysis of CO_2 and hydrogen to directly produce synthesis gas (Syngas) used in synthesis processes to produce hydrogen derivatives. SOEL can also be operated as a fuel cell if designed accordingly, which allows electricity generation from hydrogen and

could support the electricity base load supply of inflexible system components if insufficient electricity is generated. However, the technology is still developing, and large capacities are unavailable in the short term. In addition, the low load gradient makes the application with iRES difficult.(Grigoriev et al., 2020)

The PEM has the highest flexibility of the three technologies and can reach load ranges between 5% and 100%. For a short period, the PEM can *overload* to a load level of up to 130%. However, this option has the downside of increased risks of degradation and technical failures. The flexibility makes the PEM the most suitable in stand-alone hydrogen production using iRES since fast reaction on changing power levels is possible.(Martinez Lopez et al., 2023) For better comparison, Table 2.1 shows the techno-economic parameters of the three electrolysis technologies.

Table 2.1: Comparison of electrolysis technologies based on Lange et al. (2023); El-Shafie (2023); Grigoriev et al. (2020); Danish Energy Agency (2025).

	Alkaline Electrolysis	**PEM Electrolysis**	**Solid Oxide Electrolysis**
Technology maturity	Mature	Commercial	Research & Development
Investment (€/kW)			
2025	1000–1200	1860–2320	> 2000
2030	550	650	775
2050	300	350	500
Electrical efficiency (% (based on lower heating value))			
2024	68	64	85
2030	69	67	90
2050	< 74	< 74	< 83
Current Density (A/cm²)	0.2–0.5	0.8–2.5	0.26–1
Temperature Range (°C)	70–90	50–80	700–850
Part Load Range (%)	15–100	5–130	-100–100
Load Gradient (%/s)	10–50	10–90	0.1
Cold start-up time to 100% (m)	< 80	0.5	600
Warm start-up time to 100% (s)	240	< 10	600
Lifetime (h)	up to 100,000	up to 50,000	500–2000

PEM electrolysis uses a thin, solid membrane as electrolyte instead of a liquid like the AEL. This approach increases the flexibility since no evaporation or movement of liquids will occur while the travel distance of electrons is minimized. The compact modular setup, which is supported by the high current density, allows the individual control of modules, increasing the flexibility further.(Lange et al., 2023) Due to the acidic characteristic of the membrane, PEM electrolysis relies on precious metals as catalysts, like platinum and iridium. In addition, the high pressure within the stacks requires gas-tight and stable equipment.(Martinez Lopez et al., 2023)

The PEM technology is still capital-intensive, which requires significant cost reductions to allow cost competitiveness with fossil-based hydrogen. These reductions can be achieved

by improving the technology itself. For example, increasing the efficiency of the process by increasing the cell area and the power density (Fraunhofer ISE, 2021). Another potential for cost reduction is the reduction of precious materials like iridium and platinum. For example, optimized production (Taie et al., 2020) or the utilization of conductive additives (Ferner and Litster, 2024) have shown a significant reduction of precious materials while achieving a similar PEM stack performance. However, the main opportunities for cost reduction are the scale-up of capacities and production. Auxiliary components like piping, power electronics, and gas purification can be centralized, reducing their fixed cost share per installed capacity when increasing the facility's capacity. The scale-up of production would exploit the economies of scale and decrease the costs per electrolysis unit produced, especially in combination with a high level of automation.(Fraunhofer ISE, 2021)

While hydrogen covers several applications in the electricity and building sectors, other sectors like the industry and mobility rely on hydrogen derivatives produced using hydrogen combined with other feedstocks.

2.2.2 Hydrogen derivatives

The following section will introduce the hydrogen derivatives covered in this thesis and their properties, describe the main production processes and products, and provide global production quantities. Figure 2.4 presents an overview of the different hydrogen derivatives and final products.

Synthetic natural gas (SNG) represents a broad range of natural gas equivalents not produced from natural gas extraction. The different processes and feedstocks result in a gas mixture consisting mainly of methane but can contain traces of sulfur, ethane, propane, and other elements. Non-PtX processes are primarily based on the gasification of coal, biomass, and waste to generate Syngas combined with a subsequent production of SNG by methanation. PtX processes rely on CO_2 and hydrogen as feedstocks, which can be directly transformed into SNG by methanation or pre-processed beforehand using the reverse water-gas shift reaction. The similarity to natural gas is the primary advantage of SNG. Infrastructures like gas pipelines and applications could transport and utilize SNG with only minor adjustments, like removing impurities (e.g., sulfur, heavier hydrocarbons) from the gas mixture.(Biollaz and Schildhauer, 2016) The broad range of natural gas applications, from supplying heat to long-term energy storage to the chemical sector's material applications, could also be covered using SNG. However, this range could be downsized drastically since the material application is often the natural gas steam reforming process. Instead of processing hydrogen to SNG and reconverting it back to hydrogen, a direct application of hydrogen might be more suitable, depending on the hydrogen availability at the consumption location. The large-scale adoption of PtX SNG is mainly hindered due to the cost disadvantage compared to natural gas. Schlautmann et al. (2021) calculated PtX SNG production costs of 12–40 €ct/kWh in 2020 to 5–9 €ct/kWh in 2050 when renewable electricity is applied; the current German wholesale price of natural gas lies at around 3.6 €ct/kWh (Bundesnetzagentur, 2025). In addition, PtX SNG is only produced in pilot and demonstration plants in marginal quantities compared to the global natural gas extraction.

Methanol is an elemental compound of the chemical industry, produced using the methanol synthesis, and used to produce downstream products like formaldehyde, acetic acid, and

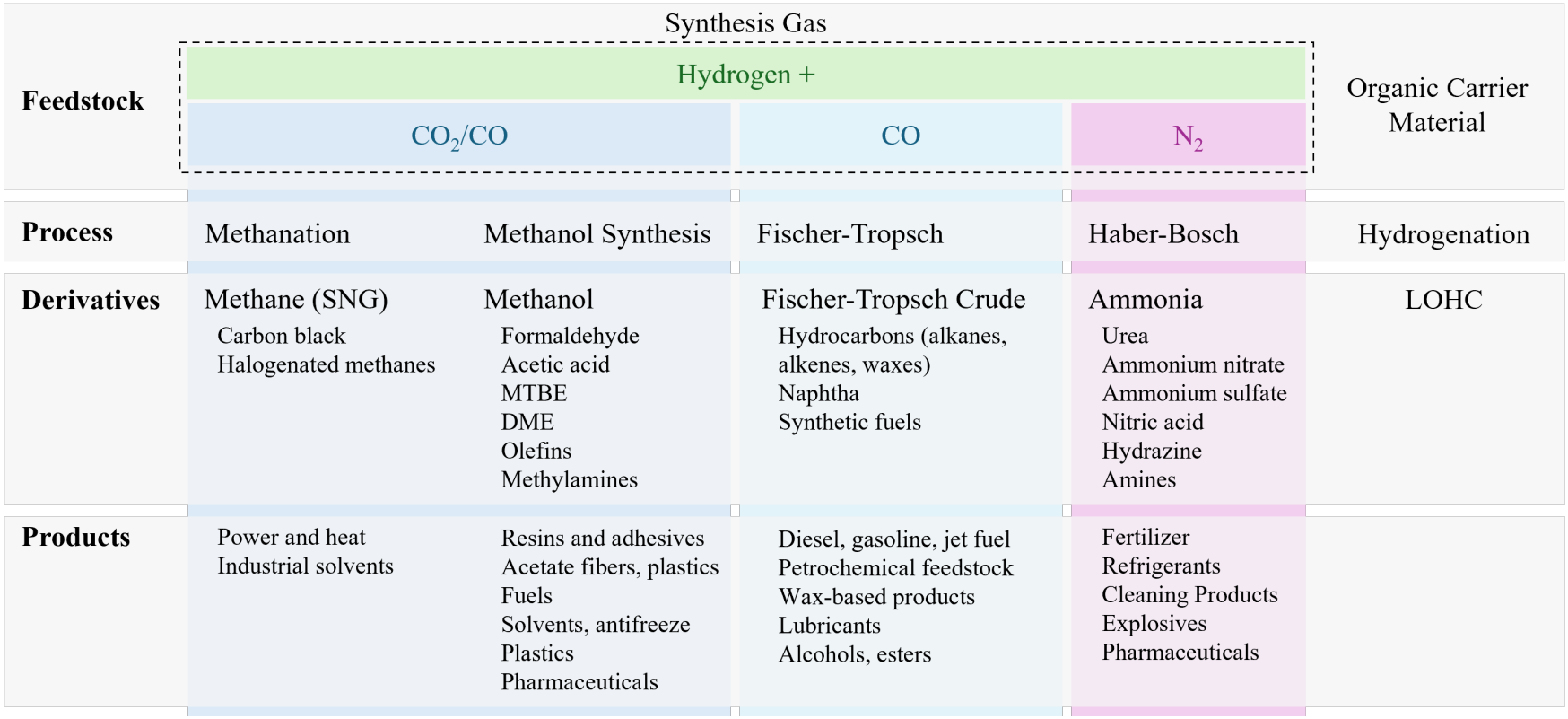

Figure 2.4: PtX hydrogen derivatives and final products. Based on IRENA and Methanol Institute (2021); The Royal Society (2020); de Klerk, Arno (2008).

plastics. In 2021, 98 million tonnes of methanol were produced, potentially increasing to 500 Mta by 2050. The current production uses natural gas reformation (65%) and coal gasification (35%), resulting in production costs of around 100–250$/t and around 0.3 Gt of GHG emissions. Currently, only 0.2% are produced using biological feedstocks. The main advantage of methanol is its storability and transportability due to its high energy density and liquid state at ambient pressure levels. These properties, in combination with the potential to blend methanol with conventional fuels, open future applications as a transport fuel for ships and other large vehicles. However, the current production costs of PtX methanol (820–2380$/t) exceed conventional production costs significantly. Here, significant cost reductions are expected with the increasing maturity of the technologies, reaching production costs of 250–630$/t.(IRENA and Methanol Institute, 2021)

Fischer-Tropsch (FT) synthesis uses carbon monoxide and hydrogen to produce FT crude. This technology was developed in 1925 to allow the production of fuels from conventional energy carriers like natural gas, lignite, and hard coal. FT crude has similar properties to conventional crude oil. It is a mixture of different hydrocarbons and, identical to its conventional counterpart, needs further upgrading to the final products. The similarity to conventional crude oil allows the same product diversity, including fuels like diesel, gasoline, and kerosene, wax-based products, lubricants, and alcohols.(de Klerk, Arno, 2008) In addition, the similarity to crude oil allows the utilization of the oil transport infrastructure, such as oil pipelines and oil carriers. Like SNG, renewable FT crude is produced on a small scale using pilot and demonstration plants. However, large-scale FT crude plants using fossil energy carriers like natural gas exist. The production costs of renewable, electricity-based kerosene could be 5–8 times higher compared to fossil-based kerosene (Pio et al., 2023).

Ammonia stands out from other hydrogen derivatives since it does not rely on carbon-containing feedstock. Instead, ammonia relies on nitrogen, which is available in the ambient air in high concentrations. The synthesis of ammonia via the Haber-Bosch process is a well-established process and has already been applied at large scales, producing around 185 Mta of ammonia in 2020 at production costs of around 200–870$/t (IEA, 2023a), depending mainly on the natural gas price. With the projected increase in population and economy, the volume could increase by 40% by 2050. Most of these volumes are produced using hydrogen from natural gas steam reforming, resulting in 0.45 Gt of GHG emissions per year. 70% of the production volume is used to produce fertilizer for the agricultural sector. Other applications are ammonia nitrates, which are used for chemical products, explosives, and chemical agents. Ammonia can be liquefied at a relatively high temperature[5] to increase the volumetric energy density, allowing low-cost transport, distribution, and storage. This property makes ammonia interesting for future applications, such as the use as a transport fuel for ships or as a hydrogen carrier. The downside of ammonia as a fuel or hydrogen carrier is the release of nitrogen in the combustion or cracking process. Nitrogen is one element of nitrogen oxides, a pollutant responsible for health issues, overfertilization, and acidification of the environment. In particular, the combustion of ammonia could result in nitrogen oxides, which would have to be treated with end-of-pipe technologies like scrubbers.(International Energy Agency (IEA), 2021)

Liquid organic hydrogen carrier (LOHC) are seen as hydrogen carriers since the liquid state at atmospheric pressure and temperature allows a low-cost transport and storage.

[5] -33°C at atmospheric pressure; 20°C at 7.5 bar

In addition, they have a much higher volumetric energy density and are relatively safe due to their non-explosive property and difficult material flammability. The carrier material, like Dibenzyltoluol or Monobenzyltoluol, is circulated between the *loading* and *unloading* location. This process has the advantage that the carrier material is recycled and does not require constant resupply. However, two main disadvantages drive the costs of LOHC transport. First, the LOHC transport vessels conduct empty trips transporting the unloaded carrier material for subsequent use. Second, the unloading process (dehydrogenation) requires significant amounts of thermal energy to release the hydrogen from the LOHC, which could require a separate heat supply or partial combustion of the transported hydrogen if insufficient heat is available.(Niermann et al., 2021) Since LOHCs are discussed mainly in the context of hydrogen transport, further information is given in Section 2.3.2.

The different hydrogen derivatives have individual properties and allow the substitution of conventional energy carriers. The majority of costs will stem from the electricity-based hydrogen supply. However, the supply of other feedstocks besides hydrogen comprises significant challenges, as described in the following section.

2.2.3 Feedstock

The following subsection provides additional information on commodities required to produce hydrogen and its derivatives, specifically water, CO_2, and nitrogen. The hydrogen production process using water electrolysis requires, by stoichiometry, at least 9 kg of treated water for each kg of hydrogen. All water electrolysis types rely on water or steam free from particles and dissolved salts to prevent any contamination of or damage to the equipment, like electrodes or membranes, which could affect the durability of the electrolysis system (Becker et al., 2023). Water supply plays a significant role in the investment decision since water is not equally distributed around the globe, excluding large shares of otherwise high-quality locations for renewable energy generation. Simoes et al. (2021) lists several potential water sources. The obvious choice is the water supply network, which generally provides good-quality water in sufficient quantities. However, such networks might not be available in the context of remote PtX facilities. Other potential water sources are surface waters like rivers, streams, and lakes, as well as groundwater and rainwater. This water source might be limited to avoid environmental impacts from water withdrawal, which could increase the water stress level (Figure 2.5). The utilization of wastewater needs additional effort, but could have a cost advantage compared to air capture or desalination (Woods et al., 2022). In addition, wastewater treatment will be mandatory in any case, particularly for stand-alone facilities, since suitable wastewater treatment infrastructure might not be available. Seawater desalination is especially interesting because it supplies large quantities of fresh water to coastal locations. This technology uses thermal or membrane desalination to separate salt and impurities from the water. However, additional energy demand is necessary to operate the desalination plant, and the brine, the salt-containing residue stream, needs to be carefully disposed of to minimize any environmental impact (Soliman et al., 2021). With sufficient humidity, freshwater could be supplied further by DAC plants since freshwater arises in the CO_2 separation process. This process is particularly interesting since the cost performance of DAC could be improved by reducing the demand for external freshwater supply (Wang et al., 2024).

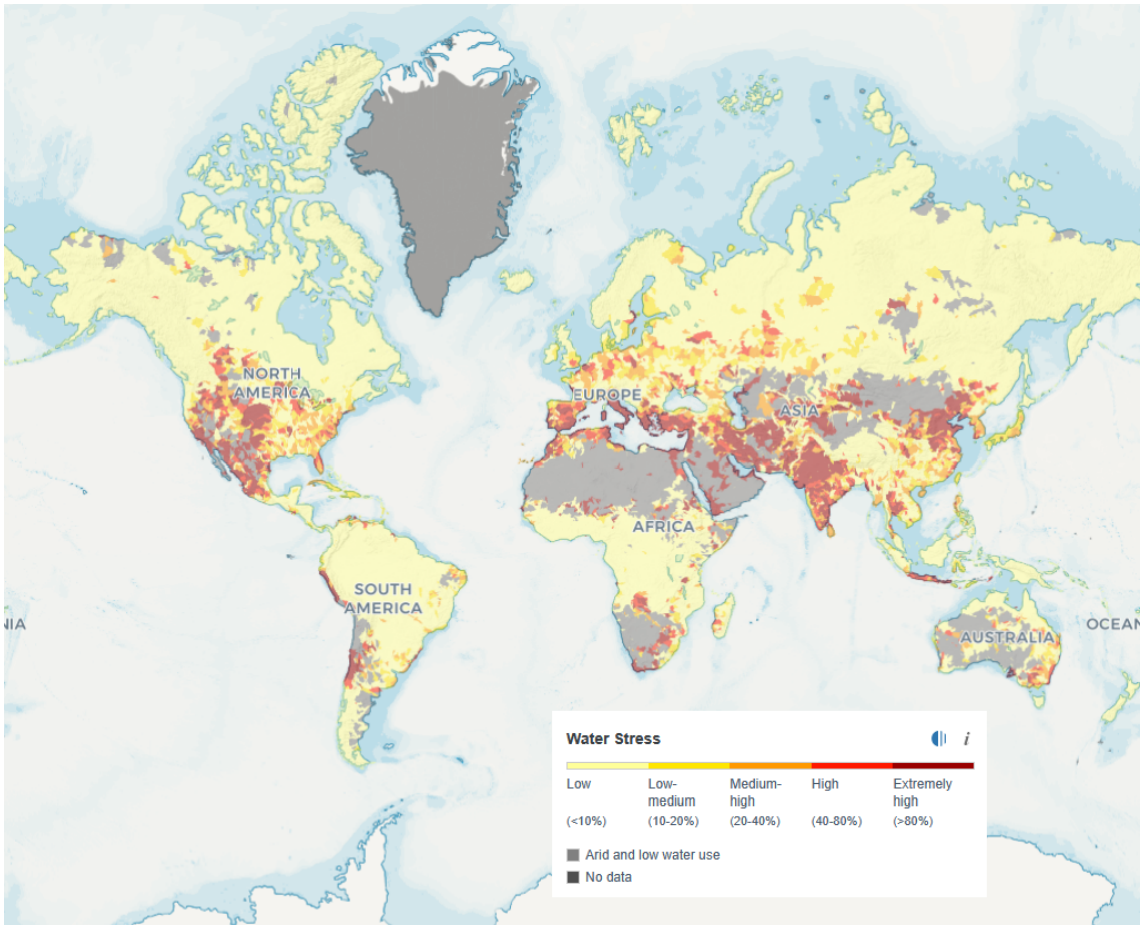

Figure 2.5: Annual global water stress level (World resources institute, 2025).

Hydrogen derivatives can be categorized by their non-hydrogen feedstock. SNG, methanol, and FT crude rely on carbon in form of carbon monoxide or CO_2. Ammonia, on the other hand, requires nitrogen. Both categories of derivatives use syngas as feedstock, which is a mix of hydrogen and the non-hydrogen feedstock in a specific ratio to achieve optimal conversion rates. Carbon monoxide is more reactive than CO_2. However, its disadvantage is the lower availability in pure form. The feedstock ratio derives from the chemical equation and is 2:1 (FT crude), 3:1 (SNG), and 2:1 (methanol) in the case of carbon monoxide and hydrogen, and 4:1 (SNG), and 3:1 (methanol) in the case of CO_2 and hydrogen. To achieve this optimal ratio or to provide carbon monoxide if only CO_2 is available and syngas using CO_2 is not applicable (FT case), the water-gas shift (Equation 2.2) and reverse water-gas shift reactions (Equation 2.3) can be applied. These reactions allow the conversion from CO_2 to carbon monoxide consuming hydrogen, and vice versa, using water.

$$CO + H_2O \rightarrow CO_2 + H_2 \qquad \Delta H = -41.1 \text{ kJ/mol} \tag{2.2}$$

$$CO_2 + H_2 \rightarrow CO + H_2O \qquad \Delta H = 41.1 \text{ kJ/mol} \tag{2.3}$$

Unlike the water-gas-shift reaction, the reverse water-gas-shift reaction is still in development and has yet to achieve maturity and commercialization (Markowitsch et al., 2023). Another obstacle is the necessary heating demand, where a temperature of 830°C and higher has to be supplied, which, however, facilitates sintering and coking, both resulting in the deactivation[6] of the catalyst (González-Castaño et al., 2021). The choice of applied fuel or energy to cover the heat demand significantly affects the process parameters. For example, recycled gas streams or by-products reduce the overall efficiency since a significant share of the produced hydrogen is not converted to the final product. Using natural gas increases the GHG footprint due to its fossil nature. To overcome this challenge, recent approaches model electric-heated reverse water-gas-shift reactors in combination with renewable energies (Basini et al., 2022).

One potential source of CO_2 is pointsource (PS) CO_2, which exists wherever carbon-containing energy carriers are used or process-related emissions occur. These include fossil-based energy carriers like coal or natural gas, biomass processing units, and emissions from cement production. Using fossil-based energy carriers could be restricted since the application of produced eFuels could emit previously captured CO_2. Biomass would allow renewable CO_2 supply but is limited in potential, similar to biogenic hydrogen (see Figure 2.1). While these limitations exist, PS could be an essential step towards PtX since the concentrated CO_2 in the flue gas is a reliable and cost-effective option for CO_2 supply (IEA, 2024), and capture technologies applied to PS are already commercialized (dena, 2021). Three approaches exist to capture CO_2 from CO_2 PS. Treating the flue gas of processes uses the post-combustion approach to separate the CO_2 from other flue gas components. This approach typically applies physical or chemical adsorption or absorption to capture the CO_2, where temperature or pressure increases and decreases alternately to capture and release the CO_2 from the sorbent material. The pre-combustion process treats the feedstock before combustion using gasification to separate the CO_2 from other components like hydrogen. Typically, the hydrogen is applied in the following combustion processes. However, the product of the gasification process could be applied as Syngas directly since hydrogen, carbon monoxide, and CO_2 emerge from the process. Finally, the oxyfuel approach uses pure oxygen in the combustion instead of ambient air to ensure a high share of CO_2 in the flue gas to avoid flue gas dilution with nitrogen and allowing a quite easy separation of CO_2 by condensing water from the flue gas stream.

Next to PS, CO_2 can also be separated from ambient air, using the DAC technology. In contrast to nitrogen, only around 0.04% of the ambient air consists of CO_2. Similar to the post-combustion process, DAC applies the adsorption (low-temperature) and absorption (high-temperature) process using the alternating increase and decrease of temperature to capture and release the CO_2 from the sorbent material. High-temperature (HT) DAC technologies have the advantage that mature technologies can be applied. However, similar to the SOEL, a cost advantage follows only if low-cost heat from other processes is available. Low-temperature (LT) technologies are less efficient, but their heat demand might be covered by low-temperature waste heat emitted from the synthesis process of the PtX facility. The main advantage of DAC compared to PS is the geographical independence, allowing the exploitation of favorable production sites globally. However, the production scales are small, resulting in high capturing costs of DAC compared to other

[6]The "progressive loss of activity or selectivity with time" (Martín et al., 2022)

technologies.(IEA, 2024) Table 2.2 shows a comparison of the most relevant CO_2 capture technologies.

Table 2.2: Parameter ranges for selected CO_2 capture technologies based on dena (2021); IEA (2024); Wang and Song (2020); Sodiq et al. (2023); Bisotti et al. (2024); Block et al. (2024).

Technology	**Cost (Forecast)** (€/tCO_2)	**Power** (MWh_{el}/tCO_2)	**Heat** (MWh_{th}/tCO_2)	**Temp.** (°C)	**TRL** (-)
Post-comb.	40–120 (<100)	0.18–1.04	0.41–1.29	100–140	9
Pre-comb.	50–100 (–)	0.32–0.41	0.36–1.04	>300	9
LT-DAC	125–500 (∼100)	0.4–0.7	1.9–2.6	80–100	3–9
HT-DAC	120–340 (<200)	0.3–0.5	1.5–2.5	∼900	7–8

Finally, ammonia production using the Haber-Bosch synthesis requires a hydrogen/nitrogen ratio of 3:1. The advantage of nitrogen compared to CO_2 is its abundant availability in ambient air, with a share of around 78%. Today, most nitrogen is produced using cryogenic air separation, where the different boiling points of the ambient air elements are utilized to separate the nitrogen from other components. Further technologies are membrane separation and pressure swing adsorption processes.(Smith and Klosek, 2001)

The next step in the supply chain before application is the transport of LC-H2D, especially if remote locations are utilized to produce low-cost products.

2.3 Transport

Transporting large quantities of energy carriers by ship and pipeline is vital to cover the global energy demand. The comparison between the transmission of electricity and the transport of energy carriers shows the advantage of energy carriers. For example, Germany's most extensive high-voltage direct current electricity transmission line has a capacity of 4 GW. With the total yearly transport quantity of 55 bn m^3 natural gas and assuming steady supply, Nordstream 2 would have had a thermal capacity of up to 67.8 GW if it had ever been commissioned. A single Ultra Large Crude Carrier class crude oil ship can transport 3.82 TWh of energy. These numbers show the advantage of gaseous, liquid, and solid energy carriers like coal, natural gas, and oil, which have high volumetric and gravimetric energy densities, making transport in large quantities cost-efficient.

LC-H2D could partially utilize the existing transport infrastructure. However, three main challenges exist. First, the technical properties of some LC-H2D differ from existing transported energy carriers, demanding the conversion of transport infrastructure in some cases. Second, some of the LC-H2D or their conventional equivalents are not yet transported in large quantities, leading to missing know-how and infrastructure. Third, the production of LC-H2D based solely on renewable energy allows the global production, and new transport routes might emerge to exploit especially favorable production locations. However, coordination between different producers and other stakeholders is required to utilize the

transport capacity. The following subsections will introduce the existing transport infrastructure and show potential future developments to allow cost-efficient transport of LC-H2D.

2.3.1 The current transport infrastructure

The most commonly transported energy carriers are crude oil, natural gas, and coal, and large consolidated infrastructures exist to connect extraction locations with consumers. Since natural gas, in contrast to crude oil, is not necessarily processed to upstream products and often distributed even into single households, it holds the longest total pipeline length with around 1 million km of pipelines in operation (Global Energy Monitor, 2025b), with the majority in North America, Europe, and China. Natural gas transport via ship using liquefied natural gas (LNG) has increased in recent years. One reason is the Russo-Ukrainian War, which partially sanctioned Russian natural gas imports into Europe. European governments expanded their LNG terminal capacities to enable the import from exporters like the United States and Qatar and to evade the import of Russian natural gas, which increased LNG imports by 60% (2021: 80 bn m^3; 2022: 130 bn m^3) while pipeline imports plummeted (IEA, 2023b). The increase in global LNG trade is also evident in the expansion of terminal infrastructure. Global Energy Monitor (2025b) states that 215 import and 165 export terminals are currently in operation, while 71 import and 41 export terminals are under construction. The major downside of LNG transport is the necessary liquefaction, which increases the volumetric energy density by around 600 times at costs of 2-3 $/MMBtu (0.68 - 1.02 €cents/kWh) (Molnar, 2022). The costs of natural gas transport lie between 0.14–0.79 $/(1000km*MMBtu) for pipeline transport, and between 0.72–2.16 $/(1000km*MMbtu) for LNG shipping (Saadi et al., 2018).

Crude oil is a raw material transported mainly via pipeline and ship from the extraction points to the refineries. Global Energy Monitor (2025a) lists more than 345,000 km of operating crude oil pipelines and another 12,000 km under construction. In addition, 8,445 crude oil tankers with a total deadweight tonnage of 565,2 Mio. t (26.1% of the total deadweight tonnage of all ships) enable the global sea-based shipping (Bundeswehr, 2023). Figure 2.6 shows the inter-area movement of the 2.1 bn t of crude oil in 2023. The central exporting countries are from the Middle East, from Russia, despite the Russo-Ukrainian War, Canada, and the United States. China, Europe, and the United States are the leading importers. The global crude oil trade is heavily affected by the Organization of the Petroleum Exporting Countries (OPEC), which is an association consisting of oil-producing countries[7] to coordinate the crude oil output to ensure a profitable trade and stable markets. They cover around 37% of global crude oil extraction and 79% of crude oil reserves (OPEC, 2024). The high volumetric and gravimetric energy density allows low-cost transport of crude oil, reaching costs of around 0.12–0-37 $/(1000km*bbl) for shipping and around 0.24–0.73 $/(1000km*bbl) for pipeline transport (Saadi et al., 2018).

Ammonia and methanol, next to the conventional energy carriers, are partially traded and transported internationally. In the case of ammonia, in 2019, a volume of 20 Mta or around 10% of the global production was traded globally with Russia, Trinidad and Tobago, and the Middle East as main exporters, and the European Union, India, and the United

[7] Members are: Algeria, Congo, Equatorial Guinea, Gabon, Iran, Iraq, Kuwait, Libya, Nigeria, Saudi Arabia, United Arab Emirates, and Venezuela

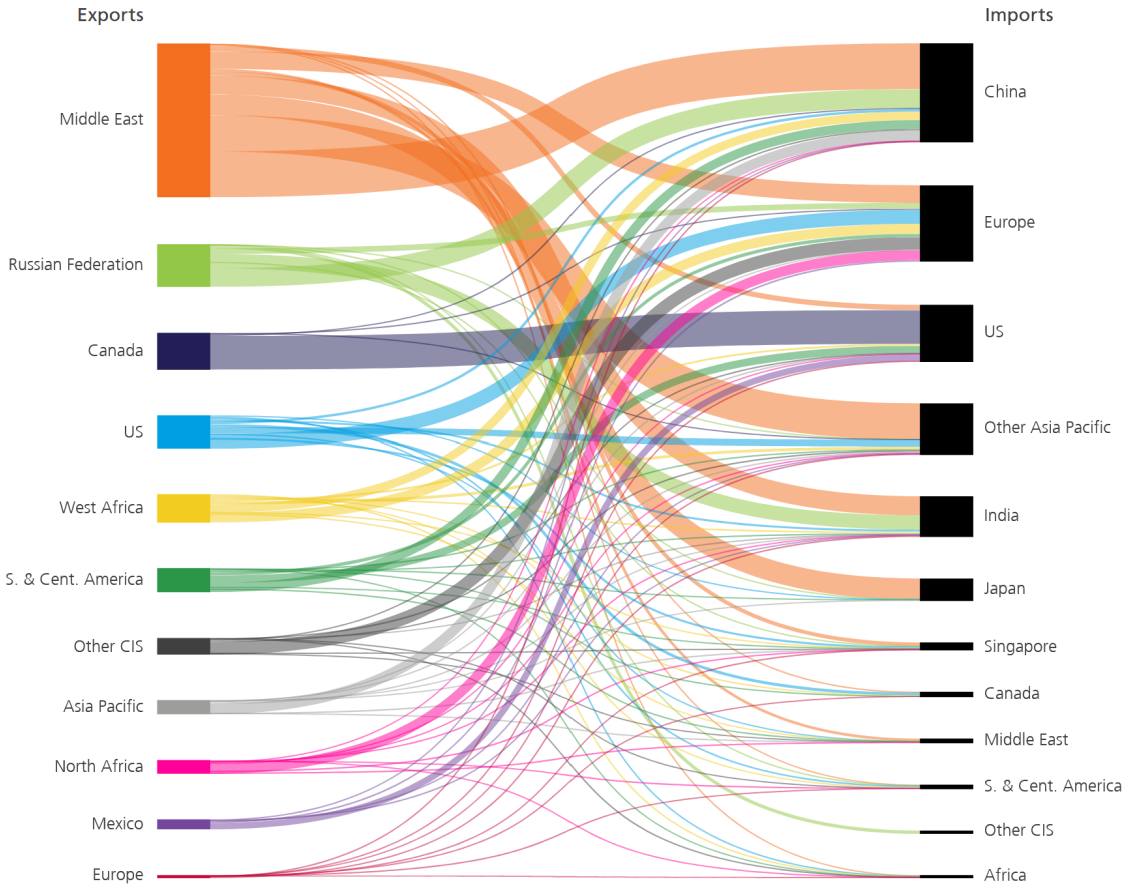

Figure 2.6: Inter-area movement of the 2.1 bn t of crude oil in 2023 (energy institute, 2024).

States as main importers (International Energy Agency (IEA), 2021). Based on The Royal Society (2020), the main ammonia pipelines exist in the United States with 4,830 km to transport and distribute ammonia from terminals to the fertilizer producers, and in Eastern Europe / Russia with 2,400 km to transport ammonia to the Black Sea for export. In addition, a fleet of around 170 ships, including 40 ships solely for ammonia transport, and around 200 harbors with ammonia terminals enable global shipping. Short-distance transport can be covered using distribution pipelines or trucks.(Egerer et al., 2023) A third of the global methanol production is shipped and traded globally (IRENA and Methanol Institute, 2021). The major exporters are Trinidad and Tobago, Saudi Arabia, and the United States, while the main importers are China, India, and the Netherlands. When traded, a share of 80–90% of the global methanol trade (IRENA and Methanol Institute, 2021) is shipped at costs of around 2.8 €/(1000km*t) (Staiß et al., 2022). Other transport, especially national transport, is conducted by railroad or short pipeline segments.

Hydrogen and the other derivatives mentioned in Section 2.2.2 are either not transported at all or only over short distances for two reasons. First, the hydrogen derivative, like LOHC, has no current application. Second, the commodity is an intermediate downstream product. In this case, the conventional energy carrier is transported to the point of use and further processed into the final product. For example, hydrogen is mainly produced

at the demand location from steam reforming, and only around 5,000 km of hydrogen pipelines exist (Lipiäinen et al., 2023). However, the future shift in the energy system might change the production method, extend the application of eFuels, and increase their global trading volumes. Therefore, significant adjustments to the transport system might be necessary.

2.3.2 Potential future developments of global energy transport

The advantage of the SNG, ammonia, and methanol is the ability to use existing transport infrastructure and the know-how to expand the infrastructure. Similar accounts for FT crude, which can use the crude oil transport infrastructure with minor treatment of the energy carrier. However, adjustments would still be necessary since the existing transport routes are constructed to connect historic production locations with demand centers. Using renewable energy might shift the production locations to regions without transport infrastructure. Therefore, new transport infrastructure might be necessary. In addition, transport volumes might increase, making larger transport capacities necessary. For example, IRENA and Methanol Institute (2021) states that the methanol production volume might increase from 100 to 500 Mta in 2050. In the case of ammonia, an increase of 40% by 2050 is possible (IEA, 2023a). The transport of eFuels such as hydrogen or LOHC still has minor dimensions, and their future potential is still being tested. Altogether, the future transport of eFuels is still in discussion, showing the necessary research demand on technologies, capacities, and locations.

The most discussed option is the transport of hydrogen via pipelines. This option would ensure that the hydrogen supply avoids costly conversion to LNG or other hydrogen derivatives, and potential losses from reconversion. The existing natural gas pipeline infrastructure and subsequent applications can handle hydrogen to a certain extent (Figure 2.7). For example, a hydrogen share of around 12% in the existing natural gas transport infrastructure is feasible. However, with an increasing share of hydrogen, the natural gas pipeline could take significant damage from embrittlement due to the high reactivity of hydrogen. In addition, transporting hydrogen using infrastructure designed for natural gas transport could be challenging since hydrogen has a higher permeation and air diffusion, and a lower density, heat value, and Wobbe Index than natural gas.(Perna et al., 2020; Télessy et al., 2024)

Figure 2.7 further shows that the existing pipelines could be repurposed, while components like compressors or valves would require replacements to handle a hydrogen share of 40% or higher. The retrofitting of existing infrastructure and the construction of new pipeline segments to enable the transport of hydrogen from hydrogen production and import locations to demand centers is the objective of the German Hydrogen Core Network (German: Wasserstoffkernnetz) and the European Hydrogen Backbone project. The Hydrogen Core Network's plan aims for 9,040 km of hydrogen pipelines (Figure 2.8) with a share of 56% retrofitted natural gas pipelines and amounting to 18.9 bn€ in investments (Bundesnetzagentur, 2024d). It can be seen as a part of the Hydrogen Backbone, which covers more than 58,000 km, needs 80–143 bn€ investment, and has the same share of around 60% of retrofitted natural gas pipelines (European Hydrogen Backbone and Gas Infrastructure Europe, 2024). Retrofitting natural gas pipelines is significantly cheaper than building new pipelines, decreasing the necessary investment demand. Based on Bundesnetzagentur

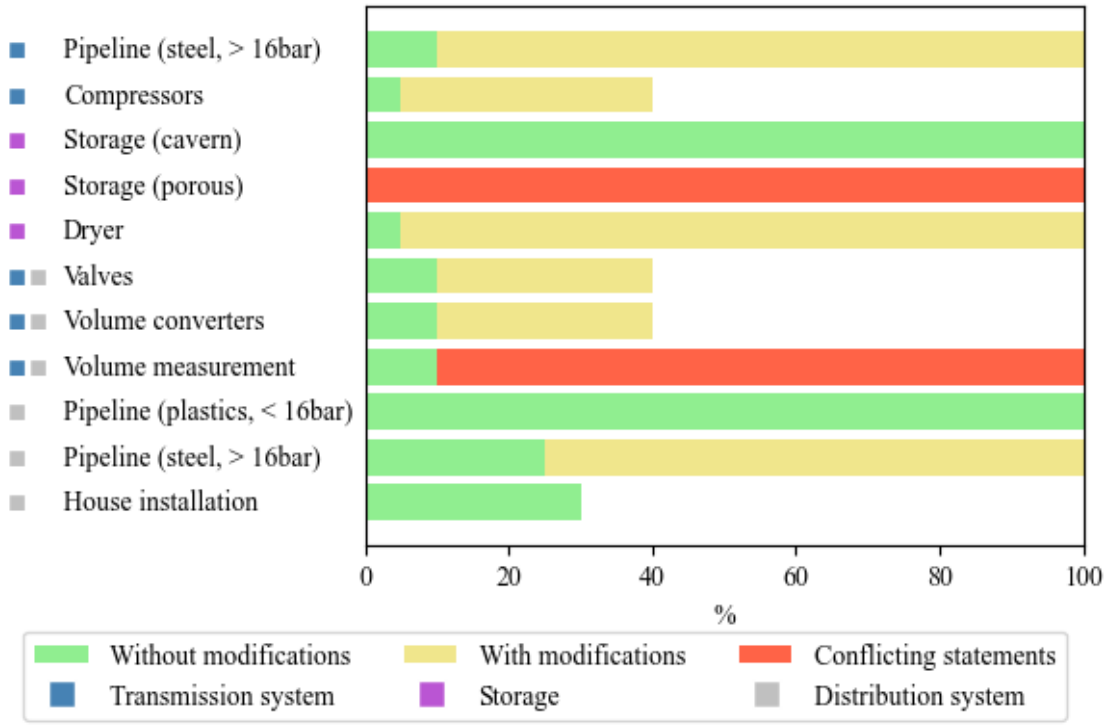

Figure 2.7: Potential share of hydrogen in the infrastructure, with modification and without modification (Bard et al., 2022). The conflicting statements bar shows additional research demand since different studies state conflicting results.

(2024a) and Bundesnetzagentur (2024b), 4,929 km of natural gas pipelines will be repurposed, which requires investments of around 3 bn€, while the new construction of around 3,816 km of hydrogen-ready pipelines requires around 16 bn€.

Pipeline transport is not the only potential hydrogen transport option. The ability to convert hydrogen into liquefied hydrogen (LH2) or hydrogen derivatives, further referred to as hydrogen carriers, and a subsequent reconversion opens manifold transport alternatives. Especially, the shipping of hydrogen carriers enables the import of hydrogen from locations disconnected from the European natural gas pipeline system, like Patagonia and Australia (Johnston et al., 2022; Müller et al., 2024). However, the different properties of the hydrogen carriers lead to other applications for each. For example, the additional energy the hydrogen carriers use takes place at various supply chain stages for each hydrogen carrier. While methanol, LNG, and LH2 need most of the energy in the conversion process before shipping, ammonia and LOHC use most of the energy in the form of heat in the ammonia cracking and LOHC dehydrogenation process after shipment to release the hydrogen from the carrier. Therefore, ammonia and LOHC are particularly suitable if waste heat exists at the import terminal, but an autothermal process, where the hydrogen carrier itself is burned to supply heat, is possible as well. Each of these hydrogen carriers comes with different transport costs and efficiencies. Therefore, distance plays another vital role when deciding which hydrogen carrier to use. Finally, while ammonia, methanol, and LNG transport are established technologies, LH2 and LOHC transport are still in development.(Sterner et al., 2024) Table 2.3 shows the technology readiness level (TRL)

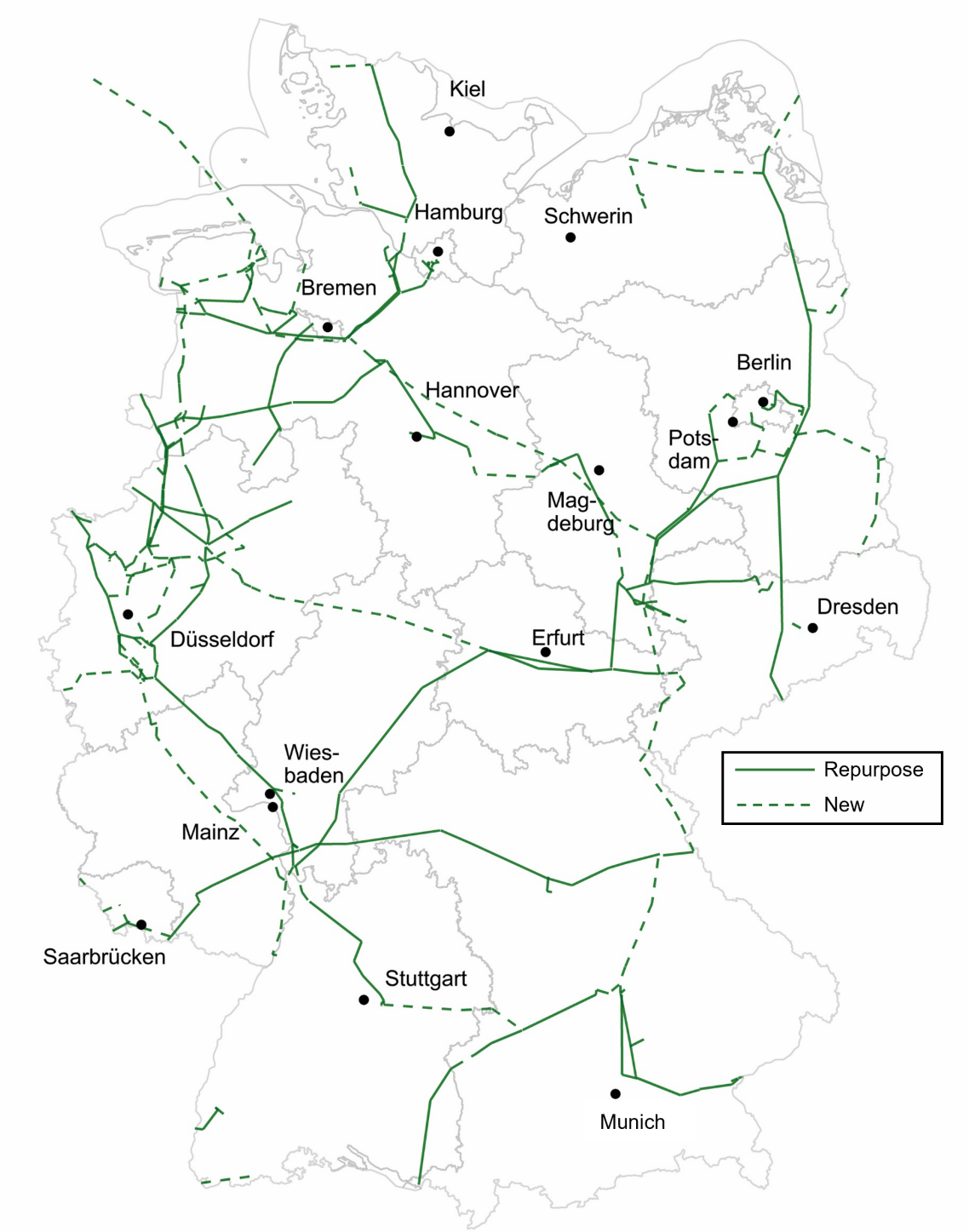

Figure 2.8: German Hydrogen Core Network (Bundesnetzagentur, 2024c).

and efficiencies of transport and the total supply chain for different eFuels using a 3,000 km pipeline and 10,000 km ship transport. The high transport TRL and efficiency are visible, looking at the direct supply of electricity-based hydrogen derivatives. The TRL stems from the already established transport on a megaton scale of their conventional

counterparts. While hydrogen carriers are a valid option to transport hydrogen, their disadvantage stands out since their total efficiency is significantly lower than the direct hydrogen supply via pipeline. However, enormous production potentials and low-cost production from favorable locations could still make these options competitive.

Table 2.3: Comparison of TRL and efficiency of different electricity-based hydrogen and hydrogen derivatives import options (Sterner et al., 2024).

Import of **hydrogen** via pipeline 3,000 km	CO_2 Source	TRL transport	Efficiency transport [%]	TRL total	Efficiency total [%]
... as hydrogen		9	90-96	8-9	57-67
... as SNG	PS	7-9	42-75	7-9	26-53
	DAC	4-9	39-67	4-9	24-48
via ship 10,000 km					
... as LH2		5-9	65-78	5-9	41-55
... as ammonia		4-9	56-86	4-9	35-60
... as methanol	PS	5-9	47-62	5-9	31-43
	DAC	4-9	43-54	4-9	28-38
... as LNG	PS	9	36-65	7-9	23-46
	DAC	9	34-59	4-9	21-41
... bound to LOHC		3-9	62-70	3-9	39-49
Import of **derivatives** (without reconversion to hydrogen) via pipeline 3,000 km					
SNG	PS	9	90-98	7-9	39-62
	DAC			4-9	36-56
via ship 10,000 km					
Ammonia		7-9	97	7-9	51-64
Methanol	PS	9	98	7-9	44-62
	DAC			4-9	40-54
SNG via LNG	PS	9	78-85	7-9	34-54
	DAC			4-9	31-48
FT crude	PS	9	99	6-9	40-45
	DAC			4-9	36-39

Developing hydrogen carrier transport infrastructure is key to achieving a low-cost supply. This development contains the expansion of transport capacities and mature transport options. For example, crude oil carriers can be converted to methanol (Schorn et al., 2021) or LOHC carriers without major modifications, or be used to transport FT crude or its products (Sterner et al., 2024). Liquefied petroleum gas carriers could partially be converted to ammonia carriers (Harmsen and Gerritse, 2024). However, with the increasing production volume, a potential increase in shipping volume might demand additional

transport capacities. The other important development is further research and scale-up of the hydrogen transport using LH2 and LOHC since the maturity of these transport options has not been reached. In the case of LOHC, especially the scale-up of the carrier medium production and the efficiency losses in the dehydrogenation are the major barriers (Sterner et al., 2024). Research, particularly on catalysts of the dehydrogenation process, could improve the efficiency of hydrogen transport using LOHC if milder reaction conditions could be achieved (Aakko-Saksa et al., 2018). The major challenge in the case of LH2 is achieving and maintaining low temperatures of around 20 K (-253.15°C). These extreme temperatures demand high cooling energy input and are technically challenging. A Japanese company built and operated the first commercial LH2 carrier with a capacity of 75 tons (2.5 GWh). The company's objective is to achieve full commercial scale of LH2 transport by 2030, including LH2 carriers with a volume of 160,000 m^3 (9,600 tons; 320 GWh) (Abraham et al., 2024).

The past sections have discussed potential applications, production, and transport of LC-H2D, covering the complete supply chain, but even though the technologies are available and the large consumption potential exists, only 4% of the announced 520 GW electrolysis projects have reached the final investment decision, and some of the most ambitious projects have been canceled (International Energy Agency (IEA), 2024). Based on expert interviews, the majority of experts see only limited (40%) or mixed (34%) progress in the hydrogen economy (Yap and McLellan, 2024) since significant barriers still exist.

2.4 Barriers to ramping up the hydrogen economy

Reasons for the low share of projects beyond the final investment decision are barriers and challenges on the supply and demand side of the hydrogen economy. These barriers and challenges are in manifold areas like technology, economics, and regulatory aspects (Table 2.4). The following sections will describe and discuss the main barriers to the hydrogen economy.

2.4.1 Regulatory framework on the production of electricity-based hydrogen and its derivatives

Before discussing the description and regulatory aspects, a description of LC-H2D policy approaches is required. In general, three approaches exist to regulate the production, transport, and application of LC-H2D. Command-and-control instruments steer the hydrogen economy by setting fixed regulations, which the affected targets[8] need to follow. These include bans, quotas, and standards. Market-based instruments regulate prices and quantities by lowering or raising taxes, implementing subsidies, using auctions to facilitate capacity installations, or implementing cap-and-trade systems. Finally, information-based or voluntary instruments increase transparency through, for example, labels and certificates to allow targets to make informed decisions, which could facilitate self-commitment to the objective (Henstra, 2016; Jänicke et al., 2003). Figure 2.9 depicts the different approaches and states some regulations on LC-H2D fitting the other approaches.

[8] "Targets are actors whose behaviour is linked to the achievement of goals, including individuals, groups, and other governments." Henstra (2016)

Table 2.4: Main barriers and challenges of the hydrogen economy based on International Energy Agency (IEA) (2024); International Renewable Energy Agency (2021); Le et al. (2024); Tarkowski and Uliasz-Misiak (2022); Bade et al. (2024); Bielefeld et al. (2023).

Barrier	Manifestation
Regulatory uncertainties	• Missing/inflexible/excessive regulatory framework • Missing financial incentives (e.g., contracts for differences, subsidies) • Missing regulatory incentives (e.g., quotas) • Licensing and permissions
Demand uncertainties	• Reserved consumers
High production costs	• High upfront investment • Operational costs from renewable electricity • Scale-up of electrolysis production • Efficiency losses
Technical challenges	• Operational challenges • Safety requirements • Abrasion, corrosion • Rare earths, expensive materials
Infrastructure	• Shortage of transport, distribution, and storage infrastructure • Uncertainty of future availability of transport infrastructure

The production standards of renewable fuels of non-biological origin
Before the final publication of the delegated act of REDII, significant uncertainties existed on how electricity supply conditions would be adopted, since the stated electricity supply conditions and the supply of CO_2 would heavily affect their potential business cases. Studies show that a strict implementation could increase production costs (Frontier Economics, 2021), could lead to over-capacities of renewable generators (Ruhnau and Schiele, 2023), and increased risk from a volatile electricity supply (Schlund and Theile, 2022). However, loose implementation could increase the utilization of fossil power generation to supply steady electricity to the production plant (Zeyen et al., 2024). Consideration of the regulatory framework is necessary to determine the impact of the electricity supply conditions on the PtX system. In addition, the interaction with the energy system needs to be analyzed to assess the benefit of the implemented regulatory framework from the system planner's perspective.

Policy type	Command-and-control instruments	Market-based instruments	Information-based / voluntary instruments
Assumptions	Targets will obey state-issued regulation due to fear of penalties or acceptance of government legitimacy	Financial incentives and disincentives motivate targets	– Targets have commitment and capacity, but lack knowledge – Targets will adapt if risks are assessable and advantage perceptible
Approaches	– Bans / prohibitions – Standards – Quotas	– Taxes / fees – Subsidies / tax deductions – Allowance trading	– Labels – Certificates – Self-commitment
Exemplary policy in RFNBO context	– Ban of conventional fuel in passenger vehicles from 2035 – reFuel Aviation kerosene quota – RFNBO standards in RED II delegated act – Hydrogen quota in RED III	– H2Global double auctions – European Hydrogen Bank subsidy auctions – Important Projects of Common European Interest (IPCEI: Hy2Tech, Hy2Use, Hy2Infra, Hy2Move)	– CertifHy – InnoFuels platform
Pros	– Clear regulation – High certainty – Potentially fast implementation	– Cost efficient – Fosters innovation – Precise targeting	– Low costs and administrative complexity – Precise targeting – Low political risks
Cons	– Low incentive of innovation – Log-in effects – Potentially cost inefficient – High political risk	– Uncertain outcome due to complex dependencies – Necessary internalization of external costs – Potentially expensive and administrative complex	– Potentially low impact – Uncertain outcome – Greenwashing

Figure 2.9: Policy approaches (Henstra, 2016; Jänicke et al., 2003) and exemplary implementations in the context of the hydrogen economy and electricity-based hydrogen and its derivatives.

The REDII delegated act (European Union, 2023a) answered the major questions on the electricity supply conditions of the RFNBO production, and the delegated act in European Union (2023b) presented the methodology to calculate the GHG emissions of the final products. These delegated acts aim to significantly reduce GHG emissions, which can only be achieved if low-carbon electricity is used. Otherwise, grid electricity based on conventional energy carriers could even result in higher GHG emissions when applying eFuels compared to conventional fuels (Alhyari et al., 2019). The second objective is that the electricity consumption of the PtX facility should not apply additional stress on the electricity network.

Regarding electricity supply, two options exist: using grid electricity or building stand-alone facilities. While the second case automatically fulfills all requirements as soon as renewable energies are used, the first case must consider the properties of the bidding zone (Table 2.5). Germany has directly adopted the European electricity supply conditions and emissions calculation method of REDII and associated delegated acts in the 37th Bundesimmisionsschutzgesetz (Deutscher Bundestag, 2024b).

Table 2.5: Bidding zone properties and electricity supply conditions of grid-connected PtX systems (European Union, 2023a).

Bidding zone properties	**Electricity supply conditions**
Annual renewable share $\geq$ 90%	Operating hours must not exceed hours of renewable supply
Carbon intensity $\leq$ 18 g CO_2-eq. / MJ	• Renewable electricity demand is covered by contracts • Geographical correlation • Temporal correlation
Redispatch necessary	Redispatch demand is reduced by the same amount as electricity consumption
Any	• Additionality • Geographical correlation • Temporal correlation

Especially the additionality, the temporal, and the geographical correlation must be met by electrolysis systems that are not located in bidding zones fulfilling the properties in Table 2.5 (e.g., Germany), which could result in the barriers mentioned in Section 2.4. The additionality condition ensures that additional renewable generator capacities are installed to produce RFNBO. Temporal correlation aims to ensure a balance between electricity generation and consumption. Here, electricity storage solutions comply with this regulation if they also charge with the temporal correlation. Geographical correlation aims to avoid any additional network congestion. Since bidding zones might change over time, this geographical correlation needs to be achieved at the time of installation. Table 2.6 explains the properties of the electricity supply to comply with the conditions.

Stand-alone PtX plants automatically fulfill the geographical and temporal correlation condition since they are directly connected to the renewable generators. These renewable generators must meet the additionality condition. The stand-alone PtX systems can be connected to the electricity grid, but smart metering must prove that no electricity from the grid was used to produce RFNBO.

With the regulation of electricity and CO_2 supply, the EU aims to reduce the GHG impact of the RFNBO production. To quantify this potential, the EU developed a calculation methodology for the production, consumption, and transport of RFNBO shown in Equation 2.4.

Table 2.6: Properties of the different electricity supply conditions (European Union, 2023a).

Electricity supply condition	Properties
Additionality	• Installation of renewable capacities not longer than 36 months before PtX system • No previous financial support for investment or operation
Temporal correlation	• Balancing of electricity generation and consumption on an hourly basis[9] • Electricity clearing price on day-ahead market for respective period $\leq$ 20 €/MWh • Electricity clearing price on day-ahead market for respective period $\leq$ CO_2 emission allowance for 1 ton in the same period $\cdot$ 0.36
Geographical correlation	• Electricity generation and consumption in same bidding zone • Electricity generation and consumption in interconnected bidding zones with consumption being in the bidding zone with lower or equal clearing prices in the day-ahead market • Electricity generation and consumption in interconnected bidding zones with generation being in an offshore bidding zone

$$E = e_{input} + e_{processing} + e_{transport\ and\ distribution} + e_{use} - e_{ccs} \tag{2.4}$$

The emission intensity does not include emissions from any machinery and equipment of the PtX system, and the carbon intensity of renewable energies is attributed with 0. This approach is applied to avoid multiple accounting of renewable energies, and deviates from the classical life cycle assessment (LCA) approach, where each component, input, and output is considered when calculating GHG emissions. Unlike renewable electricity, grid electricity must be considered when calculating the carbon footprint. The same applies to processing, transport, distribution, and usage emissions. Applying CCS allows additional reduction if excess CO_2 is stored. Overall, the RFNBO needs to achieve a carbon reduction of at least 70% compared to conventional energy carriers, which are valued with 94 gCO_2-eq. per MJ.

Finally, European Union (2003) regulates the origin of CO_2 in producing hydrogen derivatives. Potential CO_2 sources are industrial exhaust gases, natural CO_2 emissions, biomass,

or DAC. However, especially industrial exhaust gases are limited since the EU tries to reduce the overall emissions, and using carbon capture and utilization (CCU) would only shift CO_2 emissions to the following RFNBO application. Therefore, only processes listed in the EU CO_2 trading scheme can be used until 2041, except emissions from electricity generation, which are limited to 2036. Biomass, natural CO_2 emissions, and DAC can be used without limitation. However, the CO_2 emissions from the applied electricity and heat of CO_2 capturing processes are also considered.

Increasing the share of renewable fuels of non-biological origin using quotas
The major challenge of the hydrogen economy is overcoming the chicken-and-egg problem. On the demand side, one main barrier is the lack of willingness to purchase RFNBO due to high costs. Several policy instruments were developed to enforce the utilization of RFNBO to increase the demand. The principal instruments are quotas of RFNBO consumption. For example, the renewable energy directive III aims to increase the share of RFNBO hydrogen on the total industrial applied hydrogen to 42% in 2030 and 60% in 2035 (European Union, 2023c), which is a significant increase looking at the current share of RFNBO hydrogen of 0.4% in 2023 (European Hydrogen Observatory, 2024). Furthermore, quotas exist for hard-to-abate applications where policy makers agree that alternatives for RFNBO are expensive or technically infeasible. This circumstance applies to the aviation fuel kerosene, where the EU implemented quotas of RFNBO sustainable aviation fuels (at least 35% in 2050 (European Union, 2023d)). Finally, a RFNBO quota of 1% in 2030 exists for the overall transport sector (European Union, 2023c). The missing willingness to adopt RFNBO is further exacerbated by the uncertainty on infrastructure as to whether RFNBO will be available locally in the long term, and by complicated regulatory frameworks which prevent the demonstration of clear advantages of eFuels application (Yap and McLellan, 2024).

Market-based instruments to address the cost-disadvantage of renewable fuels of non-biological origin
However, the main barrier to the hydrogen economy is the missing price competitiveness of RFNBO and conventional energy carriers. Based on International Energy Agency (IEA) (2024), RFNBO hydrogen costs 1.5 to 6 times more than fossil-based hydrogen, with the main share being the high capital expenditures, electricity supply costs, and transport costs. To decrease production costs, the EU and its members have implemented several programs that use investment support as a subsidy instrument. In the EU, the *European Hydrogen Bank* or the *Important Projects of Common European Interest on Hydrogen* are used to subsidize investments in production, infrastructure, and storage of RFNBO. For example, within the *H2Infra* program, 33 projects with a nominal eligible cost of 11.509 billion € are funded with a nominal state aid of 6.905 bn €, covering around 60% of the project costs with funding. Such subsidies aim to ignite the initial spark of the hydrogen economy since decreasing RFNBO supply costs could already lift some of the existing barriers.

The regulatory framework regarding RFNBO focuses mainly on the production of RFNBO, and the electricity supply conditions of REDII need to be considered when planning and operating PtX systems. However, next to the regulative aspects, further challenges exist when planning PtX systems.

2.4.2 The challenging planning of power-to-X plants

Another major barrier is the risk in PtX plant designing when considering iRES electricity generation. Operational challenges could arise since the relatively inflexible synthesis components meet the volatile renewable electricity generation. This applies especially for stand-alone plants where a backup electricity supply, for example from the grid, might not be available. From a technical point of view, the flexible operation of synthesis units could demand ramping and partial load abilities, increase safety risks, lead to degradation of the technical equipment, and decrease product quality. Such effects would directly impact economic performance since lower efficiencies, increased maintenance, and lower utilization could cancel out the potential benefits of flexible operation.(Bielefeld et al., 2023; Iglesias González et al., 2016) However, if the system fits the flexibility demand, benefits can be significant. For example, the capacities of auxiliary equipment like hydrogen storage units could decrease, resulting in reduced investment demand (Pfeifer et al., 2020). The operational challenges further affect the planning process since the site-specific renewable electricity generation poses the challenge to plan and optimize PtX systems concerning local circumstances. Peña et al. (2024) stated that only minor flexibility properties are required to reduce production costs significantly and that a fully flexible methanol synthesis could reduce costs by 33% since over-capacities of all components would significantly decrease. These challenges and opportunities emphasize the necessary integrated planning of PtX systems to achieve minimal production costs while maintaining safe and reliable operation.

2.4.3 Transport infrastructure challenges for the hydrogen and derivative supply

Next to the challenging integration of renewable energies and a complex regulatory framework, transport plays a significant role when aiming for low-cost RFNBO supply. One current barrier regarding transport is the shortage of available infrastructure for the transport, distribution, and storage of hydrogen. Existing long-distance transport of energy carriers is mainly focused on natural gas, crude oil, coal, methanol, and ammonia, and the properties of hydrogen, like corrosion and diffusion, limit the utilization of existing infrastructure (Perna et al., 2020). Retrofitting the existing infrastructure could allow the application of RFNBO. However, uncertainty about the extent to which existing infrastructure will be retrofitted exists. For example, municipalities might decommission existing infrastructure instead of retrofitting, since other options like district heating are preferred (Südwestrundfunk, 2024). The decentralization of hydrogen production could further require new infrastructure to connect emerging production centers with the consumers. These challenges show the necessary assessment of the current transport infrastructure and potential developments in the future. Such an analysis could be the basis for policymakers to support their infrastructure planning and for investors to make investment decisions.

2.4.4 A critical discussion on the barriers

National and supranational governments address these barriers by defining hydrogen strategies to support and stimulate the ramp-up of the hydrogen economy. For example, the German national hydrogen strategy aims to ramp up domestic hydrogen production by achieving 10 GW of national electrolysis capacity by 2030, which, next to imports, covers the 95–130 TWh of LC-H2D demand projection. The strategy includes a road map to

develop the necessary infrastructure for import and transport, implement hydrogen applications, create framework conditions, and ensure the supply of low-cost and low-carbon hydrogen. Another aim of the German government is to make Germany one of the leading suppliers of hydrogen technologies.(Bundesregierung, 2023a)

However, most of the barriers mentioned above can be critically discussed, since the regulation or non-regulation is solely based on political decision-making. For example, the electricity supply conditions in REDII specifically address electrolysis units. In contrast, political regulations do not constrain other future electricity consumers, such as data centers, heat pumps, or electric vehicles. Heat pumps and electric vehicles might be partially operated flexibly, potentially increasing flexibility in the power system. However, data centers require full availability, and their electricity demand is expected to double globally by 2030, primarily driven by the application of artificial intelligence (International Energy Agency (IEA), 2025).

Banning technologies is particularly controversial, since this instrument stipulates technologies and options. One example of this instrument is banning conventional fuels in internal combustion engines (ICE) of passenger vehicles (European Union, 2023e). ICE supporters state that 2035 is too early, as a sufficient quantity of RFNBO fuels will not be available, effectively banning any new ICE passenger vehicles. Therefore, this ban is often referred to as *Verbrennerverbot* (ICE ban) in German media, even though only applying conventional fuels is forbidden. On the other side, supporters of the ban claim that without such a ban, the fossil fuel demand of passenger vehicles might not decrease, since car manufacturers have no incentive to change the propulsion of the vehicles or ensure the provision of sufficient RFNBO fuels.(Birel et al., 2024) This aspect is particularly critical since passenger vehicles have an average lifetime of 18–28 years in Europe (Held et al., 2021), and cars sold beyond 2035 might require fuel beyond 2050. A similar discussion occurs in domestic heating, where the German *Ampel* government decided to reform the *Gebäudeenergiegesetz* (Bundesregierung, 2023b), roughly translated to *Building Energy Act*. One part of this regulation implements a minimal share of renewable energy in newly installed heating systems to 65 %, starting in 2026. The amendment of the law was controversial within the different parties of the government and the general population.(Haas et al., 2025) Both laws began the discussion on the technological neutrality of political decisions. Here, supporters of LC-H2D claim that the market should decide which technology will prevail, while opponents state that public and private funding should be focused on the more efficient technologies to speed up their adoption. However, banning specific LC-H2D applications could hinder the general ramp-up of the hydrogen economy, since the hydrogen economy would benefit from learning curves and economies of scale independently of the type of RFNBO produced.(Birel et al., 2024)

The missing cost competitiveness of LC-H2D and conventional energy carriers can also be critically discussed. This missing cost competitiveness does not arise solely from the high production costs of LC-H2D. The high emissions reduction potential of LC-H2D could reduce negative externalities significantly, especially GHG emissions, and insufficiently internalizing these externalities for conventional energy carriers could build significant market entry barriers for sustainable technologies (Owen, 2006). Examples of internalizing negative externalities are cap-and-trade systems like the European Union Emissions Trading System I & II or CO_2 taxes. However, with a CO_2 emission certificate price of currently 78.55 €/ton$_{CO_2}$ (boerse.de (2025) on the 9^{th} October 2025) and the German

CO_2 tax of 55 €/ton_{CO_2} for 2025, these costs are significantly below the estimated social costs of carbon, which could reach up to 283 \$/ton_{CO_2} (Moore et al., 2024). Reasons for the discrepancy between the estimated social costs of carbon and carbon prices are manifold. For example, the actual social cost of carbon remains unknown since the damage of climate change is uncertain, and calculations heavily depend on applied models and scenarios (Pezzey, 2019). Lobbying plays another role, which can significantly dilute ambitious climate protection policies (Culhane et al., 2021). However, one major reason is the direct effect on the purchasing power of the population, since the majority of consumed goods and services, such as mobility, food, and heating, incur significant amounts of CO_2 emissions and costs would rise if CO_2 prices increase. This comprises the political risk of public opposition and decreasing approval rates (Carattini et al., 2018).

Generally speaking, climate policy is difficult. Policy makers tend to focus on urgent, short-term policies instead of long-term, overall strategic planning (Burrows and Gnad, 2018), since long-term effects of climate change are difficult to predict and the effects of policies mitigating climate change are diffuse, while policies leading to technology bans and price increases are directly noticeable. The hydrogen economy is no exception from this, explaining the political hesitation and the concentration on no-regret applications such as aviation fuels.

3 Methodology

The following chapter will provide insights into the methods developed and applied in this thesis. Paper A applies a power system modeling approach to assess the impact of the REDII electricity supply conditions on the RFNBO production (Section 3.1). The production is further assessed from a grid-independent perspective, starting with a deterministic modeling of stand-alone PtX production systems in Paper B (Section 3.2), which is developed into a robust optimization approach considering renewable electricity generation uncertainties in Paper C (Section 3.3). Finally, the modeling of the global RFNBO transport is described in Paper D (Section 3.4). Each study is briefly motivated, its methods are classified in the broader taxonomy of methods in the research field, and modeling choices are explained. Figure 3.1 shows the objective of each paper and the applied methods.

3.1 Energy system modeling

Energy system models are one of the main instruments applied in energy research to assess the interaction between technologies, stakeholders, and markets. Research applying these models started after the oil crisis and can be categorized into top-down models, which usually apply aggregated data and focus on all markets using general-equilibrium models, and bottom-up partial-equilibrium models, which mainly focus on the technological feasibility of potential energy systems without considering other markets (Lopion et al., 2018; Böhringer and Rutherford, 2008). The different model types are also distinguishable regarding the underlying mindset when implemented. Normative models aim to achieve a set goal or a desired future state of the energy system, such as carbon neutrality, 100% renewable energy supply, or full autarky of the energy system. Descriptive or predictive models aim to represent and analyze the current energy system and realistic developments based on technological, economic, and political frameworks. Explorative models account for uncertainties in their scenarios by including disruptive events, pessimistic or optimistic scenarios, and variations of prices, technology developments, and policy changes. A mix of these approaches is possible as well. For example, normative models typically rely on descriptive or explorative elements to define the framework within which the model can achieve the desired goal.(Börjeson et al., 2006)

Most energy system models are normative bottom-up partial-equilibrium models with descriptive elements. However, several modeling and methodological choices can be made, and thus, a broad spectrum of such energy system models exists. Based on Klatzer et al. (2022) and Hoffmann et al. (2024), these modeling and methodological choices include the formulation and expansion type, power flow modeling, gas flow modeling, stochasticity, spatial and temporal resolution, and the consideration of regulation. Before categorizing the model developed in Paper A, these dimensions are briefly described.

Paper A

Authors & title: Langenmayr, U. and Ruppert, M.: Renewable origin, additionality, temporal and geographical correlation – eFuels production in Germany under the RED II regime

Objective: Investigate optimal locations and operation of the eKerosene production in Germany while considering the renewable energy directive II electricity supply conditions

Applied method: Energy system modeling of the German power system including the electricity generation, electricity transmission network, and the eKerosene production

Paper B

Authors & title: Langenmayr, U., Heinzmann, P., Schneider, A., Ruppert, M., Rudi, A., and Fichtner, W.: Stand-alone power-to-X production dynamics: A multi-method approach to quantify the emission-cost reduction trade-off

Objective: Holistic modeling of stand-alone Power-to-X production to investigate technical, economic, and environmental properties as well as the trade-offs between economic and environmental objectives

Applied method: Multi-method approach including flowsheet optimization using process simulation, techno-economic assessment based on the process simulation results, life cycle assessment based on the process simulation results, and multi-objective optimization

Paper C

Authors & title: Langenmayr, U., Slednev, V., Ruppert, M., and Fichtner, W.: An adaptive robust optimization approach using scenario-based uncertainty sets for stand-alone power-to-X facilities.

Objective: Consideration of renewable electricity generation uncertainty in the planning process of stand-alone Power-to-X facilities

Applied method: Adaptive robust optimization in combination with scenario-based uncertainty sets

Paper D

Authors & title: Langenmayr, U., Schuler, J., Slednev, V., and Fichtner, W.: Mapping Tomorrow's Energy Journeys – A Global Perspective on the Transport of Synthetic Energy Carriers.

Objective: Investigation of the global RFNBO supply chain considering high-resolution data on hydrogen production costs, renewable generator capacity potential, and transport infrastructure

Applied method: Heuristic-inspired branch-and-bound solving algorithm to solve large-scale mixed-integer problems

Figure 3.1: Overview of objectives and methods in each paper.

Energy system models can be distinguished into two categories: expansion models and unit commitment problems. Expansion models usually cover generation expansion planning (GEP), transmission network expansion planning (TNEP), and the expansion of both (TNEP & GEP), and are usually applied to assess the necessary development of the energy system to achieve the overall objective. Unit commitment problems focus on the sole operation of systems with the objective of cost minimization. A differentiation can be drawn between investment-oriented operational models, which aim to investigate the impact of single technology expansions on the energy system, and strategic models, which

usually aim to achieve long-term objectives, such as carbon neutrality or a 100 % renewable energy supply. The choice of model scope is closely related to the necessary time horizon. Operational models assess and monitor the current state of the energy system, typically covering a period of a few hours to a few days. Investment-oriented operational models usually cover a single year to assess costs and technological performance. Strategic models usually apply a multi-year approach to model long-term transformation. Such multi-year approaches can be divided into perfect foresight approaches, where all considered years are processed in a single closed optimization problem. In contrast, myopic approaches divide the individual years into separate optimization problems to consider the uncertainty of future developments, such as regulations, specific investments, or developments in demand. Operational models might apply rolling horizon approaches, where a short time horizon is processed and shifted to the following time horizon. Such models often require a fine temporal resolution, frequently higher than hourly, to achieve a detailed modeling of the operation itself; therefore, a short time horizon is necessary. Strategic models usually apply hourly or even lower temporal resolutions since such models need to cover the multi-year time horizon to represent the strategic implications correctly. Another aspect to mention regarding temporal resolution is the application of representative periods. These periods aim to reduce the necessary data by concentrating on repetitive patterns of weather and demands instead of the complete time-series data. Another modeling choice is the considered components. Basic components are electricity generators and electricity transmission grid assets. These can be complemented by storage units, conversion units, as well as electricity sources and sinks. While these components can be electricity-related only, adding further commodities could shift a model from a power system to a multi-commodity system. Finally, considering uncertainty is another systematic characteristic of energy system models, including uncertainty on load demand, iRES generation, fuel prices, and economic parameters. These uncertainties can be included using multi-stage stochastic optimization, Monte Carlo-based approaches, and descriptive scenarios.

Finally, the model formulation plays an important role and mostly depends on the degree of technical detail implemented. For example, the electricity transmission grid can be implemented as a non-convex and non-linear alternating current optimal power flow (AC-OPF) model, which allows the assessment of reactive power, voltage magnitude, or phase angles. If this technical detail is not required, direct current optimal power flow (DC-OPF) models could be used instead, which allow linear optimization. This circumstance also applies to gas grids since the exact modeling of gas flows requires non-linear gas equations. Decisions are another significant driver of complexity in energy system models. They comprise the choice of transmission line to build, policy alternatives, or linearized formulations of economies of scale and learning curves of investments, and are solved using mixed-integer optimization.

Another dimension in Hoffmann et al. (2024) is the consideration of regulation. While some regulations are assessed, none of the reviewed publications considered the REDII regulations, even though the production or import of LC-H2D is assessed. For example, system-level models like Balmorel (Wiese et al., 2018), Calliope (Pfenninger and Pickering, 2018), REMix (Gils et al., 2017), OSEMoSYS (Howells et al., 2011), GENeSYS-MOD (Löffler et al., 2017), TIMES (Loulou and Labriet, 2008), or PyPSA Brown et al. (2018) all comprise studies, which cover LC-H2D topics such as the role of hydrogen in the future energy system (Kountouris et al., 2024; Tetik and Kirkil, 2024; Béres et al., 2024; Blanco et al., 2018), the impact of hydrogen infrastructure (Neumann et al., 2023; Hanto et al.,

2024; Upadhyay et al., 2025; Hofmann et al., 2025), the investigation of domestic production and LC-H2D imports (Burandt, 2021; Sasanpour et al., 2021; Wetzel et al., 2023; Slednev, 2024), or the analysis of uncertainties (Pickering et al., 2022; Pinto et al., 2024), among others. This literature overview is not exhaustive, but it shows that LC-H2D is an essential keystone of the energy system transformation towards carbon neutrality. However, these studies have in common the missing consideration of the European regulation on the production of RFNBO, even though their production is modeled to be in Europe or imported to Europe. Based on the regulation described in Section 2.4.1, the majority of LC-H2D within these models would not count as RFNBO but rather as eFuels. Even if the necessary grid conditions are met from the beginning (e.g, Sweden) or achieved within the long-term planning horizon of the energy system model, the operation of the electrolyzer units is not constrained to the renewable generation or to redispatch measurements.

Only a limited number of studies have integrated the electricity supply conditions in REDII from a national or transnational central planner perspective. One of the first studies using an energy system perspective was published by Brauer et al. (2022). The approach assesses various regulatory options regarding the electricity supply of hydrogen supply chains. They cover the German and all adjacent electricity bidding zones and apply nine scenarios, each having a different manifestation of the temporal and geographical correlation and the additionality condition. Ricks et al. (2023) assessed the impact of the hourly temporal correlation and the additionality condition, and such variations, regarding total system costs and embodied GHG emissions. The study covered the US Western Interconnection electricity system[1], which was modeled using the GenX model. The different electricity supply conditions were implemented using constraints, connecting the operation of the electrolysis unit to the renewable generators' output based on the set temporal correlation. The additionality condition was met by considering only renewable generators installed in the same period as the electrolysis unit. Zeyen et al. (2024) use the PyPSA-EUR framework covering the German electricity transmission network, which is clustered into bidding zones. Afterward, a two-step optimization is conducted to optimize the energy system without considering hydrogen production in the first optimization. In the optimized energy system, hydrogen production is integrated, and the second optimization allows only the capacity expansion of wind, solar PV, and battery storage at the locations of the electrolysis system. The analysis further implements different temporal correlations and allows relaxation of the hydrogen demand from a steady hourly supply to a fully flexible supply. The Chilean energy system was modeled using OSEMoSYS in Vargas-Ferrer et al. (2025) to calculate the production costs of hydrogen and ammonia exports while meeting the REDII requirements. Next to a monthly and hourly temporal correlation, this model implements emission thresholds, ensuring the maximal allowed carbon intensity of the product based on European regulations, and follows a long-term planning horizon up to 2060.

While these publications cover the RFNBO-aligned hydrogen production, several open questions remain. First, most studies concentrate on the temporal correlation without implementing the geographical or additionality condition. Second, the power system is aggregated to bidding zone levels, which also aggregates the renewable electricity generation. This aggregation results in portfolio effects, which could overestimate the availability and volatility of iRES generation. This is essential if the impact of the RFNBO conditions

[1]The electricity supply conditions of the Inflation Reduction Act conform to the conditions in REDII

on the electrolysis units is assessed, since actual electrolysis units might not be able to acquire private purchase agreements that are similarly diversified. Finally, while hydrogen will probably be the most produced RFNBO, the production of other RFNBO is not covered. The production of such could be more challenging, since inflexible synthesis units require a steady hydrogen supply, which affects the energy system differently than the flexible operation of electrolysis units.

Paper A aims to close this gap and conducts a system-level analysis that models the development of the power system by applying a myopic multi-period planning approach, which minimizes the total system costs for the projected years 2022, 2025, and 2030 consecutively. The model is implemented as a linear DC-OPF model. This choice was taken since alternating current models would increase the complexity of the model due to non-linearity and non-convexity, and such complexity exceeds the scope of this work, especially since the objective of the approach is not to model and assess the transmission grid in detail. The nodal resolution equals the electricity transmission grid, where each busbar represents a system node. At this resolution, the nodal-specific renewable electricity generation can be assigned to the same node's electrolysis and battery storage units, which ensures that no grid congestion exists between electricity generation and consumption, and avoids portfolio effects, which occur at aggregated models as described above. Furthermore, binary and discrete variables, which are commonly used in mixed-integer unit commitment or transmission network expansion planning problems, are avoided. However, the problem can still be assigned to transmission network expansion planning problems, since the capacity of existing transmission lines can be expanded, but the choice of adding new transmission lines is omitted. The model is also part of the generator expansion problem class, where new generators can be installed in each projected year. The RFNBO production is implemented as total demand over all nodes, and consumption or transport of the produced RFNBO is not considered. Other sectors, like transport, buildings, or industry, are not modeled explicitly, and only their electricity consumption is considered. In addition, any natural gas or hydrogen infrastructure is omitted, making the model an electricity-only system, which, furthermore, does not implement power sector instruments like demand side management or loss of load. After optimizing the system of a projected year, key parameters such as load demand, renewable electricity share, commissioning and decommissioning of components, and RFNBO demand are adjusted to consider the development over time. This affects all components of the power system, including generators and the components of the transmission grid. Next to these two component types, the RFNBO production is optimized, consisting of a battery storage, electrolysis unit, hydrogen storage, DAC unit, and synthesis unit. This setup is implemented at each node of the system. If CO_2 point sources exist at the node, a CO_2 scrubbing unit is also implemented. The temporal correlation is addressed by limiting the electrolysis and battery storage electricity consumption to the electricity generation of renewable energy sources (RES-E) generators at the same node and of the same hour. However, the electrolysis electricity consumption is further constrained to the electricity generation of RES-E generators installed in the same projected years to ensure compliance with the additionality condition. Two final remarks on the methodological characterization are the consideration of uncertainty and the model complexity. First, especially with an increasing share of iRES, electricity generation is increasingly affected by uncertainty. However, this approach aims to assess the impact of the RFNBO-aligned production on the power system and PtX system, and considering uncertainties could significantly complicate the quantification of this impact. Therefore, a

deterministic approach is chosen. Second, the temporal resolution of the applied profiles is hourly, which, in combination with the high spatial resolution, could result in significant computational complexity of the model. Therefore, weighted weekly representative profiles derived from ten years of weather and demand data are applied.

Next to system-level energy system models, which often require simplifying technical details, facility-level stand-alone PtX systems are of interest, which conduct a detailed assessment of the RFNBO production outside the energy system's boundaries.

3.2 Deterministic modeling of Power-to-X facilities

As discussed in Section 2.1, a significant share of RFNBO might not be produced domestically but imported from countries with favorable conditions for large-scale production at low costs. Next to low costs, low GHG emission intensity is required to achieve the desired GHG emission reduction compared to fossil energy carriers. Paper B addresses this research field by building a general stand-alone PtX system model, which considers production costs and GHG emissions simultaneously, while applicable to locations globally.

Outside of system-level assessments, analyses of stand-alone PtX models have been conducted using thermodynamic models using process simulations, techno-economic models, environmental studies, or a combination of different methods (Ince et al., 2021). The modeling approach depends on the objective of the study. Technological assessments require a high degree of technical detail in the process. This degree of technical detail is usually not applied in studies that assess technology integration into a broader context. In this context, high-resolution temporal and spatial data are generally used, which requires simplifications of the processes, since technological complexity could hinder the assessment due to computational burdens. Therefore, studies often choose between two approaches based on the objective: either they assess the technology and its economic or environmental performance in detail, or they assess the economic or environmental impact of the technology in the broader PtX context. In contrast to focusing on either of the objectives, Paper B conducts a detailed assessment of the technology, assesses the economic and environmental impact, and analyzes the technology within the full context of stand-alone PtX systems. The integrated modeling enables a complete understanding of the technologies within the PtX system, ensures transparency of modeling choices, and allows a consistent database since all parameters are based on own assessments and common assumptions.

The following sections outline the individual methods concisely, including process simulation to model and understand the considered chemical processes, the conducted techno-economic assessment (TEA) to assess the economic implications and to derive the economic parameters, the LCA to investigate the environmental impact and to derive environmental parameters, and the multi-criteria decision-making approach bringing the economic and environmental analysis together. Afterward, the synergies between the different methods are explained to justify the complexity of this multi-method approach.

3.2.1 Understanding the technology using process simulation

Chemical reactions are complex processes that are usually subject to thermodynamic laws. This circumstance leads to non-linear relations between physical parameters, such as pres-

sure or temperature, and conversion efficiencies. These non-linear properties limit the available methods when modeling synthesis units while keeping a high degree of technical detail. The most common approach is the application of process simulation tools like Aspen Plus® or AVEVA™. In comparison to other approaches, like non-linear optimization, these software already include the standard components of synthesis plants, which are connected to the physical and thermodynamic constraints behind chemical reactions and mechanical processes, simplifying the implementation due to the available, comprehensive, and consistent databases.

Process simulations follow a structured workflow to model and optimize chemical plants and systems. In a first step, the plant design is implemented using a flowsheet configuration, where the different modules of the system, like reactors, columns, heat exchangers, among others, are selected and connected by defining material and energy streams, allowing the computation of mass and energy balances. Each module of the flowsheet is associated with a mathematical model to simulate the typical parameters and characteristics of the operation correctly. In addition, thermodynamic models are implemented to model the chemical behavior of the different materials based on pressure, temperature, or contact times. The simulation is executed once the process is implemented, and the results are analyzed. An iterative improvement process is conducted where the process parameters of the individual modules or the system's setup can be adjusted to reduce waste energy and material, or to increase the product yield (Haydary, 2019). Figure 3.2 shows an exemplary flowsheet configuration. In this case, the developed flowsheet configuration of the FT synthesis, which was developed in Paper B. The output of process simulations is a technically optimized chemical plant flowsheet, which includes the dimensioning of the individual modules, the mass and energy balances between the modules, operation conditions, and auxiliary commodities that the process requires. At this point, economic or environmental aspects are not considered.

3.2.2 The techno-economic assessment of the technology

Based on the results of the technical analysis, a TEA is conducted to understand the system's economic impact. A broad landscape of TEA approaches exists, and to decide on a suitable approach, the objective of the TEA has to be defined. The first objective of the TEA is to derive the system's CAPEX and OPEX based on the process simulation's technical results. This objective excludes most of the TEA approaches, since they only apply CAPEX and OPEX in their assessment. The second objective of the TEA is the calculation of a benchmark based on the steady-state operation of the system, which allows the comparison of the economic performance to other steady-state systems and validates the technical and economic results. The second objective does not require any temporally resolved data, and simple spreadsheet approaches are sufficient to achieve the objective. In addition, the multi-criteria analysis will consider temporally resolved data, which makes additional complexity at this stage redundant.

Conducting TEA based on the technical parameters of the process simulation to derive CAPEX and OPEX and to calculate the economic performance is a common approach to investigate synthesis units of PtX systems (Ince et al., 2021). The derived capacities are used to calculate the equipment costs of the components, which are projected to the target year using the Chemical Engineering Plant Cost Index (CEPCI). The projected equipment costs represent only the actual production costs of the equipment and do not consider

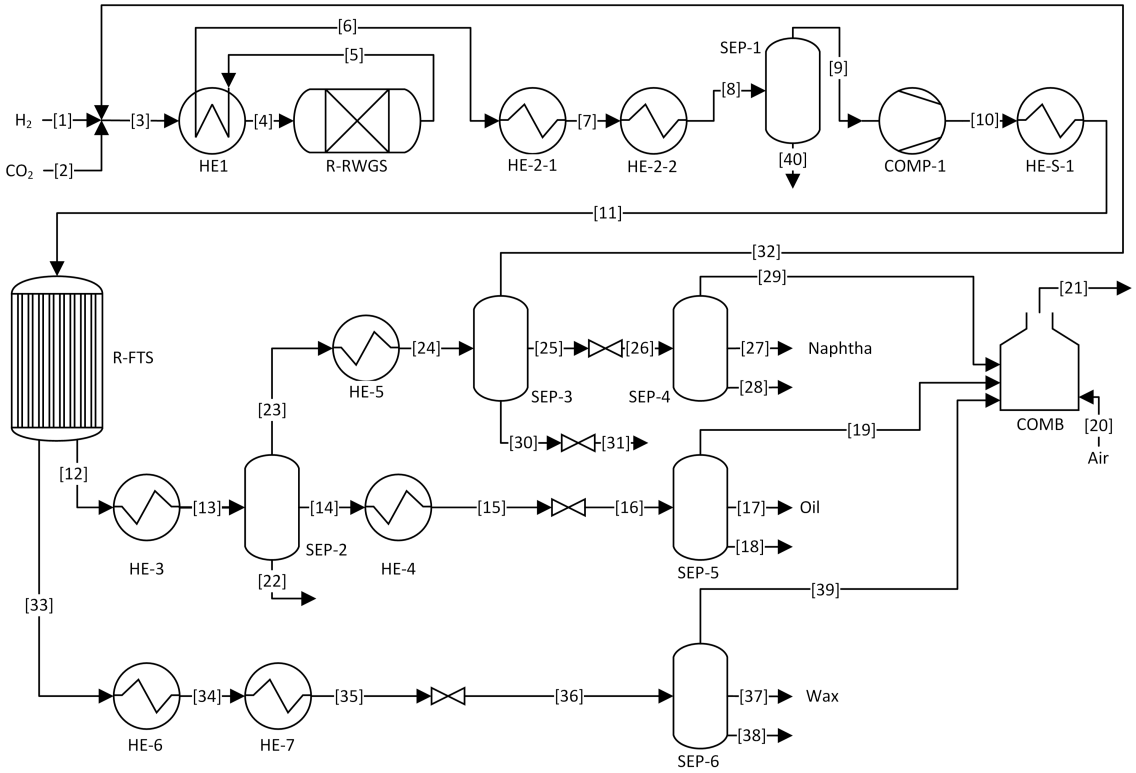

Figure 3.2: Developed flowsheet configuration of the FT synthesis (Langenmayr et al., 2025a).

surcharges like installation, piping, engineering, supervision, or uncertainties. Therefore, surcharge factors based on Peters et al. (2003) are applied to calculate the CAPEX. The process simulation covers only the synthesis plant, while the electrolysis data is based on literature values. Based on the CAPEX of all components, fixed costs are calculated, including the annualized investment, maintenance, and labor costs. Variable costs are calculated based on the utility and electricity demand of the synthesis and electrolysis, and are used to calculate the OPEX. Combined with the fixed costs, the total production costs of the setup are calculated. Figure 3.3 shows the different components and data of the conducted TEA. A volatile electricity supply is not considered since the TEA assumes steady-state operation. This circumstance results in redundancy of storage units and in high yearly capacity factors for the components, leading to low fixed costs per produced unit. Therefore, the TEA of the steady-state facility represents a lower bound of production costs.

3.2.3 The environmental assessment of the technology

LCA allows the in-depth analysis of a system regarding the environmental impact of the system and its components from different life cycle stages. The method comprises four steps (Figure 3.4). The first step includes the definition of the goal and scope of the analysis. Here, the motivation and aim are defined as well as the system boundaries, the

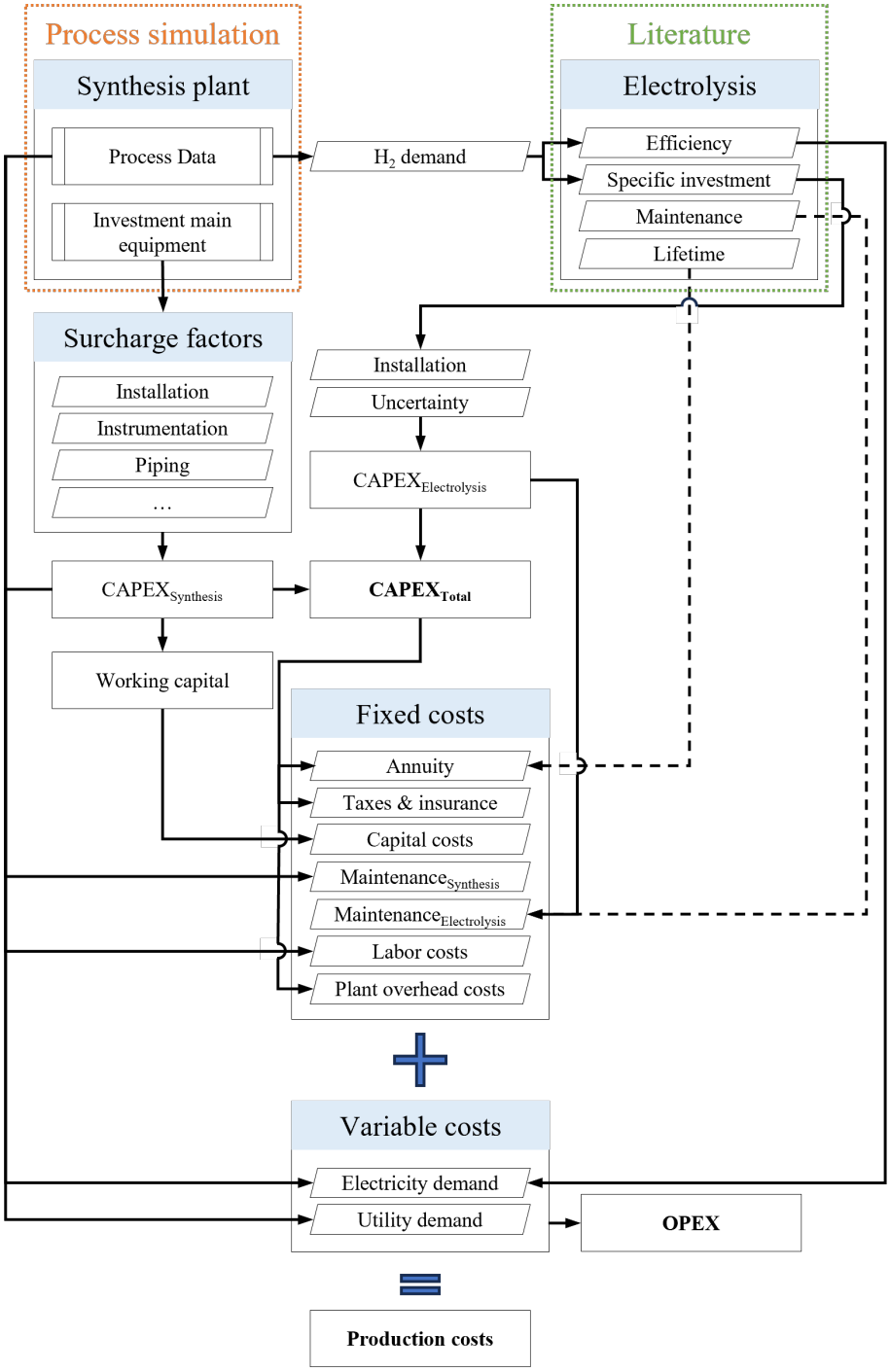

Figure 3.3: Overview of the components and data of the conducted techno-economic analysis methodology.

functional unit[2], assumptions and limitations, as well as allocation procedures if necessary. The system boundaries are usually defined based on the considered processes in the life

[2] "A functional unit is a quantified description of the function of a product that serves as the reference basis for all calculations regarding impact assessment" Traverso et al. (2020)

cycle of a system. For example, considering the system's life cycle from raw material extraction to application is called cradle-to-gate. If the disposal of the system's components is included, the system boundaries are called cradle-to-grave. Finally, only certain parts of the life cycle can be assessed, which is described as gate-to-gate system boundaries. The following life cycle inventory analysis step includes the data collection and the modeling of the product system. The data derived from the process simulations is applied here since the process simulation provides detailed information on the PtX system. Afterward, the life cycle impact assessment classifies the inventory data into the impact categories like global warming potential or acidification, followed by the characterization using category-specific factors to quantify their potential contribution to these impacts. The final step is interpreting and evaluating the results, where insights and findings can be derived to draw conclusions in line with the defined goal and scope of the analysis.(Koj et al., 2019) The output of the LCA is the full environmental impact of the system as a whole, referenced to the functional unit. Manifold LCA have been conducted in the context of PtX systems since various decisions can affect the impact indicators, including the electricity supply, CO_2 source, electrolysis technology, and synthesis process (Ince et al., 2021; Koj et al., 2019; Garcia-Garcia et al., 2021; Ajeeb et al., 2024). Similar to the steady-state TEA, the LCA will also only represent the lower bound of the environmental impact.

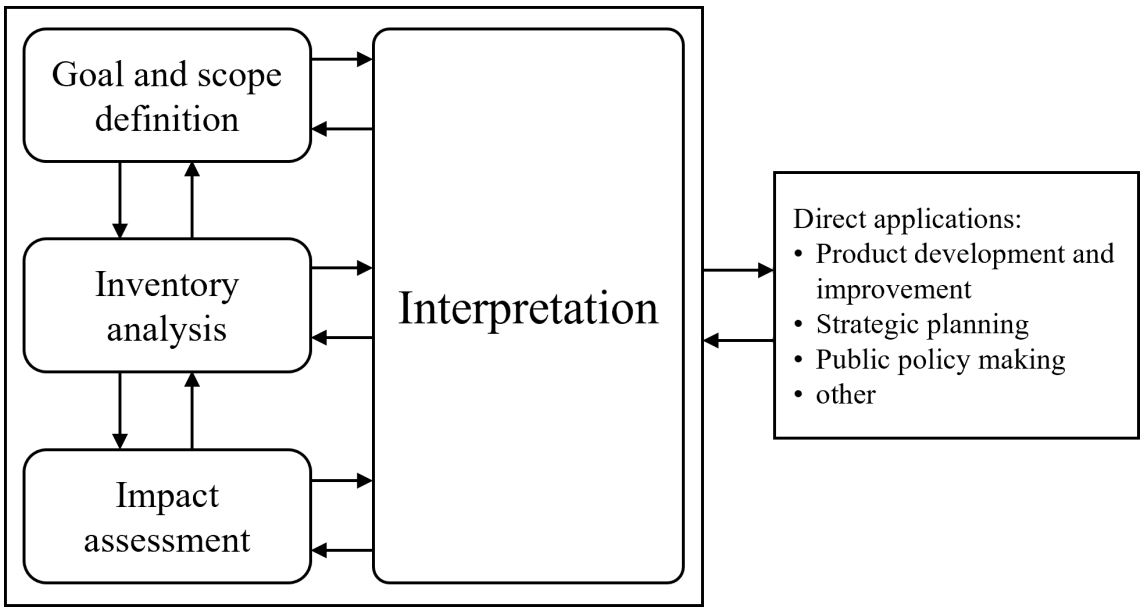

Figure 3.4: Framework of LCA based on ISO 14040 standard.

3.2.4 Multi-objective optimization

Considering multiple, often conflicting objectives simultaneously is the aim of multi-criteria decision-making and is applied to identify the most fitting solution based on the stakeholder preferences. To describe different multi-criteria decision-making approaches, the taxonomy of Pirdashti et al. (2011) is used. Multi-criteria decision-making can be categorized into multi-attribute decision-making approaches, which consider a discrete decision space with a finite number of alternatives, and multi-objective decision-making, which considers an infinite decision space with discrete and continuous variables. Multi-attribute

decision-making approaches, such as the analytic hierarchy process or the technique for order of preference by similarity to ideal solution, do not meet the study's requirements, as the applied multi-criteria decision-making aims to calculate optimal capacities, which are continuous variables. Multi-objective decision-making results in a set of Pareto efficient solutions, and the most-fitting solution is based on the stakeholders' preferences. Pareto efficient solutions have the property that an objective cannot be improved without worsening the other objective(s). Several methods have been developed to derive the set of Pareto efficient solutions. To narrow down suitable approaches, the expression of preferences is considered. A priori methods define the preferences of the stakeholder beforehand, interactive methods include the preferences while decision making, and a posteriori methods allow the application of preferences after the calculation. Paper B's objective is to present the complete set of Pareto efficient solutions to show trade-offs between objectives. Therefore, only a posteriori approaches are considered. This excludes methods like goal programming, where the deviation of different objectives from a previously defined goal is minimized. Another property of the multi-objective decision-making is the complexity of the solution space. While linear and convex problems can be solved with standard optimization algorithms, non-convex and non-linear problems are usually addressed using evolutionary algorithms. In the context of non-linear and non-convex problems, these algorithms are efficient as they do not necessarily calculate exact solutions and are robust as they are implemented to avoid local optima. However, the technical, economic, and environmental data derived from process simulation, steady-state TEA, and LCA are linear, since the non-linear processes within the components are simplified to combine high-resolution temporal and spatial data. Evolutionary algorithms are, therefore, not required.

Within MOO, further directions exist. One possible approach is the weighted-sum approach, where a single objective function sums the normalized objective function value multiplied by its weighting. The full Pareto front is derived by applying combinations of preferences, each in an individual optimization. The ε-constraint approach uses the lexicographic values of the objective functions to determine the range of objective function values. A stepwise processing of the ranges is conducted as individual optimization runs, where one objective function is optimized, while the other objectives are implemented as constraints and constrained by the previously determined objective function value e_i of the current step.(Caramia and Dell'Olmo, 2020) The MOO applied in Paper B is based on the augmented ε-constraint approach of Mavrotas (2009), which ensures strictly dominant solutions. The following equations show the general structure of the MOO problem. Since s_i is in the objective function and maximized, the objective function f_i, constrained by the previously calculated objective function value e_i, is minimized as well to ensure strictly dominant solutions. At the same time, ε is sufficiently small, so the objective function is only marginally affected. The coefficients r_i are used to adjust the dimensions of the s_i to each other, since the objective function values f_i could significantly differ.

$$\min_{x} \quad f_1(x) - \varepsilon \cdot (\frac{s_2}{r_2} + \frac{s_3}{r_3} + \cdots + \frac{s_p}{r_p}) \tag{3.1}$$

subject to

$$f_2(x) + s_2 = e_2 \tag{3.2}$$

$$f_3(x) + s_3 = e_3 \tag{3.3}$$

$$\vdots$$

$$f_p(x) + s_p = e_p \tag{3.4}$$

$$h(x) = 0 \tag{3.5}$$

$$g(x) \leq 0 \tag{3.6}$$

Some additional remarks on the optimization problem are required. The MOO considers minimal production costs and GHG emissions as objective functions. The production costs are based on the annualized investments, fixed operation and maintenance costs, and operational costs, such as utility demand or variable operation and maintenance costs. The GHG emissions are based on the specific GHG emissions of a component's production, installation, operation, and disposal. Other impact categories are not considered. The constraints of the optimization problem define the technologies' properties, such as ramping abilities, minimal load potential, and efficiencies, and the decision variables include the hourly operation of the individual components, such as conversion units, generators, and storage units, and the capacities of each component. The techno-economic assessment in the MOO is closely related to the steady-state TEA in Section 3.2.2, but has some significant differences. For example, the steady-state TEA only assesses the PtX system, whose capacities are dimensioned in the process simulation, and does not conduct an economic optimization. The MOO further includes hourly iRES electricity generation from wind and solar PV generators to accurately model the operation of the PtX system. In contrast, the steady-state TEA considers the electricity supply only in the form of electricity costs and yearly capacity factors. One advantage of conducting the steady-state TEA is the determination of scaling effects of synthesis units, which are also implemented in the mixed-integer linear optimization by linearizing the capacity-dependent investment. Finally, the MOO is implemented as a deterministic model, neglecting uncertainties from technologies or renewable electricity generation.

3.2.5 Multi-method approach to exploit synergies between process simulation, techno-economic analysis, life cycle assessment, and multi-objective optimization

Conducting process simulation and steady-state TEA as well as LCA allows consistent parameters and assumptions to be provided and applied. In contrast to this study, other studies relying on literature data could mix technical, economic, and environmental parameters without ensuring the data are based on the same technical setup. In addition, multi-method approaches can exploit synergies between and overcome the disadvantages of individual methods. Looking at the applied methods, process simulation and the TEA and LCA based on process simulation results often imply a steady-state operation of the system. This steady-state operation assumes a consistent supply of energy and auxiliary

materials, allowing the system to operate at optimal conditions. Several approaches exist to consider the volatile electricity supply from iRES. A first approach would be to conduct several discrete process simulations with different electricity supply conditions. The disadvantage lies in the necessity of conducting enough simulations to cover the infinite set of potential electricity supply conditions. In addition, this approach would optimize the technical setup, and the economic and environmental dimensions are only assessed and not optimized. The second approach is optimizing renewable generation, electrolysis, DAC, and storage units with the constraint to supply electricity and feedstock steadily to the synthesis unit (Osman et al., 2020). This approach would result in an upper bound of production costs or GHG emissions, since the potential flexibility of the synthesis unit is not exploited. To overcome these challenges, all components are modeled within the MOO to cover the infinite set of renewable electricity supply and exploit the potential flexibility of the synthesis unit. The interplay between the different methods, which helps overcome the single methods' disadvantages while exploiting their advantages, is shown in Figure 3.5.

The applied methods are conducting a deterministic analysis, and parameter uncertainties from the technologies or the iRES electricity generation are not considered. These uncertainties could push the PtX system to its limits if the calculated capacities are insufficient to supply electricity and feedstock at each moment. Therefore, a robust system setup could be more suitable for realistically implementing PtX systems.

3.3 Achieving robust Power-to-X system design

Planning PtX systems while considering iRES electricity generation faces short-term volatility and long-term availability uncertainties. Stand-alone systems, where back-up electricity is unavailable, are especially threatened with unplanned shutdowns due to insufficient electricity or feedstock supply. In addition, the volatile character of iRES generation conflicts with the relatively inflexible chemical synthesis processes, and the implementation of flexible operation faces manifold challenges, for example, the complexity of implementation, safety risks, degradation of product quality, and others (Bielefeld et al., 2023). In the worst case, an insufficient supply of feedstock might result in increased degradation of the catalysts and, therefore, reduce long-term production efficiency (Bielefeld et al., 2023; Iglesias González et al., 2016), and in the context of remote stand-alone PtX facilities, the dependence on external service providers poses another obstacle (Bielefeld et al., 2023).

To decide on suitable methods to consider the uncertainty in planning and optimizing PtX systems, a closer look at the concept of uncertainty is necessary. In Hubbard (2014), uncertainty is defined as follows: "The lack of complete certainty, that is, the existence of more than one possibility. The "true" outcome/state/result/value is not known." While future outcomes might be unknown, past applications and measurements might have created information available for assessment. Based on this information, the uncertainty can be described using uncertainty sets. Robust optimization approaches apply uncertainty sets to incorporate the uncertainty into the model and to optimize the system against the worst-case realization of the uncertain parameter. With an increase in measurements and applications, the nature of the distribution of the realizations can be assessed. Initially, an ambiguity exists, since an insufficient number of historical realizations hinders the exact determination of the distribution function. In distributionally robust optimization,

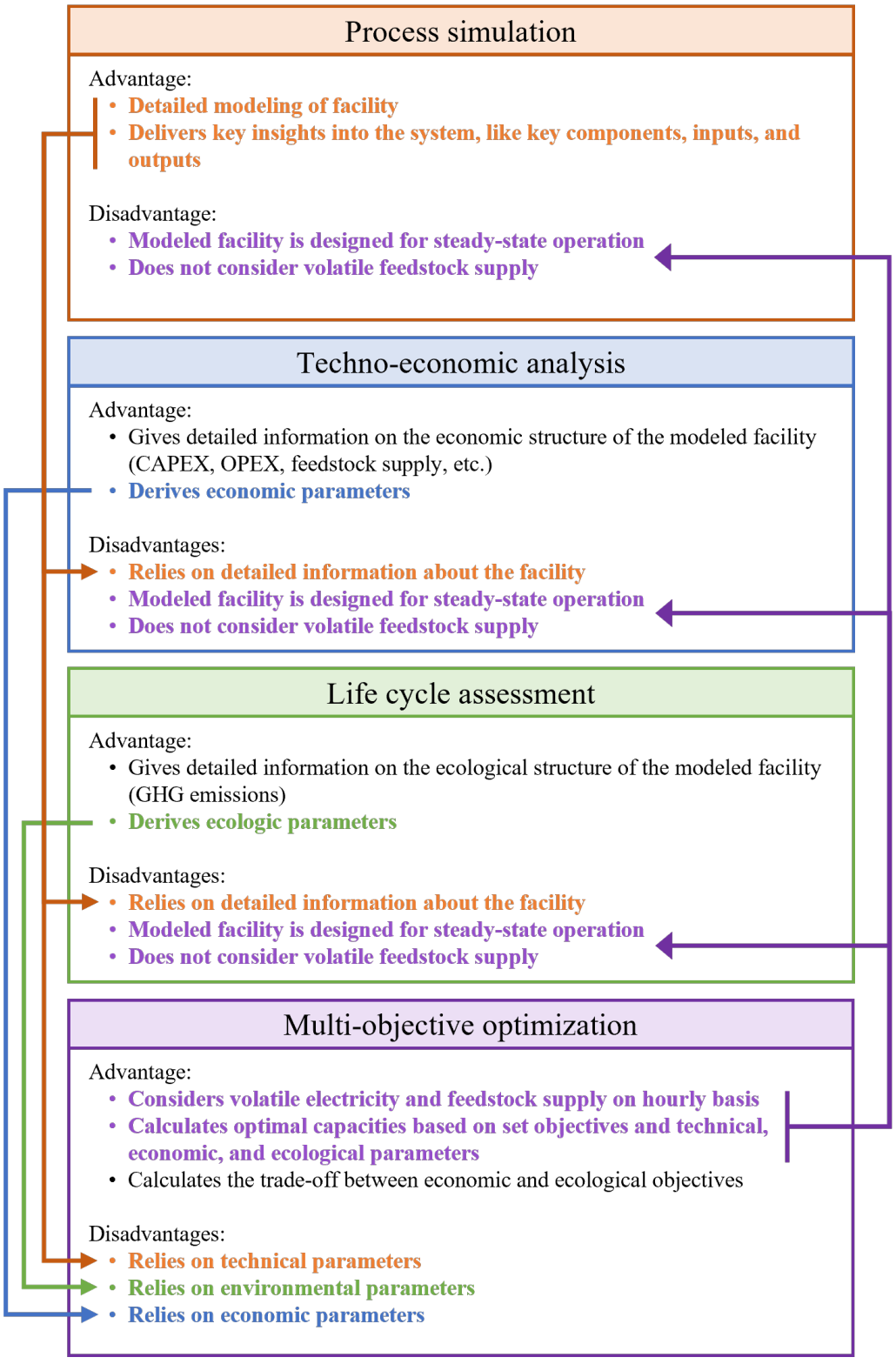

Figure 3.5: Interplay, advantages, and disadvantages of the applied methods of the multi-method approach (Langenmayr et al., 2025a).

all potential distributions are considered simultaneously by placing them in an ambiguity set and optimizing the system robustly against all possible distributions. With a further increase in realizations, the certainty of the distribution increases, and the user can apply stochastic optimization, where the derived probabilities of selected events allow the optimization of the expected value of a system affected by uncertainty.Weber et al. (2021)

PtX systems are affected by several different uncertainties when operated flexibly (Bielefeld et al., 2023; Iglesias González et al., 2016), and a selected few are classified into the categories stated in Rebennack (2016). Technology uncertainties describe uncertainties that exist due to past decisions. In the PtX context, these include the degradation of product quality and the catalyst, since the decision to use flexible operation might affect products and the catalyst at later stages. Similar accounts for the availability of the synthesis unit, where a shutdown might have been required if the feedstock supply, due to past decisions, was insufficient. Right-hand side uncertainties often represent uncertainties that arise outside of the optimized system, but do not affect the objective function. A typical example is the exogenous product demand, unaffected by the PtX system. If the products are sold on and feedstock is purchased from a global market, objective function coefficient uncertainties in the form of price uncertainties exist. These are similar to right-hand side uncertainties, but the affected parameters are only part of the objective function. Other objective function coefficient uncertainties are specific investments into equipment if insufficient information exists. Finally, recourse uncertainties describe parameter uncertainties, where the parameter itself has stochastic properties that are unaffected by past decisions or external factors. The renewable electricity generation is one example of recourse uncertainties.

The decision on which approach should be applied depends on the available data to model the considered uncertainty and the objective followed (Gorissen et al., 2015). In Paper C, only the recourse uncertainties are implemented since other uncertainties do not apply to the specific case study, or data is unavailable to model the uncertainty. For example, no global RFNBO market currently exists, and investment decisions are only taken if long-term purchase agreements are made. This approach eliminates the described right-hand side uncertainties and partially the objective function coefficient uncertainties since selling prices and demand are fixed by contracts. As a stand-alone PtX system is implemented, most feedstock is produced onsite, eliminating the feedstock price uncertainty of the most essential feedstocks. The impact of unplanned shutdowns and component degradation is difficult to quantify, since chemical systems are usually operated under steady-state conditions, and data covering these events does not exist in research literature. Hence, it is chosen to omit flexible operation outside of safe thresholds to ensure that a degradation does not occur and shutdowns are avoided. Data covering the renewable generation uncertainty is sufficiently available, and robust and stochastic modeling approaches have been used to consider the iRES electricity generation uncertainty. Therefore, the decision on which approach to use is based on the objective. The main aim of stand-alone PtX system design is reliable production at low costs, which implies the avoidance of unplanned shutdowns and component degradation. Based on this objective, a robust system design is desired, which avoids shutdowns and degradation in each scenario. Stochastic optimization achieves robust capacities against the expected value, but rare extreme scenarios might not affect capacity decisions since their probability could be low. Robust optimization calculates robust capacities based on the worst-case scenario, which is often such an extreme scenario. This circumstance leads to a decision in favor of robust optimization.

Next to the objective and the information situation, the implications of the decision have to be considered to decide on the fitting robust optimization approach. The investment into stand-alone PtX systems is complex since several components need to be dimensioned simultaneously, including renewable generators, storage units for hydrogen, CO_2, and electricity, the CO_2 supply using DAC and the hydrogen supply using electrolysis, as well as the synthesis unit itself. In addition, the dimensioning considers the interaction with the environment, for example, by considering the renewable generation profiles. The standard robust optimization approach would optimize the PtX investment against a single worst-case renewable generation scenario. However, the performance of the calculated, robust capacities against the complete data set is not assessed. New worst-case scenarios could develop, which would be particularly unfavorable for the derived robust system. Another approach would be the simultaneous consideration of all available data. However, due to increased data consideration, the complexity of this brute force approach could hinder the implementation, and the strong conservatism of the results might be undesired.

A subgroup of robust optimization is adaptive robust optimization (ARO) Bertsimas et al. (2013), which fits the desired properties since the approach uses an iterative solving process that assesses the calculated robust solution and adds only new worst-case scenarios if the robust solution does not perform within selected tolerances. In the context of investment decisions, ARO applies the following structure. In the first stage, an investment decision is taken. This is typically implemented as a minimization problem, where the investment is minimized ($\min_x c_x^\top \cdot x$) while the requirements of the system (Equations 3.8 and 3.9) have to be met. The uncertainty reveals itself (Equation 3.10) in the second stage. Here, robust optimization aims to maximize the punishment ($\max_{u \in U}$) for the initial first-stage decision taken. Finally, the system can react to the realization of the uncertainty in the third stage by operating the plant (Equations 3.11 and 3.12) in such a way that the impact of the punishment of the second stage is minimized ($\min_y c_y^\top \cdot y$). The following problem shows the closed optimization problem behind ARO. The Objective function in 3.7 and the constraints (Equations 3.8, 3.9, 3.11, and 3.12) are based on the optimization problem developed in Section 3.2.4, but the MOO is reduced to the single objective of cost minimization.

$$\min_x \quad c_x^\top \cdot x \qquad \max_{u \in U} \qquad \min_y \quad c_y^\top \cdot y \tag{3.7}$$

subject to

$$h(x) = 0 \tag{3.8}$$

$$g(x) \leq 0 \tag{3.9}$$

$$u \in U \tag{3.10}$$

$$A(x,u) \cdot y = b(x,u) \tag{3.11}$$

$$D(x,u) \cdot y \leq e(x,u) \tag{3.12}$$

This closed optimization problem is solved by separating the first stage from the second and third stage problems using decomposition, and a subsequent dualization of the third stage problem to achieve a single maximization problem as the second stage problem. The created problem comprises the first-stage problem, which minimizes the investment and calculates the robust capacities, and the second-stage problem, which reveals the

uncertainty and reacts to it. The iterative solution process (Figure 3.6) adds worst-case profiles to the first-stage problem until the second-stage cannot punish the first-stage problem's decision beyond a set stop criterion.

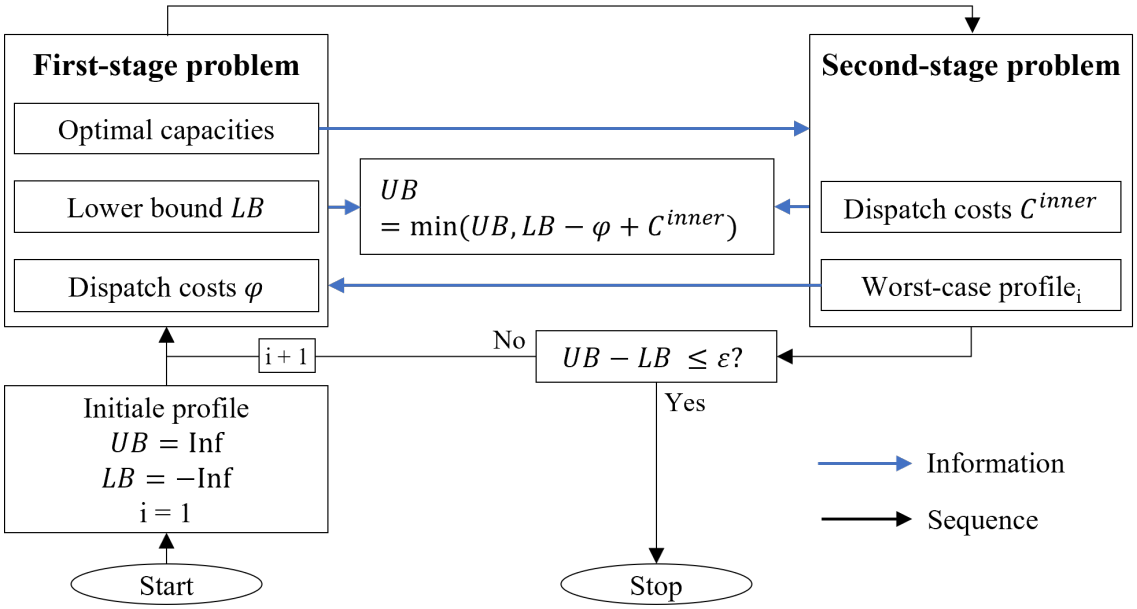

Figure 3.6: Structure of the decomposition algorithm (based on Riepin et al. (2022)). The algorithm iteratively solves the first-stage problem to calculate the optimal capacities and the second-stage problem to obtain the worst-case profile to punish the capacity decision of the current iteration. The algorithm terminates as soon as the difference between the upper bound and lower bound is below a set tolerance ε.

ARO has been improved and applied in manifold studies. Jabr (2013) used a similar framework to analyze the network expansion planning of electricity grids. Chen et al. (2014) and Ruiz and Conejo (2015) apply the column-and-constraint generation approach, developed by Zeng and Zhao (2013), to allow faster computation compared to Bender's decomposition. Mínguez and García-Bertrand (2016) improved the approach further by combining the advantageous solving of the inner problem in Jabr (2013) and the column-and-constraint generation approach in Chen et al. (2014) and Ruiz and Conejo (2015) to improve solvability further. To exploit these past improvements, the solving approach of Mínguez and García-Bertrand (2016) is applied.

Approaches focusing on strategic planning problems are primarily transmission network expansion planning problems (Baringo and Baringo, 2018; Baringo et al., 2020; Garcia-Bertrand and Minguez, 2017; García-Cerezo et al., 2023; Mahmoud et al., 2024; Riepin et al., 2022; Verastegui et al., 2019). Most of these approaches apply cardinality-constrained polyhedral uncertainty sets (Bertsimas and Sim, 2004), which use the vertexes of data in combination with budget constraints to model the underlying uncertainty. In the case of time series data, cardinality-constrained uncertainty sets have the advantage that the vertexes can be determined in advance, as they represent the minimum and maximum values of the hourly realizations of the values (Riepin et al., 2022). This uncertainty set $\mathcal{U}$ is combined with a deterministic profile to calculate a worst-case profile by deviating from

the hourly value of the deterministic profile $\bar{d}_t$ to one of the vertexes using $\hat{d}_t$ and $\check{d}_t$ and the respective decision variables $\hat{z}_t$ and $\check{z}_t$ to calculate the hourly value of the worst-case profile d_t. The total number of hourly deviations $\sum_{t\in\mathcal{T}}(\hat{z}_t + \check{z}_t)$ is limited by the budget Γ to control the conservatism of the approach.

$$\mathcal{U} = \begin{Bmatrix} d_t = \bar{d}_t + \hat{d}_t\hat{z}_t + \check{d}_t\check{z}_t, & \forall t \in \mathcal{T} \\ \hat{z}_t + \check{z}_t \leq 1, & \forall t \in \mathcal{T} \\ \sum_{t\in\mathcal{T}}(\hat{z}_t + \check{z}_t) \leq \Gamma, & \\ z_t \in [0,1], & \forall t \in \mathcal{T} \\ \hat{d}_t, \check{d}_t \in \mathbb{R}, & \forall t \in \mathcal{T} \end{Bmatrix} \tag{3.13}$$

However, the resulting profiles are difficult to interpret since the profiles might be a combination of non-related vertexes of single realizations (Velloso et al., 2020), and result, for example, in profiles with highly oscillating capacity factors that are technically infeasible. To address this challenge, scenario-based polyhedral uncertainty sets have been developed. Such uncertainty sets consider time series data not as individual realizations for each time step and combine them into a worst-case profile, but consider the whole time series as a single scenario. The scenario-based polyhedral uncertainty sets choose one vertex scenario as the worst-case scenario from all scenarios (third term). The hourly realizations equal the hourly values of the worst-case profile (first term). To control the conservatism of the approach, a minimal total capacity factor of the profile can be implemented (fourth term). This approach ensures the statistically correct representation, since the worst-case profile is chosen from historic data.

$$\mathcal{U} = \begin{Bmatrix} u_t = \sum_{p\in\mathcal{P}} \tilde{u}_{p,t} \cdot \beta_p & \forall t \in \mathcal{T} \\ \beta \in [0,1]^p & \\ \sum_{p\in\mathcal{P}} \beta_p = 1 & \\ \sum_{p\in\mathcal{P}} \sum_{t\in\mathcal{T}} \tilde{u}_{p,t} \cdot \beta_p \geq \Gamma & \end{Bmatrix} \tag{3.14}$$

This uncertainty set was first applied by Velloso et al. (2020) to a unit commitment problem. Since then, it has been used and developed in multiple studies focusing primarily on unit commitment (Jiménez et al., 2023; Lara Filho et al., 2023; Mancilla-David et al., 2020; Qu et al., 2023). One shortcoming of applying scenario-based uncertainty sets in the context of ARO is the difficult scalability of the approach. Using polyhedral uncertainty sets reduces the hourly capacity factors to the vertexes, significantly reducing the amount of considered data. In the case of scenario-based uncertainty sets, it is difficult to identify the vertex scenarios exogenously since the impact of each scenario on the system is challenging to quantify ex ante[3]. Therefore, the complete set of scenarios must be

[3] A whole research stream deals with this challenge (Abedi et al., 2019; Doss-Gollin et al., 2023)

considered to ensure that the vertexes are not ruled out. This might be less of a challenge for unit commitment problems, which are of an operational nature and have a short decision-making horizon, such as a single day or a few weeks. However, the application of scenario-based uncertainty sets on PtX investment problems, which consider long-term implications that require comprehensive data to make robust investment decisions, might be challenging. The consideration of extensive data in combination with the recursive approach of ARO impedes the straightforward, robust implementation, as real-world-sized problems become increasingly computationally expensive. To address this challenge, only parts of the time series data will be replaced by worst-case profiles to reduce the computational burden. Most time series data will be covered by deterministic representative data and their weightings, which are derived from applying k-means clustering to identify repetitive patterns in time series data. The approach implements $\mathcal{N}$ weighted clusters with deterministic representative profiles, and an additional worst-case cluster, which covers the uncertain worst-case profile. This worst-case cluster has a weighting of 1, and all other cluster weightings are adjusted to restore the overall sum of weightings. In the second-stage problem, this worst-case cluster contains all deterministic profiles, and the problem chooses the profile that punishes the investment problem of the first-stage problem the most. This worst-case profile is added to the worst-case cluster of iteration i in the first-stage problem. Figure 3.7 shows the implementation of the representative and worst-case data in the second-stage problem.

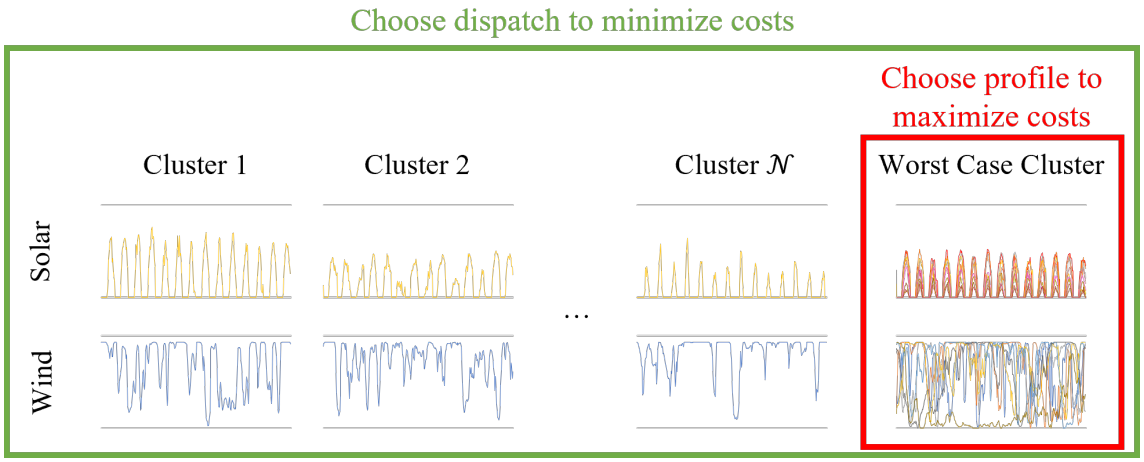

Figure 3.7: Graphical presentation of the implementation of the representative and the worst-case clusters (Langenmayr et al., 2025c). The representative clusters contain the deterministic representative profiles, while the worst-case cluster contains all historic profiles. The second-stage problem chooses the profile in the worst-case cluster, which punishes the investment decision in the first-stage problem the most.

Having designed systems that can reliably produce RFNBO under uncertainty, the next step is to consider how these products move through global supply chains, which leads this methodology chapter away from the micro perspective of the production to the macro perspective of global RFNBO transport.

3.4 Supply chain modeling

To achieve a low-cost supply, the individual properties of the RFNBO and the available transport options must be considered (Sterner et al., 2024). The low-cost transport is critical since the current production cost disadvantage of RFNBO compared to fossil energy carriers would be exacerbated if inefficient supply chains are implemented. However, optimal configuration can be complicated since each network node in the supply chain allows for different production, storage, conversion, and transport alternatives (Dagdougui, 2012). In addition, the setup of LC-H2D supply chains depends on several conditions, such as the target commodity and the available infrastructure. This complexity, combined with the global opportunity to produce RFNBO, is addressed in Paper D's conducted RFNBO supply chain study.

Research covers the topic of LC-H2D supply chains by applying three different modeling approaches. Energy system models take a whole-system scope and allow cross-sectoral optimization, but come at the cost of complex mathematical problems and necessary simplifications of the supply chain. Location-specific assessments use detailed modeling of technologies and supply chains, but are difficult to scale since case-specific assumptions are required. Supply chain models usually apply high geographical and temporal resolution data to cover large supply chain networks, but do not consider cross-sectoral effects.(Fakhreddine et al., 2025) The main result of supply chain models is the LC-H2D costs at the export terminal or the demanding location. Some research further investigates potential export quantities and the demand in the importing country to cover the supply chain fully. Parolin et al. (2022) reviewed hydrogen delivery models and categorized them based on their modeling choices. The overall objective of the model is usually the minimization of total supply or network costs. Next to this objective, objectives like minimizing the environmental impact or safety risks are followed, which are sometimes considered using MOO. In the time scale category, resolutions from snapshots to year-long time series or multi-period approaches are implemented. Geographic information system (GIS)-based data allows considering network data and other information, such as renewable capacity potential, at high spatial resolution. Approaches differ in their considered supply chain components, such as production facilities, storage units, or transport. In addition, several transport means can be implemented, including pipeline, shipping, road, or railroad transport.

The developed model in Paper D minimizes the total supply costs, including hydrogen production costs, the conversion costs of commodities, and the transport costs from the production location to the destination. To increase the computational performance, the model is separated into the preprocessing of data and the actual solving of the model (Figure 3.8), which are described in the following subsections. Here, further information is provided to categorize the model within the above-described categories.

3.4.1 Preprocessing of input data

The framework is a bottom-up model considering global data on infrastructure, hydrogen production costs, electricity generation costs, and hydrogen production potentials. Data on such a spatial resolution is typically utilized using GIS-based approaches. Global spatial weather data is processed into hourly renewable generation profiles, which are further clustered into representative weeks using k-means clustering. Using the optimization

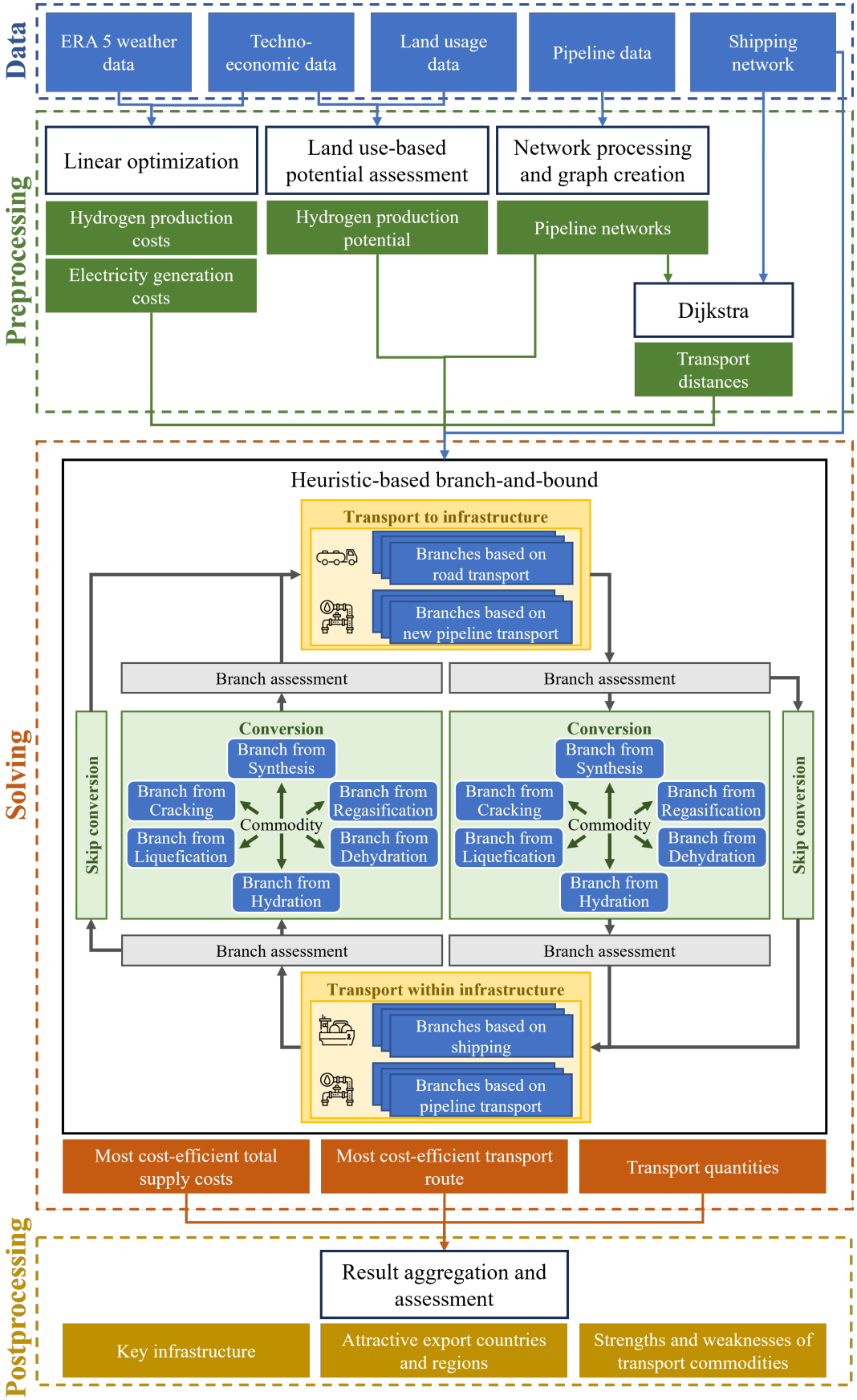

Figure 3.8: Graphical abstract of the transport modeling approach. Based on graphical abstract in Langenmayr et al. (2025b).

model described in Section 3.2, which is reduced to single-objective optimization of costs, hydrogen production and electricity generation costs are calculated for each grid cell of the covered area. The optimal capacities of each grid cell are further processed with land use and coverage data to calculate the hydrogen production potential. Origin locations can be drawn randomly based on the grid cells or created from the global grid by processing the grid cells into Voronoi cells. The oil and gas pipeline infrastructure data is prepared and processed to derive the edges and nodes of the network, which are used to create a network graph for each coherent network. A similar approach is applied to the shipping data to derive the global shipping network graph. The Dijkstra algorithm calculates the distances between the pipeline network's individual entry and exit points and between ports in the shipping network.

Considering comprehensive data on hydrogen production costs and quantities, electricity generation, and infrastructure allows a detailed assessment of the global RFNBO supply chain on high resolution. However, sophisticated solving algorithms are required to process the data without significant simplifications and aggregation.

3.4.2 Heuristic-inspired branch-and-bound solving approach

Supply chain energy system models are often implemented as closed optimization problems, which can jointly optimize the complete supply chain. However, such models are limited by their spatial scope or their spatial resolution since large-scale mixed-integer models would exceed even commercial solvers' capabilities. Two steps are conducted to handle this complexity. First, while many origin locations are possible, each is processed individually. Second, even considering only one origin location at once would result in a model where the decisions on conversion or transport build the supply chain setup and result in combinatorial binary variables. The decision on conversion or transport builds a network, where each edge is associated with either transport or conversion costs, resembling fixed charge network flow models. Instead of solving the network as a closed optimization model, an iterative approach combined with branch creation based on conversion and transport options is developed, which resembles a heuristic-inspired branch-and-bound method. The general structure of the method is the alternating option to convert a commodity and to transport a commodity. Conversion occurs at network nodes, while the transport moves the commodity along the edges. The alternating optional conversion and transport allows the endogenous calculation of the supply chain configuration. Each time a conversion or transport option is taken, a branch containing information about the current commodity, network node, and supply costs is created. Branches reaching the final destination and having the desired commodity are candidates for the most cost-efficient transport route.

The iterative processing allows the efficient utilization of parallelization and matrix calculations without exceeding computational resources. In addition, regular assessments of created branches can be conducted to prune branches early on, and this can be further used to exclude transport options before creating branches. The efficient implementation of the heuristic is the main methodological contribution of this study, since it allows solving complex, large-scale mixed-integer supply chain models on common computation infrastructure, which allows the coverage of the RFNBO supply chain beyond spatial scope and resolution of similar research in this field. At the same time, the pruning and exclusion of transport options are conducted carefully to ensure that the most cost-efficient transport route for each origin-destination combination is reached.

Pruning based on costs. The simplest approach to pruning branches is the calculation of a global upper bound, with which all branches can be compared. A feasible but not necessarily the most cost-efficient solution is calculated for each origin-destination combination. In each assessment step, all branches are compared to this upper bound and eliminated if the supply costs exceed the global upper bound. The upper bound is further updated when a branch has reached the final destination, has the desired commodity, and its total supply costs are lower than the upper bound. Next to the global upper bound, local upper bounds are implemented for each network node. The local upper bound of a network node is set as soon as a branch reaches the network node. This local upper bound is connected to the commodity of the branch, resulting in several local upper bounds for each network node. Branches reaching this network node will be compared to the local upper bound and eliminated if their supply costs exceed the local upper bound. If the supply costs are lower than the local upper bound, the local upper bound will be updated, and all branches growing out of the previous branch, which set the local upper bound, will be eliminated. Distances can be used to eliminate branches as well. Based on the direct residual distance of a branch to the final destination, the lowest possible costs to the final destination can be calculated. Together with the current supply costs of the branch at the current node, the lowest total supply costs can be approximated, and the branch can be eliminated if these costs exceed the global upper bound. A similar approach is conducted using the minimal distance to the closest network node. If the minimal costs to the closest network node, including optional conversion and transport, and the current supply costs already exceed the global upper bound, the branch can be eliminated.

Exclusion of transport options based on costs. Before even creating branches, transport options can be eliminated to avoid expensive matrix-based calculations. Branches near transport infrastructure, like pipelines and ports, are evaluated regarding their ability to use the infrastructure. For example, if the infrastructure is a gas pipeline, branches using non-gaseous commodities require conversion before using the gas infrastructure. If the lowest conversion costs to any gaseous commodity, in addition to the current supply costs of the branch, exceed the global upper bound, all gas pipelines are excluded for this branch. Similar counts for oil pipelines and shipping. Furthermore, the branch creation based on several entry points of the same infrastructure is assessed. If a branch could use several entry points of the same infrastructure in the following iteration, a preassessment of the transport to the closest entry point is conducted, and the costs of the inner-infrastructure transport to the other entry points are calculated. The costs calculated in the preassessment are compared to the costs of direct transport to the other entry points, and entry points are excluded where the direct transport costs exceed the preassessment costs. This approach follows the idea that inner-infrastructure transport is cheaper than transport between infrastructure, which typically relies on road or new pipeline transport. The exclusion of transport options is optional since branches would be eliminated based on the global and local upper bounds in the following iterations. However, removing these options early on will increase the efficiency of the matrix-based branch creation in the subsequent iteration steps since many options are not considered.

4 Overarching context and summary of papers and results

The following chapter explains the overarching connection between the different publications, followed by the introduction and summary of the four papers on which this dissertation is based. For each paper, the context of the paper is given, followed by the scientific contribution, the results, and the discussion. The papers can be found in Part II of this dissertation.

The common topic of all publications is PtX processes. However, each publication investigates different aspects of this overarching topic. Paper A analyzes the production of PtX aviation fuel in the German power system with a strong focus on the regulatory framework of producing such fuels. In addition to the PtX production within interconnected energy systems, stand-alone PtX systems are an option to produce PtX products in accordance with the regulatory framework. Paper B follows this approach, in contrast to Paper A, and conducts a multi-objective optimization to derive the trade-off between production costs and GHG emissions of different PtX products. Again, looking at stand-alone PtX systems, Paper C extends the approach of Paper B by considering the uncertainties of solar PV and wind electricity generation to calculate robust capacities of stand-alone PtX systems. Finally, Paper D focuses on the transportation of PtX products instead of the production, and derives the most cost-efficient transport routes from globally distributed export locations to chosen destinations. In this approach, the results of Paper B are used to set the initial hydrogen costs in the different export locations. Figure 4.1 shows an overview of the different papers and their connection.

4.1 Paper A: Renewable origin, additionality, temporal and geographical correlation – eFuels production in Germany under the RED II regime

Paper A with the title *Renewable origin, additionality, temporal and geographical correlation – eFuels production in Germany under the RED II regime* was published in the journal *Energy Policy* in 2023 and was co-authored with Manuel Ruppert (methodology, writing, revision). The full study can be found in Section A.

4.1.1 Motivation and objective

The idea of this paper developed with the ongoing legislative procedure of the REDII regulation on the production of eFuels. This process included several drafts and revisions of REDII. It took more than four years, leading to long-lasting regulatory uncertainty for producers and consumers of eFuels. This process was accompanied by studies and statements from industry and stakeholder groups to calculate the impact of the different

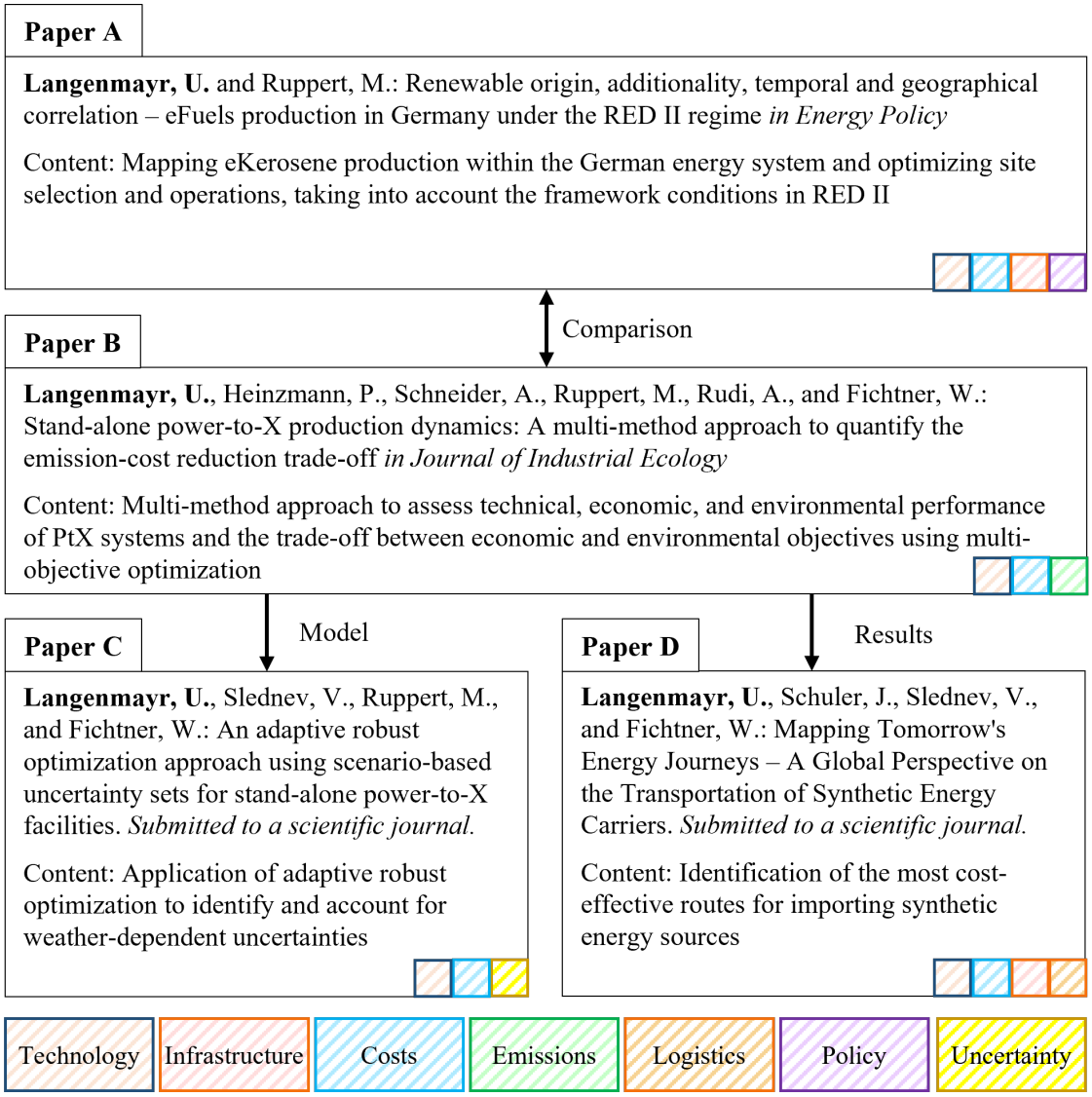

Figure 4.1: Overview of the dissertation.

electricity purchase conditions on total production costs, primarily based on the producer's point of view.

The objective of Paper A is twofold: First, the impact of the PtX production on the energy system is analyzed. These results contain the optimal placement of the PtX systems and show the necessary renewable expansion to cover the electricity demand of the electrolysis units. Second, the impact on the PtX system is assessed. This aspect includes the optimal capacities and operational parameters of the electrolysis units, which are especially interesting for eFuels producers since they can assess the profitability of their investments based on these framework conditions. Next to electricity, CO_2 point sources and DAC are implemented, which allow further analysis on utilized CO_2.

4.1.2 Methodology

Paper A applied the open source energy system framework PyPSA-EUR, which uses the PyPSA energy system model and applies European data to provide a ready European energy system. The provided data for this framework includes the European electricity network, the electricity demand, conventional and renewable generators, and pump-storage plants. The first adjustment of this model was the restriction of the spatial scope to the German energy system. Second, only the power system is considered, excluding other sectors such as mobility, industry, or heating. They are regarded within the electricity demand. Afterward, the German *Marktstammdatenregister* was used to allocate renewable generator capacities to the network transmission nodes. A myopic approach has been applied to model the development of the power system. Here, the projected years 2022, 2025, and 2030 were implemented, and the development of electricity demand and iRES targets were adjusted for each projected year. In addition, the decommission of components beyond their lifetime, the nuclear phaseout, and the coal phaseout have been modeled. REDII-admitted CO_2 point sources were added and aggregated to the nodal level of the power system. Since the aim is to investigate the impact of the REDII electricity purchase conditions, constraints were implemented to represent these different conditions, and different scenarios are calculated with these constraints active or inactive.

4.1.3 Key findings

Results show that applying REDII conditions increases electrolysis capacity requirements by 9% in 2025 and 16% in 2030, while average utilization decreases by about 700 hours annually due to stricter temporal matching between renewable generation and electrolysis operation. Renewable generator capacities, particularly solar PV, rise slightly to diversify the electricity supply, while onshore wind contributions decline. Electrolysis units concentrate in coastal regions with high renewable potential, shifting the determining factor for siting from CO_2 availability to renewable resource accessibility. CO_2 abatement costs increase by 14.3%, from 429 to 491 € per ton, mainly due to higher investments in renewable generation, hydrogen storage, and CO_2 capture systems.

While REDII constraints raise system costs and reduce utilization efficiency, their overall impact on the German power system remains moderate. Electrolysis flexibility helps integrate renewable generators and reduce curtailment. Policy-wise, early subsidies and co-location with renewable sources may enhance feasibility, and stand-alone systems in regions with higher renewable capacity factors could offer lower-cost decarbonization pathways.

4.2 Paper B: Stand-alone power-to-X production dynamics: A multi-method approach to quantify the emission-cost reduction trade-off

Paper B with the title *Stand-alone power-to-X production dynamics: A multi-method approach to quantify the emission-cost reduction trade-off* was published in the *Journal of Industrial Ecology* in 2025. The author is the lead author of the paper and was co-authored with Paul Heinzmann (process simulation, writing, revision), Alexander Schneider (LCA, writing, revision), Manuel Ruppert (methodology, writing, revision), Andreas

Rudi (methodology, writing, revision), and Wolf Fichtner (writing, revision). The full study can be found in Section B.

4.2.1 Motivation and objective

The paper was developed since the results of Paper A showed that the production of RFNBO within energy systems can be very constraining. In contrast, stand-alone PtX systems could exploit favorable locations regarding low-cost renewable electricity generation and renewable capacity potential.

When planning stand-alone PtX systems, the individual characteristics of locations regarding solar PV and wind generation capacity factors need to be considered. In addition, investors might have several objectives, with minimal production costs or minimal GHG emissions being the most popular ones. Production costs are significant since they decide on the potential commercialization of the eFuels. At the same time, the GHG emissions play an important role since the additional costs of eFuels in comparison to their conventional counterparts are only justified if sufficient GHG can be avoided using eFuels instead of conventional energy carriers. Considering the GHG emission is further necessary to produce in accordance with the REDII regulatory framework.

Paper B developed a multi-method approach to assess the trade-off between production costs and GHG emissions of various eFuels, while considering the individual location characteristics regarding solar PV and wind generation capacity factors. The multi-method approach ensured that a comprehensive, consistent, and transparent database was applied.

4.2.2 Methodology

The methodology is a multi-method approach consisting of five different steps. The first step consists of a process simulation of the FT and methanol processes and derives key technical parameters. Based on these parameters, a techno-economic assessment is conducted to derive the economic parameters. In addition, the technical data are used in a LCA to assess the system regarding GHG emissions. To consider the local iRES conditions, weather profiles of more than 238,427 global locations are generated using the open source tool atlite (Hofmann et al., 2021) and ERA 5 data (Hersbach et al., 2020) and clustered into representative profiles using k-means clustering. The technical, economic, and ecological parameters are applied in the optimization steps. The first optimization is a single-objective optimization of the hydrogen production, minimizing either production costs or GHG emissions of all 238,427 locations. The second optimization applied the ε-constraint MOO, which investigates five production locations (Chile, Saudi Arabia, Kazakhstan, Australia, and Germany) in detail, and optimizes capacities and operations of all components to minimize the production costs and GHG emissions simultaneously, which derives the location and technology-specific trade-offs. Figure 4.2 shows all applied methods and their interaction.

4.2.3 Key findings

The study finds that the environmental and economic performance of PtX systems highly depends on the renewable energy mix and the flexibility of the underlying technologies.

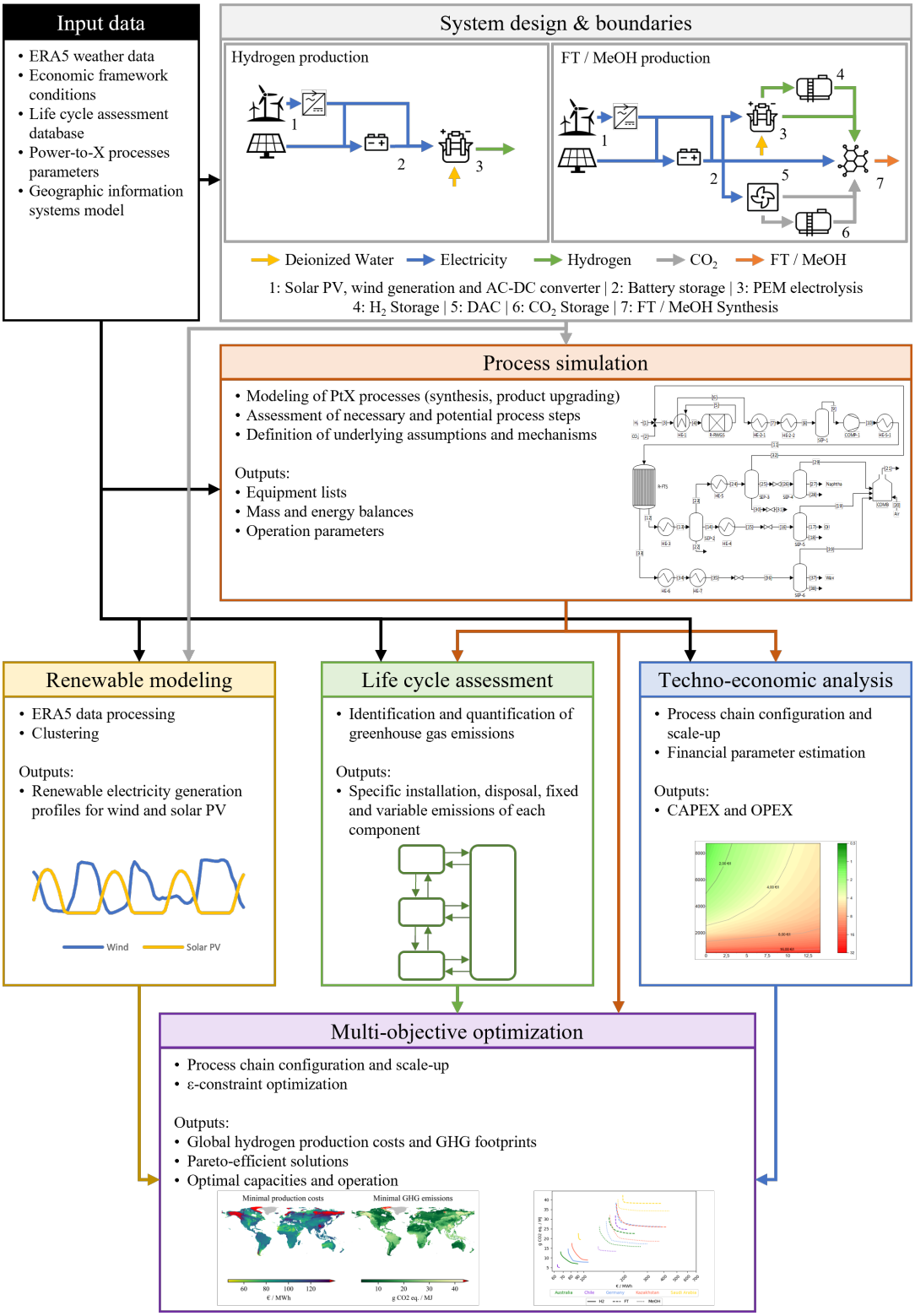

Figure 4.2: Geographical abstract of the multi-method approach modeling the hydrogen, FT, and methanol production (Langenmayr et al., 2025a).

Locations with strong wind resources, such as southern Chile, achieve the most favorable results, combining low production costs with minimal greenhouse gas emissions. Wind power's higher capacity factors and lower GHG emissions per installed capacity make it superior to solar PV, whose manufacturing remains emission-intensive. In contrast, solar-dominated regions, such as Saudi Arabia, exhibit significantly higher emissions and require additional wind capacity or battery storage investment to approach comparable environmental outcomes. Areas with balanced wind and solar conditions, such as Australia, Germany, and Kazakhstan, offer trade-offs by combining diversified renewable electricity generation and moderate storage needs.

Hydrogen production performs best among the examined PtX pathways because it involves fewer intermediate processing steps and no additional carbon feedstock. While technically viable, methanol and FT synthesis are more expensive and emission-intensive due to lower process flexibility and higher capital investment in synthesis and storage units. The MOO shows that achieving further emission reductions causes production costs to rise steeply beyond a certain threshold, underlining a clear emission–cost trade-off. Flexible operation of PtX systems mitigates this trade-off by reducing reliance on auxiliary components and enabling better adaptation to variable renewable power supply.

Overall, the discussion emphasizes that PtX investments should be guided by geographical and technological considerations. Wind-rich regions provide the most sustainable prospects for large-scale PtX deployment, while mixed renewable portfolios can yield near-optimal balances between environmental and economic performance. The findings confirm that single-method assessments underestimate these interdependencies and that integrating technological, economic, and environmental data within a dynamic optimization framework enables robust decision support for future PtX system planning.

4.3 Paper C: An adaptive robust optimization approach using scenario-based uncertainty sets for stand-alone power-to-X facilities

Paper C is titled *An adaptive robust optimization approach using scenario-based uncertainty sets for stand-alone power-to-X facilities* and was submitted to a scientific journal in 2025. The author is the main author and was supported by Viktor Slednev (methodology, writing, revision), Manuel Ruppert (methodology, writing, revision), and Wolf Fichtner (writing, revision). The full study can be found in Section C.

4.3.1 Motivation and objective

The deterministic model in Paper B allows the assessment of PtX systems based on techno-economic-ecological data and location-specific iRES profiles. However, since the MOO model uses a deterministic approach, uncertainties from iRES electricity generation are not considered. Paper C applies the model of Paper B and adjusts it to consider uncertainty to achieve robust capacities of PtX systems. A robust system setup is required since the synthesis process is sensitive to process parameters like feedstock supply, temperature, or pressure, and even minor changes could affect the products or damage the equipment. Therefore, chemical plants in the process chain of PtX processes face new challenges since the iRES electricity generation might be insufficient to supply the chemical plants steadily.

To ensure the supply of the chemical plant within the PtX processes, robust capacities of electricity generation and storage units are necessary.

4.3.2 Methodology

Paper C applies ARO in combination with scenario-based uncertainty sets and representative data. ARO derives robust capacities by iteratively identifying worst-case capacity factor profiles until the capacities are sufficiently robust to supply electricity and feedstock to the inflexible synthesis units steadily. Scenario-based uncertainty sets are applied to achieve realistic worst-case capacity factor profiles. These draw the capacity factor profiles from the historical set of all capacity factor profiles, which reflects the worst case regarding the optimized capacities of the current iteration. Since all capacity factor profiles are considered in this uncertainty set, the optimization problem is computationally complex. To address this challenge, representative periods are applied, so that the optimization draws only capacity factor profiles with the length of the representative period. The approach is tested with different representative period lengths to assess the impact of the length on computation time and quality of the robust solution.

The developed approach is applied to producing hydrogen, FT crude, and methanol. The syntheses behind these eFuels have different flexibilities, which allow the impact assessment of flexibility on the approach and results. In addition, the exact locations in Paper B (in Chile, Saudi Arabia, Kazakhstan, Australia, and Germany) are considered to assess the impact of different renewable electricity generation conditions on the robust solution. Representative period lengths from 1 to 14 days are evaluated to showcase which period length is required for each synthesis and its flexibility to achieve a robust solution. These results are compared to the approach using complete yearly capacity factor profiles.

4.3.3 Key findings

The ARO model effectively improved the reliability and profitability of stand-alone PtX facilities under uncertain renewable energy generation. Results showed that robust designs required only moderate additional investments, typically 0.5–15% for flexible systems such as hydrogen or methanol production, but up to 40% for less flexible systems like FT synthesis. Locations dominated by solar PV (e.g., Saudi Arabia) achieved robustness with minor capacity increases, since solar PV is a reliable electricity generation technology in such regions. At the same time, wind-dominated sites (e.g., Chile) required larger solar PV and storage investments to manage long-term variability.

The analysis highlighted that system flexibility strongly influences robustness: flexible systems could adapt to fluctuating renewable supply with limited cost increases, whereas inflexible systems needed additional generation and storage capacities to avoid costly feedstock shortages. Robust configurations consistently outperformed deterministic ones in stability and profit consistency by minimizing penalty electricity purchases and ensuring steady operation during adverse weather periods.

Furthermore, using representative data through temporal clustering significantly reduced computational effort without compromising robustness. Representative datasets of about two weeks provided solutions comparable to complete historical data, demonstrating the approach's computational efficiency. Overall, the ARO framework offers a practical and

scalable method for designing cost-effective, robust PtX investments across varying renewable resource conditions.

4.4 Paper D: Mapping Tomorrow's Energy Journeys – A Global Perspective on the Transport of Synthetic Energy Carriers

While Papers A, B, and C concentrate on producing eFuels, Paper D examines the transport. This paper was developed and written by the author, supported by the co-authors Julia Schuler (data research, writing, revision), Viktor Slednev (methodology, writing, revision), and Wolf Fichtner (writing, revision). It is titled *Mapping Tomorrow's Energy Journeys – A Global Perspective on the Transport of Synthetic Energy Carriers* and was submitted to a scientific journal in 2025. The full study can be found in Section D.

4.4.1 Motivation and objective

Stand-alone production of eFuels allows the exploitation of locations with excellent renewable energy conditions regarding capacity factors and land availability, enabling low-cost production in large quantities. However, such locations have often not been exploited for electricity generation since the technical constraints and the costs of large-scale electricity transmission hindered this. Compared to electricity, many energy carriers are suitable for long-distance transportation since their transport losses are minimal and their volumetric and gravimetric energy density is high. The objective of Paper D is to assess the global eFuels supply chain to draw strategic implications, comprising the identification of key transport infrastructure based on transport routes and quantities, attractive export countries and regions based on total supply costs, and the decision on produced and transported commodities based on costs and available transport infrastructure.

4.4.2 Methodology

The framework is a bottom-up model considering global data on infrastructure, hydrogen production costs, electricity generation costs, and hydrogen production potentials. To calculate hydrogen production and electricity generation costs, data and model of Paper B are applied (Section 4.2). The optimal capacities of each grid cell are further processed with land use and coverage data to calculate the hydrogen production potential (Slednev et al., 2018; Slednev, 2024). Origin locations can be drawn randomly based on the grid cells or created from the global grid by processing the grid cells into Voronoi cells.

Pipeline infrastructure data is obtained from the Global Energy Monitor (Global Energy Monitor, 2025a,b), which covers global oil and gas pipeline projects and their status. The infrastructure data is prepared and processed to derive the edges and nodes of the network, which are used to create a graph for each coherent network. A similar approach has been developed in genthalili (2022), which processes shipping data (Eurostat, 2021) to a global network graph. The Dijkstra algorithm calculates the distances between the pipeline network's individual entry and exit points and between ports in the shipping network.

The data is applied in the developed heuristic-inspired branch-and-bound algorithm, which allows efficient calculation of the most cost-efficient total supply costs and the respective route. The model uses a combination of matrix-based calculations and efficient pruning to solve the routing problem, which allows the application of high-resolution spatial

data, while considering seven eFuels and three transport means. Since large matrices are avoided, parallelization is applied to simultaneously process the 10,735 globally distributed locations.

4.4.3 Key findings

The study finds that access to existing transport infrastructure, primarily pipelines and ports, is the key determinant of low-cost supply for eFuels. Even though Europe has relatively high renewable production costs, its extensive gas pipeline network and port facilities make it competitive by minimizing the need for costly conversions and long-distance road transport. In contrast, remote regions without such infrastructure face higher costs due to additional processing and transport requirements. Retrofitting existing natural gas pipelines for hydrogen transport substantially reduces supply costs, particularly across Europe, North Africa, and Central Asia. When retrofitting is impossible, the trade shifts toward hydrogen derivatives such as ammonia and methanol, which are easier to transport but add conversion expenses. Ammonia is generally the most cost-effective carrier for maritime trade because of its low synthesis and shipping costs, while methanol is preferred for long inland routes. Methane and FT crude occupy narrower niches tied to existing gas or oil pipelines. The results also show that infrastructure availability strongly influences which regions can emerge as major exporters. Countries with direct or easily adaptable pipeline links to demand centers, such as Algeria, offer the lowest supply costs. Distant exporters like Australia and Patagonia remain viable mainly for shipping, where port access outweighs distance.

The study underscores that expanding and retrofitting global energy transport infrastructure will be crucial for an efficient hydrogen economy. Policies enabling hydrogen-ready pipelines, port retrofits for ammonia and methanol, and cross-regional connectivity can significantly lower global energy transport costs and foster new trade routes. Despite uncertainties in technology readiness and cost assumptions, the analysis provides a clear global picture: more than geography or production cost, infrastructure readiness will determine the competitiveness of future synthetic energy trade.

5 Critical reflection

The developed models, methods, and approaches in this thesis can only simulate real conditions, and the drawn results and conclusions must be understood with this circumstance in mind. Limitations comprise simplifications and trade-offs based on incomplete information and necessary modeling choices, and are discussed within this critical reflection chapter. However, each limitation discussed is complemented by potential developments in future research. This chapter will only give a broad overview, and comprehensive discussions are presented in the individual publications.

5.1 The trade-off between considered data and research scope

Quantitative models require sufficient data to allow a realistic representation of the modeled system. High-resolution temporal and spatial data allow the detailed assessment of operation and local properties necessary to make well-founded decisions. In addition, information on other sectors and markets could enrich the models by enabling the analysis of interdependencies. This accounts for all developed models within this thesis. However, significant simplifications are used to reduce computational expenses, especially in the case of the large-scale models of Papers A, C, and D.

Energy systems are usually implemented as partial equilibrium models (Section 3.1), which could be extended by modeling the interaction with other, non-energy related sectors, dependencies, or markets. In addition, technical, economic, social, and environmental dimensions could be extended (Hoffmann et al., 2024). In Paper A, only the power system is assessed, and the spatial scope is limited to Germany. This approach could be improved by extending the spatial scope and including other sectors such as heating, industry, or mobility. Notably, the hydrogen infrastructure could support the ramp-up of the eFuels production. The models developed in Paper B take a two-fold approach. The process simulation and the TEA and LCA, which were conducted based on the process simulation results, focus on the technical details, while the operation is modeled as steady-state. Modeling and optimizing the non-linear processes within the components while maintaining a high temporal resolution and a long planning horizon, required in strategic investment decisions, would result in significant computational expenses. The opposite applies to the case of the MOO. The technical processes are simplified to ramp up abilities, minimal load capability, and mass and energy balances. This simplification allows the application of the high-resolution temporal data and a long planning horizon to derive suitable PtX plant capacities, but leaves out the technical modeling. While containing high spatial resolution data, temporal resolution is reduced to a single snapshot in the heuristic-inspired branch-and-bound solving algorithm of Paper D. This approach is suitable since it aims to identify suitable transport routes and does not aim to model the exact operation of the supply chain. However, time-dependent steps in the supply chain, such as storage at logistics hubs or seasonality of demand, are not considered. These could be included

to improve the quality of the results and consider scarce storage and transport capacities during high-demand periods. The supply chain could be extended to cover eFuels and final commodities such as steel or fertilizer to see if importing such final products would be more cost-efficient than inland production (Parolin et al., 2022). Even though a high spatial resolution is implemented, the infrastructure could be assessed in more detail, including detailed planning of pipeline routing and retrofitting other infrastructure elements, such as terminals or logistics hubs (Fakhreddine et al., 2025).

Another approach to improve computation efficiency is the application of representative periods instead of complete yearly capacity factor profiles, which is conducted in all four publications. A significant share of information is lost when applying representative periods, which particularly affects the modeling of long-term storage demand (Scott et al., 2019; Teichgraeber and Brandt, 2019), which is essential in the power system analysis of Paper A. Different period lengths could be assessed to assess the impact of representative periods, such as in Paper C (Section 4.3), or different clustering methods compared (Scott et al., 2019).

5.2 Parameter uncertainty

Several parameter uncertainties exist in the developed models, which can be categorized as described in Rebennack (2016). Objective function coefficient uncertainties comprise specific equipment investment and operational costs, such as prices and revenues. Specific investments are subject to uncertainties since the key technologies, such as electrolysis and DAC, are still in development and large-scale production capacities are only starting to emerge. Sensitivity analyses and scenarios could help assess this uncertainty, but they are only addressed briefly in Paper B regarding electrolysis investment. The other publications in this thesis do not address this type of uncertainty, since this assessment is out of scope due to different scenarios and assessments being prioritized.

Recourse uncertainties are addressed in Paper C, where the uncertainties from iRES electricity generation are considered in the robust optimization. Even though this model was developed, it is not applied in Paper B, since the MOO is incompatible with the ARO, or in Paper D, since many locations are considered. iRES electricity generation uncertainties are also not considered in Paper A, as the impact of the REDII electricity purchase conditions would be challenging to assess when electricity generation uncertainties would affect the PtX system at the same time. Other recourse uncertainties, such as efficiencies, could be interesting to assess since technologies are still in development and their future performance is uncertain.

Right-hand side uncertainties, such as demand uncertainties, are not considered, which would affect the electricity demand in Paper A or the RFNBO demand in Papers B and C. Finally, technology uncertainties exist when past decisions affect the current range of actions. These uncertainties are omitted since sufficient data to model them are unavailable, such as the degradation, start-up times, and start-up costs of equipment.

In general, uncertainties are often neglected in energy system models, since their consideration would significantly increase complexity. However, approaches such as Monte Carlo simulations, stochastic programming, and robust optimization enable their consideration (Fodstad et al., 2022).

5.3 Soft-linking of the models to exploit synergies

The developed models all have limitations regarding their scope. The energy system model in Paper A considers the German power system and the kerosene production within this geographical scope. A broader scope concerning modeled eFuels, considered sectors, and geographical scope could result in insights on transforming the whole energy system. Paper B and C model individual stand-alone PtX systems, optimally dimensioning and operating the systems with a sole electricity supply from wind and solar PV. These models do not consider macroeconomic dimensions such as global demand, infrastructure, or market dynamics. The supply model in Paper D solves the problem for each location individually, and the insights need to be derived from post-processing of all solutions. This limits the model's ability to derive system-wide insights since demand, transport capacity limitations, and potential interactions between different supply chains are not considered.

These approaches would fit a potential soft-linking approach as suggested in Fakhreddine et al. (2025). The supply chain model is linked to the deterministic stand-alone PtX model by providing costs for hydrogen production and electricity generation. To avoid costly calculations, energy system models could also apply these hydrogen production and electricity generation costs as exogenous inputs instead of endogenous options. In addition, the supply cost curve could be derived from the supply chain model for each shipping or pipeline terminal to represent global imports in energy system models realistically. Finally, the impact of trading barriers, including non-technical uncertainties, could be assessed.

5.4 The social dimension of power-to-X

The United Nations Organization has defined 17 Sustainable Development Goals, with two affecting the production of eFuels. For example, providing clean water might conflict with the water demand of electrolysis units. Water sources, such as groundwater or surface water, could be at risk if additional water consumption stresses the already stressed region's water supply. This circumstance could be worsened by climate change. Therefore, such critical local properties must be taken into account in assessments. Another Sustainable Development Goal is affordable and clean energy. PtX could enable the production of low-cost and low-carbon energy carriers in remote places, potentially providing cheap and clean energy. However, production at locations with beneficial renewable electricity generation potentials and subsequent transportation to countries with LC-H2D demand is currently the focus of discussions. In addition, countries with favorable PtX locations often still rely on conventional energy carriers themselves, sparking a discussion on exploiting the best locations to produce eFuels instead of using them to generate electricity to meet local demand. These circumstances must be considered when making modeling choices.(Boretti, 2025; Kalt and Tunn, 2022) This challenge can be addressed by including the energy system of the exporting country in the assessment to consider the local electricity and LC-H2D demand, or by modeling solely the energy system of the exporting country to identify which renewable capacity potentials are required within the country.

6 Summary, conclusion and outlook

Replacing conventional energy carriers with renewable energy to generate electricity is the primary approach to reducing greenhouse gas emissions and mitigating anthropogenic climate change. However, electricity cannot replace all applications in our energy system. High-temperature heat demand, the material application of energy carriers, or the hard-to-abate applications, such as aviation, reveal the technical and economic limitations of electrification. Hydrogen and its derivatives are potential candidates for overcoming the limitations of electrification. In the so-called power-to-X process, the electrolysis unit splits water into its constituent elements, hydrogen and oxygen, using electrical voltage. The hydrogen could further be used in synthesis processes to produce hydrogen derivatives, such as Fischer-Tropsch crude, methanol, or ammonia. Combined with renewable electricity, preferably produced at favorable locations with potentially low electricity generation costs and high capacity potentials for renewable installations, the produced hydrogen and synthesized hydrogen derivatives could replace conventional energy carriers with low-carbon alternatives. However, significant barriers exist that hinder the rapid upscale of the hydrogen economy. These include complex regulatory policies, the challenging integration of volatile renewable electricity generation into inflexible synthesis processes, and uncertainties in transporting the hydrogen and its derivatives. This thesis addresses these barriers using quantitative models that assess the technical, economic, and environmental dimensions of hydrogen production and supply, as well as its derivatives.

The first contribution of this thesis is the impact assessment of the electricity supply conditions formulated in the Renewable Energy Directive II on the renewable, electricity-based kerosene production within the German power system. The four electricity supply conditions, namely additionality, renewable origin, temporal correlation, and geographical correlation, are implemented as constraints to comply with the regulations. The German power system is modeled with the geographical resolution of the electricity transmission network, using the busbars as nodes. Compared to other research, this approach ensures that the electrolysis operation has a strict temporal correlation to the renewable generation instead of a diversified renewable generation portfolio, which occurs when aggregating the transmission network. In addition, kerosene is considered the final product, which adds additional complexity due to the inflexible synthesis system. High-resolution CO_2 data was included to exploit existing CO_2 sources. The approach assesses the impact of the electricity supply conditions on producing renewable, electricity-based kerosene, including optimal location, capacity dimensions, operation, and the effect on the energy system itself.

Energy system studies state that a large share of hydrogen and hydrogen derivatives might be imported due to the limited space availability in industrialized countries like Germany. Therefore, global locations with favorable production conditions, such as sufficient renewable capacity potential and low-cost renewable electricity generation costs, could be exploited. The second contribution of this thesis consists of a multi-method approach to

model and assess stand-alone power-to-X facilities. In the first step, the technical setups of the synthesis plants are modeled and optimized to derive capacities, mass and energy balances, and utility demands. This data is applied in a techno-economic assessment to derive CAPEX and OPEX of the different system components. In addition, the technical setups are used in life cycle assessments to derive the specific greenhouse gas emissions of the facility. In the fourth step, the technical, economic, and environmental data are applied in a multi-objective optimization, which optimizes the design and operation of the power-to-X facility regarding economic and environmental objectives simultaneously. This mixed-integer linear program includes the hourly renewable electricity generation profiles of wind and solar photovoltaic of five globally-distributed locations to assess the trade-off in the form of Pareto fronts between the different objectives and the impact of the various renewable electricity generation conditions. Compared to other research, this approach derives consistent and comprehensive technical, economic, and environmental data while developing a decision-support tool that allows stakeholders, such as technology developers, investors, and policy makers, to make well-founded decisions on production costs, carbon intensity, and required capacities.

The stand-alone power-to-X model used a deterministic approach to assess the system. However, stand-alone systems could be at risk of insufficient supply of renewable electricity and feedstocks, since a backup electricity supply might not exist. Therefore, the deterministic model is developed to consider the renewable electricity generation uncertainty from solar photovoltaic and wind generators to achieve robust capacities, which can supply sufficient electricity to the system for each weather condition. The model applies the adaptive robust optimization approach, identifying worst-case weather patterns and calculating robust capacities to address these worst cases. Scenario-based uncertainty sets were used to ensure the consideration of realistic worst-case weather patterns. However, this uncertainty set type comes at the cost of considering all yearly historical weather profiles, making the approach computationally complex. To address this challenge, representative data are applied, and only two-weekly profiles are included in the uncertainty set. The results show that the developed robust capacities perform significantly better than deterministic profiles. The target product quantity is achieved for all technologies, including hydrogen, Fischer-Tropsch crude, and methanol, and robust revenues are achieved. In addition, applying representative profiles significantly reduces calculation time while containing a robust solution.

The thesis's last contribution moves away from producing renewable hydrogen and hydrogen derivatives and models their global supply chain. Low-cost power-to-X products from remote, stand-alone production locations can only be supplied if an efficient supply chain is implemented, which avoids unnecessary commodity conversions and inefficient transport routes. The developed heuristic-inspired branch-and-bound solution algorithm efficiently calculates the most cost-efficient transport and conversion of seven different commodities, while containing a high spatial resolution of production and infrastructure data, being applicable globally, and considering three means of transport. Containing high-resolution spatial data while keeping several commodity and transport mean options differentiates this approach from similar research, which usually applies significant simplifications and infrastructure aggregation to achieve efficient calculation. The results show that, from the European perspective, the European gas pipeline infrastructure is a considerable asset if retrofitting to hydrogen-ready infrastructure is conducted. The connection to neighboring regions such as Northern Africa, the Middle East, and Central Asia allows for

a low-cost hydrogen supply and high quantities. If shipping is required, ammonia and methanol are key commodities, imported from countries and regions such as the Americas and Australia.

One additional remark on the publications is the open science approach. Each approach is either based on an open source model (Paper A) or is published as an open source model (Papers B, C, and D), and is entirely based on open data. For general accessibility, each publication is open access.

Even though the presented approaches contribute significant insights and method developments, further analysis is needed. The power system analysis in Paper A could be geographically extended to cover the complete European energy system, implement hydrogen-demanding sectors, such as industry, heating, and mobility, and the production of further electricity-based hydrogen and hydrogen derivatives, next to kerosene. Papers B and C could cover additional hydrogen derivatives, such as ammonia and synthetic natural gas. Furthermore, the detailed assessment of production locations could consider additional data such as water availability, political stability, and transport infrastructure. Time-dependent information, such as storage operation, seasonal demand, and infrastructure capacity availability, could be considered in Paper D, and final products, like green steel and fertilizer, could be added to the choice of transported commodities. All papers could extend the consideration of uncertainties, which are currently only considered in Paper C. Finally, the synergies between the different models could be exploited by more closely linking methods and results.

7 References

Aakko-Saksa, P. T., Cook, C., Kiviaho, J., and Repo, T. Liquid organic hydrogen carriers for transportation and storing of renewable energy – Review and discussion. *Journal of Power Sources*, 396:803–823, Aug. 2018. ISSN 03787753. doi:10.1016/j.jpowsour.2018.04.011. URL https://linkinghub.elsevier.com/retrieve/pii/S0378775318303483.

Abedi, A., Gaudard, L., and Romerio, F. Review of major approaches to analyze vulnerability in power system. *Reliability Engineering & System Safety*, 183:153–172, Mar. 2019. ISSN 09518320. doi:10.1016/j.ress.2018.11.019. URL https://linkinghub.elsevier.com/retrieve/pii/S0951832018303041.

Abraham, E. J., Linke, P., Al-Rawashdeh, M., Rousseau, J., Burton, G., and Al-Mohannadi, D. M. Large-scale shipping of low-carbon fuels and carbon dioxide towards decarbonized energy systems: Perspectives and challenges. *International Journal of Hydrogen Energy*, 63:217–230, Apr. 2024. ISSN 03603199. doi:10.1016/j.ijhydene.2024.03.140. URL https://linkinghub.elsevier.com/retrieve/pii/S0360319924009728.

AG Energiebilanzen e.V. Auswertungstabellen zur Energiebilanz 1990 bis 2023, Mar. 2025a. URL https://ag-energiebilanzen.de/wp-content/uploads/2025/03/EBD23e_Auswertungstabellen_deutsch.xlsx.

AG Energiebilanzen e.V. Primärenergieverbrauch Jahr 2024, Mar. 2025b. URL https://ag-energiebilanzen.de/wp-content/uploads/2024/12/PEV4Q_aktualisiert.xlsx.

Agora Industry. Chemie im Wandel - Die drei Grundpfeiler für die Transformation chemischer Wertschöpfungsketten, 2023. URL https://www.agora-industrie.de/fileadmin/Projekte/2022/2022-02_IND_Climate_Positive_Chemistry_DE/A-EW_299_Chemie_im_Wandel_DE_WEB.pdf.

Agora Verkehrswende. Letzte Chance für 15 Mil- lionen E-Autos bis 2030. Wie eine schnelle Transformation zur Elektromobilität in Deutschland noch gelingen kann und warum die Einbindung chinesischer Automo- bilhersteller dabei eine wichtige Rolle spielt (Langfassung), 2024. URL https://www.agora-verkehrswende.de/fileadmin/Projekte/2024/15-Millionen-Ziel-China_mit-BCG/118_BCG-Studie_Elektroautos_Langfassung.pdf.

Ajeeb, W., Costa Neto, R., and Baptista, P. Life cycle assessment of green hydrogen production through electrolysis: A literature review. *Sustainable Energy Technologies and Assessments*, 69:103923, Sept. 2024. ISSN 22131388. doi:10.1016/j.seta.2024.103923. URL https://linkinghub.elsevier.com/retrieve/pii/S2213138824003199.

Alhyari, M., Al-Salaymeh, A., Irshidat, M., Kaltschmitt, M., and Neuling, U. The Impact of Energy Source on the Life-Cycle Assessment of Power-to-Liquid Fuels. *Journal of Ecological Engineering*, 20 (4):239–244, Apr. 2019. ISSN 2299-8993. doi:10.12911/22998993/104659. URL http://www.journalssystem.com/jeeng/The-Impact-of-Energy-Source-on-the-Life-Cycle-Assessment-of-Power-to-Liquid-Fuels,104659,0,2.html.

Arcos, J. M. M. and Santos, D. M. F. The Hydrogen Color Spectrum: Techno-Economic Analysis of the Available Technologies for Hydrogen Production. *Gases*, 3(1):25–46, Feb. 2023. ISSN 2673-5628. doi:10.3390/gases3010002. URL https://www.mdpi.com/2673-5628/3/1/2.

Bade, S. O., Tomomewo, O. S., Meenakshisundaram, A., Ferron, P., and Oni, B. A. Economic, social, and regulatory challenges of green hydrogen production and utilization in the US: A review. *International Journal of Hydrogen Energy*, 49:314–335, Jan. 2024. ISSN 03603199. doi:10.1016/j.ijhydene.2023.08.157. URL https://linkinghub.elsevier.com/retrieve/pii/S0360319923041587.

Bard, J., Gerhardt, N., Selzam, P., Beil, M., Wiemer, M., and Buddensiek, M. THE LIMITATIONS OF HYDROGEN BLENDING IN THE EUROPEAN GAS GRID A study on the use, limitations and cost of hydrogen blending in the European gas grid at the transport and distribution level. 2022. doi:10.13140/RG.2.2.30093.41448. URL https://rgdoi.net/10.13140/RG.2.2.30093.41448. Publisher: Fraunhofer Institute for Energy Economics and Energy System Technology.

Baringo, L. and Baringo, A. A Stochastic Adaptive Robust Optimization Approach for the Generation and Transmission Expansion Planning. *IEEE Transactions on Power Systems*, 33(1):792–802, Jan. 2018. ISSN 0885-8950, 1558-0679. doi:10.1109/TPWRS.2017.2713486. URL http://ieeexplore.ieee.org/document/7944676/.

Baringo, L., Boffino, L., and Oggioni, G. Robust expansion planning of a distribution system with electric vehicles, storage and renewable units. *Applied Energy*, 265:114679, May 2020. ISSN 03062619. doi:10.1016/j.apenergy.2020.114679. URL https://linkinghub.elsevier.com/retrieve/pii/S0306261920301914.

Basini, L., Furesi, F., Baumgärtl, M., Mondelli, N., and Pauletto, G. CO2 capture and utilization (CCU) by integrating water electrolysis, electrified reverse water gas shift (E-RWGS) and methanol synthesis. *Journal of Cleaner Production*, 377:134280, Dec. 2022. ISSN 09596526. doi:10.1016/j.jclepro.2022.134280. URL https://linkinghub.elsevier.com/retrieve/pii/S0959652622038525.

Becker, H., Murawski, J., Shinde, D. V., Stephens, I. E. L., Hinds, G., and Smith, G. Impact of impurities on water electrolysis: a review. *Sustainable Energy & Fuels*, 7(7):1565–1603, 2023. ISSN 2398-4902. doi:10.1039/D2SE01517J. URL https://xlink.rsc.org/?DOI=D2SE01517J.

Bertsimas, D. and Sim, M. The Price of Robustness. *Operations Research*, 52(1):35–53, Feb. 2004. ISSN 0030-364X, 1526-5463. doi:10.1287/opre.1030.0065. URL https://pubsonline.informs.org/doi/10.1287/opre.1030.0065.

Bertsimas, D., Litvinov, E., Sun, X. A., Zhao, J., and Zheng, T. Adaptive Robust Optimization for the Security Constrained Unit Commitment Problem. *IEEE Transactions on Power Systems*, 28(1):52–63, Feb. 2013. ISSN 0885-8950, 1558-0679. doi:10.1109/TPWRS.2012.2205021. URL http://ieeexplore.ieee.org/document/6248193/.

Bielefeld, S., Cvetković, M., and Ramírez, A. Should we exploit flexibility of chemical processes for demand response? Differing perspectives on potential benefits and limitations. *Frontiers in Energy Research*, 11:1190174, June 2023. ISSN 2296-598X. doi:10.3389/fenrg.2023.1190174. URL https://www.frontiersin.org/articles/10.3389/fenrg.2023.1190174/full.

Biollaz, S. M. and Schildhauer, T. J., editors. *Synthetic natural gas from coal, dry biomass, and power-to-gas applications*. Wiley, Hoboken, New Jersey, 2016. ISBN 978-1-119-19136-0 978-1-119-19125-4 978-1-119-19133-9 978-1-118-54181-4. doi:10.1002/9781119191339.

Birel, T., Breeman, G., Van Buitenen, A., and Vijver, M. Defueling the impasse: EU political discourse on e-fuels. *Energy Policy*, 187:114022, Apr. 2024. ISSN 03014215. doi:10.1016/j.enpol.2024.114022. URL https://linkinghub.elsevier.com/retrieve/pii/S0301421524000429.

Bisotti, F., Hoff, K. A., Mathisen, A., and Hovland, J. Direct Air capture (DAC) deployment: A review of the industrial deployment. *Chemical Engineering Science*, 283:119416, Jan. 2024. ISSN 00092509. doi:10.1016/j.ces.2023.119416. URL https://linkinghub.elsevier.com/retrieve/pii/S0009250923009727.

Blanco, H., Nijs, W., Ruf, J., and Faaij, A. Potential for hydrogen and Power-to-Liquid in a low-carbon EU energy system using cost optimization. *Applied Energy*, 232:617–639, Dec. 2018. ISSN 03062619. doi:10.1016/j.apenergy.2018.09.216. URL https://linkinghub.elsevier.com/retrieve/pii/S0306261918315368.

Block, S., Viebahn, P., and Jungbluth, C. Analysing direct air capture for enabling negative emissions in Germany: an assessment of the resource requirements and costs of a potential rollout in 2045. *Frontiers in Climate*, 6:1353939, Feb. 2024. ISSN 2624-9553. doi:10.3389/fclim.2024.1353939. URL https://www.frontiersin.org/articles/10.3389/fclim.2024.1353939/full.

boerse.de. Co2 Emissionsrechte, Oct. 2025. URL https://www.boerse.de/rohstoffe/Co2-Emissionsrechtepreis/XC000A0C4KJ2.

Boretti, A. Green imperialism a barrier to equitable progress in the hydrogen economy. *International Journal of Hydrogen Energy*, 105:137–147, Mar. 2025. ISSN 03603199. doi:10.1016/j.ijhydene.2025.01.195. URL https://linkinghub.elsevier.com/retrieve/pii/S0360319925002162.

Brauer, J., Villavicencio, M., and Trüby, J. Green Hydrogen: How Grey Can It Be?, 2022. URL https://fsr.eui.eu/publications/?handle=1814/74850.

Brown, T., Hörsch, J., and Schlachtberger, D. PyPSA: Python for Power System Analysis. *Journal of Open Research Software*, 6(1):4, Jan. 2018. ISSN 2049-9647. doi:10.5334/jors.188. URL https://openresearchsoftware.metajnl.com/article/10.5334/jors.188/.

Bundesnetzagentur. Anlage 3: Neubaumaßnahmen (Antrag 22.07.2024), 2024a. URL https://www.bundesnetzagentur.de/DE/Fachthemen/ElektrizitaetundGas/Wasserstoff/_DL/geaendert_Anlage3.xlsx?__blob=publicationFile&v=3.

Bundesnetzagentur. Anlage 4: Umstellungsmaßnahmen (Antrag 22.07.2024), 2024b. URL https://www.bundesnetzagentur.de/DE/Fachthemen/ElektrizitaetundGas/Wasserstoff/_DL/geaendert_Anlage2.xlsx?__blob=publicationFile&v=3.

Bundesnetzagentur. Genehmigstes Wasserstoffkernnetz, Oct. 2024c. URL https://www.bundesnetzagentur.de/DE/Fachthemen/ElektrizitaetundGas/Wasserstoff/Kernnetz/Karte.jpg?__blob=publicationFile&v=1.

Bundesnetzagentur. Genehmigung eines Wasserstoff-Kernnetzes gemäß § 28q Abs. 8 S. 1 i. V. m. § 28q Abs. 1, 2, 4, 5, 6 Satz 1 so- wie des Abs. 7 EnWG, Oct. 2024d. URL https://www.bundesnetzagentur.de/DE/Fachthemen/ElektrizitaetundGas/Wasserstoff/_DL/Genehmigung.pdf?__blob=publicationFile&v=6.

Bundesnetzagentur. Gaspreise Großhandel in EUR/MWh, May 2025. URL https://www.bundesnetzagentur.de/DE/Gasversorgung/aktuelle_gasversorgung/_svg/Gaspreise/Gaspreise.html.

Bundesregierung. Fortschreibung der Nationalen Wasserstoffstrategie NWS 2023, 2023a. URL https://www.bmbf.de/SharedDocs/Downloads/DE/20/230726-fortschreibung-nws.pdf?__blob=publicationFile&v=4.

Bundesregierung. Gesetz zur Änderung des Gebäudeenergiegesetzes, zur Änderung des Bürgerlichen Gesetzbuches, zur Änderung der Verordnung über Heizkostenabrechnung, zur Änderung der Betriebskostenverordnung und zur Änderung der Kehr- und Überprüfungsordnung, Oct. 2023b. URL https://www.recht.bund.de/bgbl/1/2023/280/VO.html.

Bundeswehr. Marinekommando Jahresbericht 2023 - Fakten und Zahlen zur maritimen Abhängigkeit der Bundesrepublik Deutschland. Technical report, 2023. URL https://www.bundeswehr.de/resource/blob/5716058/277a375f7630de85fe86fef391de90b3/jahresbericht-2023-neu--data.pdf.

Burandt, T. Analyzing the necessity of hydrogen imports for net-zero emission scenarios in Japan. *Applied Energy*, 298:117265, Sept. 2021. ISSN 03062619. doi:10.1016/j.apenergy.2021.117265. URL https://linkinghub.elsevier.com/retrieve/pii/S0306261921006814.

Burrows, M. J. and Gnad, O. Between 'muddling through' and 'grand design': Regaining political initiative – The role of strategic foresight. *Futures*, 97:6–17, Mar. 2018. ISSN 00163287. doi:10.1016/j.futures.2017.06.002. URL https://linkinghub.elsevier.com/retrieve/pii/S0016328717300083.

Béres, R., Nijs, W., Boldrini, A., and Van Den Broek, M. Will hydrogen and synthetic fuels energize our future? Their role in Europe's climate-neutral energy system and power system dynamics. *Applied Energy*, 375:124053, Dec. 2024. ISSN 03062619. doi:10.1016/j.apenergy.2024.124053. URL https://linkinghub.elsevier.com/retrieve/pii/S0306261924014363.

Böhringer, C. and Rutherford, T. F. Combining bottom-up and top-down. *Energy Economics*, 30(2):574–596, Mar. 2008. ISSN 01409883. doi:10.1016/j.eneco.2007.03.004. URL https://linkinghub.elsevier.com/retrieve/pii/S014098830700059X.

Börjeson, L., Höjer, M., Dreborg, K.-H., Ekvall, T., and Finnveden, G. Scenario types and techniques: Towards a user's guide. *Futures*, 38(7):723–739, Sept. 2006. ISSN 00163287. doi:10.1016/j.futures.2005.12.002. URL https://linkinghub.elsevier.com/retrieve/pii/S0016328705002132.

Caramia, M. and Dell'Olmo, P. Multi-objective Optimization. In *Multi-objective Management in Freight Logistics*, pages 21–51. Springer International Publishing, Cham, 2020. ISBN 978-3-030-50811-1 978-3-030-50812-8. doi:10.1007/978-3-030-50812-8_2. URL http://link.springer.com/10.1007/978-3-030-50812-8_2.

Carattini, S., Carvalho, M., and Fankhauser, S. Overcoming public resistance to carbon taxes. *WIREs Climate Change*, 9(5):e531, Sept. 2018. ISSN 1757-7780, 1757-7799. doi:10.1002/wcc.531. URL https://wires.onlinelibrary.wiley.com/doi/10.1002/wcc.531.

Chen, B., Wang, J., Wang, L., He, Y., and Wang, Z. Robust Optimization for Transmission Expansion Planning: Minimax Cost vs. Minimax Regret. *IEEE Transactions on Power Systems*, 29(6):3069–3077, Nov. 2014. ISSN 0885-8950, 1558-0679. doi:10.1109/TPWRS.2014.2313841. URL https://ieeexplore.ieee.org/document/6784363/.

Culhane, T., Hall, G., and Roberts, J. T. Who delays climate action? Interest groups and coalitions in state legislative struggles in the United States. *Energy Research & Social Science*, 79:102114, Sept. 2021. ISSN 22146296. doi:10.1016/j.erss.2021.102114. URL https://linkinghub.elsevier.com/retrieve/pii/S2214629621002073.

Dagdougui, H. Models, methods and approaches for the planning and design of the future hydrogen supply chain. *International Journal of Hydrogen Energy*, 37(6):5318–5327, Mar. 2012. ISSN 0360-3199. doi:10.1016/j.ijhydene.2011.08.041. URL https://linkinghub.elsevier.com/retrieve/pii/S0360319911019288. Publisher: Elsevier BV.

Danish Energy Agency. Technology Data Renewable Fuels - Technology descriptions and projections for long-term energy system planning - Update 2025, 2025. URL https://ens.dk/en/analyses-and-statistics/technology-data-renewable-fuels.

de Klerk, Arno. *Fischer-Tropsch Refining*. PhD thesis, University of Pretoria, Pretoria, Feb. 2008. URL https://repository.up.ac.za/server/api/core/bitstreams/1554bbdb-0ed1-402e-a5b8-e2181c94f94a/content.

dena. Technische CO2-Senken. Techno-ökonomische Analyse ausgewählter CO2-Negativemissionstechnologien - Kurzgutachten im Rahmen der dena-Leitstudie Aufbruch Klimaneutralität – Prognos AG Berlin, 2021. URL https://www.dena.de/infocenter/technische-co2-senken-techno-oekonomische-analyse-ausgewaehlter-co2-negativemissionstechnologien/.

Deutscher Bundestag. Antwort der Bundesregierung auf die Kleine Anfrage der Fraktion der CDU/CSU – Drucksache 20/13467 – Umsetzung der Kraftwerksstrategie, Nov. 2024a. URL https://dserver.bundestag.de/btd/20/136/2013645.pdf.

Deutscher Bundestag. Verordnung zur Neufassung der Siebenunddreißigsten Verordnung zur Durchführung des Bundes-Immissionsschutzgesetzes (Verordnung zur Anrechnung von strombasierten Kraftstoffen und mitverarbeiteten biogenen Ölen auf die Treibhausgasquote – 37. BImSchV), July 2024b. URL https://dserver.bundestag.de/btd/20/098/2009844.pdf.

Doss-Gollin, J., Amonkar, Y., Schmeltzer, K., and Cohan, D. Improving the Representation of Climate Risks in Long-Term Electricity Systems Planning: a Critical Review. *Current Sustainable/Renewable Energy Reports*, 10(4):206–217, Aug. 2023. ISSN 2196-3010. doi:10.1007/s40518-023-00224-3. URL https://link.springer.com/10.1007/s40518-023-00224-3.

Egerer, J., Grimm, V., Niazmand, K., and Runge, P. The economics of global green ammonia trade – "Shipping Australian wind and sunshine to Germany". *Applied Energy*, 334:120662, Mar. 2023. ISSN 03062619. doi:10.1016/j.apenergy.2023.120662. URL https://linkinghub.elsevier.com/retrieve/pii/S0306261923000260.

El-Shafie, M. Hydrogen production by water electrolysis technologies: A review. *Results in Engineering*, 20:101426, Dec. 2023. ISSN 25901230. doi:10.1016/j.rineng.2023.101426. URL https://linkinghub.elsevier.com/retrieve/pii/S2590123023005534.

Energiewirtschaftliches Institut an der Universität zu Köln (EWI). dena-Leitstudie Aufbruch Klimaneutralität: Klimaneutralität 2045 - Transformation der Verbrauchssektoren und des Energiesystems, 2021.

energy institute. Statistical Review of World Energy. Technical report, 2024. URL https://www.bpb.de/system/files/dokument_pdf/Statistical_Review_of_World_Energy_2024.pdf.

European Hydrogen Backbone and Gas Infrastructure Europe. European Hydrogen Backbone: Boosting EU Resilience and Competitiveness. Technical report, 2024. URL https://ehb.eu/files/downloads/1732103116_EHB-Boosting-EU-Resilience-and-Competitiveness-20-11-VF.pdf.

European Hydrogen Observatory. The European hydrogen market landscape, 2024. URL https://observatory.clean-hydrogen.europa.eu/sites/default/files/2024-11/The%20European%20hydrogen%20market%20landscape_November%202024.pdf.

European Union. DIRECTIVE 2003/87/EC OF THE EUROPEAN PARLIAMENT AND OF THE COUNCIL of 13 October 2003 establishing a scheme for greenhouse gas emission allowance trading within the Community and amending Council Directive 96/61/EC, Oct. 2003. URL https://eur-lex.europa.eu/LexUriServ/LexUriServ.do?uri=OJ:L:2003:275:0032:0046:en:PDF.

European Union. Commission Delegated Regulation (EU) 2023/1184 of 10 February 2023 supplementing Directive (EU) 2018/2001 of the European Parliament and of the Council by establishing a Union methodology setting out detailed rules for the production of renewable liquid and gaseous transport fuels of non-biological origin, June 2023a. URL https://eur-lex.europa.eu/legal-content/EN/TXT/PDF/?uri=CELEX:32023R1184.

European Union. Commission Delegated Regulation (EU) 2023/1185 of 10 February 2023 supplementing Directive (EU) 2018/2001 of the European Parliament and of the Council by establishing a minimum threshold for greenhouse gas emissions savings of recycled carbon fuels and by specifying a methodology for assessing greenhouse gas emissions savings from renewable liquid and gaseous transport fuels of non-biological origin and from recycled carbon fuels, June 2023b. URL https://eur-lex.europa.eu/legal-content/EN/TXT/PDF/?uri=CELEX:32023R1185.

European Union. DIRECTIVE (EU) 2023/2413 OF THE EUROPEAN PARLIAMENT AND OF THE COUNCIL of 18 October 2023 amending Directive (EU) 2018/2001, Regulation (EU) 2018/1999 and Directive 98/70/EC as regards the promotion of energy from renewable sources, and repealing Council Directive (EU) 2015/652, Oct. 2023c. URL https://eur-lex.europa.eu/legal-content/EN/TXT/PDF/?uri=OJ:L_202302413.

European Union. REGULATION (EU) 2023/2405 OF THE EUROPEAN PARLIAMENT AND OF THE COUNCIL of 18 October 2023 on ensuring a level playing field for sustainable air transport (ReFuelEU Aviation), Oct. 2023d. URL https://eur-lex.europa.eu/legal-content/EN/TXT/HTML/?uri=OJ:L_202302405.

European Union. Regulation (EU) 2023/851 of the European Parliament and of the Council of 19 April 2023 amending Regulation (EU) 2019/631 as regards strengthening the CO2 emission performance standards for new passenger cars and new light commercial vehicles in line with the Union's increased climate ambition (Text with EEA relevance), Apr. 2023e. URL https://eur-lex.europa.eu/legal-content/EN/TXT/?uri=celex:32023R0851.

Eurostat. SeaRoute [Software], Jan. 2021. URL https://github.com/eurostat/searoute. Programmers: _:n227.

Fakhreddine, J., Dodds, P. E., and Butnar, I. Global hydrogen trade pathways: A review of modelling advances and challenges. *International Journal of Hydrogen Energy*, 129:236–252, May 2025. ISSN 0360-3199. doi:10.1016/j.ijhydene.2025.04.203. URL https://linkinghub.elsevier.com/retrieve/pii/S0360319925018592. Publisher: Elsevier BV.

Ferner, K. J. and Litster, S. Composite Anode for PEM Water Electrolyzers: Lowering Iridium Loadings and Reducing Material Costs with a Conductive Additive. *ACS Applied Energy Materials*, 7(18):8124–8135, Sept. 2024. ISSN 2574-0962, 2574-0962. doi:10.1021/acsaem.4c01866. URL https://pubs.acs.org/doi/10.1021/acsaem.4c01866.

Fleiter, T., Rehfeldt, M., Neusel, L., Hirzel, S., Neuwirth, M., Schwotzer, C., Kaiser, F., and Gondorf, C. CO2-neutral process heat using electrification and hydrogen. Technical report, Fraunhofer ISI, 2024. URL https://publica.fraunhofer.de/handle/publica/472300.

Fodstad, M., Crespo Del Granado, P., Hellemo, L., Knudsen, B. R., Pisciella, P., Silvast, A., Bordin, C., Schmidt, S., and Straus, J. Next frontiers in energy system modelling: A review on challenges and the state of the art. *Renewable and Sustainable Energy Reviews*, 160:112246, May 2022. ISSN 13640321. doi:10.1016/j.rser.2022.112246. URL https://linkinghub.elsevier.com/retrieve/pii/S136403212200168X.

Fraunhofer ISE. COST FORECAST FOR LOW TEMPERATURE ELECTROLYSIS – TECHNOLOGY DRIVEN BOTTOM-UP PROGNOSIS FOR PEM AND ALKALINE WATER ELECTROLYSIS SYSTEMS A cost analysis study on behalf of Clean Air Task Force, 2021. URL https://www.google.com/url?sa=t&source=web&rct=j&opi=89978449&url=https://www.ise.fraunhofer.de/content/dam/ise/de/documents/publications/studies/cost-forecast-for-low-temperature-electrolysis.pdf&ved=2ahUKEwiX7du_iLeNAxXnB9sEHX9BCIQQFnoECAoQAQ&usg=AOvVaw37aRFQ_Ag4zm3mJWY3Bl2G.

Frontier Economics. Grünstromkriterien der RED II - Auswirkungen auf die Kosten und Verfügbarkeit Grünen Wasserstoffs in Deutschland. Technical report, July 2021. URL https://www.frontier-economics.com/media/wcmieebg/analyse-red-ii-kritieren.pdf.

Garcia-Bertrand, R. and Minguez, R. Dynamic Robust Transmission Expansion Planning. *IEEE Transactions on Power Systems*, 32(4):2618–2628, July 2017. ISSN 0885-8950, 1558-0679. doi:10.1109/TPWRS.2016.2629266. URL http://ieeexplore.ieee.org/document/7744691/.

Garcia-Garcia, G., Fernandez, M. C., Armstrong, K., Woolass, S., and Styring, P. Analytical Review of Life-Cycle Environmental Impacts of Carbon Capture and Utilization Technologies. *ChemSusChem*, 14(4):995–1015, Feb. 2021. ISSN 1864-5631, 1864-564X. doi:10.1002/cssc.202002126. URL https://chemistry-europe.onlinelibrary.wiley.com/doi/10.1002/cssc.202002126.

García-Cerezo, Baringo, L., and García-Bertrand, R. Expansion planning of the transmission network with high penetration of renewable generation: A multi-year two-stage adaptive robust optimization approach. *Applied Energy*, 349:121653, Nov. 2023. ISSN 03062619. doi:10.1016/j.apenergy.2023.121653. URL https://linkinghub.elsevier.com/retrieve/pii/S0306261923010176.

genthalili. SeaRoute [Software], Jan. 2022. URL https://github.com/genthalili/searoute-py/tree/main. Programmers: _:n264.

Gils, H. C., Scholz, Y., Pregger, T., Luca De Tena, D., and Heide, D. Integrated modelling of variable renewable energy-based power supply in Europe. *Energy*, 123:173–188, Mar. 2017. ISSN 03605442. doi:10.1016/j.energy.2017.01.115. URL https://linkinghub.elsevier.com/retrieve/pii/S0360544217301238.

Global Energy Monitor. Global Oil Infrastructure Tracker, 2025a. URL https://globalenergymonitor.org/projects/global-oil-infrastructure-tracker/.

Global Energy Monitor. Global Gas Infrastructure Tracker, 2025b. URL https://globalenergymonitor.org/projects/global-gas-infrastructure-tracker/.

González-Castaño, M., Dorneanu, B., and Arellano-García, H. The reverse water gas shift reaction: a process systems engineering perspective. *Reaction Chemistry & Engineering*, 6(6):954–976, 2021. ISSN 2058-9883. doi:10.1039/D0RE00478B. URL https://xlink.rsc.org/?DOI=D0RE00478B.

Gorissen, B. L., Yanıkoğlu, and Den Hertog, D. A practical guide to robust optimization. *Omega*, 53:124–137, June 2015. ISSN 03050483. doi:10.1016/j.omega.2014.12.006. URL https://linkinghub.elsevier.com/retrieve/pii/S0305048314001698.

Grigoriev, S., Fateev, V., Bessarabov, D., and Millet, P. Current status, research trends, and challenges in water electrolysis science and technology. *International Journal of Hydrogen Energy*, 45(49):26036–26058, Oct. 2020. ISSN 03603199. doi:10.1016/j.ijhydene.2020.03.109. URL https://linkinghub.elsevier.com/retrieve/pii/S0360319920310715.

Haas, T., Sander, H., Fünfgeld, A., and Mey, F. Climate obstruction at work: Right-wing populism and the German heating law. *Energy Research & Social Science*, 123:104034, May 2025. ISSN 22146296. doi:10.1016/j.erss.2025.104034. URL https://linkinghub.elsevier.com/retrieve/pii/S221462962500115X.

Hanto, J., Herpich, P., Löffler, K., Hainsch, K., Moskalenko, N., and Schmidt, S. Assessing the implications of hydrogen blending on the European energy system towards 2050. *Advances in Applied Energy*, 13: 100161, Feb. 2024. ISSN 26667924. doi:10.1016/j.adapen.2023.100161. URL https://linkinghub.elsevier.com/retrieve/pii/S2666792423000409.

Harmsen, J. and Gerritse, E. D3b.3 - Ammonia Tanker Fleet Analysis. Technical report, Zenodo, Oct. 2024. URL https://zenodo.org/doi/10.5281/zenodo.13895458.

Haydary, J. *Chemical process design and simulation: Aspen Plus and Aspen HYSYS applications*. Wiley, Hoboken, N.J, 2019. ISBN 978-1-119-08911-7.

Heimann, T., Argueyrolles, R., Reinhardt, M., Schuenemann, F., Söder, M., and Delzeit, R. Phasing out palm and soy oil biodiesel in the EU : What is the benefit? *GCB Bioenergy*, 16(1):e13115, Jan. 2024. ISSN 1757-1693, 1757-1707. doi:10.1111/gcbb.13115. URL https://onlinelibrary.wiley.com/doi/10.1111/gcbb.13115.

Held, M., Rosat, N., Georges, G., Pengg, H., and Boulouchos, K. Lifespans of passenger cars in Europe: empirical modelling of fleet turnover dynamics. *European Transport Research Review*, 13(1):9, Dec. 2021. ISSN 1867-0717, 1866-8887. doi:10.1186/s12544-020-00464-0. URL https://etrr.springeropen.com/articles/10.1186/s12544-020-00464-0.

Henstra, D. The tools of climate adaptation policy: analysing instruments and instrument selection. *Climate Policy*, 16(4):496–521, May 2016. ISSN 1469-3062, 1752-7457. doi:10.1080/14693062.2015.1015946. URL http://www.tandfonline.com/doi/full/10.1080/14693062.2015.1015946.

Hersbach, H., Bell, B., Berrisford, P., Hirahara, S., Horányi, A., Muñoz-Sabater, J., Nicolas, J., Peubey, C., Radu, R., Schepers, D., Simmons, A., Soci, C., Abdalla, S., Abellan, X., Balsamo, G., Bechtold, P., Biavati, G., Bidlot, J., Bonavita, M., De Chiara, G., Dahlgren, P., Dee, D., Diamantakis, M., Dragani, R., Flemming, J., Forbes, R., Fuentes, M., Geer, A., Haimberger, L., Healy, S., Hogan, R. J., Hólm, E., Janisková, M., Keeley, S., Laloyaux, P., Lopez, P., Lupu, C., Radnoti, G., De Rosnay, P., Rozum, I., Vamborg, F., Villaume, S., and Thépaut, J. The ERA5 global reanalysis. *Quarterly Journal of the Royal Meteorological Society*, 146(730):1999–2049, July 2020. ISSN 0035-9009, 1477-870X. doi:10.1002/qj.3803. URL https://rmets.onlinelibrary.wiley.com/doi/10.1002/qj.3803.

Hoffmann, M., Schyska, B. U., Bartels, J., Pelser, T., Behrens, J., Wetzel, M., Gils, H. C., Tang, C.-F., Tillmanns, M., Stock, J., Xhonneux, A., Kotzur, L., Praktiknjo, A., Vogt, T., Jochem, P., Linßen, J., Weinand, J. M., and Stolten, D. A review of mixed-integer linear formulations for framework-based energy system models. *Advances in Applied Energy*, 16:100190, Dec. 2024. ISSN 26667924. doi:10.1016/j.adapen.2024.100190. URL https://linkinghub.elsevier.com/retrieve/pii/S2666792424000283.

Hofmann, F., Hampp, J., Neumann, F., Brown, T., and Hörsch, J. atlite: A Lightweight Python Package for Calculating Renewable Power Potentials and Time Series. *Journal of Open Source Software*, 6(62): 3294, Jan. 2021. doi:10.21105/joss.03294. Number: 62.

Hofmann, F., Tries, C., Neumann, F., Zeyen, E., and Brown, T. H2 and CO2 network strategies for the European energy system. *Nature Energy*, 10(6):715–724, Apr. 2025. ISSN 2058-7546. doi:10.1038/s41560-025-01752-6. URL https://www.nature.com/articles/s41560-025-01752-6.

Howells, M., Rogner, H., Strachan, N., Heaps, C., Huntington, H., Kypreos, S., Hughes, A., Silveira, S., DeCarolis, J., Bazillian, M., and Roehrl, A. OSeMOSYS: The Open Source Energy Modeling System. *Energy Policy*, 39(10):5850–5870, Oct. 2011. ISSN 03014215. doi:10.1016/j.enpol.2011.06.033. URL https://linkinghub.elsevier.com/retrieve/pii/S0301421511004897.

Hubbard, D. W. *How to measure anything: finding the value of "intangibles in business"*. John Wiley & Sons, Hoboken, New Jersey, third edition edition, 2014. ISBN 978-1-118-53927-9 978-1-118-83644-6.

Icha, P. and Lauf, T. Entwicklung der spezifischen Treibhausgas-Emissionen des deutschen Strommix in den Jahren 1990 - 2024, Apr. 2025. URL https://www.umweltbundesamt.de/publikationen/entwicklung-der-spezifischen-treibhausgas-11.

IEA. Energy Technology Perspectives 2023, 2023a. URL https://iea.blob.core.windows.net/assets/a86b480e-2b03-4e25-bae1-da1395e0b620/EnergyTechnologyPerspectives2023.pdf.

IEA. How to Avoid Gas Shortages in the European Union in 2023: A practical set of actions to close a potential supply-demand gap, 2023b. URL https://iea.blob.core.windows.net/assets/96ce64c5-1061-4e0c-998d-fd679990653b/HowtoAvoidGasShortagesintheEuropeanUnionin2023.pdf.

IEA. Direct Air Capture A key technology for net zero, 2024. URL https://iea.blob.core.windows.net/assets/9766b4da-a5e3-4d76-874d-ea286e333956/DirectAirCapture_Akeytechnologyfornetzero.pdf.

IEA Bioenergy. Implementation of bioenergy in Brazil – 2024 update - Country Reports, 2024. URL https://www.ieabioenergy.com/wp-content/uploads/2024/12/CountryReport2024_Brazil_final.pdf.

Iglesias González, M., Eilers, H., and Schaub, G. Flexible Operation of Fixed-Bed Reactors for a Catalytic Fuel Synthesis—CO_2 Hydrogenation as Example Reaction. *Energy Technology*, 4(1):90–103, Jan. 2016. ISSN 2194-4288, 2194-4296. doi:10.1002/ente.201500259. URL https://onlinelibrary.wiley.com/doi/10.1002/ente.201500259.

Ince, A. C., Colpan, C. O., Hagen, A., and Serincan, M. F. Modeling and simulation of Power-to-X systems: A review. *Fuel*, 304:121354, Nov. 2021. ISSN 00162361. doi:10.1016/j.fuel.2021.121354. URL https://linkinghub.elsevier.com/retrieve/pii/S0016236121012333.

International Energy Agency (IEA). Ammonia Technology Roadmap - Towards more sustainable nitrogen fertiliser production. Technical report, 2021. URL https://iea.blob.core.windows.net/assets/6ee41bb9-8e81-4b64-8701-2acc064ff6e4/AmmoniaTechnologyRoadmap.pdf.

International Energy Agency (IEA). Global Hydrogen Review 2024. Technical report, Oct. 2024. URL https://iea.blob.core.windows.net/assets/89c1e382-dc59-46ca-aa47-9f7d41531ab5/GlobalHydrogenReview2024.pdf.

International Energy Agency (IEA). Energy and AI. Technical report, Apr. 2025. URL https://iea.blob.core.windows.net/assets/601eaec9-ba91-4623-819b-4ded331ec9e8/EnergyandAI.pdf.

International Renewable Energy Agency. Making the Breakthrough - Green hydrogen policies and technology costs, 2021. URL https://www.irena.org/-/media/Files/IRENA/Agency/Publication/2020/Nov/IRENA_Green_Hydrogen_breakthrough_2021.pdf?la=en&hash=40FA5B8AD7AB1666EECBDE30EF458C45EE5A0AA6.

IRENA and Methanol Institute. Innovation Outlook Renewable Methanol, 2021. URL https://www.irena.org/-/media/Files/IRENA/Agency/Publication/2021/Jan/IRENA_Innovation_Renewable_Methanol_2021.pdf.

Jabr, R. A. Robust Transmission Network Expansion Planning With Uncertain Renewable Generation and Loads. *IEEE Transactions on Power Systems*, 28(4):4558–4567, Nov. 2013. ISSN 0885-8950, 1558-0679. doi:10.1109/TPWRS.2013.2267058. URL https://ieeexplore.ieee.org/document/6547161/.

Jiménez, D., Angulo, A., Street, A., and Mancilla-David, F. A closed-loop data-driven optimization framework for the unit commitment problem: A Q -learning approach under real-time operation. *Applied Energy*, 330:120348, Jan. 2023. ISSN 03062619. doi:10.1016/j.apenergy.2022.120348. URL https://linkinghub.elsevier.com/retrieve/pii/S0306261922016051.

Johnston, C., Ali Khan, M. H., Amal, R., Daiyan, R., and MacGill, I. Shipping the sunshine: An open-source model for costing renewable hydrogen transport from Australia. *International Journal of Hydrogen Energy*, 47(47):20362–20377, June 2022. ISSN 03603199. doi:10.1016/j.ijhydene.2022.04.156. URL https://linkinghub.elsevier.com/retrieve/pii/S0360319922017281.

Jänicke, M., Kunig, P., and Stitzel, M. *Lern- und Arbeitsbuch Umweltpolitik: Politik, Recht und Management des Umweltschutzes in Staat und Unternehmen*. Dietz, Bonn, 2., aktualisierte aufl edition, 2003. ISBN 978-3-8012-0319-1.

Kalt, T. and Tunn, J. Shipping the sunshine? A critical research agenda on the global hydrogen transition. *GAIA - Ecological Perspectives for Science and Society*, 31(2):72–76, July 2022. ISSN 0940-5550. doi:10.14512/gaia.31.2.2. URL https://www.ingentaconnect.com/content/10.14512/gaia.31.2.2.

Klatzer, T., Bachhiesl, U., and Wogrin, S. State-of-the-art expansion planning of integrated power, natural gas, and hydrogen systems. *International Journal of Hydrogen Energy*, 47(47):20585–20603, June 2022. ISSN 03603199. doi:10.1016/j.ijhydene.2022.04.293. URL https://linkinghub.elsevier.com/retrieve/pii/S0360319922019668.

Koj, J. C., Wulf, C., and Zapp, P. Environmental impacts of power-to-X systems - A review of technological and methodological choices in Life Cycle Assessments. *Renewable and Sustainable Energy Reviews*, 112: 865–879, Sept. 2019. ISSN 13640321. doi:10.1016/j.rser.2019.06.029. URL https://linkinghub.elsevier.com/retrieve/pii/S1364032119304228.

Koller, F., Christian Winkler, Liedtke, G., Österle, I., Mocanu, T., Seibert, D., Deniz, Matteis, T., Bergfeld, M., Sehn, V., Kattelmann, F., Haun, M., and Dirnaichner, A. Ariadne-Report - Deutschland auf dem Weg zur Klimaneutralität 2045 Szenarien und Pfade im Modellvergleich - Verkehr, Oct. 2021.

Kopp, J., Moritz, M., Scharf, H., and Schmidt, J. Strukturwandel in der Gaswirtschaft – Was bedeutet die Entwicklung der Gas- und Wasserstoffnachfrage für die zukünftige Infrastruktur?: Eine Metaanalyse bestehender Energiesystemstudien. *Zeitschrift für Energiewirtschaft*, Dec. 2022. ISSN 0343-5377, 1866-2765. doi:10.1007/s12398-022-00335-2. URL https://link.springer.com/10.1007/s12398-022-00335-2.

Kountouris, I., Bramstoft, R., Madsen, T., Gea-Bermúdez, J., Münster, M., and Keles, D. A unified European hydrogen infrastructure planning to support the rapid scale-up of hydrogen production. *Nature Communications*, 15(1):5517, June 2024. ISSN 2041-1723. doi:10.1038/s41467-024-49867-w. URL https://www.nature.com/articles/s41467-024-49867-w.

Lange, H., Klose, A., Lippmann, W., and Urbas, L. Technical evaluation of the flexibility of water electrolysis systems to increase energy flexibility: A review. *International Journal of Hydrogen Energy*, 48(42):15771–15783, May 2023. ISSN 03603199. doi:10.1016/j.ijhydene.2023.01.044. URL https://linkinghub.elsevier.com/retrieve/pii/S0360319923000459.

Langenmayr, U. and Ruppert, M. Renewable origin, additionality, temporal and geographical correlation – eFuels production in Germany under the RED II regime. *Energy Policy*, 183:113830, Dec. 2023. ISSN 03014215. doi:10.1016/j.enpol.2023.113830. URL https://linkinghub.elsevier.com/retrieve/pii/S0301421523004159.

Langenmayr, U., Heinzmann, P., Schneider, A., Ruppert, M., Rudi, A., and Fichtner, W. Stand-alone power-to-X production dynamics: A multi-method approach to quantify the emission-cost reduction trade-off. *Journal of Industrial Ecology*, page jiec.70085, July 2025a. ISSN 1088-1980, 1530-9290. doi:10.1111/jiec.70085. URL https://onlinelibrary.wiley.com/doi/10.1111/jiec.70085.

Langenmayr, U., Schuler, J., Slednev, V., and Fichtner, W. Mapping Tomorrow's Energy Journeys – A Global Perspective on the Transport of Synthetic Energy Carriers. *Submitted to a scientific journal*, 2025b.

Langenmayr, U., Slednev, V., Ruppert, M., and Fichtner, W. An adaptive robust optimization approach using scenario-based uncertainty sets for stand-alone power-to-X facilities. *Submitted to a scientific journal*, 2025c.

Lara Filho, M. O. D., Pinto, R. S., Aquino, C. C. C. B. D., Unsihuay-Vila, C., and Tabarro, F. H. A Data-driven Robust Model for Day-ahead Operation Planning of Microgrids Considering Distributed Energy Resources and Demand Response. *Brazilian Archives of Biology and Technology*, 66:e23220245, 2023. ISSN 1678-4324, 1516-8913. doi:10.1590/1678-4324-2023220245. URL http://www.scielo.br/scielo.php?script=sci_arttext&pid=S1516-89132023000100605&tlng=en.

Le, T. T., Sharma, P., Bora, B. J., Tran, V. D., Truong, T. H., Le, H. C., and Nguyen, P. Q. P. Fueling the future: A comprehensive review of hydrogen energy systems and their challenges. *International Journal of Hydrogen Energy*, 54:791–816, Feb. 2024. ISSN 03603199. doi:10.1016/j.ijhydene.2023.08.044. URL https://linkinghub.elsevier.com/retrieve/pii/S0360319923039988.

Leung, D. Y., Caramanna, G., and Maroto-Valer, M. M. An overview of current status of carbon dioxide capture and storage technologies. *Renewable and Sustainable Energy Reviews*, 39:426–443, Nov. 2014. ISSN 13640321. doi:10.1016/j.rser.2014.07.093. URL https://linkinghub.elsevier.com/retrieve/pii/S1364032114005450.

Lipiäinen, S., Lipiäinen, K., Ahola, A., and Vakkilainen, E. Use of existing gas infrastructure in European hydrogen economy. *International Journal of Hydrogen Energy*, 48(80):31317–31329, Sept. 2023. ISSN 03603199. doi:10.1016/j.ijhydene.2023.04.283. URL https://linkinghub.elsevier.com/retrieve/pii/S0360319923021134.

Lopion, P., Markewitz, P., Robinius, M., and Stolten, D. A review of current challenges and trends in energy systems modeling. *Renewable and Sustainable Energy Reviews*, 96:156–166, Nov. 2018. ISSN 13640321. doi:10.1016/j.rser.2018.07.045. URL https://linkinghub.elsevier.com/retrieve/pii/S1364032118305537.

Loulou, R. and Labriet, M. ETSAP-TIAM: the TIMES integrated assessment model Part I: Model structure. *Computational Management Science*, 5(1-2):7–40, Feb. 2008. ISSN 1619-697X, 1619-6988. doi:10.1007/s10287-007-0046-z. URL http://link.springer.com/10.1007/s10287-007-0046-z.

Löffler, K., Hainsch, K., Burandt, T., Oei, P.-Y., Kemfert, C., and Von Hirschhausen, C. Designing a Model for the Global Energy System—GENeSYS-MOD: An Application of the Open-Source Energy Modeling System (OSeMOSYS). *Energies*, 10(10):1468, Sept. 2017. ISSN 1996-1073. doi:10.3390/en10101468. URL https://www.mdpi.com/1996-1073/10/10/1468.

Mahmoud, H. A., Sharaf, M., and El-Meligy, M. A. An adaptive robust optimization model for transmission expansion planning considering uncertain intervals. *International Journal of Electrical Power & Energy Systems*, 157:109821, June 2024. ISSN 01420615. doi:10.1016/j.ijepes.2024.109821. URL https://linkinghub.elsevier.com/retrieve/pii/S0142061524000425.

Mancilla-David, F., Angulo, A., and Street, A. Power Management in Active Distribution Systems Penetrated by Photovoltaic Inverters: A Data-Driven Robust Approach. *IEEE Transactions on Smart Grid*, 11(3):2271–2280, May 2020. ISSN 1949-3053, 1949-3061. doi:10.1109/TSG.2019.2951086. URL https://ieeexplore.ieee.org/document/8889689/.

Markowitsch, C., Lehner, M., and Maly, M. Evaluation of process structures and reactor technologies of an integrated power-to-liquid plant at a cement factory. *Journal of CO2 Utilization*, 70:102449, Apr. 2023. ISSN 22129820. doi:10.1016/j.jcou.2023.102449. URL https://linkinghub.elsevier.com/retrieve/pii/S2212982023000604.

Martinez Lopez, V., Ziar, H., Haverkort, J., Zeman, M., and Isabella, O. Dynamic operation of water electrolyzers: A review for applications in photovoltaic systems integration. *Renewable and Sustainable Energy Reviews*, 182:113407, Aug. 2023. ISSN 13640321. doi:10.1016/j.rser.2023.113407. URL https://linkinghub.elsevier.com/retrieve/pii/S1364032123002642.

Martín, A. J., Mitchell, S., Mondelli, C., Jaydev, S., and Pérez-Ramírez, J. Unifying views on catalyst deactivation. *Nature Catalysis*, 5(10):854–866, Sept. 2022. ISSN 2520-1158. doi:10.1038/s41929-022-00842-y. URL https://www.nature.com/articles/s41929-022-00842-y.

Mavrotas, G. Effective implementation of the -constraint method in Multi-Objective Mathematical Programming problems. *Applied Mathematics and Computation*, 213(2):455–465, July 2009. ISSN 00963003. doi:10.1016/j.amc.2009.03.037. URL https://linkinghub.elsevier.com/retrieve/pii/S0096300309002574.

Molnar, G. Economics of Gas Transportation by Pipeline and LNG. In Hafner, M. and Luciani, G., editors, *The Palgrave Handbook of International Energy Economics*, pages 23–57. Springer International Publishing, Cham, 2022. ISBN 978-3-030-86883-3 978-3-030-86884-0. doi:10.1007/978-3-030-86884-0_2. URL https://link.springer.com/10.1007/978-3-030-86884-0_2.

Moore, F. C., Drupp, M. A., Rising, J., Dietz, S., Rudik, I., and Wagner, G. Synthesis of evidence yields high social cost of carbon due to structural model variation and uncertainties. *Proceedings of the National Academy of Sciences*, 121(52):e2410733121, Dec. 2024. ISSN 0027-8424, 1091-6490. doi:10.1073/pnas.2410733121. URL https://pnas.org/doi/10.1073/pnas.2410733121.

Mínguez, R. and García-Bertrand, R. Robust transmission network expansion planning in energy systems: Improving computational performance. *European Journal of Operational Research*, 248(1):21–32, Jan. 2016. ISSN 03772217. doi:10.1016/j.ejor.2015.06.068. URL https://linkinghub.elsevier.com/retrieve/pii/S0377221715006013.

Müller, M., Pfeifer, M., Holtz, D., and Müller, K. Comparison of green ammonia and green hydrogen pathways in terms of energy efficiency. *Fuel*, 357:129843, Feb. 2024. ISSN 00162361. doi:10.1016/j.fuel.2023.129843. URL https://linkinghub.elsevier.com/retrieve/pii/S0016236123024572.

Neumann, F., Zeyen, E., Victoria, M., and Brown, T. The potential role of a hydrogen network in Europe. *Joule*, 7(8):1793–1817, Aug. 2023. ISSN 25424351. doi:10.1016/j.joule.2023.06.016. URL https://linkinghub.elsevier.com/retrieve/pii/S2542435123002660.

Niermann, M., Timmerberg, S., Drünert, S., and Kaltschmitt, M. Liquid Organic Hydrogen Carriers and alternatives for international transport of renewable hydrogen. *Renewable and Sustainable Energy Reviews*, 135:110171, Jan. 2021. ISSN 13640321. doi:10.1016/j.rser.2020.110171. URL https://linkinghub.elsevier.com/retrieve/pii/S1364032120304627.

OPEC. Annual Statistical Bulletin 2024, 2024. URL https://publications.opec.org/asb.

Osman, O., Sgouridis, S., and Sleptchenko, A. Scaling the production of renewable ammonia: A techno-economic optimization applied in regions with high insolation. *Journal of Cleaner Production*, 271: 121627, Oct. 2020. ISSN 09596526. doi:10.1016/j.jclepro.2020.121627. URL https://linkinghub.elsevier.com/retrieve/pii/S0959652620316747.

Owen, A. D. Renewable energy: Externality costs as market barriers. *Energy Policy*, 34(5):632–642, Mar. 2006. ISSN 03014215. doi:10.1016/j.enpol.2005.11.017. URL https://linkinghub.elsevier.com/retrieve/pii/S0301421505003174.

Parolin, F., Colbertaldo, P., and Campanari, S. Development of a multi-modality hydrogen delivery infrastructure: An optimization model for design and operation. *Energy Conversion and Management*, 266:115650, Aug. 2022. ISSN 01968904. doi:10.1016/j.enconman.2022.115650. URL https://linkinghub.elsevier.com/retrieve/pii/S0196890422004460.

Perna, A., Moretti, L., Ficco, G., Spazzafumo, G., Canale, L., and Dell'Isola, M. SNG Generation via Power to Gas Technology: Plant Design and Annual Performance Assessment. *Applied Sciences*, 10(23): 8443, Nov. 2020. ISSN 2076-3417. doi:10.3390/app10238443. URL https://www.mdpi.com/2076-3417/10/23/8443. Publisher: MDPI AG.

Peters, M. S., Timmerhaus, K. D., West, R. E., and West, R. E. *Plant design and economics for chemical engineers*. McGraw-Hill chemical engineering series. McGraw-Hill, Boston, 5. ed., international ed edition, 2003. ISBN 978-0-07-119872-1 978-0-07-239266-1.

Pezzey, J. C. V. Why the social cost of carbon will always be disputed. *WIREs Climate Change*, 10(1): e558, Jan. 2019. ISSN 1757-7780, 1757-7799. doi:10.1002/wcc.558. URL https://wires.onlinelibrary.wiley.com/doi/10.1002/wcc.558.

Peña, V., Gronemann, V., König, S., and Haag, S. e-Methanol - aber bitte flexibel! *CITplus*, 27(6):72–75, June 2024. ISSN 1436-2597, 1439-0663. doi:10.1002/citp.202400623. URL https://onlinelibrary.wiley.com/doi/10.1002/citp.202400623.

Pfeifer, P., Biffar, L., Timm, F., and Böltken, T. Influence of Power-to-Fuel Plant Flexibility Towards Power and Plant Utilization and Intermediate Hydrogen Buffer Size. *Chemie Ingenieur Technik*, 92 (12):1976–1982, Dec. 2020. ISSN 0009-286X, 1522-2640. doi:10.1002/cite.202000084. URL https://onlinelibrary.wiley.com/doi/10.1002/cite.202000084.

Pfenninger, S. and Pickering, B. Calliope: a multi-scale energy systems modelling framework. *Journal of Open Source Software*, 3(29):825, Sept. 2018. ISSN 2475-9066. doi:10.21105/joss.00825. URL http://joss.theoj.org/papers/10.21105/joss.00825.

Pickering, B., Lombardi, F., and Pfenninger, S. Diversity of options to eliminate fossil fuels and reach carbon neutrality across the entire European energy system. *Joule*, 6(6):1253–1276, June 2022. ISSN 25424351. doi:10.1016/j.joule.2022.05.009. URL https://linkinghub.elsevier.com/retrieve/pii/S2542435122002367.

Pinto, M. C., Simões, S. G., and Fortes, P. How can green hydrogen from North Africa support EU decarbonization? Scenario analyses on competitive pathways for trade. *International Journal of Hydrogen Energy*, 79:305–318, Aug. 2024. ISSN 03603199. doi:10.1016/j.ijhydene.2024.06.395. URL https://linkinghub.elsevier.com/retrieve/pii/S036031992402634X.

Pio, D., Vilas-Boas, A., Araújo, V., Rodrigues, N., and Mendes, A. Decarbonizing the aviation sector with Electro Sustainable Aviation Fuel (eSAF) from biogenic CO2 captured at pulp mills. *Chemical Engineering Journal*, 463:142317, May 2023. ISSN 1385-8947. doi:10.1016/j.cej.2023.142317. URL https://linkinghub.elsevier.com/retrieve/pii/S1385894723010483. Publisher: Elsevier BV.

Pirdashti, M., Tavana, M., Hassim, M. H., Behzadian, M., and Karimi, I. A taxonomy and review of the multiple criteria decision-making literature in chemical engineering. *International Journal of Multicriteria Decision Making*, 1(4):407, 2011. ISSN 2040-106X, 2040-1078. doi:10.1504/IJMCDM.2011.043556. URL http://www.inderscience.com/link.php?id=43556.

Prognos, Öko-Institut, Wuppertal-Institut. Klimaneutrales Deutschland 2045 - Wie Deutschland seine Klimaziele schon vor 2050 erreichen kann, 2021. URL https://www.agora-energiewende.de/fileadmin/Projekte/2021/2021_04_KNDE45/A-EW_231_KNDE2045_Langfassung_DE_WEB.pdf.

Qu, K., Zheng, X., and Yu, T. Environmental-Economic Unit Commitment With Robust Diffusion Control of Gas Pollutants. *IEEE Transactions on Power Systems*, 38(1):818–834, Jan. 2023. ISSN 0885-8950, 1558-0679. doi:10.1109/TPWRS.2022.3166264. URL https://ieeexplore.ieee.org/document/9755020/.

Rebennack, S. Combining sampling-based and scenario-based nested Benders decomposition methods: application to stochastic dual dynamic programming. *Mathematical Programming*, 156(1-2):343–389, Mar. 2016. ISSN 0025-5610, 1436-4646. doi:10.1007/s10107-015-0884-3. URL http://link.springer.com/10.1007/s10107-015-0884-3.

Ricks, W., Xu, Q., and Jenkins, J. D. Minimizing emissions from grid-based hydrogen production in the United States. *Environmental Research Letters*, 18(1):014025, Jan. 2023. ISSN 1748-9326. doi:10.1088/1748-9326/acacb5. URL https://iopscience.iop.org/article/10.1088/1748-9326/acacb5.

Riepin, I., Schmidt, M., Baringo, L., and Müsgens, F. Adaptive robust optimization for European strategic gas infrastructure planning. *Applied Energy*, 324:119686, Oct. 2022. ISSN 03062619. doi:10.1016/j.apenergy.2022.119686. URL https://linkinghub.elsevier.com/retrieve/pii/S030626192200962X.

Ruhnau, O. and Schiele, J. Flexible green hydrogen: The effect of relaxing simultaneity requirements on project design, economics, and power sector emissions. *Energy Policy*, 182:113763, Nov. 2023. ISSN 03014215. doi:10.1016/j.enpol.2023.113763. URL https://linkinghub.elsevier.com/retrieve/pii/S0301421523003488.

Ruiz, C. and Conejo, A. Robust transmission expansion planning. *European Journal of Operational Research*, 242(2):390–401, Apr. 2015. ISSN 03772217. doi:10.1016/j.ejor.2014.10.030. URL https://linkinghub.elsevier.com/retrieve/pii/S0377221714008510.

Saadi, F. H., Lewis, N. S., and McFarland, E. W. Relative costs of transporting electrical and chemical energy. *Energy & Environmental Science*, 11(3):469–475, 2018. ISSN 1754-5692, 1754-5706. doi:10.1039/C7EE01987D. URL https://xlink.rsc.org/?DOI=C7EE01987D.

Sasanpour, S., Cao, K.-K., Gils, H. C., and Jochem, P. Strategic policy targets and the contribution of hydrogen in a 100% renewable European power system. *Energy Reports*, 7:4595–4608, Nov. 2021. ISSN 23524847. doi:10.1016/j.egyr.2021.07.005. URL https://linkinghub.elsevier.com/retrieve/pii/S2352484721004704.

Schlautmann, R., Böhm, H., Zauner, A., Mörs, F., Tichler, R., Graf, F., and Kolb, T. Renewable Power-to-Gas: A Technical and Economic Evaluation of Three Demo Sites Within the STORE&GO Project. *Chemie Ingenieur Technik*, 93(4):568–579, Apr. 2021. ISSN 0009-286X, 1522-2640. doi:10.1002/cite.202000187. URL https://onlinelibrary.wiley.com/doi/10.1002/cite.202000187. Publisher: Wiley.

Schlund, D. and Theile, P. Simultaneity of green energy and hydrogen production: Analysing the dispatch of a grid-connected electrolyser. *Energy Policy*, 166:113008, July 2022. ISSN 03014215. doi:10.1016/j.enpol.2022.113008. URL https://linkinghub.elsevier.com/retrieve/pii/S0301421522002336.

Schorn, F., Breuer, J. L., Samsun, R. C., Schnorbus, T., Heuser, B., Peters, R., and Stolten, D. Methanol as a renewable energy carrier: An assessment of production and transportation costs for selected global locations. *Advances in Applied Energy*, 3:100050, Aug. 2021. ISSN 26667924. doi:10.1016/j.adapen.2021.100050. URL https://linkinghub.elsevier.com/retrieve/pii/S2666792421000421.

Scott, I. J., Carvalho, P. M., Botterud, A., and Silva, C. A. Clustering representative days for power systems generation expansion planning: Capturing the effects of variable renewables and energy storage. *Applied Energy*, 253:113603, Nov. 2019. ISSN 03062619. doi:10.1016/j.apenergy.2019.113603. URL https://linkinghub.elsevier.com/retrieve/pii/S0306261919312772.

Simoes, S. G., Catarino, J., Picado, A., Lopes, T. F., Di Berardino, S., Amorim, F., Gírio, F., Rangel, C., and Ponce De Leão, T. Water availability and water usage solutions for electrolysis in hydrogen production. *Journal of Cleaner Production*, 315:128124, Sept. 2021. ISSN 09596526. doi:10.1016/j.jclepro.2021.128124. URL https://linkinghub.elsevier.com/retrieve/pii/S0959652621023428.

Sing, N., Mahali, K., and Roy, S. An Overview on Biofuels: Advantages and Disadvantages. In Karaman, P. R., editor, *Recent Developments in Chemistry and Biochemistry Research Vol. 7*, pages 98–118. BP International, Oct. 2024. ISBN 978-93-48119-10-0. doi:10.9734/bpi/rdcbr/v7/2778. URL https://stm.bookpi.org/RDCBR-V7/article/view/16014.

Slednev, V. Development of a techno-economic energy system model considering the highly resolved conversion and multimodal transmission of energy carriers on a global scale, 2024. URL https://publikationen.bibliothek.kit.edu/1000170863. Medium: PDF.

Slednev, V., Bertsch, V., Ruppert, M., and Fichtner, W. Highly resolved optimal renewable allocation planning in power systems under consideration of dynamic grid topology. *Computers & Operations Research*, 96:281–293, Aug. 2018. ISSN 03050548. doi:10.1016/j.cor.2017.12.008. URL https://linkinghub.elsevier.com/retrieve/pii/S0305054817303088.

Smith, A. and Klosek, J. A review of air separation technologies and their integration with energy conversion processes. *Fuel Processing Technology*, 70(2):115–134, May 2001. ISSN 03783820. doi:10.1016/S0378-3820(01)00131-X. URL https://linkinghub.elsevier.com/retrieve/pii/S037838200100131X.

Sodiq, A., Abdullatif, Y., Aissa, B., Ostovar, A., Nassar, N., El-Naas, M., and Amhamed, A. A review on progress made in direct air capture of CO 2. *Environmental Technology & Innovation*, 29:102991, Feb. 2023. ISSN 23521864. doi:10.1016/j.eti.2022.102991. URL https://linkinghub.elsevier.com/retrieve/pii/S235218642200414X.

Soliman, M. N., Guen, F. Z., Ahmed, S. A., Saleem, H., Khalil, M. J., and Zaidi, S. J. Energy consumption and environmental impact assessment of desalination plants and brine disposal strategies. *Process Safety and Environmental Protection*, 147:589–608, Mar. 2021. ISSN 09575820. doi:10.1016/j.psep.2020.12.038. URL https://linkinghub.elsevier.com/retrieve/pii/S0957582020319650.

Staiß, F., Schmidt, M., Stephanos, C., Stöcker, P., and Wurbs, S. Optionen für den Import grünen Wasserstoffs nach Deutschland bis zum Jahr 2030. Technical report, acatech - Deutsche Akademie der Technikwissenschaften, 2022. URL https://energiesysteme-zukunft.de/publikationen/materialien/transportoptionen-wasserstoff-2030. Artwork Size: 151 Medium: application/pdf.

Sterchele, P., Brandes, J., Heilig, J., Wrede, D., Kost, C., Schlegl, T., Bett, A., and Henning, H.-M. Wege zu einem klimaneutralem Energiesystem - Die deutsche Energiewende im Kontext gesellschaftlicher Verhaltensweisen, Feb. 2020. URL https://www.ise.fraunhofer.de/content/dam/ise/de/documents/publications/studies/ISE_WegeKlimaneutralEnergiesystem_final.pdf.

Sterner, M., Hofrichter, A., Meisinger, A., Bauer, F., Pinkwart, K., Maletzko, A., Dittmar, F., and Cremers, C. 19 Import options for green hydrogen and derivatives - An overview of efficiencies and technology readiness levels. *International Journal of Hydrogen Energy*, 90:1112–1127, Nov. 2024. ISSN 03603199. doi:10.1016/j.ijhydene.2024.10.045. URL https://linkinghub.elsevier.com/retrieve/pii/S0360319924042368.

Südwestrundfunk. Kein Gas ab 2035 in Mannheim: MVV-Ankündigung sorgt für Unruhe. Nov. 2024. URL https://www.swr.de/swraktuell/baden-wuerttemberg/mannheim/mvv-informiert-ueber-das-ende-des-gasnetzes-in-mannheim-2035-100.html.

Taie, Z., Peng, X., Kulkarni, D., Zenyuk, I. V., Weber, A. Z., Hagen, C., and Danilovic, N. Pathway to Complete Energy Sector Decarbonization with Available Iridium Resources using Ultralow Loaded Water Electrolyzers. *ACS Applied Materials & Interfaces*, 12(47):52701–52712, Nov. 2020. ISSN 1944-8244, 1944-8252. doi:10.1021/acsami.0c15687. URL https://pubs.acs.org/doi/10.1021/acsami.0c15687.

Tarkowski, R. and Uliasz-Misiak, B. Towards underground hydrogen storage: A review of barriers. *Renewable and Sustainable Energy Reviews*, 162:112451, July 2022. ISSN 13640321. doi:10.1016/j.rser.2022.112451. URL https://linkinghub.elsevier.com/retrieve/pii/S1364032122003574.

Teichgraeber, H. and Brandt, A. R. Clustering methods to find representative periods for the optimization of energy systems: An initial framework and comparison. *Applied Energy*, 239:1283–1293, Apr. 2019. ISSN 03062619. doi:10.1016/j.apenergy.2019.02.012. URL https://linkinghub.elsevier.com/retrieve/pii/S0306261919303022.

Tetik, H. and Kirkil, G. The Role of Hydrogen in the Energy Mix: A Scenario Analysis for Turkey Using OSeMOSYS. *Energies*, 17(24):6348, Dec. 2024. ISSN 1996-1073. doi:10.3390/en17246348. URL https://www.mdpi.com/1996-1073/17/24/6348.

The Royal Society. Ammonia: zero-carbon fertiliser, fuel and energy store - Policy briefing. Technical report, The Royal Society, Feb. 2020. URL https://royalsociety.org/-/media/policy/projects/green-ammonia/green-ammonia-policy-briefing.pdf.

Traverso, M., Petti, L., and Zamagni, A., editors. *Perspectives on Social LCA: Contributions from the 6th International Conference*. SpringerBriefs in Environmental Science. Springer International Publishing, Cham, 2020. ISBN 978-3-030-06564-5 978-3-030-01508-4. doi:10.1007/978-3-030-01508-4. URL http://link.springer.com/10.1007/978-3-030-01508-4.

Télessy, K., Barner, L., and Holz, F. Repurposing natural gas pipelines for hydrogen: Limits and options from a case study in Germany. *International Journal of Hydrogen Energy*, 80:821–831, Aug. 2024. ISSN 03603199. doi:10.1016/j.ijhydene.2024.07.110. URL https://linkinghub.elsevier.com/retrieve/pii/S0360319924027812.

Tüysüz, H. Alkaline Water Electrolysis for Green Hydrogen Production. *Accounts of Chemical Research*, 57(4):558–567, Feb. 2024. ISSN 0001-4842. doi:10.1021/acs.accounts.3c00709. URL https://doi.org/10.1021/acs.accounts.3c00709. Publisher: American Chemical Society.

Umweltbundesamt. Datentabelle zu den Treibhausgas-Emissionen 2024, Mar. 2025. URL https://www.umweltbundesamt.de/sites/default/files/medien/11867/dokumente/datentabelle_zu_den_treibhausgas-emissionen_2024.xlsx.

Umweltbundesamt. Erneuerbare Energien in Deutschland - Daten zur Entwicklung im Jahre 2024, 2025. URL https://www.umweltbundesamt.de/sites/default/files/medien/479/publikationen/hgp_erneuerbareenergien_2024.pdf.

Upadhyay, A., Tröndle, T., Ganter, A., Petkov, I., Gabrielli, P., and Sansavini, G. The role of energy storage towards net-zero emissions in the European electricity system. *Energy Conversion and Management*, 338:119887, Aug. 2025. ISSN 01968904. doi:10.1016/j.enconman.2025.119887. URL https://linkinghub.elsevier.com/retrieve/pii/S019689042500411X.

Vargas-Ferrer, P., Jalil-Vega, F., Pozo, D., and Sauma, E. Complying with low-emission hydrogen standards in long-term integrated supply chains. *Energy Policy*, 198:114504, Mar. 2025. ISSN 03014215. doi:10.1016/j.enpol.2025.114504. URL https://linkinghub.elsevier.com/retrieve/pii/S0301421525000114.

Velloso, A., Street, A., Pozo, D., Arroyo, J. M., and Cobos, N. G. Two-Stage Robust Unit Commitment for Co-Optimized Electricity Markets: An Adaptive Data-Driven Approach for Scenario-Based Uncertainty Sets. *IEEE Transactions on Sustainable Energy*, 11(2):958–969, Apr. 2020. ISSN 1949-3029, 1949-3037. doi:10.1109/TSTE.2019.2915049. URL https://ieeexplore.ieee.org/document/8706676/.

Verastegui, F., Lorca, A., Olivares, D. E., Negrete-Pincetic, M., and Gazmuri, P. An Adaptive Robust Optimization Model for Power Systems Planning With Operational Uncertainty. *IEEE Transactions on Power Systems*, 34(6):4606–4616, Nov. 2019. ISSN 0885-8950, 1558-0679. doi:10.1109/TPWRS.2019.2917854. URL https://ieeexplore.ieee.org/document/8718350/.

Wang, X. and Song, C. Carbon Capture From Flue Gas and the Atmosphere: A Perspective. *Frontiers in Energy Research*, 8:560849, Dec. 2020. ISSN 2296-598X. doi:10.3389/fenrg.2020.560849. URL https://www.frontiersin.org/articles/10.3389/fenrg.2020.560849/full.

Wang, Y., Qu, L., Ding, H., Webley, P., and Li, G. K. Distributed direct air capture of carbon dioxide by synergistic water harvesting. *Nature Communications*, 15(1):9745, Nov. 2024. ISSN 2041-1723. doi:10.1038/s41467-024-53961-4. URL https://www.nature.com/articles/s41467-024-53961-4.

Weber, C., Heidari, S., and Bucksteeg, M. Coping with Uncertainties in the Electricity Sector - Methods for Decisions of Different Scope. *Economics of Energy & Environmental Policy*, 10(1), Jan. 2021. ISSN 21605882. doi:10.5547/2160-5890.10.1.cweb. URL http://www.iaee.org/en/publications/eeepaticle.aspx?id=351.

Wetzel, M., Gils, H. C., and Bertsch, V. Green energy carriers and energy sovereignty in a climate neutral European energy system. *Renewable Energy*, 210:591–603, July 2023. ISSN 09601481. doi:10.1016/j.renene.2023.04.015. URL https://linkinghub.elsevier.com/retrieve/pii/S0960148123004639.

Wiese, F., Bramstoft, R., Koduvere, H., Pizarro Alonso, A., Balyk, O., Kirkerud, J. G., Tveten, G., Bolkesjø, T. F., Münster, M., and Ravn, H. Balmorel open source energy system model. *Energy Strategy Reviews*, 20:26–34, Apr. 2018. ISSN 2211467X. doi:10.1016/j.esr.2018.01.003. URL https://linkinghub.elsevier.com/retrieve/pii/S2211467X18300038.

Woods, P., Bustamante, H., and Aguey-Zinsou, K.-F. The hydrogen economy - Where is the water? *Energy Nexus*, 7:100123, Sept. 2022. ISSN 27724271. doi:10.1016/j.nexus.2022.100123. URL https://linkinghub.elsevier.com/retrieve/pii/S277242712200078X.

World resources institute. Water risk atlas, 2025. URL https://www.wri.org/aqueduct.

Yap, J. and McLellan, B. Exploring transitions to a hydrogen economy: Quantitative insights from an expert survey. *International Journal of Hydrogen Energy*, 66:371–386, May 2024. ISSN 03603199. doi:10.1016/j.ijhydene.2024.03.213. URL https://linkinghub.elsevier.com/retrieve/pii/S0360319924010528.

Zeng, B. and Zhao, L. Solving two-stage robust optimization problems using a column-and-constraint generation method. *Operations Research Letters*, 41(5):457–461, Sept. 2013. ISSN 01676377. doi:10.1016/j.orl.2013.05.003. URL https://linkinghub.elsevier.com/retrieve/pii/S0167637713000618.

Zeyen, E., Riepin, I., and Brown, T. Temporal regulation of renewable supply for electrolytic hydrogen. *Environmental Research Letters*, 19(2):024034, Feb. 2024. ISSN 1748-9326. doi:10.1088/1748-9326/ad2239. URL https://iopscience.iop.org/article/10.1088/1748-9326/ad2239.

Part II

Research Papers

Paper A:

Renewable origin, additionality, temporal and geographical correlation – eFuels production in Germany under the RED II regime

Uwe Langenmayr[a], Manuel Ruppert[a]
[a] Karlsruhe Institute of Technology (KIT), Chair of Energy Economics, Karlsruhe, Germany

Reference
Langenmayr, U. and Ruppert, M. Renewable origin, additionality, temporal and geographical correlation – eFuels production in Germany under the RED II regime. *Energy Policy*, 183:113830, Dec. 2023. ISSN 03014215. doi:10.1016/j.enpol.2023.113830. URL `https://linkinghub.elsevier.com/retrieve/pii/S0301421523004159`

Energy Policy 183 (2023) 113830

Contents lists available at ScienceDirect

Energy Policy

journal homepage: www.elsevier.com/locate/enpol

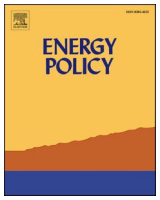

Renewable origin, additionality, temporal and geographical correlation – eFuels production in Germany under the RED II regime

Uwe Langenmayr *, Manuel Ruppert

Institute for Industrial Production, Karlsruhe Institute of Technology, Karlsruhe, Germany

ARTICLE INFO

Keywords:
eFuels
Renewable energy directive
Energy system analysis
Hydrogen
Synthesis

ABSTRACT

E-fuels are a promising technological option to reduce the carbon footprint in the transportation sector. To ensure the renewable origin of electricity-based fuels and minimize the impact of power-to-liquid facilities on the electricity grid, the European Union implemented electricity purchase conditions within the Renewable Energy Directive II. In this work, we analyze the impact of these electricity purchase conditions on the optimal placement, dimensioning and operation of facilities and the German electricity system. The results show that implementing the proposed electricity purchase conditions increases electrolysis capacity by 15.8% and reduces utilization by 672 h in 2030. With the constrained electricity supply, the power-to-liquid facilities concentrate on network nodes with high renewable potential, while the carbon dioxide supply loses importance. Overall, the German electricity system is not heavily affected by the proposed purchase conditions as the required renewable generation capacities only increase slightly. At the same time, carbon dioxide abatement costs rise by 14.3% by introducing the electricity purchase conditions.

1. Introduction

While the transition of the European electricity sector towards a lower carbon footprint is in full swing, changes in the industry, heat and transportation sectors are materializing at a much slower pace. In the transportation sector, rising transport volume and the increasing weight of passenger cars have led to growing greenhouse gas (GHG) emissions in recent years. Consequently, the European Union aims to increase the speed of transformation of the different sectors. The primary legislative implementation is the Renewable Energy Directive 2018/2001 (RED II) (European Union, 2022), which introduces a minimum share of renewable energies in final energy consumption within the transport sector of 14% by 2030. Germany aims to surpass this target and plans to achieve at least 28% renewable share within the same timeframe.

Electricity-based synthetic fuels (eFuels) are one viable technology that enables lower or even zero emissions for combustion-based mobility. Hydrogen is one of the starting products in the eFuels production process and is based on the electrolysis process, where water is split into hydrogen and oxygen using electricity. Hydrogen itself can be considered an eFuel, but it can also be processed into carbon-based eFuels for transportation like gasoline, diesel and kerosene. Here, carbon dioxide (CO_2) is obtained from local sources via CO_2 scrubbing or from the atmosphere via direct air capture (DAC). Different synthesis processes exist to convert the synthetic gas to eFuels, for example, the Fischer-Tropsch (FTS) process and the methanol-to-gasoline route. As such, eFuels can be considered a complementary technology to battery-electric transportation, and can play a significant role when meeting transportation needs where battery technology is not well suited. For example, battery storage is less favorable for long-distance (e.g., international aviation) and heavy-duty transportation (e.g., shipping). This is mainly due to the battery's low energy density, which requires large and thus heavy batteries for these types of transportation (Siegemund et al., 2017). Furthermore, as the passenger car fleet will still consist of a large amount of internal combustion engine vehicles in the future due to the inertia of the fleet (Luderer et al., 2021), eFuels might be the only alternative to achieve carbon neutrality within the existing fleet.

2. Background on the renewable energy directive II in the context of eFuel production

The Green Deal is the central climate policy initiative to achieve carbon neutrality by 2050 in the European Union. The initiative includes a 50–55% reduction of GHG emissions by 2030 compared to the GHG emission levels of 1990. The Green Deal also includes specific policy

* Corresponding author.
E-mail address: uwe.langenmayr@kit.edu (U. Langenmayr).

https://doi.org/10.1016/j.enpol.2023.113830
Received 29 September 2022; Received in revised form 4 September 2023; Accepted 21 September 2023
Available online 20 October 2023

proposals to reduce GHG emissions and increase the renewable energy share in all sectors. The European Union's adjustment of climate objectives was followed by revisions of existing policies. One of these policies, the RED II, established a legal framework and common principles to promote the use of renewable energy sources and an efficient energy system integration in the European Union. The vision of an integrated energy system includes all sectors, aiming to increase the renewable energy share not only in the electricity sector. One aspect of RED II assesses the different technologies in the transportation sector. It describes which and how technologies can be used within the integrated energy system, if quotas or limitations exist, and how national members of the European Union can use crediting systems to assess the contribution of the different technologies to national GHG reduction.

Today, eFuel production faces complex challenges. First, additional electrical demand from hydrogen production can lead to new or increased congestion in the electricity grid, especially when electricity demand from eFuel production and renewable electricity generation are spatially remote in a generally congested transmission grid environment. Second, to ensure the renewable property of eFuels, electricity needs to stem primarily or exclusively from renewable energy sources and should not lead to higher GHG emissions than the utilization of conventional fuels.

In RED II, the European Commission proposed a catalogue of requirements in Art.27(3) to assess eFuels as renewable fuels of non-biological origin (RNFBO). On one hand, the production of eFuels with grid-independent renewable energy sources (RES) is regulated in Art.4(1). This option is especially reasonable if high potentials of RES exist and eFuel production does not collide with other renewable energy targets. On the other hand, grid-connected eFuel production is defined in Art.4(2). Here, the RFNBO status is achieved if the renewable energy share in the bidding zone is at least 90% in the last calendar year and the operation time of the electrolysis does not exceed the time with renewable generation. Alternatively, sourcing electricity from the grid is possible if the emission intensity of the electricity is lower than 18 gCO_2eq/MJ.

Grid-connected eFuel production that is RFNBO-compatible is also possible in bidding zones with a lower share of renewable energy, but the requirements are more comprehensive. In the aforementioned case, the RFNBO status can be achieved by obtaining a private purchase agreement for the required amount of electricity while meeting other electricity purchase conditions. Art.4(2)(a) determines that the RES must be commissioned within the last 36 months before the commissioning of the electrolysis unit. We refer to this limitation as the additionality constraint. Art.4(2)(b) excludes all generation from RES which has received previous subsidies. The temporal correlation condition in Art.4(2)(c) specifies that for all facilities starting production before 2030 the electricity consumption of the electrolysis does not exceed the total electricity generation of the RES within the same month. From the year 2030 on, the requirement for the temporal correlation condition changes to an hourly matching requirement. Optionally, the tightening of the correlation condition can be adopted by member states even before 2030. An increase of electrolysis utilization by using electricity storage is a suitable solution considered in the proposal. Exceptions exist if the price falls below a certain level (20 €/MWh or 0.36 times the CO_2 certificate price in the respective hour). Finally, Art.4(2)(d) defines the geographical correlation. Electrolysis and RES generation must be located in the same bidding zone. Alternatively, generation can be sourced from either adjacent bidding zones with equal or higher day-ahead prices at times of electricity consumption or in adjacent offshore bidding zones. Art.27(3)(12) mentions that the requirements for spatial alignment of generation and electrolysis aim at avoiding increased congestion between electric sources and sinks in the transmission network. The presented electricity purchase criteria apply for all electrolysis units from January 1, 2027.

As the electricity purchase conditions target the placement of both new RES and electrolysis, they influence the resulting optimal placement, dimensioning and operation of eFuels production facilities. In this work, we examine two aspects of the RED II implementation: The impact of the different electricity purchase conditions on the eFuels production like capacities and capacity factors of the different components, the effect of the resulting eFuels production on the energy system in regards to generation capacities and their distribution, and finally the CO_2 abatement costs. The structure of the paper is as follows: The second chapter covers the existing literature on sector coupling approaches, including eFuels production, and presents the contributions this study will answer. The literature chapter is followed by a description of the methodology, which consists of the energy system model, the implemented eFuels production structure and the electricity purchase conditions. The case study chapter describes the considered scenarios, CO_2 sources and energy system data, and the eFuels demand. The results for the German electricity system are presented and discussed in the following chapter, followed by the policy implications of our results and a conclusion.

3. Literature review

Studies in the field of sector coupling focus either on scales like buildings (Wang et al., 2018), cities (Dahal et al., 2018; Heinisch et al., 2021; Nevens and Roorda, 2014), single countries (Bogdanov et al., 2021; Gudmundsson et al., 2018; Gils et al., 2021; Seljom and Rosenberg, 2018; Pensini et al., 2014; Kiviluoma and Meibom, 2011; Schill and Gerbaulet, 2015; Osorio-Aravena et al., 2021) or even several countries at the same time (Brown et al., 2018; Ashfaq et al., 2017; Meibom et al., 2007; Gea-Bermúdez et al., 2021; Blanco et al., 2018b; Capros et al., 2019; Pavičević et al., 2020; Helgeson and Peter, 2020). A distinction is also possible based on modelled coupled sectors such as transportation (Brand et al., 2012; Plötz et al., 2019; Kiviluoma and Meibom, 2011; Schill and Gerbaulet, 2015; Heinisch et al., 2021; Helgeson and Peter, 2020), heating (Gudmundsson et al., 2018; Bogdanov et al., 2021; Pensini et al., 2014; Meibom et al., 2007; Ashfaq et al., 2017; Jimenez-Navarro et al., 2020), or multi-sector approaches (Bogdanov et al., 2021; Brown et al., 2018; Osorio-Aravena et al., 2021; Gea-Bermúdez et al., 2021; Gils et al., 2021; Blanco et al., 2018b; Capros et al., 2019; Pavičević et al., 2020). An exhaustive review of differences and similarities among energy system analyses including sector coupling can be found in Hansen et al. (2019), Ramsebner et al. (2021) and Hanley et al. (2018).

The analysis of the effect of eFuels production in energy systems is still relatively limited (Ramsebner et al., 2021). Blanco et al. (2018a) examined the European energy system with the TIMES energy system model to research the potential of hydrogen and power-to-liquid (PtL). The approach consisted of conducting a systematic parameter analysis with several scenarios to research the development of different hydrogen and hydrocarbon technologies in a low-carbon energy system. The study of a carbon-neutral European energy system was conducted by Capros et al. (2019) using the PRIMES model with different decarbonization scenarios. Their aim was to examine the EU 2030 climate and energy framework, the viability, sustainability and affordability of carbon-neutrality by 2050, and necessary policies to achieve the carbon neutrality objective. Mesfun et al. (2017) used the mixed-integer linear energy system BeWhere Alps to examine the ability of Power-to-Gas and PtL processes to improve the integration of intermittent renewable energy generation in the Alpine region. Quarton and Samsatli (2020) used the mixed-integer programming software Value Web Model to optimize the complete carbon capture utilization (CCU) and storage value chain, including PtL. The energy system model Balmorel was used by Gea-Bermúdez et al. (2021) to minimize the discounted system costs of Northern-central Europe to investigate the role of sector coupling in the future energy system. Helgeson and Peter (2020) developed a multi-sector model to investigate the transition of the transport sector and the necessary interaction between European countries to achieve low-carbon transportation. They included several sector-linking

components to analyze the future role of power-to-x technologies, including PtL. The above-mentioned studies implement PtL facilities without consideration of the facilities' flexibility and subsequent limitations. Generally, the flexibility of PtL facilities is low compared to that of electrolysis units (Bogdanov et al., 2021). Assuming high flexibility might result in underestimated impact on the energy system (e.g., necessity of storage, inflexible demand). For Kazakhstan (Bogdanov et al., 2021) and Chile (Osorio-Aravena et al., 2021), PtL flexibility is considered and used in a linear programming energy system model to minimize the annual costs of the energy system, including industry, heat, transportation, and power sector. Based on these results, PtL processes result in additional base load due to their inflexibility. To our knowledge, no sector-coupling model considers the impact of electricity purchase conditions or describes the operation of PtL facilities with regards to their impact on the energy system in detail.

Complementary to large-scale energy system models, a quantitative analysis of the effects of temporal correlation between hydrogen production and electricity generation to electrolysis operation was conducted by Schlund and Theile (2022). Here, a mixed-integer Markov Chain model with different interval lengths of simultaneity was applied. Similarly, Ruhnau and Schiele (2022) analyzed a wind-hydrogen system and optimized the investment and operation under different regulations. The results showed that strict regulations will result in large over-investments to increase electrolysis utilization and might slow down the green hydrogen deployment. Both approaches investigated green hydrogen production on a single unit scale and did not give consideration to large energy system models.

Next to sector coupling models, qualitative analyses of electricity purchase conditions have already been conducted based on the example of the RED II directive. Scheelhaase et al. (2019) state that the development, production and use of eFuels for aviation need a regulatory framework to reduce the uncertainty of investors. Such regulations have not been implemented and RED II might be the basis for the implementation of national laws. Chiaramonti and Goumas (2019) qualitatively analyzed RED II regarding its impact on renewable fuels including advanced biofuels, recycled carbon fuels and RFNBOs. They state that RED II is not technology-neutral towards eFuels compared to electric mobility. In comparison, eFuels can be refused by EU member states or might have constraining electricity purchase conditions like the additionality or the temporal correlation with the electricity generation. They conclude that the current framework does not provide a sufficient investment environment for eFuels and that the development of future regulations will delay large-scale eFuel production.

In existing literature, no studies consider both eFuels production on an energy system level and the associated legislative implementation. On one hand, studies focusing on sector coupling including PtL do not consider the regulations of eFuels production. Their results lack a detailed representation of the actual operation of PtL facilities and their impact on the energy system. Other quantitative studies focus on single electrolysis units and their optimal individual operation, without considering the energy system integration in the context of sector coupling. On the other hand, the impact of RED II has been investigated by qualitative studies so far without any quantitative assessments. In this work, we contribute to existing research, as we present a set of feasible constraints that enables the implementation of electricity purchase conditions into an energy system model.

4. Methodology

PyPSA parameter and variables

Parameter/ variable	Unit	Description
i,j		Bus labels
u		Individual unit label for each generator and storage unit

(continued on next column)

(continued)

PyPSA parameter and variables

Parameter/ variable	Unit	Description
y		Installation year of unit
l		Branch labels
t		Snapshot /time step labels
ω_t	h	Weighting of snapshot t in objective function
$g_{u,i,y,t}$	MW	Dispatch of unit
$C_{u,i,y}$	MW	Capacity of generator
$\overline{g}_{u,i,y,t}$		Availability per unit of generator capacity
$\eta_{u,i,y}$		Efficiency of unit
$ru_{u,i,y}$	1/h	Generator ramp up limit per unit of capacity
$rd_{u,i,y}$	1/h	Generator ramp down limit per unit of capacity
$c^{fix}_{u,i,y}$	€/MW	Fixed costs
$c^{var}_{u,i,y}$	€/MWh	Variable cost
$e_{u,i,y,t}$	MWh	Storage state of charge (energy level)
$E_{u,i,y}$	MWh	Storage energy capacity
$g^{in}_{u,i,y,t}$	MW	Inflow of storage unit
$g^{spil}_{u,i,y,t}$	MW	Spillage of storage unit
$d_{i,t}$	MW	Electricity demand
$f_{l,t}$	MW	Branch active power flow
F_l	MW	Branch active power rating
c^{fix}_l	€/MW	Branch fixed cost
$\eta_{l,t}$		Efficiency loss of a branch
x_l		Reactance of line
$M_{l,c}$		Cycle matrix (here, c represents cycle label)
$K_{i,l}$		Incidence matrix
π_y		Share of renewable generation
$C^{EC,lim}_y$	MW	Capacity limitation of energy carrier

Additional parameters and variables of the eFuels production

Parameter/ variable	Unit	Description
α		Scrubber unit labels
β		Direct air capture unit labels
γ		Electrolysis unit labels
δ		Synthesis unit labels
$m^{FG,PS}_{i,t}$	$t_{flue\ gas}$	Dispatch of flue gas point source
$C_{i,FG}$	$t_{flue\ gas}$ /h	Capacity of flue gas point source
$m^{CO_2,PS}_{i,t}$	t_{CO2}	Dispatch of CO_2 point source
C_{i,CO_2}	t_{CO2} /h	Capacity of CO_2 point source
$m_{\alpha,i,y,t}$	$t_{flue\ gas}$	Dispatch of scrubber unit
$C_{\alpha,i,y}$	$t_{flue\ gas}$ /h	Capacity of scrubber unit
$c^{fix}_{\alpha,i,y}$	€/$t_{flue\ gas}$ * h	Fixed costs of scrubber unit
$c^{var}_{\alpha,i,y}$	€/$t_{flue\ gas}$	Variable cost of scrubber unit
$\mu_{\alpha,i,y}$		Lower bound capacity utilization of scrubber unit
$\eta^{FG,CO_2}_{\alpha,i,y}$		Conversion efficiency scrubber
$m^{CO_2,SC}_{i,t}$	t_{CO2}	CO_2 production from scrubber units
$p_{\beta,i,y,t}$	MW	Dispatch of DAC unit
$C_{\beta,i,y}$	MW	Capacity of DAC unit
$c^{fix}_{\beta,i,y}$	€/MW	Fixed costs of DAC unit
$c^{var}_{\beta,i,y}$	€/MWh	Variable cost of DAC unit
$\mu_{\beta,i,y}$		Lower bound capacity utilization of DAC unit
$\eta^{EL,CO_2}_{\beta,i,y}$		Conversion efficiency DAC
$m^{CO_2,DAC}_{i,t}$	t_{CO2}	CO_2 production from DAC units
$m^{CO_2}_{i,t}$	t_{CO2}	Total CO_2 production
$p_{\gamma,i,y,t}$	MW	Dispatch of electrolysis unit
$C_{\gamma,i,y}$	MW	Capacity of electrolysis unit
$c^{fix}_{\gamma,i,y}$	€/MW	Fixed costs of electrolysis unit
$c^{var}_{\gamma,i,y}$	€/MWh	Variable cost of electrolysis unit
$\mu_{\gamma,i,y}$		Lower bound capacity utilization of DAC unit
$\eta^{EL,H_2}_{\gamma,i,y}$		Conversion efficiency electrolysis
$p^{H_2}_{t,i}$	MWh	Total hydrogen production
$p^{H_2}_{\delta,i,y,t}$	MWh	Hydrogen dispatch of synthesis unit
$C_{\delta,i,y}$	MWh	Capacity of synthesis unit
$c^{fix}_{\delta,i,y}$	€/MW	Fixed costs of synthesis unit
$c^{var}_{\delta,i,y}$	€/MWh	Variable cost of synthesis unit

(continued on next page)

(*continued*)

Additional parameters and variables of the eFuels production		
Parameter/ variable	Unit	Description
$\mu_{\delta,i,y}$		Lower bound capacity utilization of synthesis unit
$\eta^{H_2,F}_{\delta,i,y}$		H_2 Conversion efficiency FTS
$m^{CO_2}_{\delta,i,y,t}$	t_{CO2}	CO_2 dispatch of synthesis unit
$\eta^{CO_2,F}_{\delta,i,y}$		CO_2 Conversion efficiency FTS
$p^{F}_{\delta,i,y,t}$	MWh	Fuel dispatch of synthesis unit
$p^{F}_{i,t}$	MWh	Total fuel production
$D^{F,tot}_{y}$	MWh	Total fuel demand
Sets		
GEN		Generators
EC		Energy carrier
HC		Hard coal power plants
RES		Renewable energy sources
HS		Hydrogen storage

4.1. Description of the energy system model

In this paper, we use the open-source energy system toolbox PyPSA (Brown et al., 2018) and the PyPSA-EUR workflow (Hörsch et al., 2018a) to implement the fundamental energy system model which we then extend to account for eFuels. PyPSA allows several applications, including ones considering electricity network restrictions based on a DC formulation using a linearized optimal power flow.

While the framework used only allows for the optimization of a static timeframe with multiple time steps, the investigation of the effect of electricity purchase conditions on the energy system requires the consideration of multiple linked years. Thus, the existing formulation is extended by a subsequent multi-year implementation to analyze the development of the energy system over the considered time frame using multiple optimization years. The implementation of the time coupling process is shown in Fig. 1. The model extension allows the detailed investigation of expansion planning of the grid, electricity generation, and eFuels production over a multi-year time horizon under the consideration of the interconnection between installation times of renewable energies and electrolysis units.

4.1.1. Objective function

In PyPSA, the total annual system costs are minimized. The system cost contains variable and fixed costs of generation, storage and transmission. In addition, we consider the capital and operating costs of eFuel production. Unit commitment is not considered. The objective function is given by Equation (1).

$$\min \sum_{l} c^{fix}_{l} \bullet F_{l} + \sum_{i}\sum_{y}\left(\sum_{u}\left(C_{u,i,y} \bullet c^{fix}_{u,i,y} + \sum_{t}\omega_{t} \bullet g_{u,i,y} \bullet c^{var}_{u,i,y}\right) + \sum_{\alpha}\left(C_{\alpha,i,y} \bullet c^{fix}_{\alpha,i,y} + \sum_{t}\omega_{t} \bullet m_{\alpha,i,y,t} \bullet c^{var}_{\alpha,i,y}\right) + \sum_{\beta}\left(C_{\beta,i,y} \bullet c^{fix}_{\beta,i,y} + \sum_{t}\omega_{t} \bullet p_{\beta,i,y,t} \bullet c^{var}_{\beta,i,y}\right) + \sum_{\gamma}\left(C_{\gamma,i,y} \bullet c^{fix}_{\gamma,i,y} + \sum_{t}\omega_{t} \bullet p_{\gamma,i,y,t} \bullet c^{var}_{\gamma,i,y}\right) + \sum_{\delta}\left(C_{\delta,i,y} \bullet c^{fix}_{\delta,i,y} + \sum_{t}\omega_{t} \bullet p^{H_2}_{\delta,i,y,t} \bullet c^{var}_{\delta,i,y}\right)\right) \quad (1)$$

4.1.2. Constraints

To model the technical constraints of the basic electrical components of the energy system, Equations (2)–(8) are used. In the case of generators and storages, Eq. (2) describes the lower and upper limit of the generator dispatch. In the case of RES generators, $\bar{g}_{u,i,y,t}$ describes the availability of the renewable energy at the location at each time step. The capacities of the generators are limited by lower and upper capacity limits (3). This equation accounts for renewable generators limited by renewable potential at the location. Eq. (4) defines the ramp-up and ramp-down limitations of the generator dispatch.

$$\underline{g}_{u,i,y,t} \bullet C_{u,i,y} \leq g_{u,i,y,t} \leq \bar{g}_{u,i,y,t} \bullet C_{u,t} \forall u, i, y, t \quad (2)$$

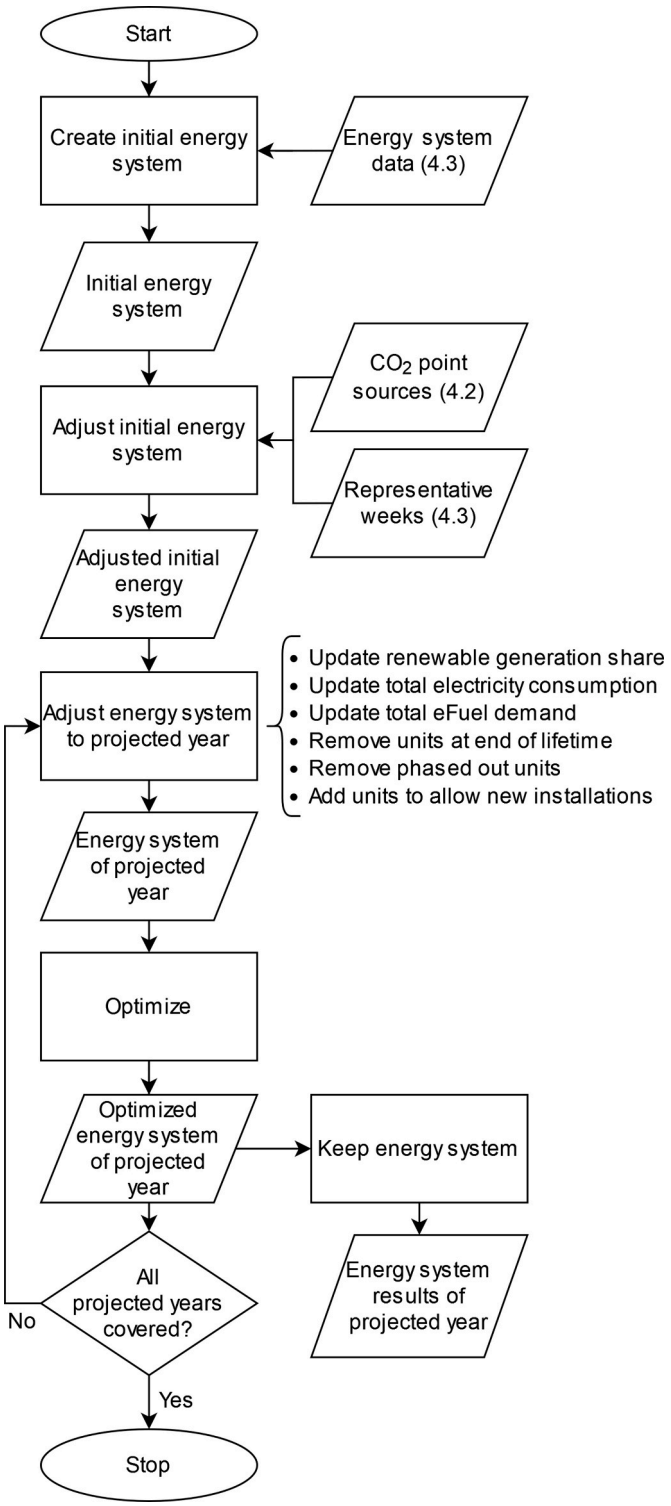

Fig. 1. Flow chart of the time coupling process.

$$\widetilde{C}_{u,i,y} \le \sum_{y} C_{u,i,y} \le \overline{C}_{u,i,y} \forall u, i \tag{3}$$

$$-rd_{u,i,y} \bullet C_{u,i,y} \le \left(g_{u,i,y,t} - g_{u,i,y,t-1}\right) \le ru_{u,i,y} \bullet C_{u,i,y} \forall u, i, y, t > 1 \tag{4}$$

For each time step, the energy level of the previous time step, the charging and discharging, as well as inflows and spillage are taken to calculate the energy level of a storage unit at the current time step (5). Eq. (6) defines the range of the energy level of each storage.

$$e_{u,i,y,t} = \eta_{u,i,y,0}^{\omega_t} \bullet e_{u,i,y,t-1} + \eta_{u,i,y,+} \bullet \omega_t \left[g_{u,i,y,t}\right]^{+} - \eta_{u,i,y,-}^{-1} \bullet \omega_t \left[g_{u,i,y,t}\right]^{-} + \omega_t \bullet g_{u,i,y,t}^{in} - \omega_t \bullet g_{u,i,y,t}^{spil} \forall u, i, y, t \tag{5}$$

$$\widetilde{e}_{u,i,y,t} \bullet E_{u,i,y} \le e_{u,i,y,t} \le \overline{e}_{u,i,y,t} \bullet E_{u,i,y} \forall u, i, y, t \tag{6}$$

Kirchhoff's current law is implemented in the energy system balance using Eq. (7). It ensures that the inelastic demand is covered by the total generator dispatch, the storage dispatch, and the flows through branches, differentiated in controllable links and passive lines from other buses at every bus and at each time step (Frysztacki et al., 2021).

$$\sum_{u} g_{u,i,y,t} + \sum_{l} K_{il} f_{l,t} = d_{i,t} \forall i, l, y, t \tag{7}$$

The link and line dispatch are limited by time-dependent availability ($\widetilde{f}_{l,t} = -1$ and $\overline{f}_{l,t} = 1$ in the case of lines) and the respective capacity (8).

$$\widetilde{f}_{l,t} \bullet F_l \le f_{l,t} \le \overline{f}_{l,t} \bullet F_l \forall l, t \tag{8}$$

Finally, Kirchhoff's voltage law is implemented with Eq. (9). The linear load flow implementation allows for a good approximation of the transmission network and the implementation, as cycle constraints have a lower computational effort compared to angle- or PTDF-based formulations (Hörsch et al., 2018b; Frysztacki et al., 2021).

$$\sum_{l} M_{l,c} \bullet x_l \bullet f_{l,t} = 0 \forall c, t \tag{9}$$

To extend on the fundamental model described in this section, additional constraints to specify the energy system's transition path are implemented. Eq. (10) limits the total capacity of generators that use a specific energy carrier. This equation allows for the implementation of a national policy aimed at reducing electricity generation from certain energy carriers. Eq. (11) further restricts the transition pathway towards renewable energy sources by defining a lower bound for renewable electricity generation share of π_y. Both parameters, the capacity limit of generators ($C_y^{EC,lim}$) and the renewable electricity generation share (π_y) depend on the currently processed projected year.

$$C_y^{EC,lim} \ge \sum_{u}^{U \in EC} \sum_{i} \sum_{y} \overline{C}_{u,i,y} \forall y \tag{10}$$

$$\pi_y \sum_{u}^{U \in GEN} \sum_{i} \sum_{y} \sum_{t} \left(g_{u,i,y,t} \bullet \omega_t\right) \le \sum_{u}^{U \in RES} \sum_{i} \sum_{y} \sum_{t} \left(g_{u,i,y,t} \bullet \omega_t\right) \tag{11}$$

4.2. eFuel production

The following chapter introduces the considered PtL route and describes its implementation in the overall modelling framework. One mandatory element of the eFuels production is the provision of CO_2. We assume that CO_2 can be obtained from point sources and DAC. Point sources have the advantage that the emitted flue gas consists of a high concentration of CO_2 or pure CO_2. Their limitation is the capacity of the point source. DAC, on the other side, allows CO_2 supply from ambient air, which provides the possibility to gather much larger quantities of CO_2. However, the lower CO_2 concentration in the air results in higher energy demands for the separation process. Scrubber units and DAC are assumed low-temperature units, allowing for heat utilization of the synthesis processes without further heat supply. The second input for eFuels production is hydrogen. Here, we model the electrolysis as a polymer electrolyte membrane (PEM), as this technology is able to react immediately to volatile electricity generation and the output hydrogen has a favorable pressure level for the following synthesis steps. The actual synthesis is implemented as a single component. This component includes the supply of synthesis gas via reverse water-gas shift reaction, the FTS step to produce the syncrude, and the product processing in the hydrocracker. The process is connected to the electricity grid and a battery storage unit can be used for more flexibility either in the energy system or the PtL process. Fig. 2 depicts the implemented PtL process.

Similar to generators, the output of the CO_2 point source m is limited by the capacity of the point source. Ramp-up and ramp-down constraints, or dispatch limitations, are not applied, as it is assumed that excess flue gas or CO_2 can be emitted if necessary. Eqs. (12) and (13) describe the limiting constraints.

$$0 \le m_{i,t}^{FG,PS} \le C_{i,flue\ gas} \forall i, t \tag{12}$$

$$0 \le m_{i,t}^{CO_2,PS} \le C_{i,CO_2} \forall i, t \tag{13}$$

The DAC utilization is limited by the capacity of the DAC (14). Heat demand is not considered as it can be covered by the exothermal reactions of the synthesis units. Furthermore, ambient air is sufficiently available and, therefore, excluded in the optimization program. The electricity consumption of the DAC unit is taken into account with Eq. (15). This demand originates mainly from the operation of the ventilators that direct the ambient air through the separation unit.

$$0 \le p_{\beta,i,y,t} \le C_{\beta,i,y} \forall \beta, i, y, t \tag{14}$$

$$m_{i,t}^{CO_2\ from\ DAC} = \sum_{\beta} \sum_{y} \left(p_{\beta,i,y,t} \bullet \eta_{\beta,i,y}^{El,CO_2}\right) \forall i, t \tag{15}$$

Similar to the utilization limitation in the case of DAC units, CO_2 scrubber units are limited as well (16). The total production of CO_2 from the scrubber units at each bus depends on the used flue gas and the conversion factor (17). Heat demand, again, is not considered. Eq. (18) limits the flue gas used by the scrubber units to the total available flue gas of all point sources at each hour and each bus. The total volume of CO_2 available at each hour and each bus is modelled in Eq. (19). The equation describes the contribution of CO_2 from DAC, point sources with scrubber unit, and point sources with direct CO_2 emissions to the total CO_2 available.

$$0 \le m_{\alpha,i,y,t}^{FG,PS} \le C_{\alpha,i,y} \forall \alpha, i, y, t \tag{16}$$

$$m_{i,t}^{CO_2,SC} = \sum_{\alpha} \sum_{y} \left(m_{\alpha,i,y,t}^{FG,PS} \bullet \eta_{\alpha,i,y}^{FG,CO_2}\right) \forall i, t \tag{17}$$

$$m_{i,t}^{FG,PS} = \sum_{\alpha} \sum_{y} m_{\alpha,i,y,t}^{FG,PS} \forall i, t \tag{18}$$

$$m_{i,t}^{CO_2} = m_{i,t}^{CO_2,PS} + m_{i,t}^{CO_2,SC} + m_{i,t}^{CO_2,DAC} \forall i, t \tag{19}$$

The operation of the electrolysis is described with Eq. (20) and Eq. (21). Eq. (20) describes the dispatch limitation of the electrolysis. Due to the high flexibility of electrolysis, the operation of the unit is only constrained by its capacity. Eq. (21) treats the conversion of electricity to hydrogen by implementing the efficiency of the electrolysis. The conversion of distilled water to hydrogen is not covered. Instead, the costs of distilled water is included in the operational costs of the electrolysis.

$$0 \le p_{\gamma,i,y,t} \le C_{\gamma,i,y} \forall \gamma, t, y, t \tag{20}$$

$$p_{i,t}^{H2} = \sum_{\gamma} \sum_{y} \left(p_{\gamma,i,y,t} \bullet \eta_{\gamma,i,y}^{El,H_2}\right) \forall i, t \tag{21}$$

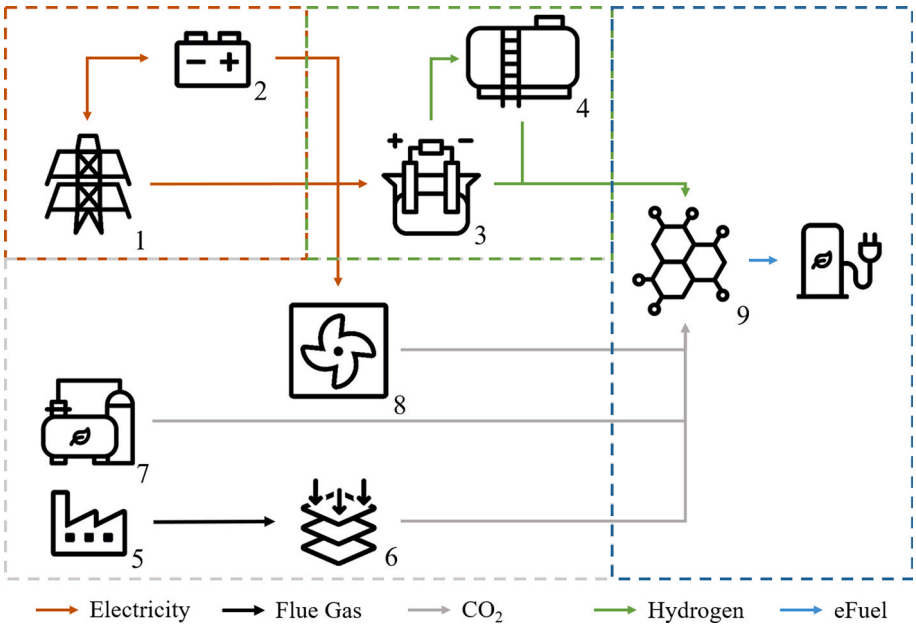

Fig. 2. Schematic structure of the power-to-liquid Fischer-Tropsch route comprising the energy system (1), battery storage (2), PEM electrolysis (3), hydrogen storage (4), flue gas point sources (5), scrubber unit (6), direct CO_2 point sources (7), direct air capture unit (8) and synthesis unit (9). The different arrow colors represent the different energy and mass flows: orange represents electricity, green represents hydrogen, black represents flue gas, grey represents CO_2 and blue represents eFuel.

Eq. (22) implements the dispatch limitation of the synthesis unit. The conversion of hydrogen to fuel is covered in Eq. (23). To connect the synthesis unit to the hydrogen storage and electrolysis, Eq. (24) balances the hydrogen at the bus using hydrogen production and consumption, and storage dispatch. Similar to the hydrogen, CO_2 conversion is covered in Eq. (25). As no CO_2 storage exists, only CO_2 production and consumptions needs to be balanced at each time step. This is implemented with Eq. (26). Finally, the total fuel production at the bus and time step is calculated using Eq. (27).

$$\mu_{\delta,i,y} \bullet C_{\delta,i,y} \leq p^{H_2}_{\delta,i,y,t} \leq C_{\delta,i,y} \forall \delta, i, y, t \tag{22}$$

$$p^{F}_{\delta,i,y,t} = p^{H_2}_{\delta,i,y,t} \bullet \eta^{H_2,F}_{\delta,i,y} \forall \delta, i, y, t \tag{23}$$

$$p^{H_2}_{i,t} + \sum_{u}^{U \in HS} \sum_{y} g_{u,i,y,t} = \sum_{\delta} \sum_{y} p^{H_2}_{\delta,i,y,t} \forall i, t \tag{24}$$

$$p^{F}_{\delta,i,y,t} = m^{CO_2}_{\delta,i,y,t} \bullet \eta^{CO_2,F}_{\delta,i,y} \forall \delta, i, y, t \tag{25}$$

$$m^{CO_2}_{i,t} = \sum_{\delta} \sum_{y} m^{CO_2}_{\delta,i,y,t} \forall i, t \tag{26}$$

$$p^{F}_{i,t} = \sum_{\delta} \sum_{y} p^{F}_{\delta,i,y,t} \forall i, t \tag{27}$$

The total yearly eFuels production of the FTS units has to be equal or larger than the total yearly demand. This constraint is implemented with Eq. (28). As hydrogen cannot be obtained from sources other than electrolysis, and CO_2 cannot be obtained from sources other than DAC, flue gas scrubber units or direct CO_2 sources, this constraint will force the optimization to calculate the optimal capacities of storages, electrolysis, CO_2 supply, and synthesis units. Additionally, the dispatch is optimized to cover the eFuels demand set in this constraint.

$$D^{F,tot}_{y} \leq \sum_{i} \sum_{t} p^{F}_{i,t} \bullet \omega_t \forall y \tag{28}$$

4.3. Electricity purchase condition constraints and implementation methods

The primary intention of this approach is to analyze the impact of electricity purchase conditions in eFuel production and the energy system. Thus, in the following subchapter we explain the implementation of the purchase conditions of origin, additionality and correlation into the presented approach.

4.3.1. Renewable origin

If the PtL facility is grid-connected, Art.4(2) defines that power purchase agreements have to be contracted to ensure the renewable origin of the eFuel. In the model formulation described above, all PtL facilities are grid-connected. Therefore, it is assumed that power purchase agreements are used for all PtL facilities.

4.3.2. Element of additionality

Eq. (11) defines that at least the share π_y of the total electricity generation is covered by renewable generation. Following only this system boundary, it would not be necessary to cover electricity demand of electrolysis units with renewable energy entirely, which does not fulfill the renewable origin criteria as a purchase criteria. Therefore, electricity consumption of electrolysis units is added to the total renewable share objective with share $(1 - \pi_y)$. This increased share satisfies two requirements simultaneously because the element of additionality as the increased electricity demand, caused solely by the electrolysis units, will be covered entirely by RES. If the electricity purchase conditions are considered, Eq. (29) replaces Eq. (11) which leads to the previously described result of fulfilling the element of additionality.

$$\pi_y \sum_{u}^{U \in GEN} \sum_{i} \sum_{y} \sum_{t} (g_{u,i,y,t} \bullet \omega_t) + (1 - \pi_y) \sum_{\gamma} \sum_{i} \sum_{y} \sum_{t} (p_{\gamma,i,y,t} \bullet \omega_t) \leq \sum_{u}^{U \in RES} \sum_{i} \sum_{y} \sum_{t} (g_{u,i,y,t} \bullet \omega_t) \tag{29}$$

4.3.3. Temporal and geographical correlation

The placement of RES generation and PtL facility in the same bidding zone is one way of defining the geographical correlation in the European electricity market. This market is characterized by multiple bidding zones which borders should largely align with congested lines of the transmission system. In this context, congestions between the supply and demand of electricity should be avoided by restricting the investment of RES generation and PtL to the same bidding zone. Currently, unified pricing areas like Germany are subject to internal congestions and are resolving these with measures of congestion management after the market has been cleared. Therefore, the approach using only bidding zones does not fully satisfy the requirements in situations where significant congestion occurs within a bidding zone. While the current legislative proposal on a European basis does not go beyond the definition of geographical correlation on bidding zone level, it seems reasonable to assume that additional constraints which further restrict placement of RES generation and PtL location will be implemented in countries with internal grid congestion like Germany. Thus, we model the geographical correlation in a more restricting way based on a nodal correlation approach. This can be achieved by limiting electrolysis electricity consumption in a network node to the available RES generation at the same network node. While this approach can be considered as a significant exceedance of the zonal restriction, it provides a much more efficient boundary to achieve the goal of the geographical correlation as a purchase condition in Europe during the transition phase towards a carbon neutral energy system.

Electrolysis units present the issue that uncontrolled electricity consumption could stress the electricity grid additionally. In addition, unconstrained electricity consumption might result in high carbon footprints of the produced hydrogen if the production takes place during hours with a high share of electricity generation from carbon-based energy carriers. The temporal correlation requirement aims to avoid both challenges. It constrains the electricity consumption of electrolysis to the electricity generation from the associated RES on an hourly basis.

Eq. (30) shows the combined temporal and geographical correlation constraint. For each network node and hour step, electricity consumption of electrolysis units at the same bus has to be smaller than or equal to electricity generation from RES at this bus. In addition, electricity consumption of electrolysis units is constrained to RES capacities that have been installed in the same projected year (considering y), adhering the electricity purchase to the additionality constraint.

$$\sum_{\gamma} p_{\gamma,i,y,t} \leq \sum_{u}^{RES} g_{u,i,y,t} \forall i,t,y \tag{30}$$

5. Case study

5.1. Scenarios

The case study consists of three scenarios, which all are investigated using the optimization approach described in Chapter 3. The three scenarios differ regarding eFuel production objective and the set of applied electricity purchase conditions. The first scenario depicts the reference case and uses neither eFuel production objectives nor electricity purchase conditions. The results can be considered as the benchmark energy system which results from no future requirement for eFuel production and subsequently no conditions for such production. The benchmark results will be used to discuss changes following the eFuel production implementation in the two other scenarios. In the second scenario, *No-RED*, the eFuel production objective is implemented as a constraint (Eq. (28)) to assure production of the desired amount of eFuels while electricity purchase conditions are not applied. Lastly, in the third scenario, *RED*, the eFuel production objective and electricity purchase conditions constraints proposed in the legislation of RED II are both added with the subsequent restrictions to the performed optimization. Here, the electricity purchase conditions apply for the projected years 2025 and 2030 to account for the transitional phase. Additionally, we implement this scenario with the hourly temporal correlation starting already before 2030 which is optional for all member states.

Eq. (30) constrains the eFuels production to RES. We further constrain Eq. (30) to wind and solar generation only, instead of all RES. Electricity from hydropower is excluded as the hydropower potential in Germany is already utilized and no further hydropower plants can be build. Biomass is excluded because the direct utilization of biomass to produce biofuels is more efficient than the route via electricity generation to produce eFuels.

All scenarios consider the phase-out of nuclear and coal power plants. Nuclear and lignite power plants are decommissioned with individual deconstruction dates based on the national phase-out schedule. The total hard coal power plant capacity is limited through Eq. (10), resulting in an optimized hard coal decommissioning schedule from an overall system perspective (see Chapter 4.3).

5.2. CO_2 sources

The availability of CO_2 sources is a fundamental element for determining the optimal location of eFuel production. While there are a large variety of potential CO_2 sources that can be utilized in the process of producing eFuels, a small number of industries and industry sectors provide the majority of this potential and are of most interest when creating a dataset of CO_2 sources. Consequently, we use a geographically matched dataset of steel factories, refineries, cement factories, bioethanol plants, and biomethane plants as available CO_2 or flue gas sources. These sources are process-related and thus especially favorable for utilization in the eFuels production process as they cannot be avoided by using renewable energy carriers. Energy-related CO_2 emissions derive from the combustion of lignite, coal, natural gas or crude oil to supply energy as heat or electricity. Using energy-relatedCO_2 emissions has several shortcomings. For one, CO_2 emissions would not be carbon neutral. Additionally, the added steps of combustion and electricity generation would reduce the overall efficiency of the PtL process further. These energy carriers could be converted directly into fuels using gasification or pyrolysis, achieving a higher efficiency. Therefore, energy-related CO_2 emissions are not considered.

To derive the final CO2 emissions, we preprocess the data of the different technologies. In the case of steel factories, refineries, and cement factories, the total yearly emissions of each facility are reduced by energy-related emissions. For bioethanol plants, no information on their emissions is available. Therefore, we use the capacities of the bioethanol plants in combination with a specific CO_2 emission of 0.96 tons of CO_2 per produced ton of bioethanol (Meisel et al., 2015) to calculate the total yearly CO_2 emissions of each bioethanol plant. The problem of missing data availability on CO_2 emissions also exists for biomethane plants. Typically, CO_2 concentration of biomethane plants lie between 25% and 45% (Fischedick et al., 2015). Based on this range, we use an average CO_2 concentration of 35% and the facility capacity to calculate the yearly CO_2 emissions. The total yearly CO_2 emissions are assumed to be equally distributed over the year, allowing for the calculation of hourly CO_2 emissions. Table 1 shows yearly and hourly CO_2 emissions of the considered emitters, and Fig. 3 shows the spatial distribution of the facilities within Germany.

5.3. Energy system input data

Data on the German transmission grid, conventional generators, distribution of electricity demand, as well as renewable generation profiles are based on the PyPSA-EUR energy system workflow (Hörsch et al., 2018a). We extended data of RES capacities based on the core energy market data (Bundesnetzagentur, 2021) of the German federal network agency and matched this data with the data provided by

Table 1
Yearly and hourly flue gas and CO_2 point source emissions.

Facility	Hourly Emissions [t/h]	Yearly Emissions [Mio. t]	Emission type	Reference
Steel factory	5165	45.24	Flue gas	www.thru.de (Deutsche Emissionshandelsstelle, 2021)
Refinery	2512	22.00	Flue gas	www.thru.de (Deutsche Emissionshandelsstelle, 2021)
Cement factory	2495	21.85	Flue gas	www.thru.de (Deutsche Emissionshandelsstelle, 2021)
Bioethanol plant	176	1.54	CO_2	Bundesverband der deutschen Bioethanolwirtschaft e. V. (2021)
Biomethane plant	142	1.24	Flue gas	Deutsche Energie-Agentur (2021)

PyPSA-EUR. To reduce the computational intensity and account for the yearly, weather-dependent variation in electricity demand and volatile RES generation, the profiles of demand and renewable capacity factors are included using representative weeks. Here, historical data from 2012 to 2019 is clustered to derive nine representative weeks for each calculated year using the clustering approach proposed in Yilmaz et al. (2019). The resulting representative week consists of load and renewable capacity factor profiles, which are individually weighted using the time step weighting ω_t to create a representative sample of the demand and generation patterns of the last seven years. Figure 4 shows the different data sets and their underlying structure for the year 2020.

To achieve the development of a high RES energy system, following time-dependent parameters are used: First, the renewable generation share of the total electricity generation. This parameter aims to steadily increase the RES capacities and generation. The net power consumption defines the total electricity consumption within the energy system. This consumption increases due to increasing consumers like heat pumps, electric vehicles, and other power-to-x applications like hydrogen and methane production (power-to-gas). The generating hard coal capacities are limited by the hard coal capacity limitation set by the German government. All described assumptions are given in Table 2.

5.4. *eFuel production in Germany*

The eFuel production in Europe heavily relies on the development of the energy system, political support and the development of eFuel production technologies. From the energy system point of view, hydrogen and eFuel production are especially useful if the renewable potential allows low-cost production. In countries like Germany, renewable potentials are limited and the eFuel production is in direct competition to the coverage of conventional load, electric mobility and other electricity-based applications. Looking at the political aspects, a general hesitation towards eFuels is noticeable. For example, the planned crediting system in RED II enables national members to develop a technology-based strategy to reduce GHG emissions. This crediting system might favor technologies like electric mobility or (advanced) biofuels as they can be credited multiple times, giving them a larger lever to reduce GHG emissions than eFuels. In addition, car manufacturers need to reduce the tail pipe emissions of their fleet to 0 g CO_2 equivalents per kilometer by 2035. eFuels are only a valid option if the

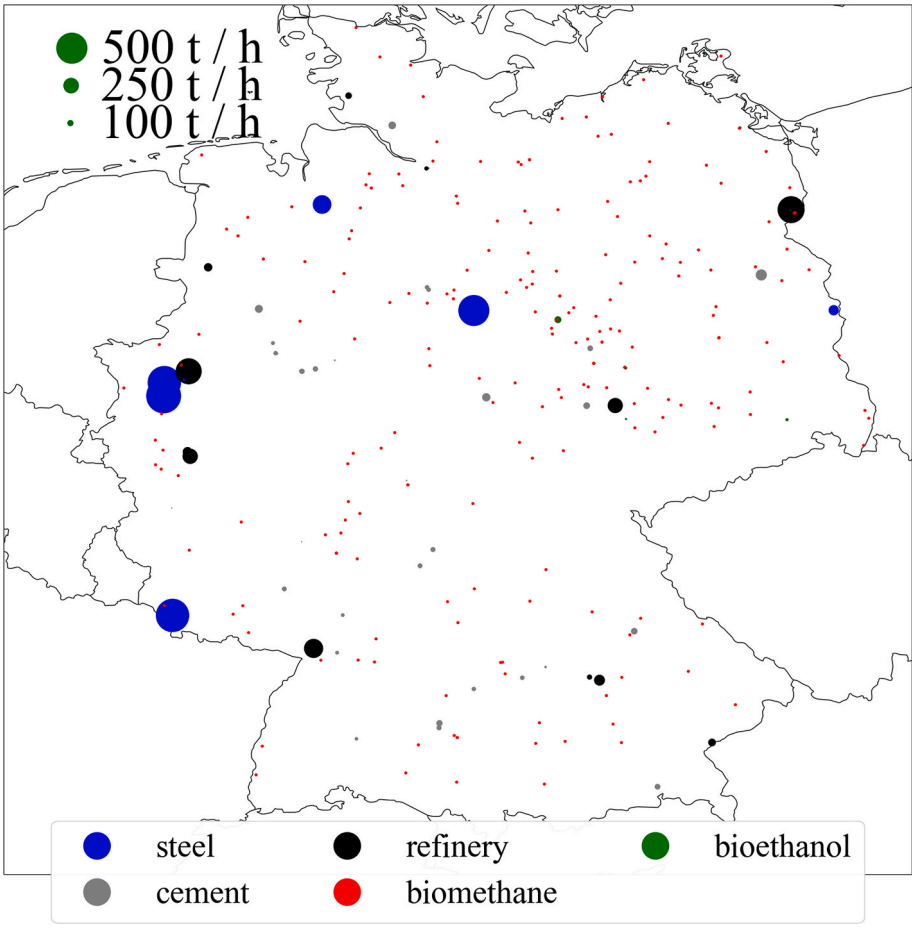

Fig. 3. Distribution of flue gas and CO_2 point source capacities in Germany.

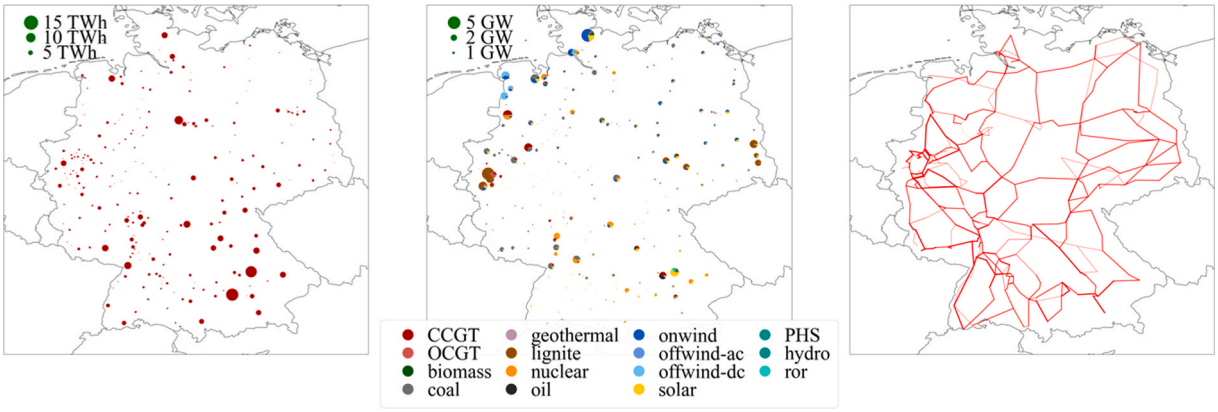

Fig. 4. Distribution of yearly spatial load demand (left), generator capacity (middle) and transmission lines (right) in 2020.

Table 2
Assumptions on renewable generation share, total power consumption and hard coal generator capacity limits.

Parameter	2020	2025	2030	Reference
Renewable generation share	40%	54%	68%	Sensfuß et al. (2021)
Net power consumption [TWh]	532,8	589,9 (interpolated)	647	Sensfuß et al. (2021)
Hard coal capacity limit	–	9.9 GW	8 GW	Bundesamt für Justiz (8/14/2020)

internal combustion engine vehicle exclusively uses eFuels, banning drop-in fuels with only a share of eFuels completely. Next to the policy aspects, technological uncertainties exist. Electrolysis and DAC are still immature technologies, which gives rise to the question if large capacities of these technologies will be available to supply large volumes of eFuels. In addition, due to the necessity of electrolysis in the eFuels production process, the production of eFuels is in direct competition to other technologies that depend on electrolysis and green hydrogen. This includes, for example, steel production, refinery processes, the pharmaceutical, chemical and agricultural industry. This situation might further reduce the support by policy makers as this competition could slow down GHG emission reduction efforts in these sectors. Furthermore, looking at the current projects in the fields of eFuels, the majority of large-scale projects are planned at locations with favorable renewable energy generation outside of Germany or even outside of Europe to achieve low production costs. Therefore, it is assumable that the majority of eFuels will be produced outside of Germany and will not be covered by domestic production. Based on the above-mentioned aspects and uncertainties, we conclude that only little domestic eFuels volume will take place in Germany and assume that larger volumes will be produced outside of Germany.

The policy framework ReFuels Aviation (European Union 4/25/2023) implements a eFuels quota of 1.2% in 2030 and 2% in 2032 in the aviation sector. It is important to mention that even this quota does not mean that the eFuels are produced in Germany. Distribution companies like refineries are obligated to distribute the quota of aviation fuels as eFuels, but are not bounded to produce these in Germany. To analyze the impact of the eFuel scale-up, we assume an eFuel production of 0.5% in 2025–2029, and 2% starting in 2030. Based on the aviation fuel demand in Germany in 2019 (434 PJ (Arbeitsgemeinschaft Energiebilanzen e.V., 2021)), and assuming that this demand remains constant, around 0.6 and 2.41 TWh of eFuel will be needed by 2025 and 2030, respectively, to meet the quota. Consequently, these values are used as the eFuel production objective for this case study.

6. Results & discussion

6.1. eFuel production facilities

6.1.1. Electrolysis, synthesis and storage capacity

Table 3 provides an overview of the total electrolysis, synthesis and storage capacities. Without any restrictions from electricity purchase conditions (No-RED), total electrolysis capacities will reach 201 MW by 2025 and 1128 MW by 2030. The increasing eFuel demand drives the growing electrolysis capacity in this scenario. In the RED scenario, this additional electricity demand has the same effect but the additional purchase conditions lead to increased total electrolysis capacities of 220 MW in 2025 and 1306 MW in 2030. Altogether, the RED II conditions result in 9.0% more electrolysis capacity in 2025 and 15.8% more electrolysis capacity in 2030.

At the same time, the total capacity of synthesis units will reach very similar levels in both scenarios. The main reason is that the synthesis is not highly flexible, and the operation is not constrained in both scenarios. However, while synthesis capacities develop almost consistently, storage capacities differ strongly. Due to low flexibility and the inability to shut down synthesis units, situations with a low electricity supply, that would result in reduced or stopped hydrogen production, need to be bridged by hydrogen supply from hydrogen storage. The resulting hydrogen storage in the No-RED scenario is capable of supplying hydrogen for the synthesis process for 30.06 h in 2025 and 55.50 h in 2030. In the RED scenario, these numbers increase to 54.8 h in 2025 and 111.2 h in 2030.

6.1.2. Operation of electrolysis units

In the No-RED scenario, electrolysis units have an average utilization of 7984 h in 2025 and 5875 h in 2030. Even though electrolysis operation is not constrained, electrolysis units are not operated at full utilization in 2025 and 2030. With decreasing fixed costs of electrolysis and an increasing share of renewable energy over the years, offering flexibility from electrolysis overcapacities becomes more attractive as average local marginal prices decrease with a higher share of RES. This decreased utilization further explains the increase of the storage capacity to synthesis capacity ratio. With lower utilization and a steady demand for synthesis, more hydrogen needs to be stored to bridge gaps

Table 3
Capacities of electrolysis, synthesis units and hydrogen storage in the No-RED and RED scenarios.

Parameter	No-RED		RED	
Year	2025	2030	2025	2030
Total Electrolysis Capacity [MW Electricity]	201	1128	220	1306
Total Synthesis Capacity [MW Hydrogen]	69	298	69	285
Total Hydrogen Storage Capacity [MWh]	2071	16,532	5860	31,646

without hydrogen production.

Purchase condition constraints result in lower utilization of electrolysis units in the RED scenario. The associated dispatch results in lower utilization of 7336 h in 2025 and 5203 h in 2030. Similarly to the No-RED scenario, this effect can be attributed to lower marginal prices and decreasing cost of electrolysis units. However, the even-higher reduction in electrolysis utilization is caused by the time-dependent availability of RES generation. Altogether, the utilization drops by 8.1% in 2025 and 11.4% in 2030.

The operation of electrolysis is illustrated in Fig. 5 (No-RED) and Fig. 6 (RED). To compare the dispatch, one network node is chosen, where the installation of electrolysis capacity is optimal in the No-RED and RED scenarios. Both figures use a logarithmic scale on the y-axis to allow for comparison of the dispatch as the renewable capacities differ.

Fig. 5 shows the dispatch of the electrolysis unit and the available RES generation at the chosen network node in the No-RED scenario without electrolysis dispatch constraints. The electrolysis unit is dispatched at maximum capacity at the majority of time steps and is not affected by the RES generation directly. Indirectly, electrolysis utilization is influenced by low marginal prices of electricity, which occur when renewable energy generation is high and conventional electricity demand is low. In addition, biomass-based electricity generation is available to operate the eFuel production facility.

Fig. 6 shows the exemplary electrolysis unit in the RED scenario and the corresponding RES generation. Corresponding RES capacities are only such, which have been commissioned in the same projected year as the electrolysis and, therefore, meet the additionality requirement. Two things are observable. On the one hand, the corresponding RES generation is much smaller than the total available RES capacities at the network node as seen in Fig. 5. This limitation derives from the additionality constraint. On the other hand, it is apparent that the operation is increasingly correlated to the corresponding RES generation, which results in shutdowns of the electrolysis unit when wind and solar generation are insufficient to satisfy the nodal electrolysis demand. This correlation derives from the temporal correlation. Even though generation of wind and solar capacities commissioned in the same projected year is sufficient during many hours to operate the electrolysis at high utilization levels, the electrolysis stops operation for short periods before and after solar generation. The volatile operation is caused by low marginal prices, which shapes the electrolysis operation curve. This can be seen by the reduction of electrolysis operation in a corresponding manner to the reduction of solar generation. Another interesting point is the high utilization of the electrolysis shown in Fig. 6 and numerically presented in Table 4. This high utilization is possible due to the ratio between electrolysis and RES capacities. The system feeds in the residual energy between RES generation and electrolysis demand into the electricity grid. This approach allows high electrolysis utilization even with limited RES potential and might be a suitable approach for eFuels production under the RED II regime.

6.1.3. CO_2 source

The results show that the application of the energy purchase conditions result in different utilization of the CO_2 production technologies. In the No-RED scenario in 2025, almost all CO_2 is obtained from direct sources, and even in 2030, direct sources supply 46.91% of the total CO_2. DAC plays no role in the No-RED scenario. In the RED scenario, the CO_2 supply is more diversified. In 2025, the major share is CO_2 from sources with flue gas (68.2%), followed by direct sources (30.6%), and DAC (1.2%). In 2030, CO_2 from direct sources does not increase, while DAC CO_2 increases by 14.307 tons. Nevertheless, the major share of CO_2 is still scrubbed from flue gas sources, accounting for 89.9% of the total CO_2.

The distribution of CO_2 production technologies in Fig. 7 shows that CO_2 sources play an important role next to the electricity supply. Without the constrained electricity supply, direct sources play a significant role and locations are chosen based on the available CO_2. With the implementation of RED II constraints, electricity purchase is more constrained, and fewer locations are attractive regarding electricity supply. Instead of implementing production facilities at direct CO_2 sources like in the No-RED scenario, the energy system in the RED scenario prioritizes the electricity supply over the CO_2 supply and accepts a less attractive CO_2 supply. Simultaneously, this shift towards prioritized electricity supply leads to the increased relevance of DAC, as CO_2 sources are often limited at the locations with the most attractive, RED II adhered electricity supply, which does not influence DAC at the same time.

6.1.4. Production facility locations

The above-mentioned aspects - low marginal prices and CO_2 supply costs - play a significant role in the decision on the location of eFuel production units. Average marginal prices are lower in northern Germany, where favorable wind circumstances exist. This tendency is clearly visible when looking at the distribution of eFuel facilities, depicted as the location and capacity of electrolysis units in Fig. 8.

When comparing spatial distributions, it is apparent that in the No-RED scenario a larger share of electrolysis units are installed further away from the German coastline, close to the Polish border and in Saxony-Anhalt. One primary reason is the availability of a direct CO_2 source at these locations, which, without the purchase conditions, proves to be the optimal solution over maximizing nodal wind energy availability.

Expectedly, the inclusion of the geographical correlation condition changes the spatial distribution of electrolysis units. The condition

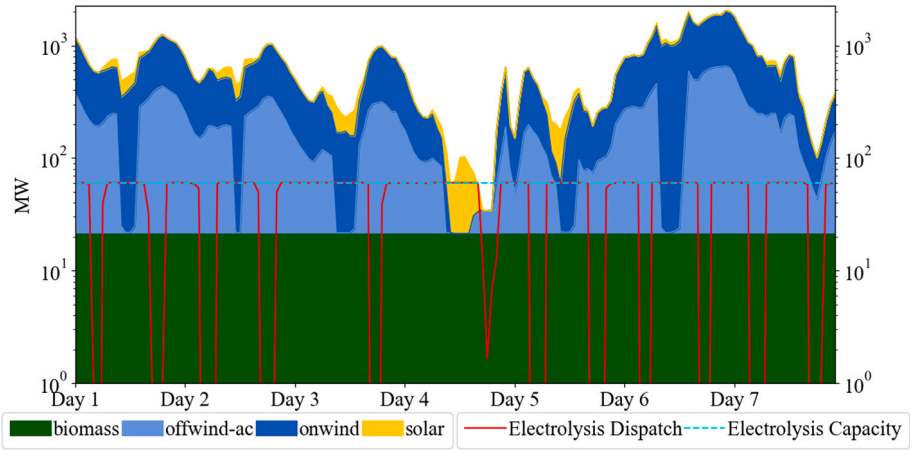

Fig. 5. Electrolysis operation of one exemplary electrolysis unit in 2030 in the No-RED scenario.

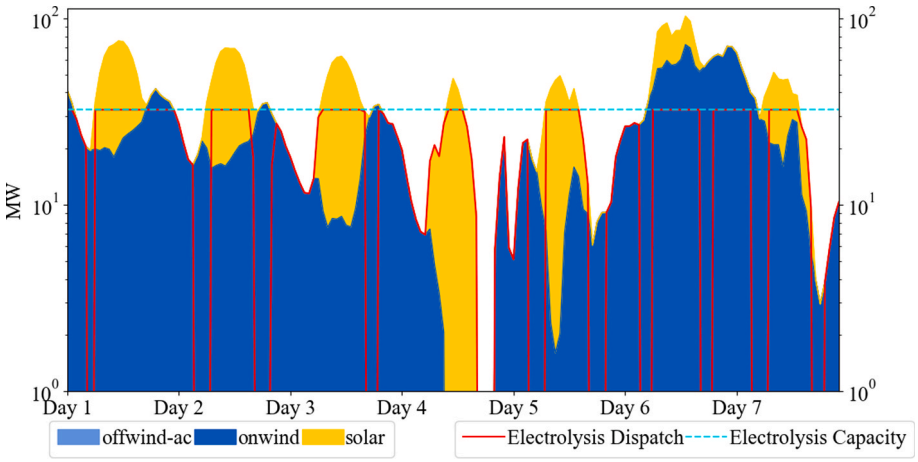

Fig. 6. Electrolysis operation of the largest electrolysis unit in 2030 in the RED scenario.

Table 4
Average utilization of the electrolysis units in the No-RED and RED scenario.

Parameter	No-RED		RED	
Year	2025	2030	2025	2030
Average Utilization [h]	7984	5875	7336	5203

removes the option of installing electrolysis capacity at network nodes without renewable generation, while also limiting viable capacities according to the available wind and solar potential at the same location. Thus, a shift from direct CO_2 sources as the primary driver in location choice towards available renewable potential and high capacity factors can be observed in the results.

6.2. Impact on the energy system

6.2.1. Renewable capacities and distribution

Table 5 shows renewable capacities in GW for each scenario in 2030. Both scenarios with additional eFuels demand unsurprisingly result in increased renewable capacities. The main driver is the increased electricity demand and the necessity to achieve the proper share of renewable energies.

Fig. 9 shows the relative change of wind and solar capacities compared to the reference scenario. The No-RED and the RED scenario both have higher wind capacities than the reference scenario. The offshore capacities differ only slightly from the reference scenario, but solar and onshore capacities increase in each. Hence, both scenarios result in higher RES capacities, mainly because of the increased electricity demand, but, in the case of the RED scenario, also because the PtL demand needs to be covered fully by RES generation.

It is further visible that the RED scenario will install more solar capacities and less wind onshore capacities. The reason might be the diversification of the electricity supply. Using solar generation might help to close gaps in the wind generation and, therefore, increase the utilization of the constrained electrolysis. This circumstance is visible in Fig. 6. As the electrolysis units are located close to the shore where solar capacity factors are lower, the solar capacities might have to be increased to achieve sufficient solar generation.

Table 6 shows the curtailment of RES in 2030 for the different scenarios. It is observable that the curtailment reduces with the installation of electrolysis units and especially reduces when constraints to increase the correlation between renewable energy generation and electrolysis electricity consumption are implemented. Therefore, the overall flexibility of electrolysis units in combination with hydrogen storage help to integrate renewable energy generation.

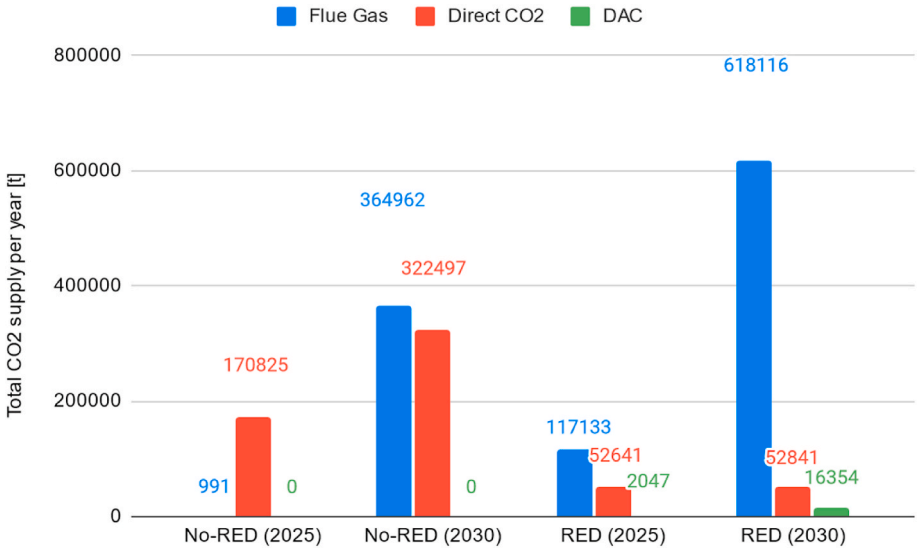

Fig. 7. CO_2 quantity covered by the flue gas route (blue), direct CO_2 route (red) and DAC route (green) in 2025 and 2030 in the No-RED and RED scenarios.

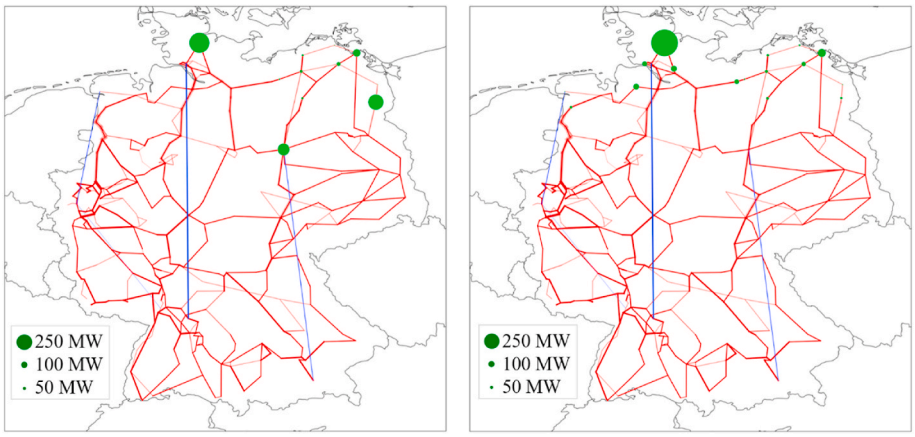

Fig. 8. Transmission lines and electrolysis capacities in 2030 in the No-RED scenario (left) and RED scenario (right).

Table 5
Installed renewable generation capacities in the reference, No-RED and RED scenario.

Scenario	Solar [GW]	Onshore Wind [GW]	Offshore Wind [GW]
Reference	144,580	95,720	13,614
No-RED	146,630	96,540	13,609
RED	147,410	96,210	13,621

6.2.2. CO_2 abatement costs

CO_2 abatement costs give information about the additional costs of energy systems to reduce CO_2 compared to energy systems without these efforts. To calculate CO_2 abatement costs, the total costs of the reference scenario are subtracted from the total costs of the No-RED or RED scenario each. The cost differences are discounted to the year 2020 and divided by the total amount of saved CO_2. Table 7 shows the CO_2 abatement costs. In the No-RED scenario, CO_2 abatement costs are 429.0 € /t CO_2. The RED scenario has CO_2 abatement costs of 490.6 € /tCO_2. While RED II conditions result in additional costs for the energy system, both CO_2 abatement costs differ by 14.3%.

The majority of additional costs in both scenarios stem from the investment in renewable generation, electrolysis, hydrogen storage and CO_2 supply. Looking at the capacities of RES and the different components of the synthesis, it is observable that the constrained purchase in the RED scenario results in higher solar, electrolysis, and storage capacities, and the utilization of DAC. These additional investments explain the difference between both abatement costs.

Fig. 10 shows the share of the different components on the abatement costs. CO_2 has only a small share, supporting the statement that the decision regarding optimal location is mainly influenced by the available electricity. Both strategies contribute to reduce the investments into the grid, but this reduction is neglectable compared to the additional costs of the energy system from eFuel production.

7. Conclusions & policy implications

In this paper, we presented an approach to investigate the impact of

Table 6
Curtailment of electricity from RES in 2030 for each scenario.

	Reference	No-RED	RED
Curtailment	7.0%	6.9%	6.8%

Table 7
CO_2 abatement costs of the No-RED and RED scenario.

	No-RED	RED
CO_2 abatement costs [€ /t]	429.05	490.58

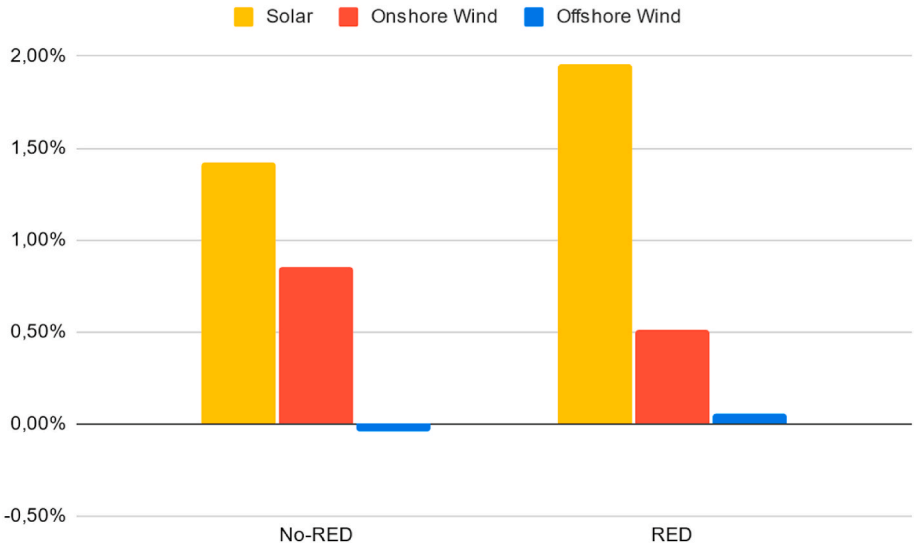

Fig. 9. Changed wind and solar capacities in % compared to the reference scenario.

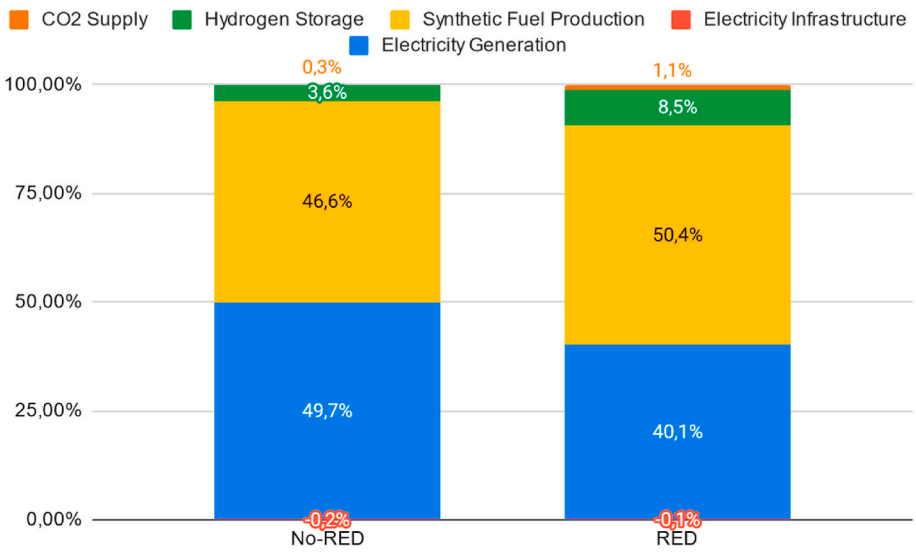

Fig. 10. Share of CO_2 supply costs (orange), hydrogen storage costs (green), eFuel production costs (yellow), electricity infrastructure costs (red) and electricity generation costs (blue) on the CO_2 abatement costs. Due to the high flexibility demand of the electrolysis and the low flexibility of the synthesis units in the RED scenario, hydrogen storage capacities increase and its share on the CO_2 abatement costs rise.

electricity purchase conditions of the Renewable Energy Directive II (RED II) on eFuels production, which is applied to a case study in the German energy system. According to the RED II, three conditions need to be met to classify eFuel as sourced from renewable sources: First, the electricity used to produce the eFuel must stem from renewable sources. Second, the additionality constraint defines that eFuel production should result in additional renewable capacities. Third, the temporal and geographical correlation between renewable electricity generation and electrolysis electricity consumption needs to be met. We used a linear optimization energy system model that accounts for the electricity transmission network as well as CO_2 sources, electrolysis, hydrogen and battery storage, and synthesis. In a second step, additional constraints accounting for the three purchase conditions were added. We compared two scenarios, with and without electricity purchase constraints, which include the objective of producing the quota of 2% aviation fuel in Germany by 2030.

The chosen approach and the case study are subject to a number of limitations. The power-to-liquid process is only investigated at from the system's perspective, and uncertainty remains whether the derived dimensioning and operation conditions are sufficient for economical operation, which might also stem from additional benefits such as balancing energy. As eFuels production technology is still developing, there are several uncertainties with regard to future development. A significant uncertainty are future investment expenditures necessary for electrolysis and DAC units, faster realization of cost reduction potentials could increase economical attractiveness. Furthermore, the uncertainties of the energy system case study itself can be mentioned. Here, the load demand, the transmission grid and several other aspects might develop differently in the long-term than assumed. From the energy system modeling perspective, several uncertainties could affect the results. Compared to conventional kerosene demand, the estimated demand to be fulfilled by electrolysis by 2030 in this work is relatively low. Higher eFuel would have a more emphasized impact on the energy system and will very likely result in a more substantial transformation of the energy system, which might be difficult to achieve by 2030. In addition, the geographical location of the eFuel demand in this work is assumed to be restricted on a national level only. Higher spatial granularity in demand modeling might affect the decision on the optimal location of production facilities. To further improve accuracy in modeling the hydrogen sector of the energy system, the existing approach could be extended to include future hydrogen infrastructure, such as pipelines, storage facilities, and major demand locations in future work. Furthermore, the input data when using representative data for future energy scenarios depends on the accuracy of the clustering approach and might differ from results using entire time-series data. Finally, the national scope of this work is limited to Germany. In future work, an extension to the central European energy system is desirable to account for the interdependencies between the interconnected systems, especially when modeling the electricity system.

The results show that the electricity purchase conditions have major impacts on dimensioning and operation of Fischer-Tropsch eFuels production. The required capacity of electrolysis increased by 9.05% (2025) and 15.77% (2030), and average electrolysis utilization drops from 5875 h to 5203 h in 2030 (7984 h to 7336 h in 2025) when electricity purchase conditions are applied. The condition of temporal correlation forces the electrolysis to adapt to volatile renewable generation. With electricity purchase conditions, locations with large capacities of newly installed renewable energies are more attractive as the ratio between renewable capacities and electrolysis capacity supports high electrolysis utilization under RED II restrictions. This aspect, along with the additional purchase condition, results in higher solar, offshore wind, and onshore wind capacities. Even with the change in optimal electrolysis location, utilization of electrolysis is lower when purchase conditions are considered. CO_2 takes a minor role regarding placement of power-to-liquid facilities, but increases in importance if electricity purchase is not constrained. In comparison to the CO_2 abatement costs in the No-RED scenario, abatement costs in the RED scenario increased by 14.34%. Conditions for electricity purchase of electrolysis increases investment, especially in solar capacities, as achieving the highest possible electrolysis utilization is the cost-optimal solution. With eFuels production and purchase conditions, the volume of curtailed electricity reduces and lower investments into the electricity grid are necessary. However, the abatement costs show that these positive effects are neglectable when compared to the additional costs from eFuels production, storage, and renewable generation.

Based on the results of this work, the following policy implications can be derived. First, the high CO_2 abatement costs of power-to-liquid applications show that their grid-connected application might be less favorable than alternatives like electric mobility. This circumstance does not necessarily mean that eFuels are less favorable in general. The production within stand-alone power-to-liquid facilities with higher renewable capacity factors might reduce the CO_2 abatement costs

significantly and might be more suitable, especially when the economic maturity of the technology is low. In addition, the increase of the CO_2 abatement costs by only 14.34% more than the scenario without electricity purchase criteria shows that the implementation of electricity purchase criteria might be a suitable approach from the energy system planner's perspective. However, the question arises if the increased investment into the power-to-liquid facility when applying electricity purchase conditions result in economic feasibility of the eFuel production. Subsidies to support producers, especially in the early stage of the upcoming green hydrogen industry, might be necessary. Altogether, it might be an efficient solution to locate early electrolysis capacities close to the renewable generators and use electrolysis as a flexible supply in later stages of the development of a hydrogen-based system where lower investment allows economical operation with lower utilization. Furthermore, the approach to dimension the electrolysis at lower capacities than the corresponding RES capacities in combination with the diversification of electricity supply by using both, wind and solar capacities, allow high utilization of electrolysis even with grid-connected systems. The advantage of this approach is that residual energy between renewable generation and electrolysis demand can be fed-in into the electricity grid and, therefore, be sold at spot markets to create an additional revenue stream.

CRediT authorship contribution statement

Uwe Langenmayr: Conceptualization, Data curation, Formal analysis, Methodology, Software, Validation, Visualization, Writing – original draft, Writing – review & editing. **Manuel Ruppert:** Conceptualization, Data curation, Formal analysis, Methodology, Validation, Writing – original draft, Writing – review & editing.

Declaration of competing interest

The authors declare that they have no known competing financial interests or personal relationships that could have appeared to influence the work reported in this paper.

Data availability

The data and code is already open source available (see references).

A. Appendix

A.1 Economic assumptions of CO2 scrubber unit, synthesis and hydrogen storage.

Component	CAPEX	Fixed O&M	Variable O&M	Lifetime	Reference
CO_2 scrubber	130911 [€ /t *h]	9 [% of investment]	0	20 [years]	Heinzmann et al. (2021)
Synthesis	1371624 [€ /MW Hydrogen]	9 [% of investment]	14.49 [€ /MW Hydrogen]	20 [years]	Heinzmann et al. (2021)
Hydrogen storage	490 [€ /kg]	1 [% of investment]	0	20 [years]	Gorre et al. (2020)

A.2 Economic assumptions of electrolysis and DAC units

	2020	2025	2030	Reference
CAPEX				
Electrolysis [€ /MW]	1000	873	810	Heinzmann et al. (2021)
DAC [€ /t_{CO2} * a	730	540	340	Fasihi et al. (2019)
Lifetime [Years]				
Electrolysis	20	20	20	Heinzmann et al. (2021)
DAC	20	20	20	Fasihi et al. (2019)
Fixed O&M [% of investment]				
Electrolysis	5	5	5	Heinzmann et al. (2021)
DAC	4	4	4	Fasihi et al. (2019)
Variable O&M				
Electrolysis [€ /MW Electricity]	0.005	0.005	0.005	Heinzmann et al. (2021)
DAC	0	0	0	Fasihi et al. (2019)

A.3 Technical assumptions of the eFuel production route

Component	Unit	2020	2025	2030	Reference
Electrolysis	Efficiency	61.2	61.6	62	Heinzmann et al. (2021)
CO_2 scrubber	t CO_2 /t Flue gas	0.286	0.286	0.286	Heinzmann et al. (2021)
DAC	t CO_2 /MW Electricity	4	4	4	Fasihi et al. (2019)
Synthesis	MW Syncrude /MW Hydrogen	60.6	60.6	60.6	Heinzmann et al. (2021)
Synthesis	t CO_2 /MWh Fuel	0.173	0.173	0.173	Heinzmann et al. (2021)

A.4 Energy system related assumptions. Other relevant assumptions are taken from Hörsch et al. (2018a).

Component	Parameter	Unit	2020	2025	2030	Reference
Wind Offshore	CAPEX	€ /kW	3467	3052	2637	Keles and Yilmaz (2020)
Wind Offshore	Fixed O&M	€ /kW*a	113	99.5	86	
Wind Offshore	Variable O&M	€ /kWh	0.5	0.5	0.5	
Wind Onshore	CAPEX	€ /kW	1619	1489	1243	
Wind Onshore	Fixed O&M	€ /kW*a	32	29.5	27	
Wind Onshore	Variable O&M	€ /kWh	0.5	0.5	0.5	
Photovoltaic	CAPEX	€ /kW	649	610	570	
Photovoltaic	Fixed O&M	€ /kW*a	1.6	1.5	1.4	
Photovoltaic	Variable O&M	€ /kWh	0.1	0.1	0.1	
Biomass	CAPEX	€ /kW	5012	4823	4634	
Biomass	Fixed O&M	€ /kW*a	136	133.5	131	
Biomass	Variable O&M	€ /kWh	0	0	0	

References

Arbeitsgemeinschaft Energiebilanzen e.V., 2021. 1 Auswertungstabellen zur Energiebilanz Deutschland. Daten für die Jahre von 1990 bis 2020. https://ag-energiebilanzen.de/wp-content/uploads/2020/09/awt_2020_d.pdf checked on 3/23/2022.

Ashfaq, Asad, Kamali, Zulqarnain Haider, Agha, Mujtaba Hassan, Arshid, Hirra, 2017. Heat coupling of the pan-European vs. regional electrical grid with excess renewable energy. Energy 122, 363–377. https://doi.org/10.1016/j.energy.2017.01.084.

Blanco, Herib, Nijs, Wouter, Ruf, Johannes, Faaij, André, 2018a. Potential for hydrogen and Power-to-Liquid in a low-carbon EU energy system using cost optimization. Appl. Energy 232, 617–639. https://doi.org/10.1016/j.apenergy.2018.09.216.

Blanco, Herib, Nijs, Wouter, Ruf, Johannes, Faaij, André, 2018b. Potential of power-to-methane in the EU energy transition to a low carbon system using cost optimization. Appl. Energy 232, 323–340. https://doi.org/10.1016/j.apenergy.2018.08.027.

Bogdanov, Dmitrii, Gulagi, Ashish, Fasihi, Mahdi, Breyer, Christian, 2021. Full energy sector transition towards 100% renewable energy supply: integrating power, heat, transport and industry sectors including desalination. Appl. Energy 283, 116273. https://doi.org/10.1016/j.apenergy.2020.116273.

Brand, Christian, Tran, Martino, Anable, Jillian, 2012. The UK transport carbon model: an integrated life cycle approach to explore low carbon futures. Energy Pol. 41, 107–124. https://doi.org/10.1016/j.enpol.2010.08.019.

Brown, Tom, Hörsch, Jonas, Schlachtberger, David, 2018. PyPSA: Python for power system analysis. J. Open Res. Software 6. https://doi.org/10.5334/jors.188. Article 4.

Bundesamt für Justiz (8/14/2020): Gesetz zur Reduzierung und zur Beendigung der Kohleverstromung* (Kohleverstromungsbeendigungsgesetz - KVBG). KVBG. Available online at: https://www.gesetze-im-internet.de/kvbg/BJNR181810020.html.

Bundesnetzagentur, 2021. Marktstammdatenregister. https://www.marktstammdatenregister.de/MaStR/Datendownload checked on 12/14/2021.

Bundesverband der deutschen Bioethanolwirtschaft e.V., 2021. Bioethanolproduktion seit 2005. https://www.bdbe.de/biokraftstoff-bioethanol/zellulose-ethanol checked on 12/14/2021.

Capros, Pantelis, Zazias, Georgios, Evangelopoulou, Stavroula, Kannavou, Maria, Fotiou, Theofano, Siskos, Pelopidas, et al., 2019. Energy-system modelling of the EU strategy towards climate-neutrality. Energy Pol. 134 (8), 110960 https://doi.org/10.1016/j.enpol.2019.110960.

Chiaramonti, David, Goumas, Theodor, 2019. Impacts on industrial-scale market deployment of advanced biofuels and recycled carbon fuels from the EU Renewable Energy Directive II. Appl. Energy 251 (August), 113351. https://doi.org/10.1016/j.apenergy.2019.113351.

Dahal, Karna, Juhola, Sirkku, Niemelä, Jari, 2018. The role of renewable energy policies for carbon neutrality in Helsinki Metropolitan area. Sustain. Cities Soc. 40 (3), 222–232. https://doi.org/10.1016/j.scs.2018.04.015.

Deutsche Emissionshandelsstelle, 2021. Treibhausgasemissionen 2020. Emissionshandelspflichtige stationäre Anlagen und Luftverkehr in Deutschland (VET-Bericht 2020). https://www.dehst.de/SharedDocs/downloads/DE/publikationen/VET-Bericht-2020.pdf;jsessionid=69E65A7F02764A76F48CD2D59B07806A.1_cid331?_blob=publicationFile&v=4 checked on 12/14/2021.

Deutsche Energie-Agentur, 2021. Biogas Einspeiseatlas Deutschland. https://www.biogaspartner.de/einspeiseatlas/ checked on 12/14/2021.

European Union, 2022. COMMISSION DELEGATED REGULATION (EU) …/… of XXX supplementing Directive (EU) 2018/2001 of the European Parliament and of the Council by establishing a Union methodology setting out detailed rules for the production of renewable liquid and gaseous transport fuels of non-biological origin 2022 (L 328/82). https://ec.europa.eu/info/law/better-regulation/have-your-say/initiatives/7046068-Production-of-renewable-transport-fuels-share-of-renewable-electricity-requirements-_en checked on 6/23/2022.

European Union (4/25/2023): Fit for 55: Parliament and Council reach deal on greener aviation fuels. Available online at: https://www.europarl.europa.eu/news/en/press-room/20230424IPR82023/fit-for-55-parliament-and-council-reach-deal-on-greener-aviation-fuels, checked on 8/22/2023..

Fasihi, Mahdi, Efimova, Olga, Breyer, Christian, 2019. Techno-economic assessment of CO2 direct air capture plants. J. Clean. Prod. 224 (3), 957–980. https://doi.org/10.1016/j.jclepro.2019.03.086.

Available online at:. In: Fischedick, Manfred, Görner, Klaus, Thomeczek, Margit (Eds.), 2015. CO2: Abtrennung, Speicherung, Nutzung. Ganzheitliche Bewertung im Bereich von Energiewirtschaft und Industrie. Springer Berlin Heidelberg, Berlin, Heidelberg http://nbn-resolving.org/urn:nbn:de:bsz:31-epflicht-1574888.

Frysztacki, Martha Maria, Hörsch, Jonas, Hagenmeyer, Veit, Brown, Tom, 2021. The strong effect of network resolution on electricity system models with high shares of wind and solar. Appl. Energy 291, 116726. https://doi.org/10.1016/j.apenergy.2021.116726.

Gea-Bermúdez, Juan, Jensen, Ida Græsted, Münster, Marie, Koivisto, Matti, Kirkerud, Jon Gustav, Chen, Yi-kuang, Ravn, Hans, 2021. The role of sector coupling in the green transition: a least-cost energy system development in Northern-central Europe towards 2050. Appl. Energy 289, 116685. https://doi.org/10.1016/j.apenergy.2021.116685.

Gils, Hans Christian, Gardian, Hedda, Schmugge, Jens, 2021. Interaction of hydrogen infrastructures with other sector coupling options towards a zero-emission energy system in Germany. Renew. Energy 180, 140–156. https://doi.org/10.1016/j.renene.2021.08.016.

Gorre, Jachin, Ruoss, Fabian, Karjunen, Hannu, Schaffert, Johannes, Tynjälä, Tero, 2020. Cost benefits of optimizing hydrogen storage and methanation capacities for Power-to-Gas plants in dynamic operation. Appl. Energy 257 (1–2), 113967. https://doi.org/10.1016/j.apenergy.2019.113967.

Gudmundsson, Oddgeir, Thorsen, Jan Eric, Brand, Marek, 2018. The role of district heating in coupling of the future renewable energy sectors. Energy Proc. 149, 445–454. https://doi.org/10.1016/j.egypro.2018.08.209.

Hanley, Emma S., Deane, J.P., Gallachóir, B.Ó.P., 2018. The role of hydrogen in low carbon energy futures–A review of existing perspectives. Renew. Sustain. Energy Rev. 82, 3027–3045. https://doi.org/10.1016/j.rser.2017.10.034.

Hansen, Kenneth, Breyer, Christian, Lund, Henrik, 2019. Status and perspectives on 100% renewable energy systems. Energy 175, 471–480. https://doi.org/10.1016/j.energy.2019.03.092.

Heinisch, Verena, Göransson, Lisa, Erlandsson, Rasmus, Hodel, Henrik, Johnsson, Filip, Odenberger, Mikael, 2021. Smart electric vehicle charging strategies for sectoral coupling in a city energy system. Appl. Energy 288, 116640. https://doi.org/10.1016/j.apenergy.2021.116640.

Heinzmann, Paul, Glöser-Chahoud, Simon, Dahmen, Nicolaus, Langenmayr, Uwe, Schultmann, Frank, 2021. Techno-ökonomische Bewertung der Produktion regenerativer synthetischer Kraftstoffe.

Helgeson, Broghan, Peter, Jakob, 2020. The role of electricity in decarbonizing European road transport – development and assessment of an integrated multi-sectoral model. Appl. Energy 262, 114365. https://doi.org/10.1016/j.apenergy.2019.114365.

Hörsch, Jonas, Hofmann, Fabian, Schlachtberger, David, Brown, Tom, 2018a. PyPSA-Eur: an open optimisation model of the European transmission system. Energy Strategy Rev. 22, 207–215. https://doi.org/10.1016/j.esr.2018.08.012.

Hörsch, Jonas, Ronellenfitsch, Henrik, Witthaut, Dirk, Brown, Tom, 2018b. Linear optimal power flow using cycle flows. Elec. Power Syst. Res. 158, 126–135. https://doi.org/10.1016/j.epsr.2017.12.034.

Jimenez-Navarro, Juan-Pablo, Kavvadias, Konstantinos, Filippidou, Faidra, Pavičević, Matija, Quoilin, Sylvain, 2020. Coupling the heating and power sectors: the role of centralised combined heat and power plants and district heat in a European decarbonised power system. Appl. Energy 270, 115134. https://doi.org/10.1016/j.apenergy.2020.115134.

Keles, Dogan, Yilmaz, Hasan Ümitcan, 2020. Decarbonisation through coal phase-out in Germany and Europe — impact on Emissions, electricity prices and power production. Energy Pol. 141 (2), 111472 https://doi.org/10.1016/j.enpol.2020.111472.

Kiviluoma, Juha, Meibom, Peter, 2011. Methodology for modelling plug-in electric vehicles in the power system and cost estimates for a system with either smart or dumb electric vehicles. Energy 36 (3), 1758–1767. https://doi.org/10.1016/j.energy.2010.12.053.

Luderer, Gunnar, Kost, Christoph, Dominika, 2021. Deutschland auf dem Weg zur Klimaneutralität 2045 - Szenarien und Pfade im Modellvergleich. Potsdam Institute for Climate Impact Research.

Meibom, Peter, Kiviluoma, Juha, Barth, Rüdiger, Brand, Heike, Weber, Christoph, Larsen, Helge V., 2007. Value of electric heat boilers and heat pumps for wind power integration. Wind Energy 10 (4), 321–337. https://doi.org/10.1002/we.224.

Meisel, Kathleen, Braune, Maria, Gröngröft, Arne, Majer, Stefan, Müller-Langer, Franziska, Naumann, Karin, Oehmichen, Katja, 2015. Technische und methodische Grundlagen der THG-Bilanzierung von Bioethanol. Handreichung. Leipzig, Dresden: DBFZ Deutsches Biomasseforschungszentrum gemeinnützige GmbH; Sächsische Landesbibliothek – staats- und Universitätsbibliothek Dresden. Available online at: https://nbn-resolving.de/urn:nbn:de:bsz:14-qucosa2-357054.

Mesfun, Sennai, Sanchez, Daniel L., Leduc, Sylvain, Wetterlund, Elisabeth, Lundgren, Joakim, Biberacher, Markus, Kraxner, Florian, 2017. Power-to-gas and power-to-liquid for managing renewable electricity intermittency in the Alpine Region. Renew. Energy 107, 361–372. https://doi.org/10.1016/j.renene.2017.02.020.

Nevens, Frank, Roorda, Chris, 2014. A climate of change: a transition approach for climate neutrality in the city of Ghent (Belgium). Sustain. Cities Soc. 10, 112–121. https://doi.org/10.1016/j.scs.2013.06.001.

Osorio-Aravena, Juan Carlos, Aghahosseini, Arman, Bogdanov, Dmitrii, Caldera, Upeksha, Ghorbani, Narges, Mensah, Theophilus Nii Odai, et al., 2021. The impact of renewable energy and sector coupling on the pathway towards a sustainable energy system in Chile. Renew. Sustain. Energy Rev. 151, 111557 https://doi.org/10.1016/j.rser.2021.111557.

Pavičević, Matija, Mangipinto, Andrea, Nijs, Wouter, Lombardi, Francesco, Kavvadias, Konstantinos, Navarro, Jiménez, Juan Pablo, et al., 2020. The potential of sector coupling in future European energy systems: soft linking between the Dispa-SET and JRC-EU-TIMES models. Appl. Energy 267, 115100. https://doi.org/10.1016/j.apenergy.2020.115100.

Pensini, Alessandro, Rasmussen, Claus N., Kempton, Willett, 2014. Economic analysis of using excess renewable electricity to displace heating fuels. Appl. Energy 131, 530–543. https://doi.org/10.1016/j.apenergy.2014.04.111.

Plötz, Patrick, Gnann, Till, Jochem, Patrick, Yilmaz, Hasan Ümitcan, Kaschub, Thomas, 2019. Impact of electric trucks powered by overhead lines on the European electricity system and CO2 emissions. Energy Pol. 130, 32–40. https://doi.org/10.1016/j.enpol.2019.03.042.

Quarton, Christopher J., Samsatli, Sheila, 2020. The value of hydrogen and carbon capture, storage and utilisation in decarbonising energy: insights from integrated value chain optimisation. Appl. Energy 257 (5), 113936. https://doi.org/10.1016/j.apenergy.2019.113936.

Ramsebner, Jasmine, Haas, Reinhard, Ajanovic, Amela, Wietschel, Martin, 2021. The sector coupling concept: a critical review. WIREs Energy Environ 10 (4), 1. https://doi.org/10.1002/wene.396.

Ruhnau, Oliver, Schiele, Johanna, 2022. Flexible green hydrogen: economic benefits without increasing power sector emissions. Available online at:. In: ZBW - Leibniz Information Centre for Economics, Kiel, Hamburg http://hdl.handle.net/10419/258999. checked on 6/23/2022.

Scheelhaase, Janina, Maertens, Sven, Grimme, Wolfgang, 2019. Synthetic fuels in aviation – current barriers and potential political measures. Transport. Res. Procedia 43, 21–30. https://doi.org/10.1016/j.trpro.2019.12.015.

Schill, Wolf-Peter, Gerbaulet, Clemens, 2015. Power system impacts of electric vehicles in Germany: charging with coal or renewables? Appl. Energy 156, 185–196. https://doi.org/10.1016/j.apenergy.2015.07.012.

Schlund, David, Theile, Philipp, 2022. Simultaneity of green energy and hydrogen production: analysing the dispatch of a grid-connected electrolyser. Energy Pol. 166, 113008 https://doi.org/10.1016/j.enpol.2022.113008.

Seljom, Pernille, Rosenberg, Eva, 2018. A scandinavian transition towards a carbon-neutral energy system. In: George, Giannakidis (Ed.), Limiting Global Warming to Well below 2 °C, Vol. 64. With Assistance of Kenneth Karlsson, Maryse Labriet, Brian Ó. Gallachóir. Springer (Lecture Notes in Energy Ser, v. 64), Cham, pp. 105–121.

Sensfuß, Frank, Lux, Benjamin, Bernath, Christiane, Kiefer, Christoph, Pfluger, Benjamin, Kleinschmitt, Chris, 2021. Langfristszenarien für die Transformation des Energiesystems in Deutschland. Treibhausgasneutrale Hauptszenarien Modul Energieangebot. Edited by Bundesministerium für Wirtschaft und Energie (BMWi). Consentec GmbH; Fraunhofer-Institut für System- und Innovationsforschung ISI; ifeu – Institut für Energie- und Umweltforschung Heidelberg. Technische Universität Berlin.

Siegemund, Stefan, Trommler, Marcus, Kolb, Ole, Zinnecker, Valentin, 2017. «E-FUELS» STUDY. The potential of electricity-based fuels for low-emission transport in the EU. An expertise by LBST and dena. Edited by Deutsche Energie-Agentur GmbH (dena). Deutsche Energie-Agentur GmbH; Ludwig-Bölkow-Systemtechnik GmbH. Berlin. https://www.dena.de/fileadmin/dena/Dokumente/Pdf/9219_E-FUELS-STUDY_The_potential_of_electricity_based_fuels_for_low_emission_transport_in_the_EU.pdf checked on 3/22/2022.

Wang, Huan, Chen, Wenying, Shi, Jingcheng, 2018. Low carbon transition of global building sector under 2- and 1.5-degree targets. Appl. Energy 222 (2), 148–157. https://doi.org/10.1016/j.apenergy.2018.03.090.

Yilmaz, Hasan Ümitcan, Fouché, Edouard, Dengiz, Thomas, Krauß, Lucas, Keles, Dogan, Fichtner, Wolf, 2019. Reducing energy time series for energy system models via self-organizing maps. IT Inf. Technol. 61 (2-3), 125–133. https://doi.org/10.1515/itit-2019-0025.

Paper B:

Stand-alone power-to-X production dynamics - A multi-method approach to quantify the emission-cost reduction trade-off

Uwe Langenmayr[a], Paul Heinzmann[a], Alexander Schneider[a], Manuel Ruppert[a], Andreas Rudi[a], Wolf Fichtner[a]

[a] Karlsruhe Institute of Technology (KIT), Chair of Energy Economics, Karlsruhe, Germany

Reference

Langenmayr, U., Heinzmann, P., Schneider, A., Ruppert, M., Rudi, A., and Fichtner, W. Stand-alone power-to-X production dynamics: A multi-method approach to quantify the emission-cost reduction trade-off. *Journal of Industrial Ecology*, page jiec.70085, July 2025a. ISSN 1088-1980, 1530-9290. doi:10.1111/jiec.70085. URL `https://onlinelibrary.wiley.com/doi/10.1111/jiec.70085`

DOI: 10.1111/jiec.70085

RESEARCH ARTICLE

JOURNAL OF INDUSTRIAL ECOLOGY WILEY

Stand-alone power-to-X production dynamics

A multi-method approach to quantify the emission-cost reduction trade-off

Uwe Langenmayr | **Paul Heinzmann** | **Alexander Schneider** | **Manuel Ruppert** | **Andreas Rudi** | **Wolf Fichtner**

Institute for Industrial Production (IIP), Karlsruhe Institute of Technology (KIT), Karlsruhe, Germany

Correspondence
Uwe Langenmayr, Institute for Industrial Production (IIP), Karlsruhe Institute of Technology (KIT), Karlsruhe, Germany.
Email: uwe.langenmayr@kit.edu

Editor Managing Review: Luk Van Wassenhove

Abstract

Power-to-X (PtX) processes allow for increased utilization of renewable energy in sectors like transportation, heat, and industry, where greenhouse gas emissions are hard to abate or irreducible. However, due to significantly higher production costs than conventional alternatives and the requirement of lower greenhouse gas footprints, PtX processes must aim for low-cost and low-emission production. This work introduces a multi-method approach by combining process simulation, techno-economic analysis, life cycle assessment, renewable electricity generation modeling, and multi-objective optimization to investigate the relationship between PtX production costs and greenhouse gas emissions to support investment decisions. The approach is applied to produce renewable hydrogen, Fischer–Tropsch crude, and methanol by considering global weather data with hourly temporal resolution. Our results show that locations with high wind capacity factors achieve the lowest costs and greenhouse gas emissions, and locations with high solar PV capacity factors perform worst in the context of greenhouse gas emissions when producing PtX products, primarily due to the emission-intensive production of solar PV modules. Locations with mixed capacity factors of wind and solar PV allow cost-efficient greenhouse gas emissions reduction since solar PV capacities can be substituted with a combination of wind generation capacities and battery storage. In addition, flexible PtX technologies reduce costs and greenhouse gas emissions significantly since fewer auxiliary components, like storage, are needed.

KEYWORDS
industrial ecology, multi-method approach, multi-objective optimization, open source, power-to-X, renewable energy carriers

1 | INTRODUCTION AND LITERATURE REVIEW

The transformation of the electricity sector is in full swing toward renewable energies. Other sectors, such as industry, heating, agriculture, and transportation, need to increase their share of renewable energy to defossilize. While electrification of processes provides suitable, cost-effective,

and efficient solutions for many processes, not all processes can be electrified. Especially if the energy carriers are used as feedstock, for example, in ammonia production, electrification is not an alternative (International Energy Agency [IEA], 2021, 2023).

Offering an option of indirect electrification, power-to-X (PtX) processes help to increase the share of renewable energy beyond the supply of renewable electricity by transforming electrical energy into chemical energy (Oyewo et al., 2024). Stand-alone PtX facilities are of particular interest, since favorable locations regarding land availability and capacity factors of the renewable generators, without the limitation of grid availability, can be chosen to produce large quantities of PtX products at low costs. Not relying on grid electricity avoids additional costs like taxes and levies, and avoids grid electricity with a potential high share of conventional energy carriers, which is necessary to comply with the European regulation of grid electricity supply to produce renewable electricity-based PtX products (European Union, 2023).

The coupling element between electric energy and chemical energy carriers in PtX facilities is mainly based on electrolysis processes, with water electrolysis as the most common technology (Rego de Vasconcelos & Lavoie, 2019). In combination with renewable electricity, power-to-gas (PtG) technologies produce green hydrogen. Hydrogen can be used directly or as an intermediate product, transported, or stored in a gaseous or liquid state. A potential large-scale off-taker of green hydrogen might be the steel industry, where the direct reduction of iron ore offers a future low-carbon alternative to blast furnace ovens (Jacobasch et al., 2021). Other PtG applications include the production of gaseous fuels and energy carriers based on hydrogen, like synthetic natural gas (SNG) (Götz et al., 2016; Tremel, 2018).

In power-to-liquid applications, green hydrogen is used as an intermediate to generate liquid fuels and energy carriers, like synthetic methanol (MeOH) or Fischer–Tropsch (FT) synthesis-based sustainable aviation fuels (SAF) (Schmidt et al., 2018; Schorn et al., 2021). Power-to-liquid and advanced PtG applications rely on the supply of additional input streams besides green hydrogen. Carbon sources, mainly CO_2, are needed to generate synthetic hydrocarbons (SNG, SAF, e-Diesel, and MeOH), while renewable ammonia production relies on nitrogen supply (Tremel, 2018). FT synthesis-based hydrocarbons offer a broad range of applications where fuels with high energy densities are needed, such as aviation, sea shipping, and chemical industries (De Klerk, 2008; Dry, 1999). MeOH is required primarily in today's chemical industries as a base chemical but can be used as an intermediate for many products in the future by applying processes like methanol-to-olefins, methanol-to-gasoline, or methanol-to-jet, or as a marine fuel (Schemme et al., 2020).

In summary, PtX concepts are as broad as their application areas. Still, even though they enable the increase of renewable energy in manifold sectors, only a few have been commercialized so far since low-cost and renewable production faces manifold challenges (IEA, 2024). PtX technologies require multidisciplinary research to investigate their potential from technological, economic, and environmental dimensions, while the interaction of different technologies also needs to be addressed. Renewable electricity generation (RES-E) volatility and region-specific renewable availability are especially new challenges for operators of conventional synthesis systems, which prevent the application of off-the-shelf solutions.

We have identified and compared studies investigating PtX plants (see Table 2 in Section A1 of Supporting Information S1). The research on PtX plants is characterized by several dimensions that can be assessed using different methodologies, approaches to consider RES-E generation, and objectives. Looking at methods, life cycle assessments (LCA) calculate the life cycle impact of defined systems to investigate criteria, such as the environmental or social impact of the system (Campos-Guzmán et al., 2019; Hoppe et al., 2018; Koj et al., 2019; Werker et al., 2019). Process simulations aim to create realistic models of chemical plants to assess technical feasibility and scalability while improving processes. They are often combined with techno-economic assessments (TEA) to estimate costs and evaluate economic feasibility using spreadsheet calculations (Albrecht et al., 2017; Heinzmann et al., 2021; Runge et al., 2020). TEAs can also be conducted solely based on literature values (Armijo & Philibert, 2020; Morgan et al., 2017) and integrated into optimization approaches like linear programming (LP) or mixed-integer linear programming (Berger et al., 2021; Maggi et al., 2020).

The definition of the system precedes the actual LCA. The same applies to TEAs based on process simulations, where the process simulation defines the system. The consumption of feedstocks is assumed to be steady and often integrated into calculations by applying constants. When studying RES-E generation, such constants are usually the levelized electricity costs and yearly capacity factors (Kadam & Yadav, 2024; Schack et al., 2016). A first approach to address the limitations of such a simplification is to consider RES-E generation in separate models. Osman et al. (2020) model hydrogen supply as an LP. Fasihi et al. (2016) overlay the RES-E generation profiles to calculate the levelized costs of electricity generation and yearly capacity factors. Both works use the results of their RES-E modeling in subsequent, separate models. However, even though the RES-E generation is considered, it is reduced to a single parameter in the main model. More advanced approaches model the RES-E generation with the PtX plant by integrating capacity factor profiles of renewable generators with a resolution of up to 1 h (Berger et al., 2021; Sherwin, 2021). Such approaches consider the volatility and availability of RES-E generation and allow for more realistic decisions.

The above-mentioned literature focuses on single objectives, like calculating production costs or environmental or social life cycle impacts. However, single objectives might ignore potential trade-offs between different objectives. Studies increasingly use multi-criteria assessment to close this research gap. In Lee et al. (2022) and Terlouw et al. (2024), production costs and greenhouse gas (GHG) emissions are considered. However, their approach assesses both objectives independently. Multi-objective optimization (MOO) is applied to consider both objectives simultaneously. For instance, whereas Farajiamiri et al. (2023) use MOO to calculate the trade-off between production costs, land use, and water use, Kenkel et al. (2021) investigate the trade-off between production costs and GHG emissions.

The review of existing literature shows a clear gap in the systematic evaluation of the entire PtX chain. Steady-state methods like LCA, process simulations, and spreadsheet-based TEAs can provide detailed information on the plant. However, the volatility of RES-E generation is reduced to a

constant. In addition, LCA and spreadsheet-based TEAs are only applicable to defined systems and cannot be used to derive optimal facility design regarding environmental or economic objectives. Conversely, approaches with more sophisticated methods of integrating RES-E generation often simplify the technical, economic, and ecological characteristics of PtX plants. Finally, most approaches concentrate on single objectives, ignoring potential inconsistencies and trade-offs of multiple objectives like production costs and GHG emissions. The identified research gap leads to the following research questions:

1. How can a systematic evaluation of the entire PtX plant be implemented?
2. How is the trade-off between production costs and GHG emissions characterized, and how can it provide decision support for PtX plant investments?
3. What are the key decisions to reduce production costs and GHG emissions of PtX products?
4. How do different technologies and locations perform compared to each other, and what are the key drivers of these performances?

Our research aims to overcome the mentioned limitations by systematically developing a holistic methodology to evaluate the entire PtX process chain. First, we use process simulation to gain in-depth information on feedstocks, auxiliary materials, chemical conversions, and plant capacity dimensions. We combine the derived information with TEA and LCA to understand the economic and environmental impact of each process chain's components. Second, we enrich the information with temporally and geographically highly resolved RES-E profiles within a multi-objective mixed-integer linear optimization to investigate each process performance in the context of volatile renewable generation. The combination of TEA, LCA, and optimization allows the calculation of optimal capacities concerning economic and environmental objectives based on the location-specific RES-E generation. With this approach, the limitations of individual methods are addressed and synergies exploited (see Figure 1 in Section A2 of Supporting Information S1). For example, the limitation of LCA regarding the necessary predefinition of the plant design and simplified RES-E consideration can be addressed, and the environmental assessment can be scaled to numerous individual locations. Similar holds for the process simulation methodology in combination with spreadsheet-based TEA. To our knowledge, such a holistic approach has not been conducted yet. This approach allows for decision support in the context of PtX investments by providing detailed insights into developing optimal production costs, greenhouse gas emissions, capacities, and operations at a high temporal and geographical resolution. Based on individual preferences, strategic decisions can be made on optimal locations, capacities, and operations while quantifying production costs and GHG emissions. The developed multi-method approach is showcased using green hydrogen, FT crude, and MeOH production. This manuscript's results and discussion section will focus mainly on the MOO, and the results and discussion of the process simulation, LCA, and TEA will be presented in Sections A3.3, A3.5, and A4.3 of Supporting Information S1.

2 | METHODOLOGY

The following chapter describes the developed method of this work, which is further depicted in the graphical abstract in Figure 1. While we apply the complete methodology to fully understand the underlying technology and derive technical, economic, and environmental parameters, while ensuring consistency, users can use only parts of the method to reduce the complexity if suitable data exists.

2.1 | Process simulation and techno-economic analysis

Next to designing new processes or modeling existing ones, process simulation in chemical engineering is used to generate mass and energy balance data of the relevant streams and unit operations of a process design to perform TEA. The process designs to be considered and analyzed have to be defined in the first stage and can be adjusted during process simulation iterations. While simple processes and flowsheets might be examined by hand calculation, process simulation tools are necessary to solve more complex problems and to supply a sufficient database for comprehensive analyses (Haydary, 2019).

Regarding potential applications, FT synthesis-based hydrocarbons and MeOH, besides the direct usage of green hydrogen, are seen as power-to-liquid products with a high chance of commercialization due to the potential to replace fossil-based production of base chemicals and fuels. FT synthesis products, MeOH, and their derivatives can substitute currently used products without or with minor application and infrastructure changes and are often called "drop-in" solutions (Schemme et al., 2020).

The applied process simulations aim to create reliable data on the production of (A) FT synthesis raw products and (B) MeOH by using mature technologies. The generated data is input for the subsequent techno-economic analysis, LCA, and the MOO. The techno-economic analysis aggregates detailed process steps into modules, providing relevant input/output correlations. Both chemical processes (A) and (B) are based on the supply of green hydrogen and gaseous CO_2. In (A), three product fractions are produced (naphtha, middle distillate, and wax) but are then brunched as one product. Further processing of the raw FT synthesis products could lead to higher-value products like SAF, diesel, and gasoline. Still, it would imply the need for additional equipment and a deeper investigation into the demand markets to find the optimal flowsheet design. Therefore, upgrading

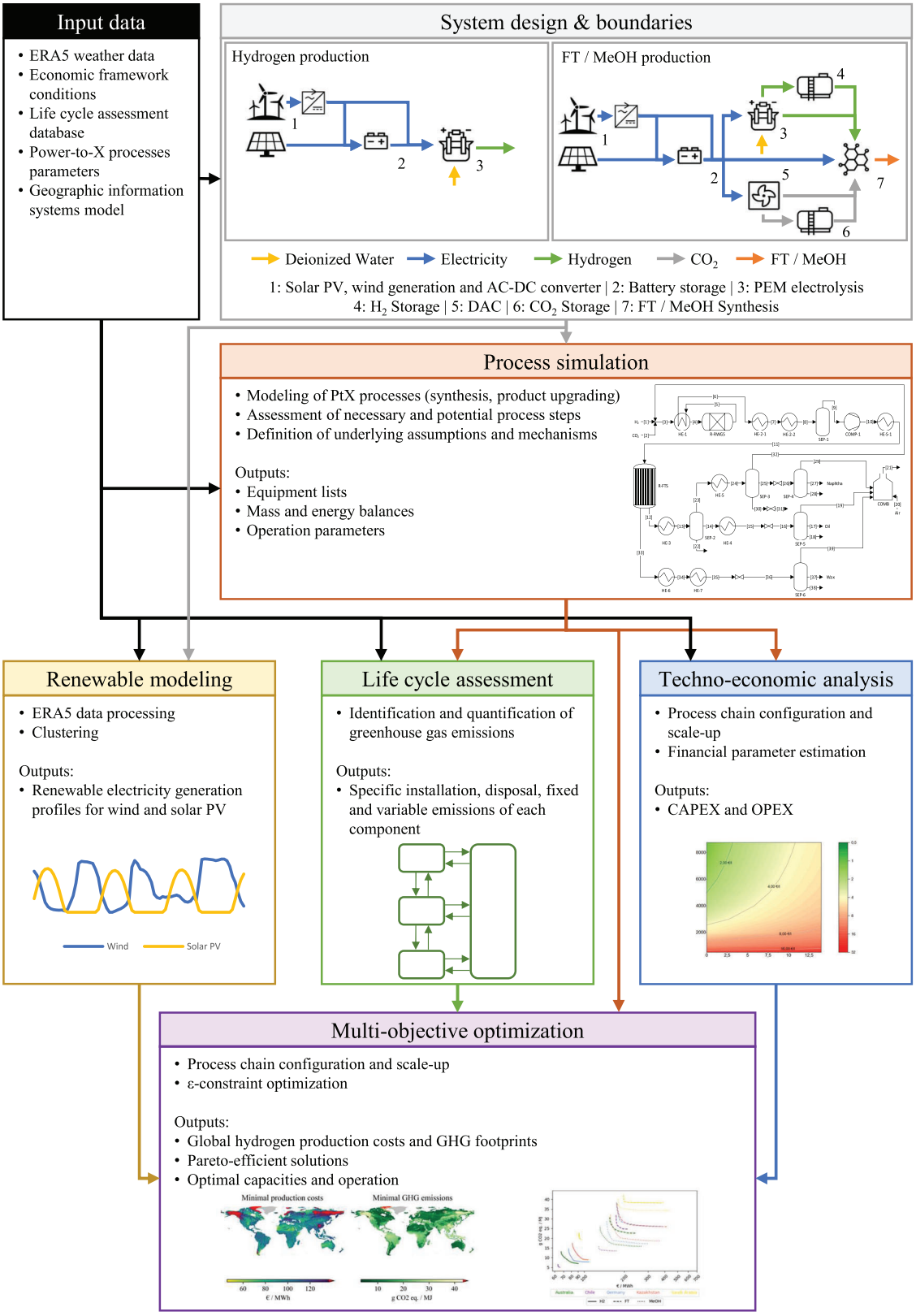

FIGURE 1 Graphical abstract of the multi-method approach.

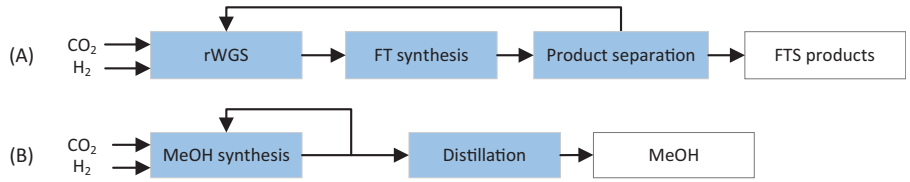

FIGURE 2 Simplified block flowsheet of the two synthesis process configurations: (a) FT synthesis-based process and (b) synthetic methanol-based process.

these raw products is outside the scope of this work. The same principle applies to process scheme (B), in which MeOH could be upgraded by applying further processes, but with the loss of generality of product application. Like in the current international structures, global trade will likely rely on primary product streams (currently petrol oil), and the upgrading or processing will be near the potential demanders.

The process setup for (A) relies on the supply of synthesis gas, a stoichiometric mixture of carbon monoxide (CO) and H_2, since the low-temperature FT synthesis applied in this work uses Cobalt (Co)-based catalysts that are not active for the conversion of CO_2 under relevant process conditions. To generate a suitable synthesis gas stream, CO_2 and H_2 are converted into synthesis gas by the reverse water gas shift reaction:

$$CO_2 + H_2 \rightleftharpoons CO + H_2O\ \Delta_R H^0 = 41\ \text{kJ/mol} \quad \text{(I)}$$

The reverse water gas shift reaction is endothermic, so heat input is required. To prevent the formation of methane and carbon deposition (e.g., by the Boudouard reaction) while securing sufficient conversion, high-temperature levels of up to 1000°C are chosen. Due to the highest energy efficiency in a power-to-liquid FT synthesis process, an electrically heated reverse water gas shift reaction reactor is assumed.

In low-temperature FT synthesis reactors, *n*-paraffins are the main product. The reaction equation for the generation of *n*-paraffins by low-temperature FT synthesis can be simplified by assuming $(CH_2)_n$ as a *n*-paraffin with the chain length *n*:

$$CO + 2H_2 \rightarrow (CH_2)_n + H_2O\ \Delta_R H^0 = -165\ \text{kJ/mol} \quad \text{(II)}$$

The process simulation assumes a particular product distribution according to the Anderson–Schulz–Flory distribution, using an alpha value of 0.9, referring to typical product distributions of low-temperature FT synthesis processes based on Co catalysts (Van De Loosdrecht et al., 2013).

For MeOH synthesis (B), no pre-processing of the incoming CO_2 and H_2 is necessary. The CO_2- and CO-based methanol synthesis reactions are represented by Equations (III) and (IV), with the consideration that the water gas shift reaction (V) and the reverse water gas shift reaction (I) is likely to occur as well, based on reactor conditions and composition:

$$CO_2 + 3H_2 \rightarrow CH_3OH + H_2O\Delta_R H^0 = -49.2\ \text{kJ/mol} \quad \text{(III)}$$

$$CO + 2H_2 \rightarrow CH_3OH\ \Delta_R H^0 = -90.8\ \text{kJ/mol} \quad \text{(IV)}$$

$$CO + H_2O \rightleftharpoons CO_2 + H_2\Delta_R H^0 = -41\ \text{kJ/mol} \quad \text{(V)}$$

Figure 2 shows a simplified flowsheet for both processes (A) and (B):

While the estimation of production costs is in the scope of the optimization in this work, the applied method demands techno-economic input parameters derived from process simulations and the literature. The results of the process simulations provide the necessary data to estimate equipment cost. This is done either by using the built-in Aspen Plus Economic Analyzer for most of the equipment needed or by applying cost correlations and data from the literature, especially for specialized equipment. To update the cost estimation to a targeted reference time of 2023, the Chemical Engineering Plant Cost Index (CEPCI) was used. The application of surcharge factors is chosen to derive the entire capital investment, using the ratio factors from Peters et al. (2004) for fluid processing plants. Details about these cost calculations can be found in Section A3 of Supporting Information S1.

2.2 | Life cycle assessment

Heeding the ISO 14040 series, LCA is applied to evaluate the environmental burdens of the considered value chains. Since the global warming potential is one of the most relevant impact categories in today's cross-sectoral decision-making, this LCA focuses on identifying and quantifying

GHG emissions. The "cradle-to-gate" approach considers GHG emissions along the process chain from mining raw materials to the produced energy carrier (on the production site) and the end-of-life treatment of the waste flows.

The process chains for producing hydrogen, FT crude, and MeOH include RES-E, a battery, and proton exchange membrane (PEM) electrolysis. In addition, next to the synthesis units (c.f. Figure 2), the pathways for producing FT crude and MeOH comprise a direct air capture (DAC) unit and buffer tanks and compressors for the intermediates (H_2 and CO_2). The LCA aims to provide the MOO model's fixed and variable CO_2 emissions. Due to the optimization of the single process steps, no functional units for the entire product system are defined. Instead, every process step is represented by one reference unit (i.e., 1 MWh of H_2 storage capacity is the reference unit for the H_2 storage tank). Excess heat/steam as a by-product in the synthesis processes is used for internal heat demands in the DAC process. Since no additional by-products are generated, the consideration of allocations in the product system is omitted.

The life cycle inventory data is primarily from the process simulations and comprises energy and mass flows and utilities like electricity and cooling water (c.f. Section A4 of Supporting Information S1). Constructional data from LCA literature are used and extrapolated to the needed magnitude. The characteristics of further flows, like operating materials and emissions, are also obtained from the literature. Correspondingly to their importance in today's energy transition approaches, LCA data on water electrolysis (Bareiß et al., 2019; Gerloff, 2021; Palmer et al., 2021; Terlouw et al., 2022) and on DAC (Chauvy & Dubois, 2022; Deutz & Bardow, 2021; Madhu et al., 2021; Terlouw et al., 2021) are detailed in the literature. While numerous LCA studies on green MeOH production (Cordero-Lanzac et al., 2022; Hank et al., 2019; Sollai et al., 2023; Zhu et al., 2022) are described in the literature, studies on FT synthesis are less abundant (Micheli et al., 2022; Rojas-Michaga et al., 2023). Completing the life cycle inventory, the underlying supply chain and background data are drawn from the ecoinvent database 3.9.1 using the modeling software openLCA 2.0.2. The underlying supply chains are connected by market processes primarily for Europe, since interests and technical know-how surrounding PtX processes are predominantly concentrated in Europe, even for global implementations. To avoid the controversial issue of allocating waste flows, the system model "Allocation at the Point of Substitution" (APOS) was chosen (Wernet et al., 2016). Detailed information on data usage and calculation for life cycle inventory is provided in Section A4.2 of Supporting Information S1.

The global warming potential is the most suitable impact category in the frame of this work regarding the relevance of the carbon footprint of a product or process in today's decision-making in the transformation and defossilization of the energy and transport sector. ReCiPe 2016 v1.03, midpoint (H), as one of the state-of-the-art impact assessment methods, provides the climate change impact as defined by the Intergovernmental Panel on Climate Change (2013), including the CO_2-equivalent of the different GHGs with a residence time of 100 years (GWP100) (Huijbregts et al., 2017).

2.3 | Multi-objective optimization

The developed mixed-integer linear program is an extension of the model of Langenmayr and Ruppert (2023) and considers multiple objectives to obtain Pareto optimal solutions. These solutions contain optimal capacities and operation of PtX plants, allowing for a comprehensive assessment of resulting production costs and GHG emissions of derived PtX products. Sets of modeling constraints based on process simulation data ensure the appropriate implementation of technological processes. Economic and environmental data are incorporated into the model according to objective functions. Finally, the model allows for considering local data (e.g., weather conditions) to customize the process for specific locations. Whereas LCA and TEA define the system boundaries for the analysis, the optimization is performed for explicit case studies within the analysis scope. Such an approach is challenging to scale to numerous locations with individual properties like RES-E capacity factors. MOO considers each location's properties and economic and environmental data simultaneously, and determines optimal capacities and operations for each location. This makes MOO especially suitable for numerous locations with individual properties, as shown in the case studies presented in Section 3.3.

The first objective function (Equations 1 and 2) minimizes the annual total costs of the PtX processes, which consist of the annualized investment (*ANN*), yearly fixed maintenance and operation costs (*FOM*), variable maintenance and operation costs (*VOM*) of each component *k*, and dispatch costs from the purchase, selling, and disposal of each commodity *c*, and start-up costs of components (*SU*). Investment *i* also includes renewed investments in components after their service life and residual values of components at the end of the PtX plant's service life.

$$\begin{aligned}\text{Total costs} = &\sum_{k}\left(i_k\left(\text{ANN}_k+\text{FOM}_k\right)+\text{SU}_k+\sum_{c}\sum_{t}x^{\text{out}}_{k,s^{MO}(k),c,t}\cdot\text{VOM}_k\cdot\text{W}_c\right)+\sum_{s^S}\left(i_{s^S}\left(\text{ANN}_{s^S}+\text{FOM}_{s^S}\right)+\sum_{c}\sum_{t}x^{\text{charge}}_{s^S,c,t}\cdot\text{VOM}_{s^S}\cdot\text{W}_c\right)\\ &+\sum_{g}\left(i_g\left(\text{ANN}_g+\text{FOM}_g\right)+\sum_{c}\sum_{t}x^{\text{generation}}_{g,s^G(g),c,t}\cdot\text{VOM}_g\cdot\text{W}_c\right)+\sum_{c}\sum_{t}\left(\sum_{s^P}x^{\text{purchase}}_{s^P,c,t}\cdot\text{P}^{\text{purchase}}_{s^P,c,t}-\sum_{s^Q}x^{\text{sell}}_{s^Q,c,t}\cdot\text{P}^{\text{sell}}_{s^Q,c,t}\right)\cdot\text{W}_c \qquad (1)\end{aligned}$$

$$f_1 = \min \text{Total costs} \qquad (2)$$

The second objective function (Equations and 4) minimizes the annual total GHG emissions of the PtX processing plant. Carbon footprints are considered in the installation of the components ($GF^{\text{installation}}$), the fixed annual operation and maintenance (GF^{FOM}), the variable operation and maintenance (GF^{VOM}), and the disposal of the components (GF^{disposal}).). In addition, the GHG footprint of purchased (GF^{purchase}) and sold (GF^{sell}) commodities are also considered.

$$\begin{aligned}\text{Total emissions} = &\sum_{k}\left(\text{cap}_k\left(\text{GF}_k^{\text{installation}}+\text{GF}_k^{\text{disposal}}+\text{GF}_k^{\text{fixed O\&M}}\right)+\sum_{c}\sum_{t}x^{\text{out}}_{k,s^{MO}(k),c,t}\cdot\text{GF}_k^{\text{variable O\&M}}\cdot\text{W}_c\right)\\&+\sum_{s^S}\left(\text{cap}_{s^S}\left(\text{GF}_{s^S}^{\text{installation}}+\text{GF}_{s^S}^{\text{disposal}}+GF_{s^S}^{\text{fixed O\&M}}\right)+\sum_{c}\sum_{t}x^{\text{charge}}_{s^S,c,t}\cdot\text{GF}_{s^S}^{\text{variable O\&M}}\cdot\text{W}_c\right)\\&+\sum_{g}\left(\text{cap}_g\left(\text{GF}_g^{\text{installation}}+\text{GF}_g^{\text{disposal}}+\text{GF}_g^{\text{fixed O\&M}}\right)+\sum_{c}\sum_{t}x^{\text{generation}}_{g,s^G(g),c,t}\cdot\text{GF}_{s^G(g)}^{\text{variable O\&M}}\cdot\text{W}_c\right)\\&+\sum_{c}\sum_{t}\left(\sum_{s^P}x^{\text{purchase}}_{s^P,c,t}\cdot\text{GF}_s^{\text{purchase}}-\sum_{s^Q}x^{\text{sell}}_{s^Q,c,t}\cdot\text{GF}_{s^Q}^{\text{sell}}\right)\cdot\text{W}_c\end{aligned}\tag{3}$$

$$f_2 = \min \text{Total emissions}\tag{4}$$

In this work, MOO combines both objective functions simultaneously to investigate the relation between costs and GHG emissions. Based on the work of Mavrotas (2009), the first step calculates the payoff table. In this payoff table, the result of f_2 when minimizing f_2 represents the GHG emission utopia value, and the result of minimizing f_2 when first minimizing f_1 represents the GHG emission nadir value approximation. We calculate the range between utopia and nadir value approximation, and separate the range into 100 intervals. In the second step, we incorporate the intervals in the optimization problem by adjusting f_1 and add a new constraint to consider the interval step.

$$f_1 = \min\left(\text{Total costs} - \text{slack}\cdot\varepsilon\right)\tag{5}$$

$$\text{Total emissions} + \text{slack} - e_i = 0\tag{6}$$

The constraint in Equation (6) ensures that the total emissions are lower than or equal to the precalculated interval value e_i. Using the slack variable in the objective function Equation (5) and in Equation (6), we ensure only efficient solutions are taken. The impact of the slack variable on the objective function is minimal since the epsilon coefficient is an adequately small number.

The constraints of the MOO represent the technical properties of the conversion units, like ramping abilities, minimal and maximal loads, and efficiencies. In addition, storage units are considered by defining their state of charge, minimal and maximal state of charge, charging and discharging efficiencies, charging and discharging power, and power-to-capacity ratios. Finally, generator units use hourly capacity factors and the capacity variable to calculate the hourly RES-E generation. Constraints concerning commodities define the option to buy, sell, emit, and obtain the individual commodity or to set total yearly demand, which the optimized PtX plant must cover. Next to technical properties, economic and environmental data are connected to the optimization problem, like scaling factors, CAPEX, and market data (purchase and selling prices and emissions). Since the setup of components and utilized options, such as purchasing and selling commodities, can be individually adjusted, the model applies to manifold processes and case studies. The complete model is presented in Section A5.1 of Supporting Information S1.

3 | RESULTS

The following section contains an excerpt of the process simulation, TEA, and LCA results. The main results stem from the MOO, which consists of a global view of green hydrogen production, a location-specific analysis of the relationship between production costs and GHG emissions, and investment decision support for the PtX production of hydrogen, FT, and MeOH. Comprehensive information and results on the other applied methods can be found in Sections A3.3, A3.5, and A4.3 of Supporting Information S1.

TABLE 1 Key results of the process simulations and the techno-economic analysis.

Parameter	(A) FT	(B) MeOH
Input	0.439 kg H_2	0.191 kg H_2
	3.138 kg CO_2	1.395 kg CO_2
	4.386 kWh electricity	0.314 kWh electricity
Output	1 kg FT crude	1 kg MeOH
I_0	167,865,923€	118,669,824€
C_0	22,767 kg_{FT}/h	52,312 kg_{MeOH}/h
δ	0.67	0.67

TABLE 2 Fixed and variable GHG emissions from life cycle assessment used in the optimization model.

Processes	Fixed emissions per capacity $GF^{installation} + GF^{FOM} + GF^{disposal}$		Variable emissions per output GF^{VOM}	
Wind turbine	1,115	kg CO_{2eq} per kW	0.19	kg CO_{2eq} per MWh
PV system	2,398	kg CO_{2eq} per kW	0.00002	kg CO_{2eq} per MWh
PEM electrolysis	114	kg CO_{2eq} per kW input	0.0009	kg CO_{2eq} per kWh input
H_2 compressor	394	kg CO_{2eq} per kg H_2/h	0	kg CO_{2eq} per kg H_2
DAC unit	18.8	kg CO_{2eq} per kg CO_2/h	0.0476	kg CO_{2eq} per kg CO_2
CO_2 compressor	2.7	kg CO_{2eq} per kg CO_2/h	0	kg CO_{2eq} per kg CO_2
FT synthesis	6,146	kg CO_{2eq} per kg FT crude/h	0.094	kg CO_{2eq} per kg FT crude
MeOH synthesis	2,685	kg CO_{2eq} per kg MeOH/h	0.028	kg CO_{2eq} per kg MeOH
LFP battery	105,645	kg CO_{2eq} per MWh	0	kg CO_{2eq} per MWh
H_2 storage vessel	69,270	kg CO_{2eq} per t H_2	0	kg CO_{2eq} per t H_2
CO_2 storage vessel	1,598	kg CO_{2eq} per t CO_2	0	kg CO_{2eq} per t CO_2

3.1 | Results of process simulation

For the MOO, the normalized inputs and outputs are of interest, as well as the investment I_0 needed for a base capacity C_0 sized synthesis unit and, if applicable, a scaling exponent δ, which adjusts the investment I to the actual capacity C by taking into account economies of scale, as displayed in Equation (7). The investment I can be calculated based on different capacities C, resulting in an investment curve. This curve is linearized into segments (c.f. Section A5.2 of Supporting Information S1) and integrated into the MOO to calculate the specific investment i_k of each component (Equation 1).

$$\frac{I}{I_0} = \left(\frac{C}{C_0}\right)^{\delta} \tag{7}$$

Table 1 sums up the process simulation and economic analysis results. The results are based on a steady-state simulation of a PtX plant with an input of 10 t/h H_2.

3.2 | Results of life cycle assessment

The MOO model needs the one-time emissions associated with the plant and site construction ($GF^{installation}$, GF^{FOM}, and $GF^{disposal}$) and the ongoing emissions (GF^{VOM}) (Equation 3). Thus, the results are divided into fixed and variable emissions, as shown in Table 2. Since disposal efforts per unit occur only once, their resulting emissions are also included in the fixed emissions. Additional information on the results, their sensitivity, and the validity of the LCA are discussed in Section A4.3 of Supporting Information S1.

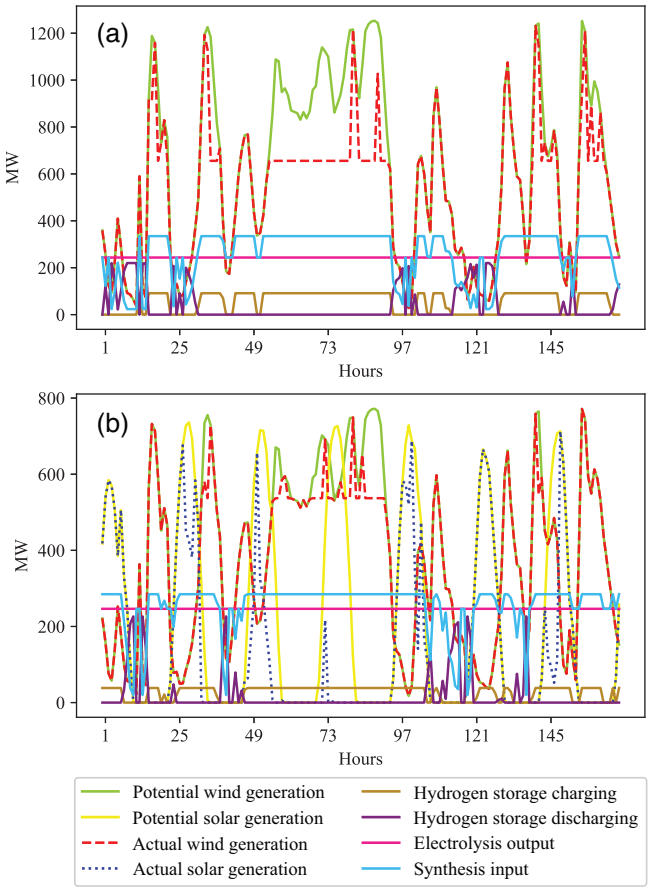

FIGURE 3 Interplay between components having green hydrogen as input or output and renewable electricity supply in the case of environmental (a) and economic (b) optimization of FT production in Australia. Numerical data of the figure is given in Supporting Information S2.

3.3 | Results of the dynamic multi-objective optimization

We apply the MOO to the production of hydrogen, FT, and MeOH in five different locations (longitude and latitude): Chile (−71.00°, −53.00°), Australia (127.75°, −30.75°), Germany (8.78°, 53.75°), Kazakhstan (50.00°, 48.50°), and Saudi Arabia (36.50°, 28.50°). These locations were chosen to analyze the impact of different CFs: Chile has excellent wind conditions, Saudi Arabia has excellent PV conditions, and Germany, Australia, and Kazakhstan have mixed CFs. In the case of hydrogen, we additionally supply a global view on minimal production costs and GHG emissions. Eleven years of weather data for each location are obtained from the ERA 5 (Hersbach et al., 2020) dataset and processed with the open-source tool atlite (Hofmann et al., 2021) to capacity factor profiles of the RES-E generators. The wind capacity factor profiles include losses from AC to DC conversion. The clustering of the data is described in Langenmayr and Ruppert (2023). Next to synthesis and PEM electrolysis, we include battery, hydrogen, and CO_2 storage, as well as necessary compressors. The CO_2 is obtained from a low-temperature DAC. Techno-economic assumptions, which the process simulations have not covered, are provided in Tables 13–15 of Supporting Information S1.

The electricity supply of the PtX plants stems from using wind and solar PV electricity generation. Based on the hourly CF, the capacities of all components are dimensioned to achieve a sufficient and secure supply of all conversion components in the plant. In addition, the operation of the system is optimized. Figure 3 showcases an excerpt of the operation of FT production in Australia in the case of GHG emissions (A) and production costs (B) minimization. The figure clearly shows how components interact with each other hourly and how different objectives affect the choice of components and the operation.

3.3.1 | A global view of green hydrogen production

Our approach allows for a two-fold analysis. First, large areas for PtX implementations can be considered based on high-resolution geographical data. The maps in Figure 4 show the results of production costs and GHG emissions minimization on a global scale. This map can be used to get a

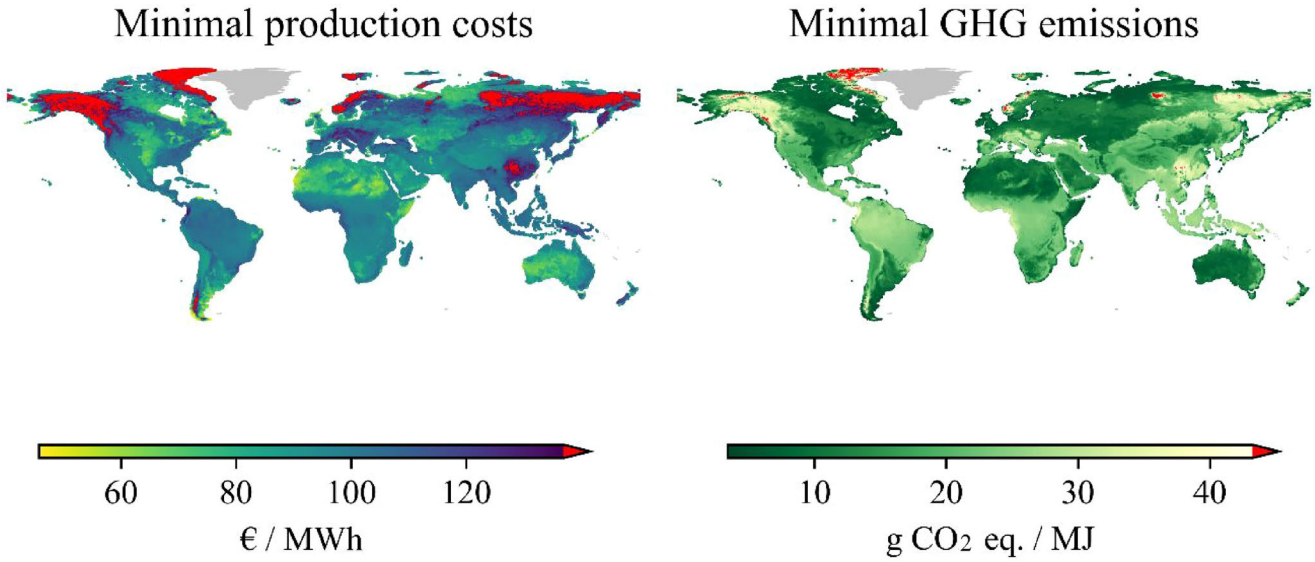

FIGURE 4 Minimal hydrogen production costs (left) and minimal GHG emissions of hydrogen production (right). Production cost and GHG emission outliers of the results are colored in red to reduce their impact on the scales. Numerical data of the figure is given in Supporting Information S2.

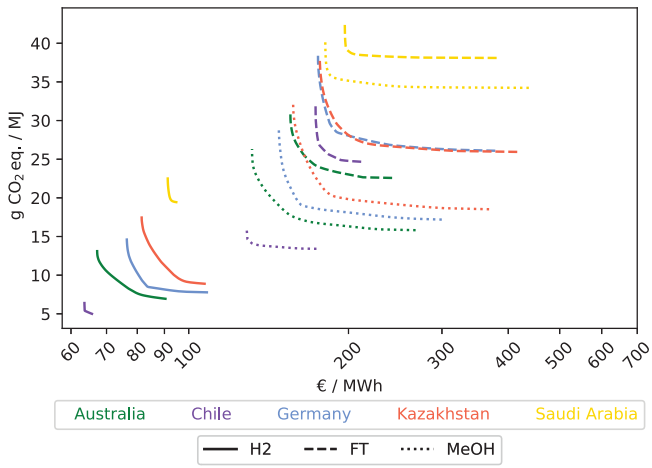

FIGURE 5 Pareto fronts for the chosen locations for producing renewable hydrogen. Numerical data of the figure is given in Supporting Information S2.

general overview of suitable PtX regions concerning minimal costs and GHG emissions. When production costs are minimized, the costs range from 45.73 to 443.42€/MWh, and in the case of GHG emission minimization, the emissions range from 3.45 to 76.68 g $CO_{2eq.}$/MJ.

3.3.2 | Detailed analysis of suitable PtX plant locations

Figure 5 shows the technology and location-specific Pareto fronts derived from the MOO. Looking at the hydrogen production Pareto fronts, it is visible that the location of Chile (CF wind: 5,093 h; CF solar: 1,116 h) performs best concerning GHG emissions and costs compared to the other locations in the case of hydrogen and MeOH production. The Pareto front in Chile is relatively narrow compared to different locations and technologies, showing that production costs and GHG emissions are predominantly aligned. As soon as locations increasingly use solar PV for electricity generation, the Pareto fronts start steeply increasing GHG emissions when aiming for lower production costs. The LCA results show that solar PV has higher GHG emissions per installed capacity than wind generation, and using solar PV to decrease production costs heavily increases GHG emissions. However, locations with mixed capacity factors, Germany (CF wind: 3,532 h; CF solar: 1,084 h), Australia (CF wind: 3,447 h; CF solar: 1,752 h), and Kazakhstan (CF wind: 2,684 h; CF solar: 1,241 h), can replace the majority of GHG emissions without significant increase of costs since

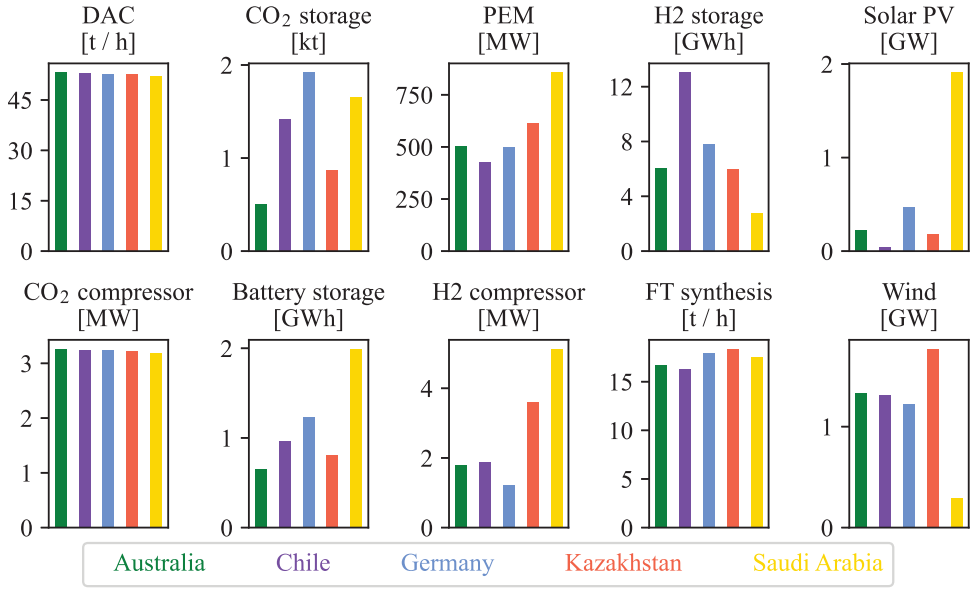

FIGURE 6 Capacities of all components of the Fischer–Tropsch production in different countries using the best trade-off capacities. Numerical data of the figure is given in Supporting Information S2.

replacing solar PV with wind generation in combination with battery storage is sufficient to cover the electricity demand. The advantage of diversification of electricity generation is less pronounced for the location of Saudi Arabia (CF wind: 1,026 h; CF solar: 1,956 h). Significant amounts of wind generation must be installed to reduce solar PV generation, increasing production costs and shortening the steep increase of GHG emissions.

Several challenges accompany the synthesis of green hydrogen into hydrogen derivatives. First, other commodities like CO_2 or heat are needed as input, next to electricity. Second, synthesis units are less flexible than PEM electrolysis, and a steady supply of inputs is necessary, which contradicts the volatile character of renewable energy. Therefore, the integration of renewable electricity is more demanding. The capital investment into the different synthesis technologies and the DAC units, in combination with overcapacities and storage units, to allow for a steady supply of inputs, results in higher costs. Like costs, GHG emissions also increase for the same reasons. The substantial cost increase is evident if the lowest possible GHG emissions are achieved. This circumstance emphasizes the need to consider both objectives when investing in hydrogen and its derivatives to avoid costly GHG abatement strategies. Comparing the course of the Pareto fronts of FT and MeOH shows an interesting aspect. While Chile's hydrogen and MeOH fronts perform better in terms of costs and emissions than all other countries, the FT front of Chile performs worse than the FT Pareto front in Australia. The reduced flexibility of the FT synthesis challenges electricity generation mainly from wind, resulting in additional auxiliary component capacities. Australia has good mixed capacity factors and can combine solar PV and wind generation capacities to supply more steady electricity.

Regarding the production costs of hydrogen as a product, the best-performing scenario (Chile) is reaching minimum costs close to the often-referred fossil reference threshold of 72€/MWh (2$/kg) (IEA, 2024). Methanol and FT crude production costs in the economically best-performing scenarios (Chile and Australia, respectively) are higher than their fossil references by a factor of three to four (Arnaiz Del Pozo et al., 2022; Hafner, 2022; IRENA and Methanol Institute, 2021; Oil & Energy Trends, 2024). The GHG emissions associated with fossil hydrogen production from natural gas or coal far exceed those of green hydrogen, even when carbon capture and storage are included. However, comparing the renewable hydrocarbon products MeOH and FT crude with their fossil references is difficult, as negative GHG emissions from DAC should be included. A more detailed comparison of the results with their fossil reference products can be found in Section A6.3 of Supporting Information S1.

The advantage of Pareto fronts is that trade-offs between production costs and GHG emissions are displayed, and investors can choose the Pareto solution that best fits their preferences regarding costs and emissions. In addition, for each trade-off, the MOO provides optimal capacities for all components and operational information to support the investment decision. Suppose a balanced relation between production costs and GHG emissions is admired. In that case, the trade-off of the Pareto front closest to the origin of the normalized coordinate system presents an appropriate choice. Using this balanced trade-off, Figure 6 shows the installed capacity, the primary decision in PtX investment, per location to produce FT. It highlights how the different CFs affect the generation unit's choice and all components' capacities. For example, the location in Saudi Arabia exploits high solar PV availability by installing large capacities of solar PV generation in combination with battery storage capacities, since solar PV can only provide a steady electricity supply during the day when storages are charged, but nighttime needs to be covered without RES-E generation. In contrast, Chile dismisses solar PV capacities since wind generation substitutes for all solar PV generation due to sufficient wind CFs. Further results and a sensitivity analysis are given in Section A6 of Supporting Information S1.

4 | SUMMARY, CONCLUSION, AND FUTURE WORK

PtX processes connect the electricity sector with other sectors like heating, transportation, and industry. This holds the opportunity to enable the energy transition toward sectoral defossilization. In the presented multi-method approach, we combined process simulations with techno-economic analysis and LCA to analyze different PtX products. The technology paths are modeled in detail by integrating necessary equipment, mass and energy balances, and economic and environmental parameters. The derived comprehensive data on producing green hydrogen, FT crude, and MeOH were applied in a dynamic MOO tool designed to model and optimize PtX pathways. The developed approach allows the determination of location-specific production costs and emissions, enables the trade-off analysis between both objectives based on optimized capacities, and successfully overcomes the limitations of the single-method approaches as commonly applied in the reviewed literature.

Our results show that wind generation is advantageous compared to solar PV generation for two reasons: First, wind electricity generation can achieve higher capacity factors, resulting in low-cost electricity generation. Second, the LCA shows that wind generation has lower specific GHG emissions per installed capacity, providing an environmental advantage compared to solar power generation. Therefore, regions with excellent wind conditions, like Patagonia in southern Chile, enable low-cost and low-emission production of renewable hydrogen and hydrogen derivatives. From a global perspective, locations with mixed renewable availability, such as Australia, Germany, and Kazakhstan, benefit from substituting wind with solar PV generation or vice versa to achieve either low-emission or low-cost production. Locations with high solar PV but low wind availability, like Saudi Arabia, show higher emissions in the production processes since large quantities of wind capacity have to be installed to reduce emissions. Based on the obtained Pareto fronts, investment decisions can be taken, and optimal capacities and operations can be determined to allow comparison of trade-off solutions. By comparing the different PtX energy carriers, we see that hydrogen performs best since auxiliary components to support the inflexible synthesis operation, like storage units, have lower capacities, and additional feedstock like CO_2 is unnecessary. The performance of FT and MeOH processes shows that individual characteristics like flexibility or heat demand derived from comprehensive process simulations affect production costs and emissions at each location individually, emphasizing the necessity for in-depth analysis and consideration of such parameters.

Even though we used an extensive multi-method approach to assess PtX processes, some methodological limitations exist. For example, uncertainties from RES-E or the PtX processes are not considered. Stochastic or robust optimization could be applied to consider such parameter uncertainties in future works. For the LCA, fixed capacities are assumed, which contradicts the variable capacities in the optimization model. Hence, conducting the LCA for different capacities could help to consider scaling effects and provide better GHG emission results. In addition, other impact categories could be included, such as water consumption or land use. Furthermore, the LCA heavily relies on life cycle inventory data, mainly affecting solar PV emissions. Long-term developments, such as producing solar PV modules with renewable electricity, are not considered in the data but could significantly reduce PV module production emissions. Furthermore, a more detailed process simulation of components could improve the modeling in the optimization context. For example, PEM electrolysis efficiency depends on the current power level and can exceed its nominal capacities for the short term. Finally, the multi-model approach only assesses the production of PtX products. However, it does not consider other important aspects such as transportation and infrastructure, water availability, or political conditions, which will further affect costs and GHG emissions and provide investment decision support.

AUTHOR CONTRIBUTIONS

Conceptualization: Uwe Langenmayr, Manuel Ruppert, and Andreas Rudi. *Methodology*: Uwe Langenmayr (renewable electricity generation modeling and multi-objective optimization), Paul Heinzmann (process simulation and techno-economic assessment), and Alexander Schneider (life cycle assessment). *Software*: Uwe Langenmayr. *Data curation*: Uwe Langenmayr, Paul Heinzmann, and Alexander Schneider. *Writing—original draft*: Uwe Langenmayr, Paul Heinzmann, Alexander Schneider, Manuel Ruppert, Andreas Rudi, and Wolf Fichtner. *Writing—review and editing*: Uwe Langenmayr, Paul Heinzmann, Alexander Schneider, Manuel Ruppert, Andreas Rudi, and Wolf Fichtner. *Visualization*: Uwe Langenmayr.

ACKNOWLEDGMENTS

Open access funding enabled and organized by Projekt DEAL.

CONFLICT OF INTEREST STATEMENT

The authors declare no conflicts of interest.

DECLARATION OF GENERATIVE AI AND AI-ASSISTED TECHNOLOGIES

To improve the readability of our work, we have applied Grammarly (v.1.2.92.1464).

DATA AVAILABILITY STATEMENT

The multi-objective optimization has been implemented in Python and is available as open source here: https://github.com/ulicious/ptx_now. All data to recreate the results in this manuscript are published with a CC by 4.0 license and can be found in Langenmayr (2025).

ORCID

Uwe Langenmayr https://orcid.org/0000-0002-3436-7228

REFERENCES

Albrecht, F. G., König, D. H., Baucks, N., & Dietrich, R.-U. (2017). A standardized methodology for the techno-economic evaluation of alternative fuels—A case study. *Fuel*, *194*, 511–526. https://doi.org/10.1016/j.fuel.2016.12.003

Armijo, J., & Philibert, C. (2020). Flexible production of green hydrogen and ammonia from variable solar and wind energy: Case study of Chile and Argentina. *International Journal of Hydrogen Energy*, *45*(3), 1541–1558. https://doi.org/10.1016/j.ijhydene.2019.11.028

Arnaiz Del Pozo, C., Cloete, S., & Jiménez Álvaro, Á. (2022). Techno-economic assessment of long-term methanol production from natural gas and renewables. *Energy Conversion and Management*, *266*, 115785. https://doi.org/10.1016/j.enconman.2022.115785

Bareiß, K., de la Rua, C., Möckl, M., & Hamacher, T. (2019). Life cycle assessment of hydrogen from proton exchange membrane water electrolysis in future energy systems. *Applied Energy*, *237*, 862–872. https://doi.org/10.1016/j.apenergy.2019.01.001

Berger, M., Radu, D., Detienne, G., Deschuyteneer, T., Richel, A., & Ernst, D. (2021). Remote renewable hubs for carbon-neutral synthetic fuel production. *Frontiers in Energy Research*, *9*, 671279. https://doi.org/10.3389/fenrg.2021.671279

Campos-Guzmán, V., García-Cáscales, M. S., Espinosa, N., & Urbina, A. (2019). Life cycle analysis with multi-criteria decision making: A review of approaches for the sustainability evaluation of renewable energy technologies. *Renewable and Sustainable Energy Reviews*, *104*, 343–366. https://doi.org/10.1016/j.rser.2019.01.031

Chauvy, R., & Dubois, L. (2022). Life cycle and techno-economic assessments of direct air capture processes: An integrated review. *International Journal of Energy Research*, *46*(8), 10320–10344. https://doi.org/10.1002/er.7884

European Union. (2023). Commission Delegated Regulation (EU) 2023/1184 of 10 February 2023 Supplementing Directive (EU) 2018/2001 of the European Parliament and of the Council by Establishing a Union Methodology Setting out Detailed Rules for the Production of Renewable Liquid and Gaseous Transport Fuels of Non-Biological Origin, 2023/1184. https://eur-lex.europa.eu/legal-content/EN/TXT/PDF/?uri=CELEX:32023R1184

Cordero-Lanzac, T., Ramirez, A., Navajas, A., Gevers, L., Brunialti, S., Gandía, L. M., Aguayo, A. T., Sarathy, S. M., & Gascon, J. (2022). A techno-economic and life cycle assessment for the production of green methanol from CO_2: Catalyst and process bottlenecks. *Journal of Energy Chemistry*, *68*, 255–266. https://doi.org/10.1016/j.jechem.2021.09.045

De Klerk, A. (2008). Fischer–Tropsch refining: Technology selection to match molecules. *Green Chemistry*, *10*(12), 1249. https://doi.org/10.1039/b813233j

Deutz, S., & Bardow, A. (2021). Life-cycle assessment of an industrial direct air capture process based on temperature–vacuum swing adsorption. *Nature Energy*, *6*(2), 203–213. https://doi.org/10.1038/s41560-020-00771-9

Dry, M. E. (1999). Fischer–Tropsch reactions and the environment. *Applied Catalysis A: General*, *189*(2), 185–190. https://doi.org/10.1016/S0926-860X(99)00275-6

Farajiamiri, M., Meyer, J.-C., & Walther, G. (2023). Multi-objective optimization of renewable fuel supply chains regarding cost, land use, and water use. *Applied Energy*, *349*, 121652. https://doi.org/10.1016/j.apenergy.2023.121652

Fasihi, M., Bogdanov, D., & Breyer, C. (2016). Techno-economic assessment of power-to-liquids (PtL) fuels production and global trading based on hybrid PV-wind power plants. *Energy Procedia*, *99*, 243–268. https://doi.org/10.1016/j.egypro.2016.10.115

Gerloff, N. (2021). Comparative life-cycle-assessment analysis of three major water electrolysis technologies while applying various energy scenarios for a greener hydrogen production. *Journal of Energy Storage*, *43*, 102759. https://doi.org/10.1016/j.est.2021.102759

Götz, M., Lefebvre, J., Mörs, F., McDaniel Koch, A., Graf, F., Bajohr, S., Reimert, R., & Kolb, T. (2016). Renewable power-to-gas: A technological and economic review. *Renewable Energy*, *85*, 1371–1390. https://doi.org/10.1016/j.renene.2015.07.066

Hafner, M., (with Luciani, G.). (2022). *The Palgrave handbook of international energy economics*. Springer International Publishing AG.

Hank, C., Lazar, L., Mantei, F., Ouda, M., White, R. J., Smolinka, T., Schaadt, A., Hebling, C., & Henning, H.-M. (2019). Comparative well-to-wheel life cycle assessment of OME 3–5 synfuel production via the power-to-liquid pathway. *Sustainable Energy & Fuels*, *3*(11), 3219–3233. https://doi.org/10.1039/C9SE00658C

Haydary, J., (with American Institute of Chemical Engineers). (2019). *Chemical process design and simulation: Aspen Plus and Aspen HYSYS applications*. Wiley.

Heinzmann, P., Glöser-Chahoud, S., Dahmen, N., Langenmayr, U., & Schultmann, F. (2021). *Techno-ökonomische Bewertung der Produktion regenerativer synthetischer Kraftstoffe*. Karlsruher Institut für Technologie (KIT). https://doi.org/10.5445/IR/1000140638

Hersbach, H., Bell, B., Berrisford, P., Hirahara, S., Horányi, A., Muñoz-Sabater, J., Nicolas, J., Peubey, C., Radu, R., Schepers, D., Simmons, A., Soci, C., Abdalla, S., Abellan, X., Balsamo, G., Bechtold, P., Biavati, G., Bidlot, J., Bonavita, M., … Thépaut, J. (2020). The ERA5 global reanalysis. *Quarterly Journal of the Royal Meteorological Society*, *146*(730), 1999–2049. https://doi.org/10.1002/qj.3803

Hofmann, F., Hampp, J., Neumann, F., Brown, T., & Hörsch, J. (2021). atlite: A lightweight Python package for calculating renewable power potentials and time series. *Journal of Open Source Software*, *6*(62), Article 62. https://doi.org/10.21105/joss.03294

Hoppe, W., Thonemann, N., & Bringezu, S. (2018). Life cycle assessment of carbon dioxide–based production of methane and methanol and derived polymers. *Journal of Industrial Ecology*, *22*(2), 327–340. https://doi.org/10.1111/jiec.12583

Huijbregts, M. A. J., Steinmann, Z. J. N., Elshout, P. M. F., Stam, G., Verones, F., Vieira, M., Zijp, M., Hollander, A., & van Zelm, R. (2017). ReCiPe2016: A harmonised life cycle impact assessment method at midpoint and endpoint level. *The International Journal of Life Cycle Assessment*, *22*(2), 138–147. https://doi.org/10.1007/s11367-016-1246-y

International Energy Agency (IEA). (2021). *Ammonia technology roadmap: Towards more sustainable nitrogen fertiliser production*. OECD. https://doi.org/10.1787/f6daa4a0-en

International Energy Agency (IEA). (2023). *Global hydrogen review 2023*. OECD. https://doi.org/10.1787/cb2635f6-en

International Energy Agency (IEA). (2024). *Global hydrogen eeview 2024*. IEA. https://www.iea.org/reports/global-hydrogen-review-2024

IRENA and Methanol Institute. (2021). Innovation Outlook : Renewable Methanol, International Renewable Energy Agency, Abu Dhabi.

Jacobasch, E., Herz, G., Rix, C., Müller, N., Reichelt, E., Jahn, M., & Michaelis, A. (2021). Economic evaluation of low-carbon steelmaking via coupling of electrolysis and direct reduction. *Journal of Cleaner Production*, *328*, 129502. https://doi.org/10.1016/j.jclepro.2021.129502

Kadam, R. S., & Yadav, G. D. (2024). Life cycle analysis of ammonia and methane production using green hydrogen and carbon dioxide. *Journal of Cleaner Production*, *449*, 141620. https://doi.org/10.1016/j.jclepro.2024.141620

Kenkel, P., Wassermann, T., Rose, C., & Zondervan, E. (2021). A generic superstructure modeling and optimization framework on the example of bi-criteria Power-to-Methanol process design. *Computers & Chemical Engineering*, *150*, 107327. https://doi.org/10.1016/j.compchemeng.2021.107327

Koj, J. C., Wulf, C., & Zapp, P. (2019). Environmental impacts of power-to-X systems—A review of technological and methodological choices in life cycle assessments. *Renewable and Sustainable Energy Reviews*, *112*, 865–879. https://doi.org/10.1016/j.rser.2019.06.029

Langenmayr, U. (2025). *Location-specific renewable profiles and Power-to-X parameters*. Zenodo. https://doi.org/10.5281/ZENODO.14848855

Langenmayr, U., & Ruppert, M. (2023). *Calculation of synthetic energy carrier production costs with high temporal and geographical resolution*. Karlsruher Institut für Technologie (KIT). https://doi.org/10.5445/IR/1000162460

Lee, H., Choe, B., Lee, B., Gu, J., Cho, H.-S., Won, W., & Lim, H. (2022). Outlook of industrial-scale green hydrogen production via a hybrid system of alkaline water electrolysis and energy storage system based on seasonal solar radiation. *Journal of Cleaner Production*, *377*, 134210. https://doi.org/10.1016/j.jclepro.2022.134210

Madhu, K., Pauliuk, S., Dhathri, S., & Creutzig, F. (2021). Understanding environmental trade-offs and resource demand of direct air capture technologies through comparative life-cycle assessment. *Nature Energy*, *6*(11), 1035–1044. https://doi.org/10.1038/s41560-021-00922-6

Maggi, A., Wenzel, M., & Sundmacher, K. (2020). Mixed-integer linear programming (MILP) approach for the synthesis of efficient power-to-syngas processes. *Frontiers in Energy Research*, *8*, 161. https://doi.org/10.3389/fenrg.2020.00161

Mavrotas, G. (2009). Effective implementation of the ε-constraint method in multi-objective mathematical programming problems. *Applied Mathematics and Computation*, *213*(2), 455–465. https://doi.org/10.1016/j.amc.2009.03.037

Micheli, M., Moore, D., Bach, V., & Finkbeiner, M. (2022). Life-cycle assessment of power-to-liquid kerosene produced from renewable electricity and CO_2 from direct air capture in Germany. *Sustainability*, *14*(17), 10658. https://doi.org/10.3390/su141710658

Morgan, E. R., Manwell, J. F., & McGowan, J. G. (2017). Sustainable ammonia production from U.S. offshore wind farms: A techno-economic review. *ACS Sustainable Chemistry & Engineering*, *5*(11), 9554–9567. https://doi.org/10.1021/acssuschemeng.7b02070

Oil and Energy Trends. (2024). Prices. *Oil and Energy Trends*, *49*(7–8), 52–54. https://doi.org/10.1111/oet.9_13128

Osman, O., Sgouridis, S., & Sleptchenko, A. (2020). Scaling the production of renewable ammonia: A techno-economic optimization applied in regions with high insolation. *Journal of Cleaner Production*, *271*, 121627. https://doi.org/10.1016/j.jclepro.2020.121627

Oyewo, A. S., Lopez, G., ElSayed, M., Galimova, T., & Breyer, C. (2024). Power-to-X economy: Green e-hydrogen, e-fuels, e-chemicals, and e-materials opportunities in Africa. *Energy Reports*, *12*, 2026–2048. https://doi.org/10.1016/j.egyr.2024.08.011

Palmer, G., Roberts, A., Hoadley, A., Dargaville, R., & Honnery, D. (2021). Life-cycle greenhouse gas emissions and net energy assessment of large-scale hydrogen production via electrolysis and solar PV. *Energy & Environmental Science*, *14*(10), 5113–5131. https://doi.org/10.1039/D1EE01288F

Peters, M. S., Timmerhaus, K. D., West, R. E., & West, R. E. (2004). *Plant design and economics for chemical engineers* (5th ed., international ed. 2004). McGraw-Hill. ISBN: 0-07-0496137-7.

Rego de Vasconcelos, B., & Lavoie, J.-M. (2019). Recent advances in power-to-X technology for the production of fuels and chemicals. *Frontiers in Chemistry*, *7*, 392. https://doi.org/10.3389/fchem.2019.00392

Rojas-Michaga, M. F., Michailos, S., Cardozo, E., Akram, M., Hughes, K. J., Ingham, D., & Pourkashanian, M. (2023). Sustainable aviation fuel (SAF) production through power-to-liquid (PtL): A combined techno-economic and life cycle assessment. *Energy Conversion and Management*, *292*, 117427. https://doi.org/10.1016/j.enconman.2023.117427

Runge, P., Sölch, C., Albert, J., Wasserscheid, P., Zöttl, G., & Grimm, V. (2020). Economic comparison of electric fuels produced at excellent locations for renewable energies: A scenario for 2035. *SSRN Electronic Journal*. https://doi.org/10.2139/ssrn.3623514

Schack, D., Rihko-Struckmann, L., & Sundmacher, K. (2016). Structure optimization of power-to-chemicals (P2C) networks by linear programming for the economic utilization of renewable surplus energy. In *Computer aided chemical engineering* (Vol. 38, pp. 1551–1556). Elsevier. https://doi.org/10.1016/B978-0-444-63428-3.50263-0

Schemme, S., Breuer, J. L., Köller, M., Meschede, S., Walman, F., Samsun, R. C., Peters, R., & Stolten, D. (2020). H_2-based synthetic fuels: A techno-economic comparison of alcohol, ether and hydrocarbon production. *International Journal of Hydrogen Energy*, *45*(8), 5395–5414. https://doi.org/10.1016/j.ijhydene.2019.05.028

Schmidt, P., Batteiger, V., Roth, A., Weindorf, W., & Raksha, T. (2018). Power-to-liquids as renewable fuel option for aviation: A review. *Chemie Ingenieur Technik*, *90*(1–2), 127–140. https://doi.org/10.1002/cite.201700129

Schorn, F., Breuer, J. L., Samsun, R. C., Schnorbus, T., Heuser, B., Peters, R., & Stolten, D. (2021). Methanol as a renewable energy carrier: An assessment of production and transportation costs for selected global locations. *Advances in Applied Energy*, *3*, 100050. https://doi.org/10.1016/j.adapen.2021.100050

Sherwin, E. D. (2021). Electrofuel synthesis from variable renewable electricity: An optimization-based techno-economic analysis. *Environmental Science & Technology*, *55*(11), 7583–7594. https://doi.org/10.1021/acs.est.0c07955

Sollai, S., Porcu, A., Tola, V., Ferrara, F., & Pettinau, A. (2023). Renewable methanol production from green hydrogen and captured CO_2: A techno-economic assessment. *Journal of CO2 Utilization*, *68*, 102345. https://doi.org/10.1016/j.jcou.2022.102345

Terlouw, T., Bauer, C., McKenna, R., & Mazzotti, M. (2022). Large-scale hydrogen production via water electrolysis: A techno-economic and environmental assessment. *Energy & Environmental Science*, *15*(9), 3583–3602. https://doi.org/10.1039/D2EE01023B

Terlouw, T., Rosa, L., Bauer, C., & McKenna, R. (2024). Future hydrogen economies imply environmental trade-offs and a supply-demand mismatch. *Nature Communications*, *15*(1), 7043. https://doi.org/10.1038/s41467-024-51251-7

Terlouw, T., Treyer, K., Bauer, C., & Mazzotti, M. (2021). Life cycle assessment of direct air carbon capture and storage with low-carbon energy sources. *Environmental Science & Technology*, *55*(16), 11397–11411. https://doi.org/10.1021/acs.est.1c03263

Tremel, A. (2018). *Electricity-based Fuels*. Springer International Publishing. https://doi.org/10.1007/978-3-319-72459-1

Van De Loosdrecht, J., Botes, F. G., Ciobica, I. M., Ferreira, A., Gibson, P., Moodley, D. J., Saib, A. M., Visagie, J. L., Weststrate, C. J., & Niemantsverdriet, J. W. (2013). Fischer–Tropsch synthesis: Catalysts and chemistry. In *Comprehensive inorganic chemistry II* (pp. 525–557). Elsevier. https://doi.org/10.1016/B978-0-08-097774-4.00729-4

Werker, J., Wulf, C., & Zapp, P. (2019). Working conditions in hydrogen production: A social life cycle assessment. *Journal of Industrial Ecology*, *23*(5), 1052–1061. https://doi.org/10.1111/jiec.12840

Wernet, G., Bauer, C., Steubing, B., Reinhard, J., Moreno-Ruiz, E., & Weidema, B. (2016). The ecoinvent database version 3 (part I): Overview and methodology. *The International Journal of Life Cycle Assessment*, *21*(9), 1218–1230. https://doi.org/10.1007/s11367-016-1087-8

Zhu, R., Wang, Z., He, Y., Zhu, Y., & Cen, K. (2022). LCA comparison analysis for two types of H_2 carriers: Methanol and ammonia. *International Journal of Energy Research*, *46*(9), 11818–11833. https://doi.org/10.1002/er.7947

SUPPORTING INFORMATION

Additional supporting information can be found online in the Supporting Information section at the end of this article.

How to cite this article: Langenmayr, U., Heinzmann, P., Schneider, A., Ruppert, M., Rudi, A., & Fichtner, W. (2025). Stand-alone power-to-X production dynamics - A multi-method approach to quantify the emission-cost reduction trade-off. *Journal of Industrial Ecology*, 1–15. https://doi.org/10.1111/jiec.70085

SUPPORTING INFORMATION FOR:

Langenmayr, U.; Heinzmann, P.; Schneider, A.; Ruppert, M.; Rudi, A.; Fichtner, W. (2024): Stand-alone Power-to-X Production Dynamics - A Multi-Method Approach to Quantify the Emission-Cost Reduction Trade-off. *Journal of Industrial Ecology*.

Summary

This supporting information provides additional declarations and insights into the conducted literature review (A1), an overview of applied methods (A2), process simulation (A3), and life cycle assessment (A4) described in the manuscript. Main assumptions, simulation design parameters, calculation steps, and life cycle inventory (LCI) data of the considered Power-to-X (PtX) value chains for the production of hydrogen, methanol (MeOH), and Fischer-Tropsch crude (FT) are described. Further information on the multi-objective optimization is given (A5). Due to the limited number of words and figures in the main script, we added further results and a sensitivity analysis (A6).

A1. Additional information on the literature review

Table 1: Abbreviations in literature review

FT	Fischer-Tropsch	GHG	Greenhouse gas
H_2	Hydrogen	LCA	Life cycle assessment
LP	Linear program	MeOH	Methanol
MILP	Mixed-integer linear program	MOO	Multi-objective optimization
O&M	Operation and Maintenance	TEA	Techno-economic assessment

Table 2 shows the key characteristics of the reviewed literature. The research gap is based on an approach to consider RES-E generation, the applied methodologies, and the overall objective. The simplified integration of RES-E is visible, where most approaches do not model RES-E generation directly in their model. Furthermore, different methodologies are applied, each with strengths and limitations. Finally, the overall objective often concentrates on a single dimension, like costs or emissions, or assesses several objectives in multi-objective optimization.

Table 2: Key characteristics of reviewed literature

Literature	Energy carrier	RES-E modeling[1]	Methodology	Overall objective
Werker et al. (2019)	H_2	Parameter	LCA (social)	Calculate life cycle impact
Hoppe, Thonemann and Bringezu (2018)	Methane, MeOH, polymers	Parameter	LCA (environmental)	Calculate life cycle impact
Kadam and Yadav (2024)	Ammonia, methane	Parameter	LCA (environmental)	Calculate life cycle impact
Albrecht et al. (2017)	FT products	Parameter	Process simulation, TEA (Spreadsheet)	Calculate production costs
Heinzmann et al. (2021)	FT products	Parameter	Process simulation, TEA (Spreadsheet)	Calculate production costs
Runge et al. (2020)	FT products	Separated	Process simulation, TEA (Spreadsheet)	Calculate production costs
Fasihi, Bogdanov and Breyer (2016)	FT products	Separated	TEA (Spreadsheet)	Calculate global production costs

[1] **Parameter**: RES-E is only considered as parameter and is not modeled; **Separated**: RES-E modeling is not part of the main method; **Integrated**: RES-E is modeled in the main method

Lee et al. (2022)	H_2	Separated	TEA (Spreadsheet), LCA (GHG emissions)	Calculate production costs and carbon footprint
Armijo and Philibert (2020)	H_2, ammonia	Separated	TEA (Spreadsheet)	Calculate production costs
Osman et al. (2020)	Ammonia	Separated	Process simulation, TEA (Spreadsheet, LP)	Calculate production costs
Schack, Rihko-Struckmann and Sundmacher (2016)	MeOH	Parameter	TEA (LP)	Maximize profit
Sherwin (2021)	FT products	Integrated (4h-resolution capacity factors)	TEA (LP)	Minimize production costs
Morgan et al. (2017)	Ammonia	Parameter	TEA (Spreadsheet)	Calculate production costs
Maggi et al. (2020)	Syngas	Parameter	TEA (MILP)	Derive system design
Berger et al. (2021)	Methane	Integrated (hourly-resolution capacity factors)	TEA (LP/MILP)	Create generic LP/MILP and calculate minimal production costs
Terlouw et al. (2024)	H_2	Integrated (hourly-resolution capacity factors)	TEA (equilibrium model, MILP)	Calculate costs and emissions of hydrogen economy; show mismatch between demand and supply

Farajiamiri et al. (2023)	FT products, MeOH	Integrated (hourly-resolution capacity factors)	TEA (MILP), MOO	Show trade-off between costs, land use, and water use
Kenkel et al. (2021)	MeOH	Parameter	Process simulation, TEA (MILP), MOO	Show trade-off between costs and GHG emissions
This work	H_2, FT, MeOH	Integrated (hourly-resolution capacity factors)	Process simulation, LCA (GHG emissions), TEA (Spreadsheet, MILP), MOO	Show trade-off between costs and GHG emissions

A2. Additional information on the interaction between the different methods

The multi-method approach uses process simulations, life cycle assessment, spreadsheet-based techno-economic analysis, and multi-objective optimization. This approach was chosen to exploit the synergy between the different methods and overcome the individual methods' disadvantages. *Figure 1* shows the different methods, their advantages and disadvantages, and how they are connected to exploit the synergies.

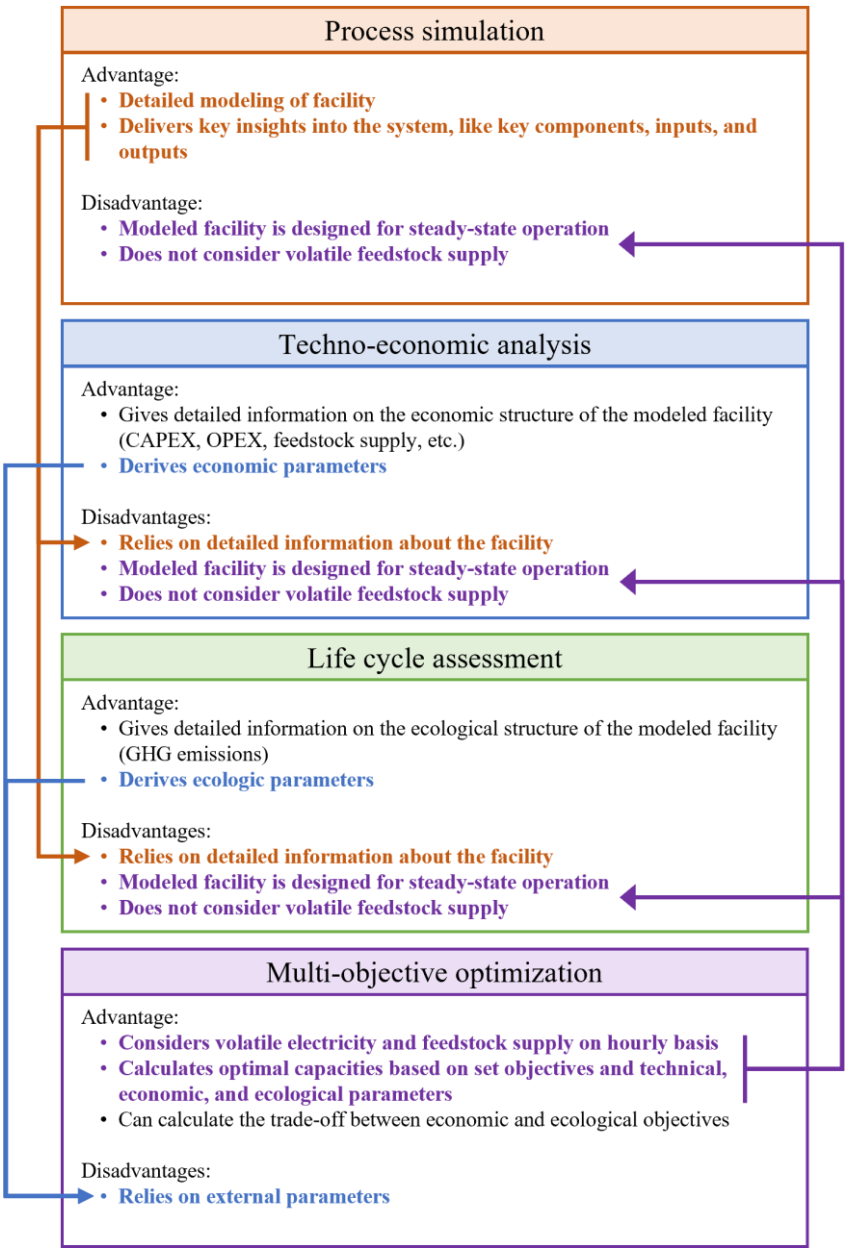

Figure 1: Advantages and disadvantages of, and synergies (arrows) between different methods

A3. Process simulation and economic analysis

The two process pathways (A) and (B) have been assessed by steady-state process simulations in Aspen Plus v14.0 to obtain technological and economic data as input to the optimization. A plant with a steady-state demand of 10t/h of hydrogen at nominal capacity has been assumed as a design basis.

3.1 Process simulation of the FT synthesis-based process pathway

Figure 2 shows the flowsheet of the simulated FT synthesis-based process pathway. The data of the referred streams is included in the Supplementary Information (SI) spreadsheet file.

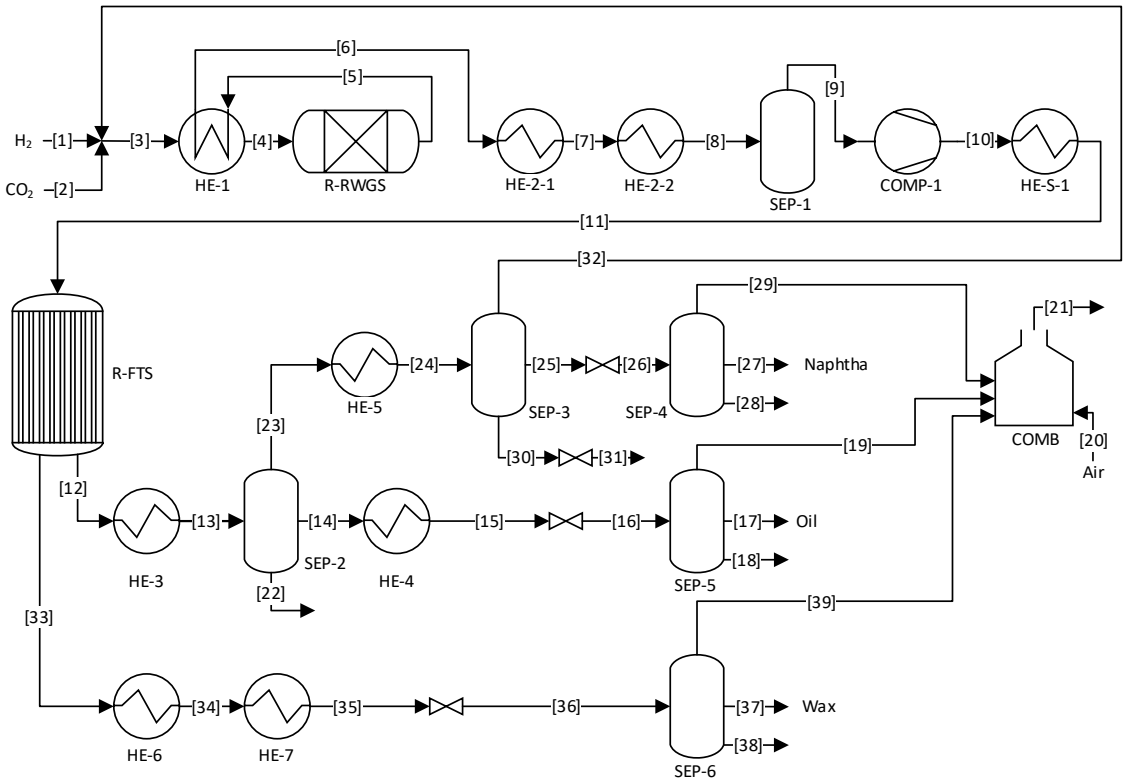

Figure 2: Flowsheet of the FT synthesis-based process pathway

Table 3 summarizes the setup and the main results of the applied model blocks in Aspen Plus.

Table 3: Simulation block modules setup and results details of the FT synthesis-based pathway

Block	Setup	Results
COMB	T_{out} = 140°C	Q = -2.80 MW

COMP-1	Isentropic, $p_{discharge}$ = 20 bar; $\eta_{Isentropic}$ = 0.85, $\eta_{Mechanical}$ = 0.95	P_{el} = 9.61 MW, T_{out} = 144°C
HE-1	T_{out} = 500°C	Q = 50.63 MW
HE-2-1	T_{out} = 135°C, Utility: LPS-G	Q = -37.31 MW
HE-2-2	T_{out} = 55°C, Utility: CW	Q = -20.69 WM
HE-S-1	T_{out} = 210°C, Utility: MPS	Q = 6.5 MW
HE-3	T_{out} = 120°C, Utility: LPS-G	Q = -27.51 MW
HE-4	T_{out} = 40°C, Utility: CW	Q = -0.44 MW
HE-5	T_{out} = 35°C, Utility: CW	Q = -11.96 MW
HE-6	T_{out} = 120 °C, Utility: LPS-G	Q = -0,84 MW
HE-7	T_{out} = 35°C, Utility: CW	Q = -0,54 MW
R-FT synthesis	T = 230°C, Δp = -1 bar, Utility: MPS-G, X_{CO} = 60%, alpha = 0,9	Q = -90.09 MW
R-RWGS	T = 900°C, Δp = -0,5 bar Utility: EL	Q = 90.26 MW
SEP-1 to SEP-6	Δp = 0 bar, duty = 0	

Several design specifications and calculator blocks support the simulation. These ensure a constant stoichiometric H2/CO-ratio of 2,0 at the reactor entrance, ensure a sufficient oxygen supply at the purge gas combustion unit (COMB) by adapting the air inlet flow, and calculate the single compound conversions of the FT synthesis-reactor based on the alpha value (assuming Anderson-Schulz-Flory distribution).

Table 4 shows the usage or generation ratios and the definition of the utilities used in the simulation of the FT synthesis-based process pathway.

Table 4: Utilities of the FT synthesis-based process pathway

Name	Definition	Results
CW	Cooling water T_{in} = 25°C, T_{out} = 30°C	Duty: 33.64 MW
EL	Electricity	Power demand: 99.87 MW
LPS	Low pressure steam, T = 110°C, full condensation	No demand inside the synthesis plant
LPS-G	Generation of LPS, T = 110°C	Duty: 68.47 MW
MPS	Medium pressure steam, T = 230°C, full condensation	Duty: 6.5 MW
MPS-G	Generation of MPS, T = 230°C	Duty: 96.1 MW

The table shows that a surplus of steam (LPS-G and MPS-G) is generated inside the plant (LPS, MPS), which can supply heat to the DAC unit. Under the assumption of a heat demand of 5.4 MJ/kg_{CO2} of the DAC (Deutz and Bardow, 2021), the FT synthesis-based synthesis plant can supply sufficient heat to the DAC.

3.2 Process simulation of the MeOH-based process pathway

Figure 3 shows the flowsheet of the simulated FT synthesis-based process pathway. The data of the referred streams is included in the spreadsheet file of the SM.

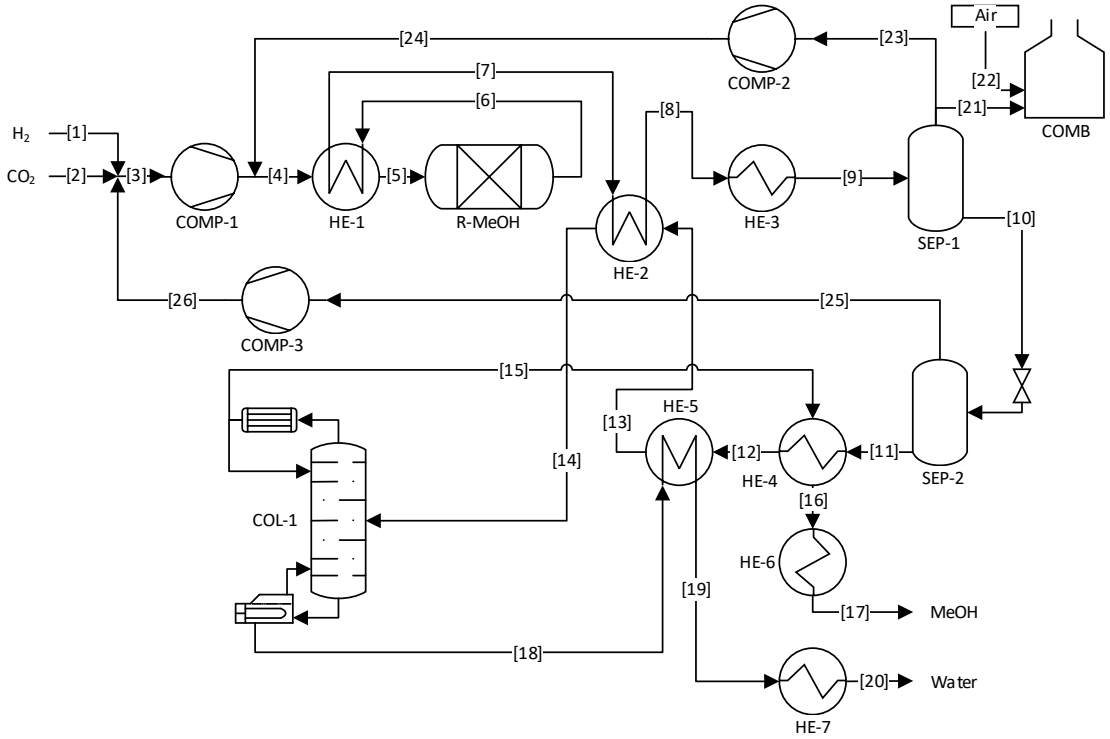

Figure 3: Flowsheet of the MeOH-based process pathway

Table 5 summarizes the setup and the main results of the applied model blocks in Aspen Plus.

Table 5: Simulation block modules setup and results details of the MeOH-based pathway

Block	Setup	Results
COL-1	15 stages, partial vapor condenser, reflux ratio = 1.49, distillate to feed ratio = 0.503, utilities: CW and LPS	$Q_{condensor}$ = -25.44 MW $Q_{reboiler}$ = 13.76 MW
COMB	T_{out} = 140°C	Q = -5.91 MW
COMP-1	Isentropic, 3 stages with intercooling to 80°C, utility: CW $p_{discharge}$ = 76 bar; $\eta_{Isentropic}$ = 0.85, $\eta_{Mechanical}$ = 0.95	P_{el} = 14.57 MW, Q = -6.98 MW
COMP-2	Isentropic, $p_{discharge}$ = 76 bar; $\eta_{Isentropic}$ = 0.85, $\eta_{Mechanical}$ = 0.95	P_{el} = 1.67 MW, T_{out} = 38°C
COMP-3	Isentropic, $p_{discharge}$ = 10 bar; $\eta_{Isentropic}$ = 0.85, $\eta_{Mechanical}$ = 0.95	P_{el} = 0.17 MW, T_{out} = 38°C
HE-1	$\Delta T_{hot\text{-}inlet\text{-}cold\text{-}outlet}$ = 10K,	Q = 50.05 MW
HE-2	T_{out} = 82.4°C	Q = 29.17 MW
HE-3	T_{out} = 30°C, Utility: CW	Q = -15,84 MW
HE-4	T_{out} = 60°C, Utility: CW	Q = -2.71 MW
HE-5	$\Delta T_{approach}$ = 10K	Q = 0.86 MW
HE-6	T_{out} = 30°C, Utility: CW	Q = -16.09 MW
HE-7	T_{out} = 40°C, Utility: CW	Q = -1.40 MW
R-MeOH	Constant thermal fluid temperature of 245°C, l = 12m, d_{tube} = 0.06m, GHSV = 10,000, Δp by Ergun correlation with roughness of 4.572e-05 m, catalyst bed voidage of 0.4, particle density of 1.775 g/cm³, Utility: MPS-G	Q = -24.69 MW, T_{max}= 256.87°C, T_{min} = 236.60°C
SEP-1	Δp = 0 bar, Q = 0	
SEP-2	Δp = 0 bar, Q = 0	

Several design specifications and calculator blocks support the simulation. By their application, a MeOH purity of 99% is secured at the head of the rectification column by adjusting the reflux ratio. The number of tubes in the methanol synthesis reactor is calculated to apply a steady GHSV.

The kinetic approach from Van-Dal and Bouallou (2013) has been applied in a RPlug module in Aspen Plus for the methanol synthesis reactor.

Table 6 shows the usage or generation ratios and the definition of the utilities used in the simulation of the MeOH-based process pathway.

Table 6: Utilities of the MeOH-based process pathway

Name	Definition	Results
CW	Cooling water, T_{in} = 25°C T_{out} = 30°C	Duty: 65.74 MW
EL	Electricity	Power demand: 16.40 MW
LPS	Low pressure steam, T = 110°C, full condensation	Duty: 13.76 MW
LPS-G	Generation of LPS, T = 110°C	Duty: 5.91 MW
MPS	Medium pressure steam, T = 245°C, full condensation	No demand
MPS-G	Generation of MPS, T = 245°C	Duty: 24.69 MW

It is assumed that the lack of LPS can be supplied by transforming MPS to LPS. Under the assumption of a heat demand of 5.4 MJ/kg_{CO2} of the DAC and due to the fact the MeOH based synthesis plant can supply only 0.83 MJ/kg_{CO2} in the form of residual MPS generated, it is assumed that the DAC unit's residual heat demand is covered by electricity in the MeOH-based process pathway. The possibility of further heat integration by supplying low temperature heat (e.g., as hot water) in the DAC unit operation loop or by implementing a heat pump system is not considered here, but might be an interesting option for future simulation work.

3.3 Process simulation results

To be able to compare the overall results to others, energy efficiency, hydrogen efficiency, and carbon efficiency are the most important KPIs, which are defined according to the following *Equations (1)*, *(2)*, and *(3)*.

$$Energetic\ efficency:\ \eta_{en,LHV} = \frac{LHV_{products} \cdot \dot{m}_{products}}{P_{Electrolyzer} + P_{Synthesis\ plant}} \quad (1)$$

$$Hydrogen\ efficency:\ \eta_{H2,LHV} = \frac{LHV_{products} \cdot \dot{m}_{products}}{\dot{m}_{H2} \cdot LHV_{H2} + P_{Synthesis\ plant}} \quad (2)$$

$$Carbon\ efficency:\ \eta_C = \frac{\dot{n}_{C,products}}{\dot{n}_{C,CO2}} \quad (3)$$

Table 7 shows the results of the efficiency parameters of the two simulated processes.

Table 7: Efficiency results of the simulated processes

Parameter	(A) FT	(B) MeOH
$\eta_{en,LHV}$	46.16%	56.08%
$\eta_{H2,LHV}$	63.92%	82.82%
η_C	98.80%	98.53%

The technological KPIs above represent the most relevant parameters of power-to-liquid processes. The process simulations performed within this work are in good correlation with reviewed literature studies (König *et al.*, 2015; EC JRC Institute for Energy and Transport, 2016; Fasihi, Bogdanov and Breyer, 2016; Albrecht *et al.*, 2017; Schemme *et al.*, 2020; Adelung, Maier and Dietrich, 2021; Herz *et al.*, 2021; Lacerda De Oliveira Campos *et al.*, 2022). Compared to biomass-based routes or power-to-liquid processes, using tail gas-fired rWGS reactor furnaces, the carbon efficiency is high and mainly influenced by the assumed purge gas ratio.

The MeOH producing process configuration (B) shows a considerably higher energy efficiency due to a more straightforward process setup without needing an energy-consuming reverse water gas shift reactor. On the one hand, one must consider that further upgrading MeOH to fuel-type hydrocarbons (e.g., via an MTG process) diminishes the advantage of higher production energy efficiency. Also, in the considered pathways, the FT synthesis process supplies enough steam from the reactor's cooling to cover the complete heat demand of the DAC unit. On the other hand, the MeOH-based process can only cover a minor share of that heat demand, resulting in additional electricity consumption in the DAC unit and lower overall system efficiency.

Deriving separate and clearly stated data from literature, while maintaining a sure consistency in applied methods, timeframe, and level of detail, is challenging. Also, the separate handling of electrolysis systems, synthesis plants, generation, and storage units within the further optimization

work is expected to enable a more precise determination of the total investment of a complete power-to-liquid plant.

3.4 Economic analysis

An index is applied to adjust the estimated equipment cost (EC) from a reference point in time (base year) to the target year, according to *Equation (4)*. The Chemical Engineering Plant Cost Index (CEPCI) transfers the estimated EC to the target year 2023.

$$EC_{target\ year} = \frac{CEPCI_{target\ year}}{CEPCI_{base\ year}} \cdot EC_{target\ year} \quad (4)$$

The estimated and adjusted EC are multiplied by surcharge factors to get to the full capital investment (FCI), according to *Equation (5)*.

$$FCI = EC \cdot \sum_i f_i \quad (5)$$

Table 8 shows the assumed surcharge factors applied to get from EC to FCI, according to Peters *et al.* (2004).

Table 8: Applied surcharge factors

Surcharge	Type	Factor
Purchased Equipment Delivered	Direct Costs	100%
Installation	Direct Costs	47%
Instrumentation and controls	Direct Costs	36%
Piping	Direct Costs	68%
Electrical systems	Direct Costs	11%
Buildings	Direct Costs	18%
Yard Improvements	Direct Costs	10%
Service facilities	Direct Costs	70%
Sum Direct Investment		**360%**
Engineering and supervision	Indirect Costs	33%
Construction expenses	Indirect Costs	41%
Legal expenses	Indirect Costs	4%
Contractor's fee	Indirect Costs	22%
Contingency	Indirect Costs	44%
Contingency Electrolysis	Indirect Costs	25%
Sum Indirect Investment		**144%**
Fixed Capital Investment		**504%**
Working Capital		46%
Total Capital Investment		**550%**

Table 9 shows the estimated equipment costs for the FT synthesis-based process pathway:

Table 9: Estimated equipment cost of the FT synthesis-based process pathway

Name	Type	Equipment cost	Source
COMB	Furnace	519,300 €	APEA
COMP-1	Compressor	6,882,500 €	APEA
HE-1	Heat exchanger	354,300 €	APEA
HE-2-1	Heat exchanger	505,700 €	APEA
HE-2-2	Heat exchanger	92,700 €	APEA
HE-3	Heat exchanger	160,700 €	APEA
HE-4	Heat exchanger	18,200 €	APEA
HE-5	Heat exchanger	108,300 €	APEA
HE-6	Heat exchanger	21,200 €	APEA
HE-7	Heat exchanger	20,000 €	APEA
HE-S-1	Heat exchanger	139,300 €	APEA
R-RWGS	El. heated tubular reactor	5,045,168 €	(König *et al.*, 2015)
R-FT synthesis	Evaporation cooled tubular reactor	19,138,362 €	(Hannula and Kurkela, 2013)
SEP-1	Flash vessel	77,900 €	APEA
SEP-2	Flash vessel	61,900 €	APEA
SEP-3	Flash vessel	59,200 €	APEA
SEP-4	Flash vessel	31,300 €	APEA
SEP-5	Flash vessel	33,000 €	APEA
SEP-6	Flash vessel	37,700 €	APEA

Table 10 shows the CAPEX distribution of the FT synthesis-based process pathway.

Table 10: CAPEX of FT synthesis-based process pathway

Equipment Costs	**33,307,000 €**
Installation	15,655,000 €
Instrumentation and controls	11,991,000 €
Piping	22,649,000 €
Electrical systems	3,664,000 €
Buildings	5,996,000 €
Yard Improvements	3,331,000 €
Service facilities	23,315,000 €
Total direct plant cost	**119,905,000 €**
Engineering and supervision	10,992,000 €
Construction expenses	13,656,000 €
Legal expenses	1,333,000 €
Contractor's fee	7,328,000 €
Contingency	14,655,000 €
Total indirect plant costs	**47,962,000 €**
Fixed Capital Investment Synthesis plant	**167,866,000 €**
Working Capital	15,261,000 €
Total Investment	**183,127,000 €**

Table 11 shows the estimated equipment costs for the MeOH-based process pathway:

Table 11: Estimated equipment cost of the MeOH-based process pathway.

Name	Type	Equipment cost	Source
COL	Column	1,050,100 €	APEA
COMB	Furnace	809,300 €	APEA
COMP-1	Compressor	8,698,400 €	APEA
COMP-2	Compressor	1,850,100 €	APEA
COMP-3	Compressor	1,246,500 €	APEA
HE-1	Heat exchanger	3,014,900 €	APEA
HE-2	Heat exchanger	1,628,500 €	APEA
HE-3	Heat exchanger	402,500 €	APEA
HE-4	Heat exchanger	70,800 €	APEA
HE-5	Heat exchanger	23,100 €	APEA
HE-6	Heat exchanger	279,000 €	APEA
HE-7	Heat exchanger	23,400 €	APEA
HE-S-1	Heat exchanger	139,300 €	APEA
R-MEOH	Evaporation-cooled tubular reactor	4,092,900 €	APEA
SEP-1	Flash vessel	200,900 €	APEA
SEP-2	Flash vessel	155,200 €	APEA

Table 12 shows the CAPEX distribution of the MeOH-based process pathway.

Table 12: CAPEX of MeOH-based process pathway

Equipment Costs	**23,546,000 €**
Installation	11,067,000 €
Instrumentation and controls	8,477,000 €
Piping	16,012,000 €
Electrical systems	2,591,000 €
Buildings	4,239,000 €
Yard Improvements	2,355,000 €
Service facilities	16,482,000 €
Total direct plant cost	84,765,000 €
Engineering and supervision	7,771,000 €
Construction expenses	9,654,000 €
Legal expenses	942,000 €
Contractor's fee	5,181,000 €
Contingency	10,361,000 €
Total indirect plant costs	33,906,000 €
Fixed Capital Investment Synthesis plant	**118,670,000 €**
Working Capital	10,789,000 €
Total Investment	**129,459,000 €**

3.5 Discussion of economic results

The difficulty in comparing TEA results lies in the harmonization of assumptions, system boundaries, currencies, timeframes, and applied methods. Since the primary focus of the performed process simulation and TEA was providing a data basis of conversions and investment demands, the evaluation of economic results with literature is focused on specific investment.

Regarding the investment needed for an FT synthesis-based plant, cost estimations generally show more deviations, which are caused by only a few typically available cost correlations for the FT

synthesis reactor system and the assumed technology (slurry or fixed bed). The resulting specific investment of the FT-based synthesis plant in this work comes down to 7.37 million €$_{2024}$/(t_{fuels}/h) or 602 €$_{2024}$/$kW_{fuels,LHV}$. This is considerably lower than the outcome of Fasihi, Bogdanov and Breyer (2016) and Albrecht *et al.* (2017), but in good correlation with Schemme *et al.* (2020). Based on further studies and literature, the overall production cost contribution of the synthesis plant CAPEX is expected to be low.

The resulting specific investment demand of a CO_2 and H_2-based MeOH synthesis plant is 2.27 million €$_{2024}$/(t_{MeOH}/h) or 410 €$_{2024}$/$kW_{MeOH,LHV}$. This is in good correlation with the results of Lacerda De Oliveira Campos *et al.* (2022), and higher than the results of Schemme *et al.* (2020), which show a relevant influence of plant size.

In contrast to researching data from open literature, one main advantage of performing the coupled work of process simulation and economic evaluation in this work is gaining a more detailed view of the cost structure and potential levers in the processes directly. Topics like the heat integration with carbon capture or DAC units can be targeted more confidently. Future potential of efficiency or flexibility gains by changes in the process configurations will be easier to asses by directly adapting the simulations and cost calculations instead of being dependent on literature data.

3.6 Further economic parameter assumptions

Table 13: Techno-economic assumptions on electricity generators (Danish Energy Agency, 2023)

	Wind Generator + AC/DC converter	Solar PV Generator
CAPEX	1,040 k€/MW	310 k€/MW
Fixed O&M	1.21 %	1%
Variable O&M	0.00135 k€/MWh	0
Lifetime	25	30

Table 14: Techno-economic assumptions on storage units

	Hydrogen Storage (Braun *et al.*, 2022)	CO_2 Storage (Svensson *et al.*, 2004)	Battery Storage (Cole and Karmakar, 2023)
CAPEX	12 k€ / MWh	45.14 k€ / t	330 k€/MWh
Fixed O&M	4 %	4 %	5.645 %
Variable O&M	0	0	0.00112 k€/MWh
Lifetime	20	20	20
Minimal SOC	0 %	0 %	10 %
Maximal SOC	100 %	100 %	90 %
Roundtrip Efficiency	100 %	100 %	85 %

Table 15: Techno-economic assumptions on conversion units

	PEM Electrolysis (Braun *et al.*, 2022)	H_2 Compressor (own)	CO_2 Compressor (own)	DAC (Fasihi, Efimova and Breyer, 2019)	FT-Synthesis	MeOH-Synthesis
CAPEX	810 k€/MW	1,590.01 k€/MW	3,241.27 k€ / MW	6,395 k€/t CO_2 / h	Cf. Table 1 in main manuscript	Cf. Table 1 in main manuscript
Fixed O&M	4 %	4 %	4 %	7 %	Cf. Table 1 in main manuscript	Cf. Table 1 in main manuscript
Variable O&M	0	0	0	0	Cf. Table 1 in main manuscript	Cf. Table 1 in main manuscript
Lifetime	20	20	20	20	20 (own)	20 (own)
Minimal Power	7 %	0 %	0	0 %	70 % (Iglesias González, Eilers and Schaub, 2016)	20 % (Mucci, Mitsos and Bongartz, 2023)
Ramp-Up	100 %/h	100 %/h	100 %/h	100 %/h	30 %/h (own)	80 %/h (own)
Ramp-Down	100 %/h	100 %/h	100 %/h	100 %/h	30 %/h (own)	80 %/h (own)
Input	1.52 MWh Electricity 0.27 t Water	0.0167 MWh Electricity	0.06134 MWh Electricity	0.5 MWh Electricity (FT) 1.77 MWh Electricity (MeOH)	Cf. Table 1 in main manuscript	Cf. Table 1 in main manuscript
Output	1 MWh Hydrogen			1 t CO_2	Cf. Table 1 in main manuscript	Cf. Table 1 in main manuscript

A4. Life cycle assessment

The following supplementary delivers background information on the conducted LCA. After the fundamentals, the different process steps are described and detailed. Furthermore, the results are shown, and the critical parameters and the model's validity are discussed.

4.1 Database and fundamentals

Building the supply chain and delivering background datasets, the ecoinvent database 3.9.1. as system model "Allocation at the point of substitution" (APOS) is used. In the following, ecoinvent processes or flows are characterized by *italic letters* to provide better reading and distinction. The LCA is modelled with the openLCA 2.0.2 software and calculated with the impact assessment method ReCiPe 2016 v1.03, midpoint (H).

Since the optimization model of this study requires the fixed and variable emissions emerging in the value chain of the different energy carriers, the approach of this LCA differs from others. By building the inventories and calculating the impacts excluding that for construction, the variable or operating emissions from water, wastewater, electricity, catalyst demand, etc., are determined. Emissions related to the construction are assessed separately by creating individual product systems for the single plant components, i.e., chemical factory, compressors, storage tanks, etc. Converting data and units to the desired target sizes, algorithms of Wolfram Alpha LLC are used for operational materials and datasheets from World Material for constructional materials. Where a lack of data requires assumptions, conservative approaches are always used, knowing the overestimation and robustness of the results. Economies of scale are generally not considered in the LCI due to a lack of data or modular design of process units, like the electrolysis and DAC plant, enabling linear scaling.

4.2 Process description and modeling

4.2.1 Electricity generation

This study considers photovoltaic modules and wind turbines to generate renewable electricity. Regarding electricity produced via photovoltaic, the ecoinvent process *market for a photovoltaic*

plant, 570kWp, multi-Si, on open ground, is chosen, representing an average global photovoltaic plant production process. The operational effort of a photovoltaic plant includes tap water and wastewater provided as stated in the process *electricity production, photovoltaic, 570kWp open ground installation* for Germany. The construction of the wind turbine system is considered with the processes *market for wind turbine, 4.5MW, onshore,* and *market for wind turbine network connection, 4.5MW, onshore*. Following the process of *electricity production, wind, >3MW turbine, onshore* for Germany, lubricating oil, waste mineral oil, and transport are required for plant operation. Taking the need for direct current specifically for battery and electrolysis into account, the electricity production by wind turbines is complemented by a converter using the most similar process of *inverter production, 500kW*. In return, the inverter, which is by default included in the photovoltaic process, is excluded, since photovoltaic modules provide direct current. While electricity from a photovoltaic plant or a wind turbine is used for all demands on the production site, upstream demands are considered as defined in supply chain processes.

4.2.2 Battery

Lithium ferrophosphate (LFP) battery is currently the most promising battery technology for stationary applications (Riegel, 2018). The appropriate ecoinvent process (*market for battery, Li-ion, LFP, rechargeable, prismatic*) is supplemented by the battery round-trip efficiency of 90% taken from Palmer et al. (2021). The end of life of batteries is included with *treatment of used Li-ion battery, hydrometallurgical treatment.*

4.2.3 Electrolysis system

The model of water electrolysis via proton exchange membrane (PEM) technology includes a feed pump, the PEM itself, the following purification in a deoxygenation (DeOxo) and water adsorption unit, a buffer tank for the storage of gaseous hydrogen, and is related to 1 MW electricity input. Process concept, energy demand, plant size, and weight come from Bareiß *et al.*, 2019. The water feed pump is modeled with *water pump production, 22 kW* linearly scaled to the needed 10 kW as described in Bareiß *et al.* (2019). With the appropriate electricity demand and stoichiometric quantity of deionized water, the operation of the feed pump is estimated. Due to PEM electrolysis and PEM fuel cell analogy, the ecoinvent process *market for fuel cell,*

polymer electrolyte membrane, 2kW electrical, future is used to depict the electrolysis stack. It is scaled to the desired capacity of 1 MW by using the mass correlations between stack and balance of plant described in Gerloff (2021). The comparison with Gerloff's detailed inventory for the PEM electrolysis shows a higher GWP contribution for the model of this study and is therefore rated as a conservative approach. The electrolysis operation is covered with *maintenance, polymer electrolyte membrane fuel cell 2kW electrical*. Water adsorption is considered by silica gel as an adsorbent, and the electricity demand for regeneration from Bareiß *et al.* (2019). Adsorbent demand is calculated by assuming an amount of 500 life cycles for one silica gel package based on the technical datasheet of Bohlender GmbH and an assumed water adsorption capacity of 20 w.-% for silica gel based on details of Waller. A cylindrical adsorption column with a volume of 1 m^3 and a wall strength of 5 mm is assumed. The DeOxo unit is conservatively modeled with the process *market for catalytic converter, oxidation, 20 liter*, which is assumed to fit the description of a platinum group-based catalytic deoxygenation as stated in Bareiß *et al.* (2019). The size of the DeOxo unit is calculated by potentially extrapolating the data from the ErreDueGas-Austria technical datasheet. The 80 bar storage tank and the electricity requirement for compression hydrogen from electrolysis, from 30 bar to 80 bar storage pressure, is modeled following the approach from Terlouw *et al.* (2022). For the first approximation, all compressors in the considered process chains are represented by the process *market for air compressor, screw-type compressor, 300kW,* adapted by linear scaling based on the appropriate power.

4.2.4 DAC

Low temperature direct air capture (LTDAC) technology is chosen cause of the possibility of integrating surplus heat from the synthesis processes at a temperature level suitable for the LTDAC process. The degree of heat demand coverage by surplus heat from synthesis is discussed in A1. Using data regarding plant construction, energy, and catalyst demand from Deutz and Bardow (2021), the model follows the process design of Climeworks technology. Constructional data for the LTDAC plant comes from personal communication with S. Deutz and couldn't be listed due to confidentiality. Madhu *et al.* (2021) provide information on wastewater and water emissions. The technical datasheet by TOMCO2 Systems (2018) delivers

a weight of 26.5 t for a 25 bar CO_2 storage tank. Analog to the hydrogen storage, the CO_2 tank is modeled assuming stainless steel as the construction material. Electricity demand of 64 kWh/t CO_2 and the size of the compressor (4.5 MW) for compressing CO_2 from 2 to 25 bar are received from the process simulation.

4.2.5 Fischer-Tropsch synthesis

Regarding Fischer-Tropsch synthesis, the process simulation (*Section 3.1*) delivers information on process design, operating conditions, plant components, and mass and energy flows (wastewater, flared purge gas, electricity, heat, water, etc.). Catalyst type (ZSM, Cobalt, Nickel), demand, and construction effort are determined as described in Rojas-Michaga *et al.* (2023). *Table 16* shows the FT synthesis inventory. The functional unit is 1 kg of FT-Crude, consisting of 16 w.-% of naphta, 38 w.-% of oil, and 46 w.-% of wax.

Table 16: LCI Data of FT synthesis

Input		Output	
Flow	Amount	Flow	Amount
Air compressor (items)	1.17E-8	Carbon dioxide (kg)	0.03603
Air compressor (items)	3.21E-9	FT-Crude (kg)	1
Carbon dioxide (kg)	3.13779	Heat, middle pressure steam (kWh)	3.93361
Chemical factory, organics (items)	1.86E-11	Heat, low-pressure steam (kWh)	3.12378
Cobalt (kg)	0.00122	Wastewater (m^3)	1.59E-6
Electricity (kWh)	4.38617	Wastewater (m^3)	0.00255
Hydrogen (kg)	0.43923	Water	2.138E-5

Nickel (kg)	3.87E-5	
Water (kg)	0.00159	
Zeolite (kg)	2.11E-5	

4.2.6 Methanol synthesis

The same procedure is pursued for methanol synthesis. Here, literature data on construction and catalysts are taken from Sollai *et al.* (2023) and Hank *et al.* (2019). The LCI of the MeOH synthesis is shown in *Table 17*.

Table 17: LCI data of MeOH synthesis

Input		Output	
Flow	Amount	Flow	Amount
Air compressor (items)	1.5E-9	Carbon dioxide (kg)	0.02782
Air compressor (items)	9E-11	Methanol (kg)	1
Air compressor (items)	8.08E-9	Wastewater (m^3)	0.00056
Air compressor (items)	8.85E-10	Water	3.18E-5
Aluminum oxide (kg)	2.2E-6	Water	4.5E-7
Carbon dioxide (kg)	1.39555	Heat, middle pressure steam (kWh)	0.32608
Chemical factory, organics (items)	2E-10		
Copper oxide (kg)	1.19E-5		

Electricity (kWh)	0.31402	
Hydrogen (kg)	0.19116	
Nickel (kg)	3.87E-5	
Water (m^3)	4.5E-7	
Zinc oxide (kg)	4.45E-6	

Modeling the construction efforts of the synthesis processes, the ecoinvent process *chemical factory construction* is assumed to be most suitable. Since this process represents a refinery based on data of a distillation unit (Hischier, 2007), which typically doesn't involve pressurized processes, compressors are added separately to the inventories of FT- and MeOH-synthesis, based on the specifications of the process simulation.

4.3 Results and discussion

4.3.1 LCA results

The GHG emissions for the installation, fixed operation and maintenance, disposal, and variable operation and maintenance are given in *Table 2* in the main manuscript. ***Fehler! Verweisquelle konnte nicht gefunden werden.*** shows the GWP of the three studied products with and without considering carbon dioxide removal (CDR). The mentioned fixed and variable emissions are combined by determining business cases and their application to three scenarios. To follow consistency, the business case for hydrogen production is set for a 20-year lifetime of the plant and 8000 annual operating hours as stated in Hank *et al.* (2019) and Rojas-Michaga *et al.* (2023). Since the electricity generation is identified as the primary influence parameter across all product systems, three scenarios are defined to examine the sensitivity of the results. The first two scenarios consider the electricity generation by photovoltaic and wind, respectively, for 50% once for Germany (A) and once for Spain(B). The third scenario depicts the electricity generation in Spain by wind only (C). The significant

influence of electricity generation is evident by a two- to threefold difference between scenarios A and C for all products.

Table 18: GWP of hydrogen, FT-Crude, and MeOH for different electricity generation scenarios. (A) electricity generation in Germany with 50% PV and 50% Wind, (B) electricity generation in Spain with 50% PV and 50% Wind, and (C) electricity generation in Spain with 100% Wind

Product	Scenario	Total GWP in kg $CO_{2,eq}$/GJ product	Total GWP w/o CDR in kg $CO_{2,eq}$/GJ product
Hydrogen, 30 bar	A	32,2	32,2
	B	21,9	21,9
	C	13,0	13,0
FT-Crude, 1 bar	A	-18,9	54,4
	B	-34,3	39,0
	C	-48,1	25,2
MeOH, 1 bar	A	-24,2	45,7
	B	-36,8	33,0
	C	-48,2	21,7

Literature values for the GWP of 1 GJ of hydrogen with a similar product system can range from 5,62 kg $CO_{2,eq}$ (Ghandehariun and Kumar, 2016) to 27,3 kg $CO_{2,eq}$ (Bareiß *et al.*, 2019). Looking at FT-products with similar process chains, Micheli *et al.* (2022) and Rojas-Michaga *et al.* (2023) determined the GWP to 13,4 and. 21,43 kg $CO_{2,eq}$ per GJ FT jet fuel, respectively. Comparable LCA studies on methanol from Maimaiti *et al.* (2023), Hoppe, Thonemann and Bringezu (2018) and Zang *et al.* (2021) show a GWP of 11, 20 and 13,6 kg $CO_{2,eq}$ per GJ MeOH, respectively. Nevertheless, there are also studies with higher GWP, like Zhu *et al.*

(2022) with 52 kg $CO_{2, eq}$ per GJ MeOH. The comparison with the literature shows that the results of this work are in the upper value range as stated in the literature by trend, which underlines the relatively conservative approach within this study. Since the GHG emissions related to the electricity generation dominate the GWP of the products, the choice of renewable electricity generation technology, location, plant lifetime, yearly full load hours, and the energy demand of the power-to-liquid facility significantly shape the results. Other studies show, for instance, a lower GWP for electricity-based methanol -75 kg CO2, eq per GJ (with negative emissions) and 15,8 kg CO2, eq per GJ (without negative emissions) using hydropower (Cordero-Lanzac *et al.*, 2022) or concentrated solar power (Moretti *et al.*, 2023). Furthermore, the supply system for carbon dioxide in this study considers DAC, which is naturally associated with a higher energy demand than the capture processes from point sources. Other studies commonly use carbon capture processes from flue gas (Uusitalo *et al.*, 2017; Cordero-Lanzac *et al.*, 2022; Fernández-González *et al.*, 2022), which are mature technologies with lower capture costs. Nevertheless, the credibility of negative GHG emissions through carbon removal from fossil sources expires according to European carbon removal certification frameworks by 2041. Credibility plays a crucial role in regulatory and admission, as well as in monetizing the value added to green or renewable products. Therefore, this study does not consider carbon capture technologies from fossil sources.

4.3.2 Validity of data

While the validity of the data from process simulation, i.e., mass and energy flows, can be verified with literature values, the used literature data for plant construction must be otherwise analyzed and evaluated. The emissions associated with the *chemical factory, organics* are determined by dividing the resulting specific GWP by the particular demand for *chemical factory, organics* as stated in Rojas-Michaga *et al.* (2023) (FT synthesis) and Hank *et al.* (2019) (MeOH synthesis). Using these specific demands, containing insufficient information about the plant's lifetime, operating hours, and capacity, isn't congruent with the general approach of this LCA study for calculating the absolute fixed emissions and thus causes an inconsistency. Since the majority of GHG emissions in the process chain of PtX-products is connected to the energy demand (electricity for electrolysis and heat for CO_2 capture) (Rojas-Michaga *et al.*, 2023a) and

the superficial focus of this LCA lies on the quantification of the GWP, this inconsistency does not lead to higher inaccuracies. This is proved by checking the sensitivity of the GWP, where the variation of the construction efforts (*chemical factory, organics,* and *air compressor)* in FT-synthesis by a factor of 10 causes a relative change of only 1,2% in GWP. Thus, the applied linear scaling for *chemical factory, organics,* and *air compressor* also doesn't lead to higher uncertainties. As the lack of quantitative data regarding the efforts to construct the synthesis plants and their components is identified as the main uncertainty in the LCA, the resulting assertions can be assessed as reliable and robust.

A5. Additional information on multi-objective optimization

5.1 Complete model description

Table 19: Model notation

Type	Description
Sets	
$s \in S$	Set of commodities
$s \in S_k^{MI}$	Subsets of S representing the main input commodity of component k
$s \in S_k^{MO}$	Subsets of S representing the main output commodity of component k
$s \in S_g$	Subsets of S representing the generated commodity of generator g
$s \in FC$	Subset of S representing freely available commodities
$s \in EC$	Subset of S representing emittable commodities

$s \in PC$	Subset of S representing purchasable commodities
$s \in QC$	Subset of S representing saleable commodities
$s \in DC$	Subset of S representing demanded commodities
$s \in DTC$	Subset of S representing total demanded commodities
$s \in SC$	Subset of S representing storable commodities
$k \in K$	Set of conversion components
$n \in N_k$	Set of investment curve segments of component k for linearization
$g \in G$	Set of generator components
$c \in C$	Set of temporal clusters
$t \in T$	Set of time steps

Variables

x_s	Quantity of mass or energy of commodity s
b	Binary variable to indicate current status
$\text{cap}_{k,n}$	Capacity of investment curve for segment *n* of conversion component *k*
$\text{cap}_k, \text{cap}_g, \text{cap}_s$	Capacity of components *k*, *g* and *s*
$\text{soc}_{s,c,t}$	State of charge of storage component for commodity *s* in cluster *c* at time *t*

i_k, i_g, i_s	Investment of components *k*, *g* and *s*
slack	Slack variable for the Pareto optimization

Parameters

$\mathrm{BC}_{k,n}^{upper}, \mathrm{BC}_{k,n}^{lower}$	Upper and lower bound of capacity segment *n* of conversion component *k*
$\mathrm{BU}^{upper}, \mathrm{BU}^{lower}$	Upper and lower bound of capacity utilization
$\mathrm{RAMP}_k^{up}, \mathrm{RAMP}_k^{down}$	Ramp-up and ramp-down rate of conversion component *k*
$\mathrm{Inv}_{k,n}^{fix}, \mathrm{Inv}_{k,n}^{var}$	Fix and variable investment of capacity segment *n* of conversion component *k*
$\mathrm{Inv}_g, \mathrm{Inv}_s$	Investment of Generator and Storage components of *g* and *s*
$\mathrm{ANN}_k, \mathrm{ANN}_g, \mathrm{ANN}_s$	Annuity Factor of components *k*, *g* and *s*
$\mathrm{FOM_k}, \mathrm{FOM_g}, \mathrm{FOM}_s$	Fixed maintenance and operation of components *k*, *g* and *s*
$\mathrm{VOM}_k, \mathrm{VOM}_g, \mathrm{VOM}_s$	Variable maintenance and operation of components *k*, *g* and *s*
$\mathrm{GF}^i, \mathrm{GF}^d, \mathrm{GF}^{fO\&M}, \mathrm{GF}^{vO\&M},$	Greenhouse gas footprint of installation, disposal, fixed and variable operation and maintenance
R_s	Ratio between storage power and capacity of storage for commodity *s*

$CF_{g,s,c,t}$	Capacity factor of generator g for commodity *s* in cluster *c* at time *t*
$\eta^{out}_{k,main\ in,s}$	Conversion factor from main input to output *s* of conversion component *k*
$\eta^{in}_{k,main\ in,s}$	Conversion factor from main input to input *s* of conversion component *k*
$\eta^{charge}_{s}, \eta^{discharge}_{s}$	Charging and discharging efficiency of storage for commodity *s*
$P^{purchase}_{s,c,t}$	Purchase price of commodity *s* in cluster *c* at time *t*
$P^{sell}_{s,c,t}$	Selling price of commodity *s* in cluster *c* at time *t*
D_s	Total demand of commodity *s*
e	Objective function value at current interval step
ε	Adequately small value to include slack in the objective function
W_c	Weighting of cluster *c*
BM	Big-M coefficient (sufficiently large number)
$D^{standby}_{k,s,c,t}$	Standby demand of commodity s for conversion component *k* in cluster *c* at time *t*
DT_k, ST_k	Shut-off state and standby state downtime of conversion component *k*

$DT_{k,c,t}, ST_{k,c,t}$	Shut-off and standby state downtime of conversion component *k* in cluster *c* at time *t*
$P_k^{start\ up}$	Start-up costs of conversion component *k*
SU_k	Start-up costs of component *k*
RPL	Representative period length

5.1.1 Objective functions

$$\begin{aligned}\min f_1 = &\sum_{k\in K}\left(i_k(ANN_k + FOM_k) + SU_k + \sum_{s\in S_k^{MO}}\sum_{c\in C}\sum_{t\in T} x_{k,s,c,t}^{out}\cdot VOM_s\cdot W_c\right)\\ &+\sum_{\hat{s}\in SC}\left(i_{\hat{s}}(ANN_{\hat{s}} + FOM_{\hat{s}}) + \sum_{c\in C}\sum_{t\in T} x_{\hat{s},c,t}^{charge}\cdot VOM_{\hat{s}}\cdot W_c\right)\\ &+\sum_{g\in G}\left(i_g(ANN_g + FOM_g) + \sum_{\tilde{s}\in S_g}\sum_{c\in C}\sum_{t\in T} x_{g,\tilde{s},c,t}^{generation}\cdot VOM_g\cdot W_c\right)\\ &+\sum_{c\in C}\sum_{t\in T}\left(\sum_{\bar{s}\in PC} x_{\bar{s},c,t}^{purchase}\cdot P_{\bar{s},c,t}^{purchase} - \sum_{\dot{s}\in QC} x_{\dot{s},c,t}^{sell}\cdot P_{\dot{s},c,t}^{sell}\right)\cdot W_c - slack\cdot\varepsilon\end{aligned} \quad (6)$$

$$\begin{aligned}&Total\ emissions\\ &=\sum_{k\in K}\left(cap_k\left(GF_k^i + GF_k^d + GF_k^{fO\&M}\right) + \sum_{s\in S_k^{MO}}\sum_{c\in C}\sum_{t\in T} x_{k,s,c,t}^{out}\cdot GF_k^{vO\&M}\cdot W_c\right)\\ &+\sum_{\hat{s}\in SC}\left(cap_{\hat{s}}\left(GF_{\hat{s}}^i + GF_{\hat{s}}^d + GF_{\hat{s}}^{fO\&M}\right) + \sum_{c\in C}\sum_{t\in T} x_{\hat{s},c,t}^{charge}\cdot GF_{\hat{s}}^{vO\&M}\cdot W_c\right)\\ &+\sum_{g\in G}\left(cap_g\left(GF_g^i + GF_g^d + GF_g^{fO\&M}\right) + \sum_{\tilde{s}\in S_g}\sum_{c\in C}\sum_{t\in T} x_{g,\tilde{s},c,t}^{generation}\cdot GF_{\tilde{s}}^{vO\&M}\cdot W_c\right)\\ &+\sum_{c\in C}\sum_{t\in T}\left(\sum_{\bar{s}\in PC} x_{\bar{s},c,t}^{purchase}\cdot GF_{\bar{s}}^{purchase} - \sum_{\dot{s}\in QC} x_{\dot{s},c,t}^{sell}\cdot GF_{\dot{s}}^{sell}\right)\cdot W_c - slack\cdot\end{aligned} \quad (7)$$

$$Total\ emissions + \text{slack} - \text{e}_i = 0 \quad (8)$$

1.1.1 Commodities

Commodities represent all mass and energy flows in the system and connect all implemented components. The basic idea is balancing all commodities during all time steps, which *Equation (6)* implements.

$$\sum_{k\in K} x_{k,s,c,t}^{out} + x_{s,c,t}^{discharge} + x_{s,c,t}^{freely\ available} + x_{s,c,t}^{purchase} + \sum_{g\in G} x_{g,s,c,t}^{generation} = \sum_{k\in K} \left(x_{k,s,c,t}^{in} + x_{k,s,c,t}^{standby}\right) + x_{s,c,t}^{charge} + x_{s,c,t}^{emit} + x_{s,c,t}^{sell} + x_{s,c,t}^{demand} \quad (9)$$

$$\forall\, s \in S, c \in C, t \in T$$

Each commodity has several sources and sinks based on the user's implementation. The two simple sources (free availability and purchase) and sinks (emission and sell) are implemented with *Equations (10), (11), (12),* and *(13)*. If the sources and sinks do not apply to a commodity, the variables equal 0 for all time steps.

$$x_{s,c,t}^{freely\ available} \geq 0 \quad \forall\, s \in FC, c \in C, t \in T \quad (10)$$

$$x_{s,c,t}^{purchase} \geq 0 \quad \forall\, s \in PC, c \in C, t \in T \quad (11)$$

$$x_{s,c,t}^{sell} \geq 0 \quad \forall\, s \in QC, c \in C, t \in T \quad (12)$$

$$x_{s,c,t}^{emit} \geq 0 \quad \forall\, s \in EC, c \in C, t \in T \quad (13)$$

Another sink of the system is the demand for the target product. The demand has to be covered over all periods (*Equation (14)*). Altogether, the implementation of the demand forces the optimization to install capacities and to operate the system to satisfy the demand.

$$\sum_{c\in C}\sum_{t\in T}\left(x_{s,c,t}^{demand} \cdot \mathrm{W}_c\right) = D_s \quad \forall\, s \in DCT \quad (14)$$

1.1.2 Conversion Components

Conversion components enable the system to convert commodities and produce the target commodity. Especially in power-to-liquid processes, scaling effects impact large-scale facilities. The investment curve is divided into several linearized segments, each associated with a binary variable, lower capacity bound, upper capacity bound, fixed investment, and variable investment. The optimization chooses one of these segments using *Equation (15)*.

$$\sum_{n \in N_k} b_{k,n} = 1 \quad \forall\, k \in K \tag{15}$$

The capacity binary is activated as soon as the corresponding capacity of the segment is greater than zero (*Equation (16)*). Each segment's upper and lower bounds are implemented with *Equation (17)*. The lower bound is only active if the segment is chosen, allowing a lower bound of zero for all unused segments. The total capacity of the conversion component is calculated with *Equation (18)*. As only one segment has a capacity greater than zero, the final capacity will equal the value of the active segment. Each linear segment is associated with a slope ($Inv_{k,n}^{var}$) and an interception with the y-axis ($Inv_{k,n}^{fix}$). The final investment can be calculated using these two parameters in combination with the final capacity and binary (*Equation (19)*). The approach of linearization is described in the SI (c.f. *A3.2*). This approach further represents components without scaling effects ($N_k = \{1\};\ Inv_{k,1}^{fix} = 0;\ b_{k,1} = 1$).

$$\mathrm{cap}_{k,n} \leq b_{k,n} \cdot \mathrm{BM} \quad \forall\, k \in K, n \in N_k \tag{16}$$

$$\mathrm{BC}_{k,n}^{lower} \cdot b_{k,n} \leq \mathrm{cap}_{k,n} \leq \mathrm{BC}_{k,n}^{upper} \quad \forall\, k \in K, n \in N_k \tag{17}$$

$$\mathrm{cap}_k = \sum_{n \in N_k} \mathrm{cap}_{k,n} \quad \forall\, k \in K \tag{18}$$

$$i_k = \sum_{n \in N_k} \left(\mathrm{cap}_{k,n} \cdot \mathrm{Inv}_{k,n}^{var} + b_{k,n} \cdot \mathrm{Inv}_{k,n}^{fix}\right) \quad \forall\, k \in K \tag{19}$$

Each conversion component has at least one conversion and, therefore, at least one input and output. One input function serves as a connection between conversions and capacity. It is referenced as main input $x_{k,s,c,t}^{in}$. *Equation (20)* defines the ratio between the main input and all outputs of the same conversion unit. *Equation (21)* uses the same approach to define the ratio between the main input and all other inputs. The parameters $\eta_{k,s,\tilde{s}}^{out}$ and $\eta_{k,s,\tilde{s}}^{in}$ equal zero if commodities are not output or input of the conversion unit.

$$x_{k,\tilde{s},c,t}^{out} = x_{k,s,c,t}^{in} \cdot \eta_{k,s,\tilde{s}}^{out} \quad \forall\, k \in K, s \in S_k^{MI}, \tilde{s} \in S, c \in C, t \in T \tag{20}$$

$$x_{k,\tilde{s},c,t}^{in} = x_{k,s,c,t}^{in} \cdot \eta_{k,s,\tilde{s}}^{in} \quad \forall\, k \in K, s \in S_k^{MI}, \tilde{s} \in S, c \in C, t \in T \tag{21}$$

A conversion component's utilization is limited by a lower and upper bound of the installed capacity (*Equation (22)*). Between the upper and lower utilization limits, the conversion component's change of capacity utilization is limited by a ramp-up and ramp-down constraint (*Equation (23)*). This helps to define the flexibility of conversion components.

$$\mathrm{cap}_k \cdot \mathrm{BU}_k^{lower} \leq x_{k,s,c,t}^{in} \leq \mathrm{cap}_k \cdot \mathrm{BU}_k^{upper} \quad \forall\, k \in K, s \in S_k^{MI}, c \in C, t \in T \tag{22}$$

$$-\mathrm{cap}_k \cdot \mathrm{RAMP}_k^{down} \leq x_{k,s,c,t}^{in} - x_{k,s,c,t-1}^{in} \leq \mathrm{cap}_k \cdot RAMP_k^{up} \quad \forall\, k \in K, s \in S_k^{MI}, c \in C, t \in \{2, \dots, T\} \tag{23}$$

Conversion components have the further ability of unit commitment. This model allows three states: operating, standby, and shut-off. The operating status defines the regular operation of the component within its capacity utilization bounds. The shut-off state defines the component without any operation. The standby state, similar to the shut-off state, implements no operation of the conversion component but is associated with a standby demand, such as heating. The advantage of the standby state is the lower start-up time back to regular operation, but at the cost of supplying the standby demand. The three different states cannot co-occur (*Equation (24)*). If unit commitment is not implemented for specific conversion components, the shutdown and standby binary variables are equal to zero. *Equations (25)* and *(26)* balance the shut-off state, and *Equations (27)* and *(28)* balance the standby state.

$$b_{k,c,t}^{on} + b_{k,c,t}^{off} + b_{k,c,t}^{standby} = 1 \quad \forall\, k \in K, c \in C, t \in T \tag{24}$$

$$b_{k,c,t}^{off} = b_{k,c,t-1}^{off} + b_{k,c,t}^{shut\ down} - b_{k,c,t}^{start\ up} \quad \forall\, k \in K, c \in C, t \in T \tag{25}$$

$$b_{k,c,t}^{shut\ down} + b_{k,c,t}^{start\ up} \leq 1 \quad \forall\, k \in K, c \in C, t \in T \tag{26}$$

$$b_{k,c,t}^{standby} = b_{k,c,t-1}^{standby} + b_{k,c,t}^{standby\ on} - b_{k,c,t}^{standby\ off} \quad \forall\, k \in K, c \in C, t \in T \tag{27}$$

$$b_{k,c,t}^{standby\ on} + b_{k,c,t}^{standby\ off} \leq 1 \quad \forall\, k \in K, c \in C, t \in T \tag{28}$$

A conversion component is defined as operating when its capacity utilization is higher than zero, activating the operation state binary (*Equation (29)*). Its utilization is limited by the installed capacity's lower and upper bounds (*Equation (30)*). The binary variable allows zero utilization if the conversion component is not operating. Between the upper and lower utilization limits, the conversion component's change of capacity utilization is limited by a ramp-up and ramp-down constraint (*Equation (31)*). This helps to define the flexibility of conversion components. This ramping constraint only becomes effective if the component is in operation. If the component changes either into shut-off or standby state or from shut-off or standby state into operation, the ramping is unlimited, allowing an immediate stop or start of the operation.

$$x_{k,s,c,t}^{in} \leq b_{k,c,t}^{on} \cdot \mathrm{BM} \qquad \forall\, k \in K, s \in S_k^{MI}, c \in C, t \in T \tag{29}$$

$$\begin{aligned} &\mathrm{cap}_k \cdot \mathrm{BU}_k^{lower} + \left(b_{k,c,t}^{on} - 1\right) \cdot \mathrm{BM} \leq x_{k,s,c,t}^{in} \leq cap_k \cdot BU_k^{upper} \\ &\forall\, k \in K, s \in S_k^{MI}, c \in C, t \in T \end{aligned} \tag{30}$$

$$\begin{aligned} &-\left(\mathrm{cap}_k \cdot \mathrm{RAMP}_k^{down} + \left(b_{k,c,t}^{shut\ down} + b_{k,c,t}^{standby\ on}\right) \cdot \mathrm{BM}\right) \\ &\leq x_{k,s,c,t}^{in} - x_{k,s,c,t-1}^{in} \leq \\ &\mathrm{cap}_k \cdot \mathrm{RAMP}_k^{up} + \left(b_{k,c,t}^{start\ up} + b_{k,c,t}^{standby\ off}\right) \cdot \mathrm{BM} \\ &\forall\, k \in K, s \in S_k^{MI}, c \in C, t \in \{2, \ldots, T\} \end{aligned} \tag{31}$$

If the conversion component switches to the shut-off or standby state, it might not be able to return to normal operation conditions immediately. Therefore, it is possible to associate a necessary downtime for the shut-off and standby state. The following equations regulate the adherence of these downtimes if the conversion component switches to the respective state. The first two equations define the downtimes of the component in each hour, and *Equations (34)* and *(35)* implement the downtimes.

$$\mathrm{DT}_{k,c,t} = \min\left(\mathrm{DT}_k, \mathrm{RPL} - \left(t - \left(\left\lfloor \frac{t}{\mathrm{RPL}} \right\rfloor \cdot \mathrm{RPL}\right)\right)\right) \quad \forall\, k \in K, c \in C, t \in T \tag{32}$$

$$\mathrm{ST}_{k,c,t} = \min\left(\mathrm{ST}_k, \mathrm{RPL} - \left(t - \left(\left\lfloor \frac{t}{\mathrm{RPL}} \right\rfloor \cdot \mathrm{RPL}\right)\right)\right) \quad \forall\, k \in K, c \in C, t \in T \tag{33}$$

$$\left(b_{k,c,t}^{off} - b_{k,c,t-1}^{off}\right) \cdot \mathrm{DT}_{k,c,t} \leq \sum_{t \in T}^{t+DT_{k,c,t}-1} b_{k,c,t}^{off} \quad \forall\, k \in K, s \in S_k^{MI}, c \in C, t \in \{2, \ldots, T\} \tag{34}$$

$$\left(b_{k,c,t}^{standby} - b_{k,c,t-1}^{standby}\right) \cdot \mathrm{ST}_{k,c,t} \leq \sum_{t \in T}^{t+ST_{k,c,t}-1} b_{k,c,t}^{standby} \quad \forall\, k \in K, s \in S_k^{MI}, c \in C, t \in \{2, \ldots, T\} \tag{35}$$

The start-up of the conversion component from the shut-off state might result in start-up costs. Therefore, the following constraints define the start-up time steps and add the associated costs to these time steps.

$$\mathrm{cap}_k \cdot P_k^{start\ up} \cdot W_c - \left(1 - b_{k,c,t}^{start\ up}\right) \cdot \mathrm{BM} \leq \mathrm{SU}_{k,c,t} \quad \forall\, k \in K, c \in C, t \in T \tag{36}$$

$$\mathrm{SU}_k = \sum_{c \in C} \sum_{t \in T} \mathrm{SU}_{k,c,t} \quad \forall\, k \in K \tag{37}$$

The following equations define the standby demand, which depends on the component's capacity and a capacity-dependent demand. To avoid the coverage of standby demand at all time steps, where the conversion component is not in the standby state, *Equation (39)* is implemented.

$$\mathrm{cap}_k \cdot \mathrm{D}_{k,s}^{standby} + \left(b_{k,c,t}^{standby} - 1\right) \cdot BM \leq x_{k,s,c,t}^{standby} \leq cap_k \cdot D_{k,s}^{standby} \quad \forall\, k \in K, s \in S, c \in C, t \in T \tag{38}$$

$$x_{k,s,c,t}^{standby} \leq b_{k,c,t}^{standby} \cdot \mathrm{BM} \quad \forall\, k \in K, s \in S, c \in C, t \in T \tag{39}$$

1.1.3 Renewable Generation Units

Equation (40) calculates the hourly generation, which is dependent on the hourly capacity factor (CF) of the renewable energy and the capacity of the generator. If the generator does not produce a commodity, the CF takes 0 for all time steps. Based on the capacity, the investment in the generator is calculated (*Equation (41)*).

$$x_{g,s,c,t}^{generation} \leq \mathrm{cap}_g \cdot \mathrm{CF}_{g,c,t} \quad \forall\, g \in G, s \in S_g, c \in C, t \in T \tag{40}$$

$$i_g = \mathrm{cap}_g \cdot \mathrm{Inv}_g \quad \forall\, g \in G \tag{41}$$

1.1.4 Storage components

Equation (42) defines storage charging and discharging activities and their impact on the hourly state of charge. The storage's initial state-of-charge (SOC) is undefined so that the system can decide the optimal level. *Equation (43)* balances all storage activities to avoid solely discharging the storage. The SOC limitations are imposed by *Equation (44)*. *Equations (45)* and *(46)* define the ratio between charging and discharging activities, as well as the capacity of the storage component. The last equation defines the investment in the storage component. *Equation (48)* sets all storage capacities to 0 if a commodity is not storable.

$$soc_{s,c,t} = soc_{s,c,t-1} + x_{s,c,t-1}^{charge} \cdot \eta_s^{charge} - \frac{x_{s,c,t-1}^{discharge}}{\eta_s^{discharge}} \tag{42}$$

$$\forall\, s \in SC, c \in C, \in \{2, \dots, T\}$$

$$\sum_{c \in C} \sum_{t \in T} x_{s,c,t}^{charge} \cdot \eta_s^{charge} \cdot W_c = \sum_{c \in C} \sum_{t \in T} \frac{x_{s,c,t}^{discharge}}{\eta_s^{discharge}} \cdot W_c \tag{43}$$

$$\forall\, s \in SC, c \in C, t \in T$$

$$\mathrm{cap}_s \cdot \mathrm{BU}_s^{lower} \leq \mathrm{soc}_{s,c,t} \leq \mathrm{cap}_s \cdot \mathrm{BU}_s^{upper} \quad \forall\, s \in SC, c \in C, t \in T \tag{44}$$

$$x_{s,c,t}^{charge} \leq \mathrm{cap}_s \cdot \mathrm{R}_s \quad \forall\, s \in SC, c \in C, t \in T \tag{45}$$

$$x_{s,c,t}^{discharge} \leq \mathrm{cap}_s \cdot \mathrm{R}_s \quad \forall\, s \in SC, c \in C, t \in T \tag{46}$$

$$i_s = \mathrm{cap}_s \cdot \mathrm{Inv}_s \quad \forall\, s \in SC \tag{47}$$

$$\mathrm{cap}_s = 0 \quad \forall\, s \in S \backslash SC \tag{48}$$

Finally, a charging and discharging binary is implemented to avoid the simultaneous charging and discharging of the storage component.

$$x_{s,c,t}^{charge} \leq b_{s,c,t}^{charge} \cdot \mathrm{BM} \quad \forall s \in SC, c \in C, t \in T \tag{49}$$

$$x_{s,c,t}^{discharge} \leq b_{s,c,t}^{discharge} \cdot \mathrm{BM} \quad \forall\, s \in SC, c \in C, t \in T \tag{50}$$

$$b_{s,c,t}^{charge} + b_{s,c,t}^{discharge} \leq 1 \quad \forall\, s \in SC, c \in C, t \in T \tag{51}$$

5.2 Implementation of scaling factors

Scaling factors are implemented by linearization of the investment curve. The investment *I* is calculated for different capacities *C* using *Equation (52)* with base investment I_0, base capacity C_0, and scaling factor δ given in *Table 1* of the manuscript.

$$\frac{I}{I_0} = \left(\frac{C}{C_0}\right)^{\delta} \tag{52}$$

The resulting investment curve is calculated until a set maximal capacity, and the range of investments is divided into ten equal segments. For each segment, the capacities and investments are fit to a Linear Regression model which returns the intercept with the y axis (=minimal investment for segment $\mathrm{Inv}_{k,n}^{fix}$) and the gradient of the line (=capacity depending investment: $\mathrm{Inv}_{k,n}^{var}$). The edges of the segment represent the lower and upper bound of the capacities of the segment ($\mathrm{BC}_{k,n}^{lower}$ and $\mathrm{BC}_{k,n}^{upper}$). The last segment is implemented without an upper bound to allow capacities higher than the set maximal capacity. *Figure 4* shows the graphical abstract of the linearization process.

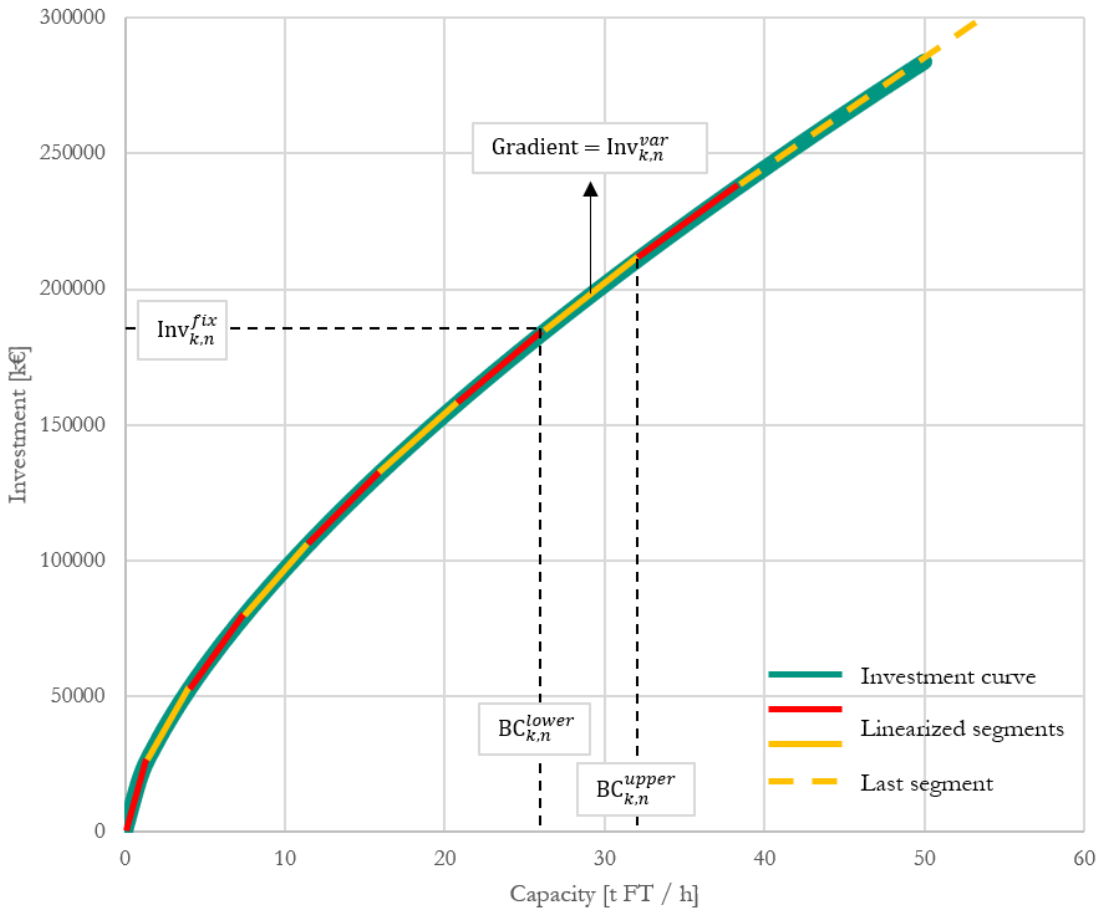

Figure 4: Graphical abstract of the investment curve linearization

A6. Further decision support results

6.1 From steady-state to flexible operation

Conventional process simulation assumes the steady-state operation of the facility. However, in combination with volatile renewable electricity generation, flexibility is needed to integrate the volatile electricity generation. To assess the impact of renewable electricity generation volatility, we apply the developed optimization tool with the objective of solely cost minimization. Here, we use the Fischer-Tropsch technology path with a steady electricity supply and compare it to the Fischer-Tropsch case applied with the renewable generation in Australia (AUS), Germany (GER), Chile (CHL), Kazakhstan (KAZ), and Saudi Arabia (SAU).

Table 20 shows how capacities and capacity factors develop in both cases. The over-capacities for all conversion components and the reduced capacity factors when renewable electricity generation is applied are visible. Notably, the PEM electrolysis is heavily affected with increased capacities of up to 861.77 MW and reduced capacity factors of 40.25%. In addition, with a fixed electricity supply, no storage units are needed. The results show that the steady-state approach is far from a realistic implementation of power-to-x production, and consideration of renewable electricity generation is indispensable.

Table 20: Capacities and capacity factors of the different components in the FT production when applying to a steady electricity supply and volatile renewable electricity generation at the best trade-off

		Fixed	AUS	SAU	GER	KAZ	CHL
Synthesis	Capacity [t FT / h]	15.6	16.92	17.02	17.69	18.84	16.31
	Capacity Factor	100.00%	92.18%	91.61%	88.15%	82.79%	95.65%
PEM Electrolysis	Capacity [MW]	346.86	453.28	861.77	487.23	491.92	426.91
	Capacity Factor	100.00%	76.52%	40.25%	71.19%	70.51%	81.25%
DAC	Capacity [t CO_2 / h]	48.94	51.95	50.67	51.09	53.21	53.40
	Capacity Factor	100.00%	94.21%	96.59%	95.80%	91.98%	91.65%
Hydrogen Storage	Capacity [MWh]	0	5,599.64	2,913.78	7,537.52	3959.73	13,165.50
Battery Storage	Capacity [MWh]	0	704.19	2,240.42	1,143.22	591.67	797.76
CO_2 Storage	Capacity [t CO_2]	0	534.49	429.02	739.99	986.93	1,398.96

6.2 Share of costs and emissions of each component on total costs and emissions

Next to the capacities in the manuscript, other information is available to support investment decisions in power-to-x facilities. *Figure 5* and *Figure 6* shows the share of each component on the total costs and emissions. Visible is the removal of solar PV to save emissions when aiming for minimal emissions. Most costs stem from the electricity supply components (wind generators, battery storage), DAC, and the PEM electrolysis, as soon as minimal emissions are achieved. Solar PV reduces electricity generation costs when aiming for minimal costs. However, using solar PV heavily increases emissions. The capacities of each scenario and country can be found in *Table 21*. As soon as costs are minimized, electricity generation, integration, and hydrogen production contribute most to total costs.

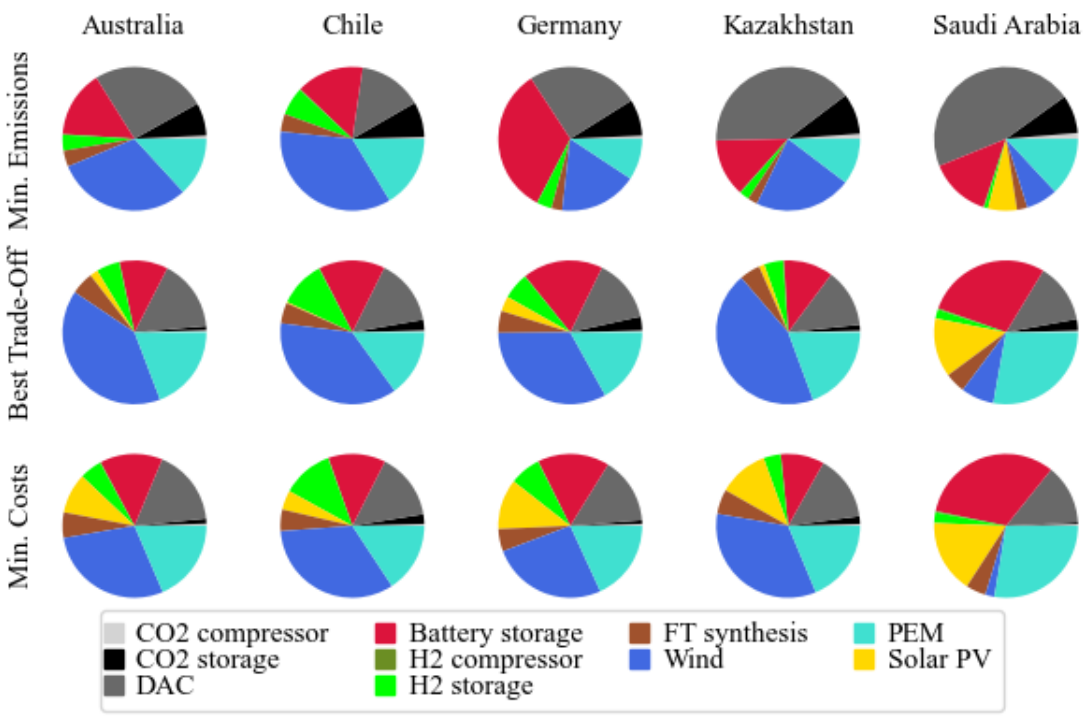

Figure 5: Shares of different components' costs on the total costs in the case of cost minimization, emissions minimization, and best trade-off. Numerical data of the figure is given in the supporting information S2

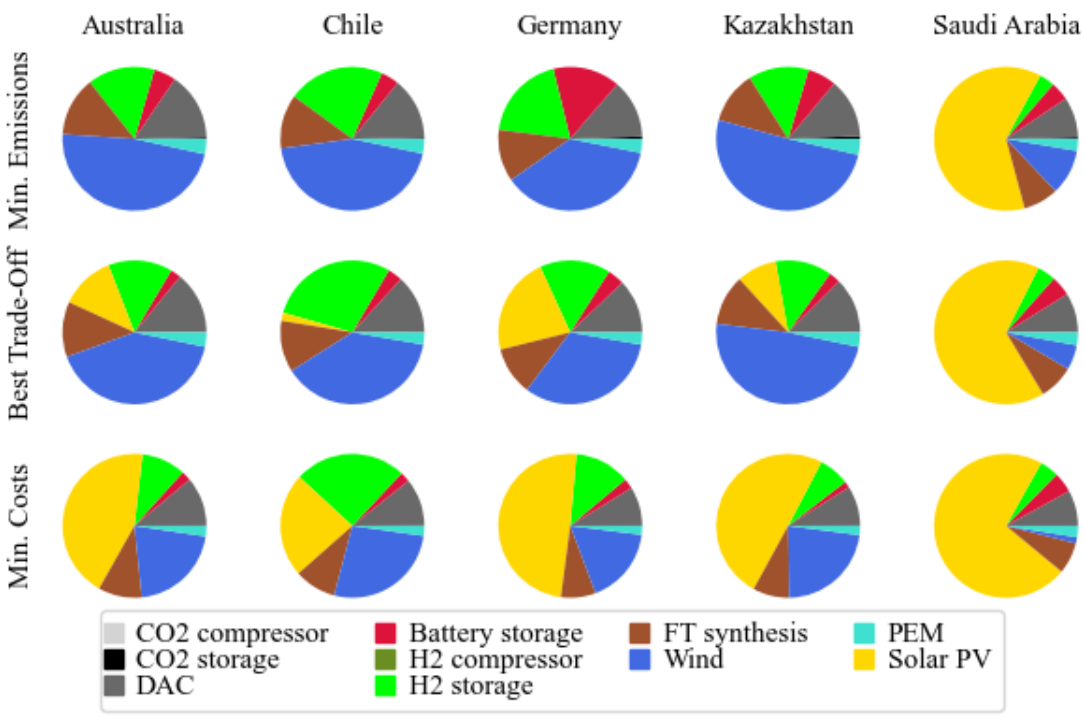

Figure 6: Share of different components' emissions on the total emissions in the case of cost minimization, emission minimization, and best trade-off. Numerical data of the figure is given in the supporting information S2

Table 21: Capacities of each component in the FT production for different countries and scenarios

Country	Scenario	CO_2 compressor [MW]	CO_2 storage [t]	DAC [t/h]	Battery storage [MWh]	H2 compressor [MW]	H2 storage [MWh]	FT synthesis [t/h]	Wind [MW]	PEM electrolysis [MW]	Solar PV [MW]
Australia	Min. GHG emissions	7.38	5,689.20	120.33	1,283.82	2.52	5,882.05	16.65	1,423.72	488.40	-
	Best Trade-Off	3.27	507.04	53.24	656.26	1.81	6,056.97	16.75	1,328.70	504.55	223.00
	Min. costs	3.14	554.72	51.17	765.44	1.96	5,264.85	16.86	858.26	440.61	1,005.79
Chile	Min. GHG emissions	3.64	5,412.66	59.39	1,152.11	3.09	9,248.71	16.34	1,456.46	535.83	-
	Best Trade-Off	3.24	1,420.32	52.89	969.76	1.87	13,046.24	16.32	1,316.53	424.45	35.66
	Min. costs	3.14	1,225.75	51.17	806.80	1.91	13,829.51	16.31	1,132.37	428.16	557.30
Germany	Min. GHG emissions	11.36	9,933.53	185.12	4,465.45	1.69	8,647.34	17.40	1,283.22	540.51	-
	Best Trade-Off	3.23	1,921.14	52.73	1,229.32	1.23	7,790.83	17.99	1,222.88	498.91	467.93
	Min. costs	3.12	467.04	50.82	1,001.51	1.62	8,361.42	16.93	886.72	489.85	1,429.08
Kazakhstan	Min. GHG emissions	19.68	12,143.60	320.77	1,905.46	4.21	6,068.94	17.67	1,743.35	658.37	-
	Best Trade-Off	3.22	865.90	52.51	813.75	3.60	5,998.15	18.38	1,771.15	614.19	184.39
	Min. costs	3.06	959.44	49.90	604.28	1.13	4,554.18	18.55	1,149.20	503.49	1,415.25
Saudi Arabia	Min. GHG emissions	20.67	10,382.59	336.97	1,825.62	4.55	2,264.77	16.73	518.62	756.70	1,768.42
	Best Trade-Off	3.19	1,653.92	51.96	1,994.12	5.13	2,761.99	17.56	287.82	857.79	1,911.19
	Min. costs	3.10	257.15	50.57	2,220.79	4.97	3,141.37	16.72	76.84	823.91	2,303.44

6.3 Comparison with fossil reference products

Regarding the production costs of Hydrogen as a product or intermediate, fossil reference production costs, based on natural gas or coal, are in the range of 0.8 to 5.7 US-$/kg$_{H2}$ (International Energy Agency (IEA), 2024), especially depending on the local availability and price of feedstock. Assuming an exchange rate of 1.08 US-$/€ (ECB, 2024) and based on the lower heating value, this leads to a production cost range of 24.7 to 166.7 €/MWh, with 61.7 €/MWh (2 US-$/kg$_{H2}$) being an often-referred threshold for industrial hydrogen production. The economically best performing scenario (Chile, cost minimized) reaches costs of 74 €/MWh, therefore being close to the referred threshold. MeOH production costs in fossil-based plants, using natural gas or coal as a feedstock, also strongly rely on their respective prices. Fossil methanol production costs, assuming average European natural gas prices, are between 45 and 48 €/MWh, depending on the technology applied (Arnaiz Del Pozo, Cloete and Jiménez Álvaro, 2022). Globally, methanol production relying on low-cost, abundant natural gas resources can reach production costs down to 16.7 €/MWh (Kang *et al.*, 2021). The economically best-performing scenario for renewable methanol production, according to our results (Chile), is at 150 €/MWh. Light crude oil is chosen as a reference product for FT-crude. Since the production costs of crude oil strongly depend on individual crude oil fields, the sole production costs are hard to determine. As an economic reference value, the global trade price of UK Brent was between 40.8 and 47.9 €/MWh in 2023 (Oil and Energy Trends, 2024). Refining crude oil usually adds costs of 5.4 €/MWh at maximum (Hafner, 2022). The economically best-performing scenario for producing renewable FT-crude (Australia) is 142 €/MWh.

Regarding the fossil reference products reported in literature, Busch et al. (2023) stated in their review mean values for GHG emissions for hydrogen production through steam methane reforming (SMR) and coal gasification (CG) of 114 g $CO_{2eq.}$ / MJ resp. 246 g $CO_{2eq.}$ / MJ. The range of hydrogen from water electrolysis for the studied regions can't be reached even by integrating (47 resp. 73 g $CO_{2eq.}$ / MJ). SMR and CG are the reference pathways for methanol production and are reported to be 22 g $CO_{2eq.}$ / MJ resp. 140 g $CO_{2eq.}$ / MJ (Kajaste *et al.*, 2018). While the CG pathway exceeds the GHG emissions of the green methanol route for

all regions, SMR-based methanol is only marginally higher ranked than the promising constellations in Chile, Australia, and Germany. Elgowainy et al. (2014) found GHG emissions of about 9 g CO2eq when looking at crude oil as a reference for FT-crude. / MJ. Its refined fossil products, gasoline, diesel, and jet fuel (22, 17 resp. 14 g $CO_{2eq.}$ / MJ), still show lower GHG emissions than the best green FT-scenario in Australia. The manuscript mentions that a fair comparison can be conducted by integrating negative GHG emissions. When considering the CO_2 removal through the direct air capture process, 64 and 68 g $CO_{2eq.}$ / MJ are chemically stored in MeOH, respectively, FT crude. This leads to an overall cradle-to-gate GHG emission reduction for both renewable hydrocarbons

6.4 Sensitivity of PEM CAPEX on Pareto fronts

PEM electrolysis installed capacities have reached 552 MW by the end of 2022 and are estimated to grow by 921 MW in 2023 (International Energy Agency (IEA), 2023). Information on projects is published scarcely, making it difficult to have robust assumptions on PEM electrolysis CAPEX. Therefore, we have conducted a sensitivity analysis regarding the PEM electrolysis CAPEX, using 75%, 100%, and 125% of the assumed CAPEX of 810 k€/MW to calculate the Pareto fronts depicted in *Figure 7*. Visible is the shift towards higher costs with increasing PEM electrolysis CAPEX. However, next to the shift, the form of the Pareto fronts changes slightly. The curve becomes more bulbous with a higher CAPEX, showing that low-emission production gets disproportionately expensive compared to lower CAPEX Pareto fronts. Finally, the approximated GHG emission nadir value increases since more expensive electrolysis results in increased focus on costs.

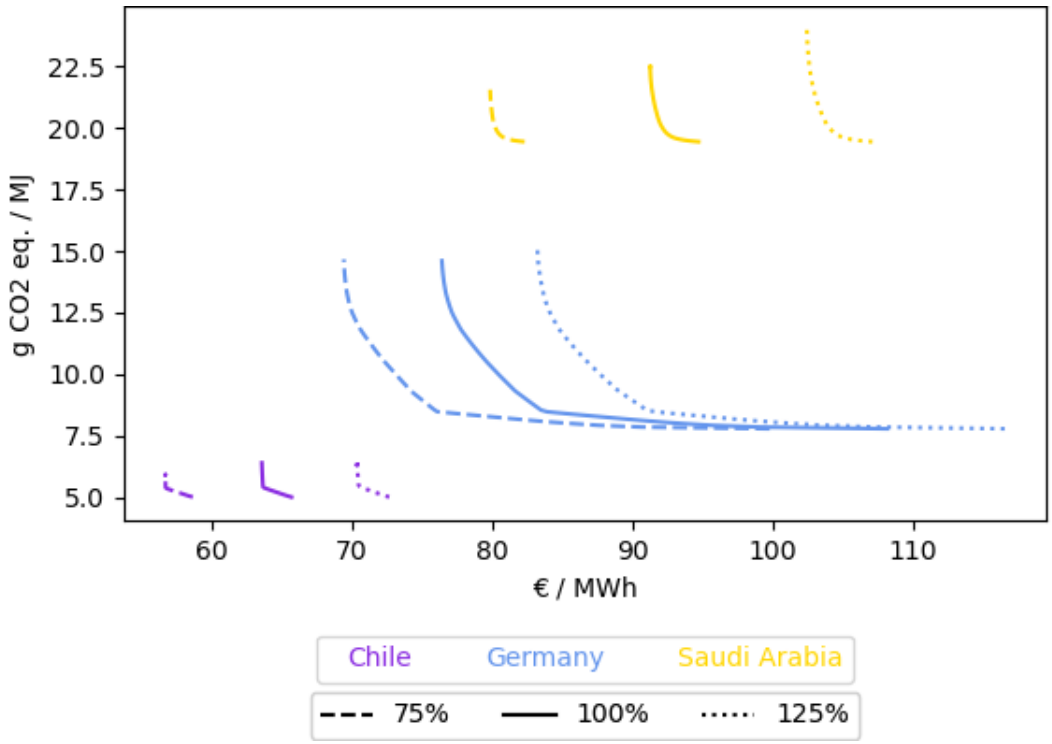

Figure 7: Pareto fronts of the hydrogen production applying sensitivity analysis on PEM electrolysis CAPEX. Numerical data of the figure is given in the supporting information S2

6.5 Sensitivity of solar PV installation emissions on Pareto fronts

The Pareto fronts of the hydrogen production in different countries, applying sensitivity analysis on the solar PV installation GHG emissions, are given in *Figure 8*. The changing emission intensity affects especially countries with high solar PV capacities in the case of cost minimization, in this case, Saudi Arabia. The GHG emissions drop or increase by around 20 g CO_2 eq. / MJ when increasing specific installation emission by +/- 25%. Interestingly, the changing amplitude to the right decreases with lower specific installation emissions. With lower specific installation emissions, emissions increase less when costs are minimized, and costs and emissions are increasingly aligned.

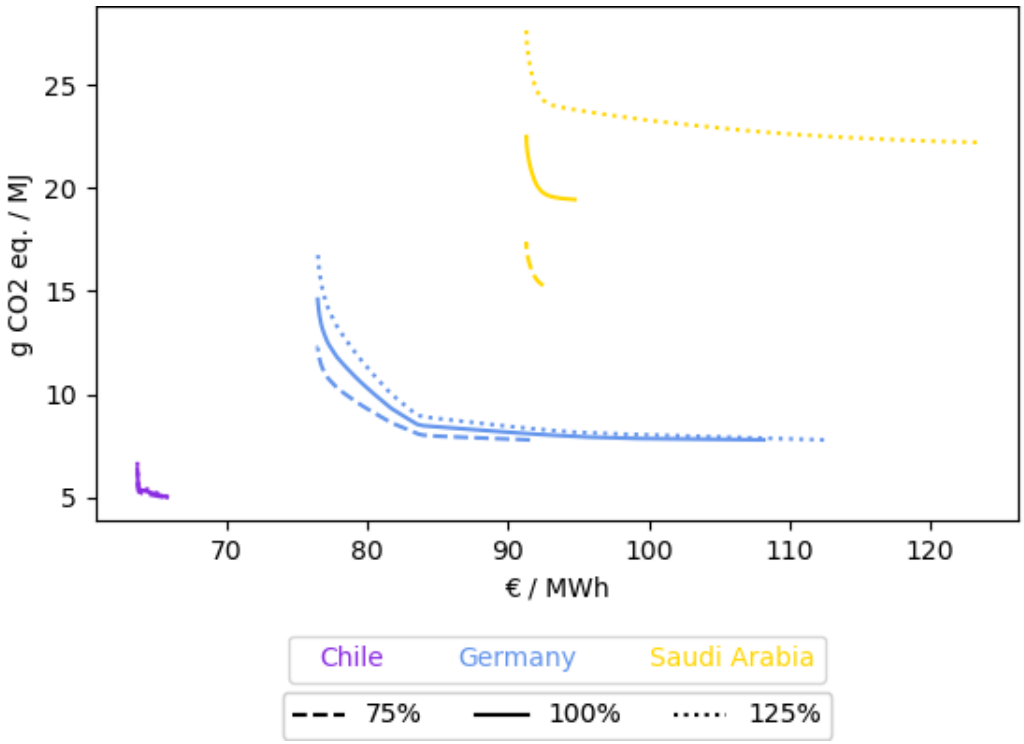

Figure 8: Pareto fronts of the hydrogen production applying sensitivity analysis on solar PV installation emissions. Numerical data of the figure is given in the supporting information S2

A7. List of references

Adelung, S., Maier, S. and Dietrich, R.-U. (2021) 'Impact of the reverse water-gas shift operating conditions on the Power-to-Liquid process efficiency', *Sustainable Energy Technologies and Assessments*, 43, p. 100897. Available at: https://doi.org/10.1016/j.seta.2020.100897.

Albrecht, F.G. *et al.* (2017) 'A standardized methodology for the techno-economic evaluation of alternative fuels – A case study', *Fuel*, 194, pp. 511–526. Available at: https://doi.org/10.1016/j.fuel.2016.12.003.

Armijo, J. and Philibert, C. (2020) 'Flexible production of green hydrogen and ammonia from variable solar and wind energy: Case study of Chile and Argentina', *International Journal of Hydrogen Energy*, 45(3), pp. 1541–1558. Available at: https://doi.org/10.1016/j.ijhydene.2019.11.028.

Arnaiz Del Pozo, C., Cloete, S. and Jiménez Álvaro, Á. (2022) 'Techno-economic assessment of long-term methanol production from natural gas and renewables', *Energy Conversion and Management*, 266, p. 115785. Available at: https://doi.org/10.1016/j.enconman.2022.115785.

Bareiß, K. *et al.* (2019a) 'Life cycle assessment of hydrogen from proton exchange membrane water electrolysis in future energy systems', *Applied Energy*, 237, pp. 862–872. Available at: https://www.sciencedirect.com/science/article/pii/S0306261919300017 (Accessed: 26 February 2024).

Bareiß, K. *et al.* (2019b) 'Life cycle assessment of hydrogen from proton exchange membrane water electrolysis in future energy systems', *Applied Energy*, 237, pp. 862–872.

Berger, M. *et al.* (2021) 'Remote Renewable Hubs For Carbon-Neutral Synthetic Fuel Production', *Frontiers in Energy Research*, 9, p. 671279. Available at: https://doi.org/10.3389/fenrg.2021.671279.

Bohlender GmbH (no date) *Grundlagen zur Regeneration von Silicagel, SICCO Trockenschränke und Exsikkatoren*. Available at: https://www.sicco.de/Technische-Infos/Trocknungsmittel-und-Luftfeuchtigkeit/Grundlagen-zur-Regeneration-von-Silicagel/ (Accessed: 7 May 2024).

Braun, J. *et al.* (2022) *Technische und risikobewertete Kosten-Potenzial-Analyse der MENA-Region. MENA-Fuels: Teilbericht 10*. Wuppertal, Stuttgart, Saarbrücken: Deutsches Zentrum für Luft- und Raumfahrt e.V.; Wuppertal Institut für Klima, Umwelt, Energie gGmbH. Available at: https://wupperinst.org/fa/redaktion/downloads/projects/MENA-Fuels_Teilbericht10_Kostenpotenziale.pdf (Accessed: 1 July 2024).

Busch, P., Kendall, A. and Lipman, T. (2023) 'A systematic review of life cycle greenhouse gas intensity values for hydrogen production pathways', *Renewable and Sustainable Energy Reviews*, 184, p. 113588. Available at: https://doi.org/10.1016/j.rser.2023.113588.

Cole, W. and Karmakar, A. (2023) *Cost Projections for Utility-Scale Battery Storage: 2023 Update*. Golden, CO: National Renewable Energy Laboratory. Available at: https://www.nrel.gov/docs/fy23osti/85332.pdf (Accessed: 27 June 2024).

Cordero-Lanzac, T. *et al.* (2022) 'A techno-economic and life cycle assessment for the production of green methanol from CO2: catalyst and process bottlenecks', *Journal of Energy Chemistry*, 68, pp. 255–266.

Danish Energy Agency (2023) *Technology Data*. Available at: https://ens.dk/sites/ens.dk/files/Analyser/technology_data_catalogue_for_el_and_dh.pdf.

Deutz, S. and Bardow, A. (2021) 'Life-cycle assessment of an industrial direct air capture process based on temperature–vacuum swing adsorption', *Nature Energy*, 6(2), pp. 203–213.

EC JRC Institute for Energy and Transport (2016) *Techno-economic and environmental evaluation of CO2 utilisation for fuel production: synthesis of methanol and formic acid*. LU: Publications Office. Available at: https://data.europa.eu/doi/10.2790/981669 (Accessed: 6 May 2024).

ECB (2024) *Euro exchange rates charts*. Available at: https://www.ecb.europa.eu/stats/policy_and_exchange_rates/euro_reference_exchange_rates/html/eurofxref-graph-usd.en.html (Accessed: 4 December 2024).

Farajiamiri, M., Meyer, J.-C. and Walther, G. (2023) 'Multi-objective optimization of renewable fuel supply chains regarding cost, land use, and water use', *Applied Energy*, 349, p. 121652. Available at: https://doi.org/10.1016/j.apenergy.2023.121652.

Fasihi, M., Bogdanov, D. and Breyer, C. (2016) 'Techno-Economic Assessment of Power-to-Liquids (PtL) Fuels Production and Global Trading Based on Hybrid PV-Wind Power Plants', *Energy Procedia*, 99, pp. 243–268. Available at: https://doi.org/10.1016/j.egypro.2016.10.115.

Fasihi, M., Efimova, O. and Breyer, C. (2019) 'Techno-economic assessment of CO2 direct air capture plants', *Journal of Cleaner Production*, 224, pp. 957–980. Available at: https://doi.org/10.1016/j.jclepro.2019.03.086.

Fernández-González, J. *et al.* (2022) 'Hydrogen Utilization in the Sustainable Manufacture of CO_2-Based Methanol', *Industrial & Engineering Chemistry Research*, 61(18), pp. 6163–6172. Available at: https://doi.org/10.1021/acs.iecr.1c04295.

Gerloff, N. (2021) 'Comparative Life-Cycle-Assessment analysis of three major water electrolysis technologies while applying various energy scenarios for a greener hydrogen production', *Journal of Energy Storage*, 43, p. 102759. Available at: https://www.sciencedirect.com/science/article/pii/S2352152X21004874 (Accessed: 22 March 2024).

Ghandehariun, S. and Kumar, A. (2016) 'Life cycle assessment of wind-based hydrogen production in Western Canada', *International Journal of Hydrogen Energy*, 41(22), pp. 9696–9704. Available at: https://doi.org/10.1016/j.ijhydene.2016.04.077.

Hafner, M. (2022) *The Palgrave Handbook of International Energy Economics*. Cham: Springer International Publishing AG.

Hank, C. *et al.* (2019) 'Comparative well-to-wheel life cycle assessment of OME 3–5 synfuel production via the power-to-liquid pathway', *Sustainable Energy & Fuels*, 3(11), pp. 3219–3233. Available at: https://pubs.rsc.org/en/content/articlehtml/2019/se/c9se00658c (Accessed: 7 March 2024).

Hannula, I. and Kurkela, E. (2013) *Liquid transportation fuels via large-scale fluidised-bed gasification of lignocellulosic biomass*. Espoo: VTT.

Heinzmann, P. *et al.* (2021) *Techno-ökonomische Bewertung der Produktion regenerativer synthetischer Kraftstoffe*. Karlsruher Institut für Technologie (KIT). Available at: https://doi.org/10.5445/IR/1000140638.

Herz, G. *et al.* (2021) 'Economic assessment of Power-to-Liquid processes – Influence of electrolysis technology and operating conditions', *Applied Energy*, 292, p. 116655. Available at: https://doi.org/10.1016/j.apenergy.2021.116655.

Hischier, R. (2007) *chemical factory construction, organics - RER - chemical factory, organics | ecoQuery, ecoinvent 3.9.1. APOS - chemical factory construction, organics*. Available at: https://ecoquery.ecoinvent.org/3.9.1/apos/dataset/8400/documentation (Accessed: 7 March 2024).

Hoppe, W., Thonemann, N. and Bringezu, S. (2018) 'Life Cycle Assessment of Carbon Dioxide–Based Production of Methane and Methanol and Derived Polymers', *Journal of Industrial Ecology*, 22(2), pp. 327–340. Available at: https://doi.org/10.1111/jiec.12583.

Iglesias González, M., Eilers, H. and Schaub, G. (2016) 'Flexible Operation of Fixed-Bed Reactors for a Catalytic Fuel Synthesis—CO_2 Hydrogenation as Example Reaction', *Energy Technology*, 4(1), pp. 90–103. Available at: https://doi.org/10.1002/ente.201500259.

International Energy Agency (IEA) (2023) *Hydrogen Production and Infrastructure Projects Database*. Available at: https://www.iea.org/data-and-statistics/data-product/hydrogen-production-and-infrastructure-projects-database (Accessed: 9 July 2024).

International Energy Agency (IEA) (2024) *Global Hydrogen Review 2024*. IEA. Available at: https://www.iea.org/reports/global-hydrogen-review-2024 (Accessed: 4 December 2024).

Kadam, R.S. and Yadav, G.D. (2024) 'Life cycle analysis of ammonia and methane production using green hydrogen and carbon dioxide', *Journal of Cleaner Production*, 449, p. 141620. Available at: https://doi.org/10.1016/j.jclepro.2024.141620.

Kajaste, R. *et al.* (2018) 'Methanol-Managing greenhouse gas emissions in the production chain by optimizing the resource base', *AIMS Energy*, 6(6), pp. 1074–1102. Available at: https://doi.org/10.3934/energy.2018.6.1074.

Kang, S. *et al.* (2021) *Innovation outlook: renewable methanol*. Edited by D. Gielen and G. Dolan. Abu Dhabi: International Renewable Energy Agency.

Kenkel, P. *et al.* (2021) 'A generic superstructure modeling and optimization framework on the example of bi-criteria Power-to-Methanol process design', *Computers & Chemical Engineering*, 150, p. 107327. Available at: https://doi.org/10.1016/j.compchemeng.2021.107327.

König, D.H. *et al.* (2015) 'Techno-economic study of the storage of fluctuating renewable energy in liquid hydrocarbons', *Fuel*, 159, pp. 289–297. Available at: https://doi.org/10.1016/j.fuel.2015.06.085.

Lacerda De Oliveira Campos, B. *et al.* (2022) 'A Detailed Process and Techno-Economic Analysis of Methanol Synthesis from H2 and CO2 with Intermediate Condensation Steps', *Processes*, 10(8), p. 1535. Available at: https://doi.org/10.3390/pr10081535.

Lee, H. *et al.* (2022) 'Outlook of industrial-scale green hydrogen production via a hybrid system of alkaline water electrolysis and energy storage system based on seasonal solar radiation', *Journal of Cleaner Production*, 377, p. 134210. Available at: https://doi.org/10.1016/j.jclepro.2022.134210.

Madhu, K. *et al.* (2021) 'Understanding environmental trade-offs and resource demand of direct air capture technologies through comparative life-cycle assessment', *Nature Energy*, 6(11), pp. 1035–1044. Available at: https://www.nature.com/articles/s41560-021-00922-6 (Accessed: 26 February 2024).

Maggi, A., Wenzel, M. and Sundmacher, K. (2020) 'Mixed-Integer Linear Programming (MILP) Approach for the Synthesis of Efficient Power-to-Syngas Processes', *Frontiers in Energy Research*, 8, p. 161. Available at: https://doi.org/10.3389/fenrg.2020.00161.

Maimaiti, S. *et al.* (2023) 'Prospective life cycle environmental impact assessment of renewable energy-based methanol production system: A case study in China', *Journal of Cleaner Production*, 425, p. 139002. Available at: https://doi.org/10.1016/j.jclepro.2023.139002.

Micheli, M. *et al.* (2022) 'Life-cycle assessment of power-to-liquid kerosene produced from renewable electricity and CO2 from direct air capture in Germany', *Sustainability*, 14(17), p. 10658.

Moretti, C. *et al.* (2023) 'Technical, economic and environmental analysis of solar thermochemical production of drop-in fuels', *Science of The Total Environment*, 901, p. 166005. Available at: https://doi.org/10.1016/j.scitotenv.2023.166005.

Morgan, E.R., Manwell, J.F. and McGowan, J.G. (2017) 'Sustainable Ammonia Production from U.S. Offshore Wind Farms: A Techno-Economic Review', *ACS Sustainable Chemistry & Engineering*, 5(11), pp. 9554–9567. Available at: https://doi.org/10.1021/acssuschemeng.7b02070.

Mucci, S., Mitsos, A. and Bongartz, D. (2023) 'Cost-optimal Power-to-Methanol: Flexible operation or intermediate storage?', *Journal of Energy Storage*, 72, p. 108614. Available at: https://doi.org/10.1016/j.est.2023.108614.

Oil and Energy Trends (2024) 'Prices', *Oil and Energy Trends*, 49(7–8), pp. 52–54. Available at: https://doi.org/10.1111/oet.9_13128.

Osman, O., Sgouridis, S. and Sleptchenko, A. (2020) 'Scaling the production of renewable ammonia: A techno-economic optimization applied in regions with high insolation', *Journal of Cleaner Production*, 271, p. 121627. Available at: https://doi.org/10.1016/j.jclepro.2020.121627.

Peters, M.S. *et al.* (2004) *Plant design and economics for chemical engineers*. 5. ed, international ed. 2004. Boston: McGraw-Hill (McGraw-Hill chemical engineering series).

Riegel, B. (2018) 'Requirements for stationary application batteries', in R. Korthauer (ed.) *Lithium-Ion Batteries: Basics and Applications*. Berlin, Heidelberg: Springer Berlin Heidelberg, pp. 393–404. Available at: https://doi.org/10.1007/978-3-662-53071-9_32.

Rojas-Michaga, M.F. *et al.* (2023a) 'Sustainable aviation fuel (SAF) production through power-to-liquid (PtL): A combined techno-economic and life cycle assessment', *Energy Conversion and Management*, 292, p. 117427. Available at: https://www.sciencedirect.com/science/article/pii/S0196890423007732 (Accessed: 7 March 2024).

Rojas-Michaga, M.F. *et al.* (2023b) 'Sustainable aviation fuel (SAF) production through power-to-liquid (PtL): A combined techno-economic and life cycle assessment', *Energy Conversion and Management*, 292, p. 117427.

Runge, P. *et al.* (2020) 'Economic Comparison of Electric Fuels Produced at Excellent Locations for Renewable Energies: A Scenario for 2035', *SSRN Electronic Journal* [Preprint]. Available at: https://doi.org/10.2139/ssrn.3623514.

Schack, D., Rihko-Struckmann, L. and Sundmacher, K. (2016) 'Structure optimization of power-to-chemicals (P2C) networks by linear programming for the economic utilization of renewable surplus energy', in *Computer Aided Chemical Engineering*. Elsevier, pp. 1551–1556. Available at: https://doi.org/10.1016/B978-0-444-63428-3.50263-0.

Schemme, S. *et al.* (2020) 'H2-based synthetic fuels: A techno-economic comparison of alcohol, ether and hydrocarbon production', *International Journal of Hydrogen Energy*, 45(8), pp. 5395–5414. Available at: https://doi.org/10.1016/j.ijhydene.2019.05.028.

Sherwin, E.D. (2021) 'Electrofuel Synthesis from Variable Renewable Electricity: An Optimization-Based Techno-Economic Analysis', *Environmental Science & Technology*, 55(11), pp. 7583–7594. Available at: https://doi.org/10.1021/acs.est.0c07955.

Sollai, S. *et al.* (2023) 'Renewable methanol production from green hydrogen and captured CO2: A techno-economic assessment', *Journal of CO2 Utilization*, 68, p. 102345. Available at: https://www.sciencedirect.com/science/article/pii/S2212982022004644 (Accessed: 7 March 2024).

Svensson, R. *et al.* (2004) 'Transportation systems for CO2—application to carbon capture and storage', *Energy Conversion and Management*, 45(15–16), pp. 2343–2353. Available at: https://doi.org/10.1016/j.enconman.2003.11.022.

Terlouw, T. *et al.* (2022) 'Large-scale hydrogen production via water electrolysis: a techno-economic and environmental assessment', *Energy & Environmental Science*, 15(9), pp. 3583–3602. Available at: https://pubs.rsc.org/en/content/articlehtml/2014/wm/d2ee01023b (Accessed: 7 March 2024).

Terlouw, T. *et al.* (2024) 'Future hydrogen economies imply environmental trade-offs and a supply-demand mismatch', *Nature Communications*, 15(1), p. 7043. Available at: https://doi.org/10.1038/s41467-024-51251-7.

TOMCO2 Systems (2018) *TOMCO Systems - Carbon Dioxide Portable Storage Units*, *TOMCO Systems*. Available at: https://tomcosystems.com/wp-content/uploads/2018/03/1.1.6.Carbon-Dioxide-Portable-Units-WEB-1.pdf (Accessed: 7 May 2024).

Uusitalo, V. *et al.* (2017) 'Potential for greenhouse gas emission reductions using surplus electricity in hydrogen, methane and methanol production via electrolysis', *Energy Conversion and Management*, 134, pp. 125–134. Available at: https://doi.org/10.1016/j.enconman.2016.12.031.

Van-Dal, É.S. and Bouallou, C. (2013) 'Design and simulation of a methanol production plant from CO2 hydrogenation', *Journal of Cleaner Production*, 57, pp. 38–45. Available at: https://doi.org/10.1016/j.jclepro.2013.06.008.

Waller, C. (no date) *Technisches Datenblatt Silikagel E mikroporöses Kieselgel (ohne Indikator)*. Available at: https://llfa.de/mwdownloads/download/link/id/89 (Accessed: 7 May 2024).

Werker, J., Wulf, C. and Zapp, P. (2019) 'Working conditions in hydrogen production: A social life cycle assessment', *Journal of Industrial Ecology*, 23(5), pp. 1052–1061. Available at: https://doi.org/10.1111/jiec.12840.

Wolfram Alpha LLC (no date) *Wolfram|Alpha: Making the world's knowledge computable*. Available at: https://www.wolframalpha.com (Accessed: 7 May 2024).

World Material (no date) *Material datasheet & equivalent of US ASTM AISI SAE, European EN, Germany DIN, British BSI, Japanese JIS & Chinese GB Standard*, *World Material*. Available at: https://www.theworldmaterial.com/ (Accessed: 7 May 2024).

Zang, G. *et al.* (2021) 'Technoeconomic and Life Cycle Analysis of Synthetic Methanol Production from Hydrogen and Industrial Byproduct CO2', *Environmental Science & Technology*, 55(8), pp. 5248–5257. Available at: https://doi.org/10.1021/acs.est.0c08237.

Zhu, R. *et al.* (2022) 'LCA comparison analysis for two types of H2 carriers: Methanol and ammonia', *International Journal of Energy Research*, 46(9), pp. 11818–11833. Available at: https://doi.org/10.1002/er.7947.

Paper C:

An adaptive robust optimization approach using scenario-based uncertainty sets for stand-alone power-to-X facilities

Uwe Langenmayr[a], Viktor Slednev[a], Manuel Ruppert[a], Wolf Fichtner[a]
[a] Karlsruhe Institute of Technology (KIT), Chair of Energy Economics, Karlsruhe, Germany

Reference
Langenmayr, U., Slednev, V., Ruppert, M., and Fichtner, W. An adaptive robust optimization approach using scenario-based uncertainty sets for stand-alone power-to-X facilities. *Submitted to a scientific journal*, 2025c

An adaptive robust optimization approach using scenario-based uncertainty sets for stand-alone power-to-X facilities

Langenmayr, Uwe[1,*]; Slednev, Viktor[1]; Ruppert, Manuel[1]; Fichtner, Wolf[1]

[1] Institute for Industrial Production (IIP), Karlsruhe Institute of Technology (KIT), Hertzstraße 16, 76187 Karlsruhe, Germany

* Corresponding author: uwe.langenmayr@kit.edu

Achieving a carbon-neutral energy system requires long-term energy storage and addressing hard-to-abate sectors, such as aviation and fertilizer production, which rely on synthetic energy carriers produced through power-to-X processes. We utilize adaptive robust optimization to optimize investment decisions under uncertainties in solar PV and wind electricity generation for various power-to-X technologies and locations. The comparison of different global locations reveals that regions with high solar PV capacity factors experience lower uncertainties, as shown by the similarity between the robust and deterministic system setup. In contrast, wind-intensive areas require significant adjustments to the deterministic system setup to achieve robustness, but can achieve low electricity generation costs due to their high wind capacity factors. Locations with mixed renewable generator capacity factors can leverage both advantages. Especially flexible power-to-X facilities, such as those for hydrogen or methanol production, can exploit these capacity factors. Inflexible systems, such as Fischer-Tropsch production, require increased auxiliary capacities, including storage or generation capacities, to achieve a sufficient supply to the synthesis, thereby reducing overall profitability. We investigate suitable representative data sets to face the computational expenses of adaptive robust optimization problems. The results demonstrate that adaptive robust optimization provides reliable solutions with representative data, minimizing losses while achieving similar high profits compared to those obtained with complete data. Our study finds that the robustness of solutions improves with longer periods, which are essential for less flexible technologies like Fischer-Tropsch synthesis, but a two-week period length is sufficient to achieve robustness for all systems.

Keywords: Adaptive robust optimization; Power-to-X; Renewable energy carriers; Process simulation; Techno-economic assessment; Life cycle assessment

Abbreviations:

ARO	Adaptive robust optimization	C&CG	Column-and-constraint generation
FT	Fischer-Tropsch crude	MeOH	Methanol

PtX	Power-to-X	PtC	Power-to-Chemicals
PtG	Power-to-Gas	PtL	Power-to-Liquids
RES-E	Renewable energy source electricity	SEC	Synthetic energy carrier

Nomenclature:

Sets	
$n \in N$	Set of deterministic temporal clusters
$n \in \widetilde{N}$	Set of worst-case cluster
$n \in M$	Union of deterministic and worst-case clusters ($M = N \cup \widetilde{N}$)
$h \in H$	Set of cluster lengths
$i \in I$	Iteration of the decomposition algorithm
$g \in G$	Set of generators
$p \in P$	Set of profiles
$q \in Q$	Set of data points
$t \in T$	Set of time steps
Variables	
x	First-stage variables
β	Second-stage variables
y	Third-stage variables
u	Uncertain variable
φ	Maximal operational costs of each iteration
λ, μ	Dual variables
π	Binary variable of the k-means clustering
ϑ	Cluster center
J	Total distance between cluster center and data points
Parameters	
x^*	Optimized variables x from the outer problem
c_x^T	Cost vector of first-stage variables
c_y^T	Cost vector of third-stage variables
$\tilde{u}$	Historic value
Γ	Threshold for historic values
A, D	Coefficient matrices
b, e, h, g	Right-hand side constants
W_n	Weighting of cluster n

1 Motivation

Synthetic energy carriers (SEC), such as green hydrogen and its derivatives, could play a significant role to achieve a low-carbon energy system. SECs can be produced through power-to-X (PtX) processes, including power-to-gas (PtG), power-to-liquids (PtL), and power-to-chemicals (PtC). Here, the key element is electrolysis, which uses electricity to split water molecules into hydrogen and oxygen. If low-carbon electricity is applied, SECs can achieve lower carbon footprints than their fossil counterparts. SECs enable long-term energy storage and support electricity supply during periods of low renewable energy source electricity (RES-E) generation, providing a solution to one of the significant challenges

of renewable electricity supply in integrated energy systems. In addition, some industrial applications rely on SECs as they are needed to provide high-temperature heat (e.g., cement production) or for material applications (e.g., fertilizer production, aviation fuel). In these hard-to-abate sectors and applications, there are currently no existing low-carbon alternatives to SECs.

The ability to produce low-carbon SECs, combined with their broad application, has led to increased analysis of their role in the future energy system. IRENA (2022) calculates a global SEC demand of more than 600 million tonnes of hydrogen and other hydrogen derivatives per year in 2050, highlighting the pivotal role of SECs. However, numerous barriers exist that limit the rapid ramp-up of SEC production, including high SEC production costs, the complexity of infrastructure projects, and demand uncertainty (International Energy Agency (IEA), 2024). Furthermore, the increased electricity demand from SEC production limits the production in regions with insufficient RES-E potentials or electricity grid capacities. Due to the availability of renewable potentials around the globe, stand-alone PtX facilities may be a suitable option to avoid the restrictions of integrated energy systems. Here, PtX facilities can be located in places with high availability of RES-E generation and sufficient land to allow low-cost production in large quantities. However, the complex operation of PtX facilities adds another barrier to the SEC economy since the volatile character of RES-E generation conflicts with the relatively inflexible chemical synthesis of PtL and PtC processes. The implementation of flexible operation faces manifold challenges, including safety risks, degradation of product quality, and others (Bielefeld et al., 2023). In the worst case, an insufficient supply of feedstock might result in increased degradation of the catalysts and, therefore, reduce long-term production efficiency (Bielefeld et al., 2023; Iglesias González et al., 2016), and in the context of remote stand-alone PtX facilities, the dependence on external service providers poses another obstacle (Bielefeld et al., 2023). Hence, a robust feedstock supply is desirable for achieving low-cost, high-quality products.

One commonly used method for modeling and analyzing conventional chemical plants is process simulation, combined with spreadsheet calculations. In the field of PtX, these calculations often assume steady electricity and feedstock supply, neglecting the volatile character of renewable energies (Albrecht et al., 2017; Heinzmann et al., 2021). To address this limitation, methods from Operations Research have been applied to calculate location-specific minimal production costs and optimal facility capacities for PtX facilities, considering local RES-E conditions. A linear optimization is applied by Osman et al. (2020) to calculate a steady hydrogen supply for an ammonia production plant. Other approaches include the complete PtX production in the optimization model, for example, for hydrogen (Terlouw et al., 2022), in PtC networks (Schack et al., 2016), and the electricity-based fuels production (Berger et al., 2021; Sherwin, 2021). Superstructures implement several alternative production routes and identify optimal plant setups next to optimal capacities and production costs (Maggi et al., 2020). In addition to single-objective optimization, multi-objective optimization is applied to consider land and water use, as well as production costs (Farajiamiri et al., 2023). However, such deterministic solutions might not be

robust against deviating weather conditions. Recent research utilizes stochastic and robust optimization of PtX facilities to account for uncertainty. However, approaches aimed at optimizing the capacity of stand-alone facilities are still rare. Wang (2025) employs a two-stage stochastic optimization approach for stand-alone ammonia production. Their results show that hydrogen storage units are being increased to react to uncertainties, resulting in rising production costs by up to 25%. To achieve resilient supply, PtX supply chains are optimized using two-stage stochastic (Mitrai et al., 2024) or two-stage robust programming (Xu et al., 2025).

Robust solutions can be achieved by applying methods of robust optimization, which allow for the inclusion of parameter uncertainty by considering worst-case scenarios. A subgroup of robust optimization with high value for real-world applications is adaptive robust optimization (ARO). This approach is practical when first-stage decisions (e.g., investments or unit commitment) are taken and applied in a second stage (e.g., operation) without the ability to adjust the first-stage decisions due to deviations from expected scenarios in the second stage. In addition, the derived solution of the ARO approach will be robust against numerous worst-case scenarios, as the recursive nature of the approach considers several worst-case scenarios simultaneously. One of the first ARO approaches was developed by Bertsimas et al. (2013), where ARO was applied to robust unit commitment planning, an approach that has been improved and applied in numerous studies. However, the application of ARO in the context of PtX investment has not been conducted to date, despite its properties aligning with the requirements. The challenge of investment problems lies in the comprehensive data requirement to put the investment decision on solid footing. This challenge is further exacerbated since the column-and-constraint (C&C) generation approach (Chen et al., 2014; Ruiz & Conejo, 2015), which is often applied in the ARO context, iteratively increases the number of constraints and variables in the optimization problem. The vast amount of data required, the increasing problem size using C&C, and the iterative solving approach of ARO result in computationally expensive optimization problems, hindering the large-scale application of this approach. Another challenge of robust optimization is the conservatism of robust solutions. Commonly applied polyhedral uncertainty sets enhance this conservatism, as the resulting time series profiles may not accurately represent realistic conditions (Velloso et al., 2020), leading to unnecessary robustness against unrealistic time series profiles.

We want to address the challenges mentioned above when dimensioning stand-alone PtX facilities. We apply our developed ARO model to investment problems in stand-alone PtX facilities, as the ARO approach meets the high operational requirements of PtX facilities, allowing for a steady and sufficient supply of feedstocks. We investigate the underlying uncertainty of different PtX facilities and RES-E generation circumstances by assessing the production paths of three different PtX energy carriers at five globally distributed locations. We ensure realistic RES-E generation profiles by applying scenario-based uncertainty sets. However, the extensive amount of required input data hinders the straightforward and robust implementation as real-world-sized problems become increasingly computationally expensive.

We use temporal clustering approaches to address the computational complexity challenge of ARO investment problems. This novel combination of methods helps to identify repetitive patterns in time series data and reduce the underlying data quantity in the ARO model to significant weather patterns.

This work is structured as follows: *Section 2* describes the general ARO solution procedure and how representative data is applied to address the computational expenses. The developed approach is applied in empirical case studies described in *Section 3.1*, followed by the results presented in *Section 3.2*. *Section 4* concludes this research, including summary, limitations and outlook.

2 Methodology

2.1 General ARO setup

The ARO optimization model consists of three stages. Generally, the first stage represents the strategic decision where costs are minimized. Afterward, the second stage represents the revelation of the uncertainty, and the strategic decision in the first stage is penalized by choosing such realization of the uncertainty, which maximizes the costs. The third stage describes the reaction phase, which enables a response to the revealed uncertainty. Here, measures can be taken to minimize the impact of the worst-case uncertainty. When applied to the problem of investment planning, the first stage represents the investment stage, where the investment x is minimized given the underlying constraints in *Equations (2)*. The worst-case scenario u is revealed in the second stage of the problem. This stage is modeled using an uncertainty set that defines the underlying uncertainty in *Equation (3)*. The last stage consists of the reaction stage, where the system operator can take corrective actions to react to the worst-case scenario using the operating variables y and the constraints in *Equations (4)*. λ and μ are the dual variables of the respective constraints.

$$\min_{x} c_x^T \cdot x \qquad \max_{u \in U} \qquad \min_{y} c_y^T \cdot y \tag{1}$$

subject to

$$h(x) = 0 \tag{2}$$
$$g(x) \leq 0$$

$$u \in U \tag{3}$$

$$A(x,u) \cdot y = b(x,u) : \lambda \tag{4}$$
$$D(x,u) \cdot y \leq e(x,u) : \mu$$

2.2 Solution procedure

The first-stage investment problem is separated from the second and third stages using the C&C generation approach. Problem *(5)* - *(10)* is often called the outer problem and represents the adjusted first-stage investment.

$$\min_{x,\varphi,y_i} c_x^T \cdot x + \varphi \tag{5}$$

subject to

$$\varphi \geq c_y^T \cdot y_i \quad \forall i \in I \tag{6}$$
$$h(x) = 0 \tag{7}$$
$$g(x) \leq 0 \tag{8}$$
$$A(x, u_i) \cdot y_i = b(x, u_i) \quad \forall i \in I \tag{9}$$
$$D(x, u_i) \cdot y_i \leq e(x, u_i) \quad \forall i \in I \tag{10}$$
$$x, \varphi, y_i \geq 0 \tag{11}$$

The outer problem minimizes the investment and the operating costs of each iteration i. The addition of worst-case scenarios is achieved through the integration of additional variables y_i (additional columns), the scenario-dependent matrices A_i and D_i, and the addition of constraints (*Equations (9)* and *(10)*). These additional constraints are added as cutting planes to the outer problem (Zeng & Zhao, 2013). Using φ, the operating costs of all iterations are considered simultaneously since it will take the value of the iteration with the highest operating costs. One major downside of the approach is the growing outer problem, as the number of variables, constants, and constraints increases with each iteration *i*. The applied outer problem is described in *Section 8.1*.

The uncertainty set (*Equation (3)*) describes the considered renewable generation uncertainties and is implemented as scenario-based uncertainty set (*Equation (12)*) (Velloso et al., 2020).

$$U_g = \left\{ u_{g,t} = \sum_{p \in P} \tilde{u}_{g,p,t} \cdot \beta_p \ \forall t, \beta \in \{0,1\}^p, \sum_{p \in P} \beta_p = 1, \sum_{p \in P} \sum_{t \in T} \tilde{u}_{g,p,t} \cdot \beta_p \geq \Gamma_g \right\} \quad \forall\, g \in G \tag{12}$$

The first term shows that the uncertainty is the product of a historical value $\tilde{u}$ and β. β represents uncertainty, which is defined as a binary in the second term, and only one historical value can be selected (third term). We implemented the uncertain parameter as binary, as it has been shown that a continuous weighting variable with bounds of 0 and 1 behaves like a binary variable (Velloso et al., 2020). Finally, the sum of uncertain parameters must exceed a certain threshold, which allows control of the solution's robustness level. Depending on the extent of the historical data and the period length of the representative data, the number of binary variables and the number of coupled variables per binary variable differ. Shorter representative period lengths result in more binary variables and shorter coupled variables, and vice versa. While the computational time of the resulting mixed-integer linear problem can vary for different configurations depending on the solver algorithm, computation infrastructure, and software used, the desired solving time needs to be considered when choosing data extent and period length. The effect on the computational time is shown in *Appendix 8.4*.

To solve the second and third stages (*Equations (3)* and *(4)*), a dualization is performed. The third-stage minimization can be transformed into a maximization problem and merged with the second-stage maximization. The single-level maximization is often referred to as the inner problem (*(13) - (16)*). This inner problem represents the facility's operation after the investment decision in the outer problem. Therefore, the optimal investment decision from the outer problem is parameterized as x^*. We present the applied inner problem in *Section 8.2.1*.

$$\max_{u,\lambda,\mu} b^T(x^*,u)\cdot\lambda + e^T(x^*,u)\cdot\mu \quad (13)$$

subject to

$$A^T(x^*,u)\cdot\lambda + D^T(x^*,u)\cdot\mu \le c_y \quad (14)$$

$$\mu \le 0 \quad (15)$$

$$u \in U \quad (16)$$

Due to the dualization of the problem and the subsequent merging of the dual variables λ and μ with the uncertainty variable u, bilinear terms appear in the objective function. Since we use binary variables in our uncertainty set, we reformulate this non-linear problem as a mixed-integer problem (see *Section 8.2.2*).

Figure 1 illustrates the solution procedure of the approach. The process starts with initializing the upper and lower bounds and optimizing the outer problem. No worst-case scenario has yet been chosen, so a random time series profile is used in the outer problem. The resulting investment decision x^* of the outer problem solution is transferred to the inner problem, where a worst-case scenario for the given investment decision x^* is derived. By incorporating this worst-case scenario into the outer problem and reverting to the determination of the investment decision, further worst-case scenarios are added to the outer problem until the difference between the upper and lower bound falls below the threshold ε which is set to 10^{-2}. In simple terms, the difference is calculated as the absolute deviation between the total costs of the outer and the inner problem. The final investment decision of the outer problem after falling below the threshold allows for robust operation under uncertain profiles since the investment decision is based on considering several worst-case scenarios, and no other scenario increases the total costs above a set threshold.

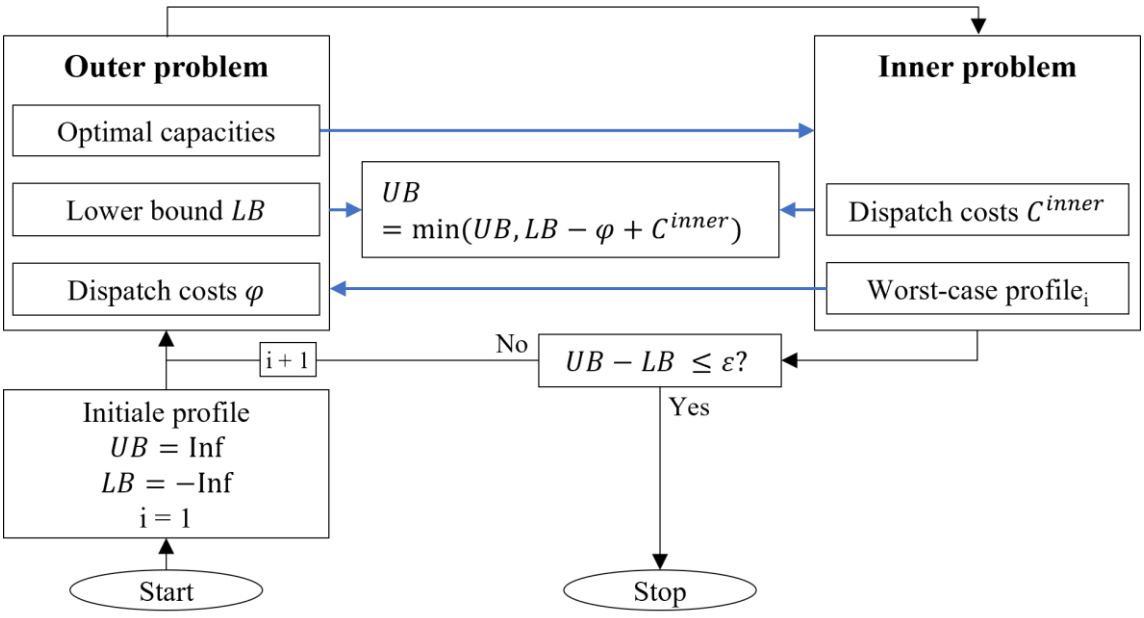

Figure 1: Flow chart of the implemented ARO process. Abbreviations are: UB = upper bound, LB = lower bound, φ = dispatch costs of outer problem, C^{inner} = dispatch costs of inner problem, ε = tolerance threshold between outer and inner problem, i = iteration (based on Riepin et al. (2022))

Long-term investments rely on sufficient information and data to make a well-founded decision. In the context of renewable energies, these data include time-series data on renewable capacity factors, which often span long periods, such as years, to provide sufficient information on potential renewable generation. However, with an increasing amount of data, the optimization model increases complexity and solving time, and the combination with the iterative approach of ARO would result in a burdensome time demand. To overcome this limitation, we cluster the underlying data to obtain representative renewable capacity factor profiles that represent most of the year. One cluster, chosen by the ARO approach from the complete data set, is added to include a worst-case period.

2.3 Complexity reduction using representative data

2.3.1 Application of k-means clustering to obtain representative data

We utilize representative data derived from data clustering to enhance computation time. The objective of representative data is to identify recurring weather conditions and condense long time series data into the primary weather conditions, weighted by their frequency of occurrence. As a clustering approach, we use k-means clustering, which has been applied in several approaches in the context of historical meteorological or capacity factor data (Hoffmann & Schlünzen, 2013; Jiang et al., 2011; Neal et al., 2016). We split the capacity factor time series for wind and solar generation into periods of length h and arrange the data in an array where each row is one period. Each column represents the hourly capacity factor of wind or solar. Before applying k-means clustering, we use principal component analysis to reduce the dimension of our data. *Equation (17)* (Bishop, 2006) shows the optimization problem behind k-means clustering. The problem minimizes the total sum of squared distances J between the different data vectors δ_q and the centers of the clusters ϑ_n by shifting the cluster centers and by setting the affiliation of the data vectors to the different clusters using the binary variables $\pi_{q,n}$.

$$\min_{\pi,\vartheta} J = \sum_{q \in Q} \sum_{n \in N} \pi_{q,n} \left\| \delta_q - \vartheta_n \right\|^2 \tag{17}$$

The number of clusters $|N_h|$ is derived via the elbow method (Thorndike, 1953), which selects the number of clusters based on the Within Cluster Sum of Squares. Here, the variability within each cluster is analyzed to assess how many clusters are necessary to cover the majority of the variability. We use the improved initialization algorithm k-means++ proposed by Arthur & Vassilvitskii (2007) to obtain more representative clustering results. The representative profiles are selected based on the centroid time series profile of each cluster. The weight of each profile is calculated by dividing the number of profiles in each cluster by the total number of profiles and then scaling it based on the period length to represent a full year (*Equation (18)*). This weighting is necessary to scale the reduced costs, due to the shortened time series, back to the original size of the time series.

$$W_n = \frac{\sum_{q \in Q} \pi_{q,n}}{\sum_{q \in Q} \sum_{n \in N} \pi_{q,n}} \cdot \frac{8760}{|N_h|} \quad \forall\, n \in N_h \tag{18}$$

2.3.2 Integration of worst-case scenarios

The combination of representative data and ARO leverages the advantages of both approaches, yielding robust solutions with significantly reduced computation time. We connect the two approaches by adding an extra cluster to the outer and inner problem, which we refer to as the worst-case cluster. We assume an occurrence of the worst case only once a year. Therefore, we implement this worst-case cluster with the weighting of 1. The weighting of all other clusters is reduced accordingly to maintain the sum of weightings ($8760/|N_h|$).

The worst-case cluster is included in all representative data clusters *M*. The weighting of the different clusters is included in the calculation of φ to set annualized investment and operation costs into the correct relation due to the shorter period length.

$$\min_{x,\varphi,y_{n,i}} c_x^T \cdot x + \varphi \tag{19}$$

subject to

$$\varphi \geq c_{y_{n,i}}^T \cdot y_{n,i} \cdot W_n \quad \forall\, n \in M, i \in I \tag{20}$$

$$h(x) = 0 \tag{21}$$

$$g(x) \leq 0 \tag{22}$$

$$A_{n,i}(x, u_i) \cdot y_{n,i} = b_{n,i}(x, u_i) \quad \forall\, n \in M, i \in I \tag{23}$$

$$D_{n,i}(x, u_i) \cdot y_{n,i} \leq e_{n,i}(x, u_i) \quad \forall\, n \in M, i \in I \tag{24}$$

$$x, y_{n,i}, \varphi \geq 0 \tag{25}$$

In the inner problem, we couple the worst-case cluster to all historical profiles in the dataset using the uncertainty set, as shown in the following equations of the adjusted inner problem. To better distinguish between deterministic and worst-case clusters, we split the deterministic clusters in set *N* and the worst-case cluster in set $\tilde{N}$. *Figure 2* shows the graphical abstract of the implementation of the representative data and the worst-case cluster in the inner problem. The union of all representative and worst-case profiles is used as a new profile given to the outer problem in the next iteration.

$$\max_{u,\lambda,\mu} \sum_{n \in N} \left({b_n}^T(x^*) \cdot \lambda_n + {e_n}^T(x^*) \cdot \mu_n \right) + \sum_{\tilde{n} \in \tilde{N}} \left({b_{\tilde{n}}}^T(x^*, u) \cdot \lambda_{\tilde{n}} + {e_{\tilde{n}}}^T(x^*, u) \cdot \mu_{\tilde{n}} \right) \tag{26}$$

subject to

$${A_n}^T(x^*) \cdot \lambda_n + {D_n}^T(x^*) \cdot \mu_n \leq c_{y_n} \cdot W_n \quad \forall\, n \in N \tag{27}$$

$${A_{\tilde{n}}}^T(x^*, u) \cdot \lambda_{\tilde{n}} + {D_{\tilde{n}}}^T(x^*, u) \cdot \mu_{\tilde{n}} \leq c_{y_{\tilde{n}}} \cdot W_{\tilde{n}} \quad \forall\, \tilde{n} \in \tilde{N} \tag{28}$$

$$\mu \leq 0 \tag{29}$$

$$u \in U \tag{30}$$

Figure 2: Graphical abstract of the optimization problem of the inner problem

The combination of ARO with the scenario-based polyhedral uncertainty set and representative profiles enables the endogenous determination of extreme weather events in the form of worst-case profiles. The choice of period length determines the duration of the extreme weather event. In addition, the approach applies to all energy systems where dualization is possible, making it a tool for determining extreme weather conditions in versatile energy system models (Velloso et al., 2020). However, it is necessary to mention that only such worst-case profiles can be chosen that make the model feasible. Therefore, each energy system needs to be analyzed to determine the required degrees of freedom for the optimization model, allowing for the utilization of all profiles. Since electricity is used to supply all conversion components and has no alternative source other than the generation from RES-E, we implement a penalty term for purchasing backup electricity. The inner problem will be able to choose such worst-case profiles that allow the RES-E generation to reach critical levels of capacity factors, which are insufficient to supply the conversion units, and the purchase of electricity is unavoidable, however, possible due to the backup electricity.

$$x^{purchase}_{Electricity,n,t} \geq 0 \quad \forall\, n \in M, t \in T \tag{31}$$

3 Empirical application

3.1 Case Study

As an optimization model, we apply the deterministic PtX optimization of Langenmayr & Ruppert (2023), which is further used to calculate the deterministic capacities (see *Appendix 8.1* for the full model). This model ensures the installation of sufficient capacities to meet the exogenously given PtX product demand while minimizing production costs by reducing the facility's annualized investment and operating costs. This work applies this model to producing hydrogen, methanol (MeOH), and Fischer-Tropsch crude (FT). The different PtX paths are used for five different locations (longitude, latitude) to consider different weather conditions: Chile (-71.00°, -53.00°), Australia (127.75°, -30.75°), Germany (8.78°, 53.75°), Kazakhstan (50.00°, 48.50°) and Saudi Arabia (36.50°, 28.50°). To consider all

available historical data, we implement a minimal capacity factor Γ_g of 0 in the uncertainty set. Each location's 40 years of weather data are obtained from the ERA5 dataset (Hersbach et al., 2020) and processed into RES-E generation profiles using the open source tool atlite (Hofmann et al., 2021). We cluster the RES-E generation profiles from 2010 to 2020 to calculate representative profiles of 336 hours in length, and use the data from 1980 to 2009 as out-of-sample data.

Renewable electricity is generated by wind and solar PV generators and used to power the proton exchange membrane (PEM) electrolysis, the direct air capture (DAC) unit, which separates CO_2 from the ambient air, and the synthesis. MeOH and FT synthesis use CO_2 and hydrogen to produce the final product. To increase the flexibility of the plant, we have included investment options for battery, CO_2, and hydrogen storage, ensuring a steady supply of feedstock even during periods of low RES-E generation. The block diagram of the PtX facility is shown in *Figure 3*. The block diagram represents hydrogen, FT, and MeOH production. However, it should be noted that this is not a co-production and that either hydrogen, FT, or MeOH is produced. Depending on the energy carrier, the corresponding techno-economic parameters are transferred to the optimization. The synthesis, the DAC, and the CO_2 and hydrogen storage units are omitted if hydrogen is produced. All the techno-economic parameters are presented in *Table 2*, *Table 3*, and *Table 4* in *Appendix 8.3*. We implement the penalty term for electricity of 10,000 € / MWh to allow electricity supply if no RES-E generation is available.

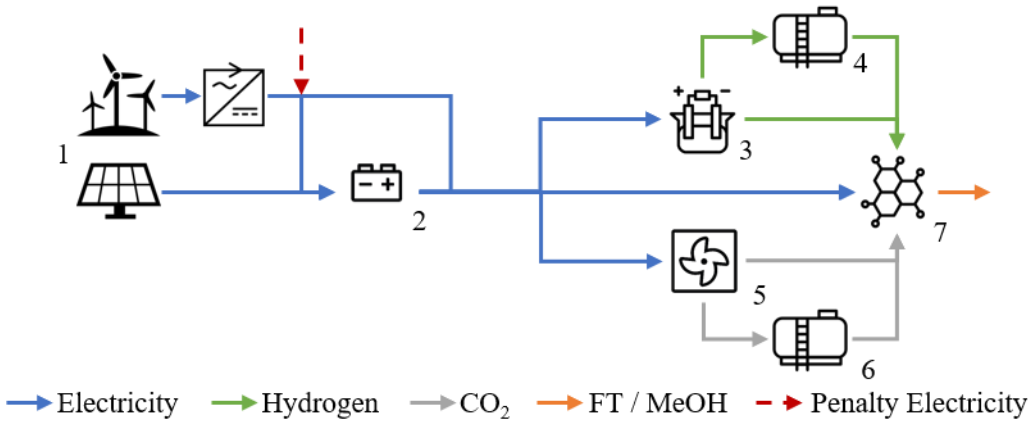

Figure 3: Schematic structure of the PtX facilities with the renewable generators wind and solar PV plus AC/DC converter (1), battery storage (2), PEM electrolysis (3), hydrogen storage (4), DAC (5), CO_2 storage (6) and synthesis unit (7). If hydrogen is produced, only the components 1-3 are required

3.2 Results

3.2.1 Additional expenditure to achieve robustness

Robustness is achieved by adjusting the facility's capacities to consider the uncertainty of RES-E generation. However, these uncertainties vary significantly between different locations, and their impact depends on the flexibility of the technology. From the differences between the deterministic and robust

investment options (*Table 1*), it is evident that robust solutions are achievable, but the additional investment depends on the location and technology. To achieve robustness, flexible facilities like hydrogen and MeOH production require higher investments, ranging from 0.5% to 15.11%, compared to the deterministic investments. FT is more challenging: In Germany, additional investments of 41.71% are necessary to achieve robustness. The difference between deterministic and robust investment reveals that locations with high solar PV availability, such as Saudi Arabia, have the lowest investment risk. In contrast, locations with high wind availability, like Chile, require additional investment to be more significant.

Table 1: Investments for the production of hydrogen, MeOH, and FT

		Chile	Australia	Germany	Kazakhstan	Saudi Arabia
Hydrogen	**Deterministic [Mio. €]**	109.84	122.04	128.56	155.71	150.84
	Robust [Mio. €]	126.43	127.72	140.37	162.61	152.23
	Difference	115.11%	104.66%	109.19%	104.43%	100.92%
MeOH	**Deterministic [Mio. €]**	260.17	272.99	290.28	334.72	346.56
	Robust [Mio. €]	292.44	284.26	317.66	351.58	348.28
	Difference	112.40%	104.13%	109.43%	105.04%	100.50%
FT	**Deterministic [Mio. €]**	367.41	321.00	338.11	387.40	350.47
	Robust [Mio. €]	490.04	351.67	479.12	448.10	362.32
	Difference	133.38%	109.55%	141.71%	115.67%	103.38%

Figure 4 shows the capacity of each component at each location and for each target energy carrier of the deterministic (dots and blue line) and robust (crosses and red dotted line) solution. For better comparison, each capacity is normalized using the maximum capacity over all components of the same type at different locations; however, this is limited to the case studies with the same target commodity.

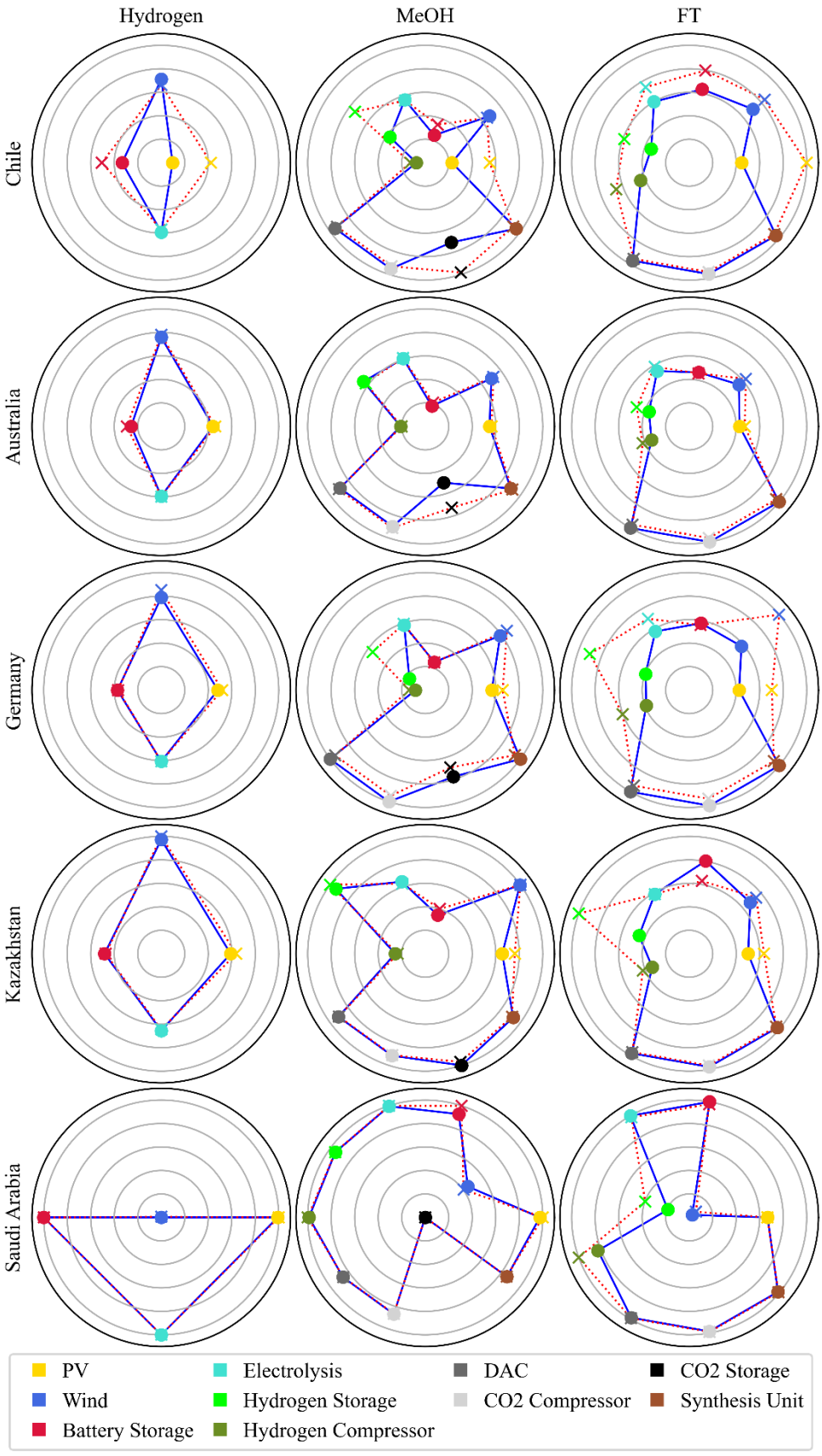

Figure 4: Normalized deterministic and robust capacities at different locations and for different target energy carrier productions

The countries differ regarding their wind and solar PV capacity factors. This circumstance results in different weather-related uncertainties and might affect the deterministic and robust solutions. Comparing other countries, it is evident that Chile's strong wind capacity factors are insufficient to supply the facilities, as wind generation may experience longer periods of low output, which resemble long-term uncertainties. The facility must increase solar PV and storage capacities to achieve robustness. Chile's robust solutions deviate the most from its deterministic solutions compared to other countries. The repetitive characteristic of solar PV resembles short-term uncertainties, making it a more reliable renewable energy source, and reducing uncertainty to a level where even deterministic solutions can be robust. However, relying mainly on solar PV increases the demand for storage and electrolysis capacities significantly, as high electricity generation is only possible during the day, and large quantities of hydrogen will be produced during these limited periods, in addition to the necessity of charging the storage units. Hence, Saudi Arabia has the highest battery storage and electrolysis capacities compared to other countries. Countries with mixed capacity factors exhibit mixed performances of their deterministic solutions and heavily depend on the energy carrier produced.

Comparing the different target energy carriers, we observe an increase in capacities when aiming for robust solutions, as flexibility decreases. Looking at hydrogen, only the Chile case increases battery storage and solar PV capacities, while robust capacities are similar to the deterministic ones at all other locations. With decreasing flexibility in the MeOH and FT production compared to hydrogen production, the impact of the RES-E generation uncertainties increasingly affects the PtX plant. While only minor adjustments of a few components are often necessary in the MeOH cases, FT cases have higher robust capacities than deterministic solutions, even in Saudi Arabia, where the robust capacities almost equal the deterministic capacities in the hydrogen and MeOH production cases. Examining the MeOH and FT cases, the figure indicates that storage and generator capacities are primarily increased to ensure a stable feedstock supply to the synthesis process, without increasing the synthesis capacity itself, which would otherwise increase the baseload feedstock demand of the synthesis unit. This circumstance clearly demonstrates the robust characteristic of the facility: larger synthesis capacities would increase the opportunity to produce, but at the cost of higher risks of insufficient feedstock supply. The robust optimization minimizes this risk and chooses lower synthesis capacities while maintaining higher storage and generator component capacities. With the higher synthesis capacity of the deterministic solution, the facility could produce higher quantities. However, the smaller capacities of storage and generator components limit such abilities. The deterministic approach is therefore the opposite of the robust solution: produce with minimal feedstock supply to reduce costs.

3.2.2 Comparing the performance of deterministic and robust solutions

The robustness of the calculated solutions can only be determined by applying the capacities to the complete data to assess their performance across different years. Critical periods with low solar PV and wind generation capacity factors are particularly concerning since electricity generation may be

insufficient to supply the system. The operation of the deterministic and robust FT production plants in Chile during one such period is presented in *Figure 5*, which shows the lower capacities of the generation units and the battery storage in the deterministic case (top). Since electricity generation is insufficient and battery storage is depleted, large quantities of penalty electricity are purchased to meet the base load demand of the FT synthesis. The robust solution (bottom) can avoid the penalty electricity since the increased capacities of battery storage and generation units, while keeping the same FT synthesis capacity, are sufficient to supply the electricity. The increased electricity supply further enables the opportunity to run the FT synthesis at higher loads, thereby increasing total production.

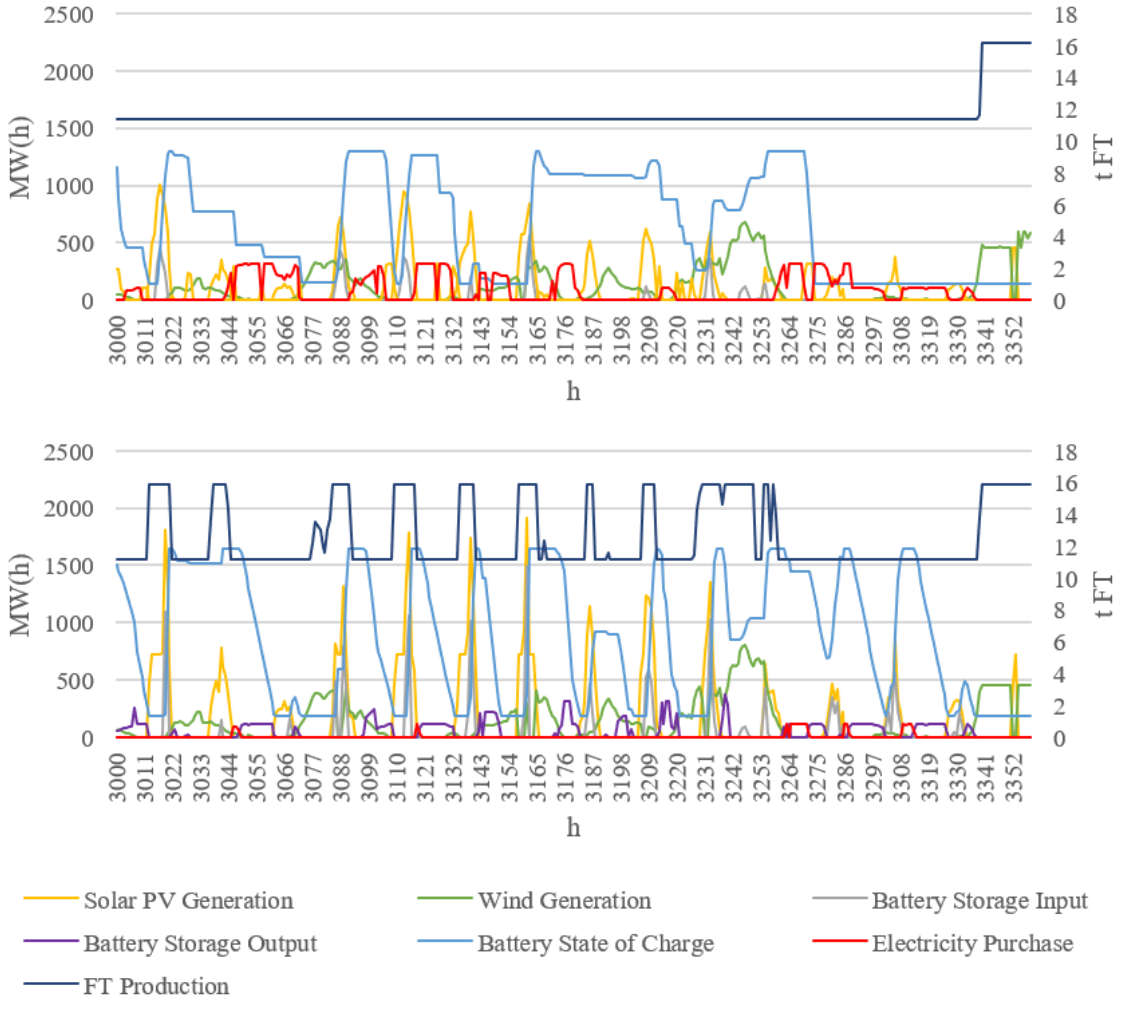

Figure 5: Operation of the FT production plant in Chile applying the deterministic (top) and robust (bottom) solution

Examining profits (*Figure 6*), Chile outperforms Saudi Arabia on average in both the hydrogen and MeOH cases. The high wind generation capacity factors allow low-cost electricity generation, and only minor additional solar PV and battery storage capacities are necessary to increase robustness, since the flexible conversion units can already absorb a significant share of the volatile wind electricity generation. However, PtX systems with lower flexibility, such as FT production, cannot absorb the volatile electricity generation. The robust solutions of Chile and Germany, both locations with good

wind conditions but low solar PV capacity factors, perform worse than those in Saudi Arabia. Locations with a good mix of wind and solar PV capacity factors tend to have the highest profits, as electricity generation can be easily diversified. The fact that the robust solutions of flexible systems perform better than the deterministic solutions, while simultaneously avoiding losses and low profits, stems from the opportunity to increase production with robust capacities in combination with the avoidance of penalty electricity purchase. This spread of profits/losses increases with decreasing flexibility of the system. Even though the produced quantities might be similar, certain penalty electricity must be procured to meet the must-run condition of the synthesis units, which reduces profits.

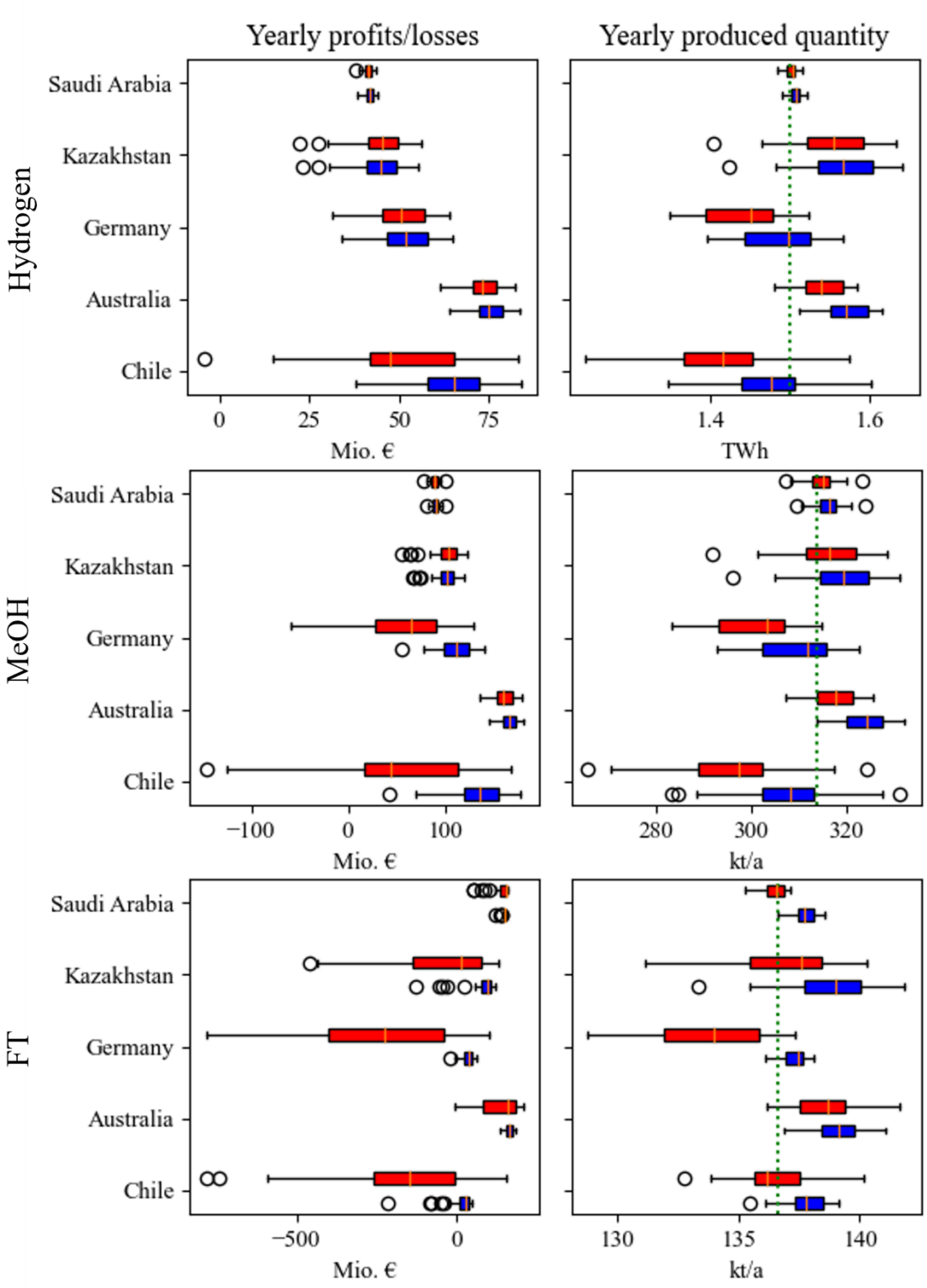

Figure 6: Yearly profits/losses and produced quantities for different products and locations. Red boxplots represent the deterministic solutions; blue boxplots represent the robust solutions. The green dotted line represents the yearly target quantity

The 11-year weather data set is sufficient to derive robust solutions for the complete data set of 40 years, shown by the performance comparison of in-sample and out-of-sample years (*Figure 7*). Only a few years in the Chilean robust case do not reach profitability. The other Chilean robust cases show only

minor profits compared to locations like Australia and Saudi Arabia due to additional investments in solar PV, storage, and electrolysis capacities. In Saudi Arabia, the deterministic quantities do not exceed robust quantities, while the deterministic profits exceed the robust ones at some point. In addition, the profits are steady compared to other locations, which indicates a lower risk of the location, as profits are more predictable even with deterministic capacities.

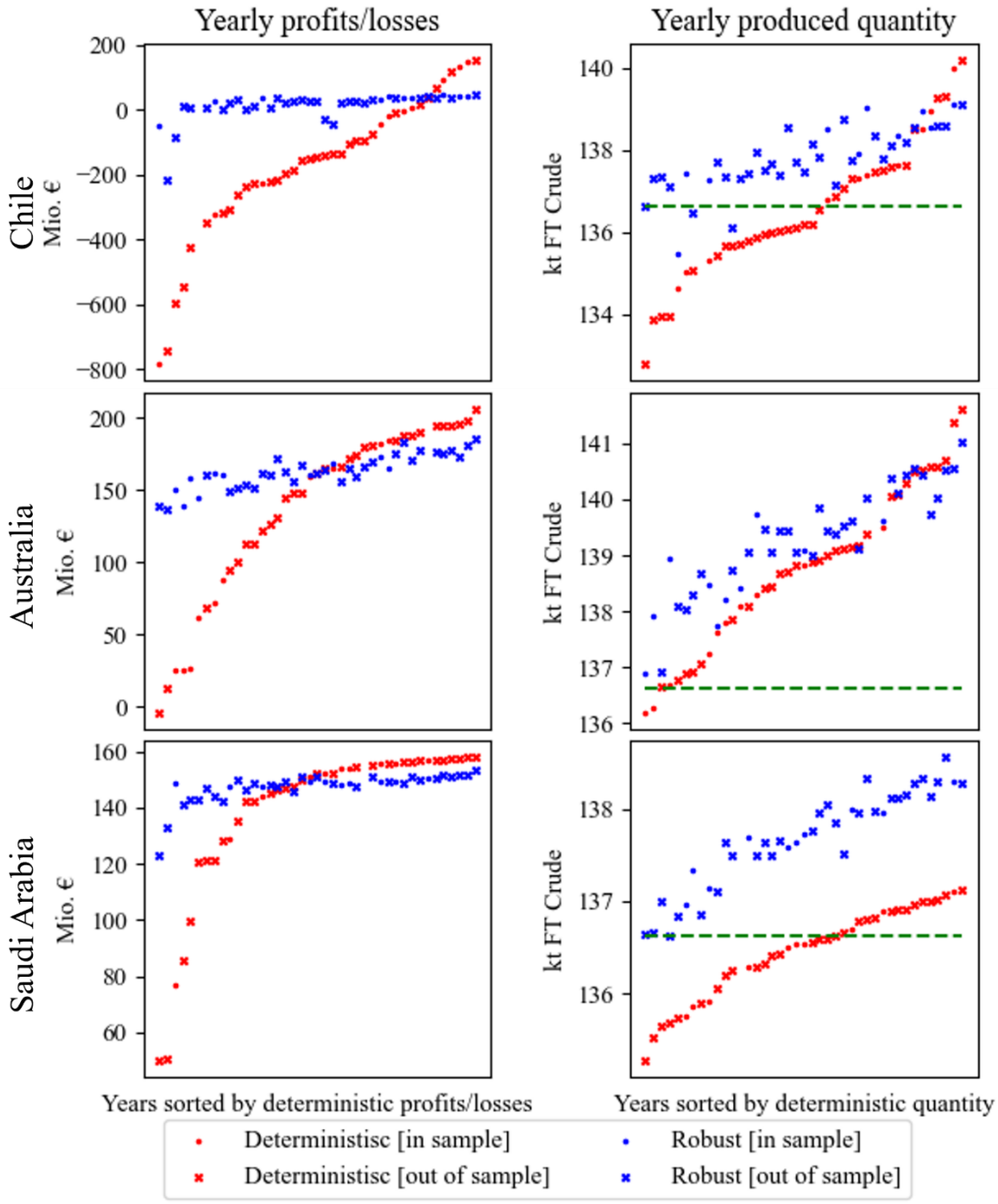

Figure 7: Comparison of profits/losses and produced quantities of in-sample and out-of-sample performance of the Saudi Arabian, Australian, and Chilean locations. The red color indicates deterministic solutions, and the blue color indicates robust solutions. The green dashed line represents the target quantity

3.2.3 Impact of representative data on the computation time and the robustness of the solution

To showcase the computation time of the approach, we use the results of the Fischer-Tropsch production in Australia for periods ranging from 24 hours to 336 hours and the entire yearly time series. *Figure 8* illustrates the individual computation time per iteration and the representative period length for the outer and inner problems. Visible is the increasing computation time with each iteration of the outer problem, showing the growing complexity. Using yearly profiles results in a cumulative computation time of the outer problem of 2,136 minutes, more than 4 times longer than the second-longest computation time (length: 288 hours, computation time: 443 minutes). In addition, the results show a general trend for longer period lengths to have more iterations. However, the trend is not explicit, as the 288-hour length has a higher computation time than the 336-hour length. This could be due to various factors, like different numbers of clusters or chosen representative profiles for each cluster, since both are derived endogenously in the clustering approach. The inner problem does not grow with each iteration. However, the underlying data in the inner problem is split differently depending on the representative period length. With a longer representative period, the number of binary variables decreases, and the length of coupled variables per binary variable increases. Examining the computation time of the inner problem for each iteration and representative period length reveals a steady computation time for the majority of representative period lengths. The lower diagram of the figure shows that the different splits of data affect the computation time; however, a clear trend is not visible. A clear outlier in the period length is the 312-hour period, which has the highest inner problem computation time. Comparing the sum of the outer and the inner problem computation time, it is visible that all representative period lengths have lower computation time than the yearly profiles.

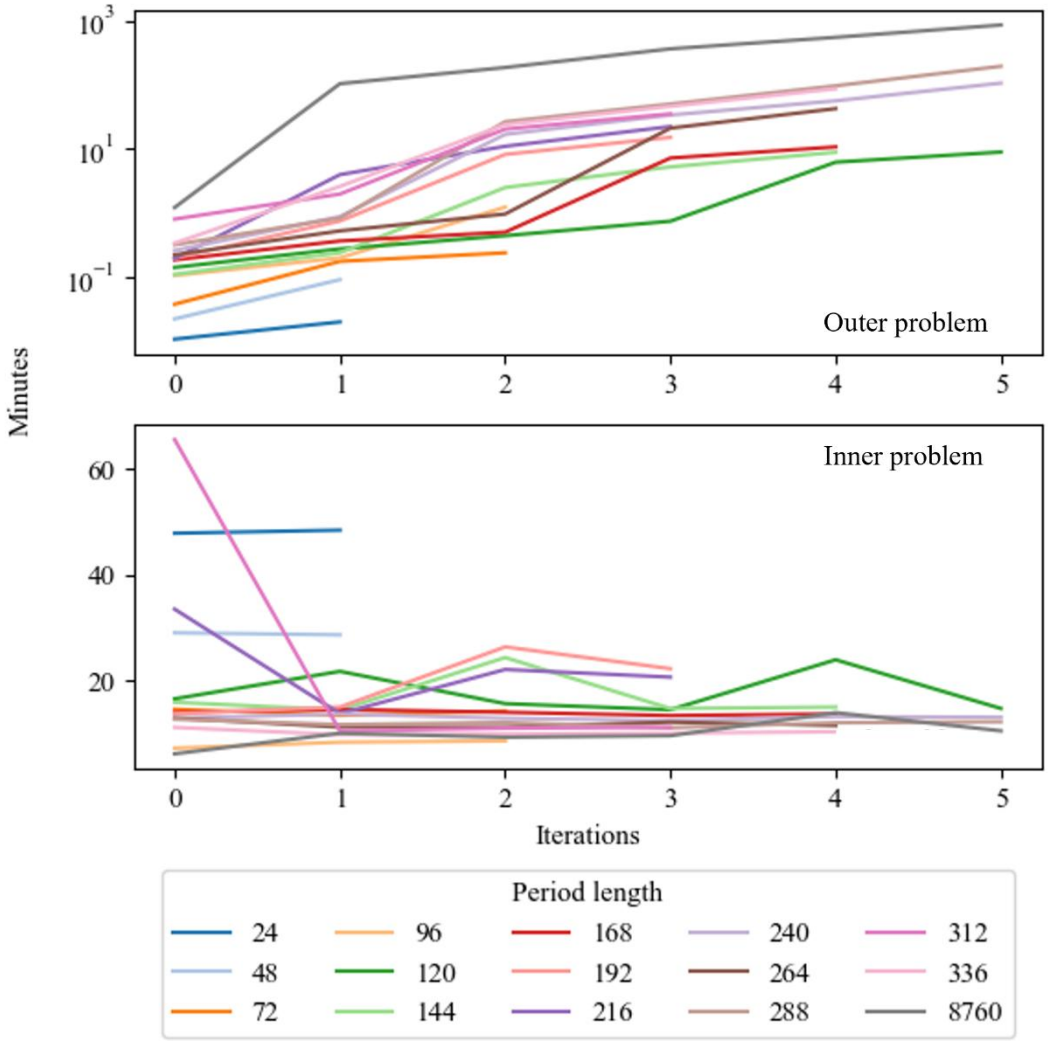

Figure 8: Calculation time per iteration and representative period length in the outer and inner problem

Next to computation time, the quality of robust solutions is essential for promoting the application of representative periods in the context of ARO energy system investment problems. *Figure 9* illustrates the total profits and losses using the complete yearly profiles, with maximizing profits as the optimization objective. The deterministic solution has mixed results, as several years result in losses, even with an increasing representative period length. This suggests that considering only a subset of information, in this case, the deterministic representative periods, is insufficient to accurately represent the weather conditions, even with increasing data length. Compared to the deterministic solutions, the robust solutions steadily improve their maximization objective. However, with a representative period length below 144 hours, even the robust solutions do not provide sufficient robustness. The reason might be that extreme weather events at the location in Australia typically do not last more than four to five days. Considering periods of this length or shorter will underestimate the frequency of extreme weather events. However, considering longer periods does not significantly affect the robust solution. Comparing the representative data to the complete data, it is visible that the full-time series data is unnecessary to

achieve robust solutions, supporting the decision to apply representative data to the ARO investment problems.

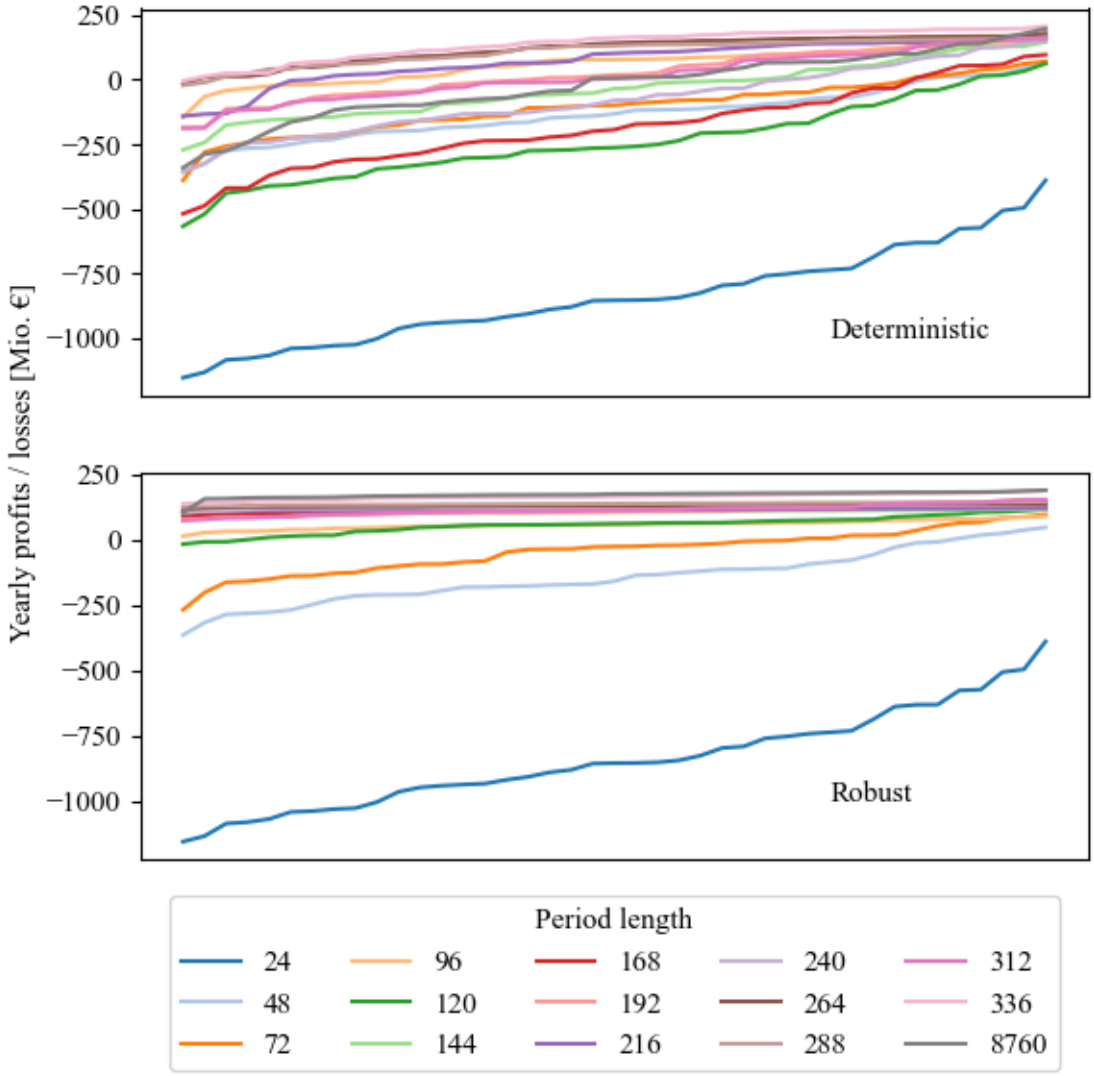

Figure 9: Yearly profits and losses for deterministic and robust solutions from different representative period lengths

4 Conclusion and outlook

Long-term energy storage is necessary to achieve a high share of renewable energy, and hard-to-abate emission sectors, such as aviation and fertilizer production, must also be addressed and might rely on synthetic energy carriers, including those produced via power-to-X. However, robust facility setups are required due to the inflexible operation of chemical facilities. In this work, we present the application of adaptive robust optimization to different power-to-X energy carrier productions and locations, aiming to achieve robust investment decisions in the face of uncertainty from solar PV and wind electricity

generation. In our approach, we contributed to recent research on adaptive robust optimization, aiming to reduce computational expenses by applying clustering approaches to the underlying historical data.

The results show the ability of our approach to achieve robust capacities tailored to the underlying PtX system, meeting the high operational requirements of PtX facilities. The robust system design of PtX plants can be achieved by adapting component capacities to account for the uncertainties in renewable electricity generation, with the extent of adjustments depending on local renewable resource characteristics and system flexibility. Locations dominated by wind energy, such as Chile, require significantly larger deviations from deterministic designs to maintain system robustness, whereas solar-heavy regions, like Saudi Arabia, achieve robustness with a minor increase in storage capacities. Furthermore, the flexibility of the production process (e.g., hydrogen vs. FT production) critically influences the extent of capacity increases needed for robustness. Here, the robust capacities of flexible systems perform similarly to the deterministic ones, while inflexible systems require additional generation and storage capacities. Although achieving robustness often requires moderate additional investment, it substantially reduces risks associated with insufficient feedstock supply and penalty electricity procurement, thereby stabilizing and enhancing long-term profitability. Systems with greater operational flexibility show improved performance under robust optimization, particularly in locations with a balanced mix of solar and wind resources. The developed approach enables PtX investors to understand the impact of uncertain RES-E electricity generation on their system, allowing them to make informed decisions to handle the uncertainty and assess the impact of these decisions on investment, profits, and losses. This ability supports future PtX investments and the transition of our energy system towards carbon neutrality.

We further show that representative data achieves similar robustness as complete data while significantly reducing computation time. Our developed approach efficiently addresses uncertainty by focusing on challenging weather periods without overcomplicating the outer problem. Although splitting the dataset into shorter periods slightly affects inner problem computation time, the impact remains manageable. More extended period lengths generally improve robustness, especially for less flexible systems, such as Fischer-Tropsch synthesis, while flexible processes, like hydrogen production, can achieve robustness with shorter periods.

While we have successfully demonstrated the applicability of our work, certain limitations remain. First, robust optimization approaches tend to produce conservative results since uncertainties are addressed without their probability. In the context of representative data, methods to derive representative data themselves have certain uncertainties. For example, the number of clusters and the chosen representative profile will affect the deterministic and robust solution, so they must be selected carefully. Additionally, the results indicate that a specific period length is necessary to achieve robust solutions. This cannot be determined beforehand and heavily depends on the underlying energy system. When examining the representative data, we should note the weighting of the worst-case cluster. In our approach, we

implement a weighting of 1, assuming the worst-case occurrence is once a year. With a more extended period, this weighting increasingly affects the solution. Other exogenous parameters also influence the approach. For example, the penalty term can significantly increase operational costs, resulting in potentially substantial deviations between upper and lower bounds in the decomposition algorithm. The chosen tolerance also affects the necessary number of iterations. The number of iterations, the approach's runtime, and the solution's robustness depend significantly on both parameters. This impact could be further investigated. Finally, several other uncertainties exist in the production of synthetic energy carriers. The complex technologies face several technological uncertainties, such as facility degradation, malfunctions, or supply disturbances, which can impact production. Such data could be included in the model, but it has been excluded since it is currently unavailable.

The approach leaves further room for improvement. First, next to the fixed power-to-X facility setup, further technologies could be applied, and their impact quantified. For example, the re-electrification of hydrogen via fuel cells or gas turbines might be a valid option to reduce the need for external electricity. Applying the scenario-based uncertainty set enables the use of accurate profiles while increasing the computational complexity of the problem. Here, approaches to investigate potential vertexes of the uncertainty set might eliminate scenarios, resulting in tighter uncertainty sets and reduced computation time. However, since it is unclear which statistical parameters comprise the uncertainty, it is difficult to identify the vertexes. This challenge could be faced by analyzing the resulting profiles of this approach to better understand the energy system’s uncertainty. Applying extreme weather events is widely used to achieve robustness in energy system analyses. Such extreme weather events could be identified using scenario-based uncertainty sets. This could be further developed to derive worst-case scenarios not only in the case of extreme weather events, but also for general parameter uncertainty. Another interesting aspect would be the development of an off-the-shelf power-to-X facility. If weather data from different locations is combined, the developed approach would identify a facility setup that is robust against various weather conditions and could be used as a standard solution.

5 Authors’ contributions

The authors of this work have contributed as follows:

Conceptualization: U.L.; Data curation: U.L.; Formal analysis: U.L.; Methodology: U.L., V.S., M.R.; Supervision: V.S., M.R., W.F.; Validation: U.L.; Visualization: U.L.; Writing - original draft: U.L., V.S., M.R., W.F.; and Writing - review & editing: U.L., V.S., M.R., W.F.

6 Declaration of interests

The authors declare no competing interests.

7 Declaration of generative AI and AI-assisted technologies

To improve the readability of our work, we have applied Grammarly (v.1.2.92.1464)

8 Appendix

Type	Description
Sets	
$s \in S$	Set of commodities
$s \in S_k^{MI}$	Subsets of S representing the main input commodity of component k
$s \in S_k^{MO}$	Subsets of S representing the main output commodity of component k
$s \in S_g$	Subsets of S representing the generated commodity of generator g
$s \in FC$	Subset of S representing freely available commodities
$s \in EC$	Subset of S representing emittable commodities
$s \in PC$	Subset of S representing purchasable commodities
$s \in QC$	Subset of S representing saleable commodities
$s \in DC$	Subset of S representing demanded commodities
$s \in DTC$	Subset of S representing total demanded commodities
$s \in SC$	Subset of S representing storable commodities
$k \in K$	Set of conversion components
$g \in G$	Set of generator components
$i \in I$	Iteration of the decomposition algorithm
$n \in N$	Set of deterministic temporal clusters
$n \in \widetilde{N}$	Set of worst-case cluster
$n \in M$	Union of deterministic and worst-case clusters ($M = N \cup \widetilde{N}$)
$p \in P$	Set of profiles
$t \in T$	Set of time steps
Variables	
$\mathrm{cap}_k, \mathrm{cap}_g, \mathrm{cap}_s$	Capacity of components *k*, *g* and *s*
$\mathrm{soc}_{s,n,t}$	State of charge of storage component for commodity *s* in cluster *n* at time *t*
y_s	Quantity of mass or energy of commodity s
λ	Dual variables
β	Binary decision to choose profile
u	Uncertain variable
Parameters	
$\mathrm{cap}_k^*, \mathrm{cap}_g^*, \mathrm{cap}_s^*$	Optimal capacity of components *k*, *g*, and *s*
$\mathrm{BU}^{upper}, \mathrm{BU}^{lower}$	Upper and lower bound of capacity utilization
$\mathrm{RAMP}_k^{up}, \mathrm{RAMP}_k^{down}$	Ramp-up and ramp-down rate of conversion component *k*
$\mathrm{Inv}_k, \mathrm{Inv}_g, \mathrm{Inv}_s$	Investment of Generator and Storage components of *g* and *s*
$\mathrm{ANN}_k, \mathrm{ANN}_g, \mathrm{ANN}_s$	Annuity Factor of components *k*, *g* and *s*
$\mathrm{FOM_k}, \mathrm{FOM_g}, \mathrm{FOM}_s$	Fixed maintenance and operation of components *k*, *g* and *s*
$\mathrm{VOM}_k, \mathrm{VOM}_g, \mathrm{VOM}_s$	Variable maintenance and operation of components *k*, *g* and *s*
$\mathrm{CF}_{g,t}$	Capacity factor of generator g at time *t* (additional indices possible)
$\eta_{k,main\ in,s}^{out}$	Conversion factor from main input to output *s* of conversion component *k*
$\eta_{k,main\ in,s}^{in}$	Conversion factor from main input to input *s* of conversion component *k*
$\eta_s^{charge}, \eta_s^{discharge}$	Charging and discharging efficiency of storage for commodity *s*
$\mathrm{P}_{s,t}^{purchase}$	Purchase price of commodity *s* at time *t* (additional indices possible)
$\mathrm{P}_{s,t}^{sell}$	Selling price of commodity *s* at time *t* (additional indices possible)

D_s	Total demand for commodity s
$\tilde{u}$	Historic value
Γ	Threshold for historic values
W_n	Weighting of cluster n
BigM	Big M coefficient

8.1 Outer problem formulation

The outer problem represents the investment stage of the ARO, where the planner determines the capacities of the various components and the operation of the PtX plants. The objective function consists of two parts: The first part is the investment itself, and the second part is the variable φ which represents the worst-case operation costs. The investment itself includes new investments after life expectancy and the residual values of components after mothballing the facility.

$$\min_{\text{cap},y,\varphi} f = \sum_{k\in K} \text{cap}_k \cdot \text{Inv}_k \cdot (\text{ANN}_k + \text{FOM}_k) + \sum_{s\in SC} \text{cap}_s \cdot \text{Inv}_s \cdot (\text{ANN}_s + \text{FOM}_s) + \sum_{g\in G} \text{cap}_g \cdot \text{Inv}_g \cdot \left(\text{ANN}_g + \text{FOM}_g\right) + \varphi \tag{32}$$

$$\varphi \geq \sum_{n\in M}\sum_{t\in T}\left(\sum_{k\in K}\sum_{s\in S_k^{MO}} y_{k,s,no,t,i}^{out} \cdot \text{VOM}_k + \sum_{\tilde{s}\in SC} y_{\tilde{s},n,t,i}^{charge} \cdot \text{VOM}_{\tilde{s}} + \sum_{g\in G}\sum_{\hat{s}\in S_g} y_{g,\hat{s},no,t,i}^{generation} \cdot \text{VOM}_g + \sum_{\bar{s}\in PC} y_{\bar{s},n,t,i}^{purchase} \cdot \text{P}_{\bar{s},n,t}^{purchase} - \sum_{\bar{s}\in QC} y_{\bar{s},n,t,i}^{sell} \cdot \text{P}_{\bar{s},n,t}^{sell}\right) \cdot \text{W}_n \quad \forall\, i \in I \tag{33}$$

All other constraints hold for both profiles in the representative data and the worst-case cluster. Constraint *(34)* balances all masses and energies in the system for each period.

$$\sum_{k\in K} y_{k,s,n,t,i}^{out} + y_{s,n,t,i}^{discharge} + y_{s,n,t,i}^{freely\ available} + y_{s,n,t,i}^{purchase} + \sum_{g\in G} y_{g,s,n,t,i}^{generation} = \sum_{k\in K} y_{k,s,n,t,i}^{in} + y_{s,n,t,i}^{charge} + y_{s,n,t,i}^{emit} + y_{s,n,t,i}^{sell} + y_{s,n,t,i}^{demand} \quad \forall\, s \in S, n \in M, t \in T, i \in I \tag{34}$$

Sources (freely available and purchased) and sinks (emissions and sales) are implemented with *Equations (35)* to *(38)*. In contrast to purchase and sale, freely available and emitted sources and sinks allow unlimited consumption (such as ambient air) or disposal (like flue gas emissions) of commodities without incurring costs or generating profits.

$$y_{s,n,t,i}^{freely\ available} \geq 0 \quad \forall\, s \in FC, n \in M, t \in T, i \in I \tag{35}$$

$$y_{s,n,t,i}^{purchase} \geq 0 \quad \forall\, s \in PC, n \in M, t \in T, i \in I \tag{36}$$

$$y_{s,n,t,i}^{sell} \geq 0 \quad \forall\, s \in QC, n \in M, t \in T, i \in I \tag{37}$$

$$y_{s,n,t,i}^{emit} \geq 0 \quad \forall\, s \in EC, n \in M, t \in T, i \in I \tag{38}$$

Over all cluster and time steps, a specific demand has to be covered, which results in the installation of capacities.

$$\sum_{n\in M}\sum_{t\in T} y_{s,n,t,i}^{demand} \geq \mathrm{D_s} \quad \forall\, \mathrm{s} \in DC, i \in I \tag{39}$$

The conversion components are regulated with the relation of educt and product in *Equations (40)* and *(41)*, as well as the upper and lower bounds for production in *Equations (42)* and *(43)*.

$$y_{k,\tilde{s},n,t,i}^{out} = y_{k,s,n,t,i}^{in} \cdot \eta_{k,s,\tilde{s}}^{out} \quad \forall\, k \in K, s \in S_k^{MI}, \tilde{s} \in S, n \in M, t \in T, i \in I \tag{40}$$

$$y_{k,\tilde{s},n,t,i}^{in} = y_{k,s,n,t,i}^{in} \cdot \eta_{k,s,\tilde{s}}^{in} \quad \forall\, k \in K, s \in S_k^{MI}, \tilde{s} \in S, n \in M, t \in T, i \in I \tag{41}$$

$$\mathrm{cap}_k \cdot \mathrm{BU}_k^{lower} \leq y_{k,s,n,t,i}^{in} \leq \mathrm{cap}_k \cdot \mathrm{BU}_k^{upper} \quad \forall\, k \in K, s \in S_k^{MI}, n \in M, t \in T, i \in I \tag{42}$$

$$-\mathrm{cap}_k \cdot \mathrm{RAMP}_k^{down} \leq y_{k,s,n,t,i}^{in} - y_{k,s,n,t-1,i}^{in} \leq \mathrm{cap}_k \cdot \mathrm{RAMP}_k^{up} \quad \forall\, k \in K, s \in S_k^{MI}, n \in M, t \in \{2,\dots,T\}, i \in I \tag{43}$$

The generation of each renewable generator is implemented with *Equation (44)*. Unlike other parameters, the capacity factor of the generators is the only parameter associated with the iteration, indicating that other capacity factors must be considered for each iteration.

$$y_{g,s,n,t,i}^{generation} \leq \mathrm{cap}_g \cdot \mathrm{CF}_{g,s,n,t,i} \quad \forall\, g \in G, s \in S_g, n \in M, t \in T, i \in I \tag{44}$$

The state of charge for each storage unit is calculated using *Equation (45)*. The charge storage state at the period's beginning and end is balanced with *Equation (46)*. Finally, *Equation (47)* implements the bounds of the storage state of charge.

$$y_{\mathrm{s},n,t,i}^{soc} = y_{\mathrm{s},n,t-1,i}^{soc} + y_{\mathrm{s},n,t-1,i}^{charge} \cdot \eta_{\mathrm{s}}^{charge} - \frac{y_{\mathrm{s},n,t-1,i}^{discharge}}{\eta_{\mathrm{s}}^{discharge}} \quad \forall\, s \in SC, n \in M, t \in \{2,\dots,T\}, i \in I \tag{45}$$

$$y_{\mathrm{s},n,0,i}^{soc} = y_{\mathrm{s},n,T,i}^{soc} + y_{\mathrm{s},n,T,i}^{charge} \cdot \eta_{\mathrm{s}}^{charge} - \frac{y_{\mathrm{s},o,T,i}^{discharge}}{\eta_{\mathrm{s}}^{discharge}} \quad \forall\, s \in SC, n \in M, i \in I \tag{46}$$

$$\mathrm{cap_s} \cdot \mathrm{BU_s^{lower}} \leq y_{\mathrm{s},n,t,i}^{soc} \leq \mathrm{cap_s} \cdot \mathrm{BU_s^{upper}} \quad \forall\, \mathrm{s} \in SC, n \in M, t \in T, i \in I \tag{47}$$

Storage binaries, which are used in Langenmayr & Ruppert (2023), are removed without replacement. This is possible since all commodities rely on electricity, and surplus commodities can be avoided without additional costs by curtailing the electricity generation, while simultaneously charging and discharging storage units to destroy the commodity will result in operational costs.

8.2 Full description of the inner problem and reformulation

8.2.1 Inner problem

The inner problem comprises the uncertainty revelation and the plant operator's reaction. Since the uncertainty only affects the worst-case cluster, we split the representative clusters into the deterministic clusters in set *N*, and the worst-case cluster in set $\widetilde{N}$.

$$\max_{\lambda,\beta_p} f = \sum_{\bar{s}\in DC} \lambda_{\bar{s}}^{demand} \cdot \mathrm{D}_{\bar{s}} + \sum_{k\in K}\sum_{n\in N}\sum_{t\in T}\sum_{s\in S_k^{MI}} \left(\lambda_{k,s,no,t}^{upper\ bound} \cdot \mathrm{BU}_k^{upper} + \lambda_{k,s,no,t}^{lower\ bound} \cdot \mathrm{BU}_k^{lower} + \lambda_{k,s,no,t}^{ramp\ up} \cdot \mathrm{RAMP}_k^{up} + \lambda_{k,s,no,t}^{ramp\ down} \cdot \mathrm{RAMP}_k^{down}\right) \cdot \mathrm{cap}_k^* + \sum_{\tilde{s}\in SC}\sum_{n\in N}\sum_{t\in T}\left(\lambda_{\tilde{s},n,t}^{upper\ bound} \cdot \mathrm{BU}_{\tilde{s}}^{upper} + \lambda_{\tilde{s},n,t}^{lower\ bound} \cdot \mathrm{BU}_{\tilde{s}}^{lower}\right) \cdot \mathrm{cap}_{\tilde{s}}^* + \sum_{g\in G}\sum_{\hat{s}\in S_g}\sum_{t\in \tilde{T}}\left(\sum_{n\in N} \lambda_{g,\hat{s},\tilde{n},t}^{generation} \cdot u_{g,t} \cdot \mathrm{cap}_g^* + \sum_{\tilde{n}\in \tilde{N}} \lambda_{g,\hat{s},\tilde{n},t}^{generation} \cdot u_{g,t} \cdot \mathrm{cap}_g^*\right) \tag{48}$$

Equation corresponding to $y^{freely\ available}$.

$$\lambda_{\mathrm{s},n,t}^{balance} \leq 0 \quad \forall\, s \in FC, n \in M, t \in T \tag{49}$$

Equation corresponding to y^{emit}.

$$-\lambda_{s,n,t}^{balance} \leq 0 \quad \forall\, \mathrm{s} \in EC, n \in M, t \in T \tag{50}$$

Equation corresponding to $y^{purchase}$.

$$\lambda_{s,n,t}^{balance} \leq \mathrm{P}_{s,n,t}^{purchase} \cdot \mathrm{W}_n \quad \forall\, \mathrm{s} \in PC, n \in M, t \in T \tag{51}$$

Equation corresponding to y^{sell}.

$$-\lambda_{s,n,t}^{balance} \leq -\mathrm{P}_{s,n,t}^{sell} \cdot \mathrm{W}_n \quad \forall\, \mathrm{s} \in QC, n \in M, t \in T \tag{52}$$

Equation corresponding to y^{demand}.

$$-\lambda_{\mathrm{s},n,t}^{balance} + \lambda_{\mathrm{s}}^{demand} \cdot \mathrm{W}_n \leq 0 \quad \forall \mathrm{s} \in DC, n \in M, t \in T \tag{53}$$

Equation corresponding to $y^{generation}$. Here we split the worst-case cluster from the rest of the representative data to integrate all selectable profiles (*Equation (55)*).

$$\lambda_{g,s,n,t}^{generation} + \lambda_{\mathrm{s},n,t}^{balance} \leq \mathrm{VOM}_g \cdot \mathrm{W}_n \quad \forall g \in G, s \in S_g, n \in N \tag{54}$$

$$\lambda_{g,s,p,t}^{generation} + \lambda_{\mathrm{s},n,t}^{balance} \leq \mathrm{VOM}_g \cdot \mathrm{W}_n \quad \forall g \in G, s \in S_g, n \in \widetilde{N}, p \in P \tag{55}$$

Equation corresponding to y^{in}.

$$-\lambda_{s,n,t}^{balance} + \lambda_{k,\mathrm{s},n,t}^{upper\ bound} + \lambda_{k,\mathrm{s},n,t}^{lower\ bound} - \lambda_{k,\mathrm{s},n,t+1}^{ramp\ up} - \lambda_{k,\mathrm{s},n,t+1}^{ramp\ down} - \lambda_{k,\mathrm{s},\tilde{\mathrm{s}},n,t}^{in} \cdot \eta_{k,s,\tilde{s}}^{in} - \lambda_{k,s,\tilde{s},n,t}^{out} \cdot \eta_{k,s,\tilde{s}}^{out} \leq 0 \quad \forall\, k \in K, s \in S_k^{MI}, \tilde{s} \in S, n \in M, t = 1 \tag{56}$$

$$-\lambda_{s,n,t}^{balance} + \lambda_{k,\mathrm{s},n,t}^{upper\ bound} + \lambda_{k,\mathrm{s},n,t}^{lower\ bound} + \lambda_{k,\mathrm{s},n,t}^{ramp\ up} + \lambda_{k,\mathrm{s},n,t}^{ramp\ down} - \lambda_{k,\mathrm{s},n,t+1}^{ramp\ up} - \lambda_{k,\mathrm{s},n,t+1}^{ramp\ down} - \lambda_{k,\mathrm{s},\tilde{\mathrm{s}},n,t}^{in} \cdot \eta_{k,s,\tilde{s}}^{in} - \lambda_{k,s,\tilde{s},n,t}^{out} \cdot \eta_{k,s,\tilde{s}}^{out} \leq 0 \quad \forall\, k \in K, s \in S_k^{MI}, \tilde{s} \in S, n \in M, t \in \{2, \dots, T-1\} \tag{57}$$

$$-\lambda_{\mathrm{s},n,T}^{balance} + \lambda_{k,\mathrm{s},n,T}^{upper\ bound} + \lambda_{k,\mathrm{s},n,T}^{lower\ bound} + \lambda_{k,\mathrm{s},n,T}^{ramp\ up} + \lambda_{k,\mathrm{s},n,T}^{ramp\ down} - \lambda_{k,\mathrm{s},\tilde{\mathrm{s}},n,\mathrm{T}}^{in} \cdot \eta_{k,s,\tilde{s}}^{in} - \lambda_{k,s,\tilde{\mathrm{s}},n,\mathrm{T}}^{out} \cdot \eta_{k,s,\tilde{s}}^{out} \leq 0 \quad \forall\, k \in K, s \in S_k^{MI}, \tilde{s} \in S, n \in M \tag{58}$$

$$-\lambda_{s,n,t}^{balance} + \lambda_{k,s,\tilde{\mathrm{s}},n,t}^{in} \leq 0 \quad \forall\, k \in K, s \in S_k^{MI}, \tilde{s} \in S \setminus S_k^{MI}, n \in M, t \in T \tag{59}$$

Equation corresponding to y^{out}.

$$\lambda_{s,n,t}^{balance} + \lambda_{k,s,\tilde{s},n,t}^{out} \leq \mathrm{VOM}_k \cdot \mathrm{W}_n \quad \forall\, k \in K, s \in S_k^{MI}, \tilde{s} \in S, n \in M, t \in T \tag{60}$$

Equation corresponding to y^{charge}.

$$-\lambda_{s,n,t}^{balance} - \lambda_{s,n,t+1}^{soc\ balance} \cdot \eta_s^{charge} \leq \mathrm{VOM}_s \cdot \mathrm{W}_n \quad \forall\, s \in SC, n \in M, t \in \{1, \dots, T-1\} \tag{61}$$

$$-\lambda_{s,n,T}^{balance} - \lambda_{s,n}^{last\ soc} \cdot \eta_s^{charge} \leq \mathrm{VOM}_s \cdot \mathrm{W}_n \quad \forall\, s \in SC, n \in M \tag{62}$$

Equation corresponding to $y^{discharge}$.

$$\lambda_{s,n,t}^{balance} + \frac{\lambda_{s,n,t+1}^{soc\ balance}}{\eta_s^{discharge}} \leq 0 \quad \forall\, s \in SC, n \in M, t \in \{1, \dots, T-1\} \tag{63}$$

$$\lambda_{s,n,T}^{balance} + \frac{\lambda_{s,n}^{last\ soc}}{\eta_s^{discharge}} \leq 0 \quad \forall\, s \in SC, n \in M \tag{64}$$

Equation corresponding to y^{soc}.

$$-\lambda_{s,n,t+1}^{soc\ balance} + \lambda_{s,n}^{last\ soc} + \lambda_{s,n,t}^{soc\ upper\ bound} + \lambda_{s,n,t}^{soc\ lower\ bound} \leq 0 \quad \forall\, s \in SC, n \in M, t = 0 \tag{65}$$

$$\lambda_{s,n,t}^{soc\ balance} - \lambda_{s,n,t+1}^{soc\ balance} + \lambda_{s,n,t}^{soc\ upper\ bound} + \lambda_{s,n,t}^{soc\ lower\ bound} \leq 0 \quad \forall\, s \in SC, n \in M, t \in \{2, \dots, T-1\} \tag{66}$$

$$\lambda_{s,n,0}^{soc\ balance} - \lambda_{s,n,T}^{last\ soc} + \lambda_{s,n,T}^{soc\ upper\ bound} + \lambda_{s,n,T}^{soc\ lower\ bound} \leq 0 \quad \forall\, s \in SC, n \in M \tag{67}$$

The scenario-based uncertainty set is implemented with *Equations (68)* to *(71)*.

$$u_{g,t} = \sum_p \tilde{u}_{g,p,t} \cdot \beta_p \quad \forall g \in G, t \in T \tag{68}$$

$$\beta \in \{0,1\}^p \quad \forall p \in P \tag{69}$$

$$\sum_{p \in P} \beta_p = 1 \tag{70}$$

$$\sum_{p \in P} \sum_{t \in T} \tilde{u}_{g,p,t} \cdot \beta_p \geq \Gamma_g \quad \forall g \in G, \tag{71}$$

8.2.2 Problem reformulation

The application of this uncertainty set results in a non-linear optimization model since the term $\sum_{g \in G} \sum_{\hat{s} \in S_g} \sum_{t \in \tilde{T}} \sum_{\tilde{n} \in \tilde{N}} \lambda_{g,\hat{s},\tilde{n},t}^{generation} \cdot u_{g,t} \cdot \mathrm{cap}_g^*$ appears in the objective function. To avoid a multiplication of the dual third stage variable with the primal second stage variable and the fixed first stage variable, *Equation (68)* is omitted and the profile dependent uncertain capacity bound on the renewable generation $y^{generation}$ is enforced through a big-M constraint:

$$y_{g,s,n,t}^{generation} \leq \mathrm{cap}_g^* \cdot \tilde{u}_{g,p,t} + \left(1 - \beta_p\right) * \mathrm{BigM} \quad \forall\, g \in G, s \in S_g, n \in \tilde{N}, t \in T, p \in P \tag{72}$$

Based on an outer approximation, the product of the binding dual variable ($\lambda_{g,s,p,t}^{generation}$) of the previous equation, which corresponds to the chosen worst-case scenario, with the chosen capacity level and profile is determined in *Equation (73)* and added to the adjusted objective function in *Equation (74)*:

$$\gamma_{g,s,t}^{generation\_uncertain} \leq \lambda_{g,s,p,t}^{generation} \cdot \mathrm{cap}_g^* \cdot \tilde{u}_{g,p,t} + (1-\beta_p) * \mathrm{BigM} \quad \forall\, g \in G, s \in S_g, t \in T, p \in P \tag{73}$$

$$\begin{aligned}\max_{\lambda,\beta_p} f = & \sum_{s^D \in DC} \lambda_{s^D}^{demand} \cdot \mathrm{D}_{s^D} \\ & + \sum_{k\in K}\sum_{n\in N}\sum_{t\in T}\Big(\lambda_{k,s^{MI}(k),n,t}^{upper\ bound} \cdot \mathrm{BU}_k^{upper} + \lambda_{k,s^{MI}(k),n,t}^{lower\ bound} \cdot \mathrm{BU}_k^{lower} \\ & + \lambda_{k,s^{MI}(k),n,t}^{ramp\ up} \cdot \mathrm{RAMP}_k^{up} + \lambda_{k,s^{MI}(k),n,t}^{ramp\ down} \cdot \mathrm{RAMP}_k^{down}\Big) \cdot \mathrm{cap}_k^* \\ & + \sum_{s^S \in SC}\sum_{n\in N}\sum_{t\in T}\Big(\lambda_{s^S,n,t}^{upper\ bound} \cdot \mathrm{BU}_{s^S}^{upper} + \lambda_{s^S,n,t}^{lower\ bound} \cdot \mathrm{BU}_{s^S}^{lower}\Big) \cdot \mathrm{cap}_{s^S}^* \\ & + \sum_{g\in G}\sum_{s\in S_g}\sum_{n\in N}\sum_{t\in T} \lambda_{g,s,n,t}^{generation} \cdot \mathrm{CF}_{g,n,t} \cdot \mathrm{cap}_g^* \\ & + \sum_{g\in G}\sum_{s\in S_g}\sum_{t\in T} \gamma_{g,s,t}^{generation\ uncertain}\end{aligned} \tag{74}$$

8.3 Parameter assumptions

Table 2: Techno-economic assumptions on conversion units

	PEM Electrolysis (Braun et al., 2022)	H_2 Compressor (Heinzmann, 2024)	CO_2 Compressor (Heinzmann, 2024)	DAC (Fasihi et al., 2019)	FT-Synthesis (Heinzmann, 2024)	MeOH-Synthesis (Heinzmann, 2024)
CAPEX	810 k€/MW	1,590 k€/MW	3,241 k€ / MW	6,395 k€/t	8,279 k€/t/h	3,000 k€/t/h
Fixed O&M	4 %	4 %	4 %	7 %	8%	8%
Lifetime	20	20	20	20	20	20
Minimal Power	7 %	0 %	0	0 %	70 % (Iglesias González et al., 2016)	20 % (Mucci et al., 2023)
Ramp-Up	100 %/h	100 %/h	100 %/h	100 %/h	30 %/h	80 %/h
Ramp-Down	100 %/h	100 %/h	100 %/h	100 %/h	30 %/h	80 %/h
Input	1.52 MWh Electricity 0.27 t Water	0.0167 MWh Electricity	0.06134 MWh Electricity	0.5 MWh Electricity (FT) 1.77 MWh Electricity (MeOH)	3.138 t CO_2 4.386 MWh Electricity 14.63 MWh H_2	1.395 t CO_2 0.327 MWh Electricity 6.366 MWh H_2
Output	1 MWh H_2	-	-	1 t CO_2	1 t FT	1 t MeOH

Table 3: Techno-economic assumptions on electricity generators (Danish Energy Agency, 2023)

	Wind Generator	Solar PV Generator
CAPEX	1,040 k€/MW	310 k€/MW
Fixed Operation and Maintenance	1.21 % of CAPEX	1% of CAPEX
Variable Operation and Maintenance	1.35 €/MWh	0
Lifetime	25	30

Table 4: Techno-economic assumptions on storage units

	H_2 Storage (Braun et al., 2022)	CO_2 Storage (Svensson et al., 2004)	Battery Storage (Cole & Karmakar, 2023)
CAPEX	12 k€ / MWh	45.14 k€ / t	330 k€/MWh
Fixed Operation and Maintenance	4 %	4 %	5.65 %
Variable Operation and Maintenance	0	0	1.12 €/MWh
Lifetime	20	20	20
Minimal SOC	0 %	0 %	10 %
Maximal SOC	100 %	100 %	90 %
Roundtrip Efficiency	100 %	100 %	85 %

8.4 Additional results

8.4.1 Solving environment and problem size

The underlying hardware used for our calculations was an AMD Ryzen Threadripper 3990X 64-Core Processor, operating at 2.9 GHz, which enabled the utilization of up to 128 CPUs. The system has 256 GB of memory, and the operating system is Ubuntu 20.04.6 LTS.

We used PyCharm 2024.1 as an integrated development environment and Python 3.11.9 as a programming language. We read and processed the data with the Python packages PyYAML 6.0.1 and pandas 2.2.2. To set up the optimization problems, we used the Python package gurobipy 11.0.3 and Gurobi 11.0.3 (academic license) as a solver. The solver was run with a configuration at the default settings, except that the number of available threads was set to 120.

Considering the size of the optimization problems, we need to distinguish between the outer and inner problem. *Table 5* presents the number of variables in the outer problem for the case of FT production in Australia. Visible is the increasing number of variables with each iteration, due to the addition of weather data.

Table 5: Number of variables in the outer problem (FT production in Australia)

		Iteration					
		0	**1**	**2**	**3**	**4**	**5**
Period length	**24**	17,981	35,936	-	-	-	-
	48	43,883	87,740	-	-	-	-
	72	71,774	143,522	215,270	-	-	-
	96	103,649	207,272	310,895	-	-	-
	120	129,545	259,064	388,583	518,102	647,621	777,140
	144	131,531	263,036	394,541	526,046	657,551	-
	168	167,390	334,754	502,118	669,482	836,846	-
	192	207,233	414,440	621,647	828,854	-	-
	216	233,129	466,232	699,335	-	-	-
	240	278,948	557,870	836,792	1,115,714	1,394,636	-
	264	263,006	525,986	788,966	1,051,946	1,314,926	-

288	358,631	717,236	1,075,841	1,434,446	1,793,051	-
312	284,915	569,804	854,693	1,139,582	-	-
336	334,718	669,410	1,004,102	1,338,794	-	-
8,760	727,109	1,454,192	2,181,275	2,908,358	3,635,441	4,362,524

Table 6 shows the number of continuous and binary variables in the inner problem for all technologies using Australia's weather data. Since the data split is always the same, the number of continuous and binary variables does not change with each iteration step. An unintuitive number of variables stems from the use or non-use of technologies like storage units, which is decided in the outer problem. In addition, since the number of clusters is determined endogenously, it is possible that lower period lengths have a higher number of continuous variables.

Table 6: Continuous and binary variables in the inner problem for all technologies using the weather data of Australia

Period length	Hydrogen	MeOH	FT	Binaries
24	196,147	225,109	220,132	4,004
48	201,815	272,589	260,434	2,002
72	207,385	323,185	307,633	1,331
96	214,875	382,133	353,416	1,001
120	218,427	427,493	391,600	792
144	218,903	431,181	394,738	660
168	228,841	499,009	452,629	572
192	235,419	524,981	512,488	495
216	241,083	566,837	552,784	440
240	251,069	701,337	624,043	396
264	249,241	616,753	600,901	363
288	268,447	847,357	747,982	330
312	254,615	714,525	635,578	308
336	265,465	805,777	733,201	286
8,760	367,923	1,541,765	1,340,284	11

To achieve high transparency and facilitate future research, we provide code and data of this work here: https://github.com/ulicious/ptx_now_robust

9 References

Albrecht, F. G., König, D. H., Baucks, N., & Dietrich, R.-U. (2017). A standardized methodology for the techno-economic evaluation of alternative fuels – A case study. *Fuel*, *194*, 511–526. https://doi.org/10.1016/j.fuel.2016.12.003

Arthur, D., & Vassilvitskii, S. (2007). k-means++: The advantages of careful seeding. *SODA '07: Proceedings of the eighteenth annual ACM-SIAM symposium on Discrete algorithms*. Eighteenth annual ACM-SIAM symposium on Discrete algorithms, New Orleans, Louisiana, USA.

Berger, M., Radu, D., Detienne, G., Deschuyteneer, T., Richel, A., & Ernst, D. (2021). Remote Renewable Hubs For Carbon-Neutral Synthetic Fuel Production. *Frontiers in Energy Research*, *9*, 671279. https://doi.org/10.3389/fenrg.2021.671279

Bertsimas, D., Litvinov, E., Sun, X. A., Zhao, J., & Zheng, T. (2013). Adaptive Robust Optimization for the Security Constrained Unit Commitment Problem. *IEEE Transactions on Power Systems*, *28*(1), 52–63. https://doi.org/10.1109/TPWRS.2012.2205021

Bielefeld, S., Cvetković, M., & Ramírez, A. (2023). Should we exploit flexibility of chemical processes for demand response? Differing perspectives on potential benefits and limitations. *Frontiers in Energy Research*, *11*, 1190174. https://doi.org/10.3389/fenrg.2023.1190174

Bishop, C. M. (2006). *Pattern recognition and machine learning*. Springer.

Braun, J., Kern, J., Scholz, Y., Hu, W., Moser, M., Schillings, C., & Simon, S. (2022). *Technische und risikobewertete Kosten-Potenzial-Analyse der MENA-Region. MENA-Fuels: Teilbericht 10*. Deutsches Zentrum für Luft- und Raumfahrt e.V.; Wuppertal Institut für Klima, Umwelt, Energie gGmbH. https://wupperinst.org/fa/redaktion/downloads/projects/MENA-Fuels_Teilbericht10_Kostenpotenziale.pdf

Chen, B., Wang, J., Wang, L., He, Y., & Wang, Z. (2014). Robust Optimization for Transmission Expansion Planning: Minimax Cost vs. Minimax Regret. *IEEE Transactions on Power Systems*, *29*(6), 3069–3077. https://doi.org/10.1109/TPWRS.2014.2313841

Cole, W., & Karmakar, A. (2023). *Cost Projections for Utility-Scale Battery Storage: 2023 Update*. National Renewable Energy Laboratory. https://www.nrel.gov/docs/fy23osti/85332.pdf

Danish Energy Agency. (2023). *Technology Data* (Nummer 0013). https://ens.dk/sites/ens.dk/files/Analyser/technology_data_catalogue_for_el_and_dh.pdf

Farajiamiri, M., Meyer, J.-C., & Walther, G. (2023). Multi-objective optimization of renewable fuel supply chains regarding cost, land use, and water use. *Applied Energy*, *349*, 121652. https://doi.org/10.1016/j.apenergy.2023.121652

Fasihi, M., Efimova, O., & Breyer, C. (2019). Techno-economic assessment of CO2 direct air capture plants. *Journal of Cleaner Production*, *224*, 957–980. https://doi.org/10.1016/j.jclepro.2019.03.086

Heinzmann, P. (2024). *Results of process simulation and techno-economic assessment of the Fischer-Tropsch and methanol synthesis* (S. 341,2 kB) [Application/x-tar]. Karlsruhe Institute of Technology. https://doi.org/10.35097/T4ZT3ZW2AZ01X8BQ

Heinzmann, P., Glöser-Chahoud, S., Dahmen, N., Langenmayr, U., & Schultmann, F. (2021). *Techno-ökonomische Bewertung der Produktion regenerativer synthetischer Kraftstoffe*. Karlsruher Institut für Technologie (KIT). https://doi.org/10.5445/IR/1000140638

Hersbach, H., Bell, B., Berrisford, P., Hirahara, S., Horányi, A., Muñoz-Sabater, J., Nicolas, J., Peubey, C., Radu, R., Schepers, D., Simmons, A., Soci, C., Abdalla, S., Abellan, X., Balsamo, G., Bechtold, P., Biavati, G., Bidlot, J., Bonavita, M., … Thépaut, J. (2020). The ERA5 global reanalysis. *Quarterly Journal of the Royal Meteorological Society*, *146*(730), 1999–2049. https://doi.org/10.1002/qj.3803

Hoffmann, P., & Schlünzen, K. H. (2013). Weather Pattern Classification to Represent the Urban Heat Island in Present and Future Climate. *Journal of Applied Meteorology and Climatology*, *52*(12), 2699–2714. https://doi.org/10.1175/JAMC-D-12-065.1

Hofmann, F., Hampp, J., Neumann, F., Brown, T., & Hörsch, J. (2021). atlite: A Lightweight Python Package for Calculating Renewable Power Potentials and Time Series. *Journal of Open Source Software*, *6*(62), Article 62. https://doi.org/10.21105/joss.03294

Iglesias González, M., Eilers, H., & Schaub, G. (2016). Flexible Operation of Fixed-Bed Reactors for a Catalytic Fuel Synthesis—CO ₂ Hydrogenation as Example Reaction. *Energy Technology*, *4*(1), 90–103. https://doi.org/10.1002/ente.201500259

International Energy Agency (IEA). (2024). *Global Hydrogen Review 2024*. IEA. https://www.iea.org/reports/global-hydrogen-review-2024

IRENA. (2022). *Global hydrogen trade to meet the 1.5°C climate goal: Part I – Trade outlook for 2050 and way forward*. International Renewable Energy Agency.

Jiang, Griffiths, & Dirks. (2011). Linking synoptic weather types to daily rainfall in Auckland. *Weather and Climate*, *31*, 50. https://doi.org/10.2307/26169717

Langenmayr, U., & Ruppert, M. (2023). *Calculation of Synthetic Energy Carrier Production Costs with high Temporal and Geographical Resolution*. Karlsruher Institut für Technologie (KIT). https://doi.org/10.5445/IR/1000162460

Maggi, A., Wenzel, M., & Sundmacher, K. (2020). Mixed-Integer Linear Programming (MILP) Approach for the Synthesis of Efficient Power-to-Syngas Processes. *Frontiers in Energy Research*, *8*, 161. https://doi.org/10.3389/fenrg.2020.00161

Mitrai, I., Palys, M. J., & Daoutidis, P. (2024). A Two-Stage Stochastic Programming Approach for the Design of Renewable Ammonia Supply Chain Networks. *Processes*, *12*(2), 325. https://doi.org/10.3390/pr12020325

Mucci, S., Mitsos, A., & Bongartz, D. (2023). Cost-optimal Power-to-Methanol: Flexible operation or intermediate storage? *Journal of Energy Storage*, *72*, 108614. https://doi.org/10.1016/j.est.2023.108614

Neal, R., Fereday, D., Crocker, R., & Comer, R. E. (2016). A flexible approach to defining weather patterns and their application in weather forecasting over Europe. *Meteorological Applications*, *23*(3), 389–400. https://doi.org/10.1002/met.1563

Osman, O., Sgouridis, S., & Sleptchenko, A. (2020). Scaling the production of renewable ammonia: A techno-economic optimization applied in regions with high insolation. *Journal of Cleaner Production*, *271*, 121627. https://doi.org/10.1016/j.jclepro.2020.121627

Riepin, I., Schmidt, M., Baringo, L., & Müsgens, F. (2022). Adaptive robust optimization for European strategic gas infrastructure planning. *Applied Energy*, *324*, 119686. https://doi.org/10.1016/j.apenergy.2022.119686

Ruiz, C., & Conejo, A. J. (2015). Robust transmission expansion planning. *European Journal of Operational Research*, *242*(2), 390–401. https://doi.org/10.1016/j.ejor.2014.10.030

Schack, D., Rihko-Struckmann, L., & Sundmacher, K. (2016). Structure optimization of power-to-chemicals (P2C) networks by linear programming for the economic utilization of renewable surplus energy. In *Computer Aided Chemical Engineering* (Bd. 38, S. 1551–1556). Elsevier. https://doi.org/10.1016/B978-0-444-63428-3.50263-0

Sherwin, E. D. (2021). Electrofuel Synthesis from Variable Renewable Electricity: An Optimization-Based Techno-Economic Analysis. *Environmental Science & Technology*, *55*(11), 7583–7594. https://doi.org/10.1021/acs.est.0c07955

Svensson, R., Odenberger, M., Johnsson, F., & Strömberg, L. (2004). Transportation systems for CO2––application to carbon capture and storage. *Energy Conversion and Management*, *45*(15–16), 2343–2353. https://doi.org/10.1016/j.enconman.2003.11.022

Terlouw, T., Bauer, C., McKenna, R., & Mazzotti, M. (2022). Large-scale hydrogen production via water electrolysis: A techno-economic and environmental assessment. *Energy & Environmental Science*, *15*(9), 3583–3602.

Thorndike, R. L. (1953). Who belongs in the family? *Psychometrika*, *18*(4), 267–276. https://doi.org/10.1007/BF02289263

Velloso, A., Street, A., Pozo, D., Arroyo, J. M., & Cobos, N. G. (2020). Two-Stage Robust Unit Commitment for Co-Optimized Electricity Markets: An Adaptive Data-Driven Approach for Scenario-Based Uncertainty Sets. *IEEE Transactions on Sustainable Energy*, *11*(2), 958–969. https://doi.org/10.1109/TSTE.2019.2915049

Wang, S. (2025). Optimal sizing of Power-to-Ammonia plants: A stochastic two-stage mixed-integer programming approach. *Energy*, *318*, 134838. https://doi.org/10.1016/j.energy.2025.134838

Xu, J., Li, Q., & Zheng, L. (2025). A Robust Model for Hydrogen Supply Chain Network Design in China Under Renewable Energy Uncertainty. *Journal of Computing and Information Science in Engineering*, *25*(3), 031001. https://doi.org/10.1115/1.4067214

Zeng, B., & Zhao, L. (2013). Solving two-stage robust optimization problems using a column-and-constraint generation method. *Operations Research Letters*, *41*(5), 457–461. https://doi.org/10.1016/j.orl.2013.05.003

Paper D:

Mapping Tomorrow's Energy Journeys – A Global Perspective on the Transport of Synthetic Energy Carriers

Uwe Langenmayr[a], Julia Schuler[a], Viktor Slednev[a], Wolf Fichtner[a]
[a] Karlsruhe Institute of Technology (KIT), Chair of Energy Economics, Karlsruhe, Germany

Reference
Langenmayr, U., Schuler, J., Slednev, V., and Fichtner, W. Mapping Tomorrow's Energy Journeys – A Global Perspective on the Transport of Synthetic Energy Carriers. *Submitted to a scientific journal*, 2025b

Mapping Tomorrow's Energy Journeys – A Global Perspective on the Transport of Synthetic Energy Carriers

Langenmayr, Uwe[1,*]; Schuler, Julia[1]; Slednev, Viktor[1]; Fichtner, Wolf[1]

[1] Institute for Industrial Production (IIP), Karlsruhe Institute of Technology (KIT), Karlsruhe, Germany

* Corresponding author: uwe.langenmayr@kit.edu

Abstract

The global energy transition faces the challenge of bridging long distances between regions rich in renewable energy sources and major energy demand hubs, requiring the production and transport of sustainable liquid and gaseous energy carriers. This study introduces an open-source global energy transport model to optimize energy trade routes and commodity choices. It incorporates seven hydrogen-based synthetic energy carriers and related Power-to-X conversion processes, local hydrogen production, and electricity generation costs for 238,427 grid cells covering the global land area, multimodal transport options, and existing global transport infrastructure. Applied to 10,735 energy export locations worldwide with five different scenarios, we derive major implications for future energy imports, and our results highlight the pivotal value of pipeline and port infrastructure and its impact on the economic viability of various energy carriers.

Abbreviations

CAPEX	Capital Expenditure	OPEX	Operational Expenditure
DAC	Direct Air Capture	PtX	Power-to-X
DBT	Dibenzyltoluene	PV	Photovoltaics
FTC	Fischer-Tropsch Crude	RES	Renewable Energy Sources
LOHC	Liquid Organic Hydrogen Carrier	SEC	Synthetic Energy Carrier
MCH	Methylcyclohexane	TM	Transport Mean
MENA	Middle East and North Africa	WACC	Weighted Average Cost of Capital
MeOH	Methanol	SI	Supplementary Information

Introduction

The Paris Agreement established a global consensus to limit the average global surface temperature increase to below 2 °C. While the increase of renewable electricity generation can be a first option to cover electricity demand, direct electrification is not possible or cost-efficient in many sectors. Especially for shipping, aviation, heavy-duty transport, and industrial applications, the need for liquid and gaseous fuels with high energy content persists.[1–3] Emissions in these sectors can be reduced using fossil fuels combined with carbon capture and storage, biogenic feedstocks, and Power-to-X (PtX) technologies. Using PtX, electricity is applied to power processes that provide the feedstock (e.g., hydrogen, carbon dioxide, nitrogen) for subsequent syntheses. If powered by renewables or nuclear, the synthesis products have a low carbon intensity.[4,5]

The cost-efficient, large-scale, and renewable production of PtX-based synthetic energy carriers (SECs) requires regions with ample land and favorable meteorological conditions for renewable electricity generation, surpassing local energy demands. As these regions are often far from major energy demand centers, electrical interconnectors are economically unviable, and pipeline or ship-based transport of SECs is required. Ammonia[2], methane[6,7], Fischer-Tropsch crude (FTC) or methanol (MeOH)[8–10] are proposed as hydrogen-based SECs, with their fossil-based counterparts already traded globally on a megaton scale.[11] This established trade supports the adoption of SECs, as initial smaller-scale projects can utilize existing infrastructure. The high technology readiness further facilitates infrastructure scaling to accommodate potential large-scale SEC trade, leveraging existing regulatory frameworks and vast expertise.[12,13] In contrast, hydrogen lacks a fossil counterpart in international trade. However, existing pipeline infrastructures could be retrofitted to enable hydrogen transport.[1] Sea-based liquid hydrogen transport is possible, but liquid hydrogen carrier ships are not expected to become widely available before the 2030s.[14] In summary, the large-scale deployment of SECs will depend on the ability to produce them globally and to transport them using existing or adapted infrastructure. This development suggests a potential transformation of the global energy trading system, as new export regions may emerge, and raises critical questions regarding the future geography of global energy flows, the suitability and availability of transport infrastructure, and the types of SECs that will dominate long-distance trade.

The transport of SECs is included in numerous publications, using energy system models like Balmorel, PyPSA, Enertile, FINE, COMPETES, or ESDP, where PtX transport routes are typically aggregated as connections between model regions rather than representing individual ports or pipelines.[15–22] Publications with greater emphasis on the transport of SECs are often case studies focusing on specific bi-national energy trade routes.[23–29] While some studies consider multiple countries as potential exporters[30,31], they typically remain limited to country-level resolution, overlooking intranational energy transport, local infrastructure, and renewable electricity generation potentials. Additionally, the scope of transport means and SEC conversion options is often restricted. Other publications investigate multimodal energy transport between abstract, undefined energy exporting and importing regions, identifying optimal energy carrier and transport mode choices, but without consideration of local contexts.[13,32–34]

To contribute to the existing literature and to close still existing research gaps, we developed a heuristic based on a mixed-integer optimization model to efficiently calculate the most cost-efficient transport routes and transport costs from 10,735 globally distributed energy export locations to the import countries Germany, Japan, China, India, and the United States.[35] The accompanying dataset includes global shipping and pipeline infrastructure, as well as geographically high-resolved hydrogen production and electricity generation costs from solar PV and onshore wind. Based on a literature review, we calculated transport and conversion costs for our target year 2030 for seven different SECs (hydrogen, ammonia, methanol, synthetic natural gas, FTC, Methylcyclohexane (MCH), and Dibenzyltoluene (DBT)) and four transport means (ship, truck, and existing and newly built pipelines). Our results aim to provide decision support for three stakeholders: The ability to calculate the most cost-efficient transport routes supports PtX plant investors in their choice of location and produced SECs. Policy makers can identify attractive export regions, key infrastructure, and necessary repurposing. Additionally, researchers and market analysts may utilize the provided data, model, and supply curves for in-depth investigations, such as regional case studies or the development of comprehensive market models.

Results

This results section presents four key findings based on the analysis of five scenarios (*Table 1*). First, proximity to transport infrastructure is a critical factor in minimizing supply costs, enabling even less

favorable production locations, such as those in Europe, to remain competitive through existing pipelines and reduced conversion needs. Second, retrofitting existing natural gas pipelines for hydrogen transport significantly reduces total supply costs, particularly for locations within or near Europe, and influences the optimal choice of transported energy carriers. Third, the availability of infrastructure has the most significant impact on the most attractive export regions, where cost-efficient supply is most sensitive to changes in pipeline connectivity. Finally, different infrastructure configurations create distinct niches for each SEC, with specific energy carriers favored depending on transport distance, conversion costs, and the type of infrastructure available along the supply chain.

Table 1: Overview of applied scenarios

Scenario	**Commodity at destination?**	**Retrofit of natural gas pipelines?**	**Free heat supply at all nodes?**
H2-Retrofit	H_2	Yes	No
H2-No-Retrofit	H_2	No	No
All-Retrofit	Any	Yes	No
All-No-Retrofit	Any	No	No
All-Retrofit-Heat	Any	Yes	Yes

Scenario explanation: All scenarios consider 10,735 equally distributed energy export locations around the globe. In three of these scenarios ("All" scenarios), we do not define which SEC is supplied to the final destination (hydrogen (gaseous G-H2 and liquid L-H2), ammonia (NH3), methanol (MeOH), synthetic methane (G-CH4, L-CH4), DBT, MCH, and FTC). In the other two scenarios ("H2" scenarios), gaseous hydrogen is set as the target commodity at the destination. Furthermore, in three scenarios, the value of existing gas infrastructure is incorporated by allowing the utilization of natural gas pipelines with gaseous hydrogen, including certain retrofit costs ("Retrofit" scenarios). In the main paper, Germany is applied as the import destination. However, to demonstrate the broader applicability of our approach, results for Japan, China, India, and the United States as import destinations[35] are provided in the Supplementary Information (SI). We further investigate the impact of waste heat availability for conversion processes in a fifth scenario (*All-Retrofit-Heat*), whose results are also shown in the SI.

Proximity to transport infrastructure is critical for low supply costs

Our first key finding stems from the analysis of the *All-Retrofit* scenario. The results show that unfavorable hydrogen production costs in Europe are compensated with low-cost transport due to existing pipeline infrastructure and the avoidance of conversions, achieving competitive supply costs (*Figure 1-A)*. This circumstance allows European production locations to compete with locations outside Europe, where

renewable electricity generation conditions might be much more favorable. Available pipeline infrastructure or proximity to ports affects the supply costs (cf. *SI-Figure 11*), which increase when proximity to infrastructure is not given and road transport, with respective conversions, is needed.

Our results further show the choice of transport mode, transport route, and energy carrier of all export locations (*Figure 1-B*). If pipeline infrastructure is available, we see its utilization to transport gaseous hydrogen directly to Germany or the coasts, with subsequent conversion to ammonia and shipping to Germany. Depending on the road transport distance to the next pipeline, liquid hydrogen (e.g., MENA) or liquid methane (e.g., Mongolia, Northern Canada, MENA) is used. Compared to hydrogen, methane has the advantage of cheaper road and pipeline transport, and is used as soon as combined road and pipeline distances are far. Liquid hydrogen is used for medium road distances since the conversion from gaseous to liquid hydrogen is more efficient than the conversion to methane. Gaseous hydrogen implies high road transport costs and is only used near close pipelines. If no pipeline infrastructure is nearby, depending on the distance to the coast, either ammonia or methanol is produced and transported via road to the next port, then shipped to Germany. Methanol involves lower road transport costs (cf. *SI-Table 5*) but higher conversion costs (cf. *SI-Table 3*) compared to ammonia, making it attractive for inland regions with long road transport to the coast (*Figure 1-C*). In addition to cost jumps resulting from changes in transported commodities, *Figure 1-C* shows that transport costs can remain notably low despite great transport distances, e.g., when cost-efficient shipping is the only required mean of transport (e.g., Patagonia) or shipping can effectively be combined with existing pipeline infrastructure (e.g., North America). Our results indicate that from the German point of view, European neighbors should be the first address for energy trade since import costs are low compared to other countries due to proximity and existing transport infrastructure. Next, countries in Northern Africa, Central Asia, and the Middle East connected to the European oil or natural gas pipelines allow for low-cost imports. Countries and regions with high renewable electricity generation potential without connection to the European natural gas and oil infrastructure could supply SECs beyond hydrogen, since conversion is needed for cost-efficient ship transport. These regions and countries include North America, Patagonia, coastal areas of Africa, and Australia. Low inland supply costs depend on the availability of pipeline infrastructure in these regions. However, with increasing distances between Germany and the producing countries, other SEC-demanding

countries might have the advantage of achieving lower import costs due to closer proximity. High-resolution versions of these figures can be found in the SI.

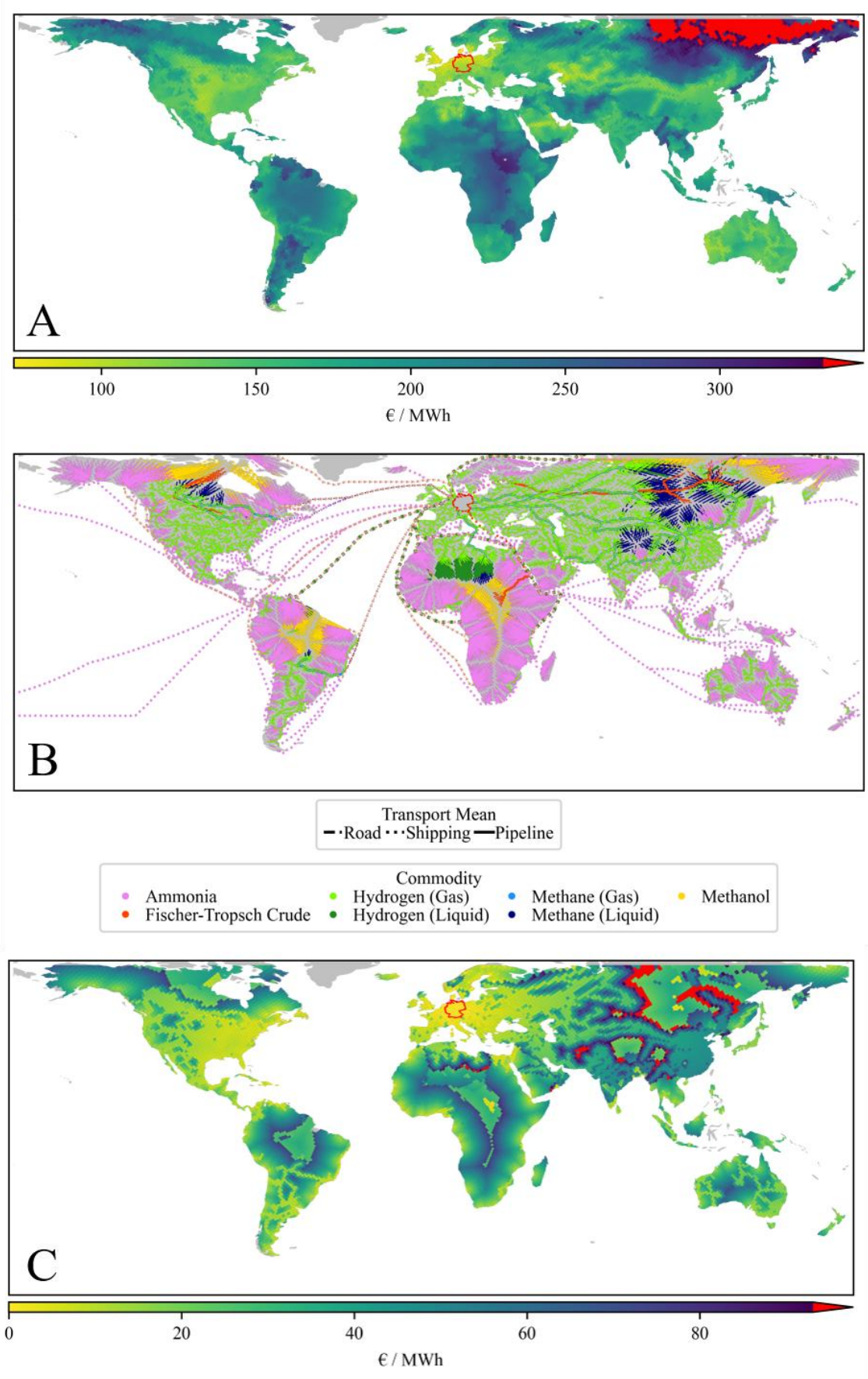

Figure 1: Supply costs, transport routes, and transport costs for SECs from global export regions to Germany under the All-Retrofit scenario. A*: Map of total supply costs including transport and*

conversion, showing that despite comparatively high hydrogen production costs, European regions remain competitive due to the availability of existing pipeline infrastructure and avoided conversions. ***B****: Most frequently selected transport modes and SECs across export locations, highlighting the strong role of pipelines for hydrogen transport from proximate regions, while ammonia, methanol, and methane are selected for longer, multimodal supply chains involving road and maritime transport.* ***C****: The transport cost component of total supply costs indicates that low costs can still be achieved from distant regions such as Patagonia or North America, where shipping dominates or combines effectively with pipeline infrastructure. Areas without nearby infrastructure rely on more costly road transport and additional conversion steps. High-resolution versions of these maps are available in the Supplementary Information.*

Total supply costs are insufficient to assess transport routes and potential export regions since SEC production locations are only developed if sufficient quantities can be produced at low supply costs. To determine both, we use the total supply costs in *Figure 1-A* and weight each location's most cost-efficient transport route by the location's potential export quantity. We cluster the locations by their total supply costs into six cost ranges and sum potential export quantities of shared infrastructure for each cluster (*Figure 2*).

Next to low total supply costs, Central Asia, the Middle East, and Northern Africa show high SEC production potentials, underlining their favorable properties for future imports to Germany (*Figure 2*, top left). Combined with the existing transport infrastructure, these regions could secure the future supply of SECs to Germany. Other locations with low total supply costs, like Australia and North America, are also attractive (*Figure 2*, top right), but the sea-based transport of SECs is less tied to infrastructure, allowing global supply and opening international competition (cf. *SI-Section 1* to *SI-Section 4*). Hinterland locations often show high renewable potential but at higher total supply cost since transport infrastructure is unavailable (*Figure 2*, center left to the bottom right). These locations will probably not be utilized due to the sufficient potential of other locations, but could be used for local supply.

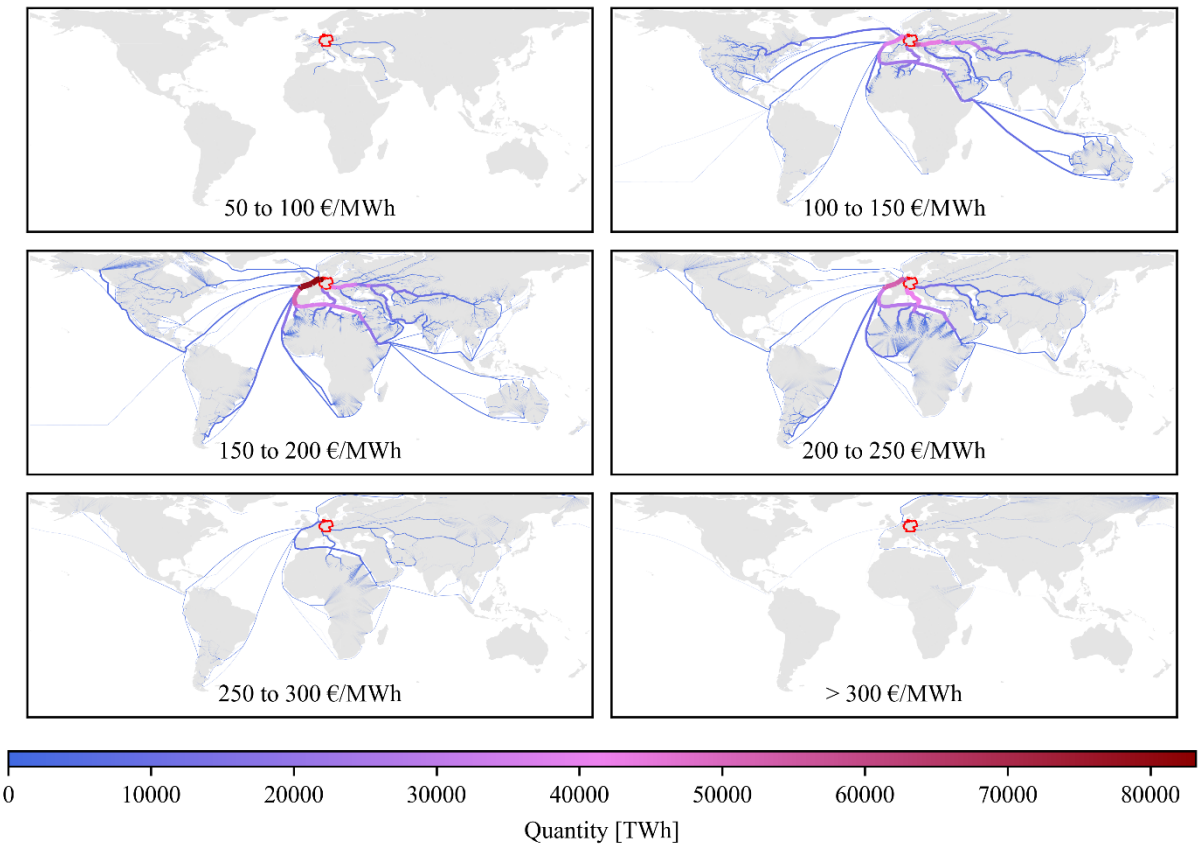

Figure 2: Export potential and supply costs of SECs to Germany, clustered by transport cost and shared infrastructure. *Export locations are grouped into six total supply cost clusters, and potential export quantities are aggregated along shared transport infrastructure. Central Asia, the Middle East, and Northern Africa combine low supply costs with high production potentials, making them prime candidates for future SEC imports. Australia and North America offer competitive supply options, mainly sea-based routes. In contrast, inland regions without infrastructure exhibit higher supply costs and are less likely to contribute significantly to international trade.*

Pipeline retrofitting significantly reduces supply costs

A comparison of results for the first four scenarios is presented to analyze the impact of retrofitting the natural gas infrastructure and the choice of target commodity at the destination. The observation that costs are lower for regions with existing pipeline infrastructure in scenarios allowing for their reuse for hydrogen transport (*Figure 3-A*, right column) compared to scenarios without reuse (*Figure 3-A*, left column) is unsurprising. This is particularly apparent for locations within Europe and adjacent regions, and underlines the importance of preparing the natural gas infrastructure to transport gaseous hydrogen. Not allowing for the reuse requires the transport of hydrogen derivatives, which results in higher costs due to conversions.

In scenarios where the delivered commodity to Germany remains unspecified, costs tend to be generally lower as no conversion to gaseous hydrogen is necessary at the destination (*Figure 3-A*, lower row), and the variety of used SECs is much broader in these scenarios (*Figure 3-B,* lower row). If gaseous hydrogen is the target commodity, mainly ammonia with low conversion and reconversion costs to gaseous hydrogen is applied for coastal regions, whereas inland regions lacking pipeline infrastructure start with liquid hydrogen due to lower road transport costs than ammonia (*Figure 3-B*, upper row).

If the target commodity is not defined and the existing infrastructure is not hydrogen-ready (*All-No-Retrofit*), ammonia plays the most crucial role due to low conversion, road transport, and shipping costs. Locations with higher distances to coastal regions use methanol if no pipeline infrastructure exists and shipping is needed in a subsequent transport step. Inland areas with available natural gas infrastructure (Central Asia, North America, and North Africa) utilize gaseous (for pipeline) and liquid (for road and shipping) methane. Finally, FTC is used if only oil pipelines exist in combination with longer road distances.

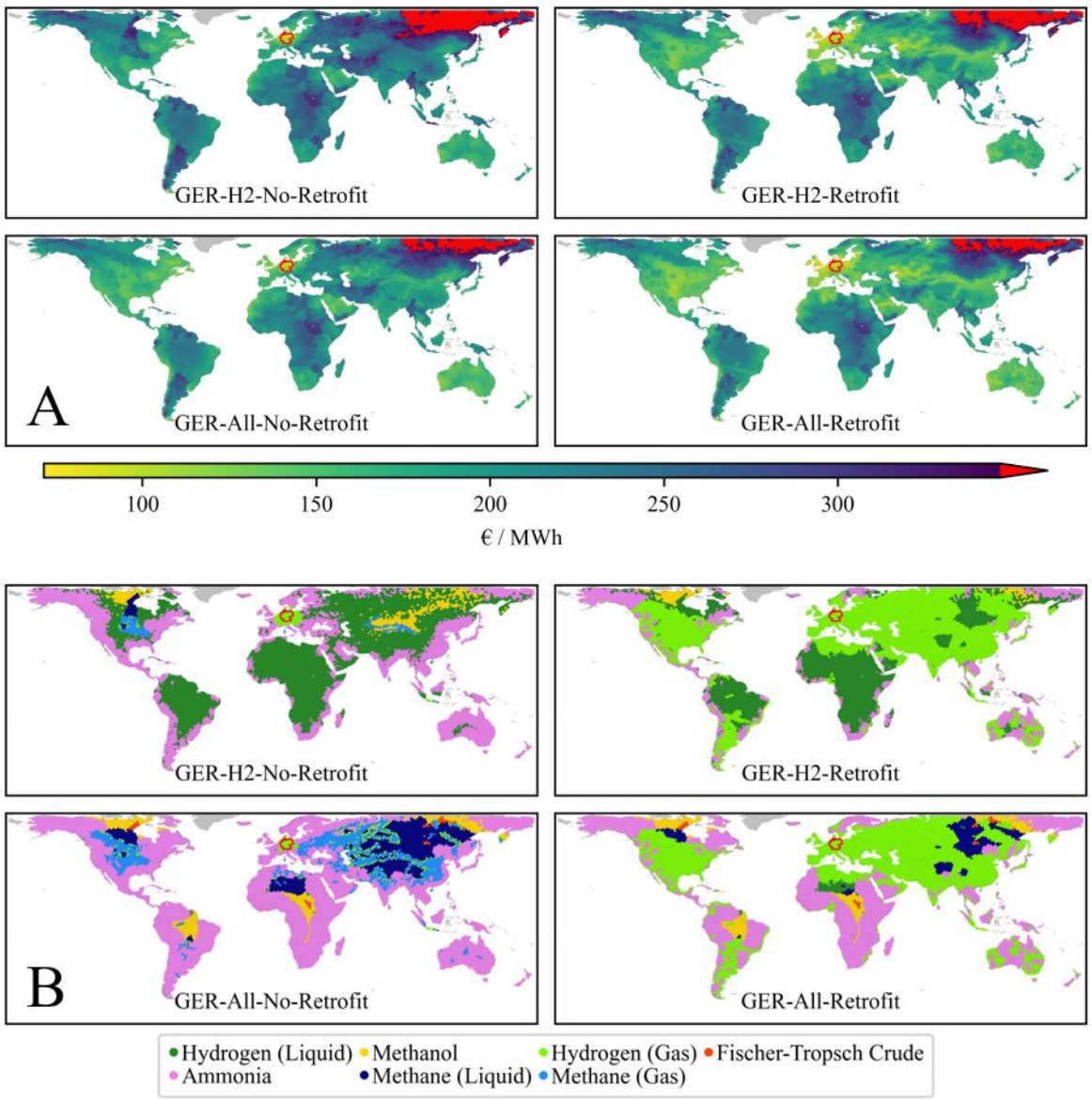

Figure 3: Impact of pipeline retrofitting and target commodity specification on energy supply costs and selected SECs. A*: Total supply costs from global export regions to Germany under four scenarios, comparing cases with and without retrofitting of existing natural gas pipelines (left vs. right columns), and scenarios with flexible vs. fixed hydrogen delivery at the destination (top vs. bottom rows). Allowing pipeline retrofitting significantly reduces supply costs, especially in Europe, North Africa, and Central Asia.* ***B:*** *Preferred SECs under the same scenarios as in A. When the imported commodity is fixed to gaseous hydrogen, ammonia dominates coastal routes, while liquid hydrogen is used in inland areas. In scenarios with flexible commodity choice, ammonia and methanol are favored depending on road distance to ports, and methane or FTC are selected when pipeline infrastructure is available or when long road transport is required.*

Infrastructure availability affects especially the most attractive export locations

Supply curves give insights into export regions' cost and quantity structure, allow comparison between the different export locations, and show in which order locations should be exploited to achieve the most cost-efficient supply. Furthermore, they will enable the impact assessment of various scenarios on costs

and quantities of the region, and changes on the left-hand side of each supply curve are especially of interest since these potentials would be exploited first. Countries with pipeline infrastructure connected to the destination, such as Algeria, profit from low transport costs and the direct transport of hydrogen, visible in the *All-Retrofit* and *H2-Retrofit* scenarios of the Algeria-to-Germany supply curve (*Figure 4)*. However, as soon as existing pipeline infrastructure is unavailable (*All-No-Retrofit* and *H2-No-Retrofit* scenarios), costs increase significantly, especially for locations that achieve low total supply costs in the *All-Retrofit* setting due to necessary conversions and reconversions. Besides increasing costs, quantities decrease due to efficiency losses from conversions and reconversions.

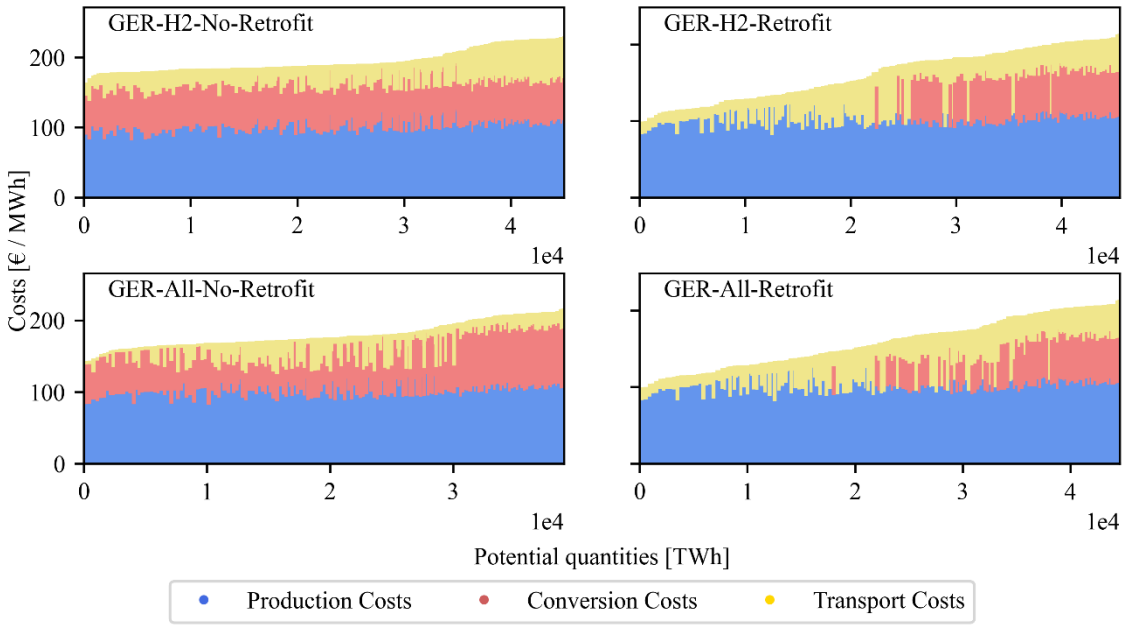

Figure 4: Supply curves for SEC transport from Algeria to Germany under four scenarios. *Supply curves display the cumulative quantities and associated costs of SEC imports from Algeria, allowing assessment of how infrastructure availability and target commodity choice affect supply potential. In scenarios enabling retrofitting existing pipeline infrastructure (All-Retrofit and H2-Retrofit), supply costs are significantly lower, and quantities are higher due to the direct transport of gaseous hydrogen. In contrast, scenarios without retrofitting (All-No-Retrofit and H2-No-Retrofit) lead to sharp cost increases and reduced supply volumes due to additional conversion and reconversion requirements.*

If no pipeline connection between the exporting country and the destination exists, supply curves are less affected by changes in the availability of infrastructure. In such cases, conversions to hydrogen derivatives are necessary to bridge large road and shipping distances, reducing the impact of infrastructure availability. Such a behavior can be seen by looking at the Australia-to-Germany supply curve (*Figure 5*).

However, even here, a slight cost increase can be seen comparing the left-hand sides of the different scenarios, since domestic pipeline transport of hydrogen is possible in Australia in the *Retrofit* scenarios.

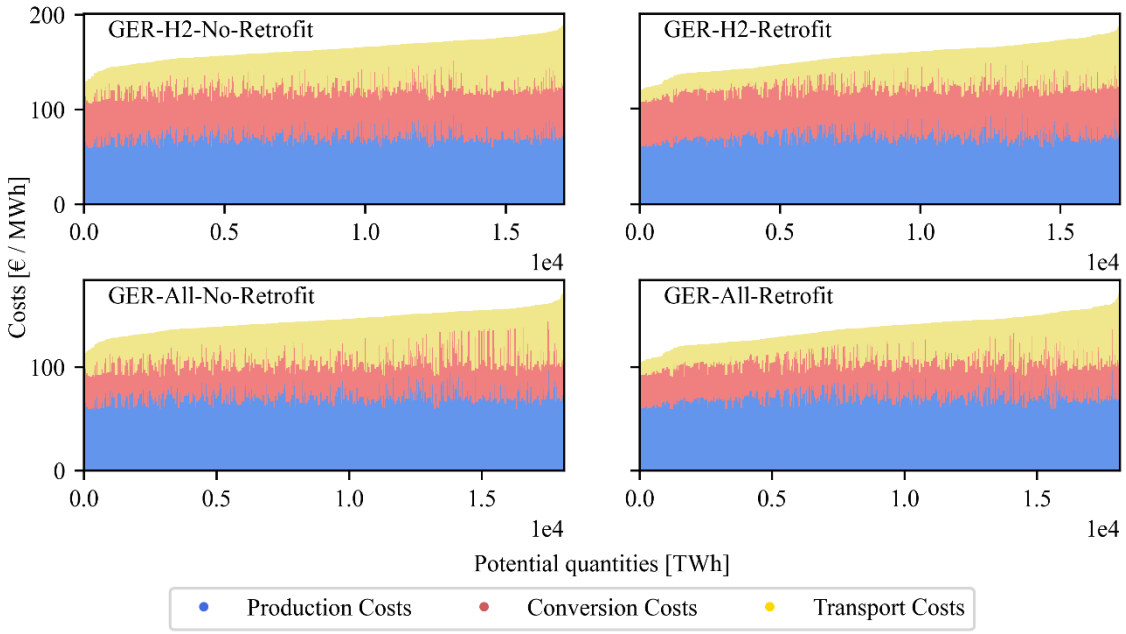

Figure 5: Supply curves for SEC transport from Australia to Germany under four scenarios. *In contrast to pipeline-connected regions, Australia's supply curves show relatively small differences between scenarios, as long-distance transport requires conversions to hydrogen derivatives regardless of infrastructure retrofitting. Nonetheless, slight cost advantages are visible in the Retrofit scenarios due to the use of domestic pipelines within Australia for initial hydrogen transport before conversion.*

Different infrastructure settings create a niche for each energy carrier

Returning to the *All-Retrofit* scenario, we analyze the selection of SECs and transport means for different transport distances. The transport of hydrogen is possible via truck, ship, and pipeline. However, due to the low volumetric energy density and energy-intensive liquefaction, only transport via pipeline is economically feasible for long distances. Road and new gas pipelines allow transport to existing pipelines. However, new gas pipelines are limited to 100 km distances, hence the abrupt limit at 100 km (*Figure 6, Hydrogen (Gas)*). While gaseous hydrogen road transport is used for distances of up to 500 km, longer distances of up to 2,000 km are covered with liquid hydrogen trucks, as the energy savings during transport outweigh the energy losses from liquefaction (*Figure 6, Hydrogen (Liquid)*).

Low synthesis costs significantly advantage ammonia over other SECs (cf. *SI-Table 3*). The combination of low conversion and moderate transport costs makes ammonia a prioritized SEC as soon as pipeline infrastructure is not available. The main application of ammonia is at locations where distances up to

2,000 km have to be covered via road transport to the next port, with subsequent shipping over a broad range of distances (*Figure 6, Ammonia*). Liquid methane is used for road transport, with subsequent shipping or pipeline transport of gaseous methane (*Figure 6, Methane (Gas) and Methane (Liquid)*). Methanol closes the gap if long-distance onshore transport is necessary to reach a port, but no pipeline infrastructure exists. It has lower road and shipping transport costs than ammonia and liquid methane, but its production is more expensive. This circumstance leads to the utilization of methanol if shipping transport is necessary and preceded by long-distance (> 1,750 km) road transport (*Figure 6, Methanol*). The high conversion costs make FTC only viable if large distances must be covered by different means of transport, including existing oil pipelines (*Figure 6: FTC*).

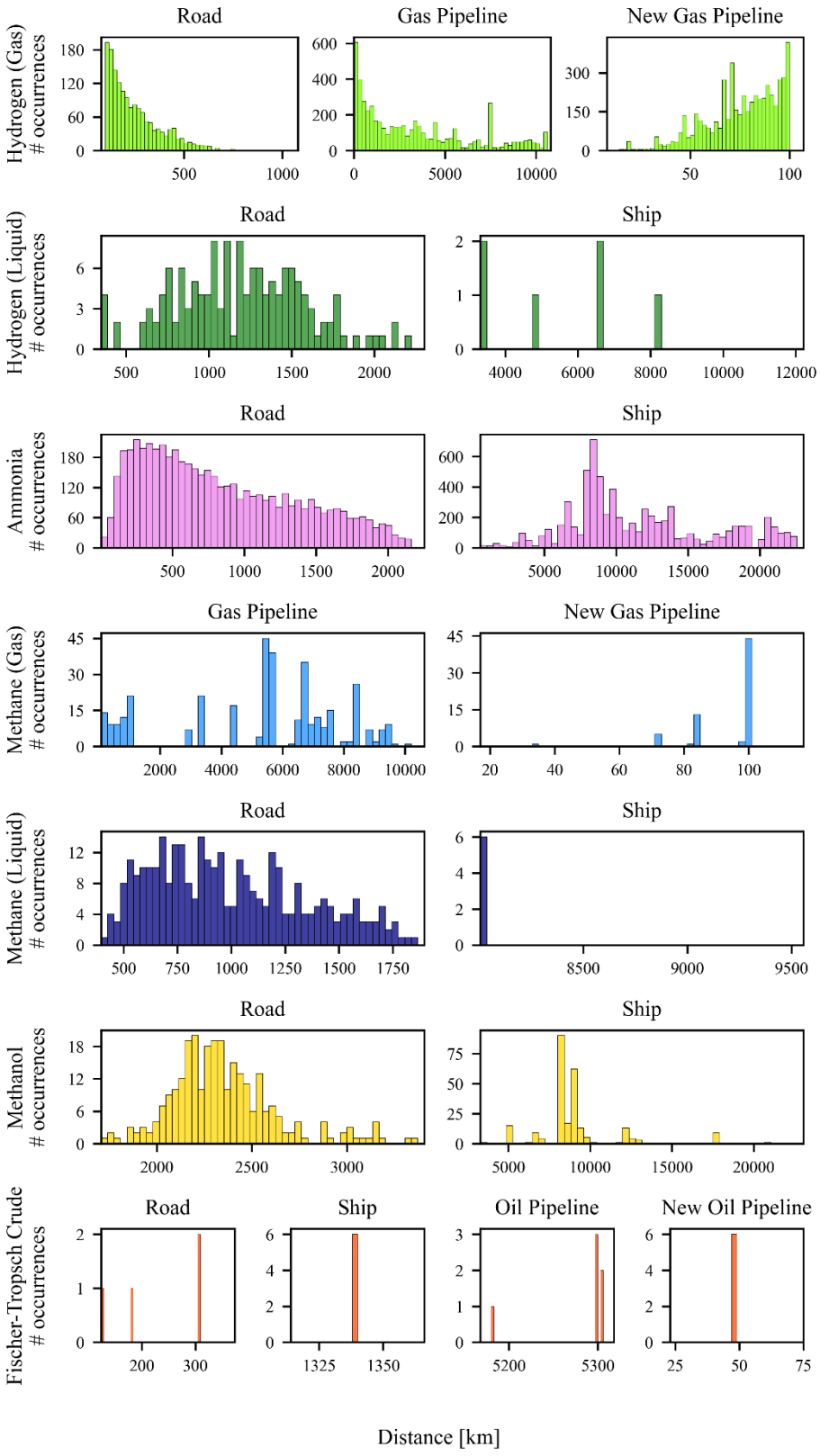

Figure 6: Transport distances and selected means of transport for various SECs under the All-Retrofit scenario. *Histograms show the distribution of transport distances by mode for each SEC. Gaseous hydrogen is primarily transported via pipeline or short-range trucking (<500 km), while liquid hydrogen covers up to 2,000 km of medium-range routes. Ammonia is used where moderate road transport to ports is followed by shipping, benefiting from low synthesis and conversion costs. Methanol becomes favorable for remote inland regions with long road distances due to its lower transport costs despite higher synthesis*

costs. Depending on infrastructure and distance, methane is applied in gaseous and liquefied form. At the same time, FTC is selected for complex, multimodal routes, including oil pipelines, where long distances justify its high conversion cost.

Discussion

We present a novel approach to assess future global transport of SECs, considering global production sites, multiple energy commodities, their interconversion, and various means of transport to calculate the most cost-efficient routes. The model features highly resolved infrastructure datasets to consider global gas and oil pipelines and ports, and applies to any combination of import and export locations worldwide. It is publicly available on GitHub, along with comprehensive global input data.

We demonstrate the model's functionality through case studies examining the supply of SECs from 10,735 locations worldwide to Germany. Analyzing five scenarios in our main paper, we identify conditions under which specific SECs constitute efficient energy transport options. Our results underscore that the availability of transport infrastructure is decisive in enabling cost-efficient transport. For instance, Europe's extensive pipeline network allows for a low-cost supply of gaseous hydrogen, which is competitive with derivative imports from regions with lower renewable electricity costs. Yet, distant exporters can also be cost-effective if located near coastlines (e.g., Patagonia) or have a well-established, retrofit-ready pipeline infrastructure (e.g., North America, Australia). Without retrofitting natural gas pipeline infrastructure, low-cost hydrogen may be limited to a few coastal locations while the production of derivatives becomes more critical. For ship-based energy transport, our results support the utilization of ammonia and methanol. SECs with high conversion costs, namely methanol and methane, are selected only for long transport distances, as their transport costs are lower than for hydrogen and ammonia. These results align with recent research.[20,21,24,27,36] Liquid hydrogen is preferably used when shipping is required, and hydrogen is the demanded commodity at the import location.

The modeling results suggest several policy implications. First, countries should accelerate the retrofit of natural gas infrastructure to enable hydrogen transport. This will allow a low-cost supply of SECs and the implementation of a SEC market since such requires the transport of commodities. Second, pipeline networks should be extended to connect major demand and supply locations, e.g., Europe with neighboring countries in Northern Africa, the Middle East, and Central Asia. Third, terminals must be

retrofitted to allow the import of sufficient quantities of SECs, mainly ammonia and methanol. Fourth, the selection of ammonia and methanol instead of hydrogen for maritime trade encourages the concentration on higher value chain products for sea-based imports that require the development of a basic chemical feedstock industry in exporting regions.

The developed approach is subject to the following limitations. As it applies heuristics to solve complex optimization problems, the optimality of the solutions cannot be formally guaranteed. However, we are confident that our results are optimal or near-optimal by carefully terminating branches based on benchmark costs. Our analyses present a snapshot for 2030 with critical input parameters of transport infrastructure and conversion plants, such as conversion efficiencies, CAPEX, and OPEX, based on a thorough literature review. Some of these technologies have a low technology readiness level, and their availability and development by 2030 remain uncertain. For example, only one carrier, one import, and one export terminal exist worldwide in the case of liquid hydrogen. Other key processes, including hydrogen liquefaction, ammonia cracking, LOHC dehydrogenation, and DAC, are currently available at smaller scales but have yet to achieve industrial-scale implementation.[37–40] However, sensitivity analyses were omitted to maintain focus and clarity in the presented results. Our global scope limits the possibility of including more detailed transport and conversion data, such as capacities of ports, pipelines, and ships, boil-off gases, loading and unloading processes, waste heat availability in ports, canal and port fees, or economies of scale for conversion plants. Road transport routes and new pipeline segments are calculated using as-the-crow-flies distances adjusted by a detour factor, since more detailed information like geographical or street map data would substantially increase computational complexity.

Methods

The applied methodology in this work aims to solve a mixed-integer optimization problem to find the most cost-efficient energy transport route from pre-defined starting points to desired locations. The model's input data includes hydrogen production and electricity generation costs as well as hydrogen production potentials for each cell of the grid, techno-economic data for all conversion units and transport modes, and infrastructure data of ports and oil and gas pipelines. Based on these data, the model decides on transport routes, transport modes, and conversions to achieve the most cost-efficient transport route.

Considering the overwhelming number of conversion and transport options in spatially highly resolved real-world applications, a closed solution of the previously defined mixed-integer problem is out of scope, even for the most advanced solver and computational resources. Therefore, we developed an iterative branching algorithm, which allows for a good approximation of the initial problem. *Figure 7* depicts the graphical abstract of the developed methodology, and the following sections describe the approach in detail. The modeling of the renewable profiles and the calculation method of the costs of hydrogen production, electricity generation, conversion, and transport are described in the SI.

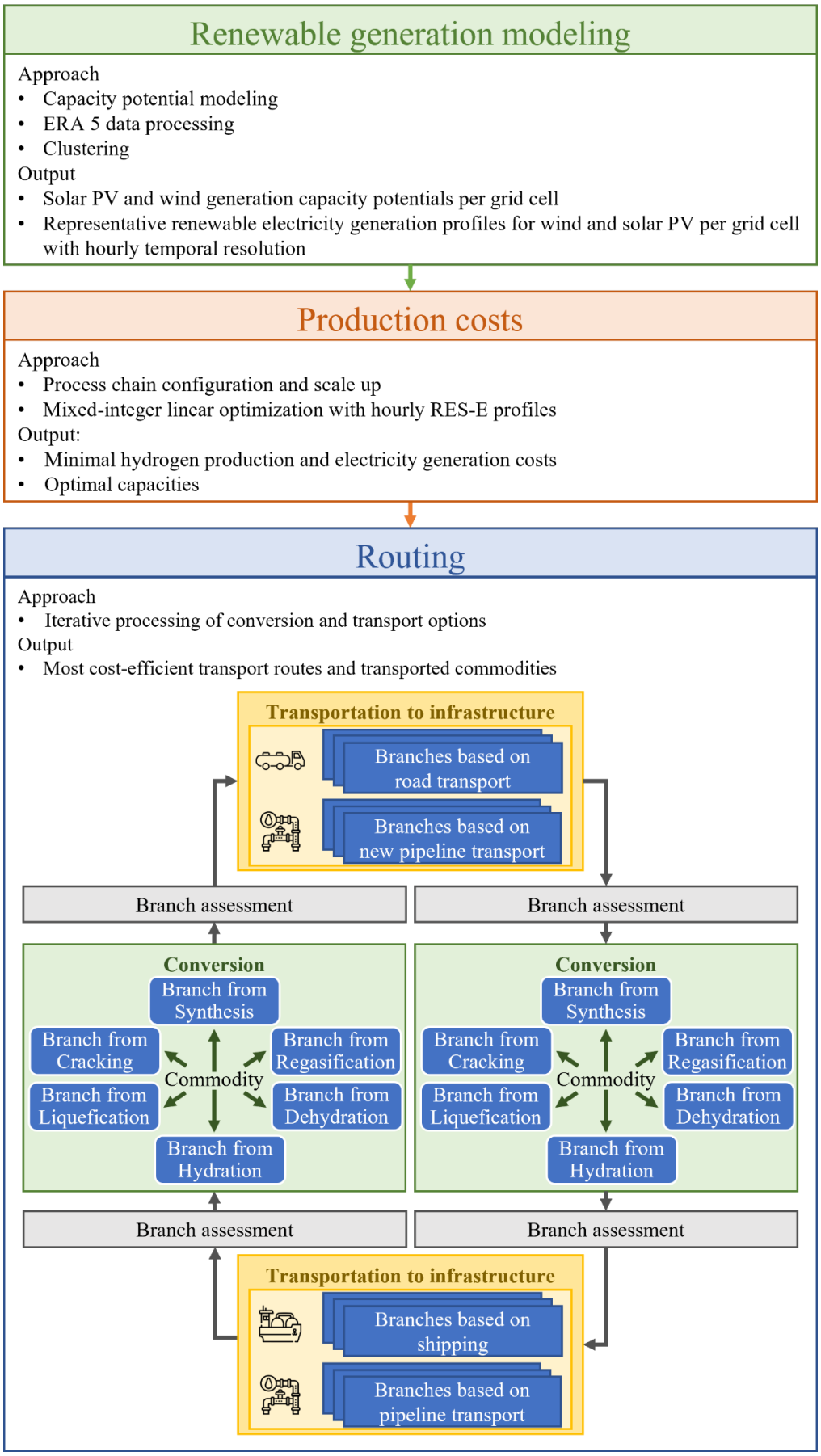

Figure 7: Graphical abstract of approach

General problem

Indexes and sets	
$n, n' \in N$	Nodes of the transport system
$n^s, n^e \in N$	Start node (n^s)
$n^e \in N^e$	Subset of potential end nodes (n^e) (e.g., nodes of a target country)
$c, c' \in C$	Commodities for transport and conversion
$t \in T$	Transport systems
$t \in T^g$	Subset of transport systems based on a graph for modeling existing pipelines and shipping routes
$t \in T^a$	Subset of transport systems based on an air distance point-to-point connection for modeling new pipelines and road transport
$(c', c) \in \Omega_n^C$	Set of edges for modeling the available conversion processes at node n from c' to c
$(n', n) \in \Omega_{t,c}^g$	Edges of the transport graph of transport system $t \in T^g$ for commodity $c \in C$
$(n', n), (n, n') \in \Omega_{n,t,c}^a$	Edges the transport system $t \in T^a$ for the air distance point-to-point transport of commodity $c \in C$ to or from node $n \in N$, which are defined based on the distance matrix $D_{n,n'}$ with $D_{n,n'} \leq \widehat{D}$
$i \in I$	Iteration index
$b \in B$	Set of branches
$(n, c) \in \Omega_b^{NC}$	Set of node-commodity tuples included in branch $b \in B$
Parameters	
$D_{n,n'}$	Distance Matrix for modelling the point-to-point transport of new pipelines and roads
$\widehat{D}$	Maximal distance
U_{n^s,n^s,c^s}	Initial costs for producing the start commodity $c^s \in C$ at start node $n^s \in N$
$\vartheta_{c',c}^{CC}$	Conversion costs [€/MWh] for producing commodity $c \in C$ from $c' \in C$
$\eta_{c',c}$	Conversion efficiency for modelling the material loss of a conversion process
$\vartheta_{n',n,c,t}^{gTC}$	Costs for the transport of commodity $c \in C$ over an edge (n', n) of the graph distance-based transport system $t \in T^g$
$\vartheta_{n',n,c,t}^{aTC}$	Costs for transporting commodity $c \in C$ over an edge (n', n) of the air distance-based transport system $t \in T^a$
Variables	
$u_{n^s,n,c}$	Cumulated conversion and transport costs for providing commodity $c \in C$ at node $n \in N$ starting from node n^s
$x_{n,c',c}$	Binary for modelling the existence of a conversion process at node n from c' to c
$x_{n',n,c,t}$	Binary for modelling the existence of a transport route of commodity c from node n' to node n via the transport system $t \in T$

Given a set of commodities $c \in C_{n^s}^S$ at any start node $n^s \in N$, the goal of the developed approach is to find a cost-optimal conversion and transport path such that the total costs for delivering a SEC to one node of the subset of potential end nodes $n^e \in N^e$ are minimized. In this context, multiple target commodities $c \in C_{n^e}^e$ for any node of a specific target region $n^e \in N^e$ can be specified, which might be either directly delivered via multiple transport systems or converted from multiple intermediate transport commodities, which themselves are allowed to be transported by multiple means. In a closed optimization, this problem can be formulated as the following mixed integer problem:

$$min \sum_{n^e \in N^e} \sum_{c \in C_{n^e}^e} u_{n^s,n^e,c} \tag{1}$$

$$s.t \quad \frac{u_{n^s,n,c'} + \vartheta_{c',c}^{CC}}{\eta_{c',c}} - u_{n^s,n,c} \leq \left(1 - x_{n,c',c}\right) * BigM \quad \forall n \in N, c \in C, (c',c) \in \Omega_n^C \tag{2}$$

$$u_{n^s,n\prime,c} + \vartheta_{n',n,c,t}^{gTC} - u_{n^s,n,c} \leq \left(1 - x_{n',n,c,t}\right) * BigM \quad \forall n \in N, c \in C, t \in T^g, (n',n) \in \Omega_{t,c}^g \tag{3}$$

$$u_{n^s,n\prime,c} + \vartheta_{n',n,c,t}^{aTC} - u_{n^s,n,c} \leq \left(1 - x_{n',n,c,t}\right) * BigM \quad \forall n \in N, c \in C, t \in T^a, (n',n) \in \Omega_{n,c,t}^a \tag{4}$$

$$\sum_{(n',n) \in \Omega_{t,c}^g} x_{n',n,c,t} + \sum_{(n',n) \in \Omega_{n,t,c}^a} x_{n',n,c,t} + \sum_{(n,c',c) \in \Omega_n^C} x_{n,c',c} = \sum_{(n,n') \in \Omega_{t,c}^g} x_{n,n\prime,c,t} + \sum_{(n,n') \in \Omega_{n,t,c}^a} x_{n,n',c,t} + \sum_{(n,c,c') \in \Omega_n^C} x_{nc,c\prime} \quad \forall n \in N/\{n^s, n^e\}, c \in C, t \in T \tag{5}$$

$$\sum_{t \in T} \sum_{c \in C} \sum_{(n',n) \in (\Omega_{t,c}^g \cup \Omega_{n,t,c}^a)} x_{n',n,c,t} + \sum_{(c\prime,c) \in \Omega_n^C} x_{n,c',c} \leq 1 \quad \forall n \in N \tag{6}$$

$$\sum_{t \in T} \sum_{c \in C} \sum_{(n,n') \in (\Omega_{t,c}^g \cup \Omega_{n,t,c}^a)} x_{n,n',c,t} + \sum_{(c,c\prime) \in \Omega_n^C} x_{n,c,c\prime} \leq 1 \quad \forall n \in N \tag{7}$$

$$\sum_{c \in C_{n^s}^S} \sum_{t \in T} \sum_{(n^s,n') \in (\Omega_{t,c^s}^g \cup \Omega_{n^s,t,c^s}^a)} x_{n^s,n',c^s,t} + \sum_{(c^s,c') \in \Omega_{n^s}^C} x_{n^s,c^s,c\prime} = 1 \tag{8}$$

$$\sum_{t \in T^{gr}} \sum_{c \in C_{n^e}^e} \sum_{(n',n^e) \in \Omega_{t,c}^{gr}} x_{n',n^e,c,t} + \sum_{c \in C_{n^e}^e} \sum_{(n',n) \in \Omega_n^{pp}} x_{n',n^e,c} + \sum_{(c',c) \in \Omega_{n^e}^C \wedge c \in C_{n^e}^e} x_{n^e,c',c} = 1 \tag{9}$$

Eq. (1) minimizes the total conversion and transport costs for multiple target commodities $c \in C_{n^e}^e$ at the optimal end node within a target region. Conversion and transport cost restrictions are modeled in *Eq. (2) - Eq. (4)* based on Big-M inequalities. The conversion costs restriction of *Eq. (2)* states that in case of a conversion from commodity $c' \in C$ to $c \in C$ at node $n \in N$ ($x_{n,c',c} = 1$), the current total costs is lower bounded by the previous total costs for delivering commodity $c' \in C$ to the current node, adjusted by the

conversion efficiency, plus the costs for the actual conversion. In case of a transport of commodity $c \in C$ from node $n' \in N$ to node $n \in N$ ($x_{n',n,c,t} = 1$) via existing pipelines or shipping routes, *Eq. (3)* ensures that the current total costs are lower bounded by the previous total cost for delivering commodity $c \in C$ to the predecessor node n', plus the transport costs $\vartheta^{gTC}_{n',n,c,t}$. Analogously, *Eq. (4)* demands that in case of a transport of commodity $c \in C$ from node $n' \in N$ to node $n \in N$ ($x_{n',n,c,t} = 1$) based on an air distance point-to-point connection for modelling new pipelines and road transport, the current total costs are lower bounded by the previous total costs for delivering commodity $c \in C$ to the predecessor node n', plus the transport costs $\vartheta^{aTC}_{n',n,c,t}$. For all nodes except of the start and end node, *Eq. (5)* ensures a nodal balance of conversion paths by demanding that the number of binaries for indicating incoming active transport and conversion options equal the number of outgoing binaries. To ensure that each node is visited only once on the route from the start to the end node, *Eq. (6)* and *Eq. (7)* restrict the number of incoming and outgoing conversion and transport options to one, respectively. Finally, *Eq. (8)* defines the starting and *Eq. (9)* the ending condition that exactly one conversion or transport option is chosen at the start and end node. The methods to calculate transport and conversion costs are given in *Sections 10.4* and *10.5* in the supplementary information.

Iterative processing of branches

Our approach is a multi-commodity multi-mean transport algorithm capable of finding the most cost-efficient transport route from pre-defined starting points to a desired location. If only one commodity is specified as the target commodity in the input parameter set, the algorithm will find the most cost-efficient route for that commodity. Specifying multiple eligible commodities and respective conversion processes allows the algorithm to select the route and the commodities to be transported. This reduces transport costs as the algorithm can take advantage of low transport costs for certain commodities. Finally, suppose the production costs of the different commodities at the starting location are specified. In that case, the algorithm will provide the total supply costs, considering production, transport, and conversion costs.

The algorithm generates possible solutions for transport from a starting point to the final destination through an iterative process. Decisions are continuously taken based on eligible conversions and routes, leading to a decision tree where each branch is created based on the choice of conversion or transport.

Branches b include information on the current geographic position or node n, the commodity c, and the total costs $u_{n^s,n,c}$ for delivering the commodity c to the current node. Furthermore, information on past nodes is also stored to avoid circulating between nodes. After each conversion or transport step, each branch is assessed to remove branches that violate set benchmarks. The overall objective of the approach is the minimization of the total costs at the final destination $\hat{n}$ for all branches whose commodity is one of the target commodities in $c \in C_{n^e}^e$. The branching procedure is described based on the following pseudocode:

Initialize
-Iteration counter i=1
-Start branches $b \in B^i$ including only the node-commodity tuple $(n^s, c^s) \in \Omega_b^{NC}$
-Set the benchmarks for the cumulated costs $u_{n^s,n,c}$ based on pre-heuristic calculations for all $(n,c) \neq (n^s, c^s)$ and the initial costs $u_{n^s,n^s,c^s} = U_{n^s,n^s,c^s}$

---

while $B^i \neq \emptyset$:

Conversion branching I

for each branch $b \in B^i$, with $(\tilde{n}, \tilde{c}) \in \Omega_b^{NC}$ denoting the leaf of the current branch

for each potential conversion edge $(\tilde{c}, c') \in \Omega_{\tilde{n}}^C$ at the current leaf

if $u_{n^s,\tilde{n},c'} > \frac{u_{n^s,\tilde{n},\tilde{c}} + \vartheta_{\tilde{c},c'}^{CC}}{\eta_{\tilde{c},c'}}$:

set $u_{n^s,\tilde{n},c'} = \frac{u_{n^s,\tilde{n},\tilde{c}} + \vartheta_{\tilde{c},c'}^{CC}}{\eta_{\tilde{c},c'}}$

if $u_{n^s,\tilde{n},c'} < \min_{n^e \in N^e} \min_{c \in C_{n^e}^e} u_{n^s,n^e,c}$:

Create new branch b′ consisting of the transport edges: $\Omega_{n,c,t,b}^a$, $\Omega_{t,c,b}^g$ and conversion edges $\Omega_{n,b}^C$ of the existing branch and add to $B^{i,1}$

Add current conversion edge and leaf to the new branch: $\Omega_{\tilde{n},b'}^C = \Omega_{\tilde{n},b}^C \cup (\tilde{c}, c')$, $\Omega_{b'}^{NC} = \Omega_b^{NC} \cup (\tilde{n}, c'))$

Delete all existing branches $b \in B^i$, with $(\tilde{n}, c') \in \Omega_b^{NC}$

Repeat conversion branching for each branch $b' \in B^{i,1}$ and add leaves to $B^{i,2}$

Transport branching I (for air distance-based modeling of new pipelines and road routes)

for each branch $b \in (B^i \cup B^{i,1} \cup B^{i,2})$, where $(\tilde{n}, \tilde{c}) \in \Omega_b^{NC}$ is a leaf of the current branch

for each potential transport edge (ñ, n′) $\in \Omega_{\tilde{n},\tilde{c},t,b}^a$

if $u_{n^s,n\prime,\tilde{c}} > u_{n^s,\tilde{n},\tilde{c}} + \min_{t \in T^a} \vartheta_{\tilde{n},n',\tilde{c},t}^{aTC}$:

set $u_{n^s,n\prime,\tilde{c}} = u_{n^s,\tilde{n},\tilde{c}} + \min_{t \in T^a} \vartheta_{\tilde{n},n',\tilde{c},t}^{aTC}$

if $u_{n^s,\tilde{n},c'} < \min_{c \in C_{n^e}^e} u_{n^s,n^e,c}$:

Create new branch b′ consisting of the transport edges: $\Omega_{n,c,t,b}^a$, $\Omega_{t,c,b}^g$ and conversion edges $\Omega_{n,b}^C$ of the existing branch and add to $B^{i,3}$

Add current transport edge and leaf to the new branch: $\Omega_{\tilde{n},\tilde{c},t,b'}^a = \Omega_{\tilde{n},\tilde{c},t,b}^a \cup (\tilde{n}, n')$, $\Omega_{b'}^{NC} = \Omega_b^{NC} \cup (n', \tilde{c})$

Delete all existing branches $b \in (B^i \cup B'^1 \cup B^{i,2})$, with $(\tilde{n}, \tilde{c}) \in \Omega_b^{NC}$

Conversion branching II for $b \in B^{i,3}$ analog to **Conversion branching I** defining $B^{i,4}$ and $B^{i,5}$

Transport branching II (for graph-based modeling of existing pipelines and shipping routes)

for each branch $b \in (B^i \cup B'^1 \cup B^{i,2} \cup B^{i,3} \cup B^{i,4} \cup B^{i,5})$, with $(\tilde{n}, \tilde{c}) \in \Omega_b^{NC}$ denoting the leaf of the current branch

for each potential transport edge $(\tilde{n}, n') \in \Omega_{t,c}^g$ at the current leaf

if $u_{n^s,n\prime,\tilde{c}} > u_{n^s,\tilde{n},\tilde{c}} + \min_{t \in T^g} \vartheta_{\tilde{n},n',\tilde{c},t}^{gTC}$:

set $u_{n^s,n\prime,\tilde{c}} = u_{n^s,\tilde{n},\tilde{c}} + \min_{t \in T^g} \vartheta_{\tilde{n},n',\tilde{c},t}^{aTC}$

if $u_{n^s,\tilde{n},\tilde{c}} < \min_{n^e \in N^e} \min_{c \in C_{n^e}^e} u_{n^s,n^e,c}$:

Create new branch b′ consisting of the transport edges: $\Omega_{n,c,t,b}^a$, $\Omega_{t,c,b}^g$ and conversion edges $\Omega_{n,b}^C$ of the existing branch and add to $B^{i,6}$: $\Omega_{t,\tilde{c},b'}^g = \Omega_{t,\tilde{c},b}^g \cup (\tilde{n}, n')$, $\Omega_{b'}^{NC} = \Omega_b^{NC} \cup (n', \tilde{c})$

Set and iteration update: $B^{i+1} = B^{i,6}$ and i=i+1

Implementation remarks

The pseudocode is an approach to heuristically implementing the mixed-integer optimization program. However, this pseudo-code will still require a huge computation time to solve the problem. To increase efficiency, we implement the approach with parallel computation matrices to allow simultaneous processing of locations.

Constraining potential transport options

We constrain the approach by forbidding consecutive point-to-point transport for two reasons: First, if a maximal distance for point-to-point transport is set, consecutive point-to-point transport would allow breaching this maximal distance by adding connected point-to-point routes in each iteration. Second, if no maximal distance is implemented, point-to-point distance to any node is possible, and using detours via other nodes will not achieve lower costs than direct point-to-point transport. Furthermore, we constrain the approach by allowing only a single utilization of transport systems like pipelines for each branch. Since we apply Dijkstra to calculate the shortest paths through pipeline systems for all nodes of the pipeline system and create one branch for each node, we cover all possible routes at once. Consecutive traversing of the pipeline system will not result in cheaper costs and will only increase the number of necessary iterations.

Upper bounds and local benchmarks

We apply a pre-heuristic to calculate an upper bound for the main heuristic. The upper bound is a valid but not necessarily the most cost-efficient solution of the approach. It allows the termination of branches if they exceed the upper bound, even before they reach the destination. In this pre-heuristic, we use the combinations start + point-to-point + shipping + point-to-point + destination; start + point-to-point + pipeline + point-to-point + destination; start + point-to-point + pipeline + point-to-point + pipeline + point-to-point + destination; start + point-to-point + pipeline + point-to-point + shipping + point-to-point + destination and start + point-to-point + destination to create routes. For all routes, we always use the closest available infrastructure (closest port to start, closest pipeline system to destination, etc.) and all combinations of available commodities to cover these routes. Branches reaching the destination and having lower total supply costs than the upper bound will update the upper bound. Potential branches can

be terminated based on the upper bound by using cost approximations. These include, for example, calculating the cheapest transport costs of the residual route to the destination, or calculating minimal additional costs for using a target infrastructure (based on residual distance to infrastructure, necessary conversions to use infrastructure, etc.). Combined with the total costs of the traveled route, such costs can be compared to the upper bound. Finally, subproblems are processed to assess potential branches. For example, suppose several branches aim for a common infrastructure network, it might be useful to process the closest branch to the infrastructure first to calculate local benchmarks of the network nodes. Other branches might exceed these local benchmarks since their transportation costs might already be higher than the transportation costs of the branch closest to the infrastructure network.

Data availability

All used data is published here under the following DOI: **10.5281/zenodo.15350282**

Code availability

The model HERMES – **H**ydrogen **E**conomy **R**outing **M**odel for cost-**e**fficient **S**upply is implemented in Python and available here: https://github.com/ulicious/hermes. The folder further contains all the necessary data applied in our case studies. Further documentation can be found here: https://hermes-h2.readthedocs.io/en/main/

Corresponding author

Further information and requests for resources should be directed toward and will be fulfilled by the lead contact, Uwe Langenmayr (uwe.langenmayr@kit.edu)

Author contributions

Conceptualization: U.L.; methodology: U.L.; software: U.L.; data curation: U.L., J.S.; validation: U.L., J.S.; writing – original draft: U.L., J.S., V.S., W.F.; writing – review and editing: U.L., J.S., V.S., W.F.; visualization: U.L.

Declaration of interests

The authors declare no competing interests.

Declaration of generative AI and AI-assisted technologies

To improve the readability of our work, we have applied Grammarly (v.1.2.92.1464)

References

1. International Energy Agency (2023). Global Hydrogen Review 2023.

2. International Energy Agency (IEA) (2021). Ammonia Technology Roadmap: Towards more sustainable nitrogen fertiliser production (OECD) https://doi.org/10.1787/f6daa4a0-en.

3. Stolz, B., Held, M., Georges, G., and Boulouchos, K. (2022). Techno-economic analysis of renewable fuels for ships carrying bulk cargo in Europe. Nat Energy *7*, 203–212. https://doi.org/10.1038/s41560-021-00957-9.

4. Sillman, J., Havukainen, J., Alfasfos, R., Elyasi, N., Lilja, M., Ruuskanen, V., Laasonen, E., Leppäkoski, L., Uusitalo, V., and Soukka, R. (2024). Meta-analysis of climate impact reduction potential of hydrogen usage in 9 Power-to-X pathways. Applied Energy *359*, 122772. https://doi.org/10.1016/j.apenergy.2024.122772.

5. IEA (2019). The Future of Hydrogen: Seizing today's opportunities (International Energy Agency).

6. Götz, M., Lefebvre, J., Mörs, F., McDaniel Koch, A., Graf, F., Bajohr, S., Reimert, R., and Kolb, T. (2016). Renewable Power-to-Gas: A technological and economic review. Renewable Energy *85*, 1371–1390. https://doi.org/10.1016/j.renene.2015.07.066.

7. Tremel, A. (2018). Electricity-based Fuels (Springer International Publishing) https://doi.org/10.1007/978-3-319-72459-1.

8. De Klerk, A. (2008). Fischer–Tropsch refining: technology selection to match molecules. Green Chem. *10*, 1249. https://doi.org/10.1039/b813233j.

9. Dry, M.E. (1999). Fischer–Tropsch reactions and the environment. Applied Catalysis A: General *189*, 185–190. https://doi.org/10.1016/S0926-860X(99)00275-6.

10. Schemme, S., Breuer, J.L., Köller, M., Meschede, S., Walman, F., Samsun, R.C., Peters, R., and Stolten, D. (2020). H2-based synthetic fuels: A techno-economic comparison of alcohol, ether and hydrocarbon production. International Journal of Hydrogen Energy *45*, 5395–5414. https://doi.org/10.1016/j.ijhydene.2019.05.028.

11. Johnston, C., Ali Khan, M.H., Amal, R., Daiyan, R., and MacGill, I. (2022). Shipping the sunshine: An open-source model for costing renewable hydrogen transport from Australia. International Journal of Hydrogen Energy *47*, 20362–20377. https://doi.org/10.1016/j.ijhydene.2022.04.156.

12. Abraham, E.J., Linke, P., Al-Rawashdeh, M., Rousseau, J., Burton, G., and Al-Mohannadi, D.M. (2024). Large-scale shipping of low-carbon fuels and carbon dioxide towards decarbonized energy systems: Perspectives and challenges. International Journal of Hydrogen Energy *63*, 217–230. https://doi.org/10.1016/j.ijhydene.2024.03.140.

13. Sterner, M., Hofrichter, A., Meisinger, A., Bauer, F., Pinkwart, K., Maletzko, A., Dittmar, F., and Cremers, C. (2024). 19 Import options for green hydrogen and derivatives - An overview of efficiencies and technology readiness levels. International Journal of Hydrogen Energy *90*, 1112–1127. https://doi.org/10.1016/j.ijhydene.2024.10.045.

14. Stargardt, M., Kress, D., Heinrichs, H., Meyer, J.-C., Linßen, J., Walther, G., and Stolten, D. (2024). Global Shipyard Capacities Limiting the Ramp-Up of Global Hydrogen-based Transportation. Preprint at arXiv, https://doi.org/10.48550/arXiv.2403.09272 https://doi.org/10.48550/arXiv.2403.09272.

15. Husarek, D., Schmugge, J., and Niessen, S. (2021). Hydrogen supply chain scenarios for the decarbonisation of a German multi-modal energy system. International Journal of Hydrogen Energy *46*, 38008–38025. https://doi.org/10.1016/j.ijhydene.2021.09.041.

16. Caglayan, D.G., Heinrichs, H.U., Robinius, M., and Stolten, D. (2021). Robust design of a future 100% renewable european energy supply system with hydrogen infrastructure. International Journal of Hydrogen Energy *46*, 29376–29390. https://doi.org/10.1016/j.ijhydene.2020.12.197.

17. Morales-España, G., Hernández-Serna, R., Tejada-Arango, D.A., and Weeda, M. (2024). Impact of large-scale hydrogen electrification and retrofitting of natural gas infrastructure on the European power system. International Journal of Electrical Power & Energy Systems *155*, 109686. https://doi.org/10.1016/j.ijepes.2023.109686.

18. Lux, B., Deac, G., Kiefer, C.P., Kleinschmitt, C., Bernath, C., Franke, K., Pfluger, B., Willemsen, S., and Sensfuß, F. (2022). The role of hydrogen in a greenhouse gas-neutral energy supply system in Germany. Energy Conversion and Management *270*, 116188. https://doi.org/10.1016/j.enconman.2022.116188.

19. Kountouris, I., Bramstoft, R., Madsen, T., Gea-Bermúdez, J., Münster, M., and Keles, D. (2024). A unified European hydrogen infrastructure planning to support the rapid scale-up of hydrogen production. Nat Commun *15*, 5517. https://doi.org/10.1038/s41467-024-49867-w.

20. Neumann, F., Zeyen, E., Victoria, M., and Brown, T. (2023). The potential role of a hydrogen network in Europe. Joule *7*, 1793–1817. https://doi.org/10.1016/j.joule.2023.06.016.

21. Hampp, J., Düren, M., and Brown, T. (2022). Import options for chemical energy carriers from renewable sources to Germany. PLoS ONE 18(2): e0262340. https://doi.org/10.1371/journal.

22. Hofmann, F., Tries, C., Neumann, F., Zeyen, E., and Brown, T. (2025). H2 and CO2 network strategies for the European energy system. Nat Energy. https://doi.org/10.1038/s41560-025-01752-6.

23. Raab, M., Maier, S., and Dietrich, R.-U. (2021). Comparative techno-economic assessment of a large-scale hydrogen transport via liquid transport media. International Journal of Hydrogen Energy *46*, 11956–11968. https://doi.org/10.1016/j.ijhydene.2020.12.213.

24. Hank, C., Sternberg, A., Köppel, N., Holst, M., Smolinka, T., Schaadt, A., Hebling, C., and Henning, H.-M. (2020). Energy efficiency and economic assessment of imported energy carriers based on renewable electricity. Sustainable Energy Fuels *4*, 2256–2273. https://doi.org/10.1039/D0SE00067A.

25. Kim, A., Kim, H., Lee, H., Lee, B., and Lim, H. (2021). Comparative Economic Optimization for an Overseas Hydrogen Supply Chain Using Mixed-Integer Linear Programming. ACS Sustainable Chem. Eng. *9*, 14249–14262. https://doi.org/10.1021/acssuschemeng.1c05446.

26. Lux, B., Gegenheimer, J., Franke, K., Sensfuß, F., and Pfluger, B. (2021). Supply curves of electricity-based gaseous fuels in the MENA region. Computers & Industrial Engineering *162*, 107647. https://doi.org/10.1016/j.cie.2021.107647.

27. Johnston, C., Ali Khan, M.H., Amal, R., Daiyan, R., and MacGill, I. (2022). Shipping the sunshine: An open-source model for costing renewable hydrogen transport from Australia. International Journal of Hydrogen Energy *47*, 20362–20377. https://doi.org/10.1016/j.ijhydene.2022.04.156.

28. Niermann, M., Timmerberg, S., Drünert, S., and Kaltschmitt, M. (2021). Liquid Organic Hydrogen Carriers and alternatives for international transport of renewable hydrogen. Renewable and Sustainable Energy Reviews *135*, 110171. https://doi.org/10.1016/j.rser.2020.110171.

29. Heuser, P.-M., Ryberg, D.S., Grube, T., Robinius, M., and Stolten, D. (2019). Techno-economic analysis of a potential energy trading link between Patagonia and Japan based on CO2 free hydrogen.

International Journal of Hydrogen Energy *44*, 12733–12747. https://doi.org/10.1016/j.ijhydene.2018.12.156.

30. Moritz, M., Schönfisch, M., and Schulte, S. (2023). Estimating global production and supply costs for green hydrogen and hydrogen-based green energy commodities. International Journal of Hydrogen Energy *48*, 9139–9154. https://doi.org/10.1016/j.ijhydene.2022.12.046.

31. Collis, J., and Schomäcker, R. (2022). Determining the Production and Transport Cost for H2 on a Global Scale. Front. Energy Res. *10*. https://doi.org/10.3389/fenrg.2022.909298.

32. d'Amore-Domenech, R., Leo, T.J., and Pollet, B.G. (2021). Bulk power transmission at sea: Life cycle cost comparison of electricity and hydrogen as energy vectors. Applied Energy *288*, 116625. https://doi.org/10.1016/j.apenergy.2021.116625.

33. Crandall, B.S., Brix, T., Weber, R.S., and Jiao, F. (2022). Techno-Economic Assessment of Green H 2 Carrier Supply Chains. Energy Fuels. https://doi.org/10.1021/acs.energyfuels.2c03616.

34. Di Lullo, G., Giwa, T., Okunlola, A., Davis, M., Mehedi, T., Oni, A.O., and Kumar, A. (2022). Large-scale long-distance land-based hydrogen transportation systems: A comparative techno-economic and greenhouse gas emission assessment. International Journal of Hydrogen Energy *47*, 35293–35319. https://doi.org/10.1016/j.ijhydene.2022.08.131.

35. Hydrogen Council, and McKinsey & Company (2022). Global Hydrogen Flows: Hydrogen trade as a key enabler for efficient decarbonization.

36. Brändle, G., Schönfisch, M., and Schulte, S. (2020). Estimating Long-Term Global Supply Costs for Low-Carbon Hydrogen. EWI Working Paper No 20/04.

37. Andersson, J., and Grönkvist, S. (2019). Large-scale storage of hydrogen. International Journal of Hydrogen Energy *44*, 11901–11919. https://doi.org/10.1016/j.ijhydene.2019.03.063.

38. acatech, and BDI (2021). A Meta-Analysis towards a German-Australian SupplyChain for Renewable Hydrogen: Working Paper HySupply.

39. IRENA, and Methanol Institute (2021). Innovation Outlook: Renewable Methanol (International Renewable Energy Agency).

40. Madhu, K., Pauliuk, S., Dhathri, S., and Creutzig, F. (2021). Understanding environmental trade-offs and resource demand of direct air capture technologies through comparative life-cycle assessment. Nat Energy *6*, 1035–1044. https://doi.org/10.1038/s41560-021-00922-6.

SUPPLEMENTARY INFORMATION

For: Langenmayr, Uwe; Schuler, Julia; Slednev, Viktor; Fichtner, Wolf (2025): Mapping Tomorrow's Energy Journeys – A Global Perspective on the Transport of Synthetic Energy Carriers

SUMMARY:

This supplementary information provides additional content as follows:

1. Additional results calculated for the destinations: the United States, China, Japan, and India
2. Breakdown of total supply costs of the *All-Retrofit* scenario
3. High-resolution version of the used transport routes and transported commodities (*Figure 1-B* in the main manuscript)
4. Results of the *All-Retrofit-Heat* scenario
5. Description of computation infrastructure and computation time
6. Applied data in the approach, including:
    a. Global transport infrastructure
    b. Solar PV and wind onshore generation capacity potentials
    c. Methods and data for the calculation of hydrogen production and electricity generation costs on high geographical resolution
    d. Methods and data for the calculation of conversion costs
    e. Methods and data for the calculation of transport costs
    f. Country specific weighted costs of capital

1 Case Study USA

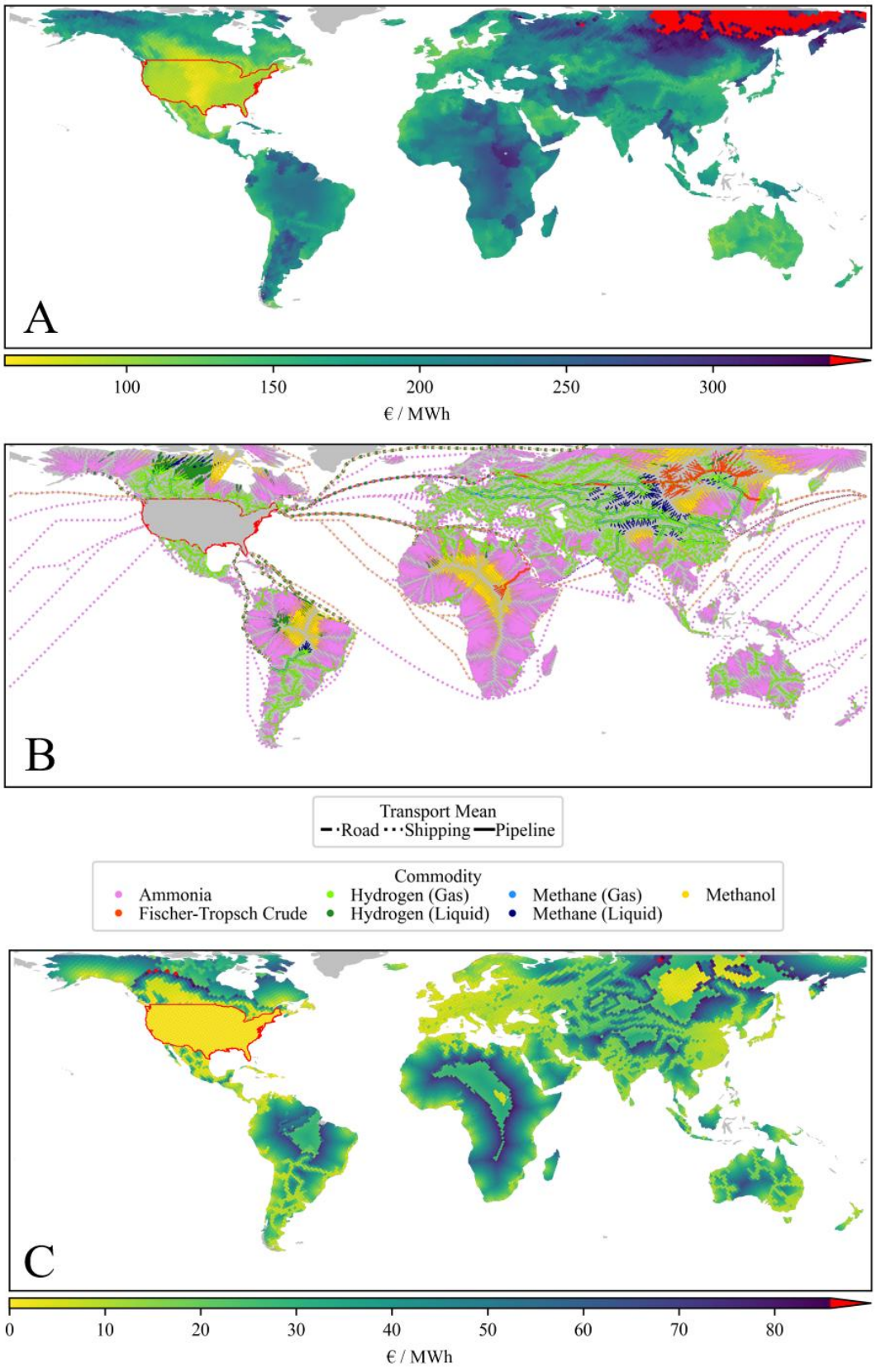

Figure 1: Total supply costs, routes, and transported SECs, and transport costs using the All-Retrofit scenario and the USA (without Hawaii, Alaska, and other oversea territories) as destination

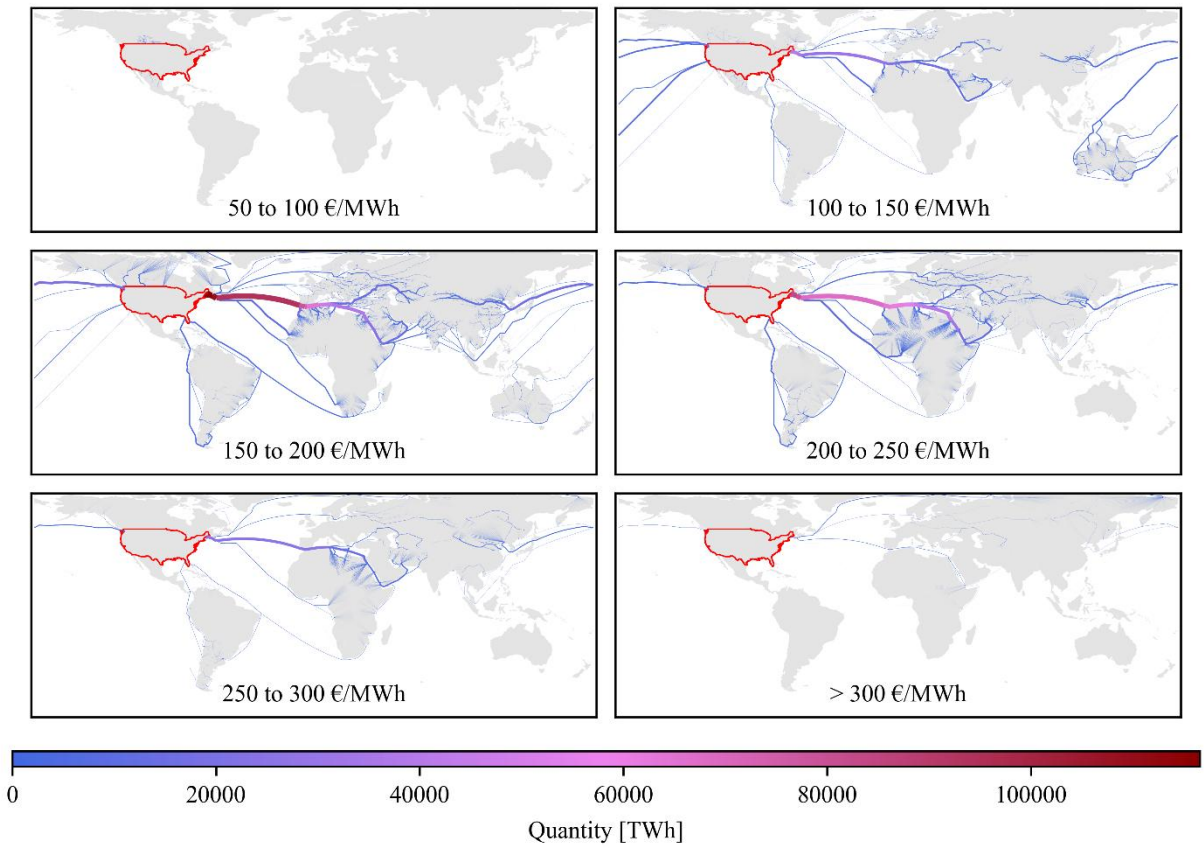

Figure 2: Most used transport routes to the USA in the All-Retrofit scenario, categorized by total supply costs and weighted by potential production quantities

2 Case Study China

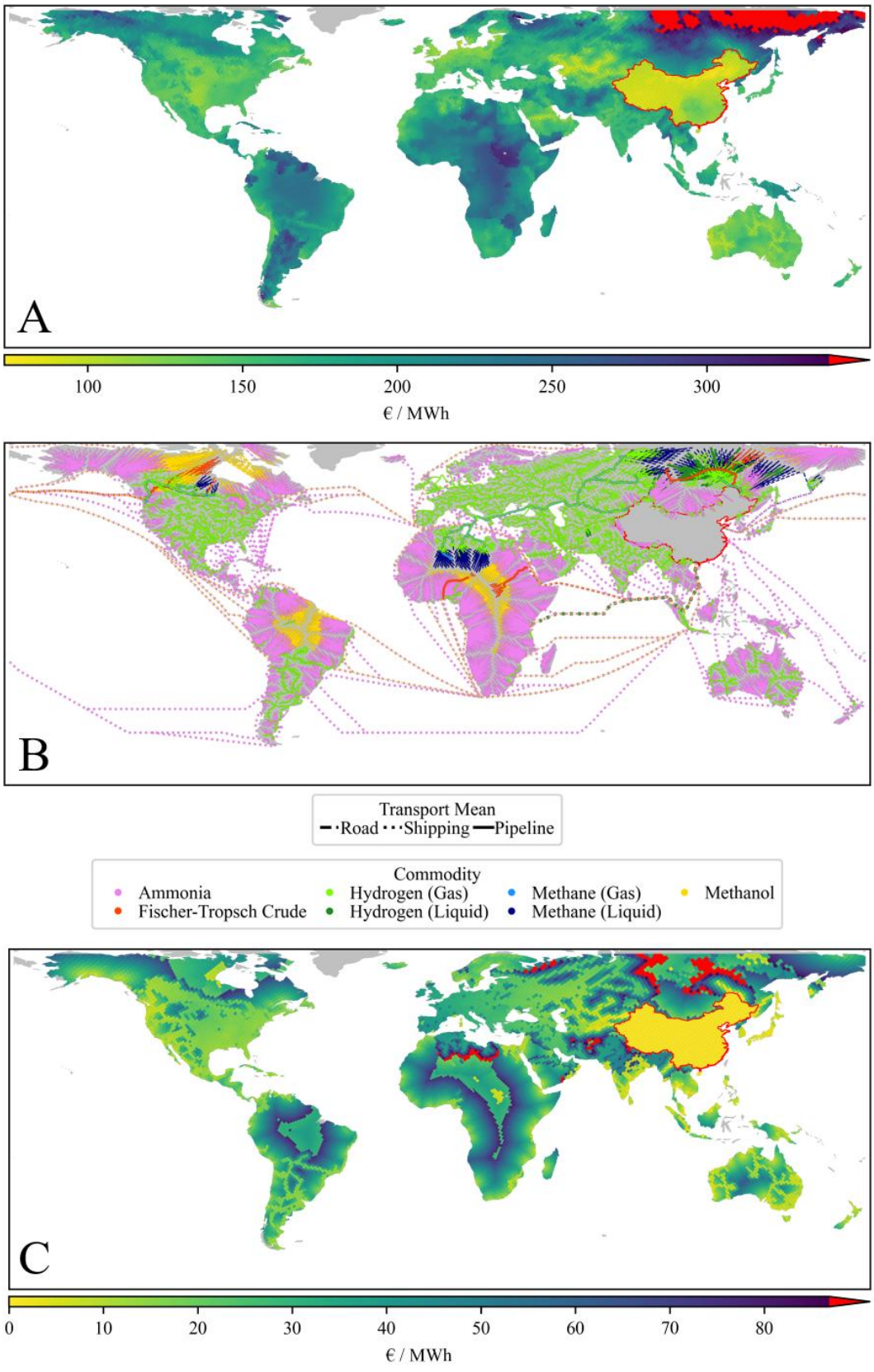

Figure 3: Total supply costs, routes, and transported SECs, and transport costs using the All-Retrofit scenario and mainland China as destination

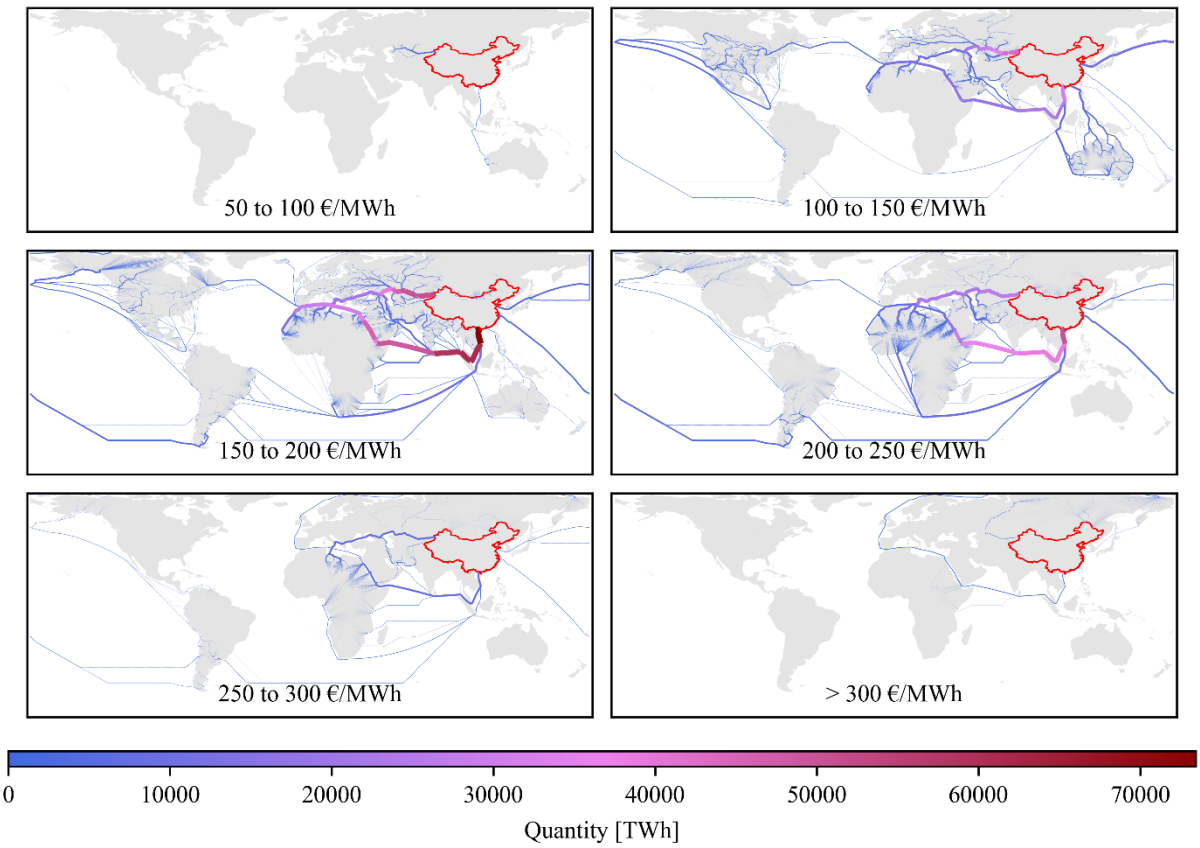

Figure 4: Most used transport routes to the People's Republic of China in the All-Retrofit scenario, categorized by total supply costs and weighted by potential production quantities

3 Case Study Japan

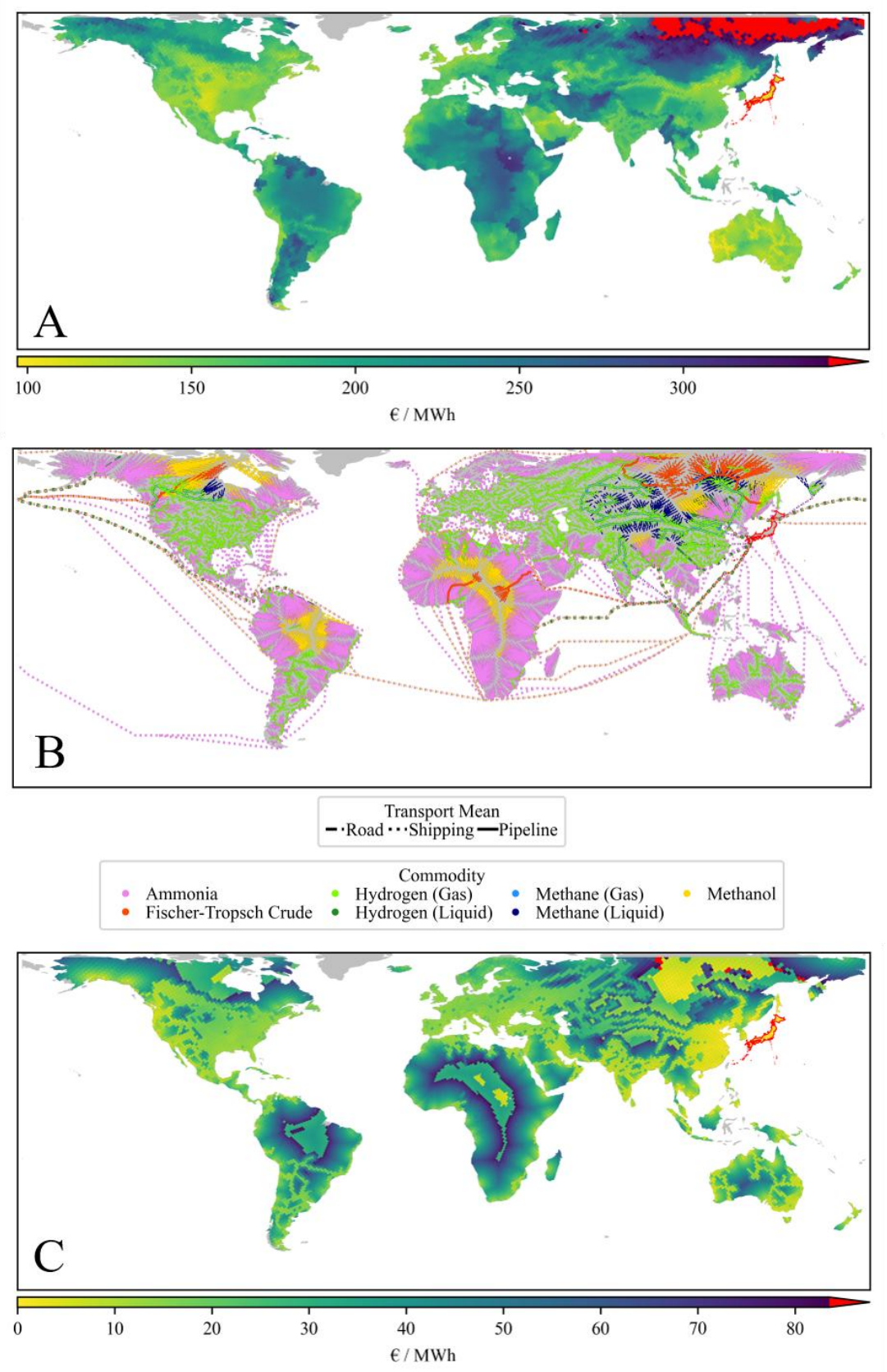

Figure 5: Total supply costs, routes, and transported SECs, and transport costs using the All-Retrofit scenario and Japan as destination

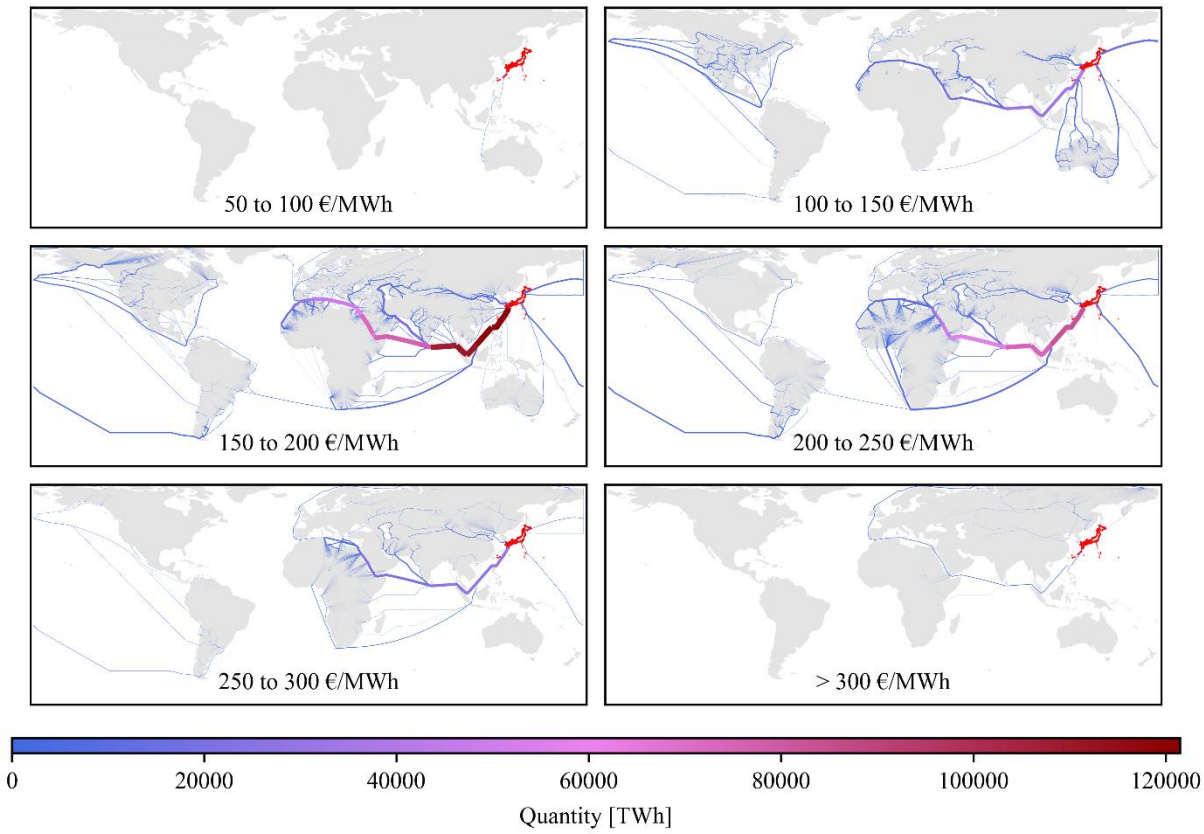

Figure 6: Most used transport routes to Japan in the All-Retrofit scenario, categorized by total supply costs and weighted by potential production quantities

4 Case Study India

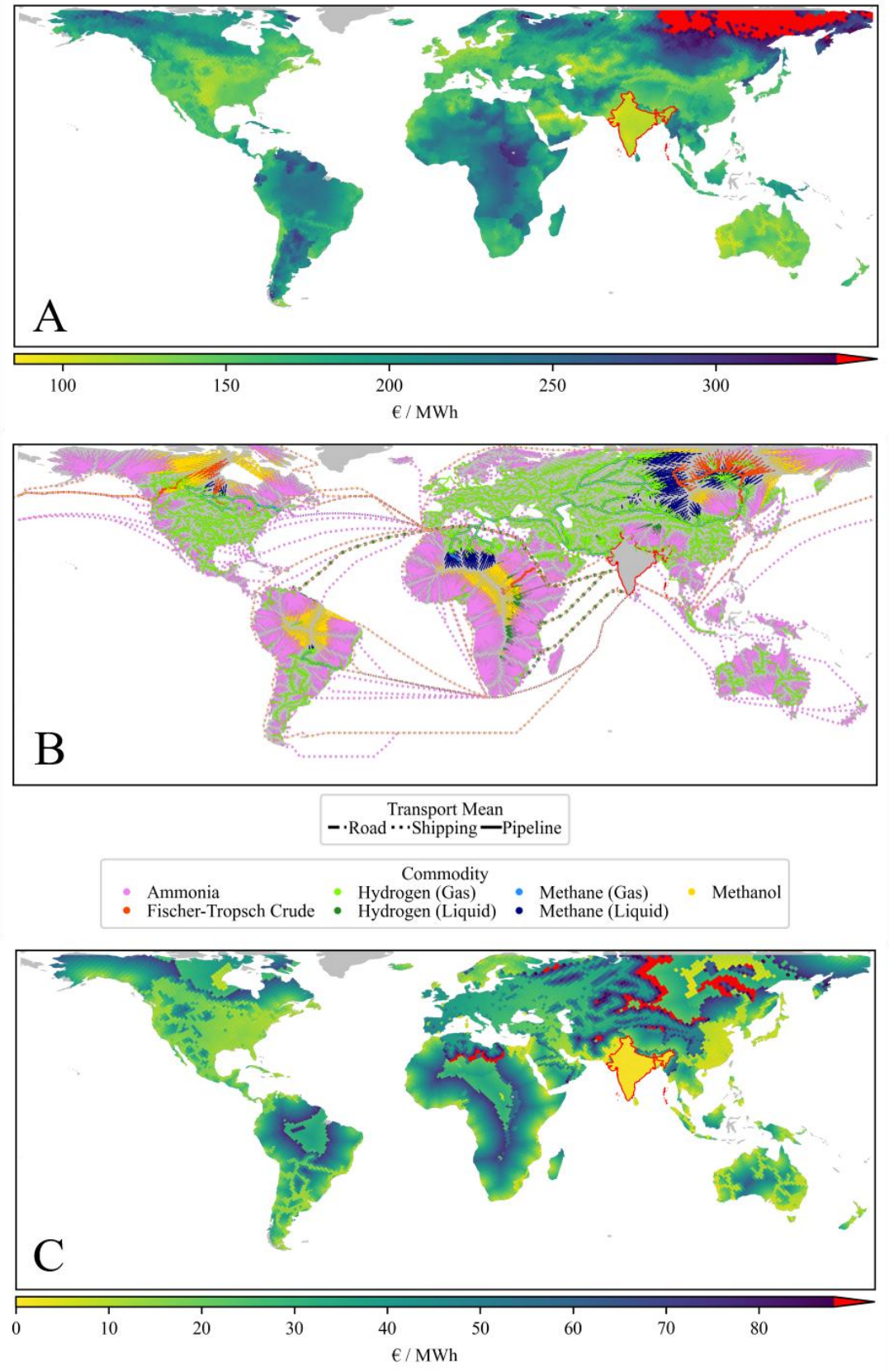

Figure 7: Total supply costs, routes, and transported SECs, and transport costs using the All-Retrofit scenario and India as destination

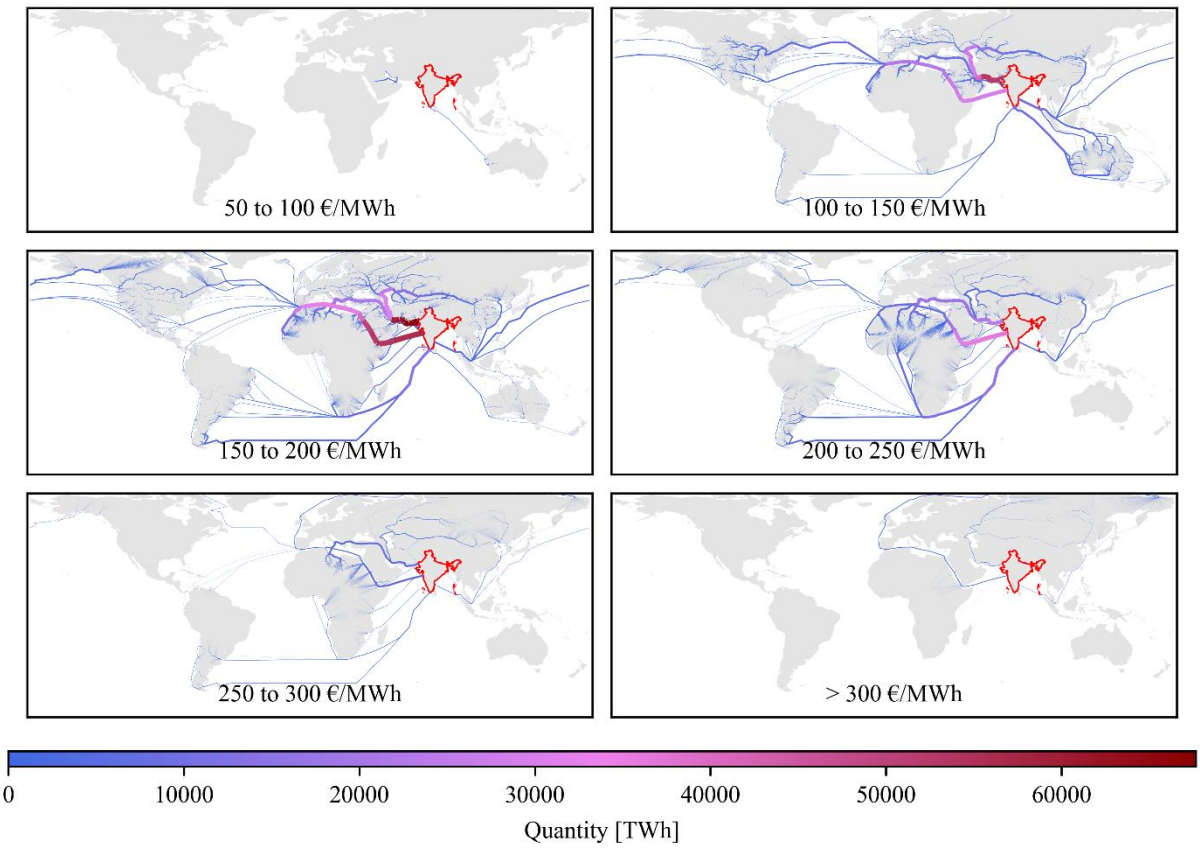

Figure 8: Most used transport routes to India in the All-Retrofit scenario, categorized by total supply costs and weighted by potential production quantities

5 Comparison of all cost types of the All-Retrofit scenario

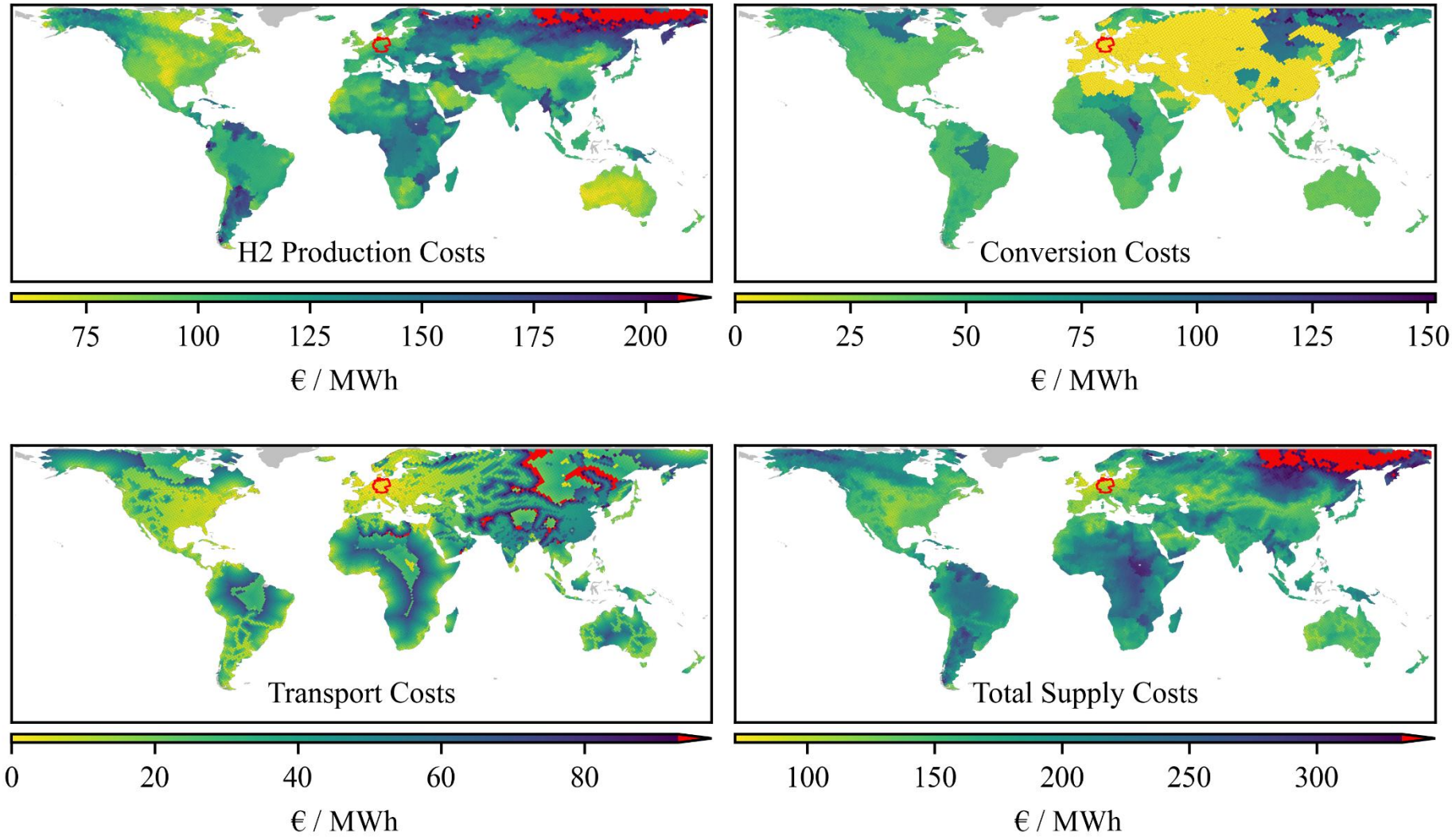

6 Used transport routes and commodities of the All-Retrofit scenario

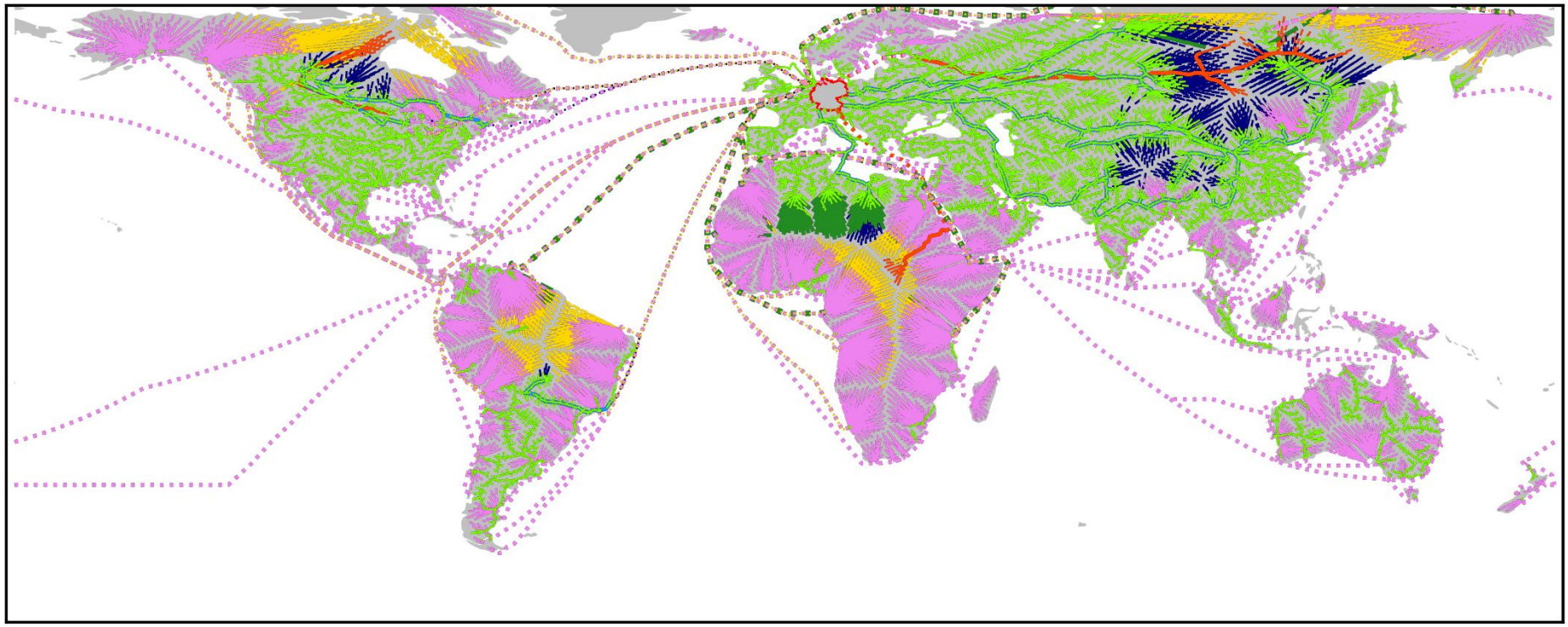

7 All-Retrofit-Heat scenario

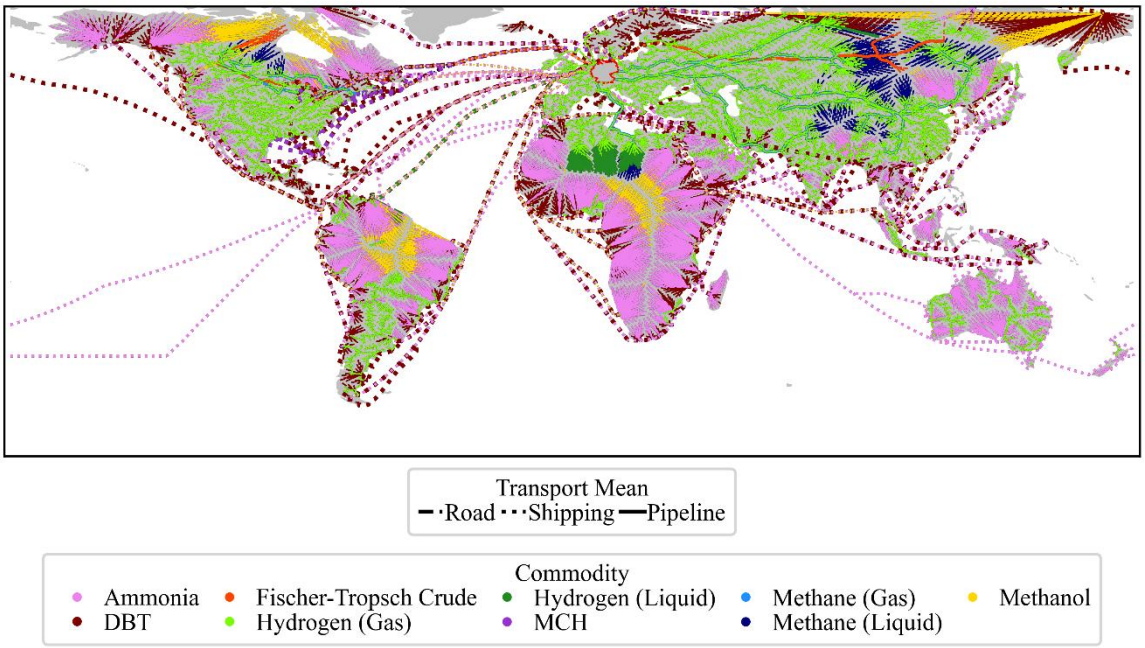

Figure 9: Taken routes and applied SECs in the GER-All-Retrofit-Heat scenario

The dehydrogenation of LOHCs is very heat-intensive: The efficiency of the process in the case of DBT lies at about 65 %, and without a low-cost heat supply, autothermal processes are necessary. To assess the utilization of SECs with high heat demand, we calculated the *All-Retrofit-Heat* scenario, which implements free heat supply at the start location, all ports, and the destination. This scenario leads to using DBT for routes containing shipping transport. *Figure 9* shows all taken routes and applied SECs in the *All-Retrofit-Heat* scenario. In contrast to *Figure 1-B*, we see the choice of DBT instead of ammonia for short-distance road transport, mainly below 1,000 km, and subsequent shipping. DBT, in comparison to ammonia, offers the advantage of a very efficient conversion from hydrogen. In regions with high electricity costs, DBT performs better than ammonia, and covered road distances increase. This is visible in northeastern Russia. Although the hydrogenation of MCH is less expensive than that of DBT, and the transportation costs by ship and truck are comparable to those of DBT, MCH is rarely utilized as the electricity demand for hydrogen release is significantly higher. The utilization of LOHCs only in this scenario shows the central challenge of LOHCs: Without a free or low-cost heat supply, they are at an economic disadvantage compared to other SECs if they are used to supply hydrogen.

8 Infrastructure and calculation time

The heuristic is implemented to achieve high computational efficiency without terminating the most cost-efficient solution. The processor is an AMD Ryzen Threadripper 3990X 64-Core at 2.9 GHz, allowing us to utilize up to 128 CPUs. The system has 256 GB of RAM. The installed operating system is Ubuntu 20.04.6 LTS. This system achieved the computation times per location, as shown in *Figure 10*.

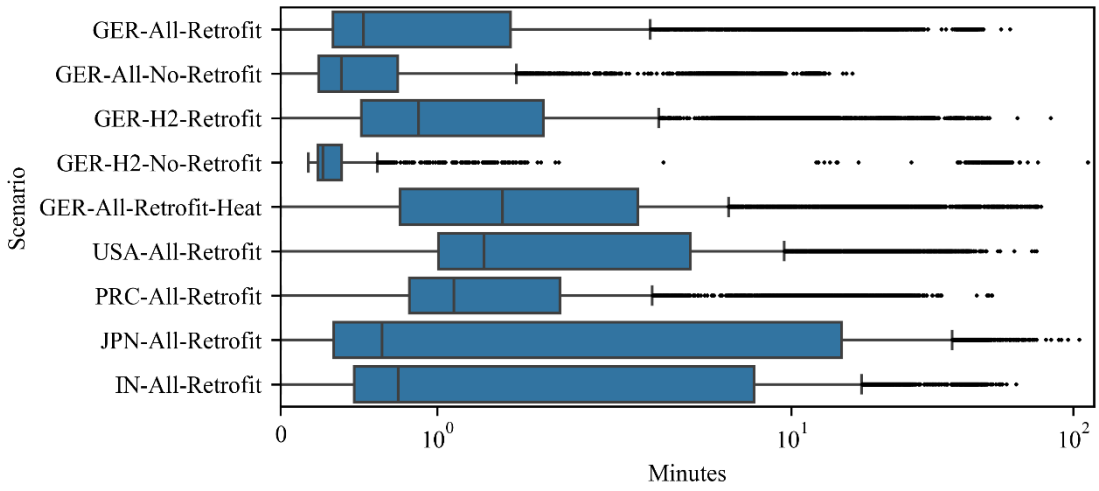

Figure 10: Calculation times per scenario

9 Data

9.1 Global energy carrier infrastructure data

All the underlying infrastructure data is open data. The *Global Energy Monitor* supplies global oil pipeline[1] and gas pipeline[2] infrastructure data. Sea routes are based on the Python package *SeaRoute*[3], which utilizes *Eurostat* data[4] to calculate international shipping routes. Ports are based on the *World Bank*[5] database. *Figure 11* shows the existing infrastructure and shipping network.

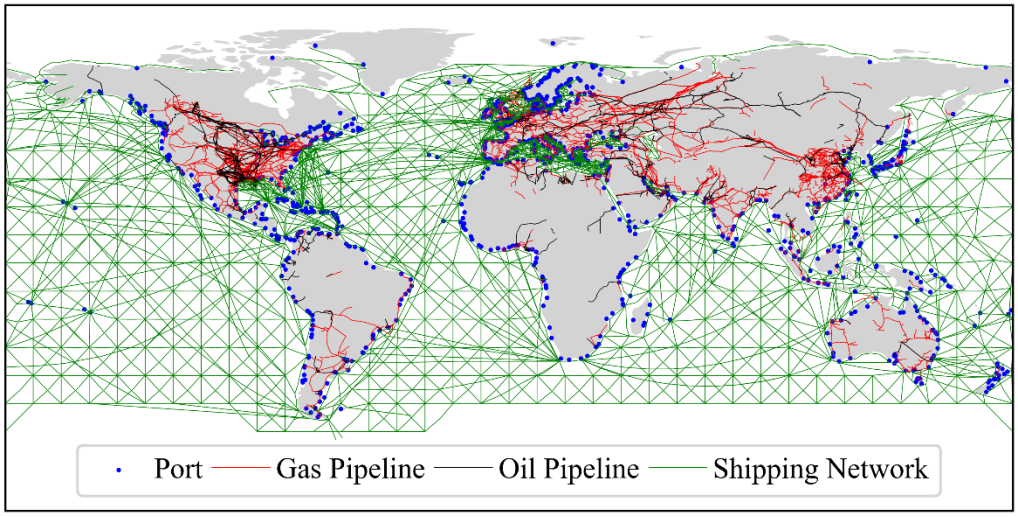

Figure 11: Depiction of port, gas, and oil pipeline data

The data is further processed to apply to the approach. Data exists as independent pipeline segments for pipelines, while more extensive networks are not reported. The individual segments are evaluated for connections and intersections to derive networks from the dataset, and connected segments are grouped into networks. Only such pipeline segments in operation or under construction are considered in this process. We increase the number of access points to the pipeline infrastructure to ensure at least one every 50 kilometers. The resulting networks are then modeled as undirected graphs where the access points and intersections represent the nodes, and the pipelines segment the edges, which are weighted by their length.

The infrastructure itself does not change during the execution of the main algorithm. Therefore, distances and shortest paths between infrastructures are consistent, and the number of shortest path options is limited. Taking advantage of this, the shortest paths within networks are calculated using the Dijkstra algorithm[6]. Distances between ports are derived using the Python package *SeaRoute*[3].

9.2 Global solar PV and onshore wind generation capacity potentials

The definition of the global ground-mounted PV and wind onshore capacity potentials follows the approach described in Slednev et al. (2018)[7] for Europe and extended by Slednev (2024)[8] on a global scale. The general aim of this publication was to define the remaining technical potential for new installations in 2030 concerning land cover suitability restrictions and to exclude areas already exploited for these generation types in 2023. While a detailed description of the various processing steps, the utilized

data, and the assumed restrictions are given in Slednev (2024)[8], the main data sources and restrictions for defining the potentials are listed in the following table:

Table 1: Central assumptions and parameters for the calculation of global solar PV and wind generation capacities

Land use-related restrictions based on Copernicus Global Land Cover		
LandCoverClass	Wind: [Buffer [m], Suitability [-]]	PV: [Buffer [m], Suitability [-]]
Closed forest, evergreen needleleaf	[-, 0.100]	[300, 0]
Closed forest, deciduous needle leaf	[-, 0.100]	[300, 0]
Closed forest, evergreen, broadleaf	[-, 0.100]	[300, 0]
Closed forest, deciduous broadleaf	[-, 0.100]	[300, 0]
Closed forest, mixed	[-, 0.100]	[300, 0]
Closed forest, unknown	[-, 0.100]	[300, 0]
Open forest, evergreen needleleaf	[-, 0.100]	[300, 0]
Open forest, deciduous needle leaf	[-, 0.100]	[300, 0]
Open forest, evergreen broadleaf	[-, 0.100]	[300, 0]
Open forest, deciduous broadleaf	[-, 0.100]	[300, 0]
Open forest, mixed	[-, 0.100]	[300, 0]
Open forest, unknown	[-, 0.100]	[300, 0]
Shrubs	[-, 0.650]	[-, 0100]
Herbaceous vegetation	[-, 0.650]	[-, 0100]
Herbaceous wetland	[1000, 0.100]	[1000, 0]
Moss and lichen	[-, 0.650]	[-, 0.325]
Bare / sparse vegetation	[-, 0.800]	[-, 0.400]
Cultivated and managed vegetation/agriculture (cropland)	[-,0.525]	[-,0.262]
Urban/built-up	[1000,0]	[-,0]
Snow and Ice	[-, 0]	[-, 0]
Permanent water bodies	[400,0]	[-,0]
Open sea	[1000,0]	[1000,0]

Topology-related restrictions based on GTOPO30		
Type	Wind	PV
Altitude	>1800m	>2500m
Slope	>20°	>15° & > 3° if not in SW to SE orientated on NH or NW to NE in SH

Infrastructure-related restrictions based on OpenStreetMap		
Type	Wind: Buffer [m]	PV: Buffer [m]
Pipeline	150	150
Highway	200	0
Overhead line	200	0

Rail	150	0
Waterway	400	100

Protected areas related restrictions based on UNEP-WCMC and IUCN (2021)		
Type	Wind	PV
All	1000	150

Regarding excluding existing wind onshore and ground-mounted PV installations, we relied on an internal database of existing power generators, which is parametrized from various sources, including an open street map, Global Energy Monitor, and IRENA 2023, among others.

9.3 Global hydrogen and electricity production costs and hydrogen production potentials

ERA 5[9] uses a global grid with a resolution of 0.25°x 0.25° to provide high-resolution weather data. Using the open source tool atlite[10], hourly capacity factor profiles for wind and solar PV electricity generation of 11 years are derived for each grid cell and clustered to obtain representative data. Other electricity generation technologies are not considered since we aim for SECs that meet the requirements to count as renewable fuels of non-biological origin (RFNBO)[11]. These requirements define the electricity origin to stem from renewable generators or low-carbon electricity grids, and the generators must be installed explicitly to produce RFNBOs, excluding already installed RES-E capacities or nuclear power. Large hydrogen storage options are unnecessary since we assume a steady hydrogen supply to conversion units, and the demand itself is implemented as total demand per year without considering temporal volatility. A mixed-integer linear optimization is applied to calculate the minimal production costs of 1 GWh of hydrogen for each ERA 5 cell. The optimization minimizes production costs based on annualized investments, fixed and variable operation and maintenance of each component, and purchase, revenues, and disposal costs. The decision variables include individual capacities, each component's operation (conversions, storage, generation), and decisions on purchasing, selling, and disposal. The constraints represent the technical properties of all components (e.g., ramping constraints, minimal and maximal load, efficiencies of conversions, storage operation) and the exchange with markets (purchase, selling, disposal) and environment (emissions, use of ambient air, RES-E generation capacity factors). The operation of the facility and all exchanges with markets and the environment have an hourly resolution, allowing the consideration of the RES-E generation volatility. We do not consider scaling factors for hydrogen production via water electrolysis, making the model linear. This enables scaling the optimal capacities to

capacity potentials to calculate hydrogen production potentials while maintaining minimal production costs. These minimal production costs are integrated into our approach to assess the relation between hydrogen production, conversion to other commodities, and transport, and to provide insights into potential import costs to the destination. A detailed explanation of the calculation of hydrogen production costs can be found in Langenmayr & Ruppert[12]. The country-specific WACCs are based on the work of Kleinschmitt et al.[13]. Since the data are based on the year 2021, we used the correlation between the given WACC and the worldwide governance indicators[14] to consider the development of 2022 (e.g., Russo-Ukrainian War). The production of hydrogen is assumed to take place at the location of electricity generation using a stand-alone production facility, excluding the option of large-scale electricity transmission in our model. The hydrogen production system comprises a proton exchange membrane (PEM) electrolysis, battery storage, and wind and solar PV generator (techno-economic data in *Table 2*). The production plant is depicted in *Figure 12*.

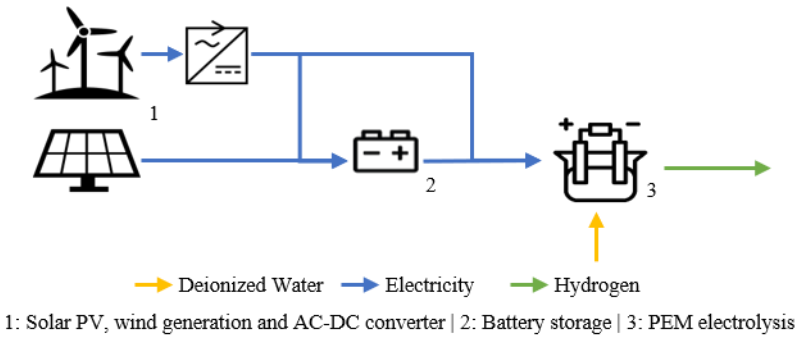

Figure 12: System boundaries of the implemented hydrogen production plant

Figure 13 shows the global hydrogen production costs.

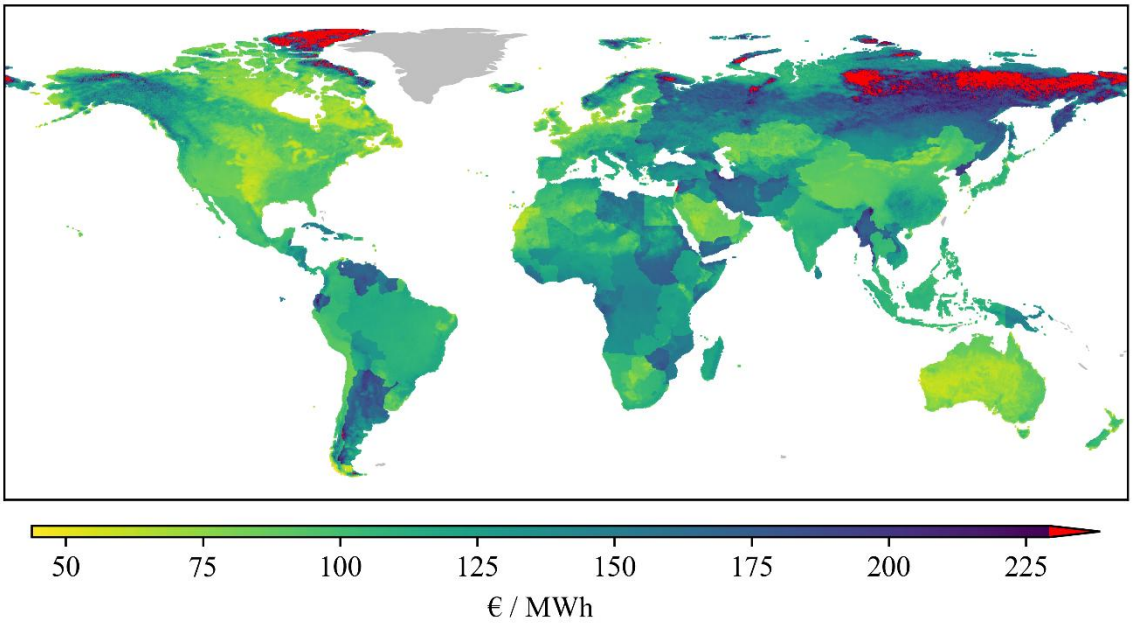

Figure 13: Hydrogen production costs for all grid cells

In addition to hydrogen production, electricity is needed to supply the synthesis processes for the conversion of hydrogen to other SECs. We use the same weather and techno-economic data to calculate electricity generation costs for each grid cell. Since the electricity is only used to supply the synthesis units, we smooth the electricity output to achieve a steady supply since synthesis units are less flexible and process conditions must be maintained to achieve desired efficiencies and outputs. Smoothed electricity output is achieved by implementing a dummy conversion with an efficiency of 100%, without any investment or operating costs, but with a minimal load of 80%. The setup is shown in *Figure 14*. The optimization model's output electricity curve will operate between 80% and 100%. However, we only use the resulting minimal generation costs to calculate conversion costs. The setup of the electricity generation is shown in *Figure 14*.

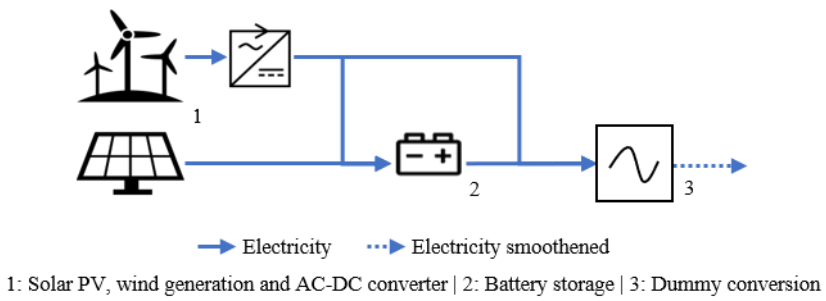

Figure 14: System boundaries of the implemented electricity generation

Table 2: Techno-economic assumptions on wind and solar generators[15], PEM electrolysis[16], and battery storage[17]

Technology	Wind	Solar	PEM electrolysis	Battery storage
Nominal investment	1,040 [€/kW]	310 [€/kW]	810 [€/kW]	330 [€/kWh]
Fixed O&M [%]	1.21	1	4	5.645
Variable O&M [€/kWh]	0.00135	0	0	0.00112
Lifetime [years]	25	30	20	20
Conversion efficiency [%]	-	-	62	-
Minimal load [%]	-	-	7	-
Minimal state of charge [%]	-	-	-	10
Maximum state of charge [%]	-	-	-	90
Round-trip efficiency [%]	-	-	-	85

The uncertainty of renewable generation concerning volatility is typically considered using stochastic or robust optimization methods. Neither sensitivity analysis nor advanced optimization methods have been applied in this work, as substantial computation time increases accompany these methods since they intensify the complexity of the optimization.

9.4 Conversion costs

Eq. (1) shows the method for calculating the specific costs of conversion processes in euros per megawatt hour energy content of the respective product, based on its lower heating value (LHV). Included are investment-related costs, CAPEX, annual operation expenditures, OPEX, as a percentage of CAPEX (cf. *Table 4*), and costs for respective precursors (nitrogen, carbon dioxide, and electricity). An annuity factor, ANF, is used to calculate annuities as presented in *Eq. (2)*, where *dp* stands for the depreciation period of the respective infrastructure in years and WACC for the weighted average costs of capital.

$$Conversion\ costs\ \left[\frac{€}{MWh}\right] = \frac{CAPEX}{Operating\ hours\ p.a.} * (ANF + OPEX) + (electricity, N_2, CO_2)\ demand * costs \quad (1)$$

$$ANF\ [a^{-1}] = \frac{WACC * (1 + WACC)^{dp}}{(1 + WACC)^{dp} - 1} \quad (2)$$

One option for the supply of heat required for endothermal dehydrogenation or cracking processes is either through autothermal processes by combusting the feedstock/reactant, except in the case of DBT and MCH dehydrogenation, where the product hydrogen is combusted. This results in a proportional reduction in

the material stream corresponding to the required heat. *Eq. (3)* shows the conversion efficiency calculation owing to reaction heat provision for ammonia cracking, methanol and methane steam reforming, or for DBT and MCH dehydrogenation. Pre-heating demands of exothermal synthesis processes are neglected, assuming process-internal heat recovery.

$$\eta_{c,c'} := \begin{cases} 1 - \dfrac{\text{heat demand}}{\text{heating value } H_2} & \text{for DBT and MCH dehydrogenation} \\ 1 - \dfrac{\dfrac{\text{heat demand}}{\text{heating value}}}{\text{stoichiometric ration} + \dfrac{\text{heat demand}}{\text{heating value}}} & \text{else} \end{cases} \quad (3)$$

The second option is the supply via waste heat utilization. If this option is set in the configuration, no additional heat is needed from autothermal processes, and the conversion efficiency is 1.

Table 3 indicates the costs associated with conversion processes between all SECs, based on literature (cf. *Table 4*) and calculated as in *Eq. (1)*, targeting 2030. Since uniform WACC and electricity costs are applied to estimate the parameters in the table, but location-specific electricity costs and/or WACC are applied in the heuristic, this table approximates the parameters used. Nitrogen (55 €/t_{N_2}[18]) and carbon dioxide costs (145 €/t_{CO_2}[18]) are uniform for all cases. When converting from one hydrogen derivative to another, it is assumed that it is converted to hydrogen first, and then the synthesis happens in the next step. FTC is not expected to be further converted. All plants have the same annual utilization of 8,000 h. The WACCs are based on the values in *Table 9*. Material costs of the LOHC substances DBT and MCH are neglected following the assumption that they can be recycled indefinitely.

Table 3: Approximation of conversion costs in €/MWh_{Prod} based on uniform electricity generation (45 €/$MWh_{Electricity}$), nitrogen (55 €/t_{N_2}), and carbon dioxide costs (145 €/t_{CO_2}[18]), as well as a WACC of 6%. Values are calculated using Eq. (1) and parameter assumptions presented in Table 4.

from	to	Costs [€/MWh_{Prod}]	from	to	Costs [€/MWh_{Prod}]	from	to	Costs [€/MWh_{Prod}]
G-H_2	L-H_2	40.5	G-H_2	MCH	2.8	G-CH_4	G-H_2	6.0
G-H_2	NH_3	18.6	G-H_2	FTC	81.4	DBT	G-H_2	4.6
G-H_2	MeOH	48.9	L-H_2	G-H_2	0.9	MCH	G-H_2	8.1
G-H_2	G-CH_4	32.6	NH_3	G-H_2	5.2	G-CH_4	L-CH_4	12.1
G-H_2	DBT	4.2	MeOH	G-H_2	4.6	L-CH_4	G-CH_4	0.004

The column "Loss of Material" in *Table 4* illustrates the material loss during conversion steps. Bold values are losses due to auto thermal processes, calculated using *Eq. (3)* based on the heat requirements listed in

Table 4, column “Heat Demand”, for ammonia cracking, methanol, and methane steam reforming (stoichiometric ratios for the respective chemical reactions: 5.63 kg_{NH3}/kg_{H2}, 5.29 kg_{MeOH}/kg_{H2}, and 2.65 kg_{CH4}/kg_{H2}), as well as for DBT and MCH dehydrogenation. Other values represent literature-based losses not related to the provision of reaction heat.

Table 4: Literature values and references for the calculation of conversion costs

	Capital costs CAPEX		Operating costs OPEX [$\%_{CAPEX}$/a]		Deprec. period [a]		Electricity demand		Heat demand		Loss of material [%]		Precursor demand	
$GH_2 \rightarrow LH_2$	1,497,967 €/MW_{H2}	[19]	8.00	[19]	20	[19]	6.78 MWh/t_{H2}	[19]	none		1.65	[19]		
$GH_2 \rightarrow NH_3$	15,000 k€/(tH_2/h)	[18]	3.00	[20]	20	[18]	1.5 MWh/t_{H2}	[18]	none/exotherm				4.63 tN_2/tH_2	[18]
$GH_2 \rightarrow$ MeOH	1,090 k€/MW_{MeOH}	[21]	1.75	[19]	30	[21]	0.1 MWh/t_{MeOH}	[21]	none/exotherm				0.25tCO_2/MWh_{MeOH}	[19]
$GH_2 \rightarrow$ G-CH_4	278 k€/MW_{CH4}	[19]	4.00	[19]	30	[19]	none		none/exotherm				0.20 tCO_2/MWh_{CH4}	[19]
$GH_2 \rightarrow$ DBT	256 k€/(30 kg_{H2}/h)	[22]	4.00	[22]	20	[23]	0.1 MWh/t_{H2}	[22]	none/exotherm		0.1	[22]		
$GH_2 \rightarrow$ MCH	157 k€/(30 kg_{H2}/h)	[22]	4.00	[22]	20	[23]	0.2 MWh/t_{H2}	[22]	none/exotherm		0.1	[22]		
$GH_2 \rightarrow$ FTC	1,600 k€/MW_{FTC}	[19]	3.00	[19]	25	[19]	0.02 MWh/MWh_{FTC}	[19]	none/exotherm				0.41tCO_2/MWh_{FTC}	[19]
$LH_2 \rightarrow GH_2$	4,320 €/MW_{H2}	[19]	3.00	[19]	10	[19]	0.6 MWh/t_{H2}	[19]	none					
$NH_3 \rightarrow GH_2$	8,800 k€/(tH_2/h)	[18]	3.00	[20]	20	[18]	0.95 MWh/t_{H2}	[18]	6.65 MWh/t_{H2}	[20]	**18.60**			
MeOH $\rightarrow GH_2$	16,318 €/MW_{H2}	[19]	4.00	[19]	20	[19]	3.2 MWh/t_{H2}	[19]	4.5 MWh/t_{H2}	[19]	**12.73**			
G-$CH_4 \rightarrow GH_2$	470,085 €/MW_{H2}	[19]	3.00	[19]	30	[19]	none		0.8 $kgCH_4/kg_{H2}$	[19]	**23.19**			
DBT $\rightarrow GH_2$	282 k€/(30 kg_{H2}/h)	[22]	4.00	[22]	20	[23]	0.1 MWh/t_{H2}	[22]	11.6 MWh/t_{H2}	[23]	**34.80**			
MCH $\rightarrow GH_2$	127 k€/(30 kg_{H2}/h)	[22]	4.00	[22]	20	[23]	4.5 MWh/t_{H2}	[22]	13.5 MWh/t_{H2}	[23]	**40.50**			
GCH4 $\rightarrow$ L-CH_4	740 €/kW_{CH4}	[19]	3.50	[19]	25	[19]	0.5 MWh/t_{CH4}	[19]	none					
L-$CH_4 \rightarrow$ G-CH_4	280 €/MW_{CH4}	[19]	3.50	[19]	30	[19]	none		none		2.0	[19]		

9.5 Transport costs and assumptions

The model includes ship transport for all liquid energy carriers and pipeline transport via existing or new pipelines for gaseous hydrogen, gaseous methane, and FTC. All energy carriers can be transported by truck, except for methane in gaseous form, due to a lack of techno-economic data. While shipping and pipeline transport costs are obtained from the literature, road transport costs *RTC* are calculated using *Eq. (4)*, with annual operating hours *aoh*, average speed *avs*, trailer capacity *trc*, fuel consumption *fuc*, fuel price *fup*, and hourly operating costs *hoc*. The trailer capacity *trc* is halved to account for the empty return trip.

$$RTC\left[\frac{€}{MWh * 1{,}000\ km}\right] = \frac{[CAPEX * (ANF + OPEX)]_{Truck} + [CAPEX * (ANF + OPEX)]_{Trailer} + aoh * (avs * fuc * fup + hoc)}{aoh * avs * trc/2} \quad (4)$$

For all transport means, we assume the marginal user approach. This means that the supplier of SECs is using existing infrastructure only by paying a certain "fee" without arranging investments. *Table 5* displays the transport costs for all SECs and respective eligible modes of transport.

*Table 5: Transport costs in €/(MWh*1,000 km)*

	G-H_2	**L-H_2**	**NH_3**	**MeOH**	**G-CH_4**	**L-CH_4**	**DBT**	**MCH**	**FTC**
New pipeline	4.9				1.4				0.4
Existing pipeline	3.1				0.9				0.2
Ship incl. invest		1.4	0.7	0.5		0.9	1.3	1.3	0.1
Truck incl. invest	126.6	23.0	33.6	15.1		16.7	42.6	43.3	7.5

Pipeline transport costs are adopted from Saadi et al.[24], with a 36-inch pipeline diameter and flow velocities of 10 m/s for hydrogen and methane pipelines and 1 m/s for oil pipelines (used for FTC). The mean of the daily closing exchange rate, averaged over the publication year 2018, 0.85 €/$, is used for the conversion from dollar to euro. *Table 6* contains literature values used for pipeline transport and liquid methane shipping. Other shipping costs are obtained from the Excel calculation tool provided for download with the publication of Staiß et al.[18] based on a shipping distance of 15,000 kilometers. Ship sizes range from a total tonnage of 75,000 t for chemical tankers handling ammonia, methanol, DBT, and MCH to 130,000 t for liquid gas tankers for hydrogen and 318,000 t for huge crude carriers (VLCC) for FTC.

Parameters for the calculation of road transport costs *RTC* as in *Eq. (4)*, are adopted from Niermann et al.[22], comprising 3,500 hours annual truck operation *aoh* at an average speed *avs* of 60 km/h, a 30 l/100km fuel consumption *fuc*, a fuel price *fup* of 1.19 €/l, and hourly operating costs *hoc* of 35 €/h. *Table 7* provides further literature values for calculating specific *RTC* for gaseous and liquid hydrogen, ammonia, DBT, and MCH. Since they are liquid hydrocarbons with similar handling requirements, methanol and FTC costs are derived from DBT/MCH *RTC* using heating values (*Table 8*). An expert interview yielded truck transport costs for liquid methane.

Further assumptions are that the maximum distance for newly built pipelines is 100 km, since infrastructure planning is complex and larger interregional projects are beyond the scope. For road transport, we assume no maximum distance for our model runs. However, it is possible to implement this in the model. Not limiting the maximum distance of road transport allows for calculating transport costs even for remote locations with no infrastructure. For road transport and newly built pipeline infrastructure, distances are multiplied by 150% to account for obstacles in the route. This reduces the newly built pipelines' as-the-crow-flies distance to 2/3 of 100 km.

Table 6: Literature values for the calculation of pipeline and methane ship transport costs (all Saadi et al.[24])

	Transport costs [$/(km*J)]
$G\text{-}H_2$	
New pipeline	$1.6/10^{12}$
Existing Pipeline	$(1.6\text{-}0.58)/\ 10^{12}$
$G\text{-}CH_4$	
New pipeline	$0.47/10^{12}$
Existing Pipeline	$(0.47\text{-}0.18)/\ 10^{12}$
FTC	
New pipeline	$0.12/10^{12}$
Existing Pipeline	$(0.12\text{-}0.04)/\ 10^{12}$
$L\text{-}CH_4$	
Ship	$0.30/10^{12}$

Table 7: Literature values for the calculation of truck transport costs (Niermann et al.[22], unless otherwise specified)

	Capital costs CAPEX [€]	**Operating costs OPEX [%/a]**	**Life span [a]**	**Trailer capacity [t]**
Truck	160,000	12	8	-
Trailer				
$G\text{-}H_2$	550,000	2	12	0.72

L-H_2	860,000		2		12		4.5	
NH_3	220,000	[25]	2	[25]	20	[25]	14.6	[25]
DBT	150,000		2		12		28.5	[26]
MCH	150,000		2		12		28.5	[26]
MeOH, FTC	analogous to DBT							

Table 8: Lower heating values and hydrogen contents

	Lower heating value[kWh/kg]	**Hydrogen content [wt.-%]**
H_2	33.33	100
NH_3	5.17	17.7
MeOH	5.83	12.5
DBT	-	6.2
MCH	-	6.16
FTC	11.75	-
CH_4	13.9	25

The electricity transmission infrastructure is not considered a transport option, which could improve our approach.[19,27] We have taken this decision since the consideration would shift the focus from the transportation and supply of SECs to a broader view of the energy transition across all sectors. In addition, the model and parameter uncertainties of such a large-scale model could further affect the quality of the transport model.

9.6 WACC

Table 9: Country-specific WACC based on [13]and [14]

Country/Territory	WACC	Country/Territory	WACC
Aruba	0.063	Liberia	0.121
Andorra	0.12	Libya	0.164
Afghanistan	0.164	St. Lucia	0.08
Angola	0.12	Liechtenstein	0.047
Anguilla	0.08	Sri Lanka	0.12
Albania	0.091	Lesotho	0.102
United Arab Emirates	0.052	Lithuania	0.059
Argentina	0.163	Luxembourg	0.047
Armenia	0.082	Latvia	0.059
American Samoa	0.062	Kosovo	0.0916
Antigua and Barbuda	0.08	Macau	0.075
Australia	0.047	Morocco	0.071
Austria	0.051	Monaco	0.059
Azerbaijan	0.076	Moldova	0.11
Burundi	0.164	Madagascar	0.092
Belgium	0.053	Maldives	0.11
Benin	0.101	Mexico	0.063
Burkina Faso	0.109	Marshall Islands	0.062
Bangladesh	0.082	North Macedonia	0.082
Bulgaria	0.063	Mali	0.12

Bahrain	0.101	Malta	0.055
Bahamas	0.076	Myanmar	0.1467
Bosnia and Herzegovina	0.11	Mongolia	0.11
Belarus	0.122	Montenegro	0.091
Belize	0.144	Mozambique	0.134
Bermuda	0.055	Mauritania	0.092
Bolivia	0.101	Martinique	0.059
Brazil	0.076	Mauritius	0.063
Barbados	0.12	Malawi	0.121
Brunei	0.075	Malaysia	0.059
Bhutan	0.075	Namibia	0.082
South Sudan	0.164	Niger	0.11
Botswana	0.055	Nigeria	0.101
Central African Republic	0.121	Nicaragua	0.11
Canada	0.047	Netherlands	0.047
Switzerland	0.047	Norway	0.047
Chile	0.054	Nepal	0.092
China	0.054	Nauru	0.062
Côte d'Ivoire	0.082	New Zealand	0.047
Cameroon	0.101	Oman	0.082
Republic of the Congo	0.134	Pakistan	0.11
Colombia	0.066	Panama	0.063
Comoros	0.102	Palau	0.075
Cape Verde	0.101	Peru	0.059
Costa Rica	0.101	Philippines	0.066
Cuba	0.134	Papua New Guinea	0.101
Cayman Islands	0.053	Poland	0.055
Cyprus	0.076	Puerto Rico	0.08
Czechia	0.053	North Korea	0.164
Germany	0.047	Portugal	0.069
Djibouti	0.092	Paraguay	0.071
Dominica	0.08	Qatar	0.053
Denmark	0.047	Réunion	0.059
Dominican Republic	0.082	Romania	0.069
Algeria	0.092	Russia	0.121
Ecuador	0.144	Rwanda	0.101
Egypt	0.101	Samoa	0.062
Eritrea	0.164	Saudi Arabia	0.054
Spain	0.063	Sudan	0.164
Estonia	0.054	Senegal	0.082
Ethiopia	0.101	Singapore	0.047
Finland	0.051	Solomon Islands	0.11
Fiji	0.082	Sierra Leone	0.121
France	0.052	El Salvador	0.11
Micronesia	0.062	San Marino	0.059
Gabon	0.12	Somalia	0.164
United Kingdom	0.053	São Tomé and Principe	0.102
Georgia	0.076	Suriname	0.144
Ghana	0.11	Slovakia	0.055
Guinea	0.092	Slovenia	0.059
Gambia	0.102	Sweden	0.047
Guinea-Bissau	0.102	Eswatini	0.102
Equatorial Guinea	0.102	Seychelles	0.102
Greece	0.082	Syria	0.164
Grenada	0.08	Chad	0.121
Guatemala	0.071	Togo	0.11

French Guiana	0.059	Thailand	0.063
Guam	0.08	Tajikistan	0.11
Guyana	0.121	Turkmenistan	0.121
Hong Kong	0.053	Timor-Leste	0.121
Honduras	0.091	Tonga	0.062
Croatia	0.071	Trinidad and Tobago	0.071
Haiti	0.121	Tunisia	0.101
Hungary	0.069	Turkey	0.101
Indonesia	0.066	Tuvalu	0.062
India	0.069	Taiwan	0.053
Ireland	0.055	Tanzania	0.101
Iran	0.164	Uganda	0.101
Iraq	0.12	Ukraine	0.11
Iceland	0.055	Uruguay	0.066
Israel	0.054	United States of America	0.047
Italy	0.069	Uzbekistan	0.091
Jamaica	0.101	St. Vincent and the Grenadines	0.08
Jordan	0.091	Venezuela	0.153
Japan	0.054	Virgin Islands (U.S.)	0.047
Kazakhstan	0.069	Viet Nam	0.082
Kenya	0.101	Vanuatu	0.062
Kyrgyz Republic	0.101	West Bank and Gaza	0.121
Cambodia	0.101	Jersey, Channel Islands	0.047
Kiribati	0.062	Yemen	0.164
St. Kitts and Nevis	0.08	Serbia	0.082
South Korea	0.052	South Africa	0.076
Kuwait	0.054	The Democratic Republic of the Congo	0.12
Laos	0.134	Zambia	0.096
Lebanon	0.239	Zimbabwe	0.164

10 References

1. Global Energy Monitor (2023). Global Oil Infrastructure Tracker [Data].

2. Global Energy Monitor (2023). Global Gas Infrastructure Tracker [Data].

3. genthalili (2022). SeaRoute [Software].

4. Eurostat (2021). SeaRoute [Software].

5. The World Bank (2020). Global - International Ports [Data].

6. Hagberg, A., Schult, D., and Swart, P. Exploring Network Structure, Dynamics, and Function using NetworkX.

7. Slednev, V., Bertsch, V., Ruppert, M., and Fichtner, W. (2018). Highly resolved optimal renewable allocation planning in power systems under consideration of dynamic grid topology. Computers & Operations Research *96*, 281–293. https://doi.org/10.1016/j.cor.2017.12.008.

8. Slednev, V. (2024). Development of a techno-economic energy system model considering the highly resolved conversion and multimodal transmission of energy carriers on a global scale. Preprint at Karlsruher Institut für Technologie (KIT), https://doi.org/10.5445/IR/1000170863 https://doi.org/10.5445/IR/1000170863.

9. Hersbach, H., Bell, B., Berrisford, P., Hirahara, S., Horányi, A., Muñoz-Sabater, J., Nicolas, J., Peubey, C., Radu, R., Schepers, D., et al. (2020). The ERA5 global reanalysis. Quart J Royal Meteoro Soc *146*, 1999–2049. https://doi.org/10.1002/qj.3803.

10. Hofmann, F., Hampp, J., Neumann, F., Brown, T., and Hörsch, J. (2021). atlite: A Lightweight Python Package for Calculating Renewable Power Potentials and Time Series. JOSS *6*, 3294. https://doi.org/10.21105/joss.03294.

11. European Union (2024). Directive (EU) 2018/2001 of the European Parliament and of the Council of 11 December 2018 on the promotion of the use of energy from renewable sources (recast).

12. Langenmayr, U., and Ruppert, M. (2023). Calculation of Synthetic Energy Carrier Production Costs with high Temporal and Geographical Resolution (Karlsruher Institut für Technologie (KIT)) https://doi.org/10.5445/IR/1000162460.

13. Kleinschmitt, C., Fragoso García, J., Franke, K., Teza, D., Seidel, L., Ebner, A., and Baier, M. (2022). Weltweite Potenziale erneuerbarer Energien. HYPAT Working Paper 03/2022.

14. Kaufmann, D., and Kraay, A. Worldwide Governance Indicators - 2023 Update.

15. Danish Energy Agency (2023). Technology Data.

16. Smolinka, T., Wiebe, N., Sterchele, P., Palzer, A., Lehner, F., Jansen, M., Kiemel, S., Miehe, R., Wahren, S., and Zimmermann, F. (2018). Studie IndWEDe: Industrialisierung der Wasserelektrolyse in Deutschland: Chancen und Herausforderungen für nachhaltigen Wasserstoff für Verkehr, Strom und Wärme: im auftrag von Bundesministerium für Verkehr und digitale Infrastruktur (BMVI).

17. Cole, W., and Karmakar, A. (2023). Cost Projections for Utility-Scale Battery Storage: 2023 Update (National Renewable Energy Laboratory).

18. Staiß, F., Adolf, J., Ausfelder, F., Erdmann, C., Hebling, C., Jordan, T., Klepper, G., Müller, T., Palkovits, R., Poganietz, W.-R., et al. (2022). Optionen für den Import grünen Wasserstoffs nach Deutschland bis zum Jahr 2030: Transportwege - Länderbewertungen - Realisierungserfordernisse (acatech - Deutsche Akademie der Technikwissenschaften) https://doi.org/10.48669/esys_2022-8.

19. Hampp, J., Düren, M., and Brown, T. (2022). Import options for chemical energy carriers from renewable sources to Germany. PLoS ONE 18(2): e0262340. https://doi.org/10.1371/journal.

20. Collis, J., and Schomäcker, R. (2022). Determining the Production and Transport Cost for H2 on a Global Scale. Front. Energy Res. *10*. https://doi.org/10.3389/fenrg.2022.909298.

21. Danish Energy Agency (2023). Technology Data for Renewable Fuels: Version 10, 08/2023.

22. Niermann, M., Timmerberg, S., Drünert, S., and Kaltschmitt, M. (2021). Liquid Organic Hydrogen Carriers and alternatives for international transport of renewable hydrogen. Renewable and Sustainable Energy Reviews *135*, 110171. https://doi.org/10.1016/j.rser.2020.110171.

23. Johnston, C., Ali Khan, M.H., Amal, R., Daiyan, R., and MacGill, I. (2022). Shipping the sunshine: An open-source model for costing renewable hydrogen transport from Australia. International Journal of Hydrogen Energy *47*, 20362–20377. https://doi.org/10.1016/j.ijhydene.2022.04.156.

24. Saadi, F.H., Lewis, N.S., and McFarland, E.W. (2018). Relative costs of transporting electrical and chemical energy. Energy Environ. Sci. *11*, 469–475. https://doi.org/10.1039/C7EE01987D.

25. International Energy Agency (2019). The Future of Hydrogen: Seizing today's opportunities.

26. Reuß, M.E. (2019). Techno-Economic Analysis of Hydrogen Infrastructure Alternatives (RWTH Aachen University) https://doi.org/10.18154/RWTH-2019-07432.

27. Neumann, F., Zeyen, E., Victoria, M., and Brown, T. (2023). The potential role of a hydrogen network in Europe. Joule *7*, 1793–1817. https://doi.org/10.1016/j.joule.2023.06.016.